SPACE SCIENCES SERIES OF ISSI

Origin and Early Evolution of Comet Nuclei

H. Balsiger, K. Altwegg, W. Huebner,
T. Owen, R. Schulz (Eds.)

Springer

INTERNATIONAL SPACE SCIENCE INSTITUTE

H. Balsiger · K. Altwegg · W. Huebner · T. Owen · R. Schulz
Editors

Origin and Early Evolution of Comet Nuclei

Workshop honouring Johannes Geiss on the occasion of his 80th birthday

Previously published in *Space Science Reviews* Volume 138, Issues 1–4, 2008

Springer

H. Balsiger
Universität Bern
Physikalisches Institut
Bern Switzerland

K. Altwegg
Universität Bern
Physikalisches Institut
Bern Switzerland

W. Huebner
Space Research Division
Southwest Research Institute (SWRI)
San Antonio, TX, USA

T. Owen
University of Hawaii
Institute for Astronomy
Honolulu, HI, USA

R. Schulz
European Space Agency (ESA)
Noordwijk, The Netherlands

Cover illustration: Composite image of the nucleus of comet Halley taken by the Halley Multicolour Camera onboard ESA's Giotto spacecraft during the flyby on 14 March 1986.

Library of Congress Control Number: 2008936039

ISBN-978-0-387-85454-0 e-ISBN-978-0-387-85455-7

Printed on acid-free paper.

1

springer.com

Contents

Foreword

Originally published in the journal Space Science Reviews, Volume 138, Nos 1–4.
DOI: 10.1007/s11214-008-9412-6

In 2006 Johannes Geiss celebrated his 80th birthday. His many impressive achievements as a scientist and pioneer of European and Swiss space science have been celebrated at several occasions. The Workshop on "Origin and Early Evolution of Comet Nuclei" was the last of these celebrations and for several reasons an especially appropriate one. Not only did it take place in the city—Bern—where Geiss spent the most part of his scientific life but also at the institute—ISSI—which was established after his retirement from the University of Bern according to his ideas. And finally cometary science possibly is the field that most clearly brings together all the disciplines in which Johannes Geiss has been active during his long and successful career. His contributions in geosciences, meteoritics, cosmology, origin of the solar system and the evolution of the Sun and the planets would all find new experimental nourishment if the origin and evolution of the most primitive bodies in the solar system—the comets—would be better known. Geiss was so convinced that comets were an important clue in his puzzle that he fought hard for the European Giotto mission when it was threatened to be abandoned for lack of interest by NASA and the US scientists. And he was one of the fathers of the HORIZON 2000 plan of ESA, which included the Comet Sample Return Cornerstone, a mission that was finally implemented in reduced form as Comet Rendezvous Mission Rosetta (now on its way to Comet Churyumov-Gerasimenko).

The closing session of the workshop was held as open lectures at Johannes Geiss' former home institution—the Physikalisches Institut—and was well attended by students, former collaborators, faculty and a broader public.

This reflected the fact that in Bern Johannes Geiss as a teacher and scientist has not only been one of the most well known personalities but also one of the most popular. He has built today's Department for Space Research and Planetology out of a small Group for Mass Spectrometry and developed it into the centre for experimental space physics in Switzerland. Due to many successful novel instrument designs coming out of Bern, Swiss space research achieved a leading role within the European Space Agency. A star without star manners Johannes Geiss achieved this by being an exceptionally good team player. He knew that you could request almost anything from your collaborators as long as you are an example in dedication. And dedicated to science he was and still is.

H. Balsiger et al. (eds.), *Origin and Early Evolution of Comet Nuclei*
DOI: 10.1007/978-0-387-85455-7_1

With this same dedication he even led his football team of physicists to become runner-up at the University's yearly championship.

All the Workshop participants, his former collaborators at the University and at ISSI and many of his friends present wished Johannes all the best for a happy and productive future and joined in a very warm applause.

October 2006
Hans Balsiger
e-mail: hans.balsiger@space.unibe.ch

Participant List

1. Kathrin Altwegg
2. Walter Huebner
3. Michael DiSanti
4. Hans Balsiger
5. Sophie Delanoye
6. Hervé Cottin
7. Michael A'Hearn
8. Anita Kilchenmann
9. Stephan Graf
10. Thomas Stephan
11. Elmar Jessberger
12. Tra-Mi Ho
13. Peter Eberhardt
14. Fritz Bühler
15. Martin Duncan
16. Peter Hoppe
17. François Robert
18. Steven Charnley
19. Julio Fernandez
20. Akiva Bar-Nun
21. Björn Davidsson
22. Stephen Fuselier
23. Diane Wooden
24. Samuel Gulkis
25. Jens Biele
26. Annette Jäckel
27. Timm Riesen
28. Horst-Uwe Keller
29. Hans Rickman
30. Dominique Bockelée-Morvan
31. Dina Prialnik
32. Jochen Kissel
33. Rita Schulz
34. Claudia Alexander

Participants not pictured:
André Balogh
Johannes Benkhoff
Roger Maurice Bonnet
Otto Eugster
Kate Fishbaugh
Johannes Geiss
Ernest Kopp
Tobias Owen
Gerhard Schwehm
Nicolas Thomas
Rudolf von Steiger
Sandra Wüthrich

Introductions

Origins of Cometary Materials

W.F. Huebner

Originally published in the journal Space Science Reviews, Volume 138, Nos 1–4.
DOI: 10.1007/s11214-007-9299-7

Abstract In this introductory presentation, material is categorized according to our state of knowledge: What do we know, what do we *think* we know but don't know certainly, and what do we not know but often describe it as if it were a well-established fact about comets, their nuclei, their composition, and processes within comets and their nuclei. The material is presented not with the intend to criticize laboratory work simulating condition in comet nuclei, or observers analyzing their observations, nor modelers using data from both these sources to improve our understanding and make predictions. The intent is to provoke discussion and dialog between these groups to avoid overstating the results.

What is a Comet? A comet is a diffuse appearing celestial phenomenon moving in an orbit about the Sun. The central body, the nucleus, is composed of ice and dust. It is the source of all cometary activity, including comae and tails. We distinguish between molecular (including atoms and ions) and dust comae. At heliocentric distances of about 1 AU and less, the hydrogen coma typically has dimensions larger than the Sun. The tails are composed of dust, neutral atoms and molecules, and plasma.

Keywords Comet nuclei · Atomic and molecular constituent · State of matter · Physico-chemical processes

1 Comets and Solar System Objects Related to Comet Nuclei

We distinguish between various classes and families of comets. Comets with an orbital period $P < 200$ years are defined as short-period (SP) comets. They are composed of the Jupiter family and the Halley family of comets. These two families are defined by the values

W.F. Huebner (✉)
Southwest Research Institute, San Antonio, TX 78228-0510, USA
e-mail: whuebner@swri.edu

of their Tisserand parameters

$$T_J = a_J/a + 2[(1 - e^2)a/a_J]^{1/2} \cos(i),$$

where a is the comet's orbital semi-major axis, e the orbit's eccentricity, i the inclination of the orbit with respect to the ecliptic, and J stands for Jupiter. Jupiter-family comets have $T_J > 2$ and are close to the ecliptic (small values of i). Halley-family comets have $T_J < 2$, and their orbital plane is typically out of the ecliptic. SP comets appear to have their origin in the trans-Neptunian region at heliocentric distances of about 10 to 50 AU (see Fernandez, this conference). Closely related to the Halley-family of comets are the Damocloids; they have comet-like orbits with $T_J < 2$, but do not show a coma.

Comets with an orbital period $P > 200$ years are defined as long-period (LP) comets. Their orbital planes and aphelia have random distributions. They appear to come from the Oort cloud, a spherical shell of comet nuclei at heliocentric distances of several times 10^4 AU (see Duncan, this conference). The Oort cloud of comet nuclei is bound to the Sun by gravity and thus forms the outer region of the solar system, just inside the boundary between the solar system and the rest of the galaxy. Since the Oort cloud is well outside of the heliopause, which modulates the cosmic ray flux, nuclei of LP comets may have been exposed over billions of years to more energetic galactic radiation than SP comet nuclei. Thus, we might expect some subtle differences between SP and 'dynamically young' LP comet nuclei, at least in their surface layers.

Closely related to comet nuclei are the trans-Neptunian objects at heliocentric distances of 30 to 50 AU. They consist of the classical Kuiper belt objects that lie in the ecliptic plane and the scattered disk objects that can be found out of the ecliptic plane. As already mentioned, Oort cloud objects have a spherical distribution with semi-major axes between 50,000–100,000 AU. Centaurs are icy bodies between Jupiter and Neptune.

Solar composition icy planetesimals (SCIPs) are a class of objects that are conjectured to have formed Jupiter (see Owen, this conference). The Galileo probe found a chemical composition for elements heavier than hydrogen that is solar, but the ratio of these elements relative to hydrogen is about three. This composition differs significantly from that of comets, particularly in the abundances of N, Ne, and isotopes.

2 The Importance of Comets

Comet nuclei were thought to be the building blocks for the outer planets. Comet nuclei in the Oort cloud form the boundary layer of the solar system, beyond which the true interstellar space of the galaxy exists. It is worthwhile to note that interstellar molecules may also be found within the solar system, beyond the heliopause. They are intruders that occupy solar system space.

Comet nuclei brought water and pre-biotic molecules into the inner solar system. Originally, most of the terrestrial planets were barren and lacked these substances because volatiles did not readily condense in the hot inner solar nebula. However, it appears that not all water on Earth came from comet impacts in the early life of the inner planets. Some water may have been brought by asteroids and much of the water may have been bound in rocks. The pre-biotic molecules brought by comet nuclei to Earth may be the source material for the origins of life. But just as comets may have contributed to the origins of life, they may also have contributed to mass extinctions. Some comets are near-Earth objects (NEOs). That is, they cross the orbit of the Earth and as potentially hazardous objects (PHOs) may

cause catastrophic impacts. Potentially hazardous long-period comets are rare, but they are more dangerous since they enter the inner solar system with higher speeds and are usually more massive than short-period comets. One of the comets that came close to the Earth is C/1983 H1 IRAS-Araki-Alcock. It was detected in April 1983, and approached the Earth within 0.05 AU within two weeks of its discovery. Some NEOs may be 'stealth comets' whose nuclei have the appearance of carbonaceous asteroids.

3 Composition and Place of Origin of Comet Nuclei

Now we turn to the main topic of this conference. Can comets be traced by their composition or other properties to their places of origin, e.g., a planet sub-nebula in the early solar system? First we note that most comet nuclei appear to be chemically heterogeneous within their own structure and composition. These comet nuclei cannot be traced to their place of origin based on their composition and structure (see also DiSanti, this conference). If, on the other hand, some chemically nearly homogeneous comet nuclei can be identified, then, perhaps they can be traced to their places of origin. Each such nucleus may release chemical species peculiar to their place of origin. I will call such comets allopatric comets: They reveal different properties based on their place of origin (their 'fatherland').

4 Comparison of Some Comet Nuclei

To date, several spacecraft have visited and imaged four comets, all short-period comets and three of them Jupiter-family comets. The Soviet spacecraft Vega 1 and Vega 2 and the ESA spacecraft Giotto flew through the coma of Comet 1P/Halley at the subsolar side at distances of 8890 km, 8030 km (Sagdeev 1988) and 596 km (Curdt et al. 1988), respectively. Three spacecraft flew in front of Halley's comet at still larger distances from the nucleus: the Japanese spacecraft Suisei and Sakigake, and the NASA spacecraft ICE. Of all the 1P/Halley investigations, the Halley Multi-Colour Camera (HMC) on Giotto gave the most detailed images (Reinhard 1988). The Deep Space 1 spacecraft imaged 19P/Borrelly in 2001. The nucleus of Comet 81P/Wild 2 was imaged by the Stardust spacecraft in 2004, and the nucleus of Comet 9P/Tempel 1 was imaged by the Deep Impact spacecraft in 2005.

All these images present an opportunity for the most detailed comparison to date. Comet nuclei are considered to be among the most primitive bodies in the solar system. Their surfaces also have aged: They have been exposed to cosmic radiation, solar heat causing erosion from the loss of volatiles (sublimation of ice from discrete active areas), collisions in the Kuiper belt, buildup of a dust mantle, change in porosity, and refreezing of gases flowing inward into a porous nucleus (see also Thomas, this conference). All these changes can alter their strength, and detailed surface features including changes in the moments of inertia and angular momentum that can lead to vibrational distortions, stresses, and loss of structural integrity. In extreme cases, it can even lead to splitting and disintegration of the nucleus.

We note immediately that all four comet nuclei appear to be different. However, they also have some common features such as smooth appearing valleys and slopes. The nuclei of 1P/Halley (Fig. 1) and 19P/Borrelly (Fig. 2) are very elongated. They may be composed of several large sub-nuclei that may have merged to form one body. The nucleus of 1P/Halley shows several crater-like features with effective diameters of several hundred meters. There are mountainous features as well as smooth appearing valleys. The nucleus of 19P/Borrelly

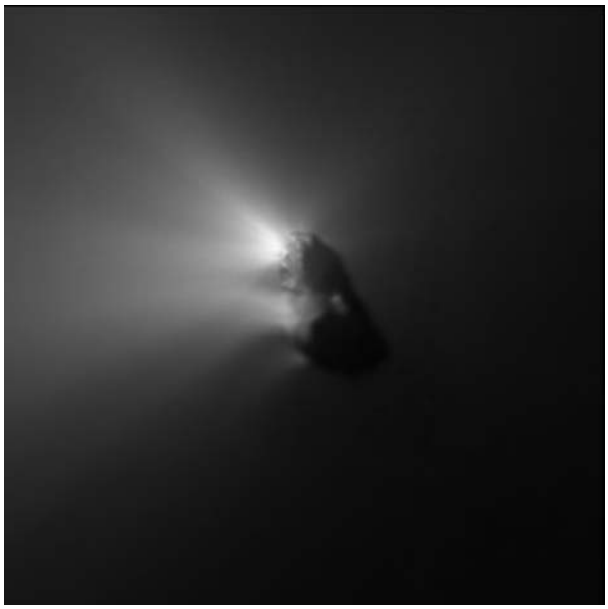

Fig. 1 Nucleus of Comet 1P/Halley. The dimensions of the nucleus are about $15.5 \times 8.5 \times 8$ km. The spatial resolution for two pixels is 100 m at the top of the image of the nucleus. (Courtesy H.U. Keller et al., Giotto, 1986)

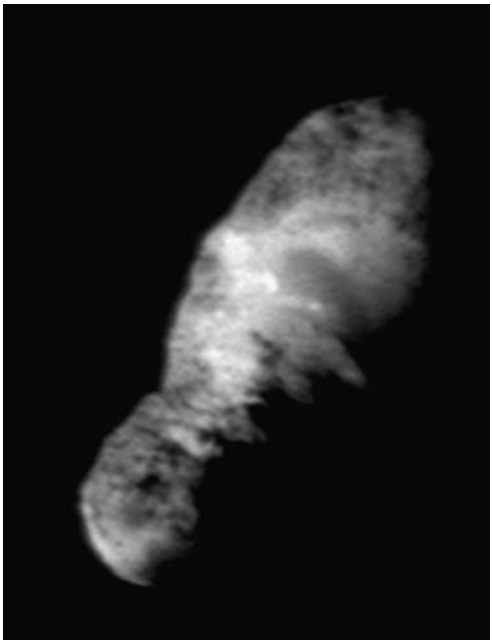

Fig. 2 Nucleus of Comet 19P/Borrelly. The dimensions of the nucleus are about $8 \times 4 \times 4$ km. The spatial resolution for two pixels is 90 m. It is not significantly better than for Comet 1P/Halley, but is for most of the nucleus. (Courtesy L. Soderblom et al., DS1 spacecraft, 2001)

shows high ridges along a jagged terminator as well as several dark patches and a small series of parallel grooves. A smooth, broad basin contains brighter features and mesa-like structures.

The nuclei of 81P/Wild 2, (Fig. 3) and 9P/Tempel 1 (Fig. 4) appear to be more spherical. They may have accreted more uniformly from smaller bodies (sub-nuclei) in the primary

Fig. 3 Nucleus of Comet 81P/Wild 2. The dimensions of the nucleus are $2.75 \times 2.00 \times 1.65$ km. The spatial resolution for two pixels is 20 m. (Courtesy D. Brownlee et al., Stardust spacecraft, 2004)

size-distribution. The nucleus of 81P/Wild 2 is particularly strongly eroded, possibly because of prolonged exposure to the Sun. This must have occurred some time ago, because the nucleus was captured from an orbit with a distant perihelion only a few decades ago.

While valleys and hills are visible in all four images, the nucleus of Comet 9P/Tempel 1 shows a very large smooth area in the top left of Fig. 4. It implies a young surface area. The surface appears to be layered. Belton (2007) and Belton et al. (2007) argue that layering is primordial and an essential element of the internal structure of nuclei of Jupiter family comets produced in the accumulation phase of gently colliding bodies. Because the collisions were gentle, they did not significantly increase the density. The differences in observed topography may be the result of environmental changes during agglomeration phases. This layering, they suggest, is present in the interior of the nucleus. The original surface may have eroded by sublimation. The arguments are based on observations of some surface layers that are bounded by scarps estimated to be 20 m high while some other surfaces show linear outcroppings on slopes. Different layers have diverse topographic features: one is "cratered," bright spots characterize another, while still another shows very rough topography. However, overall the surface of the nucleus is uniform in brightness and color. Some layers appear to have been "exhumed." Smooth layers appear in topographic low areas (see also A'Hearn, this conference). Belton suggests that random layers of materials are superposed on the original material in the core of the nucleus. The core may consist of a gently interpenetrated fractal aggregate as suggested by Donn (1991).

How this model might affect composition is not known. However, if it does affect composition, then the surface layer may be different from the deep interior even before long-term exposure to cosmic radiation or solar heat.

Several circular features, based on their shape, form, and size distribution, appear to be impact craters. However, impact craters have not been identified on other comet nuclei; thus, this interpretation must await further examination.

The question arises whether the observed surface features on the nucleus of 9P/Tempel 1 date to the primordial origin of the nucleus or are the result of evolution. Can a connection

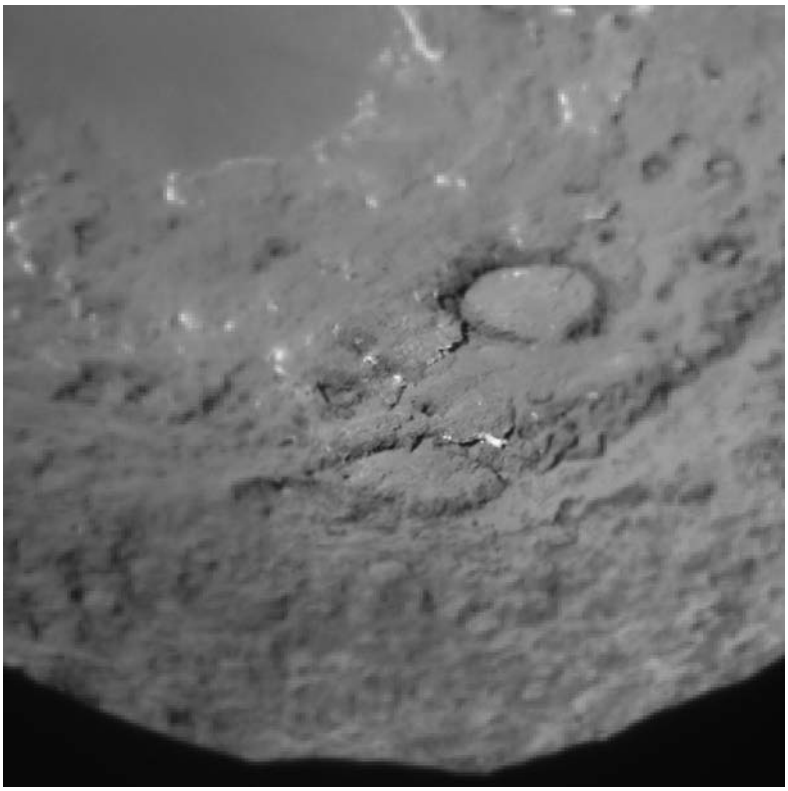

Fig. 4 Nucleus of Comet 9P/Tempel 1. The nucleus is approximately 3.1 × 2.3 km. The third dimension was not determined from spacecraft images. The spatial resolution for two pixels is 2.5 m. (Courtesy M.F. A'Hearn et al., Deep Impact spacecraft, 1995)

be made between these features and the chemical composition? Are the layered structures different in chemical composition and physical strength from each other and from the underlying core?

The layered pile model of Belton et al. (2007) is based in part on laboratory experiments of collisions between dust aggregates by Wurm et al. (2005) in which, for relative impact speeds between 13 and 25 m/s, about half of the projectile mass sticks to the target and the rest is ejected at small angles from the impact site. This "splashing" is the basis of the layered pile model. It deserves close attention and further scrutiny in conjunction with the work of Wurm et al. (2005) and Sirono and Greenberg (2000).

An opposing view is that the layered structure is the result of evolution. In active areas, gas emerges from the nucleus in jet-like features entraining dust particles. The smallest dust particles are most easily entrained; larger dust particles fall back to the surface (as we will show below) or are not entrained and remain on the surface. Volatile ices below the surface sublimate causing a gas flow outward as well as inward. The inward diffusing gas condenses again at cooler regions in the pores. The combination of coarser dust particles and refreezing gas builds a crust that is stronger (less porous) and therefore more resistant to future erosion. These layers may form the observed mesa-like structures observed on the nuclei of Comets 19P/Borrelly and 9P/Tempel 1. Since they are caused by inhomogeneities of more volatile ices in the nucleus, this would also explain the appearance of activity at their edges.

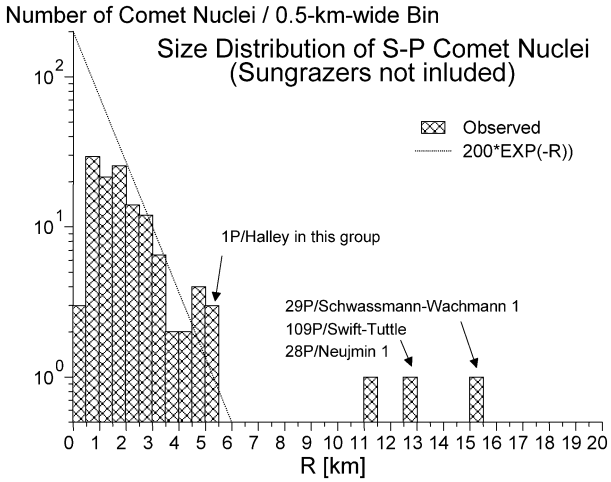

Fig. 5 Distribution of the mean radii of short-period comet nuclei, based primarily on ground-based observations. The *dotted line* is shown only to guide the eye

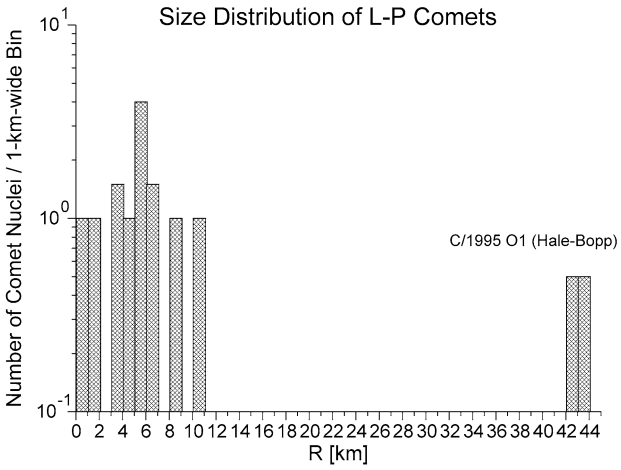

Fig. 6 Distribution of the mean radii of long-period comet nuclei, based primarily on ground-based observations. Comet Hale-Bopp (43 km) is spread over two bins

Thus, layering may be a natural result of preferential sublimation of the more volatile ice components because of thermal and gas diffusion in comet nuclei. Not only are the outer layers on a comet nucleus depleted of the more volatile ices through losses into the coma, in part these gases also diffuse inward and refreeze in pores, making a harder and possibly smoother crust (Huebner et al. 2006; see also Prialnik, this conference). Except for the four comets that were visited by spacecraft, data for the size distributions of comet nuclei are taken from websites at JPL http://neo.jpl.nasa.gov/orbits, Gonzalo Tancredi http://www.fisica.edu.uy/∼gonzalo/catalog/node17.html, and a few other sources. Only a few comets have large nuclei. The dotted line shown in Fig. 5 is shown only to guide the eye, but it might suggest an evolutionary trend. Note also that sungrazing comets are not included. These sungrazing comet nuclei would fill in the graph at the smallest mean radii. It could be argued that such comet nuclei are the result of splitting of a few larger nuclei, but we do not know the history of the other comet nuclei. They too may be fragments of larger nuclei. Note that the gap also exists when mean radii are plotted vs. perihelion distance q in Fig. 7.

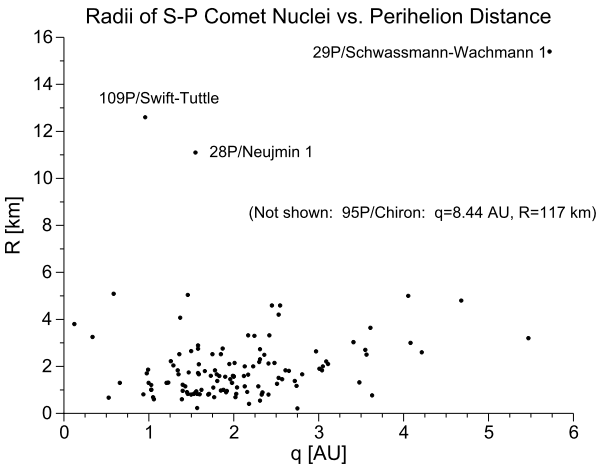

Fig. 7 Distribution of mean radii of short-period comet nuclei vs. perihelion distances

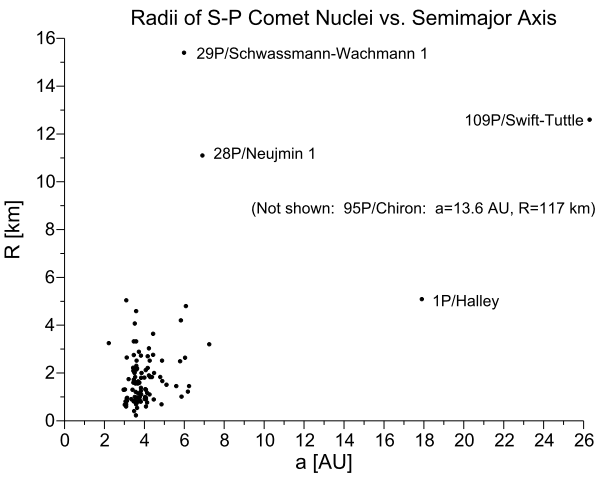

Fig. 8 Distribution of mean radii of short-period comet nuclei vs. semi-major axis of their orbits

In contrast to the nuclei of short-period comets, data for nuclei of long-period comets (see Fig. 6) are much sparser and they extend to much larger mean radii. Note that the size distribution is quite flat. If observations of mean radii for additional long-period comets do not change this distribution, then we might expect a difference in the history and composition between this comet group and short-period comets.

The size distribution of comet nuclei vs. semi-major axes, as shown in Fig. 8, suggests an observational bias for comets near the Earth. All comets observed at large distances are large and therefore can be expected to be brighter.

The next step is to relate relative abundances. Here, however, we have to be very careful. The interstellar radiation field, which affects dissociation and ionization and therefore chemical reactions involving radicals, molecules, and ions, is very different from the solar radiation field. This was one reason why we excluded ions from Table 1.

The comparison of gas-phase molecules shown in Table 1 suggests that cometary molecules may have an interstellar origin. We note that with just a few exceptions, every molecule that has been identified in a comet has also been identified in the interstellar medium. The ex-

Table 1 Comparison of identified cometary and interstellar neutral molecules

Molecule	Comet	PS	Molecule	Comet	PS	Molecule	Comet	PS	Molecule	Comet	PS	Molecule	Comet	PS
Diatomics			KCl*		×	HC_2H	×	×	C_5*		×	CH_3OCHO	×	×
H_2		×	**Triatomics**			H_2CN		×	C_4Si*		×	CH_3COOH		×
CH	×	×	CH_2	×	×	H_2CO	×	×	**Hexatomics**			CH_2OHCHO		×
NH	×	×	NH_2	×	×	HNCO	×	×	$H_2C_2H_2$*		×	CH_3C_2CH		×
OH	×	×	H_2O	×	×	*l*-C_3H		×	CH_3OH	×	×	C_7H*		×
HF		?	C_2H		×	*c*-C_3H		×	CH_3CN	×	×	H_7C_6		×
C_2	×	×	HCN	×	×	HCCN		×	CH_3NC		×	HC_6H*		×
CN	×	×	HNC	×	×	H_2CS	×	×	NH_2CHO	×	×	$OH(CH)_2OH$	×	×
CO	×	×	HCO	×	×	C_4		×	CH_2CHO	×	×	**Enneatomics**		
N_2	×		HNO		×	C_3N		×	H_2CCCC		×	CH_3CH_2OH		×
NO		×	H_2S	×	×	C_3O		×	CH_3SH		×	C_8H		×
SiH		?	C_3*	×	×	HNCS		×	HC_4H*		×	CH_3OCH_3		×
SH		×	C_2O		×	C_3S		×	HC_2CHO		×	HC_7N		×
HCl		×	CO_2	×	×	*c*-SiC_3		×	C_5H		×	CH_3CH_2CN	?	×
SiC*		×	N_2O		×	**Pentatomics**			C_5N		×	CH_3C_4H		×
C_5OSiN		×	NaCN*		×	CH_4*	×	×	C_5O		×	CH_3COCH_3		×
CP*		×	MgCN*		×	SiH_4*		×	C_5S		×	**Decatomics**		
CS	×	×	MgNC*		×	CH_2NH		×	**Heptatomics**			NH_2CH_2COOH		?
PN		×	AlNC*		×	*l*-C_3H_2		×	CH_3NH_2		×	CH_3C_4CN		?
SiO		×	*c*-SiC_2		×	*c*-C_3H_2		×	CH_3CCH		×	**Hendecatomis**		
AlF*		×	SiCN*		×	CH_2CN		×	CH_3CHO		×	HC_9N		×
NS	×	×	C_2S		×	NH_2CN		×	*c*-CH_2OCH_2		×	**Dodecatomics**		
SO	×	×	OCS	×	×	CH_2CO		×	CH_2CHOH		×	$C_2H_5OCH_3$		×
NaCl*		×	SO_2	×	×	HCOOH	×	×	CH_2CHCN		×	C_6H_6*		×
AlCl*		×	CS_2	×		C_4H	×	×	C_6H		×	**Triskaidecatomics**		
Molecule	Comet	PS	Molecule	Comet	PS	Molecule	Comet	PS	Molecule	Comet	PS	Molecule	Comet	PS
SiS		×	**Tetratomics**			HC_3N	×	×	HC_5N		×	$HC_{11}N$		×
S_2	×		CH_3		×	HCCNC		×	**Octatomics**					
FeO		?	NH_3	×	×	HNCCC		×	C_2H_6	×				

PS . . . Protostars
∗ . . . Only in envelopes of evolved stars
? . . . Tentative identification
c- . . . Cyclic molecules
l- . . . linear molecules

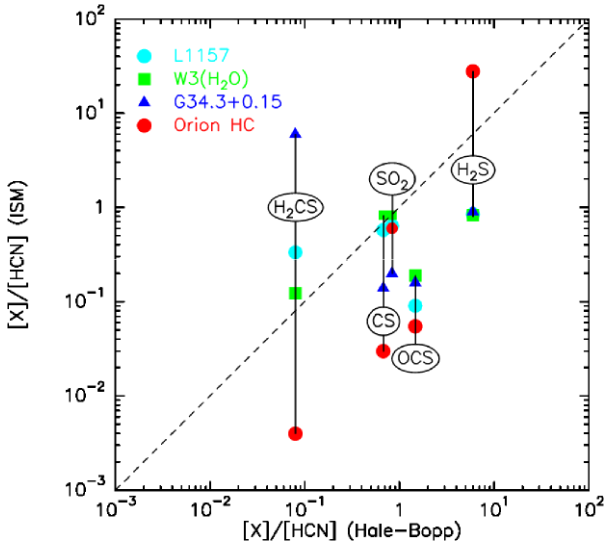

Fig. 9 Comparison of abundances of some sulfur bearing interstellar and cometary molecules. (Courtesy D. Bockelée-Morvan)

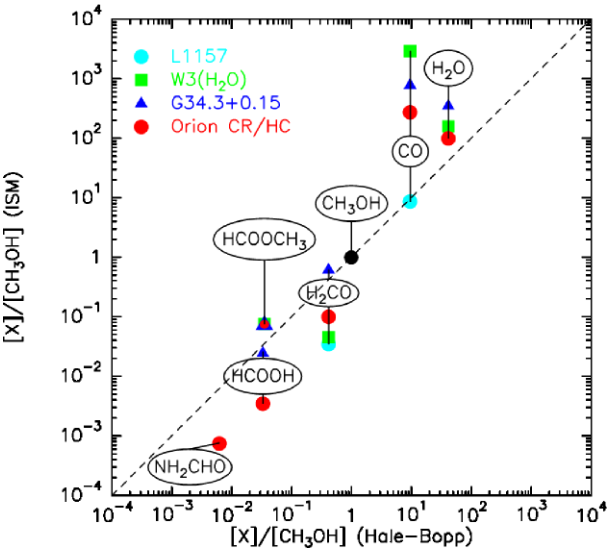

Fig. 10 Comparison of abundances of some oxygen bearing interstellar and cometary molecules. (Courtesy D. Bockelée-Morvan)

ceptions are H_2, N_2, S_2, CS_2, and C_2H_6. All of these exceptions are homonuclear diatomic or symmetric molecules, that is, molecules that do not have a permanent dipole moment. Most interstellar molecules are identified from their radio spectra. Since radio spectra depend on a strong dipole moment, these molecules have not yet been found in the interstellar medium. However, this does not mean that they do not exist in the interstellar medium.

Figures 9, 10, and 11 compare abundances of sulfur-, oxygen-, and nitrogen-bearing gas-phase molecules identified in comet comae with their interstellar abundances in four different source regions: L157, W3(H_2O), G34.3+0.15, and Orion HC. The comparison is not only striking, it is compelling. This comparison of relative abundances of three groups of molecules is still more convincing then just listing the molecules. The relationship between

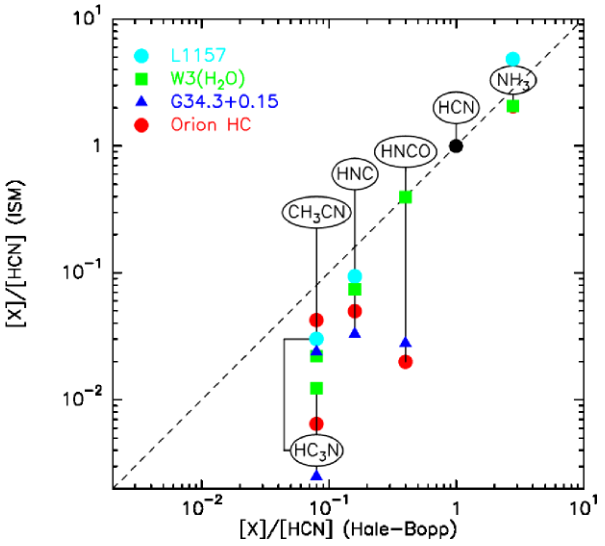

Fig. 11 Comparison of abundances of some nitrogen bearing interstellar and cometary molecules. (Courtesy D. Bockelée-Morvan)

cometary molecules and interstellar molecules suggests that these species may also have existed in the solar nebula before and during the formation of comet nuclei.

A still more meaningful comparison of cometary molecules with interstellar molecules would result if we also considered relative abundances of cometary and interstellar ices. However, as we have pointed out (Huebner and Benkhoff 1999), the relative abundances of the ices in a comet nucleus are not easily related to the relative abundances observed in the coma because of the different volatilities of the ices. Abundance data of interstellar ices is now becoming available (Ehrenfreund and Charnley 2000). In addition, when making the comparisons of interstellar (and in particular dark cloud) molecules with solar system molecules, one must also consider that the Sun is a G2 star for which the relative abundance of elements O to C is about 2. Thus, comparisons of comet compositions with dark interstellar cloud compositions are only meaningful for clouds with $O/C \approx 2$. Finally, data on interstellar molecules is based primarily on observations of high-mass protostars. High-mass protostars evolve differently than low-mass protostars, such as the Sun. Until very recently, low-mass protostars were too faint for detailed molecular observations with available instruments. The advent of 8-m class telescopes changes this now, making meaningful observations of weak near-IR features of ice components possible for the first time.

The highest column density of ice observed so far, including regions with high-mass protostars and background field stars, is for solid CO in the edge-on class I object CRBR 2422.8-3423 in Ophiuchus. The majority of the observations of CO in various source regions, including many protostars, suggest a nearly pure form of the ice. Many other interstellar ices have been identified by their spectral absorption features. Among them are H_2O, CO, ^{13}CO, CO_2, $^{13}CO_2$, OCS, NH_3, H_2CO, HCOOH, CH_3OH, and CH_3HCO. A. Boogert (private communication) compiles and updates a list of detected interstellar ice absorption features as a function of wavelength and source region together with references on a website http://spider.ipac.caltech.edu/~aboogert/icefeatures.html. Most of the absorption features are attributed to vibrational modes of the ices. The references are of the original discovery papers of the absorption features in the spectra of protostars and background stars in interstellar molecular clouds.

5 Unresolved Issues About Amorphous Ice and Clathrate Hydrates in Comet Nuclei

Amorphous water ice has been produced in the laboratory at low temperatures and fast rates of condensation. For recent papers see, e.g., Bar-Nun and Laufer (2003), Laufer et al. (2005), and Bar-Nun et al. (2006). A fast rate of condensation appears to be necessary so that the water molecules do not have time to orient their dipoles to form crystals (Kouchi et al. 1994). One of the first to suggest that amorphous water ice may exist in comet nuclei was Smoluchowski (1976, 1981). Two forms of amorphous water ice are known: a high-density form and a low-density form. High-density amorphous water ice transforms to the low-density form in the temperature range from 38 to 68 K (Jenniskens and Blake 1994). On warming from about 35 to 120 K, amorphous ice releases trapped gases at a slow continuous rate during annealing (restructuring) of the ice.

Following the suggestions of Delsemme and Swings (1952), Smoluchowski (1988) proposed that clathrate hydrates are present in comet nuclei. Clathrate hydrates also trap gases, but in cage-like crystalline structures of water ice. Figures 13 and 14 illustrate two types of clathrate hydrates. A third type of clathrate hydrate exists, but is not thought to be important for comet nuclei. Bar-Nun et al. (1988) mention a transformation of amorphous ice with trapped gases to clathrate hydrates in their laboratory experiments. However, it was Blake et al. (1991) who showed quantitatively, using an electron microscope, the transformation of amorphous ice to clathrate hydrates under near vacuum conditions. They used various mixtures of H_2O and CH_3OH to form amorphous ice and warmed it gradually. At about 120 K, a type II clathrate formed that contained close to the ideal ratio for type II clathrates of 17 H_2O molecules for each CH_3OH molecule. Since CH_3OH is a large molecule, type I clathrate hydrate is not expected to form.

Laboratory experiments, including those for amorphous ice and for clathrate hydrates, are very important for understanding properties of comet nuclei. There are strong, but indirect arguments and circumstantial evidence suggesting that amorphous water ice and clathrate hydrates may exist in comets. Some of these include:

(1) Comet nuclei are formed at low temperatures (typically 20 to 35 K) in the solar nebula.
(2) Many other species exist in the solar nebula, notably CO, CO_2, CH_4, NH_3, CH_3OH, Ar, etc. that could be trapped in the ice.
(3) A phase transition from the amorphous to crystalline state is exothermic and could explain observed comet outbursts at large heliocentric distances where the existence of other processes is difficult to explain.
(4) Gases observed in the comae of comets can be trapped in amorphous water ice as demonstrated by laboratory experiments.

In spite of these apparent "proofs," amorphous water ice or clathrate hydrates have not been detected in interstellar clouds, star-forming regions, or outer solar system objects. Perhaps condensation of water on grains in the solar nebula is too slow. However, it is quite possible that amorphous ice cannot survive very long on surfaces. Many processes, such as cosmic radiation, interstellar photons or sunlight, and collisions with particles, may cause very local warming that may initiate an irreversible phase transition. Clathrate hydrates are known to exist in nature on Earth below the ocean bed and cold under ground regions such as Siberia. However, they tend to disintegrate at low pressure.

The absence of the 1.65 μm absorption feature normally found in crystalline (hexagonal) water ice in the infrared spectra of Comet Hale-Bopp (C/1995 O1) at 7 AU heliocentric distance (Davies et al. 1997) and in icy grains in the coma of Comet C/2002 T7 (LINEAR) at 3.52 AU heliocentric distance (Kawakita et al. 2004) have been interpreted to *suggest* the

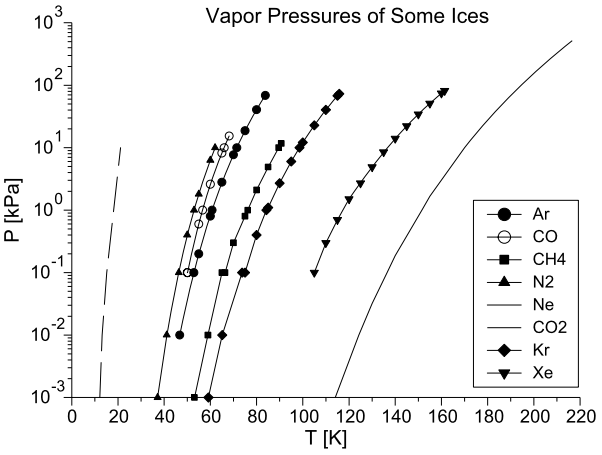

Fig. 12 Vapor pressures of pure ices. Lines are fits to data represented by various symbols. Note the proximity of the curves for N_2, CO, and Ar

presence of amorphous water ice in comets. However, the *absence* of a spectral feature of crystalline water ice in a broad and shallow spectrum does not *prove* the *presence* of amorphous water ice. There may be other explanations, such as core-mantle particles, admixtures in the ice, and temperature-dependence, particularly since Kawakita et al. also point to other features at 2.2 μm that are not well understood. Mathematical addition of spectra of pure substances is not equivalent to the spectra of real mixtures. The shapes of absorption bands become more smooth with increasing temperature of the ice, band centers tend to shift to shorter wavelengths, strengths of some bands decrease, and absorption at continuum wavelengths increases.

Laboratory experiments with amorphous water ice simulating conditions in interstellar space suggest that water vapor does not condense on refractory materials (e.g., silicate grains) until the temperature is very low. This is not the usual sequence for condensation of materials with differing enthalpies of sublimation. The usual sequence is that materials condense sequentially as temperatures decrease; gases with higher enthalpies of sublimation condense first. That would suggest that water condenses at much higher temperatures where it is more likely to form crystalline ice. Might this be the reason that the detection of water ice in interstellar clouds does not show amorphous ice?

Another puzzle is the high abundance of CO relative to N_2 and Ar in comets. Figure 12 shows that the vapor pressures of these three ices are very similar. Yet, N_2 and N-bearing compounds are under-abundant in comets relative to solar abundances of C and O and their compounds. We note that CO has a dipole moment, while N_2 and Ar do not. Could it be that trapping guest molecules in amorphous ice is enhanced for species with a dipole moment?

The thermal conductivity of amorphous water ice is a critical quantity for understanding the physics of comet nuclei. It controls the heat flow from the surface warmed by the Sun into the nucleus. However, the conductivity of amorphous ice is very poorly understood; measurements differ by many orders of magnitude (see, e.g., Huebner and Altwegg 2005) and theory does not resolve the uncertainties.

A clathrate hydrate is a crystalline lattice of water molecules that incorporates guest molecules in its cage-like structure. Two types of hydrates are relevant for our discussions here: Types I and II, as illustrated in Figs. 13 and 14, respectively. They are stable at high pressures. The guest molecules must fit inside the crystalline cages. From the work of Blake et al. (1991), it appears the presence and size of the guest molecule determines the formation of clathrate hydrates and their type. For example, the presence of CH_3OH in amorphous ice

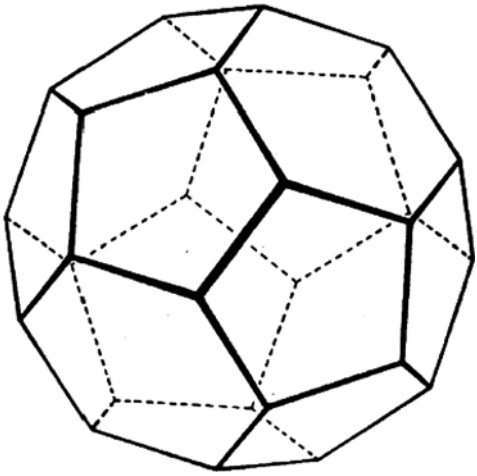

Fig. 13 Hydrate I, in which a pentagonal dodecahedron (20 water molecules) is surrounded by tetrakaidecahedra (24 water molecules each) with 2 hexagonal faces and 12 pentagonal faces. The lattice size is 1.2 nm

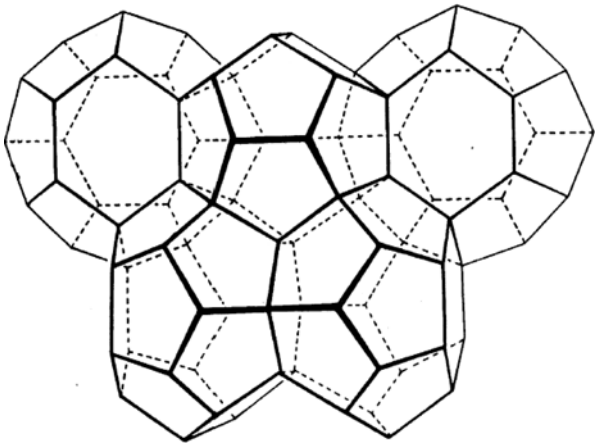

Fig. 14 Hydrate II, in a hexakaidecahedron (28 water molecules) configuration with four hexagonal faces and twelve pentagonal faces. The lattice size is 1.7 nm

initiates type II clathrate formation. Blake et al. also report a shift of the ν_3 asymmetric stretching band of CO_2 from about 234,000 to 234,600 m^{-1} as the amorphous ice doped with CO_2 is warmed from 115 K to over 120 K, i.e., as the clathrate of type II forms. This could possibly be used as a test for the transformation in comet nuclei. However, they will rapidly disintegrate in the low-pressure environment of a comet nucleus.

Typical guest molecules forming type I hydrates are CO_2 and CH_4. Type II hydrates are formed by gases like O_2 and N_2. A third hexagonal structure has been observed (type H), but is of no interest here.

6 Unresolved Issues About Comet Dust

Most siliceous comet dust is amorphous in structure. Cometary dust particles appear to be clusters of sub-micrometer sized interstellar grains, possibly held together by hydrocarbon polycondensates. However, a fraction of small silicate grains reveals a crystalline signature in their infrared spectra. The origin of the crystalline silicates is not clear. The annealing

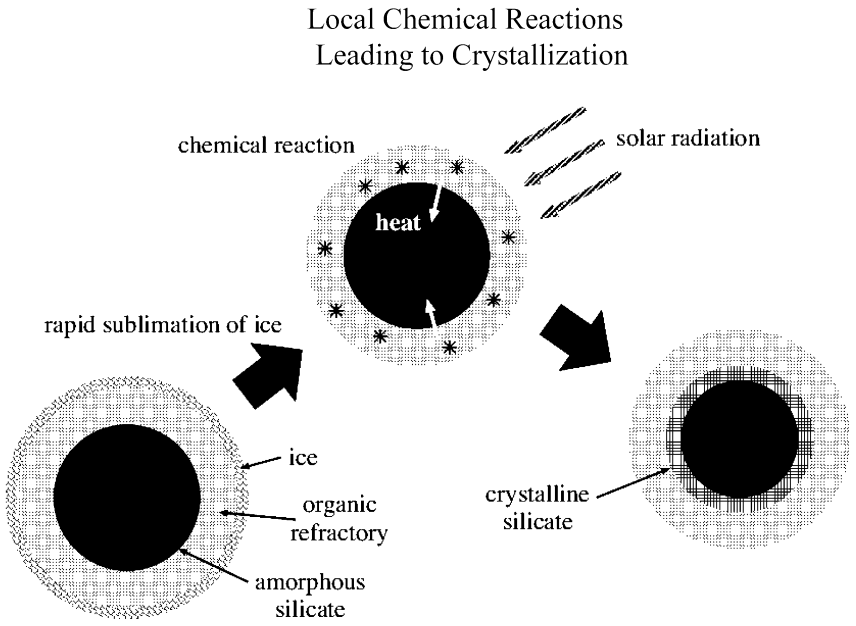

Fig. 15 A scenario for local crystallization of silicate particles. (Courtesy T. Yamamoto)

of amorphous to crystalline silicates requires high temperatures ($T \sim 1000$ K). However, comets have not been exposed to high temperatures. Two possibilities exist: Either the dust particles, or more likely some of their constituent grains, were heated before they were incorporated into the comet nucleus, or some small fractions of the grains are crystallized after they are entrained by the sublimating ices when the comet is in the inner solar system, close to the Sun.

In the first case, the bipolar outflow from the proto-Sun may have carried crystalline silicates from the hot inner solar nebula out to the comet forming region where they were mixed with other, local dust and ice to form larger dust particles. Thus, aggregation of dust particles may occur after some grains have been crystallized (see Wooden, this conference). The alternative of turbulent mixing can be ruled out because it requires gas entraining the dust moving it closer to the Sun where the dust particles crystallize when exposed to high temperatures. They must then again be entrained by gas and moved out to colder regions where comet nuclei can form. This means that the gas is also exposed to high temperatures, which would change its chemical composition. However, there is no evidence that the frozen gases in the nucleus have ever been exposed to high-temperature chemical reactions.

The second scenario is more complicated and involves local chemical reactions on particle surfaces (see Fig. 15). The model of Greenberg et al. (1996) is that amorphous silicate grains in a comet are covered by organic refractory mantles, which in turn are covered by ice mantles. After the ice on a dust particle is sublimated by solar radiation, some of the organic refractory material may get photodissociated by solar UV. These radicals can then react chemically releasing energy very locally on a grain and heat that spot to anneal some of the amorphous silicate and form a small crystalline spot.

7 Jet-Like Features, Dust Entrainment, and Their Influence on the Nucleus Surface

When solar radiation sublimates ice on the surface of a comet nucleus, the gas molecules leave the surface with a speed of approximately $v_g = 3\pi v_T/8$, where v_T is the mean thermal speed at temperature T (Huebner and Markiewicz 2000). The escaping gas entrains dust particles. The efficiency of entrainment depends on the cross section, σ_d, of the dust particle and on its mass m_d, and on the speed and flux of the gas, as indicated by the following equation for the acceleration of a dust particle

$$a_d = (C_D/2)(\sigma_d/m_d)\rho_g(v_g - v_d)|v_g - v_d| - (MG/R^2 - \omega^2 R\cos^2\theta).$$

Here C_D is the drag coefficient, which depends on the Reynolds number, ρ_g the mass density of the gas, and v_g and v_d are the speed of the gas and the dust, respectively. The second term in the equation represents the gravitational attraction of the nucleus corrected for centrifugal force caused by its spin with angular speed ω. M is the mass of the nucleus, G the universal gravitational constant, R the radial distance of a dust particle on the surface (measured from the center of gravity), and θ the angle of the location of the dust particle as measured from the equator. Note that close to the nucleus surface neither the shape of the nucleus nor of the dust particle enters the equation. For larger distances from the nucleus, multipoles of the gravitational field must be taken into account. The equation is only valid for Knudsen flow (see Davidsson, this conference), i.e., when the collision mean free path between gas molecules is large compared to the size of a dust particle. This is the usual case for comet dust particles. In the opposite extreme, Poisson flow needs to be invoked and for the intermediate case, slip flow.

Jet-like features of gas and dust may form in the coma because of topography and chemical inhomogeneity on the surface of the nucleus. These "jets" are collimated beams of gas and dust. Active areas of ice sublimation are extended sources (as opposed to point sources) on the nucleus surface. Figure 16 illustrates two opposing types of active areas: a depression and a hill.

Since the main flow of gas is initiated normal to the surface, a concave surface feature focuses (tends to increase the gas density, ρ_g) and intensifies the gas flow, producing a jet-like feature. The dust follows the gas flow. However, particles with a large ratio of cross section to mass, σ_d/m_d, which are usually smaller particles, are more easily entrained. Particles for which this ratio is very small may not be entrained at all; they remain on the surface, unless the gas flow intensifies. Particles with intermediate values of cross section to mass ratio may fall back to the surface, particularly if they are near the edge of the flow. Note that the flow issuing from the neighboring flatter area will be less intense, unless that area has ices that are more volatile. In that case, a valley, produced by erosion, may develop soon in such a place.

For a convex surface feature, the gas flow tends to diverge, which decreases ρ_g and decreases the entrainment with distance above the surface. Consequently, particles will tend to fall back to the surface. The rim, which does not have to be raised around a cavity will be convex and will cause the flow to diverge. This causes the jet-like feature to be sharper in shape.

The left panel of Fig. 16 illustrates the case with the Sun directly overhead. However, the situation does not change materially as the nucleus spins. The right panel illustrates the case when the nucleus has turned about 45°. The net result is that active areas tend to remain active and build up debris, i.e., a layer of dust particles around them. If the surface features are on a sloped area, relative to the direction to the center of gravity of the nucleus, then a

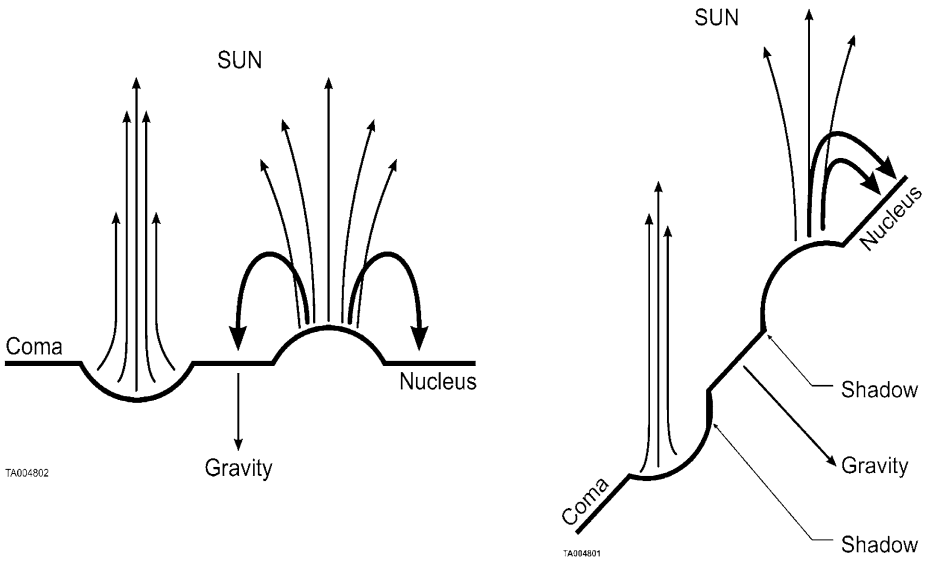

Fig. 16 Gas flow and dust entrainment from a valley (concave surface area) and a hill (convex surface feature). Thick curves represent particles with small vales of σ_d/m_d. *Left panel*: Features near the subsolar point and the surface normal to the direction of gravity. *Right panel*: The spinning nucleus has turned about 45° counter clock-wise. This also applies for a sloped surface (relative to the center of gravity)

dust layer may build up that eventually may be subject to avalanche conditions. Avalanches were observed in the KOSI experiments (Grün et al. 1993). This may lead to covering and smoothing of surface areas and may be a possible explanation of the observed smooth areas on Comet 9P/Tempel 1. Avalanche experiments should be carried out using Space Station, where the remaining air drag, equivalent to gravity, compares favorably with gravity on the surface of a comet nucleus.

Mantle formation has been considered in various models. In some models, particles with the smallest σ_d/m_d values are not entrained by the escaping gas and remain on the surface (Rickman et al. 1990). At the same time they "choke" the sublimation process and thus the gas flow. Thus, the dust layer cannot build up because the layer gets "blown away" as the comet approaches the Sun and the gas flux increases again. Building a mantle of dust particles that fall back to the surface can continue to build up to significant thickness *around* the active areas and therefore is not as likely to be "blown" away as a comet approaches the Sun. This may explain the observed persistence of a more "permanent" mantle and (relatively) active and inactive areas on the nucleus.

The dust in the coma consists of two main constituents: silicates and hydrocarbon polycondensates. These polycondensates form a distributed[1] source for coma gas. The best known is the disintegration of formaldehyde oligomer in the coma to produce CO in addition to the CO that is emitted as a gas from the nucleus

$$-(\mathrm{H_2CO})-_n \;\rightarrow\; n\mathrm{H_2} + n\mathrm{CO}.$$

[1]We emphasize the difference between distributed and extended sources: A distributed source refers to gas production in the coma. It is three dimensional. An extended source refers to gas production on the nucleus surface. e.g., an active area. It is two dimensional.

An important question is whether the gas composition from the nucleus in the "jets" is the same in all "jets" and between "jets." If this is the case, then comet nuclei are chemically homogeneous in composition but differ in abundance of some volatiles (e.g., C_2H_2, C_2H_6, etc.) depending on their place of origin in a planetary subnebula or the regular solar nebula and it may be possible to group them according to their place of origin (allopatric comet nuclei).

A'Hearn et al. (1995) analyzed the chemical composition of comets from ground-based observations of 85 comets and tried to link them to groups of comet orbits (e.g., Jupiter family, Halley family, or dynamically new comets). Their analysis met with some success, but there also were a number of exceptions (e.g., long-chain carbon molecules vs. other carbon-bearing molecules) that did not fit neatly into any of the groups. Mumma et al. (2001) proposed that some comets might form in the subnebulae of the giant planets (see also Mumma et al. 2002). On the other hand, Mumma and Reuter (1990) also concluded that some chemical species were related to specific jet-like features. "Jets" and shells of specific composition have also been reported (Cosmovici et al. 1988; Clairemidi et al. 1990; Klavetter and A'Hearn 1992; Schulz and A'Hearn 1995). *Thus, the question whether comets are diverse objects that can be grouped according to their place of origin or whether each comet is intrinsically inhomogeneous, remains unanswered*. In the latter case large-scale mixing and inelastic collisions of subnuclei, leading to inhomogeneous (rubble pile type) nuclei, may have occurred in the solar nebula—similar to the collisions of comet nuclei in the Kuiper belt as suggested by Stern (1988).

The MIRO experiments on the Rosetta mission may shed light on the internal chemical composition of comet nuclei. As ices sublimate, the speed distribution of their molecules above the surface of the nucleus is in a half-space, with an outward direction. The speed distribution function is asymmetric, and a Knudsen layer is formed in the coma because collisions are rare (see Skorov and Rickman 1998; Davidsson and Skorov 2004; Davidsson, this conference). Molecular line emissions in the microwave region will reflect the asymmetric speed distribution of the escaping gases. The MIRO instrument can resolve the asymmetry in the line profiles and give information about the nucleus interior, for example from observations of the CO line profile. A narrow CO line profile may indicate a lower temperature in the interior where the CO is sublimated. The heating of the CO and its rate of sublimation will depend on the accommodation coefficient.

8 Unidentified Spectral Lines in the Comae of Comets

Several catalogues of unidentified cometary spectral lines exist for several comets. For example, Brown et al. (1996) list 559 unidentified lines for Comets 109P/Swift-Tuttle and 23P/Brorsen-Metcalf, Cochran and Cochran (2002) list 4055 unidentified lines for Comet 122P/de Vico, and Zhang et al. (2001) 73 unidentified lines for Comet Hale-Bopp (C/1995 O1). In addition, Wyckoff et al. (1999) list unidentified bands in the plasma tail of C/1996 B2 (Hyakutake). It may be possible to identify some of these lines using computerized searches and the list of interstellar molecules, given in Table 1, as a guide.

9 Isotopes, Isomers, Enantiomers, and Dust-to-Ice Ratios

Isotopes and their ratios, determined from coma spectra, of D/H, $^{12}C/^{13}C$, $^{14}N/^{15}N$, $^{16}O/^{18}O$, $^{32}S/^{34}S$, give important clues about the origin of comet nuclei and their relationship to other

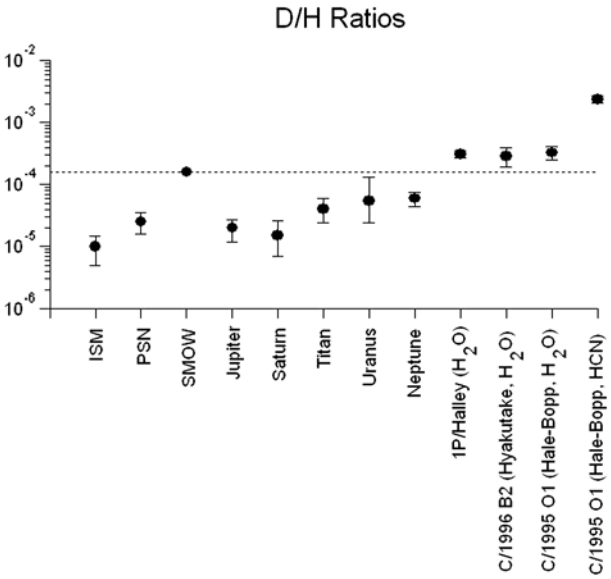

Fig. 17 Comparison of the D/H ratio in the interstellar medium (ISM), the pre-solar nebula (PSN), standard mean ocean water (SMOW), three outer planets including the Saturn moon Titan, and four comets

Table 2 Comparison of isotope ratios in comets and in the solar system

Isotope	Ratio	Comet	Isotope	Solar system ratio
$H^{12}CN/H^{13}CN$	109 ± 22	C/1995 O1 (Hale-Bopp)	$^{12}C/^{13}C$	90
$H^{12}CN/H^{13}CN$	111 ± 12	C/1995 O1 (Hale-Bopp)		
$HC^{14}N/HC^{15}N$	330 ± 98	C/1995 O1 (Hale-Bopp)	$^{14}N/^{15}N$	272
$HC^{14}N/HC^{15}N$	323 ± 46	C/1995 O1 (Hale-Bopp)		
$C^{14}N/C^{15}N$	140 ± 30	C/1995 O1 (Hale-Bopp)		
		C/2000 WM1 (LINEAR)		
$H_2^{16}O/H_2^{18}O$	518 ± 45	1P/Halley	$^{16}O/^{18}O$	499
$H_2^{16}O/H_2^{18}O$	470 ± 40	1P/Halley		
$C^{32}S/C^{34}S$	27 ± 3	C/1995 O1 (Hale-Bopp)	$^{32}S/^{34}S$	22.6
$^{32}S/^{34}S$	23 ± 6	1P/Halley		

solar system bodies. So far, isotopes are only available for long-period and Halley-family comets. Figure 17 illustrates the D/H ratio for various solar system bodies including four comets. Upper limits obtained for some comets are not shown. Table 2 summarizes the most important isotopes detected in comets and compares them with solar system values.

The large value for D/H ratio determined from the abundances of DCN and HCN in the spectra of the coma of Comet C/1995 O1 (Hale-Bopp) is probably the result of ion-molecule reactions, which enhance the ratio.

Several isomers, such as HCN and HNC, or $H_2C_3H_2$ and CH_3C_2H, may exist. HCN and HNC have been identified in the coma. Preliminary model calculations indicate that both HCN and HNC come directly from the nucleus, although not all possibilities for producing HNC in the coma have been investigated. For a recent review of CN production in comets, see Fray et al. (2005) and Cottin (this conference). The existence of isomers encourages the

search for biological precursor molecules such as NH_2CH_2COOH, and other amino acids and their enantiomers.

The mass ratio of dust to ice is poorly known. Almost all estimates are based on the ratio of dust to gas observed in the coma. However, a smaller number of larger, more massive dust particles may give the impression that a comet is nearly dust-free. Such statements should be considered with suspicion. Dust is a very important constituent of comets. Without dust, gases cannot condense. A unique way of measuring the dust-to-ice ratio is to observe the spectra of sungrazing comets. Comparing the intensity of spectra of siliceous materials relative to OH will give quantitative measures of the dust-to-ice ratio. It may also yield information about other elements such as P, Ar, etc. in comet nuclei.

10 Summary

Foremost for all data analyses from comet observations and from comet missions the basic data should be reviewed carefully for accuracy and completeness. The large uncertainties in the thermal conductivity of pure and gas-laden amorphous water ice are unacceptable. The experiments of Bar-Nun et al. (1988) indicate large releases of trapped gases from amorphous ice upon heating at about 60 K, 145 K, and 180 K. On the other hand, Blake et al. (1991) mention only one release of trapped gas at about 120 K, associated with the formation of clathrate hydrate. While many laboratory experiments on amorphous ice have been carried out and its transformation into clathrate hydrates at about 120 K has been investigated, there is still no *direct* proof of their existence in comet nuclei. This does not mean that modeling of comet nuclei assuming amorphous ice and experiments using it should be abandoned. On the contrary, a direct proof of amorphous ice in comet nuclei should be viewed as a challenge for further investigations. However, we caution that experimental results using amorphous ice and models assuming amorphous ice should not overstate its possible existence in comet nuclei. Its existence in comet nuclei still needs to be proven. It is regrettable that after years of planning, no experiment on the lander of the Rosetta mission to Comet 67P/Churyumov-Gerasimenko will test for amorphous ice. A possible test is the shift of the ν_3 asymmetric stretching band of CO_2 as amorphous ice, doped with CO_2, is warmed to about 120 K during its conversion into a clathrate (Blake et al. 1991).

Analyses of coma observations still lack many fundamental data. Among them are rate coefficients for electron impacts. Rate coefficients for charge exchange, protonation, and for electron impact and solar photo processes (ionization and dissociation) should be updated. Branching ratios for many of these processes are poorly known and in many cases totally unknown. Data for many molecular and atomic species are sparse.

In situ measurements on a comet nucleus (e.g., Rosetta) may turn into real revelations (see also Gulkis and Biele, this conference). Will there be new evidence for amorphous ice? How thick is the inactive mantle layer? How does the "jet-like" activity work? Are there pre-biotic molecules? Do they have chirality? It will be important to study a wide variety of comets and to study one comet thoroughly.

References

M.F. A'Hearn, R.L. Millis, D.G. Schleicher, D.J. Osip, P.V. Birch, Icarus **118**, 223–270 (1995)
A. Bar-Nun, D. Laufer, Icarus **161**, 157–163 (2003)
A. Bar-Nun, I. Kleinfeld, E. Kochavi, Phys. Rev. B **38**, 7749–7754 (1988)
A. Bar-Nun, I. Pat-El, D. Laufer, Icarus **187**, 321–325 (2006)

M.J.S. Belton, in *International Seminar on Nuclear War and Planetary Emergencies, 33rd Session* (World Scientific, Singapore 2007, in press)
M.J.S. Belton, P. Thomas, J. Veverka, P. Schultz, M.F. A'Hearn, L. Feaga, T. Farnham, O. Groussin, J.-Y. Li, C. Lisse, L. McFadden, J. Sunshine, K.J. Meech, W.A. Delamere, J. Kissel, Icarus **187**, 332–344 (2007)
D. Blake, L. Allamandola, S. Sandford, D. Hudgin, F. Freund, Science **254**, 548–551 (1991)
M.E. Brown, A.H. Bouchez, H. Spinrad, C.M. Johns-Krull, Astron. J. **112**, 1197–1202 (1996)
J. Clairemidi, G. Moreels, V.A. Krasnopolsky, Icarus **86**, 115–128 (1990)
A.L. Cochran, W.D. Cochran, Icarus **157**, 297–308 (2002)
C.B. Cosmovici, G. Schwarz, W.-H. Ip, Nature **332**, 705–709 (1988)
W. Curdt, K. Wilhelm, A. Craubner, E. Krahn, H.U. Keller, Astron. Astrophys. **191**, L1–L3 (1988)
B.J.R. Davidsson, Y.V. Skorov, Icarus **168**, 163–185 (2004)
J.K. Davies, T.L. Roush, D.P. Cruikshank, M.J. Bartolomew, T.R. Geballe, T. Owen, C. De Bergh, Icarus **127**, 238–245 (1997)
A.H. Delsemme, P. Swings, Annal. Astrophys. **15**, 1–6 (1952)
B. Donn, The accumulation and structure of comets, in *Comets in the Post-Halley Era*, ed. by R.I. Newburn Jr., M. Neugebauer, J. Rahe (Kluwer Academic, Dordrecht, 1991), pp. 335–360
P. Ehrenfreund, S.B. Charnley, Ann. Rev. Astron. Astrophys. **38**, 427–483 (2000)
N. Fray, Y. Bénilan, H. Cottin, M.-C. Gazeau, J. Crovisier, Planet. Space Sci. **53**, 1243–1262 (2005)
J.M. Greenberg, A. Li, T. Yamamoto, T. Kozasa, in *Physics, Chemistry and Dynamics of Interplanetary Dust*, ed. by B.A.S. Gustafson, M.S. Hanner. ASP Conf. Ser., vol. 104 (1996), pp. 497–506
E. Grün, J. Gebhard, A. Bar-Nun, J. Benkhoff, H. Düren, G. Eich, R. Hische, W.F. Huebner, H.U. Keller, G. Klees, H. Kochan, G. Kölzer, H. Kroker, E. Kührt, P. Lämmerzahl, E. Lorenz, W.J. Markiewicz, D. Möhlmann, A. Oehler, J. Scholz, K.J. Seidensticker, K. Rössler, G. Schwehm, G. Steiner, K. Thiel, H. Thomas, J. Geophys. Res. **98**, 15091–15104 (1993)
W.F. Huebner, K. Altwegg, in *The Solar System and Beyond: Ten Years of ISSI*, ed. by J. Geiss, B. Hultqvist. ISSI Scientific Report, SR-003 (2005), pp. 197–210
W.F. Huebner, J. Benkhoff, Earth Moon Planets **77**, 217–222 (1999)
W.F. Huebner, W.J. Markiewicz, Icarus **148**, 594–596 (2000)
W.F. Huebner, J. Benkhoff, M.T. Capria, A. Coradini, C. De Sanctis, R. Orosei, D. Prialnik, *Heat and Gas Diffusion in Comet Nuclei*. ISSI Scientific Report SR-004 (ESA Publication, Noordwijk, 2006)
P. Jenniskens, D.F. Blake, Science **265**, 753–756 (1994)
H. Kawakita, J. Watanabe, T. Ootsubo, R. Nakamura, T. Fuse, N. Takato, S. Sasaki, T. Sasaki, Astrophys. J. **601**, L191–L194 (2004)
J.J. Klavetter, M.F. A'Hearn, Icarus **95**, 73–85 (1992)
A. Kouchi, T. Yamamoto, T. Kozasa, T. Kuroda, J.M. Greenberg, Astron. Astrophys. **290**, 1009–1018 (1994)
D. Laufer, I. Pat-El, A. Bar-Nun, Icarus **178**, 248–252 (2005)
M.J. Mumma, D. Reuter, BAAS **22**, 1088 (1990)
M.J. Mumma, N. Dello Russo, M.A. DiSanti, K. Magee-Sauer, R.E. Novak, S. Brittain, T. Rettig, I.S. McLean, D.C. Reuter, L.-H. Xu, Science **292**, 1334–1339 (2001)
M.J. Mumma, M.A. Disanti, N. dello Russo, K. Magee-Sauer, R. Gibb, R. Novak, in *Proceedings of Asteroids, Comets, Meteors—ACM*, ed. by B. Warmbein. ESA SP-500, Noordwijk, Netherlands (2002), pp. 753–762
R. Reinhard, in *Exploration of Halley's Comet*, ed. by M. Grewing, F. Praderie, R. Reinhard (Springer, Berlin, 1988), p. 949
H. Rickman, J.A. Fernández, B.A.S. Gustafson, Astron. Astrophys. **237**, 524–535 (1990)
R.Z. Sagdeev, in *Exploration of Halley's Comet*, ed. by M. Grewing, F. Praderie, R. Reinhard (Springer, Berlin, 1988), p. 959
R. Schulz, M.F. A'Hearn, Icarus **115**, 191–198 (1995)
S.-I. Sirono, J.M. Greenberg, Icarus **145**, 230–238 (2000)
Y.V. Skorov, H. Rickman, Planet Space Sci. **46**, 975–996 (1998)
R. Smoluchowski, in *Comets, Asteroids, Meteorites, Interrelations, Evolution, and Origins*, ed. by A.H. Delsemme. IAU Coll., vol. 39 (1976), pp. 47–49
R. Smoluchowski, Astrophys. J. **244**, L31–L34 (1981)
R. Smoluchowski, Mon. Not. Roy. Astron. Soc. **235**, 343–348 (1988)
S.A. Stern, Icarus **73**, 499–507 (1988), **76**, 385
G. Wurm, G. Paraskov, O. Krauss, Icarus **178**, 253–263 (2005)
S. Wyckoff, R.S. Heyd, R. Fox, Astrophys. J. **512**, L73–L76 (1999)
H.W. Zhang, G. Zhao, J.Y. Hu, Astron. Astrophys. **367**, 1049–1055 (2001)

Origin of Comet Nuclei and Dynamics

Julio A. Fernández

Originally published in the journal Space Science Reviews, Volume 138, Nos 1–4.
DOI: 10.1007/s11214-007-9274-3

Abstract We present a review of the main physical features of comet nuclei, their birthplaces and the dynamical processes that allow some of them to reach the Sun's neighborhood and become potentially detectable. Comets are thought to be the most primitive bodies of the solar system although some processing—for instance, melting water ice in their interiors and collisional fragmentation and reaccumulation—could have occurred after formation to alter their primordial nature. Their estimated low densities (a few tenths $\mathrm{g\,cm^{-3}}$) point to a very fluffy, porous structure, while their composition rich in water ice and other highly volatile ices point to a formation in the region of the Jovian planets, or the trans-neptunian region. The main reservoir of long-period comets is the Oort cloud, whose visible radius is $\sim 3.3 \times 10^4$ AU. Yet, the existence of a dense inner core cannot be ruled out, a possibility that would have been greatly favored if the solar system formed in a dense galactic environment. The trans-neptunian object Sedna might be the first discovered member that belongs to such a core. The trans-neptunian population is the main source of Jupiter family comets, and may be responsible for a large renovation of the Oort cloud population.

Keywords Comets · Oort cloud · Transneptunian belt

1 Introduction

Comets are considered to be the most pristine bodies in the solar system, formed in the coldest regions of the protoplanetary disk beyond the "snowline", i.e., the distance from the Sun at which the temperature of the protoplanetary disk was low enough for water to condense. Therefore planetesimals that formed at such distances were ice-rich. Even though there is at present a general agreement on this concept, there are still some open questions. For example, how well preserved is the comet material since it was first accreted in the protoplanetary disk? Do most comets come from the Uranus-Neptune region and the trans-neptunian belt, or from other zones closer to the Sun, e.g., around Jupiter and Saturn or the outer asteroid

J.A. Fernández (✉)
Facultad de Ciencias, Departamento de Astronomía, Iguá 4225, 11400 Montevideo, Uruguay
e-mail: julio@fisica.edu.uy

H. Balsiger et al. (eds.), *Origin and Early Evolution of Comet Nuclei*
DOI: 10.1007/978-0-387-85455-7_3

belt? The answer to these questions depends on whether the Sun formed in a dense galactic environment and remained there during the early massive scattering of residual planetesimals and buildup of a comet reservoir (Fernández 1997). Another important issue, relevant to the physical processing of comet material, is the content (if any) of short-lived radioisotopes like ^{26}Al and ^{60}Fe, with half-lives of 0.71 Myr and ∼1.5 Myr, respectively, that could have baked and melted the water ice in the interiors of icy bodies. Liquid water chemically interacted with the minerals producing hydrated silicates in C-type asteroids (e.g., Jewitt et al. 2007). The aim of this work will be to analyze these important questions and others related to the origin of comet nuclei and how dynamics shaped their current space distribution and delivery to the inner planetary region.

2 Some Observed Orbital Features of the Comet Population

Marsden and Williams's (2005) catalogue contains 2,221 observed comets of which 1,880 are of long-period (LP) (orbital periods $P > 200$ yr) and the remaining 341 are "periodic" ($P < 200$ yr). The sample of LP comets include the special group of more than 1,000 sungrazers mainly discovered from space-borne observatories, which come from a few parent comets tidally disrupted by the Sun. Automated search programs of near-Earth objects, like LINEAR, LONEOS, NEAT, Catalina, and Siding Spring, implemented during the last ten years, are playing a very active role in the discovery of comets.

Most periodic comets belong to the Jupiter family (JF), characterized as having Tisserand constants $T > 2$ and orbital periods $P < 20$ yr. The rest of the periodic comets are of Halley-type (HT), and they have, in general, $T < 2$ and orbital periods mostly in the range $20 < P < 200$ yr. The Tisserand constant can be derived from the restricted circular three-body problem, and can be approximately applied to the case of Sun–Jupiter–comet. It is defined as

$$T = \frac{a_J}{a} + 2\left[\frac{q}{a_J}\left(2 - \frac{q}{a}\right)\right]^{1/2} \cos i, \tag{1}$$

where q, a and i are the perihelion distance, semimajor axis and inclination of the comet, and a_J is the radius of Jupiter's orbit assumed to be circular. In the restricted circular three-body problem, T is a constant of the motion. In the case Sun–Jupiter–comet, T will vary because Jupiter's orbit is not circular and the other planets also perturb the comet, though T will vary very slowly as compared with the orbital parameters q, a and i, so it can still be approximately taken as a constant of motion.

We note that a large proportion of LP comets have near-parabolic orbits with original semimajor axes $a_{\rm orig} > 10^4$ AU, or orbital binding energies $x_{\rm orig} \equiv 1/a_{\rm orig} < 10^{-4}$ AU^{-1}. The word *original* is applied to the orbital parameters the comet has before entering the planetary region, i.e., before being perturbed by the planets. The orbit of the comet observed near the Sun, called *osculating*, is computed backwards in time in the barycentric frame of reference until it is far away from the Sun. In this moment we get the original unperturbed orbital elements.

The observed distribution of original orbital energies of LP comets shows a spike at near-zero energies ($0 < x_{\rm orig} \lesssim 10^{-4}$ AU^{-1}) in an otherwise smooth $x_{\rm orig}$-distribution. Comets in the spike come from a vast reservoir called the Oort cloud that stretches to distances of several 10^4 AU. Because Oort cloud comets that cross Jupiter's orbit are subject to average perturbation by Jupiter that is well above their original energy (see Sect. 3.1), they are more likely to be in their first visit. For this reason they were called "new" by Oort (1950).

The original perihelia of such comets were very likely located before beyond Saturn, and were decreased by external perturbers (to be analyzed in the following). A few comets have slightly hyperbolic original orbits, but these may be accounted for by observational errors and/or nongravitational forces (i.e., a jet reaction on the comet nucleus produced by the sublimating gases).

From the observed flux of new comets in Earth-crossing orbits, we can derive a passage rate down to a limiting absolute total magnitude $H_T = 10.5$ (that roughly corresponds to a diameter $D \simeq 1$ km)

$$\dot{n}_{\rm new}(H_T < 10.5) \sim 3 \text{ Earth-crossing new comets every 4 yr}$$

(Fernández 2005). This result is in quite good agreement with the value of ∼0.8 per unit perihelion per year brighter than $H_T = 10.9$ derived by Francis (2005) using data exclusively from the Lincoln Near-Earth Asteroid Research (LINEAR).

A fraction of the new comets will return to the inner planetary region as evolved LP comets with larger binding energies (greater x) (e.g., Fernández 1981). The total number of LP comets in Earth-crossing orbits with diameters $D \gtrsim 1$ km can be estimated to be about seven per year, i.e., there are about 10 evolved LP comets per each new comet.

A more detailed analysis of the spike of near-parabolic comets in narrower bins shows a maximum at $x \simeq 30$ (in units of 10^{-6} AU^{-1}), so the "radius" of the *visible* Oort cloud is $\sim 3.3 \times 10^4$ AU that corresponds to the greatest concentration of semimajor axes of new comets. These comets give the place where external perturbers are more efficient in driving comet perihelia into the inner planetary region. Such a radius does not necessarily have to coincide with the circumsolar region of the greatest concentration of comets. A much larger comet population may be stored at smaller distances to the Sun, but it remains essentially hidden to us because external perturbers are usually too weak to inject some of its members into the inner planetary region. Over geologic time scales, very close stellar passages and penetrating encounters with giant molecular clouds will perturb such an inner core of the Oort cloud and trigger "comet showers", i.e., sharp increases in the influx rate of new comets (Hills 1981).

Figure 1 shows the distribution of the observed comets in the parametric plane of orbital energy versus Tisserand constant. This plot allows us to distinguish the different dynamical classes of comets. Thus, LP comets fall at the left-hand side of the diagram, HT comets fall in the middle and JF comets fall at the upper-right corner. We also note that, whereas new and LP comets have more or less random inclinations, JF comets are strongly concentrated toward the ecliptic plane. We see that for most LP and HT comets the Tisserand constant is $T < 2$. This is easy to understand if we consider, for instance, a comet in a near-parabolic orbit ($a \to +\infty$) lying in the ecliptic plane ($i = 0$), with a typical perihelion distance $q = 1.5$ AU. In this case we get $T \simeq 1.52$. If we consider inclinations $i > 0$, T will be even smaller.

3 Perturbing Forces Acting on Comets

3.1 Planetary Perturbations

When comets move within the planetary region they are subject to planetary perturbations, the equation of motion is

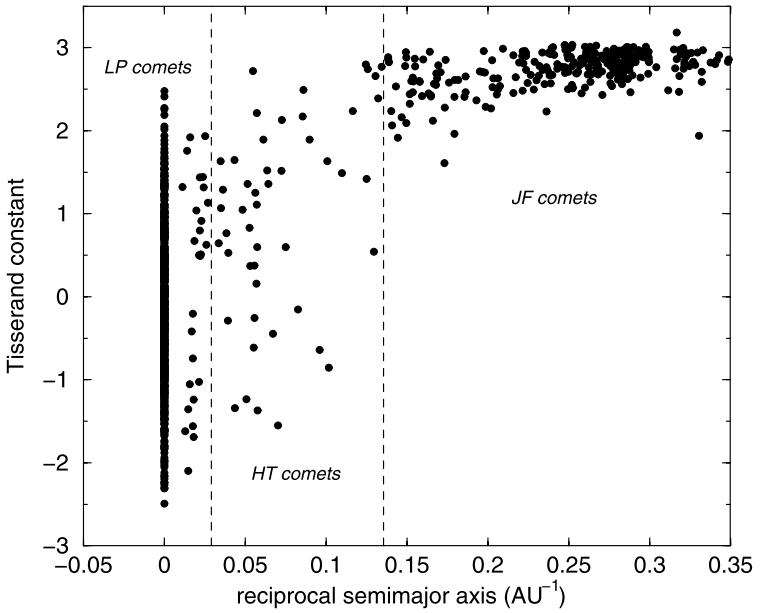

Fig. 1 The Tisserant constant versus the orbital energy (or reciprocal semimajor axis) of comets appearing in Marsden and William's (2005) catalogue. The *dashed lines* separate the three main dynamical classes of comets. LP comets with $e > 0.98$ were assumed to move on parabolic orbits ($x = 0$). This is the reason why most LP comet appear aligned along the axis $x = 0$. Sungrazers were removed from the sample

$$\frac{\mathrm{d}^2\vec{r}}{\mathrm{d}t^2} = -\frac{GM_\odot \vec{r}}{r^3} + \nabla\mathcal{R}, \tag{2}$$

where $\vec{r}$ is the Sun–comet radius vector expressed in the heliocentric frame of reference, and $\mathcal{R}$ is the disturbing function describing the perturbations of the planets of masses m_i on the comet's orbit where

$$\mathcal{R} = G\sum_i m_i\left(\frac{1}{d_i} - \frac{x_c x_i + y_c y_i + z_c z_i}{r_i^3}\right) \tag{3}$$

d_i, r_i being the distances of planet i to the comet and the Sun, respectively, and (x_c, y_c, z_c), (x_i, y_i, z_i) are the heliocentric coordinates of the comet and planet i, respectively. In some cases, a better solution can be obtained for the original orbit with the inclusion in (2) of an extra term that takes into account the nongravitational force.

The orbital parameter most affected by planetary perturbations is the semimajor axis a (or the energy x). The average change in the comet's energy per orbital revolution (expressed in AU^{-1}) under the main perturbing influence of Jupiter is of the order $(M_J/M_\odot) \sim 10^{-3}$, where M_J is Jupiter's mass. For Oort cloud comets coming for the first time to the inner planetary region, whose original binding energies are $x \simeq 10^{-4}$ AU^{-1}, a change $\delta x \sim 10^{-3}$ AU^{-1} will be in relative terms very large, so they will be very likely either ejected to interstellar space, or placed into a much more tightly bound orbit.

3.2 Stellar Perturbations

Besides the planets, comets are subject to *external* perturbers, i.e., those that do not belong to the solar system. External perturbers acting at large heliocentric distances will mainly affect the comet's angular momentum (i.e., the perihelion distance q and the inclination i), while a will be kept almost unchanged. We will start by analyzing the action of passing stars. Let us compute the perturbation of a passing star of mass M and relative velocity V on a comet at a distance r to the Sun. By assuming that the comet is at rest in a heliocentric frame of reference during the star passage and that the star's path is only slightly perturbed by the Sun's gravity, so it can be taken as a straight line, we can easily compute the change in the comet's velocity v_c due to the star passage as

$$\Delta v_c = \int_{-\infty}^{+\infty} F_* \mathrm{d}t = \int_{-\infty}^{+\infty} \frac{GM}{(D^2+u^2)^{1/2}} \frac{\mathrm{d}u}{V} = \frac{2GM}{VD}, \tag{4}$$

where u is the distance of the star to the point of closest approach to the comet, and D is the star–comet distance at the point of closest approach. We note that the impulse vector $\Delta\vec{v}_c$ follows the direction $\vec{D}$. The star will also impart an impulse to the Sun that can be computed in the same manner as (4) and changing D to $D_\odot$, where $D_\odot$ is the distance of closest approach of the star to the Sun.

The net impulse on the comet with respect to the Sun is

$$\Delta\vec{v} = \Delta\vec{v}_c - \Delta\vec{v}_\odot = \frac{2GM}{VD}\frac{\vec{D}}{D} - \frac{2GM}{VD_\odot}\frac{\vec{D}_\odot}{D_\odot}. \tag{5}$$

Now, during an orbital revolution of period P a near-parabolic comet will receive many perturbations from passing stars. Let $s(D_\odot)\,\mathrm{d}D_\odot = 2\Phi_* D_\odot\,\mathrm{d}D_\odot$ be the rate of stellar passages with impact parameters in the range $(D_\odot, D_\odot + \mathrm{d}D_\odot)$, where Φ_* is the stellar flux in the Sun's neighborhood. Since stellar perturbations occur at random, the cumulative impulse $\Delta v_{*,P}$ during an orbital revolution P will sum quadratically, thus we can write

$$\Delta v_{*,P}^2 = P\int_{D_m}^{D_M} \Delta v^2 s(D_\odot)\mathrm{d}D_\odot, \tag{6}$$

where $\Delta v^2 = \Delta\vec{v}\times\Delta\vec{v}$ is given by (5); $D_m = (2\Phi_* P)^{-1/2}$ is the minimum distance of closest approach of a star to the Sun expected during P; and D_M is the maximum distance at which a passing star may have some dynamical influence on Oort cloud comets which can be taken as infinity as a good approximation. The stellar flux is $\Phi_* = n_* V \simeq 7$ stars Myr^{-1} within one parsec (pc) for stars of average mass $\sim$0.5 $\mathrm{M}_\odot$ and a typical velocity with respect to the Sun $V \simeq 30$ km s^{-1} (Fernández 2005).

3.3 Galactic Tidal Forces

Comets are also subject to galactic tidal forces. The galactic potential can be approximately divided between that of the galactic bulge and that of the disk. The galactic disk potential is dominant, so we will concentrate on it and neglect that of the bulge. The galactic disk can be approximately modeled as a homogeneous disk of density ρ_{disk} in the mid-plane of the Galaxy, so its potential can be expressed as (e.g., Heisler and Tremaine 1986)

$$U = U_o + 2\pi G\rho_{\mathrm{disk}} z^2, \tag{7}$$

where U_o is a constant and z is the distance to the galactic mid-plane. We shall adopt in the following a value $\rho_{\rm disk} = 0.10\ {\rm M}_\odot\ {\rm pc}^{-3}$, which corresponds to that measured in the Sun's vicinity (Holmberg and Flynn 2000), though we should bear in mind that this is the value measured *at present*. In the past, the mass density of the galactic disk in the Sun's vicinity probably oscillated up and down around the current value, as the Sun experienced galactic radial and vertical excursions.

From the above potential, the tidal force of the galactic disk acting on a comet at a galactic latitude ϕ is

$$\vec{F}_{\rm disk} = \left[({\rm d}U/{\rm d}z)_c - ({\rm d}U/{\rm d}z)_\odot\right]\hat{z} = 4\pi G\rho_{\rm disk} r \sin\phi\hat{z}, \tag{8}$$

where r is the Sun–comet distance, $r\sin\phi = z_c - z_\odot$ is the difference between the distances of the comet and the Sun to the galactic mid-plane, and $\hat{z}$ is the unit vector perpendicular to the galactic plane.

The change in the perihelion distance per orbital revolution of an Oort cloud comet of semimajor axis a caused by the tidal force $\vec{F}_{\rm disk}$ is (Fernández 2005)

$$q_f^{1/2} = q_i^{1/2} + 4.5\sqrt{2}\pi^2 M_\odot^{-1}\rho_{\rm disk} a^{7/2}\cos\alpha\sin 2\phi, \tag{9}$$

where q_i, q_f are the initial and final perihelion distances, respectively, and α is the angle between the orbital plane and the plane perpendicular to the galactic disk that contains the radius Sun–comet. In the integration we assume that the other orbital elements of the comet, as well as α and ϕ, remain constant during P.

We can write $q_f = q_i + (\Delta q)_{{\rm disk},P}$, and if $(\Delta q)_{{\rm disk},P} \ll q_i$, then (9) becomes

$$(\Delta q)_{{\rm disk},P} = 12.7\pi^2 M_\odot^{-1}\rho_{\rm disk} q^{1/2} a^{7/2}\cos\alpha\sin 2\phi, \tag{10}$$

where $q \sim q_i$.

Equations (9) and (10) show that the change of the perihelion distance is maximum for a galactic latitude $\phi = 45°$, and negligible near the galactic poles and the galactic equator. The aphelion points of the observed LP comets show a concentration at mid-galactic latitudes (Delsemme 1987), thus confirming the dominant role of the tidal force of the galactic disk in driving the perihelia of Oort cloud comets into the planetary region. We also stress that $(\Delta q)_{{\rm disk},P}$ strongly depends on the semimajor axis (it is $\propto a^{7/2}$). For comets with semimajor axes $a \lesssim 10^4$ AU the change $(\Delta q)_{{\rm disk},P}$ will be negligible, so they will form an inner core of the dynamically active Oort cloud that will remain almost unperturbed, unless a very close star passage or a penetrating encounter with a molecular cloud occurs.

3.4 Penetrating Encounters with Giant Molecular Clouds

The importance of interstellar molecular clouds as major perturbers of the Oort cloud during penetrating encounters was first addressed by Biermann (1978) and Napier and Clube (1979). These encounters could have disrupted the outer portions of the Oort cloud, thus requiring a replenishment source from an inner core or the trans-neptunian belt (see Sect. 7). The largest molecular structures in interstellar space are called Giant Molecular Clouds (GMCs) and they are concentrated in the spiral arms of the Galaxy. They have typical masses of the order of 1–2 $\times\ 10^5\ {\rm M}_\odot$, mean diameters ~45 pc, and temperatures 10–20 K (van Dishoeck et al. 1993). Their typical densities are 50 H_2 molecules cm^{-3} though they exhibit a clumpy structure in which most of their mass concentrates in dense cores with densities 10^3–10^5 H_2 cm^{-3} that are active regions of star formation The mean separation among GMCs at the Sun's distance to the galactic center is ~500 pc (Blitz 1993), and the relative

velocity of the Sun with respect to GMCs is $v_{GMC} \sim 20$ km s^{-1}. Therefore, the frequency of penetrating encounters of the solar system with GMCs is not more than a few over the solar system age.

4 Where Did Comets Form?

The residual planetesimals left after the formation of the planets are considered to be the progenitors of comets, so to learn about the place where comets formed we need first a sound physical model of the protoplanetary disk. The standard model assumes a temperature profile $T(r) \propto T_o r^{-1}$ (r in AU), so if $T_o = 700$ K at $r = 1$ AU, $T = 135$ K at Jupiter's distance, $T \sim 28$ K in the Uranus–Neptune zone, and $T \sim 17$ K in the trans-neptunian belt (Goldreich and Ward 1973). This range of temperatures allows water to condense from Jupiter's zone (the "snowline") outwards, while other more volatile substances like NH_3, CO_2, CO, NH_2 and N_2 could have condensed farther away in the Uranus–Neptune zone and the trans-neptunian belt. The chemical composition of comets should reflect the conditions of pressure and temperature of the medium in which they formed and, since they are rich in water and carbon compounds (see Table 1), they had to form beyond the snowline. Their ice-rich composition contrasts with that of the rocky asteroids devoid of water ice formed in the region interior to Jupiter. In the outer asteroid belt, water molecules form chemical bonds with silicates in hydrated minerals, pointing to the early presence of liquid water (e.g., Jewitt et al. 2007).

How highly volatile ices, like CO, CH_4, N_2 or CO_2, were incorporated into the comet material is still a matter of debate. One possibility is that they condensed in the protoplanetary disk and were then accreted by the planetesimals as solids. Another possibility is that they were incorporated within clathrate forms, or absorbed by amorphous ice. The existence of clathrate structures was proposed by Delsemme and Swings (1952), who argued that some substances, like water, can form crystal structures with cavities large enough to permit occupancy by noble gas atoms or other molecular species. On the other hand, Bar-Nun and Kleinfeld (1989) showed that water may have condensed as amorphous ice, which acts as a thick woolen carpet, able to trap enormous amounts of gas at low temperatures. The trapping efficiency is strongly dependent on the considered gaseous species for temperatures $T \gtrsim 30$ K. For gases like CH_4, CO, N_2 and Ar, it is very high for a low temperature of 20 K (a factor of ten in the ratio of gas to ice), but at a higher temperature $T \sim 75$ K it drops to negligible factors in the range 3×10^{-3}–6×10^{-5}, depending upon the gas. In this regard, icy planetesimals formed in Jupiter's region would carry much less nitrogen (most of it in the form of NH_3) and heavy noble gases than icy planetesimals formed in the

Table 1 Relative abundances of parent molecules in comets(*)

Molecule	Mass fraction
H_2O	~100
CO	~7–8
CO_2	~3
H_2CO (formaldehyde)	~0–5
NH_3	~1–2
HCN	$\lesssim$0.02–0.1
CH_3OH (methanol)	~1–5

(*)From Fernández (2005)

trans-neptunian belt. In order to trap the observed proportion of ∼7% CO in amorphous ice, Bar-Nun and Kleinfeld (1989) concluded that comet Halley had to be formed at ∼50 K, i.e., in the Saturn–Uranus region.

Noble gas (He, Ne, Ar and Kr) content in comets may also give strong clues to the place where comets formed. Unfortunately, the detection of noble gases in comets has been extremely difficult because all of them have resonance transitions only in the far- and extreme-ultraviolet. From the failure to detect the 630 Å line of Ne, Krasnopolsky et al. (1997) found that comet Hale–Bopp was depleted in neon by more than 25 times relative to cosmogonic proportions, indicating that the ice was warmed above 25 K, since Ne is not trapped at higher temperatures.

It is still possible that the outer portions of the asteroid belt is the dwelling of cometary bodies that normally remain inactive. Water ice cannot be exposed on their surfaces, since any exposed ice should have sublimated very quickly, but it may remain below an insulating mineral crust. Collisions with meteoroids could leave exposed zones of fresh ice, thus triggering a sudden activity. This is at least the explanation provided by Hsieh and Jewitt (2006) for the dust activity observed in objects 133P/Elst-Pizarro, P/2005 U1 (Read) and 118401 (1999 RE_{70}), all of them having orbits typical of main-belt asteroids ($a \sim 3.2$ AU, $e \sim 0.16$–0.25, and $i \sim 0.24$–1.4 degrees). If this interpretation is correct, the snowline would have been 2 AU closer to the Sun than Jupiter, at least during a certain time. In this regard it is interesting to mention that models of minimum-mass protoplanetary disks around a protostar of 0.5 $M_\odot$ with no or moderate mass accretion (10^{-8} $M_\odot\,yr^{-1}$) bring the snowline as close as 1 AU from the central star (Sasselov and Lecar 2000).

As a summary, we can say that the scant chemical evidence available suggests that the cometary water ice condensed in a region of the nebula with temperatures in the range ∼25–50 K. According to the standard model of the protoplanetary disk, this range will correspond to the outer region beyond Saturn. Yet, given the uncertainties, we still cannot rule out any region beyond the snowline as a source of comets. The uncertainty also involves the heliocentric distance of the snowline: it could have always been around Jupiter's orbital radius, it could have been closer to the Sun than Jupiter, or it could have shifted up and down with time as the conditions of temperature and pressure in the protoplanetary disk changed. In the latter two cases, even bodies in the outer asteroid belt may have a comet (icy) nature below their inert surfaces.

5 How Pristine Are Comet Nuclei?

Could comets be the unaltered relics of the planetesimals formed in the protoplanetary disk and scattered by the giant planets? Or could they have been subject to different physical processes that altered their primordial structure? Irrespective of the physical processing experienced, the elemental abundances of comets are the closest to the solar (and cosmic) abundances as compared to other known solar system bodies, though some fractionation did occur. The most obvious fractionation was the depletion of hydrogen and helium, since these gases require extreme low temperatures (<10 K) either to condense or to be trapped in significant amounts by amorphous ice. Such low temperatures were very likely never reached in the protoplanetary disk.

Most of the cometary material seems to be very porous, fragile and of low-density. Grains accreting at low encounter velocities will form low-density aggregates of $\lesssim 0.5$ g cm^{-3} with a fractal structure (e.g., Donn 1990). The determination of masses and bulk densities of comet material, even though it is still very uncertain, points to very low values of about 0.2–0.8 g cm^{-3} for comet-sized objects (Davidsson and Gutiérrez 2004,

2005, 2006; Richardson and Melosh 2006; Marchis et al. 2006; Snodgrass et al. 2006; Lacerda and Jewitt 2007). This suggests that most of the cometary material has not been compacted by high pressures and baking in warm interiors of large parent bodies, as occurred with larger bodies with diameters greater than a few hundred km (Lacerda and Jewitt 2007).

The degree of compaction will depend on the internal strength of the material and the pressure attained in the inner regions of the comet nucleus by self-gravity. The central pressure of a body of density ρ (assumed to be uniform) and radius R is

$$P_c = \frac{2\pi}{3} G\rho^2 R^2, \tag{11}$$

which shows that the central pressure increases with the squared radius of the body. A typical one-kilometer radius icy planetesimal of density $\rho = 0.5\ \mathrm{g\,cm^{-3}}$ would attain $P_c = 3.5 \times 10^2\ \mathrm{dyn\,cm^{-2}}$, i.e., too low to compress the fluffy material. Therefore, if such icy planetesimals were the progenitors of comets, we should expect that their pristine low-density, low-strength structure would be preserved. Some or most comets may be the products of collisional cascades from large parent bodies (discussed later), which may have suffered different degrees of compaction of the material. From (11) we see that bodies with sizes in the range 10–100 km reach central pressures in the range 3.5×10^4–$3.5 \times 10^6\ \mathrm{dyn\,cm^{-2}}$, which may be large enough to crush and compact the internal material. Therefore, if some comets are fragments from much larger parent bodies, these may consist of hardened and denser material.

Let us now analyze the effect of radioactive heating in the baking and melting of comet material. For this, let us consider a spherical cometary nucleus of radius R_N and density ρ, heated by ^{26}Al decay at an average heating rate $\bar{Q} \sim 2 \times 10^{-3}\ \mathrm{erg\,g^{-1}\,s^{-1}}$. The energy produced within a volume of radius $r (\leq R_N)$ will be transferred outwards by thermal conduction, so if we neglect other energy sinks, the energy balance equation can be simply expressed

$$\frac{4}{3}\pi r^3 \rho \bar{Q} \simeq 4\pi r^2 K \frac{\mathrm{d}T}{\mathrm{d}r}, \tag{12}$$

where K is the thermal conductivity. By integrating (12) between the limits $0 < r < R_N$ we get

$$T(r) \simeq T_o + \frac{\bar{Q}\rho}{6K}\left(R_N^2 - r^2\right). \tag{13}$$

Wallis (1980) adopted $K = 1.67 \times 10^4\ \mathrm{erg\,cm^{-1}\,s^{-1}\,K^{-1}}$ for loose snow, and $\rho = 0.25\ \mathrm{g\,cm^{-3}}$, and $K = 2.93 \times 10^5\ \mathrm{erg\,cm^{-1}\,s^{-1}\,K^{-1}}$ and $\rho = 1\ \mathrm{g\,cm^{-3}}$ for solid ice + dust (at ~200 K). By introducing reasonable numerical values for the physical parameters of (13) we find that interior temperatures in a 10-km comet nucleus could rise above the melting point of ice (273 K). We must also check that the interior pressure be above the triple point ($\gtrsim 6 \times 10^3\ \mathrm{dyn\,cm^{-2}}$). From (11) we find that a 10-km radius nucleus has a central pressure of $\sim 10^4\ \mathrm{dyn\,cm^{-2}}$, which is just above that required for keeping liquid water. The internal heat will be lost by thermal conduction so, once the radioactive heat source is exhausted, the internal temperature will drop to the level of the equilibrium surface temperature. The conduction cooling time is (Jewitt et al. 2007)

$$\tau_c \sim \frac{R^2}{\kappa}, \tag{14}$$

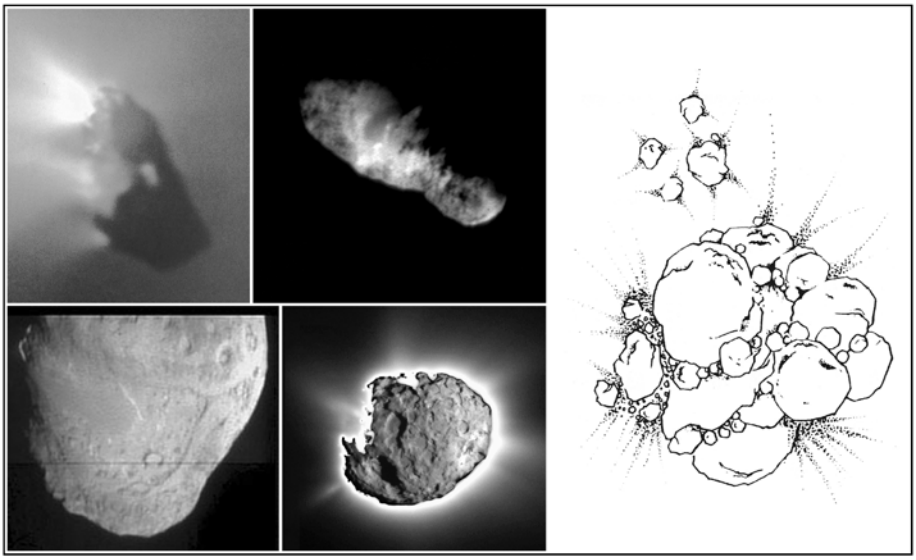

Fig. 2 Close-up images of comet nuclei observed from spacecrafts. Clockwise from the *upper-left panel* we have: 1P/Halley (ESA/Max-Planck Institut für Aeronomie), 19P/Borrelly (NASA/JPL), 81P/Wild 2 (NASA/JPL), and 9P/Tempel 1 (NASA/JPL). *Right panel*: Weissman's (1986) rubble-pile model

where $\kappa = K/(\rho C)$ is the thermal diffusivity and $C \sim 10^7$ erg g^{-1} K^{-1} is the specific heat of the comet material (Fernández 2005; Jewitt et al. 2007). By substituting the appropriate numerical values we have $\kappa \sim 10^{-2}$ cm^2 s^{-1}. Therefore, the cooling time of a comet nucleus of $R \sim 10$ km will be $\tau_c \sim 3$ Myr, i.e., very short as compared to the solar system age. Yet, TNOs or icy satellites of the outer planets with radii $R \gtrsim 10^2$ km could have kept melted cores for most of the solar system age or even until present.

Podolak and Prialnik (1997) re-evaluated the melting of ice in the cometary interior and its maintenance, shedding some doubts on the previous conclusions. They argued that efficient cooling mechanisms, such as heat conduction through the ice and heat carried off by the flow of gas through the porous nucleus, would have made it difficult to reach the conditions for core melting. Therefore, we cannot be very conclusive about the existence of cores of liquid water in icy bodies, but it remains as a very interesting possibility for large comets, icy satellites or trans-neptunian objects.

Mutual collisions might have played an important role in the physical evolution of comets in all the environments they are assumed to have formed, so that fragmentation and reaccumulation of part of the debris might have led to rubble piles like the model proposed by Weissman (1986) for the comet nucleus (Fig. 2). For kilometer-sized objects formed in the region of the Jovian planets (5–30 AU), Stern and Weissman (2001) estimated erosional lifetimes (due to mutual collisions and collisions with small debris) much shorter than the time scales for dynamical ejection under a wide range of possible cosmogonical scenarios. Therefore, they concluded that most comet-sized planetesimals were ground down to dust particles before they were scattered to the Oort cloud. If this was the case, most of the comets we observe today would be the fragments of larger parent bodies, or reaccumulation of fragments of parent bodies collisionally disrupted.

Let us consider a protoplanetary disk where the Jovian planets have already accreted most of their mass. Let Σ_p be the surface density of the residual planetesimals of typi-

cal eccentricities e and inclinations i, which are distributed in the disk with a scale height $H_p \sim i \times r$. The average mass of the planetesimals is $\bar{m} = 4/3\pi R^3 \rho$, ρ being their bulk density. The collisional time scale of bodies in the protoplanetary disk can be roughly computed if we assume that all the residual mass left after the formation of the Jovian planets was in comet-sized planetesimals of one-km radius, and that the total residual mass was about the same as the solid mass incorporated into the Jovian planets (e.g., Fernández and Ip 1996). The number of collisions n_c experienced by one of the planetesimals during a time span τ is

$$n_c = \sigma u \frac{\Sigma_p}{\bar{m} H_p} \tau, \tag{15}$$

where $\sigma \simeq \pi R^2$ is the cross-section, and $u \simeq (e^2 + i^2)^{1/2} v_c$ is the encounter velocity at infinity, v_c being the heliocentric circular velocity at a distance r.

Let us adopt $\Sigma_p = \Sigma_o (r/r_o)^{-3/2}$, with $\Sigma_o = 50\ \mathrm{g\,cm^{-2}}$ at $r_o = 1.5 \times 10^{13}$ cm (= 1 AU), valid for the region beyond the snowline (i.e., the region where water condensed and accreted into solid bodies). Thus at Neptune's distance we get $\Sigma_p \simeq 0.3\ \mathrm{g\,cm^{-2}}$ which is roughly the value obtained by smearing out the masses of Uranus and Neptune in their accretion zones (Greenberg et al. 1984). Furthermore, we can adopt $\rho = 0.5\ \mathrm{g\,cm^{-3}}$.

With these numerical values and setting the condition $n_c = 1$, we obtain the collision time scale of planetesimals beyond the snowline

$$\tau_{\mathrm{coll}} = \frac{i r \bar{m}}{\sigma (e^2 + i^2)^{1/2} (\mu/r)^{1/2} \Sigma_o (r/r_o)^{-3/2}} \simeq 150 r^3\ \mathrm{yr}, \tag{16}$$

where r is expressed in AU.

From (16) we derive collisional time scales of $\sim 2.1 \times 10^4$ yr for Jupiter's region, and $\sim 4 \times 10^6$ yr for Neptune's region, i.e., well below the dynamical time scales for ejection from their respective accretion zones, which agrees with Stern and Weissman's (2001) conclusion.

These results, pointing to an early strong erosive process by mutual collisions, were challenged by Charnoz and Morbidelli (2007, 2003). They developed a numerical model that considers both the dynamical evolution of a swarm of planetesimals and collisional erosion. They found that under certain initial conditions the erosion could not be so severe, and that it will be difficult to reconcile a strong erosion of the primordial Kuiper belt with little erosion of the Oort cloud and scattered disk population. Yet, their results are very sensitive to the initial size distribution of the planetesimals and other parameters related to the cosmogonic scenario. In conclusion, the problem appears very complex: comets may have undergone a collisional process leading to fragmentation and reaccumulation without reaching the point of decimation (otherwise we would not observe comets nowadays!). In this scenario most kilometer-size comets would correspond to fragments or rubble piles from the collisonal disruption of parent icy planetesimals.

6 How the Early Galactic Environment Shaped the Oort Cloud

As we know, the solar system is currently in a region of the Galaxy with a rather low density of stars. But what can we tell about the early galactic environment when the solar system formed? Since stars tend to form in clusters within molecular clouds, it is then likely that the early solar system was not isolated as it is now, but it was a member of a star cluster embedded in a molecular cloud. This is what is commonly observed in star-forming regions, such

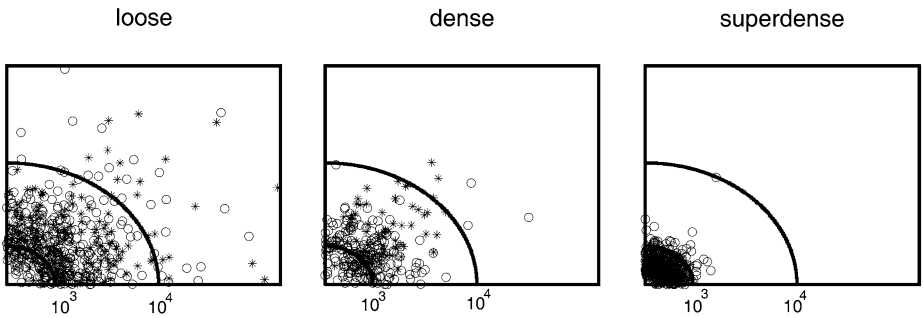

Fig. 3 Projection onto the ecliptic plane of the positions of comets at a given time trapped in the Oort cloud by the strong perturbations of stars assumed to belong, together with the early Sun, to a star cluster. The cluster models have different initial star densities: "loose" (10 stars pc^{-3}), "dense" (25 stars pc^{-3}) and "superdense" (100 stars pc^{-3}). The symbols are for bodies from the Jupiter–Saturn zone (*stars*) and for bodies from the Uranus–Neptune zone (*open circles*). The distances are expressed in AU (Fernández and Brunini 2000)

as the Orion molecular cloud complex (Lada et al. 1993). From a survey of young stellar groups within 1 kpc from the Sun, Porras et al. (2003) found that about 80% of the stars are in large clusters with more than 100 members. The fact that Jupiter and Saturn contain substantial amounts of hydrogen and helium, and Uranus and Neptune a small quantity of these gases, indicates that they grew fast enough to be able to capture gas from the nebula before its dispersal by the strong solar wind during the T Tauri phase of the early Sun. The required time scale could have been $\sim 10^7$ yr, as suggested by the sharp drop in the fraction of premain sequence stars surrounded by disks at that age (e.g., Strom 1995). The massive scattering of the residual planetesimals that followed the accretion of the Jovian planets would have lasted a few tens of Myr, so it is quite possible that most or a large fraction of the scattered planetesimals reached the Oort cloud while the solar system was still in a dense galactic environment (Fernández 1997). Adams et al. (2006) performed N-body simulations of large star clusters with 100–1,000 members. They found that the typical closest distance of binary encounters is $\sim$1,000 AU, unable to disrupt a planetary system like ours, but able to greatly perturb a swarm of planetesimals scattered by the accreted planets.

The buildup of the Oort cloud in a dense galactic environment has been simulated numerically by Fernández and Brunini (2000) and Brasser et al. (2006). Their calculations show that if the Sun was a member of an open cluster, the strong perturbations of other cluster stars would have decoupled comets from the planetary region already for semimajor axes of a few 10^3 AU. We note that the typical relative velocities among cluster stars in virial equilibrium ($\sim$1 km s^{-1}) is much smaller than among field stars ($\sim$30 km s^{-1}) which greatly enhances the perturbing effect of passing stars (cf. (4)). Figure 3 shows numerical results of comets trapped in the Oort cloud, assuming that the early Sun was within a star cluster with a dissolution time of 10^8 yr. The radius of the formed comet cloud is finely tuned to the number density of stars (and thus to the strength of the field of external perturbers); the more dense the star cluster, the more compact the core of trapped comets is. A loose star cluster (10 stars pc^{-3}) will form a rather loose comet cloud of radius $\sim 10^4$ AU, a dense star cluster (25 stars pc^{-3}) will form a more compact core of a few 10^3 AU, while a superdense star cluster (100 stars pc^{-3}) will form a very compact core of radius $\sim 10^3$ AU.

Therefore, the possible existence of an inner core of the Oort cloud of radius of a few 10^3 AU or less may give clues to the early galactic environment where the Sun formed. The discovery of 2003 VB_{12} (Sedna), moving in a kind of orbit expected for objects of the inner

core (preliminary orbital elements: $q = 76 \pm 4$ AU, $a = 480 \pm 40$ AU $i = 11.^{\circ}93$), might represent the first observed member of such a putative core. With a size very close to Pluto's (diameter ~1300–1,800 km), it suggests that a large mass might be enclosed in the inner core, including ~500 Sedna-sized objects (Brown et al. 2004), and in fact Brasser et al. (2006) found that the formation of the Oort cloud in star clusters with mean star densities $\gtrsim 10^3$ stars pc^3 will produce bodies in Sedna-like orbits. To trap bodies within an inner core of radius $a_{\rm core} \sim 10^3$ AU, they must fall within the energy range $\Delta x_{\rm core} = 1/a_{\rm core} - 1/a_{\infty} \sim 10^{-3}$ AU^{-1}, i.e., of the order of the typical energy change of bodies scattered by Jupiter (see Sect. 3.1). This suggests that Jupiter and Saturn might have also been able to place a large number of bodies from their own accretion zones in such an inner core, besides Uranus and Neptune. In this scenario, planetesimals scattered by Jupiter and Saturn will be about as likely to fall in the broadened energy range $\Delta x_{\rm core}$ as to overshoot it to interstellar space. Therefore, the inner core of the Oort cloud might have a significant mixing of bodies from different regions of the protoplanetary disk: from the Jupiter (or even the asteroidal) zone to the trans-neptunian belt, thus providing a heterogeneous population of Oort cloud comets with different contents of volatile materials.

7 The Trans-neptunian Population as a Source of Oort Cloud Comets and Jupiter Family Comets

As of February 2007, more than 1,000 trans-neptunian objects (TNOs) have been discovered. We can distinguish the following dynamical classes: (1) the *classical* belt composed of TNOs in nonresonant orbits with semimajor axes in the range $42 \lesssim a \lesssim 48$ AU in low inclination and low eccentricity orbits; (2) objects with higher inclinations in mean motion resonances (MMRs) with Neptune and semimajor axes $a < 50$ AU, the *Plutinos* in the 2 : 3 MMR being the most populated resonance; and (3) the *scattered disk* (SD) composed of bodies on highly eccentric orbits, perihelia beyond Neptune ($q > 30$ AU) and semimajor axes $a > 50$ AU (Luu et al. 1997). The SD population is of particular interest for the present study since their members dynamically evolve on time scales in general much shorter than the solar system age, either to the Oort cloud or to the Jupiter's zone where they become Jupiter family comets (Duncan and Levison 1997).

Given the uncertainties in the size distribution of TNOs (e.g., Trujillo et al. 2001; Bernstein et al. 2004; Petit et al. 2006), the mass of the scattered disk might be estimated with an accuracy of no more than an order of magnitude, let us say somewhere in between 0.01–0.1 $M_{\oplus}$. This does not include the mass contained in the inner core of the Oort cloud, which is beyond our current detection capability, but Sedna appears to be the most promising candidate.

SDOs will slowly diffuse outwards under the action of planetary perturbations until they reach the Oort cloud, with a dynamical half-life (Fernández et al. 2004)

$$t_{\rm dyn} \simeq 10^{(q-33.5)/4.7} \ \ {\rm Gyr}, \tag{17}$$

where q is expressed in AU. From (17) we get for the SDOs a lifetime $\bar{t}_{\rm dyn} \sim 1.8 \times 10^9$ yr averaged over the range of perihelion distances $31 < q < 36$ AU.

When SDOs get close to Neptune's orbit, they suffer strong perturbations. Neptune acts as a dynamical barrier that favors scattering outwards as compared to scattering inward within the planetary region. From numerical simulations, Fernández et al. (2004) found that about 60% of the bodies inserted in the Oort cloud have perihelia in the range $31 < q < 36$ AU.

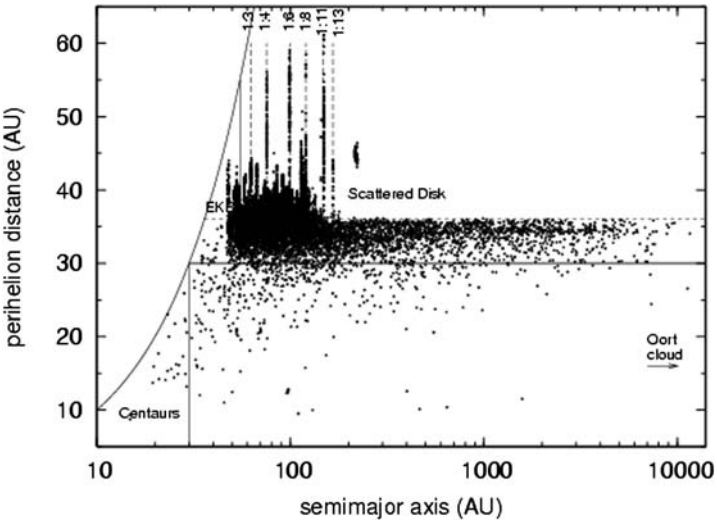

Fig. 4 Perihelion distance versus semimajor axis of SDOs (real objects + clones) plotted every 50 Myr. We can see that many objects get trapped in mean motion resonances with Neptune where the Kozai resonance acts raising their perihelia (Fernández et al. 2004)

Figure 4 shows the dynamical evolution of fictitious bodies in the parametric plane (a, q). We can see that the diffusion to the Oort cloud takes place only for bodies with $q < 36$ AU. Why do not we see SDOs with $q \gtrsim 36$ AU diffusing outward? Probably because when they fall in MMRs, planetary perturbations are too weak to dislodge them from such resonances, thus preventing their further diffusion to near-parabolic orbits. Within the MMRs the Kozai resonance may also act raising the perihelia of the bodies, placing them far from the perturbing action of Neptune and the other Jovian planets, so they can be stored there for very long time scales (Gomes et al. 2005).

The current injection rate of SDOs with radii $R > 1$ km into the Oort cloud can be computed from the estimated SD population and the dynamical lifetime of SDOs (Fernández et al. 2004), namely

$$\nu \simeq \frac{N_{SDO}}{\bar{t}_{\rm dyn}} \simeq 4 \ {\rm yr}^{-1}. \tag{18}$$

This should represent the current value, but the average rate $\bar{\nu}$ over the age of the solar system should be greater bearing in mind that the primordial SD population could have been at least 10^2 times greater (e.g., Stern 1996). Thus, a somewhat greater value $\bar{\nu} \sim 10$ should give at least the correct order of magnitude. We cannot assess yet if this injection rate is large enough to have forced a large renovation of the active Oort cloud throughout the solar system lifetime, but we leave open the possibility that it may not be so primordial as originally thought (Oort 1950), but subject to a steady replenishment of bodies.

As said earlier, a fraction of the SDOs will be transferred to the planetary region evolving as *Centaurs*, namely objects with $q < 30$ AU. Once the perihelia of SDOs reach Neptune's orbit, their perihelia can be handed down from one planet to the next inside until reaching Jupiter's zone where they may be discovered as JF comets. About one third of them will become Jupiter-crossers on time scales of $\sim 4 \times 10^7$ yr (Levison and Duncan 1997; Fernández et al. 2004). For every ~ 4 SDOs that leave the SD for the Oort cloud, ~ 2

objects are transferred to the Jupiter's zone (Fernández et al. 2004). For an estimated average lifetime of JFCs of $\sim 10^4$ yr, the steady state population of JFCs should be $\sim 2 \times 10^4$ in agreement with some previous estimates (e.g., Fernández et al. 1999). Therefore the trans-neptunian population is also a suitable source of JFCs (Fernández 1980; Duncan et al. 1988).

8 Concluding Remarks

We can summarize the main conclusions of this work in the following points:

1. New comets seem to come from a reservoir with the greatest concentration of semimajor axes around $\sim 3.3 \times 10^4$ AU. This is actually the observable part of the Oort cloud or, as we can also say, the dynamically active Oort cloud.
2. The existence of a massive inner core of the Oort cloud still remains in the theoretical realm. However, Sedna may be the first detected member of such a core.
3. The formation of a massive inner core could have been greatly facilitated if the massive scattering of planetesimals by the Jovian planets occurred while the solar system was still embedded in a dense galactic environment.
4. From their elemental composition, comets may still be considered the most primitive unprocessed bodies. Their estimated low bulk densities support this presumption, suggesting a fluffy and porous structure.
5. Nevertheless radioactive decay of short-lived radioisotopes might have led to melting of water ice in the interior of large comets.
6. Catastrophic collisions might have led to fragmentation and reaccumulation of a large proportion of the comet population, so rather than considering comets as primordial unaltered planetesimals, they may actually be assemblages of unprocessed fragments, or fragments of large parent bodies.
7. The trans-neptunian population, via the scattered disk, may be a replenishment source of Oort cloud comets, as well as the main source of JF comets.

References

F.C. Adams, E.V. Proszkow, M. Fatuzzo, P.C. Myers, Astrophys. J. **641**, 504 (2006)
A. Bar-Nun, I. Kleinfeld, Icarus **80**, 243 (1989)
G.M. Bernstein, D.E. Trilling, R.L. Allen, M.E. Brown, M. Holman, R. Malhotra, Astron. J. **128**, 1364 (2004)
L. Biermann, in *Astronomical Papers Dedicated to Bengt Stromgren*, ed. by A. Reiz, T. Anderson (Copenhagen Observatory, 1978), p. 327
L. Blitz, in *Protostars and Planets III*, ed. by E.H. Levy, J.I. Lunine (Univ. Arizona Press, Tucson, 1993), p. 125
R. Brasser, M.J. Duncan, H.F. Levison, Icarus **184**, 59 (2006)
M.E. Brown, C. Trujillo, D. Rabinowitz, Astrophys. J. **617**, 645 (2004)
S. Charnoz, A. Morbidelli, Icarus **166**, 141 (2003)
S. Charnoz, A. Morbidelli, Icarus **188**, 468 (2007)
B.J.R. Davidsson, P.J. Gutiérrez, Icarus **168**, 392 (2004)
B.J.R. Davidsson, P.J. Gutiérrez, Icarus **176**, 453 (2005)
B.J.R. Davidsson, P.J. Gutiérrez, Icarus **180**, 224 (2006)
A.H. Delsemme, Astron. Astrophys. **187**, 913 (1987)
A.H. Delsemme, P. Swings, Ann. Astrophys. **15**, 1 (1952)
B. Donn, Astron. Astrophys. **235**, 441 (1990)
M.J. Duncan, H.F. Levison, Science **276**, 1670 (1997)
M. Duncan, T. Quinn, S. Tremaine, Astrophys. J. Lett. **328**, L69 (1988)

J.A. Fernández, Mon. Not. R. Astr. Soc. **192**, 481 (1980)
J.A. Fernández, Astron. Astrophys. **96**, 26 (1981)
J.A. Fernández, Icarus **129**, 106 (1997)
J.A. Fernández, *Comets. Nature, Dynamics, Origin, and their Cosmogonic Relevance* (Springer, Dordrecht, 2005)
J.A. Fernández, A. Brunini, Icarus **145**, 580 (2000)
J.A. Fernández, T. Gallardo, A. Brunini, Icarus **172**, 372 (2004)
J.A. Fernández, W.-H. Ip, Planet. Space Sci. **44**, 431 (1996)
J.A. Fernández, G. Tancredi, H. Rickman, J. Licandro, Astron. Astrophys. **352**, 327 (1999)
P.J. Francis, Astrophys. J. **635**, 1348 (2005)
P. Goldreich, W.R. Ward, Astrophs. J. **183**, 1051 (1973)
R.S. Gomes, T. Gallardo, J.A. Fernández, A. Brunini, Celest. Mech. Dyn. Astron. **91**, 109 (2005)
R. Greenberg, S.J. Weidenschilling, C.R. Chapman, D.R. Davis, Icarus **59**, 87 (1984)
J. Heisler, S. Tremaine, Icarus **65**, 13 (1986)
J.G. Hills, Astron. J. **86**, 1730 (1981)
J. Holmberg, C. Flynn, Mon. Not. R. Astr. Soc. **313**, 209 (2000)
H.H. Hsieh, D. Jewitt, Science **312**, 561 (2006)
D. Jewitt, L. Chizmadia, R. Grimm, D. Prialnik, in *Protostars and Planets V*, ed. by B. Reipurth, D. Jewitt, K. Keil (Univ. Arizona Press, Tucson, 2007, in press)
V.A. Krasnopolsky, M.J. Mumma, M. Abbott, B.C. Flynn, K.J. Meech, D.K. Yeomans, P.D. Feldman, C.B. Cosmovici, Science **277**, 1488 (1997)
P. Lacerda, D.C. Jewitt, Astron. J. **133**, 1393 (2007)
E.A. Lada, K.M. Strom, P.C. Myers, in *Protostars and Planets III*, ed. by E.H. Levy, J.I. Lunine (Univ. Arizona Press, Tucson, 1993), p. 245
H.F. Levison, M.J. Duncan, Icarus **127**, 13 (1997)
J. Luu, B.G. Marsden, D. Jewitt, C.A. Trujillo, C.W. Hergenrother, J. Chen, W.B. Offutt, Nature **387**, 573 (1997)
F. Marchis, D. Hestroffer, P. Descamps, J. Berthier, A.H. Bouchez, R.D. Campbell, J.C.Y. Chin, M.A. van Dam, S.K. Hartman, E.M. Johansson, R.E. Lafon, D. Le Mignant, I. de Pater, P.J. Stomski, D.M. Summers, F. Vachier, P.L. Wizinovich, M.H. Wong, Nature **439**, 565 (2006)
B.G. Marsden, G.V. Williams, *Catalogue of Cometary Orbits*, 16th edn. (Smithsonian Astrophysical Observatory, Cambridge, 2005)
W.M. Napier, S.V.M. Clube, Nature **282**, 455 (1979)
J.H. Oort, Bull. Astr. Inst. Neth. **11**, 91 (1950)
J.-M. Petit, M.J. Holman, B.J. Gladman, J.J. Kavelaars, H. Scholl, Mon. Not. R. Astr. Soc. **365**, 429 (2006)
M. Podolak, D. Prialnik, in *Comets and the Origin and Evolution of Life*, ed. by P.J. Thomas, C.F. Chyba, C.P. McKay (Springer, New York, 1997), p. 259
A. Porras, M. Christopher, L. Allen, J. Di Francesco, T. Megeath, P.C. Myers, Astron. J. **126**, 1916 (2003)
J.E. Richardson, H.J. Melosh, Lunar and Planetary Institute, XXXVII, Abstract No. 1836, 2006
D.D. Sasselov, M. Lecar, Astrophys. J. **528**, 995 (2000)
C. Snodgrass, S.C. Lowry, A. Fitzsimmons, Mon. Not. R. Astr. Soc. **373**, 1590 (2006)
S.A. Stern, Astron. J. **112**, 1203 (1996)
S.A. Stern, P.R. Weissman, Nature **401**, 589 (2001)
S.E. Strom, Rev. Mex. Astron. Astrof. **1**, 317 (1995)
C.A. Trujillo, D.C. Jewitt, J.X. Luu, Astron. J. **122**, 457 (2001)
E.F. van Dishoeck, G.A. Blake, B.T. Draine, J.I. Lunine, in *Protostars and Planets III*, ed. by E.H. Levy, J.I. Lunine (Univ. Arizona Press, Tucson, 1993), p. 163
M.K. Wallis, Nature **284**, 431 (1980)
P.R. Weissman, Nature **320**, 242 (1986)

Section I: Reservoirs for Material

Reservoir for Comet Material: Circumstellar Grains

Peter Hoppe

Originally published in the journal Space Science Reviews, Volume 138, Nos 1–4.
DOI: 10.1007/s11214-007-9238-7

Abstract Primitive meteorites and interplanetary dust particles contain small quantities of dust grains with highly anomalous isotopic compositions. These grains formed in the winds of evolved stars and in the ejecta of stellar explosions, i.e., they represent a sample of circumstellar grains that can be analyzed with high precision in the laboratory. Such studies have provided a wealth of information on stellar evolution and nucleosynthesis, Galactic chemical evolution, grain growth in stellar environments, interstellar chemistry, and the inventory of stars that contributed dust to the Solar System. Among the identified circumstellar grains in primitive solar system matter are diamond, graphite, silicon carbide, silicon nitride, oxides, and silicates. Circumstellar grains have also been found in cometary matter. To date the available information on circumstellar grains in comets is limited, but extended studies of matter returned by the Stardust mission may help to overcome the existing gaps.

Keywords Solar system: formation · Comets: general · Meteors, meteoroids · Circumstellar matter · Dust, extinction · Nuclear reactions, nucleosynthesis, abundances

1 Introduction

Our Solar System formed from the collapse of an interstellar gas and dust cloud some 4.6 billion years ago. Only a small fraction of the solid matter that went into the making of the Solar System survived the earliest stages of Solar System formation. These relict samples ("presolar grains") are found in small quantities in primitive meteorites and interplanetary dust particles (IDPs). Presolar grains can be distinguished from solids that formed in the Solar System by their highly anomalous (with respect to average Solar System matter) isotopic compositions. They formed in the winds of evolved stars or in the ejecta of supernova explosions, i.e., they represent a sample of circumstellar grains that can be studied with a variety of high-precision analytical techniques in the laboratory. The study of presolar grains

P. Hoppe (✉)
Max-Planck-Institute for Chemistry, Particle Chemistry Department, P.O. Box 3060, 55020 Mainz, Germany
e-mail: hoppe@mpch-mainz.mpg.de

H. Balsiger et al. (eds.), *Origin and Early Evolution of Comet Nuclei*
DOI: 10.1007/978-0-387-85455-7_4

has opened a new window to astronomy. It complements astronomical observations and it permits us to obtain unique astrophysical information.

Comets are generally assumed to represent the most primitive solid matter in the Solar System. Recently, about 1 mg of matter from the comet Wild 2 was brought to Earth by the Stardust mission (Brownlee et al. 2006). The preliminary examination of these samples indicates that the matter in Wild 2 is a mixture of presolar materials and of solids that formed in the Solar System itself. These analyses demonstrated that comet Wild 2 contains circumstellar grains, although with lower concentrations than expected (McKeegan et al. 2006). Since the study of Stardust samples is only at the beginning, the information on the presence and nature of presolar grains in comets is very limited (only one presolar grain was found to date). Thus, in this paper I will focus on presolar (circumstellar) grains found in meteorites and IDPs as a potential reservoir for cometary material. I will give a brief overview of the different types of presolar grains, and will describe their isotopic compositions and stellar sources. The topic of presolar grains was described in detail in several review papers (Anders and Zinner 1993; Ott 1993; Bernatowicz and Zinner 1997; Zinner 1998, 2004; Hoppe and Zinner 2000; Nittler 2003; Lodders and Amari 2005) and the interested reader is referred to these papers for more in-depth information and a full list of references.

1.1 Presolar Minerals

Table 1 lists the presolar minerals identified to date. Pictures of presolar grains are displayed in Fig. 1. Most abundant are the diamonds which are found with concentrations of

Table 1 Presolar minerals found in meteorites and interplanetary dust particles

Mineral	Size (μm)	Abundance[a] (ppm)	Stellar source	Relative contribution[b]
Diamond	~0.0026	1500	Supernovae	?
Silicon carbide	0.1–10	30	AGB stars	>90%
			J-type C stars?	<5%
			Supernovae	1%
			Novae	0.1%
Graphite	1–10	10	Supernovae	<80%
			AGB stars	>10%
			J-type C stars?	<10%
			Novae	2%
Silicon nitride	~1	0.002	Supernovae	100%
Oxides	0.1–5	50	RGB/AGB stars	>90%
($MgAl_2O_4$, Al_2O_3,			Supernovae	1%
$CaAl_{12}O_{19}$, TiO_2)				
Silicates	0.1–1	200 (Met.)	RGB/AGB stars	>90%
		800 (IDPs)	Supernovae	<10%

[a]Reported maximum values from different meteorites are given.

[b]Note uncertainty about actual fraction of diamonds that are presolar and for the relative fractions of graphite grains that are attributed to AGB stars and supernovae.

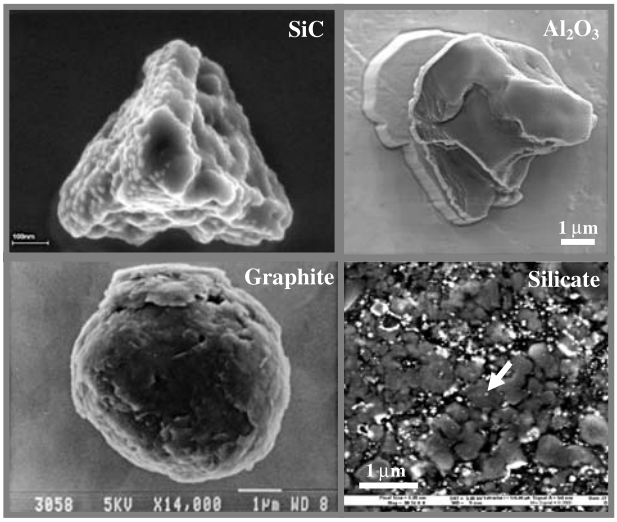

Fig. 1 Scanning electron microscopy images of circumstellar (presolar) dust found in meteorites. The circumstellar SiC, Al_2O_3 and graphite grains were chemically extracted from meteorites; the circumstellar silicate grain was found in situ in the matrix of the Acfer 094 meteorite by ion imaging. The graphite photo courtesy of S. Amari

up to 1,500 ppm (by weight) in the most primitive meteorites. What fraction of the diamonds is actually presolar is still a matter of debate. Diamonds are only 2–3 nm in size, too small for single-grain isotopic measurements. Bulk diamond samples exhibit isotopically normal (i.e., close-to-solar) C, but isotopically anomalous Xe (Lewis et al. 1987) and Te (Richter et al. 1998) which suggests that some (unknown) fraction of them is presolar. The next most abundant presolar minerals are silicates (variable composition) that are present with concentrations of up to several 100 ppm and which were discovered only recently, first in IDPs (Messenger et al. 2003) and later also in meteorites (Nguyen and Zinner 2004; Mostefaoui and Hoppe 2004). Presolar refractory oxides, namely, spinel ($MgAl_2O_4$), corundum (Al_2O_3), hibonite ($CaAl_{12}O_{19}$), and TiO_2 (Hutcheon et al. 1994; Nittler et al. 1994; Choi et al. 1998), silicon carbide (SiC) (Bernatowicz et al. 1987), and graphite (Amari et al. 1990) are found with concentrations of more than 10 ppm. Like the diamonds, SiC and graphite can be separated from meteorites in almost pure form by chemical processing. Very rare are silicon nitride (Si_3N_4) grains (Nittler et al. 1995).

1.2 Astrophysical Information

Figure 2 shows the path of presolar grains from their stellar source to the laboratory. Their isotopic compositions are those in the atmosphere or in the ejecta of their stellar sources. These are determined from the compositions at stellar birth and the nucleosynthetic processes during stellar evolution. After passage through the interstellar medium (ISM) such grains became part of the molecular cloud from which our Solar System formed. A small fraction of the most refractory of those grains survived the period of enhanced temperatures in the solar nebula and was incorporated into growing planetesimals. In small planetary bodies, such as the asteroids and comets, they escaped subsequent destruction by planetary metamorphism. Finally, they are carried to the Earth by meteorites, IDPs, and sample return missions (Stardust). The refractory oxides and the carbonaceous grains can be separated by chemical and physical treatments which were invented by Ed Anders and co-workers at the University of Chicago (Amari et al. 1994); presolar silicates can be recognized by ion imaging techniques (see below).

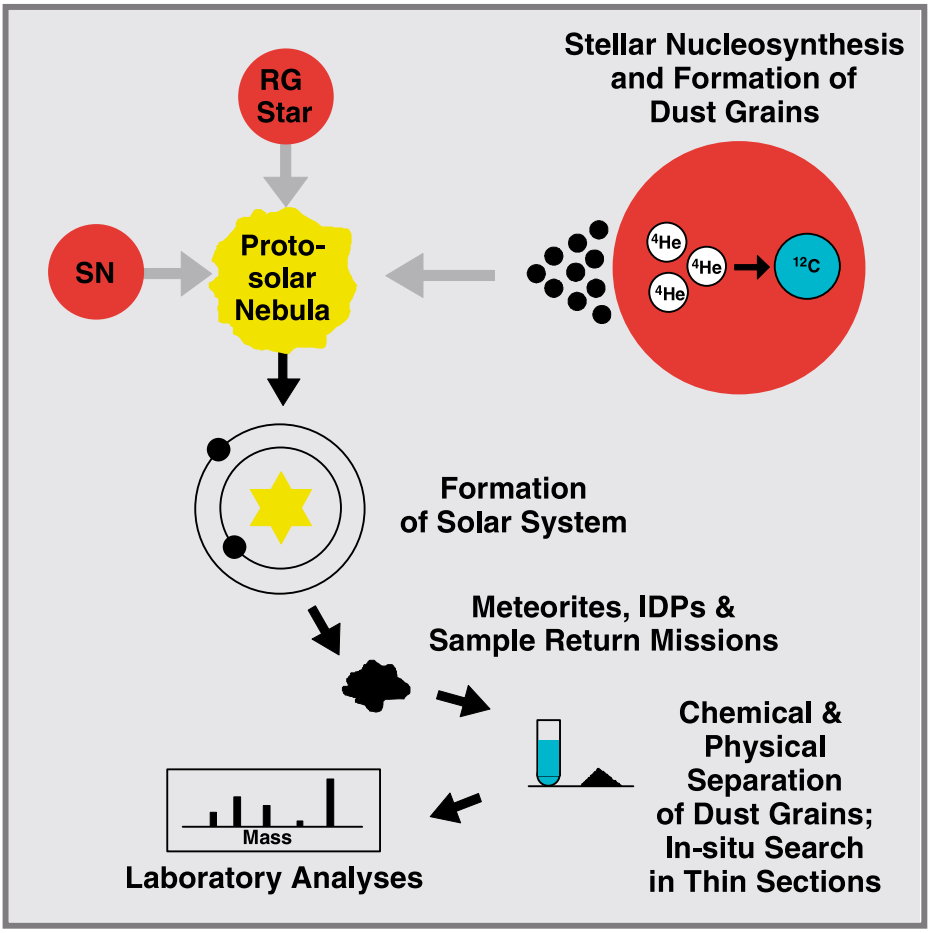

Fig. 2 The path of circumstellar grains from their stellar source to the laboratory. The grains can be either chemically and physically separated from primitive solar system materials or recognized in situ by isotope ion imaging

Important tools for the laboratory study of presolar grains are Secondary Ion Mass Spectrometry (SIMS) and Resonance Ionization Mass Spectrometry (RIMS) for isotope measurements of single grains, and Transmission Electron Microscopy (TEM) for investigations of structure and mineralogy. The laboratory study of presolar grains has provided a wealth of astrophysical information, such as on stellar nucleosynthesis and evolution, Galactic chemical evolution (GCE), mixing in supernova ejecta, grain formation in stellar environments, the chemistry in the ISM, and the types of stars that contributed dust to the Solar System.

1.3 Astronomical Observations

The types of presolar grains identified in primitive Solar System matter can be compared to astronomical observations of circumstellar dust (for an overview see Molster and Waters 2002). Most of the known presolar minerals are also observed in various stellar environments: Features of silicates (amorphous and crystalline) are seen in the spectra of young

Fig. 3 Gas and dust emission from late-type stars: Hubble Space Telescope images of Eta Carinae (*left*) and the Cat's Eye Nebula (*right*). Eta Carinae is one of the most massive stars in our Galaxy ($\sim$100 $\times$ heavier than our Sun) and suffered a giant outburst about 150 years ago. The evolved AGB star in the center of the Cat's Eye Nebula ejected its mass in a series of pulses at 1,500-year intervals. Photo credits: NASA/J. Morse (Eta Carinae), ESA, NASA, HEIC and the Hubble Heritage Team (STScI/AURA) (Cat's Eye Nebula)

stars, C- and O-rich asymptotic giant branch (AGB) stars, post-AGB stars, planetary nebulae, and massive stars. Refractory oxides are present in the atmosphere of O-rich AGB stars, carbonaceous dust around C-rich AGB stars, post-AGB stars, and planetary nebulae. Silicates and carbonaceous dust are also detected in the ISM. Other dust species such as MgS and FeS are observed in stellar spectra but have not been found as presolar grains yet. Figure 3 shows two examples of dust and gas emission from evolved stars. The most prolific suppliers of dust (O- and C-rich) to the ISM are AGB stars during different stages of their evolution (for an overview see Gail 2002). Other significant sources of dust are red supergiants, Wolf-Rayet stars and novae. Not much is known about dust from supernovae. However, some of the presolar grains found in meteorites and IDPs clearly come from supernovae (discussed later).

2 Silicon Carbide

Silicon carbide is the best-studied presolar mineral. Isotopic data are available not only for the major elements C and Si but also for a large number of minor elements that are contained in the SiC grains. This includes N, Mg, Ca, Ti, the noble gases, and heavy refractory elements (Sr, Zr, Mo, Ba, Nd, Sm, Dy). Based on the isotopic compositions of C, N, and Si and the abundance of radiogenic ^{26}Mg (from the decay of radioactive ^{26}Al which has a half life of 700,000 years), SiC was divided into six different populations (Hoppe and Ott 1997; Fig. 4): The mainstream grains which make up the majority of presolar SiC (>90% of all grains), type A&B grains, including the sub-population of the rare nova grains, type Y&Z grains, and type X grains. There is strong evidence that the majority of presolar SiC grains formed in carbon stars, late-type AGB stars in which the C/O ratio is >1 in the envelope:

(i) The distribution of C-isotopic ratios in presolar SiC grains is similar to that measured for carbon stars.

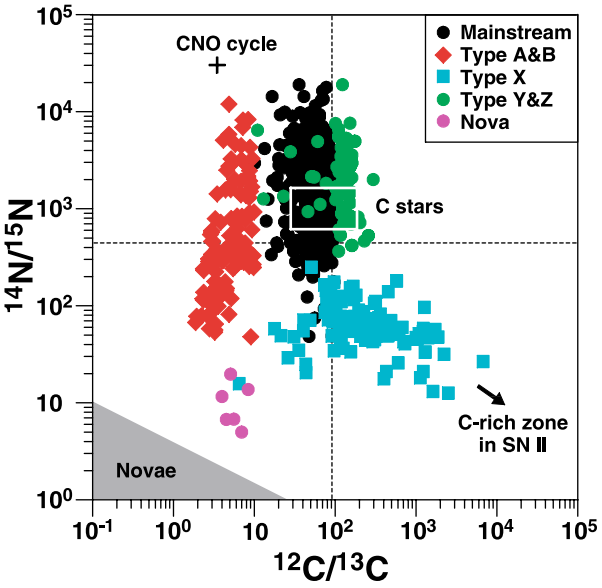

Fig. 4 C- and N-isotopic compositions of distinct presolar SiC populations. The *dashed lines* represent the solar ratios. Note that for the solar $^{14}N/^{15}N$ ratio the value inferred for Jupiter is taken (Owen et al. 2001). Data sources: Hoppe et al. (1994, 1996a, 1996b, 1997, 2000), Nittler et al. (1995), Gao and Nittler (1997), Huss et al. (1997), Amari et al. (2001a, 2001b, 2001c), and Nittler and Hoppe (2005)

(ii) The AGB star-specific signature of s-process nucleosynthesis is seen in the isotopic patterns of intermediate-mass to heavy elements.
(iii) SiC is observed in stellar spectra (see Molster and Waters 2002).
(iv) Carbon stars are the most prolific injectors of dust into the ISM (see Gail 2002).

2.1 Mainstream Grains

The mainstream grains have $^{12}C/^{13}C$ ratios between 10 and 200 and $^{14}N/^{15}N$ ratios between 50 and 20,000 (Fig. 4). Most grains are characterized by enhanced ^{13}C and ^{14}N compared to solar isotopic abundances. This is qualitatively the signature of H burning by the CNO cycle. The isotopic compositions of AGB star envelopes are changed during the star's evolution in three so-called dredge-up episodes when matter that experienced H and He burning and the s-process is mixed into the envelope. In the third dredge-up events the C/O ratio eventually exceeds unity and such stars become carbon stars. Predicted $^{12}C/^{13}C$ ratios in carbon stars are in the range of most mainstream grains. Many mainstream grains, however, have higher $^{14}N/^{15}N$ ratios than predicted by the canonical models for carbon stars. Higher $^{14}N/^{15}N$ ratios can be achieved if "cool bottom processing" (CBP) is considered (Wasserburg et al. 1995). During CBP, which occurs subsequent to the first dredge-up, deep circulation currents transport matter from the non-burning bottom of the convective envelope down to regions where some H burning can occur. Other signatures of H and He burning in SiC mainstream grains are the former presence of radioactive ^{26}Al (Hoppe et al. 1994; Huss et al. 1997) and large isotopic overabundances of ^{22}Ne (e.g., Lewis et al. 1994; Heck et al. 2007).

The isotopic patterns of the intermediate-mass to heavy elements show the imprints of s-process (slow neutron capture) nucleosynthesis (e.g., Nicolussi et al. 1997, 1998; Savina et al. 2003; Marhas et al. 2007), in agreement with theoretical predictions for 1–3 $M_\odot$ AGB stars (Lugaro et al. 2003). It is interesting to note in this context that the detection of the radioactive s-process isotope ^{99}Tc (half life 200,000 years) in the spectra of AGB stars (Merrill 1952) has been the first direct evidence that the chemical elements are produced in the interior of stars. Fingerprints of ^{99}Tc have recently also been found in the isotopic pattern of Ru

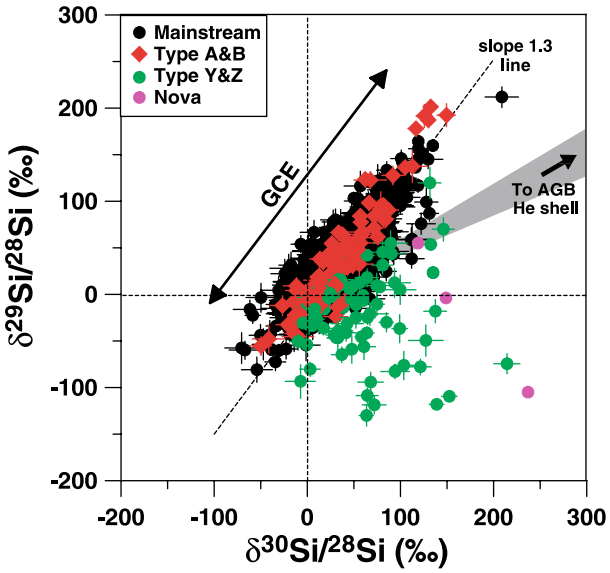

Fig. 5 Si-isotopic compositions of the distinct presolar SiC populations (except the X grains) given as permil deviation from the solar $^{29}Si/^{28}Si$ and $^{30}Si/^{28}Si$ ratios. Predictions for the evolution of the envelope of AGB stars with successive dredge-up of s-process Si is shown for comparison. Data sources: Hoppe et al. (1994), Gao and Nittler (1997), Amari et al. (2001c), and Nittler and Alexander (2003)

in SiC mainstream grains (Savina et al. 2004). The isotopic abundances of ^{99}Ru are higher than predicted for carbon stars, even if uncertainties in nuclear reaction rates are considered, but can be satisfactorily explained by contributions from now-extinct ^{99}Tc.

Although Si is affected by the s-process, its isotopic composition is changed only marginally in the envelope of solar-metallicity AGB stars with progressive third dredge-up events. Most of the mainstream grains exhibit enrichments in the neutron-rich isotopes ^{29}Si and ^{30}Si of up to 200‰ and in a Si three-isotope representation the data plot along a line with slope ~1.3 (Fig. 5). The preferred interpretation of this line is that it reflects primarily the GCE, both in time and space, of the Si isotopes and represents a range of Si starting compositions of a large number of stars and not the effects of the stellar nucleosynthesis in the grain's parent stars (Alexander 1993; Gallino et al. 1994; Timmes and Clayton 1996; Lugaro et al. 1999).

2.2 Type Y and Z Grains

The abundance of type Y and Z grains increases with decreasing grain size, from about 1% for grains >2 μm to about 5–7% for grains of 0.5 μm (Zinner et al. 2007). While $^{12}C/^{13}C$ ratios in type Y grains (Amari et al. 2001a) are higher than in mainstream grains, in type Z grains they are similar to those of mainstream grains (Hoppe et al. 1997; Nittler and Alexander 2003; Zinner et al. 2007) (Fig. 4). The type Y and Z grains have N-isotopic compositions (Fig. 4) and ^{26}Al abundances that are indistinguishable from those of the mainstream grains. In the Si three-isotope representation the type Y and Z grains plot to the ^{30}Si-rich side of the Si mainstream line (Fig. 5). This and the observed large excesses in ^{50}Ti are compatible with an origin in low-metallicity (1/3 to 1/2 solar) AGB stars.

2.3 Type A and B Grains

The minor type A and B grains have $^{12}C/^{13}C$ ratios <10 (Amari et al. 2001b). Many of these grains have lower than solar $^{14}N/^{15}N$ ratios (Fig. 4). Their Si isotopic ratios are compatible

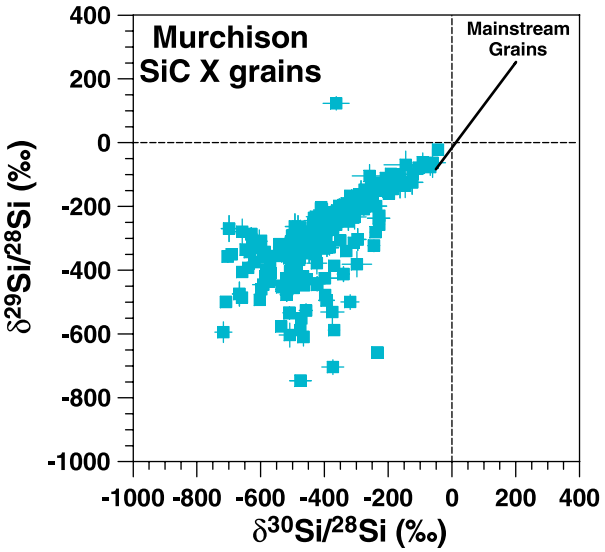

Fig. 6 Si-isotopic compositions of presolar SiC grains of type X. The range of SiC mainstream grains is shown for comparison. Data sources: Nittler et al. (1995), Hoppe et al. (2000), Besmehn (2001), Besmehn and Hoppe (2003), and Nittler and Alexander (2003)

with those of the mainstream grains (Fig. 5) except for the sub-population of the nova grains (Amari et al. 2001c; Nittler and Hoppe 2005) which plot to the ^{30}Si-rich side of the Si mainstream line. Besides novae for grains with very large ^{15}N excesses, J-type carbon stars and born-again AGB stars have been proposed as potential stellar sources for the type A and B grains. Both types of stars are poorly understood at present.

2.4 Type X Grains

SiC X grains are very rare (about 1% of all presolar SiC grains). By ion imaging in the ion microprobe (Nittler et al. 1997; Hoppe et al. 2000) X grains can be efficiently identified and a large isotope data base exists for X grains (e.g., Amari et al. 1992; Nittler et al. 1996; Hoppe et al. 2000; Hoppe and Besmehn 2002; Besmehn and Hoppe 2003; Nittler and Alexander 2003). The X grains have ^{12}C/^{13}C ratios between 6 and 7,000 and ^{14}N/^{15}N ratios between ~10 and 250 (Fig. 4). All grains have isotopically heavy N and most of them have higher than solar ^{12}C/^{13}C ratios. It is interesting to note that the in situ isotope measurements of matter ejected by comet Halley yielded C-rich particles with isotopically light C having ^{12}C/^{13}C ratios of up to ~5,000 (Jessberger and Kissel 1991) which falls in the range of the SiC X grains. The Si-isotopic compositions of X grains are displayed in Fig. 6. The X grains exhibit depletions in the neutron-rich isotopes ^{29}Si and ^{30}Si, or alternatively speaking, enrichments in ^{28}Si. This signature can be explained only by a contribution of matter that experienced advanced nuclear burning stages. This makes supernova explosions the most likely sources of the X grains. Supernovae (SNe) of Type II are preferred (Hoppe et al. 2000), but SNe of Type Ia cannot fully be ruled out (Clayton et al. 1997). Another characteristic feature of X grains are very high ^{26}Al/^{27}Al ratios of up to 0.6, much higher than those observed in grains from AGB stars.

Many of the X grains show large excesses in ^{44}Ca and ^{49}Ti which are best explained by the decay of radioactive ^{44}Ti (half life 60 years) and ^{49}V (half life 330 days). These isotopes are produced in the innermost Ni- and Si-rich zones of Type II SNe (Woosley and Weaver 1995) and their presence is considered a proof for a SN origin of the X grains. Since ^{49}Ti excesses are positively correlated with V/Ti ratios, ^{49}V must have been alive when the

X grains condensed. This constrains the time of grain formation to several months after SN explosion (Hoppe and Besmehn 2002), which is consistent with astronomical observations of dust formation in SN1987a (Wooden 1997).

One X grain with $^{12}C/^{13}C = 6$ and $^{14}N/^{15}N = 16$ plots in the range generally attributed to nova grains. Its Si-isotopic signature, $^{26}Al/^{27}Al$ ratio, and ^{44}Ca excess, however, points to a supernova origin (Nittler and Hoppe 2005). This suggests coupled synthesis of ^{13}C and ^{15}N not only in nova explosions but also in Type II SNe.

In grains from SNe, the isotopic patterns of heavy elements are expected to show the effects of the r-process (rapid neutron capture) nucleosynthesis. This, however, could not be confirmed. Measurements of Mo in X grains by RIMS revealed large excesses in ^{95}Mo and ^{97}Mo (Pellin et al. 1999). In the classical r-process the largest excesses are expected for ^{100}Mo. The observed pattern can be explained with a neutron burst in shocked He-rich matter (Meyer et al. 2000). The occurrence of this kind of neutron burst is a natural consequence of Type II SN explosions (Rauscher et al. 2002). This gives further support that X grains are from Type II SNe, and not from Type Ia, because this kind of neutron burst is not expected to occur in Type Ia SNe.

Presolar Si_3N_4 grains show the same isotopic signatures as X grains: Low $^{29}Si/^{28}Si$ $^{30}Si/^{28}Si$ and $^{14}N/^{15}N$ ratios, and high $^{26}Al/^{27}Al$ ratios (Nittler et al. 1995). This points to a close relationship between these two types of grains, making Type II SNe the most likely sources of presolar Si_3N_4.

3 Graphite

Presolar graphite grains are round, typically >1 μm in size, and have a range in density (1.6–2.2 g/cm^3) (Amari et al. 1990). Many grains contain small internal grains, mostly TiC (Bernatowicz et al. 1991), but also Mo- and Zr-rich carbides (Bernatowicz et al. 1996) and kamacite, cohenite, and iron grains (Bernatowicz et al. 1999; Croat et al. 2003). TiC, kamacite, cohenite, and iron grains have been observed in grains of likely SN origin (see below).

The range of $^{12}C/^{13}C$ ratios of graphite grains (2–7,000) is similar to that seen in presolar SiC; the distribution of $^{12}C/^{13}C$ ratios, however, is clearly different (Fig. 7). Most graphite grains have higher than solar $^{12}C/^{13}C$ ratios, as similarly observed for the SiC X grains. Most of the low-density graphite grains appear to come from SNe, as indicated by excesses in ^{15}N, ^{18}O, ^{28}Si, and high $^{26}Al/^{27}Al$ ratios (Amari et al. 1995a; Travaglio et al. 1999). Strong support for a SN origin also comes from evidence for now-extinct ^{44}Ti (Nittler et al. 1996) and ^{41}Ca (half life 105,000 years; Amari et al. 1996) observed in a few grains. Internal TiC grains show large excesses in ^{49}Ti (Stadermann et al. 2005a), as similarly observed for X grains, suggestive of decay of ^{49}V. Surprisingly, TiC sub-grains are rich in O (Stadermann et al. 2005a). They exhibit large excesses in ^{18}O and the $^{18}O/^{16}O$ ratios are even more extreme than that of the host graphite.

Some (unknown) fraction of high-density graphite grains appear to originate from AGB stars. This is indicated by the presence of internal refractory carbide grains (especially TiC), most of which have significant concentrations of Zr, Mo, and Ru in solid solution (Croat et al. 2005), and by the s-process isotopic patterns of Mo and Zr in several graphite grains (Nicolussi et al. 1998), as similarly observed in SiC mainstream grains. Further support for AGB stars comes from Kr isotope data of graphite bulk samples that show the AGB star-specific s-process pattern (Amari et al. 1995b).

A small fraction of the graphite grains probably comes from novae. Presolar graphite is the carrier of the noble gas component Ne-E(L), which consists of almost pure ^{22}Ne

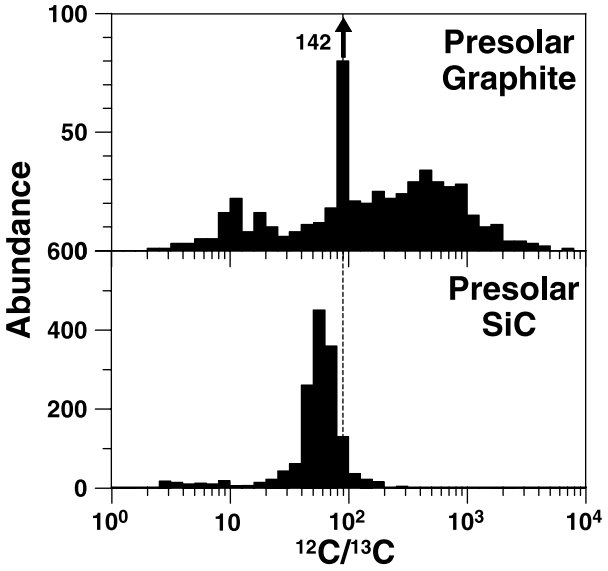

Fig. 7 Histograms of $^{12}C/^{13}C$ ratios of presolar graphite and SiC grains. Data for graphite are from Hoppe et al. (1995), those for SiC from Hoppe et al. (1994, 1996a)

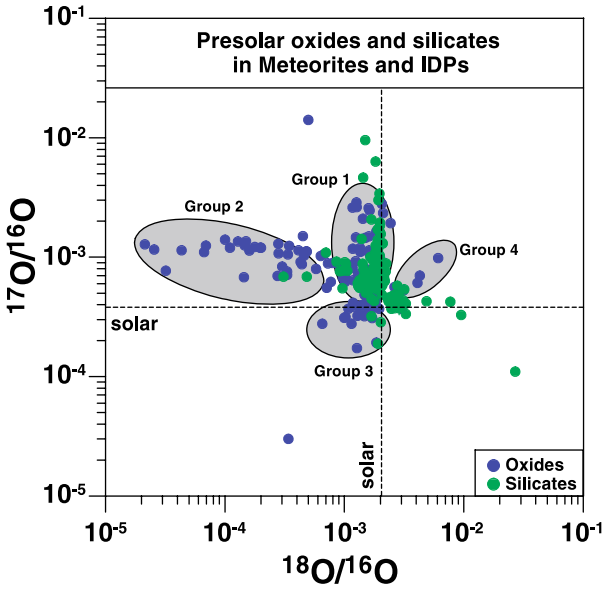

Fig. 8 O-isotopic compositions of presolar oxide and silicate grains. The solar ratios are given by the *dashed lines*. The four isotope groups of O-rich presolar dust are indicated by the *grey-shaded ellipses*. Data sources: Nittler et al. (1994, 1997, 1998), Messenger et al. (2003, 2005), Mostefaoui and Hoppe (2004), Nguyen and Zinner (2004), Hoppe et al. (2005), Stadermann et al. (2005b), Zinner et al. (2005), Floss et al. (2006), Marhas et al. (2006), Yada et al. (2006), Nguyen et al. (2007), and Vollmer et al. (2007)

(Amari et al. 1990). The low $^{20}Ne/^{22}Ne$ ratio of Ne-E(L) has been attributed to an origin in novae where ^{22}Ne is produced by the decay of radioactive ^{22}Na (half life 2.6 years) (Clayton 1975). Noble gas measurements on single graphite grains by laser heating revealed three grains with low $^{20}Ne/^{22}Ne$ and low $^{12}C/^{13}C$ ratios compatible with an origin in novae (Nichols et al. 1992,1994; Heck et al. 2007). However, as SNe also produce ^{22}Na and as a SN SiC X grain with the C- and N-isotopic signature of nova grains was found (see Sect. 2.4), a SN origin for the three graphite grains with low $^{20}Ne/^{22}Ne$ and low $^{12}C/^{13}C$ ratios cannot be ruled out.

4 Oxides

Based on their O-isotopic compositions, the oxide grains (corundum, spinel, hibonite) were divided into four groups (Nittler et al. 1997; see Fig. 8). Comparisons between the grain data and spectroscopic observations as well as stellar model predictions suggest RGB and AGB stars as the most likely stellar sources for the majority of the grains. Group 1 grains have enhanced $^{17}O/^{16}O$ ratios and close-to-solar or slightly lower than solar $^{18}O/^{16}O$ ratios. This is the signature of core H burning in low- to intermediate-mass (1–2.5 $M_\odot$) stars followed by dredge-up of core material into the envelope. While the $^{17}O/^{16}O$ ratios are mostly determined by stellar mass, the varying $^{18}O/^{16}O$ ratios reflect different metallicities of the parent stars (e.g., Boothroyd and Sackmann 1999). Group 2 grains show higher than solar $^{17}O/^{16}O$ ratios and strong depletions in ^{18}O. This signature has been explained by CBP (Wasserburg et al. 1995; Nollett et al. 2003) in low-mass (<1.65 $M_\odot$) stars during the AGB phase. Group 3 grains have lower than solar $^{17}O/^{16}O$ and $^{18}O/^{16}O$ ratios, pointing to low-mass stars with lower than solar metallicity as stellar sources. Group 4 grains exhibit enrichments in ^{17}O and ^{18}O. Proposed stellar sources for these grains include high-metallicity AGB stars and Type II SNe for grains with large ^{18}O excesses. The majority of O-rich grains from Type II SNe is expected to show strong enrichments in ^{16}O. To date only one grain with this O-isotopic signature was observed (Fig. 8, Nittler et al. 1998). Many grains from all four groups carry radiogenic ^{26}Mg from the decay of now extinct ^{26}Al. Because ^{26}Al is produced by shell H burning during the thermal pulsing AGB phase, grains with evidence for ^{26}Al must have formed during the AGB phase, those without during the preceding RGB phase.

5 Silicates

While presolar carbonaceous and oxide grains can be separated by harsh chemical treatments, this does not hold for silicates. The absence of silicates among the known reservoir of presolar grains in meteorites has been an unsatisfactory fact for a long time because silicates are the major constituent of O-rich dust around stars (see Sect. 1.3). Only the invention of the NanoSIMS ion microprobe made the discovery of presolar silicates possible. The first silicates were found by NanoSIMS ion imaging on an interplanetary dust particle by Messenger et al. (2003). In this technique a focused Cs^+ ion beam (<100 nm) is rastered over areas

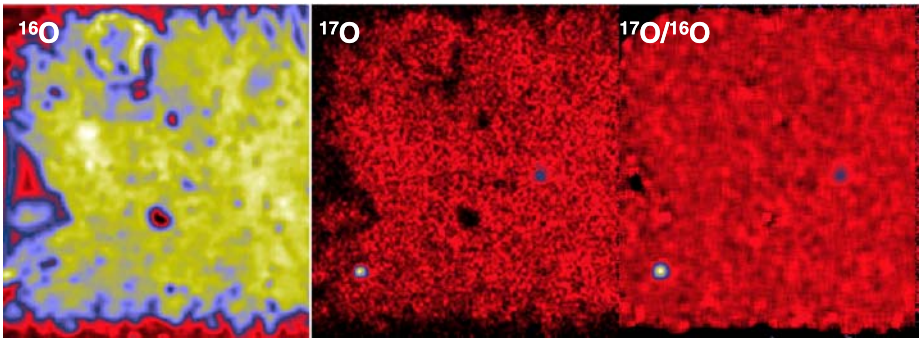

Fig. 9 NanoSIMS ion images of ^{16}O, ^{17}O, and $^{17}O/^{16}O$ in an area 9×9 μm^2 in size in the matrix of the Acfer 094 meteorite. Two presolar silicate grains can be recognized by strong enrichments in ^{17}O (from Hoppe et al. 2005)

typically some 100 μm^2 in size and simultaneous ion images of selected isotopes (e.g., ^{16}O, ^{17}O, ^{18}O) are acquired to search for local isotopic anomalies. An example is shown in Fig. 9, where two presolar silicate grains, about 300 nm in size, are seen as hotspots in the ^{17}O and ^{17}O/^{16}O ion images of an area in the matrix of the Acfer 094 meteorite (Hoppe et al. 2005).

Most presolar silicates are enriched in ^{17}O and have close-to-solar or slightly lower than solar ^{18}O/^{16}O ratio (Fig. 8) as it is similarly observed for the presolar oxides, i.e., they belong to Group 1. Grains of Group 2 are apparently rare. This, however, could be an observational bias from in situ ion imaging because small contributions from the surrounding meteorite matrix to the ion signal from the presolar grains would increase ^{18}O/^{16}O ratios considerably (Nguyen et al. 2007). As it was concluded for the presolar oxide grains, most presolar silicate grains apparently formed in the winds of RGB and AGB stars and contributions from SNe are rare. Only one grain, the one with the lowest ^{17}O/^{16}O and highest ^{18}O/^{16}O ratios (Fig. 8), clearly can be attributed to a SN source. This is based not only on its unusual O-isotopic signature but also on its Si-isotopic signature which is similar to that of the SiC X grains (Messenger et al. 2005).

Information on the detailed mineralogy of the presolar silicates is limited to date. This is because the presolar silicates are not easily accessible to Transmission Electron Microscopy investigations. Among the 10 grains analyzed to date are four so-called GEMS

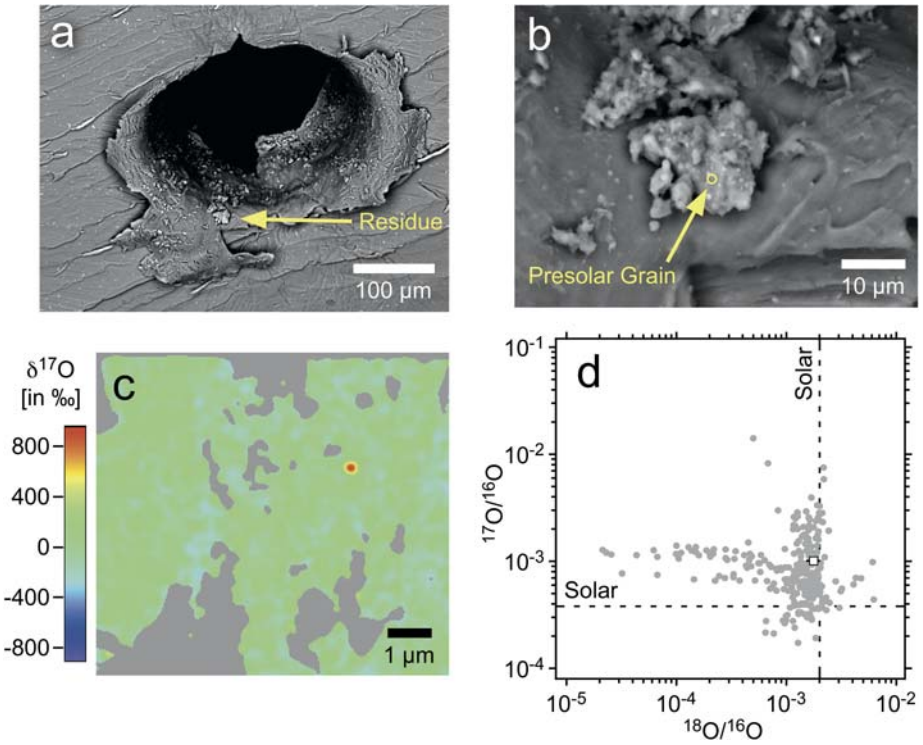

Fig. 10 The only circumstellar grain from the Stardust mission identified to date. (**a**) SEM image of an impact crater in the Al foil where the circumstellar grain was found. (**b**) Projectile residue in crater lip. (**c**) δ^{17}O map acquired with the NanoSIMS. The circumstellar grain is clearly seen as a red hotspot. (**d**) O-isotopic ratios of the circumstellar grain (*open square*) and literature data for circumstellar oxide grains from meteorites. Figure taken from McKeegan et al. (2006)

("glass with embedded metal and sulfides"), two amorphous Fe-rich silicates, two olivines ($(Mg, Fe)_2SiO_4$), one $MgSiO_3$ with a perovskite-like structure, and a composite grain with an Al-rich core (probably Al_2O_3) which is surrounded by a silicate mantle (e.g., Messenger et al., 2003, 2005; Floss et al. 2006; Vollmer et al., 2006, 2007).

6 Implications for Comets

Most comets formed in the outer fringe of our Solar System. They incorporated primitive solar system matter which remained largely unaffected since the time the comets formed. In view of the results obtained for primitive meteorites, presolar (circumstellar) grains can thus be expected to be important ingredients of comets. In fact, in situ studies onboard the Giotto spacecraft of matter from comet Halley indicated solid C-rich particles with isotopically light C (Jessberger and Kissel 1991), a signature observed in many presolar graphite and SiC SN grains. Matter from comet Wild 2, captured by the Stardust spacecraft and returned to Earth recently, can be studied in the laboratory with the best available instrumentation. Only a single circumstellar grain could be identified during the first analysis phase (Fig. 10; McKeegan et al. 2006; Stadermann et al. 2007), which represents some 20 ppm of the analyzed cometary matter. The detailed mineralogy of the grain is not known but it is likely to be an oxide or silicate. It is characterized by a strong enrichment in ^{17}O and slight depletion in ^{18}O with respect to solar isotopic abundances with $^{17}O/^{16}O \sim 0.001$ and $^{18}O/^{16}O \sim 0.0018$, i.e., it belongs to Group 1 of O-rich presolar dust (cf. Fig. 8) and likely formed in the wind of a RGB/AGB star. It should be emphasized that the detection efficiency for presolar grains in Wild 2 material is clearly less than 100% and that the true abundance of circumstellar grains could be much higher. The analysis of Stardust material is just at the beginning and it is hoped that extended laboratory studies of cometary matter will reveal more and possibly new presolar minerals not known from meteorites. This will help to get a detailed look at the starting material from which the comets formed.

Acknowledgements I thank the International Space Science Institute at Bern, Switzerland, for organizing the workshop "Origin and Evolution of Comet Nuclei" where this paper was presented.

References

C.M.O.D. Alexander, Geochim. Cosmochim. Acta **57**, 2869–2888 (1993)
S. Amari, E. Anders, A. Virag, E. Zinner, Nature **345**, 238–240 (1990)
S. Amari, P. Hoppe, E. Zinner, R.S. Lewis, Astrophys. J. **394**, L43–L46 (1992)
S. Amari, R.S. Lewis, E. Anders, Geochim. Cosmochim. Acta **58**, 459–470 (1994)
S. Amari, E. Zinner, R.S. Lewis, Astrophys. J. **447**, L147–L150 (1995a)
S. Amari, R.S. Lewis, E. Anders, Geochim. Cosmochim. Acta **53**, 1411–1426 (1995b)
S. Amari, E. Zinner, R.S. Lewis, Astrophys. J. **470**, L101–L104 (1996)
S. Amari, L.R. Nittler, E. Zinner, R. Gallino, M. Lugaro, R.S. Lewis, Astrophys. J. **546**, 248–266 (2001a)
S. Amari, L.R. Nittler, E. Zinner, K. Lodders, R.S. Lewis, Astrophys. J. **559**, 463–483 (2001b)
S. Amari, X. Gao, L.R. Nittler, E. Zinner, Astrophys. J. **551**, 1065–1072 (2001c)
E. Anders, E. Zinner, Meteoritics **28**, 490–514 (1993)
T.J. Bernatowicz, E. Zinner (eds.), *Astrophysical Implications of the Laboratory Study of Presolar Materials*, New York. AIP Conf. Proc., vol. 402, p. 750 (1997)
T.J. Bernatowicz, G. Fraundorf, T. Ming, E. Anders, B. Wopenka, E. Zinner, P. Fraundorf, Nature **330**, 728–730 (1987)
T.J. Bernatowicz, S. Amari, E. Zinner, R.S. Lewis, Astrophys. J. **373**, L73–L76 (1991)
T.J. Bernatowicz, R. Cowsik, P.C. Gibbons, K. Lodders, B. Fegley Jr., S. Amari, R.S. Lewis, Astrophys. J. **472**, 760–782 (1996)

T.J. Bernatowicz, J. Bradley, S. Amari, S. Messenger, R.S. Lewis, Lunar Planet. Sci. **30** (1999). Abstract 1392 (CD-ROM)
A. Besmehn, Ph.D. thesis, Johannes-Gutenberg-Universität, Mainz (2001)
A. Besmehn, P. Hoppe, Geochim. Cosmochim. Acta **67**, 4693–4703 (2003)
A.I. Boothroyd, I.-J. Sackmann, Astrophys. J. **510**, 232–250 (1999)
D.E. Brownlee et al., Science **314**, 1711–1716 (2006)
B.-G. Choi, G.R. Huss, G.J. Wasserburg, R. Gallino, Science **282**, 1284–1289 (1998)
D.D. Clayton, Nature **257**, 36–37 (1975)
D.D. Clayton, W.D. Arnett, J. Kane, B.S. Meyer, Astrophys. J. **486**, 824–834 (1997)
T.K. Croat, T.J. Bernatowicz, S. Amari, S. Messenger, F.J. Stadermann, Geochim. Cosmochim. Acta **67**, 4705–4725 (2003)
T.K. Croat, F.J. Stadermann, T.J. Bernatowicz, Astrophys. J. **631**, 976–987 (2005)
C. Floss, F.J. Stadermann, J.P. Bradley, Z.R. Dai, S. Bajt, G. Graham, A.S. Lea, Geochim. Cosmochim. Acta **70**, 2371–2399 (2006)
H.-P. Gail, in *Astromineralogy*, ed. by T. Henning (Springer, New York, 2002), pp. 55–120
X. Gao, L.R. Nittler, Lunar Planet. Sci. **28**, 393–394 (1997)
R. Gallino, C.M. Raiteri, M. Busso, F. Matteucci, Astrophys. J. **430**, 858–869 (1994)
P.R. Heck, K.K. Marhas, P. Hoppe, R. Gallino, H. Baur, R. Wieler, Astrophys. J. **656**, 1208–1222 (2007)
P. Hoppe, A. Besmehn, Astrophys. J. **576**, L69–L72 (2002)
P. Hoppe, U. Ott, in *Astrophysical Implications of the Laboratory Study of Presolar Materials*, ed. by T.J. Bernatowicz, E. Zinner (AIP, New York, 1997), pp. 27–58
P. Hoppe, E. Zinner, J. Geophys. Res.-Space Phys. **105**, 10371–10385 (2000)
P. Hoppe, S. Amari, E. Zinner, T. Ireland, R.S. Lewis, Astrophys. J. **430**, 870–890 (1994)
P. Hoppe, S. Amari, E. Zinner, R.S. Lewis, Geochim. Cosmochim. Acta **59**, 4029–4056 (1995)
P. Hoppe, R. Strebel, P. Eberhardt, S. Amari, R.S. Lewis, Geochim. Cosmochim. Acta **60**, 883–907 (1996a)
P. Hoppe, T.A. Kocher, R. Strebel, P. Eberhardt, S. Amari, R.S. Lewis, Lunar Planet. Sci. **27**, 561–562 (1996b)
P. Hoppe, P. Annen, R. Strebel, P. Eberhardt, R. Gallino, M. Lugaro, S. Amari, R.S. Lewis, Astrophys. J. **487**, L101–L104 (1997)
P. Hoppe, R. Strebel, P. Eberhardt, S. Amari, R.S. Lewis, Meteorit. Planet. Sci. **35**, 1157–1176 (2000)
P. Hoppe, S. Mostefaoui, T. Stephan, Lunar Planet. Sci. **36** (2005). Abstr. #1301 (CD-ROM)
G.R. Huss, I.D. Hutcheon, G.J. Wasserburg, Geochim. Cosmochim. Acta **61**, 5117–5148 (1997)
I.D. Hutcheon, G.R. Huss, A.J. Fahey, G.J. Wasserburg, Astrophys. J. **425**, L97–L100 (1994)
E. Jessberger, J. Kissel, in *Comets in the Post-Halley Era*, ed. by R.L. Newburn, M. Neugebauer, J. Rahe (Kluwer Academic, Dordrecht, 1991), pp. 1075–1092
R.S. Lewis, M. Tang, J.F. Wacker, E. Anders, E. Steel, Nature **326**, 160–162 (1987)
R.S. Lewis, S. Amari, E. Anders, Geochim. Cosmochim. Acta **58**, 471–494 (1994)
K. Lodders, S. Amari, Chemie der Erde **65**, 93–166 (2005)
M. Lugaro, E. Zinner, R. Gallino, S. Amari, Astrophys. J. **527**, 369–394 (1999)
M. Lugaro, A.M. Davis, R. Gallino, M.J. Pellin, O. Straniero, F. Käppeler, Astrophys. J. **593**, 486–508 (2003)
K.K. Marhas, P. Hoppe, F.J. Stadermann, C. Floss, A.S. Lea, Lunar Planet. Sci. **37** (2006). Abstr. #1959 (CD-ROM)
K.K. Marhas, P. Hoppe, U. Ott, Meteorit. Planet. Sci. (2007, in press)
K.D. McKeegan et al., Science **314**, 1724–1728 (2006)
P.W. Merrill, Astrophys. J. **116**, 21–26 (1952)
S. Messenger, L.P. Keller, F. Stadermann, R.M. Walker, E. Zinner, Science **300**, 105–108 (2003)
S. Messenger, L.P. Keller, D.S. Lauretta, Science **309**, 737–741 (2005)
B.S. Meyer, D.D. Clayton, L.-S. The, Astrophys. J. **540**, L49–L52 (2000)
F.J. Molster, L.B.F.M. Waters, in *Astromineralogy*, ed. by T. Henning (Springer, New York, 2002), pp. 121–170
S. Mostefaoui, P. Hoppe, Astrophys. J. **613**, L149–L152 (2004)
A.N. Nguyen, E. Zinner, Science **303**, 1496–1499 (2004)
A.N. Nguyen, F.J. Stadermann, E. Zinner, R.M. Stroud, C.M.O.D. Alexander, L.R. Nittler, Astrophys. J. **656**, 1223–1240 (2007)
R.H. Nichols Jr., C.M. Hohenberg, P. Hoppe, S. Amari, R.S. Lewis, Lunar Planet. Sci. **23**, 989–990 (1992)
R.H. Nichols Jr., K. Kehm, R. Brazzle, S. Amari, C.M. Hohenberg, R.S. Lewis, Meteoritics **29**, 510–511 (1994)
G.K. Nicolussi, A.M. Davis, M.J. Pellin, R.S. Lewis, R.N. Clayton, S. Amari, Science **277**, 1281–1283 (1997)
G.K. Nicolussi, M.J. Pellin, R.S. Lewis, A.M. Davis, S. Amari, R.N. Clayton, Geochim. Cosmochim. Acta **62**, 1093–1104 (1998)

L.R. Nittler, Earth Planet. Sci. Lett. **209**, 259–273 (2003)
L.R. Nittler, C.M.O.D. Alexander, Geochim. Cosmochim. Acta **67**, 4961–4980 (2003)
L.R. Nittler, P. Hoppe, Astrophys. J. **631**, L89–L92 (2005)
L.R. Nittler, C.M.O.D. Alexander, X. Gao, R.M. Walker, E.K. Zinner, Nature **370**, 443–446 (1994)
L.R. Nittler, P. Hoppe, C.M.O.D. Alexander, S. Amari, P. Eberhardt, X. Gao, R.S. Lewis, R. Strebel, R.M. Walker, E. Zinner, Astrophys. J. **453**, L25–L28 (1995)
L.R. Nittler, S. Amari, E. Zinner, S.E. Woosley, R.S. Lewis, Astrophys. J. **462**, L31–L34 (1996)
L.R. Nittler, C.M.O.D. Alexander, X. Gao, R.M. Walker, E. Zinner, Astrophys. J. **483**, 475–495 (1997)
L.R. Nittler, C.M.O.D. Alexander, J. Wang, X. Gao, Nature **393**, 222 (1998)
K.M. Nollett, M. Busso, G.J. Wasserburg, Astrophys. J. **582**, 1036–1058 (2003)
U. Ott, Nature **364**, 25–33 (1993)
T. Owen, P.R. Mahaffy, H.B. Niemann, S. Atreya, M. Wong, Astrophys. J. **553**, L77–L79 (2001)
M.J. Pellin, A.M. Davis, R.S. Lewis, S. Amari, R.N. Clayton, Lunar Planet. Sci. **30** (1999). Abstr. #1969 (CD-ROM)
T. Rauscher, A. Heger, R.D. Hoffman, S.E. Woosley, Astrophys. J. **576**, 323–348 (2002)
S. Richter, U. Ott, F. Begemann, Nature **391**, 261–263 (1998)
M.R. Savina, A.M. Davis, C.E. Tripa, M.J. Pellin, R.N. Clayton, R.S. Lewis, S. Amari, R. Gallino, M. Lugaro, Geochim. Cosmochim. Acta **67**, 3201–3214 (2003)
M.R. Savina, A.M. Davis, C.E. Tripa, M.J. Pellin, R. Gallino, R.S. Lewis, S. Amari, Science **303**, 649–652 (2004)
F.J. Stadermann, T.K. Croat, T.J. Bernatowicz, S. Amari, S. Messenger, R.M. Walker, E. Zinner, Geochim. Cosmochim. Acta **69**, 177–188 (2005a)
F.J. Stadermann, C. Floss, P.A. Bland, E.P. Vicenzi, D. Rost, Lunar Planet. Sci. **36** (2005b). Abstr. #2004 (CD-ROM)
F.J. Stadermann, P. Hoppe, C. Floss, P.R. Heck, F. Hörz, J. Huth, A.T. Kearsley, J. Leitner, K.K. Marhas, K.D. McKeegan, T. Stephan, Meteorit. Planet. Sci. (2007, in press)
F.X. Timmes, D.D. Clayton, Astrophys. J. **472**, 723–741 (1996)
C. Travaglio, R. Gallino, S. Amari, E. Zinner, S. Woosley, R.S. Lewis, Astrophys. J. **510**, 325–354 (1999)
C. Vollmer, P. Hoppe, F.F. Brenker, R.M. Stroud, C. Holzapfel, Meteorit. Planet. Sci. **41**, A184 (2006)
C. Vollmer, P. Hoppe, F. Brenker, C. Holzapfel, Lunar Planet. Sci. **38** (2007). Abstr. #1262 (CD-ROM)
G.J. Wasserburg, A.I. Boothroyd, I.-J. Sackmann, Astrophys. J. **447**, L37–L40 (1995)
D. Wooden, in *Astrophysical Implications of the Laboratory Study of Presolar Materials*, ed. by T.J. Bernatowicz, E. Zinner (AIP, New York, 1997), pp. 317–378
S.E. Woosley, T.A. Weaver, Astrophys. J. Suppl. **101**, 181–235 (1995)
T. Yada, F.J. Stadermann, C. Floss, E. Zinner, T. Nakamura, T. Noguchi, A.S. Lea, Lunar Planet. Sci. **37** (2006). Abstr. #1470 (CD-ROM)
E. Zinner, Ann. Rev. Earth Planet. Sci. **26**, 147–188 (1998)
E. Zinner, in *Treatise in Geochemistry*, ed. by K.K. Turekian, H.D. Holland, A.M. Davis (Elsevier, Oxford/San Diego, 2004), pp. 17–39
E. Zinner, L.R. Nittler, P. Hoppe, R. Gallino, O. Straniero, C.M.O.D. Alexander, R.S. Lewis, Geochim. Cosmochim. Acta **69**, 4149–4165 (2005)
E. Zinner, S. Amari, R. Guinness, C. Jennings, A.F. Mertz, A.N. Nguyen, R. Gallino, P. Hoppe, M. Lugaro, L.R. Nittler, R.S. Lewis, Geochim. Cosmochim. Acta (2007, in press)

Interstellar Reservoirs of Cometary Matter

S.B. Charnley · S.D. Rodgers

Originally published in the journal Space Science Reviews, Volume 138, Nos 1–4.
DOI: 10.1007/s11214-008-9331-6

Abstract We review the evidence for the products of interstellar chemistry in volatile cometary matter. We compare the organic inventory of star-forming cores with that measured in various comets and point out the similarities and differences. The conditions necessary to fractionate interstellar molecules in the heavier isotopes of H, C, O and N are summarised and compared to the measured fractionation ratios in cometary ices. We give a list of future measurements that would shed further light on the putative connection between cometary and interstellar molecules.

Keywords Comets · Radio lines: solar system · ISM: molecules · Solar system: formation · Astrochemistry

1 Introduction

The volatile composition of comets exhibits many similarities to the molecular composition of the interstellar medium (ISM), suggesting a link between interstellar matter and comets. Recent cometary observations and space missions show that some cometary material underwent significant thermal processing in the protosolar nebula (e.g., A'Hearn 2006; Brownlee 2006), in contrast to the view that comets consist of pristine interstellar ice and dust (e.g., Greenberg 1982). Nevertheless, signatures of interstellar chemistry may be preserved in cometary material in the form of isotope ratios, molecular spin ratios, and the abundances of specific organic molecules. Currently, the amount of alteration caused by nebular processing is an open question, with important implications for understanding the origin of our solar system and the volatile inventory of the early Earth (e.g., Ehrenfreund and Charnley 2000; Ehrenfreund et al. 2004).

Understanding the connection between interstellar chemistry and cometary composition will allow several important scientific questions to be addressed. What is the complement

S.B. Charnley (✉) · S.D. Rodgers
Space Science & Astrobiology Division, MS 245-3, NASA Ames Research Center, Moffett Field, CA 94035-1000, USA
e-mail: charnley@dusty.arc.nasa.gov

H. Balsiger et al. (eds.), *Origin and Early Evolution of Comet Nuclei*
DOI: 10.1007/978-0-387-85455-7_5

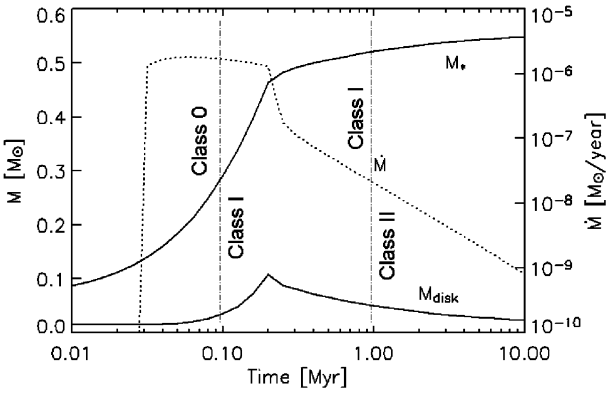

Fig. 1 Evolution of protostellar and disk masses (from van Dishoeck and Jørgensen 2008)

of pristine interstellar organic material in comets? Is it possible to reconstruct the physical and chemical history of interstellar material in the nebula from observations of its processed end-state in comets? Does the chemical composition of a comet nucleus reflect its formation zone in the nebula? Do different cometary materials (dust, ices, organic particles) originate from markedly different environments? If so, is this the case for all comet families and what are its implications for the physics of nebula evolution?

2 Formation of Protostars and Disks in Molecular Clouds

Low-mass stars such as the Sun are created from the collapse of dense pre-stellar cores, which in turn form within dark molecular clouds. Observations of many pre- and proto-stellar cores have allowed them to be classified according to their spectral energy distribution, which is a measure of their evolutionary state (Lada and Shu 1990; Bachiller 1996). Pre-stellar cores are cold, centrally condensed globules, and many appear to be on the verge of gravitational collapse (e.g., Kandori et al. 2005). The most dense regions of these cores contain 'depletion zones'—regions in which gas phase molecules (e.g., CS, CO, N_2) are selectively frozen out to form icy mantles on the dust grains (e.g., Bergin and Tafalla 2007). Class 0 sources contain a deeply embedded protostar which is still rapidly accreting material from the surrounding cocoon of gas and dust. This material will be heated by the luminous central protostar as it collapses onto the disk, and may experience a violent accretion shock at the disk surface. By the Class I stage a massive protostellar disk has built up, and the accretion rate from the remaining envelope falls dramatically (e.g., Fig. 1; Hueso and Guillot 2005), in part due to powerful outflows. Material in the disk gradually spirals into the central protostar, and turbulent mixing within the disk may also transport material processed in the inner nebula outwards to the comet-forming zones. Since comets and planetesimals probably formed fairly late in this sequence, the molecules present in primitive solar system materials are the survivors, or derivatives, of material that accreted during the Class I and II stages, before the nebular gas was lost. Thus, although we expect that comet nuclei should not consist *entirely* of pristine interstellar material, it is possible that some may survive and exhibit chemical characteristics that originated in the ISM.

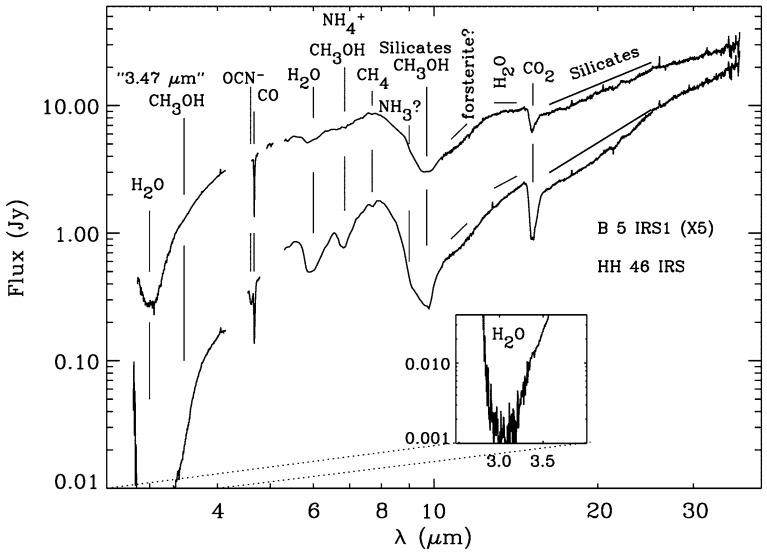

Fig. 2 Ice absorption spectra towards B5 IRS1 and HH 46 IRS (Boogert et al. 2004)

3 Interstellar Chemistry and Cometary Composition

3.1 Organics

In dark clouds, gas phase chemistry, involving ion-neutral and neutral-neutral processes, appears to favour the formation of long carbon chain molecules (Wooden et al. 2004). Atoms and molecules stick to and react on dust grains and the resulting dirty icy mantles can be probed by IR spectroscopy towards background field stars or protostars embedded in the cloud. Figure 2 shows VLT-Spitzer spectra of the Class I protostar B5 IRS 1 (Boogert et al. 2004). The major components of interstellar ice mantles are H_2O, CO, CO_2, NH_3 and CH_3OH, with CH_4, HCOOH, OCS, OCN^-, H_2CO and NH_4^+ present at trace levels. Primary interstellar ice mantles formed by accretion and cold grain-surface reactions (Wooden et al. 2004) and can also undergo secondary energetic processing by UV photons and cosmic rays (Ehrenfreund et al. 2001). Larger complex organics are thus undoubtedly present in these ices but unfortunately at abundance levels that render them undetectable in the IR.

Complex organic chemistry is found in the hot cores containing massive protostars and growing number of Class 0 sources have been shown to be very rich in organic molecules. These molecules are understood to be present in small 'hot corinos', in which icy grain mantles have been evaporated. Several of these 'hot corinos' have now been identified: IRAS 16293-2422 (Cazaux et al. 2003; Kuan et al. 2004; Bottinelli et al. 2004a), NGC1333-IRAS4A (Bottinelli et al. 2004b), NGC1333-IRAS4B (Sakai et al. 2006; Bottinelli et al. 2007) and NGC1333-IRAS2A (Jørgensen et al. 2005, Bottinelli et al. 2007). In hot cores and hot corinos, mantle evaporation into the gas means that trace organics can be detected by microwave spectroscopy. Apart from unambiguous mantle chemistry products, such as methanol and formic acid, other organics could be formed from the mantle molecules after their evaporation by ion-molecule reactions in the warm gas (Charnley et al. 1992); for example, methyl ethyl ether and other large ethers (Charnley et al. 1995, 2001; Fuchs et al. 2005).

Space missions have allowed the *refractory* organic material in comets to be studied. In situ measurements at comet Halley discovered a population of organic CHON particles (Kissel et al. 1986). Disintegration of CHON particles and various specific organic polymers have been proposed as the origin of the extended distributions of specific simple molecules in cometary comae, such as CO, H_2CO, CN, HNC, and CS (e.g., Boehnhardt et al. 1990; Kissel et al. 1997; Rodgers et al. 2004; Fray et al. 2006; Lis et al. 2008). Radio observations

Table 1 Observed molecular abundances in several comets and interstellar sources

Molecule	Comet[a] Halley	Comet[a] Hale-Bopp	Comet[a] Hyakutake	Comet[a] Lee	Comet[a] Ikeya-Zhang	L134N[b]	IRAS 16293	Sgr B2(N)[c]
CO	3.5–11	12–23	14–30	1.8–4	4–8	33,000	30,000	1,000
CO_2	3–4	6	…	…	…	…	…	…
CH_4	<0.8	1.5	0.8	0.8	0.5	…	…	…
C_2H_2	0.3	0.1–0.3	0.2–0.5	0.27	0.18	…	…	…
C_2H_6	0.4	0.6	0.6	0.67	0.62	…	…	…
CH_3OH	1.8	2.4	2	2.1–4	2.5	1	9	2
H_2CO	4	1.1	1	1.3	0.4	8	0.02	>0.005
HCOOH	…	0.09	…	…	…	0.1	<0.01	>0.003
$HCOOCH_3$	…	0.08	…	…	…	…	6	0.02
CH_3CHO	…	0.02	…	…	…	0.3	<0.003	0.002
$(CH_2OH)_2$	…	0.25	…	…	…	…	…	0.001
CH_3OCH_3	…	<0.5	…	…	…	…	2.2	0.03
NH_2CHO	…	0.015	…	…	…	…	<0.001	0.002
NH_3	1.5	0.7	0.5	…	…	80	6	…
HCN	0.1	0.25	0.1–0.2	0.1–0.3	0.1–0.2	1.7	0.06	>0.05
HNCO	…	0.1	0.07	…	…	…	0.005	0.006
HNC	…	0.04	0.01	0.01	0.005	2.7	0.004	>0.001
CH_3CN	…	0.02	0.01	…	0.01	…	0.01	0.3
HC_3N	…	0.02	…	…	<0.01	0.07	0.03	0.05
H_2S	0.4	1.5	0.8	<0.9	0.8	0.3	0.04	…
CS	…	0.1	0.1	0.08	…	0.2	0.03	…
OCS	…	0.4	0.1		<0.2	0.7	0.2	>0.02
SO	…	0.3	…	…	…	7	15	…
SO_2	…	0.2	…	…	…	0.2	2.8	0.3
CS_2	0.2	0.2	0.1	0.08	0.06–0.1	…	…	…
H_2CS	…	0.02	…	…	…	0.3	0.005	0.2
NS	…	0.02	…	…	…	…	0.02	…
S_2	…	…	0.005	0.002	0.004	…	…	…

Abundances are expressed in per cent relative to water. Adapted from Bockelée-Morvan et al. (2004), Charnley et al. (2002), and Ehrenfreund and Charnley (2000), with additional data for IRAS 16293 from Mundy et al. (1990), Blake et al. (1994), and Chandler et al. (2005)

[a]Full designations are: 1P/Halley, C/1995 O1 (Hale-Bopp), C/1996 B2 (Hyakutake), C/1999 H1 (Lee), and 153P/Ikeya-Zhang

[b]Lower limits as H_2O is not detected in this source

[c]Upper limits as the H_2O abundance is not well constrained

detected many new *volatile* organic molecules in the coma of Hale-Bopp, and upper limits were obtained for many more, including isotopologues (Crovisier et al. 2004a; Bockelée-Morvan et al. 2004). The relative abundances of specific molecules have been employed to develop a taxonomic chemical classification for comets (e.g., Mumma et al. 2003; Biver et al. 2006). Table 1 lists the volatile compositions of five comets compared to a dark cloud (L134N), a low-mass (binary) hot corino (IRAS 16293-2422) and a massive hot core (Sgr B2(N)).

The compositional similarities strengthen the connection between interstellar molecules and those found in comets. Figure 3 indicates that a defining feature of interstellar grain catalysis is the growth of linear chains by single atom additions and their subsequent saturation (Charnley 2001). Clearly, many interstellar and cometary molecules appear to share a common origin in grain-surface chemistry. However, there are discrepancies. For example, the abundance of methanol in comets is never above a few per cent, whereas its abundance in interstellar ices can lie in the range 10–40%. Nevertheless, discovery of ethylene glycol ($HOCH_2CH_2OH$) in Hale-Bopp (Crovisier et al. 2004b), at a relative abundance higher than in hot cores, leads us to expect that other organic molecules, already known in the ISM, may also be present and detectable in comets. For example, preliminary analyses of the Stardust samples from comet 81P/Wild 2 (Sandford et al. 2006) produced the surprising result that a significant quantity of the organic nitrogen appears to be contained in some form of aliphatic carbon. The aliphatic amines CH_3NH_2 and $CH_3CH_2NH_2$ are the major carriers identified and their abundance ratio is ~ 1. Future observations of hot cores may allow us to know whether this ratio is an interstellar signature.

3.2 Deuterium Fractionation

Deuterium is highly enriched in interstellar molecules because ion-molecule reactions at low temperatures lead to the preferential retention of D in molecular ion products

$$H_3^+ + HD \rightleftharpoons H_2D^+ + H_2 \quad (1)$$

$$H_2D^+ + HD \rightleftharpoons HD_2^+ + H_2 \quad (2)$$

$$HD_2^+ + HD \rightleftharpoons D_3^+ + H_2 \quad (3)$$

These deuterated molecular ions can readily transfer deuterons to other neutral molecules (Roberts 2006); their electron dissociative recombination leads to enhanced atomic D/H ratios in the gas, and hence to the formation of fractionated molecules by atom addition reactions on cold dust grains (Tielens 1983). Roberts et al. (2003) have shown that selective depletion of heavy molecules like CO on to grains in ultradense prestellar gas leads to D_3^+ and HD_2^+ ions being significantly enhanced. In the depleted gas, deuterium fractionation by gas and grain-surface processes are considerably more efficient, leading to enormous D/H ratios (~ 0.1–1) and the formation of various multideuterated isotopologues. Consequently, organic molecules formed in grain-surface schemes like Fig. 3 should also exhibit these deuteration characteristics (Charnley et al. 1997) and, in hot corinos, this is believed to be the origin of the multideuteration observed in formaldehyde, methanol (e.g., CD_2OH and CD_3OH; Parise et al. 2002, 2004) and other species (Roberts 2006; Ceccarelli 2006).

Table 2 is a summary of the deuterated molecules observed in comets, and compares the cometary D/H ratios with the relevant interstellar values. The water ratios are at the lower end of the range determined for the low-mass protostellar binary system IRAS 16293-2422 (2×10^{-4}–3×10^{-2}, Stark et al. 2004; Parise et al. 2005; Butner et al. 2007) and are

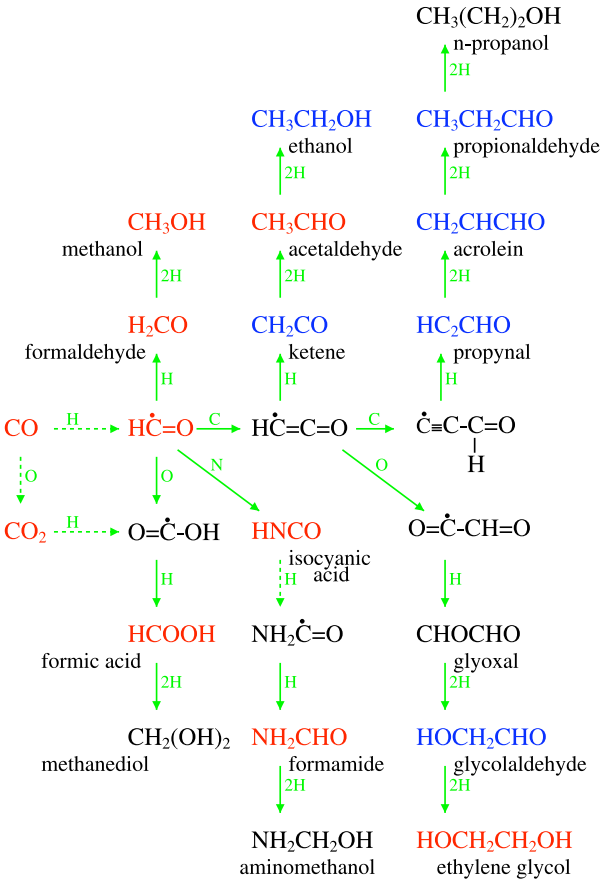

Fig. 3 Grain surface reaction scheme forming interstellar organics via atom addition reactions (see Charnley and Rodgers 2006). Molecules in *red* are detected both in comets and in interstellar/protostellar sources, whereas those in *blue* are found only in the latter. Species in *black* are not yet detected in space

consistent with the low values found in hot cores near massive protostars like those in Orion-KL (Jacq et al. 1990). The DCN/HCN ratio was 0.002 in Hale-Bopp (Meier et al. 1998b), a value again consistent with hot core measurements (0.003), but at least a factor ten lower than found around low-mass protostars (Roberts et al. 2002). Both the measured HDO/H_2O and DCN/HCN ratios are compatible with ion-molecule chemistry in gas at about 25–35 K (Millar et al. 1989).

Interplanetary dust particles are understood to originate from comets and large D/H ratios, some 50 times the terrestrial value have been measured (Messenger et al. 2003). Hence the organic carbon component of comet dust may contain higher D/H ratios than measured in simple molecules like water and HCN. The derived HDCO/H_2CO ratio in comet C/2002 T7 (LINEAR) is about 30% (Kuan et al. 2008), almost double observed interstellar ratios (Roberts 2006; Ceccarelli et al. 2007), and suggestive of an origin on 10 K dust grains in highly depleted gas.

3.3 Nitrogen Isotopic Fractionation

Although the possibility of ^{15}N fractionation in ion-molecule reactions was well-established experimentally (Adams and Smith 1981), and various isotopologues shown to be relatively easy to detect (e.g., Wilson and Rood 1994), there was little motivation from astronomical

Table 2 Deuterium fractionation in comets and the interstellar medium

Isotopologue Ratio[a]	Cometary Ratio	Comet	Interstellar Ratio[b]	Refs.[b]
HDO/H_2O	0.0006	Several[c]	0.0004–0.01	1–3
DCN/HCN	0.002	Hale-Bopp	0.01–0.1	4
$HDCO/H_2CO$	0.28	C/2002 T7	0.07–0.3	5
$HDCO/H_2CO$	< 0.1	Hale-Bopp	0.07–0.3	6
NH_2D/NH_3	< 0.1	Hale-Bopp	0.01–0.08	6
CH_3OD/CH_3OH	< 0.03	Hale-Bopp	0.01–0.06	6
CH_2DOH/CH_3OH	< 0.02	Hale-Bopp	0.04	6
HDS/H_2S	< 0.2	Hale-Bopp	0.01–0.1	6
CH_3D/CH_4	< 0.04	C/2001 Q4	< 0.06	7

[a]The values in the table are the abundance ratios of the isotopologues, and not the corresponding D/H ratios, which will differ depending on the number of hydrogen atoms in the molecule

[b]Representative interstellar values are from Roueff and Gerin (2003), where a complete list can be found

[c]HDO/H_2O ratios were measured in comets Halley, Hyakutake, & Hale-Bopp with three further tentative detections in Ikeya-Zhang, Lee, & C/2001 A2 (LINEAR) (Gibb et al. 2002)

References: (1) Eberhardt et al. (1995); (2) Bockelée-Morvan et al. (1998); (3) Meier et al. (1998a); (4) Meier et al. (1998b); (5) Kuan et al. (2008); (6) Crovisier et al. (2004a); (7) Kawakita et al. (2005)

observations to explore nitrogen isotope chemistry in detail (see however Ikeda et al. 2002). As with deuterium, bulk enhancements and ^{15}N-rich hotspots are seen in meteoritic and IDP samples (e.g., Messenger et al. 2003; Busemann et al. 2006) and the likelihood that these are also the product of fractionation from ion-molecule chemistry in cold gas has led to several recent theoretical studies.

Terzieva and Herbst (2000) explored several possible fractionation reactions which could lead to elevated $^{15}N/^{14}N$ ratios, but found only minor enhancements under typical dark cloud conditions ($\sim 25\%$). This is due to the fact that nitrogen is continually cycled between the two main reservoirs—N and N_2 (see Fig. 4). Charnley and Rodgers (2002) subsequently demonstrated that, in regions where CO is selectively depleted from the gas phase this coupling is removed, the N_2 abundance collapses, and much larger ^{15}N enhancements are possible for N_2 and ammonia in such depletion cores. Figure 5 shows that, in this case, the higher N/N_2 ratio means that ^{15}N atoms can efficiently fractionate $^{14}N_2H^+$; this is transferred to $^{14}N^{15}N$ upon recombination, He^+ releases more $^{15}N^+$ which is rapidly incorporated into NH_3 and NH_2, then frozen out in ammonia-rich ice layers. These calculations (see Fig. 5) could account for the bulk δ^{15}N values found in primitive materials, assuming subsequent processing to combine the $^{15}NH_3$-rich layers with the organic component, as well as the apparently widespread absence of N_2 in comets. However, the exact degree of fractionation possible depends on the dissociative recombination of N_2H^+. Experimental results reported by Geppert et al. (2004) indicated that dissociative recombination of N_2H^+—previously thought to produce only N_2 and H—may also produce N + NH as the dominant channel. This recouples the N – N_2 system, reducing the maximum fractionation. In light of the Geppert et al. results, Rodgers and Charnley (2004) modelled the ^{15}N chemistry and showed that large ^{15}N enhancements could be produced if either (i) there exist an abundance of PAHs available for proton transfer or, (ii) the reaction of N and NH forming N_2 has a barrier. However, recent experiments show that the branching ratios determined by Geppert et al. are in error (Molek et al. 2007). Calculations using the re-measured upper limits to the branching

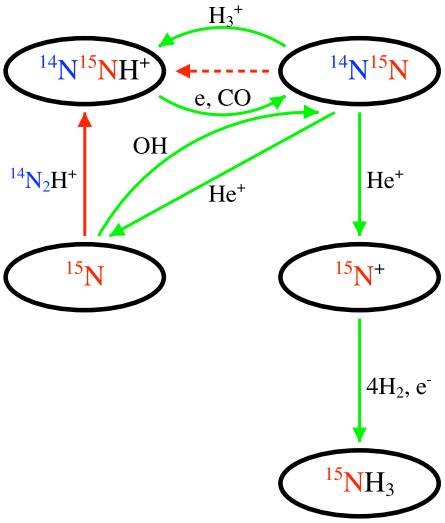

Fig. 4 Simplified chemical scheme for nitrogen in dark clouds. *Red arrows* indicate fractionation reactions which lead to ^{15}N enhancements in N_2H^+, N_2, and ultimately NH_3

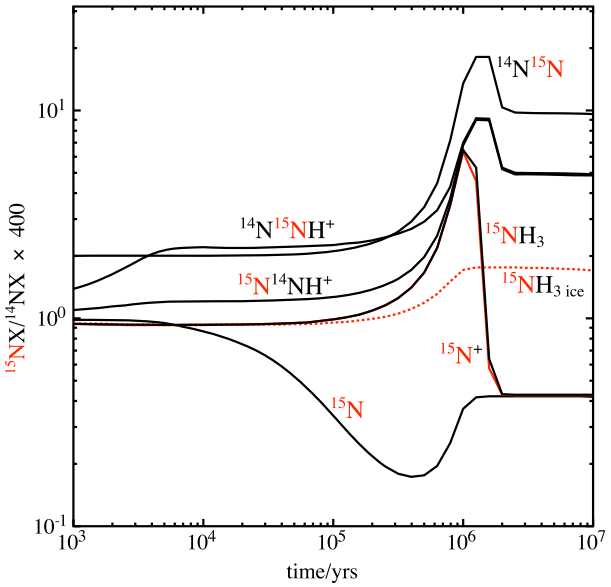

Fig. 5 ^{15}N fractionation as a function of time in a dense cloud depleted in CO. From Charnley and Rodgers (2002).

ratio for the N + NH channel effectively recovers the results of the original model (Rodgers and Charnley 2008).

Interestingly, an anomalously large, and constant, $C^{15}N/C^{14}N$ ratio has been observed in comets from the Oort Cloud (OC) population and the Jupiter Family, with a $^{15}N/^{14}N$ ratio approximately twice the terrestrial value (Arpigny et al. 2003; Hutsemékers et al. 2005; Manfroid et al. 2005). This is larger than the ratio in cometary HCN (e.g., Jewitt et al. 1997; Ziurys et al. 1999), the expected parent of CN. It appears that the isotopically-heavier CN is produced via the degradation of ^{15}N-rich organic refractory material in the coma (see Festou 1999); this material may be connected to that found in IDPs and meteorites. If interstellar ion-molecule chemistry in cold depletion cores is the origin of this ^{15}N fractionation then,

since it preferentially occurs in ammonia ice, a subsequent phase of energetic processing would be required to incorporate it into carbonaceous material (Lis et al. 2008). This would presumably have occurred in the protosolar nebula.

3.4 Oxygen and Carbon Isotopic Fractionation

Carbon and oxygen fractionation by ion-molecule reactions in the ISM were first extensively modelled by Langer et al. (1984). They showed that, compared to D and ^{15}N, relatively small fractionation will occur. Almost all the ^{13}C enrichment occurs in CO at the expense of other organic molecules and Charnley et al. (2004) showed that the subsequent freeze-out and hydrogenation of CO (see Fig. 3) and other species could preserve this $^{13}C/^{12}C$ discrepancy in more complex species formed on the surfaces of dust grains.

Isotopes of oxygen and carbon in cometary molecules can be observed at radio and optical wavelengths. The molecular $^{18}O/^{16}O$ ratios in Halley and Ikeya-Zhang, as well as the $^{13}C/^{12}C$ ratios of C_2, CN, and HCN in several comets, all indicate that the ratios are consistent with terrestrial values (Balsiger et al. 1995; Wyckoff et al. 2000; Lecacheux et al. 2003; Altwegg and Bockelée-Morvan 2003).

3.5 Molecular Spin States

Quantum-mechanically, some molecules can exist in either of two distinct states depending upon the relative alignment (parallel or antiparallel) of the spins of their H nuclei (e.g., H_2, H_2CO, CH_2CO, *c*-C_3H_2, H_2CCC), giving rise to *ortho* and *para* forms. Radiative and collisional transitions between spin states are strictly forbidden and so, when set, the ortho:para spin ratios (OPRs) can in principle persist over very long time-scales.

Interstellar molecules formed in exothermic gas-phase chemistry should generally possess an OPR thermalised at the so-called 'high-temperature limit', where it is set by the ratio of the nuclear spin statistical weights. The nuclear spin ratio of a cometary molecule defines the spin temperature $T_{\rm spin}$. Lower OPRs imply lower $T_{\rm spin}$ values and these can occur, for example, if the molecule was thermalised on cold dust subsequent to formation. Furthermore, interstellar OPR values can be transferred and altered in ion-molecular reactions (e.g., Kahane et al. 1984; Park et al. 2006). Thus, molecular OPRs, and the associated spin temperatures, offer the prospect of extracting important cosmogonic information regarding the formation environment of cometary molecules.

Ortho:para ratios have been measured in water for several comets by ground-based observations of vibrational hot bands (see Bockelée-Morvan et al. 2004; Dello Russo et al. 2005). Kawakita et al. (2002) have measured the OPR in NH_2 and, since strict selection rules constrain the OPR in photodaughters as a function of the OPR in their parents, these observations can be used as a surrogate for the OPR in ammonia. Figure 6 shows the measured and equilibrium ortho:para ratios of molecules detected in comets as a function of the spin temperature. The observed ratios imply formation temperatures for cometary ice molecules of typically 25–35 K, similar to the formation temperature implied by the D/H ratios in water and hydrogen cyanide.

4 Discussion: Interstellar Molecules in Comets?

The cometary characteristics discussed here, when taken individually, present a puzzling picture and appear to indicate that comets contain materials from very different chemical

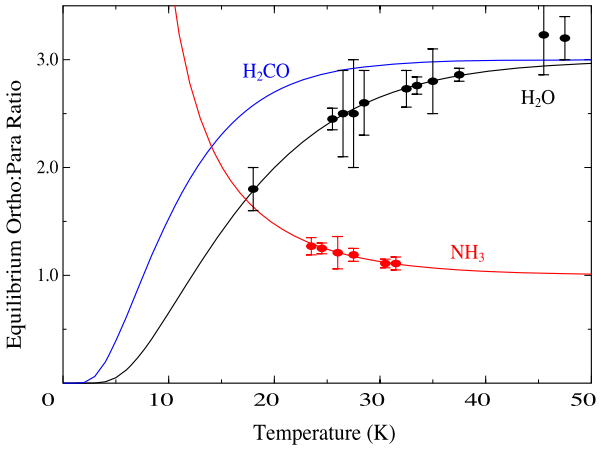

Fig. 6 Equilibrium ortho:para ratios in water, ammonia and formaldehyde as a function of temperature. The observed values are plotted for water and ammonia in ten comets. In two cases, the water OPR is > 3, larger than the equilibrium ratio at any temperature. However, the error bars on these measurements are consistent with an OPR of ≈ 3, implying a spin temperature of $\gtrsim 40$ K. Data compiled from Mumma et al. (1987, 1989), Crovisier et al. (1997), Crovisier and Bockelée-Morvan (1999), Dello Russo et al. (2005), Kawakita et al. (2001, 2002, 2004, 2006, 2007), Bonev et al. (2007)

environments. Crystalline silicate dust is common in comets (Wooden 2002) and this must have experienced temperatures in excess of about 800 K in the inner nebula. The organic inventory shows strong compositional agreement with that expected from interstellar grain-surface chemistry at around 10 K, although there are significant differences in the relative abundances. The differences in the isotopic ratios and spin temperatures are more subtle but also indicative of physically distinct environments. The D/H ratios and spin ratios in cometary water and ammonia both indicate formation in gas with temperatures of $\approx$ 25–35 K. The similarity of the OPRs in both JF and OC comets seems to suggest that both families contain material from a common reservoir. The D/H ratio in formaldehyde indicates formation on 10 K dust grains in an environment where most of the gas has frozen out. A similar cold and depleted environment, but in which N_2 can remain in the gas, is necessary to explain the $^{14}N/^{15}N$ fractionation by gas phase reactions.

4.1 Key Future Measurements

Our discussion of the possible connection between interstellar and cometary matter has been limited to recent measurements. In the specific areas of organic composition and isotopic signatures there are several future observations and laboratory studies that would test this putative connection. A (necessarily incomplete) wish-list would be

1. The detection of ethylene glycol ($HOCH_2CH_2OH$) in a comet (Crovisier et al. 2004b) suggests that searches for other organic molecules known in the ISM should be fruitful. For example, interstellar grain chemistry (see Fig. 3) indicates that glycolaldehyde and ethanol should also be present. It would also be of interest to discover if any large organics believed to be form in gas-phase chemistry reactions (e.g., ethers, amino acids, higher cyanopolyynes) are present in comets, as their absence would greatly constrain the chemical history of pre-cometary material.

2. A molecule of great potential interest is the simple organic ring cyclopropenylidene (c-C_3H_2). c-C_3H_2 is ubiquitous in the interstellar medium (Matthews and Irvine 1985) but, as it is highly reactive, it would be an unlikely remnant of interstellar chemistry. However, c-C_3H_2 may be produced in the coma through the photolytic decomposition of aromatic compounds, as proposed for interstellar photodissociation regions (e.g., Pety et al. 2005). Strong ortho and para line emission (e.g., Takakuwa et al. 2001; Bell et al. 1988) means that both the c-C_3H_2 spin ratio and the C_3HD/c-C_3H_2 ratio could be measured in suitable comets. Cyclopropenylidene could plausibly serve as a surrogate with which to probe the nature of cometary aromatic material and hence be an important tool for investigations of cometary origins.
3. The Stardust organic sample data (Sandford et al. 2006) suggests that aliphatic amines could be a significant organic reservoir in comets. Methylamine emission near 3 mm has been detected in the interstellar medium (Kaifu et al. 1974) but has not been observed in comets. Future cometary searches for CH_3NH_2 will now be possible with higher frequency spectroscopic data (Ilyushin et al. 2005). If the Stardust ratio of CH_3NH_2 : $CH_3CH_2NH_2 \sim 1$ is a general property of comets, then $CH_3CH_2NH_2$ may also be detectable in the coma. Energetic processing of ices containing NH_3, CH_4 and C_2H_6 might produce these molecules, as well as perhaps also some organic polymers. Cometary CH_4/C_2H_6 ratios are in the right range (see Table 1) but this needs to be tested in the laboratory by ice irradiation experiments. The detection of CH_3NH_2 and $CH_3CH_2NH_2$ in both comets and hot cores would allow a test of whether the Stardust sample results are evidence of interstellar chemistry.
4. Determinations of the HDO/H_2O and DCN/HCN ratios in more comets are needed to understand if the four existing measurements are typical of the other $\sim 10^{11}$ objects. Detection of cometary molecules with D/H ratios above 10%, as well as evidence for multideuteration, would significantly favour a direct interstellar/prestellar core origin (e.g., Ceccarelli et al. 2007). It is therefore of considerable importance to know if low D/H fractionation ratios, of a few percent, are common in a larger sample of comets. The widespread presence of formaldehyde in comets means that the $HDCO/H_2CO$ ratio offers a new probe of cometary organic matter. For the $HDCO/H_2CO$ ratio measured by Kuan et al. (2008), both grain-surface and gas-phase chemical schemes predict large D_2CO abundances (Rodgers and Charnley 2002), and we expect that D_2CO may be detectable in bright comets. Future searches for the isotopologues of formaldehyde and methanol in comets are needed, the upper limits of Crovisier et al. (2004a) notwithstanding.
5. A measurement of the formaldehyde OPR in a comet could provide important information on the origin of cometary organic matter. Successful measurements would allow comparison of the H_2CO OPRs with those of water, ammonia and methane ice. Interstellar H_2CO ratios are much lower and indicate H_2CO formation on grains at temperatures of about 10–15 K (Dickens and Irvine 1999). Hence, one could ascertain if some organic molecules in comets had a significantly colder formation environment than other molecules (see Fig. 6). For example, a finding of different OPRs in H_2CO and CH_4 would suggest two different organic reservoirs: interstellar and nebular.
6. The determination of $^{15}N/^{14}N$ ratios in different species in the same comet would allow us to constrain the source of cometary CN and HNC, and to test the theory that ^{15}N fractionation is a relic of low-temperature ISM chemistry. The differing $^{15}N/^{14}N$ ratios in cometary CN and HCN apparently confirms that photodissociation of HCN cannot be the main source of CN in the coma. Observing $HC^{15}N$, $H^{15}NC$, and $C^{15}N$ simultaneously would severely constrain hypothesised parent-daughter relationships between these species, and determining the $^{15}NH_2/^{14}NH_2$ ratio would yield the isotopic ratio in the ammonia ices, which are thought to be the interstellar carriers of ^{15}N enhancements.

7. Direct observation of the chemistry in protoplanetary disks is necessary to allow comparison with that of prestellar cores. The current observational data indicates that protoplanetary disks do show emission from well-known 'interstellar' molecules confined to the relatively warm inner and upper regions (see for example Blake 2006; Bergin et al. 2007; Dutrey et al. 2004, 2007; Piétu et al. 2007; Najita et al. 2007). New, more refined, models of isotopic chemistry in disks are also necessary to understand how various interstellar fractionation patterns could be altered (e.g., Markwick and Charnley 2004; Ceccarelli and Dominik 2005; Ciesla and Charnley 2006; Willacy 2007; Yurimoto et al. 2007).

5 Conclusions

We have briefly reviewed the details of the putative connection between interstellar and cometary matter. The connection seems to be strongest between the volatile organic inventories and the apparent need, as evidenced by the enhanced $^{15}N/^{14}N$ ratios found in many comets, to have a large region of very cold, selectively-depleted, gas. This scenario may also contribute to very high D/H ratios in some cometary organic molecules and is, we suggest, more likely to have occurred in the presolar core. Comets do have marked differences with ISM material; for example, they contain primarily crystalline silicate dust, and the methanol abundances and D/H ratios are both lower (Ehrenfreund et al. 2004).

However, to reliably trace the origin of cometary matter through isotopic fractionation, it will be necessary to measure isotopic ratios in several different molecules. Analysis of macromolecular organic matter from comets and IDPs has led to both nebular (Remusat et al. 2006) and interstellar chemistries being proposed as its origin (Alexander et al. 2007). Future analyses of the very primitive organic component discovered in the Stardust samples (Sandford et al. 2006) may allow this debate to be settled.

Interstellar chemistry in the prestellar core/hot corino phases of evolution is probably most relevant for the ISM-comet connection. How this chemistry evolves spatially while the central protostar evolves to the Class 0/I transition may be critical for understanding any direct interstellar contribution to cometary composition. At the minimum, this chemistry sets the initial conditions for that in the protoplanetary disk and so comparison with disk observations and chemical models is necessary. As most of the interstellar material accreted during the Class 0 phase ($\sim 10^5$ years) is consumed by the forming protostar, a meaningful comparison between interstellar and comet chemistries probably requires detailed studies of the composition of the envelopes and disks of Class I sources, e.g., those of Barnard 5 (Langer et al. 1996) and IRS46 (Lahuis et al. 2006). In the near future, our understanding of the depth of this connection will be revolutionised when the *Atacama Large Millimetre Array (ALMA)* comes online (e.g., van Dishoeck and Jørgensen 2008).

Acknowledgements This work was supported by NASA's Origins of Solar Systems, Planetary Atmospheres and Exobiology Programs and by the NASA Goddard Center for Astrobiology.

References

N.G. Adams, D. Smith, Astrophys. J. **247**, L123 (1981)
M.F. A'Hearn, Science **314**, 1708 (2006)
C.M.O'D. Alexander et al., Geochim. Cosmochim. Acta. **71**, 4380 (2007)
K. Altwegg, D. Bockelée-Morvan, Space Sci. Rev. **106**, 139 (2003)

C. Arpigny, E. Jehin, J. Manfroid, D. Hutsemékers, R. Schulz, J.A. Stüwe, J.-M. Zucconi, I. Ilyin, Science **301**, 1522 (2003)
R. Bachiller, Annu. Rev. Astron. Astrophys. **34**, 111 (1996)
H. Balsiger, K. Altwegg, J. Geiss, J. Geophys. Res. **100**, 5827 (1995)
M.B. Bell et al., Astrophys. J. **326**, 924 (1988)
E.A. Bergin, M. Tafalla, Annu. Rev. Astron. Astrophys. **45**, 339 (2007)
E.A. Bergin, Y. Aikawa, G.A. Blake, E.F. van Dishoeck, in *Protostars and Planets V*, ed. by B. Reipurth et al. (University of Arizona Press, Tucson, 2007), p. 751
N. Biver et al., Astron. Astrophys. **449**, 1255 (2006)
G.A. Blake, in *Astrochemistry: Recent Successes and Current Challenges*, ed. by D.C. Lis et al. (Cambridge University Press, Cambridge, 2006), p. 365
G.A. Blake, E.F. van Dishoek, D.J. Jansen, T.D. Groesbeck, L.G. Mundy, Astrophys. J. **428**, 680 (1994)
D. Bockelée-Morvan et al., Icarus **133**, 147 (1998)
D. Bockelée-Morvan, J. Crovisier, M.J. Mumma, H.A. Weaver, in *Comets II*, ed. by M. Festou, H.U. Keller, H.A. Weaver (University of Arizona Press, Tucson, 2004), p. 391
H. Boehnhardt, H. Fechtig, V. Vanysek, Astron. Astrophys. **231**, 543 (1990)
B. Bonev et al., Astrophys. J. **661**, L97 (2007)
A.C.A. Boogert et al., Astrophys. J. Suppl. Ser. **154**, 359 (2004)
S. Bottinelli et al., Astrophys. J. **617**, L69 (2004a)
S. Bottinelli et al., Astrophys. J. **615**, 354 (2004b)
S. Bottinelli, C. Ceccarelli, J.P. Williams, B. Lefloch, Astron. Astrophys. **463**, 601 (2007)
D. Brownlee, Science **314**, 1711 (2006)
H. Busemann, A.F. Young, C.M.O'D. Alexander, P. Hoppe, S. Mukhopadhyay, L.R. Nittler, Science **312**, 727 (2006)
H.M. Butner, S.B. Charnley, C. Ceccarelli, S.D. Rodgers, J.R. Pardo, B. Parise, J. Cernicharo, G.R. Davis, Astrophys. J. **659**, L137 (2007)
S. Cazaux, A.G.G.M. Tielens, C. Ceccarelli, A. Castets, V. Wakelam, E. Caux, B. Parise, D. Teyssier, Astrophys. J. **593**, L51 (2003)
C. Ceccarelli, in *Astrochemistry: Recent Successes and Current Challenges*, ed. by D.C. Lis et al. (Cambridge University Press, Cambridge, 2006), p. 1
C. Ceccarelli, C. Dominik, Astron. Astrophys. **440**, 583 (2005)
C. Ceccarelli, P. Caselli, E. Herbst, A.G.G.M. Tielens, E. Caux, in *Protostars and Planets V*, ed. by B. Reipurth, D. Jewitt, K. Keil (University of Arizona Press, Tucson, 2007), p. 47
C.J. Chandler, C.L. Brogan, Y.L. Shirley, L. Loinard, Astrophys. J. **632**, 371 (2005)
S.B. Charnley, in *The Bridge Between the Big Bang and Biology*, ed. by F. Giovannelli (Consiglio Nazionale delle Ricerche President Bureau, Rome, 2001), p. 139. Special volume
S.B. Charnley, S.D. Rodgers, Astrophys. J. **569**, L133 (2002)
S.B. Charnley, S.D. Rodgers, in *Astrochemistry Throughout the Universe*: *Recent Successes and Current Challenges*, ed by D.C. Lis, G.A. Blake, E. Herbst. Proceedings of IAU Symposium, vol. 231, CUP (2006), p. 237
S.B. Charnley, A.G.G.M. Tielens, T.J. Millar, Astrophys. J. **399**, L71 (1992)
S.B. Charnley, M.E. Kress, A.G.G.M. Tielens, T.J. Millar, Astrophys. J. **448**, 432 (1995)
S.B. Charnley, A.G.G.M. Tielens, S.D. Rodgers, Astrophys. J. **482**, L203 (1997)
S.B. Charnley, P. Ehrenfreund, Y.-J. Kuan, Spectrochim. Acta **57**, 685 (2001)
S.B. Charnley, Y.-J. Kuan, M.-L. Peng, H.-C. Huang, S.D. Rodgers, in *Proceedings of Asteroids, Comets, Meteors—ACM* 2002, ESA SP-500 (2002), p. 763
S.B. Charnley, P. Ehrenfreund, T.J. Millar, A.C.A. Boogert, A.J. Markwick, H.M. Butner, R. Ruiterkamp, S.D. Rodgers, Mon. Not. R. Astron. Soc. **347**, 157 (2004)
F.J. Ciesla, S.B. Charnley, in *Meteorites and the Early Solar System II*, ed. by D.S. Lauretta, H.Y. McSween Jr. (University Arizona Press, Tucson, 2006), p. 209
J. Crovisier et al., Science **275**, 1904 (1997)
J. Crovisier, D. Bockelée-Morvan, Space Sci. Rev. **90**, 19 (1999)
J. Crovisier et al., Astron. Astrophys. **418**, 1141 (2004a)
J. Crovisier, D. Bockelée-Morvan, N. Biver, P. Colom, D. Despois, D.C. Lis, Astron. Astrophys. **418**, L35 (2004b)
N. Dello Russo et al., Astrophys. J. **621**, 537 (2005)
J. Dickens, W.M. Irvine, Astrophys. J. **518**, 733 (1999)
A. Dutrey et al., in *COMETS II*, ed. by M. Festou, H.U. Keller, H.A. Weavers (University of Arizona Press, Tucson, 2004), p. 81
A. Dutrey et al., in *Protostars and Planets V*, ed. by B. Reipurth et al. (University Arizona Press, Tucson, 2007), p. 495

P. Eberhardt, M. Reber, D. Krankowsky, R.R. Hodges, Astron. Astrophys. **302**, 301 (1995)
P. Ehrenfreund, S.B. Charnley, Annu. Rev. Astron. Astrophys. **38**, 427 (2000)
P. Ehrenfreund, L. d'Hendecourt, S.B. Charnley, R. Ruiterkamp, J. Geophys. Res. **106**, 33291 (2001)
P. Ehrenfreund, S.B. Charnley, D. Wooden, in *COMETS II*, ed. by M. Festou, H.U. Keller, H.A. Weaver (University Arizona Press, Tucson, 2004), p. 115
M. Festou, Space Sci. Rev. **90**, 53 (1999)
N. Fray et al., Icarus **184**, 239 (2006)
G.W. Fuchs, U. Fuchs, T.F. Giesen, F. Wyrowski, Astron. Astrophys. **444**, 521 (2005)
W.D. Geppert et al., Astrophys. J. **609**, 459 (2004)
E.L. Gibb, M.J. Mumma, M.A. Disanti, N. Dello Russo, K. Magee-Sauer, in *Asteroids, Comets, and Meteors 2002*, ed. by B. Warmbein (ESA, Noordwijk, 2002), p. 705
J.M. Greenberg, in *COMETS*, ed. by L.L. Wilkening (University Arizona Press, Tucson, 1982), p. 131
R. Hueso, T. Guillot, Astron. Astrophys. **442**, 703 (2005)
D. Hutsemékers et al., Astron. Astrophys. **440**, L21 (2005)
M. Ikeda, T. Hirota, S. Yamamoto, Astrophys. J. **575**, 250 (2002)
V.V. Ilyushin, E.A. Alekseev, S.F. Dyubko, R.A. Motiyenko, J.T. Hougen, J. Mol. Spectrosc. **229**, 170 (2005)
T. Jacq et al., Astron. Astrophys. **271**, 276 (1990)
D.C. Jewitt, H.E. Matthews, T. Owen, R. Meier, Science **278**, 90 (1997)
J.K. Jørgensen, T.L. Bourke, P.C. Myers, F.L. Schöier, E.F. van Dishoeck, D.J. Wilner, Astrophys. J. **632**, 973 (2005)
C. Kahane, M.A. Frerking, W.D. Langer, P. Encrenaz, R. Lucas, Astron. Astrophys. **137**, 211 (1984)
N. Kaifu, M. Morimoto, K. Nagane, K. Akabane, T. Iguchi, K. Takagi, Astrophys. J. **191**, L135 (1974)
R. Kandori et al., Astron. J. **130**, 2166 (2005)
H. Kawakita et al., Science **294**, 1089 (2001)
H. Kawakita, J. Watanabe, T. Fuse, R. Furusho, S. Abe, Electron. Manuf. Procure. **90**, 371 (2002)
H. Kawakita, J.-i Watanabe, R. Furusho, T. Fuse, M.T. Capria, M.C. De Sanctis, G. Cremonese, Astrophys. J. **601**, 1152 (2004)
H. Kawakita et al., Astrophys. J. **623**, L49 (2005)
H. Kawakita et al., Astrophys. J. **643**, 1337 (2006)
H. Kawakita, E. Jehin, J. Manfroid, D. Hutsemékers, Icarus **187**, 272 (2007)
J. Kissel et al., Nature **321**, 336 (1986)
J. Kissel, F.R. Krueger, K. Roessler, in *Comets and the Origins and Evolution of Life*, ed. by P.J. Thomas et al. (Springer, Berlin, 1997), p. 69
Y.-J. Kuan et al., Astrophys. J. **616**, L27 (2004)
Y.-J. Kuan et al. (2008 in preparation)
C.J. Lada, F.H. Shu, Science **248**, 564 (1990)
F. Lahuis et al., Astrophys. J. **636**, L145 (2006)
W.D. Langer et al., Astrophys. J. **277**, 581 (1984)
W.D. Langer et al., Astrophys. J. **468**, L41 (1996)
A. Lecacheux et al., Astron. Astrophys. **402**, L55 (2003)
D. Lis, D. Bockelée-Morvan, J. Boissier, J. Crovisier, N. Biver, S. Charnley, Astrophys. J. (2008 in press)
J. Manfroid, E. Jehin, D. Hutsemékers, A. Cochran, J.-M. Zucconi, C. Arpigny, R. Schulz, J.A. Stüwe, Astron. Astrophys. **432**, L5 (2005)
A.J. Markwick, S.B. Charnley, in *Astrobiology: Future Perspectives*, ed. by P. Ehrenfreund et al. (Kluwer, Dordrecht, 2004), p. 33
H.E. Matthews, W.M. Irvine, Astrophys. J. **298**, L61 (1985)
R. Meier et al., Science **279**, 842 (1998a)
R. Meier et al., Science **279**, 1707 (1998b)
S. Messenger, F.J. Stadermann, C. Floss, L.R. Nittler, S. Mukhopadhyay, Space Sci. Rev. **106**, 155 (2003)
T.J. Millar, A. Bennett, E. Herbst, Astrophys. J. **340**, 906 (1989)
C.D. Molek, J.L. McLain, V. Poteyra, N.G. Adams, J. Phys. Chem. A **111**, 6760 (2007)
M.J. Mumma, H.A. Weaver, H.P. Larson, Astron. Astrophys. **187**, 419 (1987)
M.J. Mumma, W.E. Blass, H.A. Weaver, H.P. Larson, in *Formation and Evolution of Planetary Systems*, ed. by H.A. Weaver, L. Danly (Cambridge University Press, Cambridge, 1989), p. 157
M.J. Mumma, M.A. DiSanti, N. Dello Russo, K. Magee-Sauer, E. Gibb, R. Novak, Adv. Space Res. **31**, 2563 (2003)
L.G. Mundy, H.A. Wootten, B.A. Wilking, Astrophys. J. **352**, 159 (1990)
J.R. Najita, J.S. Carr, A.E. Glassgold, J.A. Valenti, in *Protostars and Planets V*, ed. by B. Reipurth et al. (University Arizona Press, Tucson, 2007), p. 507
B. Parise et al., Astron. Astrophys. **393**, L49 (2002)

B. Parise, A. Castets, E. Herbst, E. Caux, C. Ceccarelli, I. Mukhopadhyay, A.G.G.M. Tielens, Astron. Astrophys. **416**, 159 (2004)
B. Parise et al., Astron. Astrophys. **431**, 547 (2005)
I.H. Park, V. Wakelam, E. Herbst, Astron. Astrophys. **449**, 631 (2006)
J. Pety et al., Astron. Astrophys. **435**, 885 (2005)
V. Piétu, A. Dutrey, S. Guilloteau, Astron. Astrophys. **467**, 163 (2007)
L. Remusat, F. Palhol, F. Robert, S. Derenne, C. France-Lanord, Earth Planet. Sci. Lett. **243**, 15 (2006)
H. Roberts, in *Astrochemistry: Recent Successes and Current Challenges*, ed. by D.C. Lis et al. (Cambridge University Press, Cambridge, 2006), p. 27
H. Roberts, G.A. Fuller, T.J. Millar, J. Hatchell, J.V. Buckle, Astron. Astrophys. **381**, 1026 (2002)
H. Roberts, T.J. Millar, E. Herbst, Astrophys. J. **591**, L41 (2003)
S.D. Rodgers, S.B. Charnley, Planet. Space Sci. **50**, 1125 (2002)
S.D. Rodgers, S.B. Charnley, Mon. Not. R. Astron. Soc. **352**, 600 (2004)
S.D. Rodgers, S.B. Charnley, Mon. Not. R. Astron. Soc. (2008 in press)
S.D. Rodgers, S.B. Charnley, W.F. Huebner, D.C. Boice, in *COMETS II*, ed. by M. Festou, H.U. Keller, H.A. Weaver (University of Arizona Press, Tucson, 2004), p. 505
E. Roueff, M. Gerin, Space Sci. Rev. **106**, 61 (2003)
N. Sakai, T. Sakai, S. Yamamoto, Publ. Astron. Soc. Jpn. **58**, L15 (2006)
S. Sandford et al., Science **314**, 1720 (2006)
R. Stark et al., Astrophys. J. **608**, 341 (2004)
S. Takakuwa et al., Publ. Astron. Soc. Jpn. **53**, 251 (2001)
R. Terzieva, E. Herbst, Mon. Not. R. Astron. Soc. **317**, 563 (2000)
A.G.G.M. Tielens, Astron. Astrophys. **119**, 177 (1983)
E.F. van Dishoeck, J.K. Jørgensen, Astrophys. Space Sci. **313**, 15 (2008)
K. Willacy, Astrophys. J. **660**, 441 (2007)
T.L. Wilson, R. Rood, Annu. Rev. Astron. Astrophys. **32**, 191 (1994)
D.H. Wooden, Electron. Manuf. Procure. **89**, 247 (2002)
D.H. Wooden, S.B. Charnley, P. Ehrenfreund, in *Comets II*, ed. by M. Festou, H.U. Keller (University of Arizona Press, Tucson, 2004), p. 33
S. Wyckoff, M. Kleine, B.A. Peterson, P.A. Wehinger, L.M. Ziurys, Astrophys. J. **535**, 991 (2000)
H. Yurimoto, K. Kuramoto, A.N. Krot, E.R.D. Scott, J.N. Cuzzi, M.H. Thiemens, J.R. Lyons, in *Protostars and Planets V*, ed. by B. Reipurth et al. (University of Arizona Press, Tucson, 2007), p. 849
L. Ziurys et al., Astrophys. J. **527**, L67 (1999)

Cometary Refractory Grains: Interstellar and Nebular Sources

D.H. Wooden

Originally published in the journal Space Science Reviews, Volume 138, Nos 1–4.
DOI: 10.1007/s11214-008-9424-2

Abstract Comets are heterogeneous mixtures of interstellar and nebular materials. The degree of mixing of interstellar sources and nebular sources at different nuclear size scales holds the promise of revealing how cometary particles, cometesimals, and cometary nuclei accreted. We can ascribe cometary materials to interstellar and nebular sources and see how comets probe planet-forming process in our protoplanetary disk.

Comets and cometary IDPs contain carbonaceous matter that appears to be either similar to poorly-graphitized (amorphous) carbon, a likely ISM source, or highly labile complex organics, with possible ISM or outer disk heritage. The oxygen fugacity of the solar nebula depends on the dynamical interplay between the inward migration of carbon-rich grains and of icy (water-rich) grains. Inside the water dissociation line, OH^- reacts with carbon to form CO or CO_2, consuming available oxygen and contributing to the canonical low oxygen fugacity. Alternatively, the influx of water vapor and/or oxygen rich dust grains from outer (cooler) disk regions can raise the oxygen fugacity. Low oxygen fugacity of the canonical solar nebula favors the condensation of Mg-rich crystalline silicates and Fe-metal, or the annealing of Fe-Mg amorphous silicates into Mg-rich crystals and Fe-metal via Fe-reduction. High oxygen fugacity nebular conditions favors the condensation of Fe-bearing to Fe-rich crystalline silicates.

In the ISM, Fe-Mg amorphous silicates are prevalent, in stark contrast to Mg-rich crystalline silicates that are rare. Hence, cometary Mg-rich crystalline silicates formed in the hot, inner regions of the canonical solar nebula and they are the touchstone for models of the outward radial transport of nebular grains to the comet-forming zone. *Stardust* samples are dominated by Mg-rich crystalline silicates but also contain abundant Fe-bearing and Fe-rich crystalline silicates that are too large ($\gg$0.1 μm) to be annealed Fe-Mg amorphous silicates.

By comparison with asteroids, the *Stardust* Fe-bearing and Fe-rich crystalline silicates suggests partial aqueous alteration in comet nuclei. However, aqueous alteration transforms

D.H. Wooden (✉)
NASA Ames Research Center, MS 245-3, Moffett Field, CA 94035-1000, USA
e-mail: diane.h.wooden@nasa.gov

D.H. Wooden
e-mail: dwooden@mac.com

H. Balsiger et al. (eds.), *Origin and Early Evolution of Comet Nuclei*
DOI: 10.1007/978-0-387-85455-7_6

Fe-rich olivine to phyllosilicates before Mg-rich olivine, and *Stardust* has Mg-rich and Fe-rich olivine and no phyllosilicates. Hence, we look to a nebular source for the moderately Fe-rich to nearly pure-Fe crystalline silicates. Primitive matrices have Mg-Fe silicates but no phyllosilicates, supporting the idea that Mg-Fe silicates but not phyllosilicates are products of water-rich shocks. Chondrule-formation is a late stage process in our protoplanetary disk. *Stardust* samples show comet 81P/Wild 2 formed at least as late to incorporate a few chondrules, requiring radial transport of chondrules out to perhaps >20 AU. By similar radial transport mechanisms, collisional fragments of aqueously altered asteroids, in particular achondrites that formed earlier than chondrules, might reach the comet-forming zones. However, *Stardust* samples do not have phyllosilicates and chondrules are rare. Hence, the nebular refractory grains in comet 81P/Wild 2, as well as other comets, appear to be pre-accretionary with respect to asteroid parent bodies. By discussing nebular pathways for the formation of Fe-rich crystalline silicates, and also phyllosilicates and carbonates, we put forth the view that comets contain both the interstellar ingredients for and the products of nebular transmutation.

Keywords Comets: general · Asteroids · Solar system: formation · Accretion disks · ISM: dust · Cosmic rays

1 Introduction

1.1 Synopsis

Comet dust grain properties provide insights into physical conditions and processes in our protoplanetary disk, not only in the regions where nuclei accreted but also in the warmer regions of the disk inside the water snow line. The insights arise when we undertake four ventures: (1) distinguish between 'interstellar' and 'nebular' sources for cometary refractory grains; (2) identify the presence of cometary-like refractory grains in chondritic (asteroidal) materials; (3) understand in detail how 'nebular' sources form by primary processes in the disk; and, (4) understand how 'nebular' sources are modified by secondary processes in the protoplanetary disk (e.g., in shocks with or without water vapor) or by secondary processes in parent bodies (e.g., aqueous alteration in comets or asteroids). At journeys' end, the insights are far-reaching: we assert that the 'nebular' component of cometary grains may be ascribed to pre-accretionary material, i.e., material that existed prior to the accretion of chondrites (asteroids with chondrules). For example, *Stardust* samples of comet 81P/Wild 2 contain a few chondrules but lack phyllosilicates, which suggests that this comet accreted after chondrule-formation was initiated but this comet nucleus was not aqueously altered nor did it accrete aqueously altered asteroidal grains released into the disk by asteroid collisions. Comet 81P/Wild 2 appears to contain abundant nebular grains that formed in the inner solar nebula, suggesting radial transport was very efficient. On the other hand, other comets appear to contain refractory 'interstellar' and 'nebular' grains in more equal proportions (Sects. 2.3.2, 2.3.3, e.g., 9P/Tempel 1, Hale-Bopp, C/2001 Q4(NEAT)). We examine together the dominant refractory grain species in comets, existing models for condensation in the nebula under varying oxidation conditions, and radial transport models for solar-analog protoplanetary disks. By this investigation and comparison, we see that cometary refractory grains considered to be from 'interstellar' sources contribute to driving key processes that produce a variety of 'nebular' refractory grains that are seen in comets in varying amounts. Inward and outward radial transport in the disk, with varying degrees of efficiency, is important to explaining the composition of cometary refractory grains.

1.2 Cometary Refractory Grains and Disk Processes

Comet nuclei are amongst the least altered bodies in our solar system. Comets form amongst the giant planets and are reservoirs of materials that existed in the icy cold regions of our protoplanetary disk. By ascribing the origins of cometary materials to interstellar sources (stellar atmospheres, supernovae, or interstellar clouds) or to the protoplanetary disk, we ascertain that comets are heterogeneous mixtures of interstellar materials with materials that form or are transformed in the protoplanetary disk.

In the processing of making new materials in the protoplanetary disk, some interstellar materials are destroyed or *transformed*. When relatively abundant interstellar amorphous carbon is delivered into the hotter inner regions of the solar nebula where water is dissociated to OH^-, carbon is combusted (oxidized) into CO or CO_2. Carbon combustion consumes available oxygen and can contribute to the low oxygen fugacity[1] ($H_2O/H_2 \sim 5\times10^{-4}$) of the canonical solar nebula (Sect. 1.4.1). On the other hand, the inward transport of ice or silicate dust grains interior to the silicate evaporation front, be they either ISM grains or grains condensed at larger disk radii, can contribute oxygen to the gas phase, raising the oxygen fugacity (Wood and Hashimoto 1993). The reduction-oxidation conditions in the solar nebula depends on many factors (Wood and Hashimoto 1993). Several studies focus on how oxygen fugacity fluctuates depending on concentrations of dust and ice (Cuzzi and Zahnle 2004; Fedkin et al. 2008) and carbon (Connolly et al. 1994), and muse over the interplay between these oxidizing and reducing constituents (Cuzzi et al. 2005a, 2005b).

At $\gtrsim$1450 K, low oxygen fugacity gases favor the *condensation* of Mg-rich crystalline silicates and Fe-metal grains. At $\gtrsim$1000 K, low oxygen fugacity gases also favor the *annealing* (devitrification) *and Fe-reduction* of Fe-Mg amorphous silicates into Mg-rich silicate crystals with surface Fe-metal (Davoisne et al. 2006; Connolly et al. 1994; Sect. 2.3.4). Thus, the consumption of amorphous carbon, an interstellar source (Sect. 2.5.1), contributes to nebular gas-phase environments conducive to the formation of Mg-rich crystalline silicates by condensation or annealing. Hence, cometary Mg-rich crystalline silicates provide direct evidence for the outwards radial migration of high temperature refractory nebular grains to the regime of icy planetesimal formation (Bockelée-Morvan et al. 2002; Wehrstedt and Gail 2008). Moreover, cometary Mg-rich crystalline silicates are a profound example of the interplay between interstellar sources and nebular processes. Comets contain both the ingredients for and the by-products of nebular processing.

1.3 Recent discoveries: *Stardust* and *Deep Impact*

Recent discoveries in comets of extremely high temperature minerals and grain species akin to aqueously-altered minerals deepens our appreciation of comets as treasuries of nebular products. Calcium-aluminum minerals are found in *Stardust Mission* return samples from comet 81P/Wild 2 (Brownlee et al. 2006).

Before their discovery in *Stardust* samples (Sect. 2.2; Brownlee et al. 2006; Schmitz et al. 2008; Chi et al. 2008), calcium-aluminum inclusions (CAIs) were only found in chondrites (e.g., Kita et al. 2005).[2] The mineralogies of *Stardust* CAIs are consistent with their being CAI primary condensates (M. Zolensky, private communication).

[1] Fugacity is the vapor pressure of a vapor assumed to be an ideal gas.

[2] Chondrules are $\sim$1 mm-sized once-molten droplets that were combined with matrix material to make chondrites or asteroid parent bodies (Hewins 1997).

Exceptionally rare CAIs (the so-called relict CAIs) are found inside chondrules (Krot et al. 2006). These relict CAIs and the short-lived and long-lived isotope chronologies (Kita et al. 2005; Krot et al. 2005) argue that CAI formation predates chondrule formation. CAIs are the highest temperature (>1400–2000 K), earliest condensates of the solar nebula, forming as a result of evaporation and condensation processes; some CAIs (so-called igneous CAIs) were subsequently melted. By association, cometary CAI-type minerals in *Stardust* samples (Sect. 2.2) are nebular condensates (Brownlee et al. 2006).

Stardust samples from comet 81P/Wild 2 also contain chondrule fragments, of which 4 olivine/pyroxene grains have measured oxygen isotope abundances (Nakamura et al. 2008). The range of oxygen isotope ratios, and major and minor element concentrations of silicates mineralogy is similar to type I (magnesian) and type II (ferrous) chondrules in carbonaceous chondrites (Nakamura et al. 2008). In one *Stardust* chondrule, named "Gozen-sama", two sub-round olivine cores set in low-Ca pyroxene have disparate oxygen isotopic concentrations: one is ^{16}O-poor like typical chondrules, and one is enriched in ^{16}O relative to ^{17}O and ^{18}O, similar to what is considered the most primitive solar system materials, like CAIs (e.g., Krot et al. 2005).[3]

Early reports of *Stardust* sample analyses reported magnesian silicates and rebuked the presence of any minerals that could be associated with aqueous alteration, namely, Fe-rich crystalline silicates, carbonates, and phyllosilicates (Brownlee et al. 2006). Time and effort has revealed one indigenous Mg, Fe-carbonate (Mikouchi et al. 2007) in *Stardust* samples, a few nearly pure-Fe crystalline silicates (fayalite), and numerous moderately Fe-rich crystalline silicates (Zolensky et al. 2007, 2008). The one small (∼0.2 μm-size) indigenous cometary Mg-Fe (Ca-free) carbonate grain is associated with amorphous silica and Fe sulfide (Mikouchi et al. 2007). There are abundant teeny-tiny (∼0.02 μm-sized) Ca-carbonate grains whose origins in 81P/Wild 2 (Flynn et al. 2008; Sect. 2.8) or as aerogel contaminants is still debatable (M. Zolensky, private communication). Although, these tiny Ca-carbonates (calcite) are of a similar size to Mg-carbonates Halley's coma (Fomenkova et al. 1992a; Sect. 2.8), supporting the possibility that they might be nebular condensates from lower pressure regimes closer to the disk photosphere (Sect. 2.8). Carbonates derived from aqueous alteration typically are larger with coarser grain textures (M. Zolensky, private communication).

The full suite of (crystalline) silicate minerals discovered in *Stardust* to date include: olivine, ortho- and clino-pyroxene, feldspar, gehlenite, and tridymite (Zolensky et al. 2008); nepheline (M. Zolensky and D. Brownlee, private communication); and probably richterite, roedderite, and eifelite (Joswiak et al. 2007). There are large enough numbers of olivine and pyroxene grains to be compared with meteoritic samples and anhydrous and hydrous interplanetary dust particles (IDPs) (Zolensky et al. 2007, 2008). *Stardust* contains abundant extremely Mg-rich crystalline silicates, forsterite ($(Mg_x,Fe_{1-x})_2SiO_4$, $1 \geq x \geq 0.9$) and enstatite ($(Mg_y,Fe_{1-y})SiO_3$, $1 \geq y \geq 0.9$) and significant numbers of silicate crystals, namely olivine $(Mg_x,Fe_{1-x})_2SiO_4$ and pyroxene $(Mg_y,Fe_{1-y})SiO_3$, that span the range from Mg-rich ($x \lesssim 0.95$, $y \lesssim 0.98$) to moderately Fe-rich (x, $y \simeq 0.5$) (Zolensky et al. 2007, 2008). Moderately Fe-rich and Fe-rich crystalline silicates have been discussed as evidence for aqueous alteration on comet 81P/Wild 2 (Zolensky et al. 2007, 2008). In this context, there are un-aqueously altered nebular grains with a range of Fe-contents: type II chondrules consist of ferrous olivine and pyroxene and are not aqueously altered. In the

[3]It probably represents a fragment of a ^{16}O-rich amoeboid olivine aggregate (AOA). AOAs are refractory objects genetically related to CAIs, i.e., they formed in the same nebular region under similar physio-chemical conditions (S. Krot, private communication).

following paragraphs, we will begin to make reference to the nebular formation scenarios for Fe-bearing crystalline silicates because it makes more sense to this author that nebular refractory grains, which formed in regions of highly different water vapor content, migrated and aggregated into particles and then accreted into comet nuclei, rather than aqueous alteration occurred selectively on submicron scales to aggregate grains within the comet nucleus.

Fe-bearing crystalline silicates and carbonates in comet 81P/Wild 2, as well as phyllosilicates in *Deep Impact*-coma of comet 9P/Tempel 1, are often ascribed as products of aqueous alteration on asteroids (Krot et al. 1995, 2000). However, there are many asteroidal aqueous alteration products (Sect. 1.4.3) that are not present in substantial quantities or do not exist in *Stardust* samples and in other cometary materials. Moreover, anhydrous minerals and minerals regarded as possible products of hydrous processing are found in the same *Stardust* track and presumably existed as subgrains of a larger aggregate particle (Flynn 2008). Hence, only pieces of aggregate grains appear 'aqueously altered'. This could mean that comet grains are disequilibrated aggregates of interstellar grains, nebular grains, and/or selective bits of asteroidal bodies, or that aqueous alteration in cometesimals is selective on submicron scales (further discussed below).

To date, no phyllosilicates are detected in *Stardust* samples (Zolensky et al. 2008; M. Zolensky and D. Brownlee, private communication). In aqueous alteration experiments, Fe-rich olivines are the first to transformed to phyllosilicates, then Mg-rich olivines, and lastly, Ca-pyroxenes and diopside are transformed (Wogelius and Walther 1992; Zolensky et al. 2008). Hydrous interplanetary dust particles (IDPs) have a more limited range of Fe-contents for olivine and pyroxene ($\mathrm{Mg}/[\mathrm{Mg}+\mathrm{Fe}] \lesssim 0.25$) than anhydrous IDPs because the high Fe-content olivine and pyroxene grains have been transformed by aqueous alteration to phyllosilicates (Zolensky et al. 2008; M. Zolensky, private communication). The fact that *Stardust* samples contain crystalline silicates with a broader range of Fe-contents than hydrous IDPs, spanning Fe-contents from ~0% to 50%, with a few near 100% (pure-Fe), *yet Stardust contains no phyllosilicates* implies that comet 81P/Wild 2 was not aqueously altered.

Moreover, comet 81P/Wild 2 does not contain fragments of aqueously altered asteroids because there are no phyllosilicates. Since 81P/Wild 2 was not aqueously altered and does not contain aqueously altered asteroidal grains, we discuss the range of oxygen fugacities necessary to yield Fe-bearing crystalline silicates by nebular processes.

The anhydrous nature of *Stardust* minerals agrees with the results from thermal emission models for the infrared spectra of comet comae (Hanner et al. 1994; Wooden et al. 2000, 2005, 2007; Wooden 2002; a comparison of models for Hale-Bopp is given in Sect. 2.3.3). Specifically, no more than 1% by mass montmorillonite could be fitted into the *ISO* spectrum of comet Hale-Bopp (Wooden et al. 1999). In contrast, linear mixing models fitting the same *ISO* spectrum of Hale-Bopp and the *Spitzer* spectra of the *Deep Impact*-induced coma of comet 9P/Tempel 1 identify pure-Fe crystalline silicates (in *Deep Impact* but not in Hale-Bopp), carbonates, and the phyllosilicate smectite nontronite (Lisse et al. 2006, 2007) at the level of ~10% of the surface area-weighted mass fraction.

Aqueous alteration of comets, because of their low thermal conductivity was thought to require large nuclei ($R_{\mathrm{nuc}} \geq 200$ km, Prialnik and Podolak 1999), but more recent models show liquid water may occur in moderately-sized nuclei ($R_{\mathrm{nuc}} \geq 20$ km, Merk and Prialnik 2006; Prialnik et al. 2008; see review by McKinnon et al. 2008). The present-day mean size of comet nuclei is only 1–2 km (Lamy et al. 2005). From imaging studies by the *Deep Impact* primary craft, comet 9P/Tempel 1 is thought to have retained its primordial surface topography, revealing its formation by the layering of smaller cometesimals (Belton et al.

2007). So comet 9P/Tempel 1 appears to not be a collisional fragment of a large differentiated Kuiper Belt Object (KBO). However, each comet that has been visited by spacecraft looks different, so we may or may not be confident in extending this hypothesis to other comets. Dynamical models for ecliptic comets say statistically they cannot be collisional fragments of KBOs because collisional grinding would be so efficient that to get the population of ecliptic comet nuclei inferred to be present in the scattered disk today would require so many KBOs that the surface density of the disk would have had to be much greater expected mass surface density of the solar nebula (Charnoz and Morbidelli 2007). Note that Desch (2008) argues that the minimum mass solar nebula is 3–4 times greater than the currently accepted value. With that said, recent models for the asteroid belt imply rapid accretion to 100 km-size bodies that were then collisionally eroded. If these ideas extend to the comet-forming regime, most comets might be collisional fragments. Collisional erosion of achondrites, i.e., asteroids that formed prior to chondrules, which suffered prevalent aqueous alteration, could release aqueously altered asteroidal particles into the disk (S. Krot, private communication). If the accretion of comet nuclei persisted long enough to accrete a few chondrules, as evidenced by *Stardust* samples of comet 81P/Wild 2, then it is not inconceivable that comets might have accreted aqueously altered asteroidal grains. The time scales for asteroidal collisional grinding, outward radial transport, and comet nuclei accretion play into whether asteroids are a feasible source for the (as yet skeptical) presence of cometary phyllosilicates.

We discuss a scenario for the formation of Fe-bearing crystalline silicates, and mention phyllosilicate formation, under different than canonical nebular conditions, namely, increases in oxygen fugacity. We revisit models for the formation of Fe-rich crystalline silicates and phyllosilicates under high oxygen fugacity conditions, i.e., high water vapor, in the solar nebula (Sects. 2.3.6, 2.6). We refer to constraints on the f_{CO_2} fugacity in the solar nebula and point to possible conditions in which carbonates could have formed at lower than mid-plane pressures and at moderate temperatures (Sect. 2.8). We postulate that Mg-rich and Fe-rich crystalline silicates, phyllosilicates, and carbonates are products of the solar nebula under variable reduction-oxidation (redox) conditions.

1.4 The Evolving Protoplanetary Disk

The protoplanetary disk evolves in time (Cassen 1997; Chick and Cassen 1997): the disk went from hot to cold radially, vertically, and temporally (Bell et al. 1997, 2000). Ice and dust grains and gas underwent substantial radial excursions (Fig. 1; Keller and Gail 2004; Kley and Lin 1992). Accumulation of solids started early (‘0’–0.3 Myr) for the calcium-aluminum [mineral] inclusions (CAIs) and persists for a long time (∼1.5–3 Myr for chondrule formation) (Kita et al. 2005). Weather occurs, including changes in water vapor content, dust-to-gas ratio, oxidation state, and pressure and temperature (Cassen 1997; Cuzzi and Zahnle 2004; Cuzzi et al. 2005a, 2005b; Scott and Krot 2005a; Krot et al. 2000; Wood and Hashimoto 1993). Physical conditions in the protoplanetary disk happen (a) over long times and near steady-state and near chemical and thermodynamic equilibrium, which most clearly delineates the canonical ‘solar nebula’; (b) within a vapor cloud of fluctuating weather (pressure, temperature, water vapor content) within the nebula, perhaps due to collisions or the transport of icy cometesimals inwards of the snow line (Fig. 2); (c) within a short-lived transient event such as a shock; or (d) within a region of distinctly different conditions such as a wind, or the surface of the disk exposed to the Sun, high energy particles or x-rays.

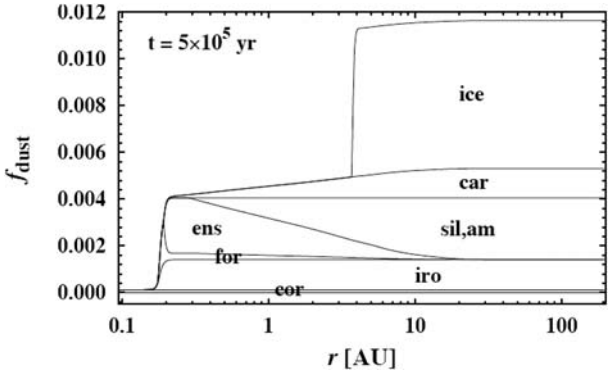

Fig. 1 Radial distribution of principal grain species for a time-dependent model of an accreting protoplanetary disk. Cumulative plot of the dust-to-gas mass ratios (f_{dust}) versus heliocentric distance after 5×10^5 yr of disk evolution for a 2-dimensional radial transport model with a meridional flow. Interstellar amorphous silicates (*sil*, *am*) and amorphous carbon (*car*) from the outer disk accrete into the inner disk. In the inner disk, condensation or annealing forms Mg-rich crystalline silicates (*for*sterite, *en*statite) and Fe-grains (*iron*). *Cor*undum represents a high temperature condensate (cf., Ebel and Grossman 2000), but actually is rare in CAIs and only mentioned in one *Stardust* track (Zolensky et al. 2006a). (Fig. 7 from Wehrstedt and Gail 2008)

1.4.1 The Canonical Reducing (Low f_{O_2}) Solar Nebula

A long hiatus ($\gtrsim$1.2 Myr) occurs between the formation of CAI-type materials (0–0.3 Myr) and the major chondrule- and matrix-formation events (1.5–3 Myr). Models for protoplanetary disks with mass accretion rates spanning 10^{-6}–$10^{-7} M_\odot$ yr^{-1} show the inner region of the early solar nebula is a reducing and not an oxidizing environment. Figure 1 shows the radial distribution of grain species for an accretion disk with inward and outward radial transport via meridional flows at 0.5 Myr (Wehrstedt and Gail 2008). Radial transport moves crystalline silicates outward, and amorphous carbon inwards. Amorphous carbon (and amorphous silicates) are destroyed by carbon combustion in the inner most regions where Mg-rich crystalline silicates are forming (Wehrstedt and Gail 2008).

The duration of mass accretion rates high enough ($10^{-7} M_\odot$ yr^{-1}) to allow silicate condensation in the disk mid-plane out to 1 AU persists for only $1–2\times10^5$ yr (Bell et al. 1997, 2000; Wooden et al. 2007). Chondrule-forming events at larger distances ($\gtrsim$2.5 AU) from the young Sun require transient heating: shocks are the favored mechanism for forming chondrules (Ciesla et al. 2003). Likewise, shocks provides high enough temperatures to condense Mg-rich crystalline silicates along with disequilibrium fine-grained Mg-Fe glasses in primitive chondrite matrixes (e.g., Acfer 094) (Scott and Krot 2005a; Wooden et al. 2005). Note that these fine-grained glasses in primitive chondrite matrixes do not look like the radiation-damaged coarse-grained Mg-Fe amorphous silicates (GEMS, Sect. 2.3.1) in cometary chondritic porous (CP) IDPs (M. Zolensky, private communication). Weaker shocks can anneal amorphous silicates (Harker and Desch 2002), and potentially provide conditions for Fe-reduction of small (0.1–1 μm-sized) Mg-Fe amorphous silicates to more Mg-rich crystals (Wooden et al. 2007).

1.4.2 Fluctuating Water Vapor and Dust-Enrichment (High f_{O_2})

A radial gradient in the water vapor, and hence the oxygen fugacity, is established in similar disk models incorporating chemical reactions (Tscharnuter and Gail 2007). The in-

ward migration of icy cometesimals and comet-like grains rich in carbon causes an interplay between oxidizing and reducing components (reviewed by Cuzzi et al. 2005b). The ice evaporation front moves inwards as the mass accretion rate declines with time (Cyr et al. 1998). For the models producing Fig. 1, the ice line begins at 6.5 AU at 10^5 yr and moves inwards to 2.5 AU by 10^6 yr due to the decline in mass accretion rate (Wehrstedt and Gail 2008). Variability in the disk mass accretion rate on smaller time scales, such as commonly produces variability in solar-analog star + disk systems (Bell et al. 1997), will move the location in the snow line on smaller time scales. Hence, the radial gradient in oxygen fugacity likely fluctuates (Cuzzi et al. 2005a, 2005b) with time scales and size scales discussed by Cuzzi and Zahnle (2004).

Inward mass accretion brings 'interstellar' Fe-Mg amorphous silicates (Sect. 2.3.1) from the outer disk into the hot inner disk where these grains are vaporized. Low oxygen fugacity nebular gases thermodynamically favor the condensation of Mg-rich silicates crystals (*for*sterite and *ens*tatite, Sect. 2.3.3) and Fe-grains (*iro* in Fig. 1). Also, low oxygen fugacity gases promote Fe-reduction, i.e., the inter-diffusion of Mg^{2+} with Fe^{2+} so that interior Fe atoms diffuse to the surface and become Fe-metal 'blebs' (Lemelle et al. 2001). In low oxygen fugacity environs, Fe-Mg amorphous silicates can be *transformed* into Mg-rich crystalline silicates with surface Fe-metal (Davoisne et al. 2006; Wooden et al. 2007). The redox conditions in the solar nebula are controlled by the abundances of gaseous H_2O and H_2, so the oxygen fugacity is defined $f_{O_2} \equiv pH_2O/pH_2$ (Wasson 1997; see Fedkin and Grossman 2006).

On the other hand, there is enough free oxygen that elemental carbon (transported from the outer disk to the inner disk as a grain component) 'combusts' to CO and CO_2, and carbon atoms in the gas-phase do not condense into carbon grains (Gail 2001, 2002, 2004). In this way, the solar nebula is very different than the grain-condensing cool atmospheres of asymptotic giant branch (AGB) stars, which are either O-rich (where silicates with a range of Fe/Mg contents can form; Gail and Sedlmayr (1999)), or C-rich (where carbon grains form; Gail and Sedlmayr 1988; Cherchneff 1995).

Gas-phase condensation can form pure-Fe crystalline silicates, after 90% of Mg is condensed into Mg-silicates and if the water vapor content is enhanced by factors of 100–1000 (Fig. 3; Palme and Fegley 1989; Weinbruch et al. 1990). Vaporization of a region enriched in dust compared to solar composition yields raises the f_{O_2} so that slightly Fe-enriched grains can condense (Fedkin and Grossman 2006; Sect. 1.4.1). If shock regions have enhanced water vapor and dust-enrichments of 550× and 300× solar composition, respectively, then the Fe-content in crystalline silicates can be raised to 60% (Fedkin et al. 2008). An Fe-content of 60% covers the range of most but not all *Stardust* Fe-bearing crystalline silicates (Zolensky et al. 2007, 2008; Sect. 1.3). The inward radial excursion of icy bodies can cause the water vapor content to fluctuate to these high values (Fig. 2; Cuzzi and Zahnle 2004). Gas-phase condensation of Fe-rich silicates at high oxygen fugacity caused by high water vapor content can explain the presence of Fe-rich silicates in comets (Sects. 2.3.5, 2.3.6).

Gas-phase condensation of Fe-rich silicates at high oxygen fugacity can explain only minor aspects of Fe-silicates in chondrules (Krot et al. 2000; S. Krot, private communication). Fe-rich silicate rims on Mg-rich crystals are seen embedded in some chondrules. A steep compositional gradient between the Fe-rich rim that surrounds the Mg-rich crystal argues for gas-phase condensation of the rim (Weinbruch et al. 1990). However, it is also argued that these Fe-rich rims most likely formed as a result of fluid-rock interactions (Krot et al. 2004). In contrast to rims around Mg-rich crystals, Fe-rich rims around Mg-rich chondrules are most likely a result of asteroidal alteration, not gas-solid reactions in the solar nebula (Krot et al. 2004).

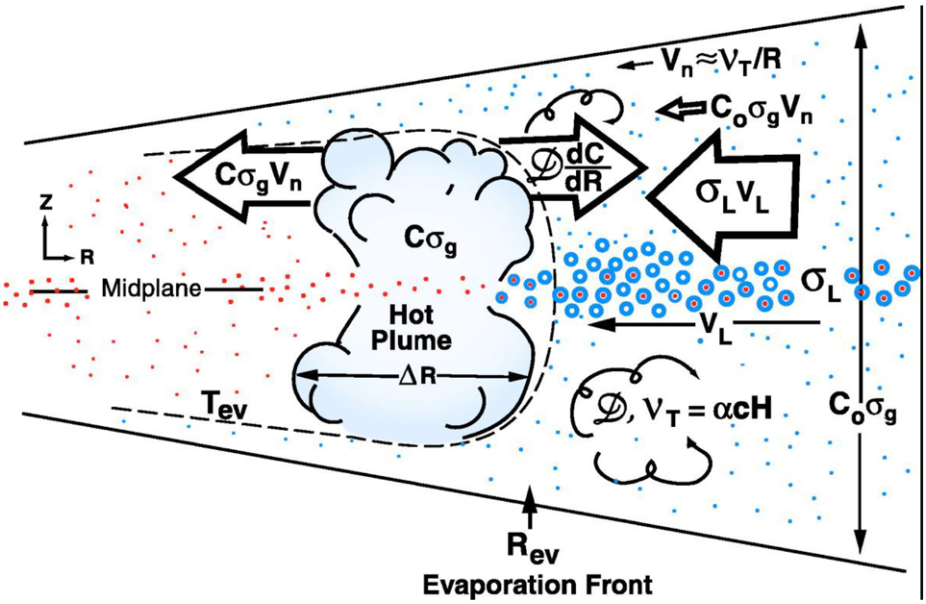

Fig. 2 Sketch of inwardly drifting cometesimals (*blue circles*) crossing the water ice evaporation front R_{ev}, with midplane temperature T_{ev}. The more refractory material (*red dots*) continues drifting inwards. (Fig. 2 from Cuzzi and Zahnle 2004)

1.4.3 High Water Vapor Nebula or Parent Body Aqueous Alteration?

The presence of water vapor or liquid water drives the formation of oxidized silicates, i.e., FeO-rich (or equivalently Fe-rich) silicates (e.g., Wasson 1997; Krot et al. 1995, 2000). Whether the aqueous alteration occurs in the nebula through gas-phase condensation, gas-grain reactions or inside asteroid bodies has been debated for a few decades (Zolensky and Browning 1997).

In parent bodies with water (as ice or in hydrated silicates), the oxygen fugacity can be raised easily because the partial pressure of H_2O is greater inside a body than in the gas-phase (Wasson 1997; Krot et al. 1995). In the gas phase, the oxygen fugacity can be raised by the vaporization of chondritic dust, which liberates oxygen bound in silicates into the gas phase (Wood and Hashimoto 1993; Fedkin and Grossman 2006). Alternatively, the oxygen fugacity can be raised by an increase in water vapor (Fegley and Palme 1985), which upon dissociation liberates OH^- (Gail 2002).

Parent body aqueous alteration forms distinct products of 'secondary processing' besides Fe-rich silicates: phyllosilicates, hydroxides, tochilinites (hydrated sulfides), sulfates, oxides, and carbonates (Zolensky and Browning 1997). A main point is that many of these secondary processing products of the parent body aqueous alteration are rare or absent in comets.

Small mass fractions of Fe-rich silicates and carbonates, and to a lesser extent oxides (Sect. 2.7) and phyllosilicates (Sect. 2.6), are found in cometary materials as investigated through IR spectroscopy, *in situ* measurements of Halley (Fomenkova et al. 1992a, 1992b), cometary anhydrous CP IDPs (Wooden 2002; Rietmeijer 1998) or *Stardust* samples (Brownlee et al. 2006; Flynn et al. 2008; Flynn 2008). We hypothesize that Fe-

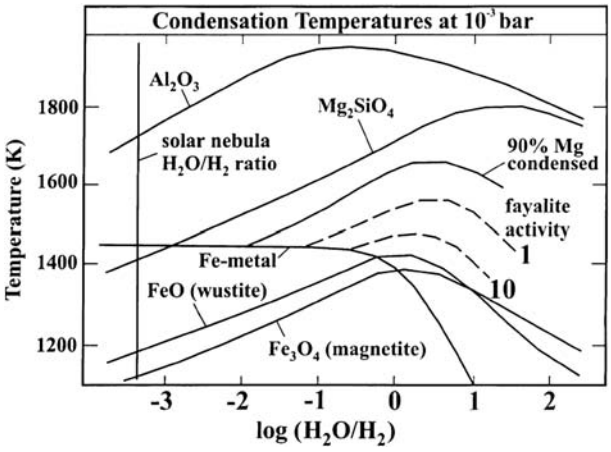

Fig. 3 Condensation of Mg-rich crystalline olivine (Mg_2SiO_4, forsterite) and Fe-rich crystalline olivine (Fe_2SiO_4, fayalite) as a function of $\log(H_2O/H_2)$ ratios. A *vertical line* denotes the canonical solar nebula [$\log(H_2O/H_2) < -3$]. Fe-rich crystalline silicates (fayalite) can form only at water vapor enrichments of several hundred and after 90% of Mg is condensed into forsterite. (Fig. 6 from Krot et al. 2000; redrawn from Palme and Fegley 1989; Weinbruch et al. 1990)

rich silicates (Sects. 2.3.5, 2.3.6), and possibly some types of phyllosilicates (Sect. 2.6), are refractory grains formed in nebular environments rich in water vapor.

We focus on enriched water vapor rather than extremely enriched dust without water vapor (Fedkin and Grossman 2006) because water vapor enrichments by the required factors are a natural consequence of the inward migration of icy bodies (Cuzzi et al. 2005a); even the modelers are concerned that dust enrichment factors of 1000 might be difficult to obtain (Fedkin and Grossman 2006). However, *we recognize that ice and dust both migrate inwards*, causing the greatest fluctuations if within small bodies such as cometesimals (Cuzzi and Zahnle 2004; Cuzzi et al. 2005a, 2005b). Cometesimals may have a ∼1:1 ratio of dust:ice, as deduced for *Deep Impact* (A'Hearn et al. 2005; Küppers et al. 2005; Keller et al. 2005). For simplicity, we refer to water vapor from here on.

We hypothesize that carbonates are nebular condensates from high carbon dioxide fugacity regions, which are spawned by carbon combustion and outward radial transport (Sect. 2.8). By invoking nebular sources for these cometary refractory grain species, we remove the need for selective aqueous alteration in cometary bodies on submicron scales.

1.4.4 Cometary Refractory Nebular Grains are Pre-Accretionary

Radial transport from the inner, hotter regions of the disk to the comet-forming regions, i.e., the trans-Neptune region (Morbidelli 2006), takes time: to enrich the disk at 20 AU takes ∼0.3 Myr (Bockelée-Morvan et al. 2002) to ∼0.5–1 Myr (Wehrstedt and Gail 2008; Wooden et al. 2007), depending on the disk model. Also, as the disk ages, the inward mass accretion rate and the outward mass transport rate declines (Wehrstedt and Gail 2008). Hence, the efficiency of incorporation of low *vs.* high oxygen fugacity products into cometary nuclei depends on the interplay between the duration of low *vs.* high water vapor content, the time-dependent outward mass transport rate, and the distance(s), range of radial migration, and duration of cometesimal accretion and nuclei accumulation.

Stardust samples contain products of high oxygen fugacity, but products of low oxygen fugacity are considerably more abundant. *Stardust* grains are often referred to as anhydrous. Other comets also contain abundant low oxygen fugacity products (Mg-rich crystals). In comparison, chondrites contain high abundances of both high oxygen fugacity and low

oxygen fugacity products, as well as parent-body aqueous alteration products. If comets do not contain materials that are aqueously altered on asteroidal parent bodies, then comets contain nebular grains that existed prior to asteroid accretion, i.e., comets contain *pre-accretionary* nebular grains.

2 Ascribing Cometary 'Interstellar' & 'Nebular' Grains and Their Plausible Formation Pathways

2.1 Focus on Refractory Grains

The compositions of comet grains are revealed by remote sensing observations (photometry, polarimetry, IR spectroscopy), by *in situ* flyby mass spectrometry of comet 1P/Halley, by laboratory examinations of *Stardust Mission* return samples from comet 81P/Wild 2, and by laboratory studies of anhydrous chondritic porous interplanetary dust particles (CP IDPs) of probable cometary origins (Hanner and Bradley 2004; Brownlee et al. 1995; Bradley 1988). From these studies, we find that comets are a combination of 'interstellar' (pre-protoplanetary disk) materials and 'nebular' materials that form or are significantly altered in the protoplanetary disk.

A clear distinction between interstellar and nebular materials occurs for cometary refractory dust species because in the protoplanetary disk grains form or are altered at high temperatures in the hot, inner regions or in shocks at 2–10 AU, and these conditions are not met in the interstellar medium or in interstellar clouds. On the other hand, for semi-refractory organics (having finite comae lifetimes), volatiles, and supervolatiles, the distinction between interstellar and nebular sources is less clear because cold, dense conditions occur in the outer protoplanetary disk as well as in the prenatal molecular cloud core (Ehrenfreund et al. 2004). Volatile cometary species are reviewed elsewhere (e.g., Fegley 1999; Irvine et al. 2000; Ehrenfreund and Charnley 2000; Ehrenfreund et al. 2004; Crovisier 2007; Charnley 2008). The evidence, interplay, and significance of interstellar and nebular refractory grain components is the focus of this review.

Cometary refractory dust grains are those species that formed at high temperatures and that are composed of rock forming elements (C, O, Mg, Al, Si, S, Fe). These grains do not experience alteration in cometary coma because in sunlight their radiative equilibrium temperatures are insufficient to cause any chemical, petrographic, or structural changes in these grains.[4] Cometary refractory dust grains represent those grains extant in the cold (and vast) regions of our protoplanetary disk where cometesimals formed, migrated, and aggregated into comet nuclei.

Cometary refractory grains include calcium-aluminum (CAI-type) minerals (Sect. 2.2), amorphous silicate-type (olivine-type, pyroxene-type) grains (Sect. 2.3.1), Mg-rich crystalline silicate minerals (Mg-rich olivine or forsterite, Mg-rich pyroxene or enstatite) (Sect. 2.3.3), amorphous carbon (Sect. 2.5.1), iron-nickel sulfides (FeS) (Sect. 2.4), as well as minor contributions from Fe-rich crystalline silicates (Sect. 2.3.5) and carbonates (Sect. 2.8), and possibly phyllosilicates (Sect. 2.6) and oxides (Sect. 2.7). Six of the nine

[4] A recent model, based on experiment, suggests amorphous silicates coated with amorphous carbon and organics undergo non-thermal crystallization in the coma, and this can produce cometary IR features (Kimura et al. 2008). However, the experiment, which demonstrated surface crystallization. did not detect any changes in the IR features (Kaito et al. 2007). The implications are not definitive.

refractory dust species (amorphous carbon, amorphous olivine-type, amorphous pyroxene-type, Mg-rich crystalline olivine, Mg-rich crystalline pyroxene, and FeS) are identified frequently in anhydrous CP IDPs or in IR spectroscopy of cometary comae. In this section, our goal is to improve and savor the complexities of our picture of the protoplanetary disk (such as Fig. 1) by critically investigating the evidence for and the sources of cometary refractory grain species.

2.1.1 Interstellar Heritage May not be Identifiable as Presolar

Interstellar materials may be descendants from stellar atmospheres or supernovae, or be grains processed in interstellar clouds or in the interstellar medium (ISM). The classification of specific cometary materials as *presolar*, which means 'interstellar with a traceable heritage', is unequivocal if the isotopic signature is significantly different from solar composition.[5] For example, in cometary anhydrous CP IDPs on submicron scales there are deuterium enrichments of a few thousand ‰ (Messenger et al. 1996). Deuterium enrichments occur by grain-gas surface reactions in a cold ($\sim$10 K) cloud over long times, so these cometary organics are 'interstellar'. Conditions in the outer, cold regions of our protoplanetary disk (10–100 K) can enhance deuterium (Robert 2006), but not to the extreme localized values seen in anhydrous CP IDPs (thousands of ‰ Messenger et al. 1996).

Out of hundreds of IDP subgrains measured, a handful have presolar oxygen isotopic signatures; two are GEMS (amorphous silicates) and one is a forsterite (extremely Mg-rich crystalline silicate in the olivine group), all of which are ^{16}O-poor and thus originate in O-rich AGB stars (Messenger et al. 2003). However, much of cometary materials are not specifically presolar. Instead, classification of cometary constituents as interstellar is based often on circumstantial evidence, i.e., they are seen in the ISM but lack presolar signatures. Sources for interstellar grains, including the possibility that 40% of ISM grains are 'solar composition' by their heritage in previous generations of protoplanetary disks, is reviewed Tielens et al. (2005). The presence of interstellar grains without presolar signatures is consistent with our notions of grain processing in the ISM through shocks and, probably, through previous generations of protoplanetary disks.

2.2 CAI-Type Minerals

To date, CAI-type minerals only have been detected in *Stardust Mission* return samples (Brownlee et al. 2006). *Stardust* CAI-type minerals are consistent with minerals predicted to be the "first condensates" from cooling solar nebula gases (Brownlee et al. 2008), and hence *cometary CAI-type minerals are refractory nebular grains.* The first CAI-like fragment is named "Inti" (Brownlee et al. 2006; Chi et al. 2008), and two more are named "Authur" and "Marvin" (Schmitz et al. 2008). "Init" contains minerals that include: TiN, gehlenite, diopside, spinel, V-bearing osbornite, anorthite, Ca-, Al-, Ti-rich clinopyroxene (fassaite), corundum, FeS, osbornite, and probably perovskite (Schmitz et al. 2008; Chi et al. 2008). The TiN in "Inti" suggests a low oxygen fugacity (rather than TiO), similar to CAIs in Allende (Chi et al. 2008). The formation of TiN suggests C/O$>$0.85, which is higher than solar nebula composition (e.g., C/O $\simeq$ 0.5, Fedkin and Grossman 2006). Chi et al. (2008) point out that, according to Dyl et al. (2005), such a high C/O suggests it originated close to the young Sun (0.3 AU). "Marvin" and "Author" contain hibbonite and gehlenite. All three

[5]Typically, solar composition is taken to be the composition of type CI chondrites.

appear to have, in the same fragment, several high temperature mineral phases. To become incorporated into comet 81P/Wild 2, the CAIs had to be radially transported out to beyond the snow line. More specifically, the CAIs may have been transported out to as far as 25–35 AU, to the trans-Neptune region, from which ecliptic comets are thought to have been preferentially scattered to their long term residences in the scattered disk beyond the Kuiper Belt (Charnoz and Morbidelli 2007).

2.3 Silicate Mineralogy, Crystallinity and Amorphousness

In comets, silicates have two recognizably different structures—amorphous and crystalline—and two compositions—olivine and pyroxene. The ratio of (Mg+Fe) to Si determines the composition: 2 for olivine and 1 for pyroxene. Crystalline silicates are olivines $[(Mg_x,Fe_{1-x})_2SiO_4]$ and pyroxenes $[(Mg_y,Fe_{1-y})SiO_3]$. Mineralogists define forsterite as Mg-rich crystalline olivine $[(Mg_x,Fe_{1-x})_2SiO_4,\ 1 \geq x \geq 0.9]$ or [Fo100–Fo90], and enstatite as Mg-rich crystalline pyroxene $[(Mg_y,Fe_{1-y})SiO_3,\ 1 \geq y \geq 0.9]$ or [En100–En90] (Henning et al. 2005). The Fe-end members of olivine and pyroxene are fayalite $[x = 0]$ or [Fa100] and ferrosilite $[y = 0]$ or [Fs], respectively. In contrast, amorphous silicates have disordered (glassy) structures and non-stiochiometric compositions, that is, their compositions do not specifically match members of a mineral sequence. Olivine-type or pyroxene-type grains form out of thermal equilibrium, such as in a rapidly cooling stellar wind or a shock (Sect. 2.3.2; Colangeli et al. 2003; Wooden et al. 2005). Degradation of stoichiometry can also occur by ion bombardment in the ISM (Sect. 2.3.2). IR spectroscopy of comets and studies of anhydrous CP IDPs indicate that typically half or more of cometary silicates are amorphous (Sect. 2.3.1). In contrast, *Stardust* samples appear to be dominantly crystalline.

2.3.1 Evidence for Fe-Mg Amorphous Silicates

By their radiative equilibrium temperatures in cometary comae, amorphous silicates have about equal abundances of Fe and Mg (Harker et al. 2002).[6] Even though the IR spectra of comets are well-fitted by laboratory IR spectra of amorphous minerals (e.g., formed by flash cooling at ∼2000°C/s, Dorschner et al. 1995; Colangeli et al. 2003), that does not indicate that cometary amorphous silicates are minerals with amorphous forms. Hence, we refer to amorphous silicates as olivine-type and pyroxene-type rather than olivine and pyroxene because of their non-stoichiometric compositions.

In anhydrous CP IDPs, the amorphous olivine-type and amorphous pyroxene-type grains are non-stoichiometric assemblages of siliceous materials (Keller et al. 2005), designated Glasses with Embedded Metal and Sulfides (GEMS) (Bradley et al. 1992; Brownlee et al. 1999; Keller and Messenger 2004). GEMS contain nanophase FeS (Bradley 1994b; Brownlee et al. 1999). The absorption feature from GEMS-rich anhydrous CP IDP material has a similar shape as the ISM absorption feature (Bradley et al. 1998, 1999a, 1999c). For more than a decade, GEMS have been considered as the prototypical ISM Fe-Mg amorphous silicate (Hanner and Bradley 2004).

Alternatively, a fraction of GEMS could have condensed by rapid-cooling, and at later phases of the solar nebula evolution based on their solar oxygen isotope compositions, i.e., ^{16}O relative to ^{17}O and ^{18}O (Keller and Messenger 2008). Krot et al. (2005) discuss how at the earliest times, when the highest temperature CAIs formed, the gas was ^{16}O-rich, but

[6] The Mg-contents of isolated pyroxene and olivine grains range from $0.6 \lesssim Mg/(Mg + Fe) \lesssim 0.4$ for 'equilibrated' meteorite Allende (see Zolensky and Barrett 1994; Zolensky et al. 2007).

less than 0.8 Myr later gas in the inner solar nebula became ^{16}O-poor. A detailed look at the isotopic signatures *and composition* of GEMS comes to a different conclusion, namely that GEMS may be ISM, and more work in called for (Matzel et al. 2008). An earlier report of a ^{16}O-rich GEMS-rich IDP (Engrand et al. 1999), suggested the GEMS could be from an earlier nebular or presolar reservoir. As yet, these are small number statistics on isotopic signatures in GEMS.

Amorphous silicates indigenous to cometary anhydrous CP IDPs are rare in *Stardust* samples (Chi et al. 2007; Ishii et al. 2008). The amorphous silicates found in *Stardust* samples are attributable to the dissolution (or crystallization) of amorphous/crystalline silicates *and* FeS upon impact in the aerogel capture medium (Ishii et al. 2008; Zolensky et al. 2006b), which itself is an extremely low density SiO_2 glass. The scarcity of indigenous amorphous silicates appears to be a surprising result of the *Stardust Mission*, and may indicate that comet 81P/Wild 2 has less interstellar refractory grains and more nebular refractory grains than other comets (Ishii et al. 2008). Except for *Stardust* samples, amorphous silicates are a ubiquitous component of cometary anhydrous CP IDPs and IR spectral energy distributions (SEDs).

2.3.2 'Interstellar' rather than 'Nebular' Sources for Amorphous Silicates

Cometary amorphous silicates are classified as interstellar largely by circumstantial evidence. Along lines-of-sight through the ISM, silicate absorption features are well-matched by both spherically-shaped Fe-Mg amorphous olivine and pyroxene (Kemper et al. 2004, 2005), and by non-spherically shaped pure-Mg amorphous olivine and pyroxene (Min et al. 2007). Detailed analysis of the ISM extinction curve implies the presence of Fe-Mg amorphous silicates (Li and Draine 2001). Studies of the depletion of gas-phase atoms into dust grains in Galactic diffuse ISM clouds show Fe, Mg, and Si are depleted together in grains, and in increasing amounts for denser clouds (Fig. 4 of Jones 2000; Savage and Sembach 1996). Only in clouds in the Galactic halo are there Mg, Si grains (without Fe) (Jones 2000). Depletion studies taken together with models for the shape of the 10 μm absorption feature imply that Galactic disk ISM silicates are Fe-Mg amorphous olivine-type and pyroxene-type grains.

Sources for ISM Fe-Mg amorphous silicates include O-rich AGB stars and supernovae. O-rich AGB stars primarily shed Fe-Mg amorphous silicates. The nucleation and growth of amorphous silicate grains requires rapid cooling in non-thermodynamic equilibrium conditions (Gail and Sedlmayr 1999; Colangeli et al. 2003). In a cooling gas, if vapor saturation is high enough then atoms, ions, and molecules start nucleating into clusters and cluster growth ensues. If there is enough time and energy for cluster rearrangement then crystals grow (Colangeli et al. 2003). Otherwise, highly disordered (amorphous) particles grow.[7]

Amorphous silicates also can form by the vitrification of crystalline silicates via ion bombardment in the ISM. Although O-rich AGB stars primarily contribute amorphous silicates to the ISM, as much as 4–20% of their siliceous grains might be Mg-rich crystalline silicates (Kemper et al. 2001). However, bombardment by low energy Galactic cosmic rays (few–50 keV H^+ or He^+ ions) probably efficiently amorphizes crystalline silicates (Carrez et al. 2002; Jäger et al. 2003; Brucato et al. 2004; Bradley 1994a; Dukes et al. 1999), with chemical composition alteration occurring at $\lesssim$20 keV (Carrez et al. 2002; Bradley 1994a). Also, low energy (4–10 keV) cosmic-ray exposure can reduce iron from

[7] See reviews of laboratory preparation techniques for amorphous silicates (Colangeli et al. 2003; Wooden et al. 2005) and annealing experiments (Wooden et al. 2005).

its stioichiometric inclusion in an amorphous Fe-Mg silicate mineral grain to nanophase Fe metal embedded within the Mg-rich amorphous silicate grain (Carrez et al. 2002), such as seen in GEMS (Bradley 1994a). Compared to keV cosmic rays, higher energy MeV cosmic rays travel farther distances from supernovae shocks (~2 pc, Spitzer and Jenkins 1975). Experiments with high energy, heavy cosmic rays (1.5 MeV Kr^+ ions) show amorphization yields are sufficient to account for interstellar amorphous silicates. Moreover, heavy cosmic ray bombardment amorphizes at one-quarter the dose for Fe-rich crystalline olivine (Fe_2SiO_4) compared to Mg-rich crystalline olivine ($Mg_{0.88}$,$Fe_{0.12})_2SiO_4$ (Jäger et al. 2003). We note another potential source for amorphizing cosmic rays may include a supernova in the vicinity of the young Sun that donated short-lived ^{60}Fe to the protoplanetary disk (e.g., Kita et al. 2005).

Transient heating and rapid cooling in nebular shocks (Connolly et al. 2006; Boss and Durisen 2005) provides a non-equilibrium rapid-cooling environment for chondrule formation (Desch and Connolly 2002), including the growth of glassy-to-microcrystalline mesostasis that surrounds crystalline silicates (Connolly and Love 1998). Amorphous materials in the matrixes of primitive chondrites also probably form in shocks (Scott and Krot 2005a; Nuth et al. 2005). These amorphous ferromagnesian (Fe-Mg-Si-O) matrix materials have more Fe than GEMS and lack the cosmic ray tracks that are characteristic of GEMS' ISM exposure (Scott and Krot 2005a).

Some GEMS potentially form in shocks in the solar nebula (Keller and Messenger 2008). We describe some of the specific circumstances that might need to occur for GEMS to be solar nebula products as follows. It is feasible that radiation damage might occur by the low energy solar cosmic rays produced by energetic X-ray flares (Wolk et al. 2005) caught within the heliopause. Low energy solar cosmic rays (~50 keV H^+) are capable of amorphizing small isolated grains (Brucato et al. 2004; Carrez et al. 2002), but do not penetrate much below the disk surface since they are so efficiently stopped by the grains, in a similar way that they penetrate only a thin skin on larger bodies (Strazulla et al. 2003). So, solar system GEMS probably need to have been close to the disk surface to become radiation damaged. In meteoritic samples, a single proto-GEMS has been found in Ningqiang, showing radiation damaged glasses surrounding silicate crystals with the same composition (Zolensky et al. 2003; Nakamura et al. 2003).

GEMS would have to escape to comet-forming regimes before they experience a reheating event. Experimental heating GEMS at ~1000 K for a few hours or at 1200 K (in flowing N_2 gas, albeit an uncontrolled f_{O_2} environment) yields moderately Fe-rich crystalline silicates and igneous textures (Brownlee et al. 2005). Heating of GEMS-like materials at ~1000 K in low f_{O_2} gases forms Mg-rich crystalline silicates and surface Fe-metal blebs (Davoisne et al. 2006). Even though experimental heating of actual GEMS is yet to be done for a controlled range of f_{O_2}, the existing experimental data indicate GEMS never saw temperatures above ~1000 K. Many lines of circumstantial evidence say a high fraction of GEMS have interstellar origins (Alexander et al. 2007; Matzel et al. 2008), even though they do not have presolar isotopic signatures (Tielens et al. 2005).

2.3.3 Evidence for Mg-rich Crystalline Silicates

Mg-rich crystalline silicates are present in many comet IR SEDs (Kelley and Wooden 2008), and are predominant in *Stardust* samples and cometary anhydrous CP IDPs. Mg-rich crystalline silicates comprise the matrixes of the most primitive chondrites (non-thermally and non-aqueously altered chondrites, e.g., Acfer 094, Wooden et al. 2005; Nuth et al. 2005;

Zolensky et al. 2007), and are present as *relic* grains in chondrules (Bradley et al. 1999b; Weinbruch et al. 2000). Crystalline silicates are predominantly Mg-rich and Fe-poor, in contrast to Fe-Mg amorphous silicates.

Laboratory spectra of Mg-rich crystalline silicates (Koike et al. 2003; Chihara et al. 2002) match well the wavelengths of the peaks of resonant features in cometary IR SEDs (SEDs are plots of $\log[\lambda F_\lambda]$ *vs.* $\log[\lambda]$) (Crovisier et al. 1997; Wooden et al. 1999, 2005; Harker et al. 2002, 2007: Kelley and Wooden 2008). Some of the highest Mg-content crystals found in solar nebula bodies are the forsterite and enstatite crystals in anhydrous CP IDPs (Bradley et al. 1999b) and in *Stardust* samples (Zolensky et al. 2006b, 2007). In *Stardust* samples, the frequency peak is at Fo98 [$x = 0.98$] and En95 [$y = 0.95$] (Zolensky et al. 2007). Submicron and micron-size single crystals of Mg-rich pyroxene and Mg-rich olivine can constitute 5–50% of mass (5–50 wt%) of an anhydrous CP IDP (Wooden et al. 2007; Alexander et al. 2007). IDP L2009*E2 has 5–10 wt% Mg-rich silicate crystals (Keller et al. 2000).

In many nearly isotropic (long-period Oort cloud) comets and in some ecliptic (short-period Jupiter Family) comets, the fraction of cometary silicates that are Mg-rich silicate crystals is significant ($f_{\rm cryst} \simeq$ 0.3–0.8). A high $f_{\rm cryst}$ in some comets,[8] e.g., ∼30% in *Deep Impact* (Harker et al. 2007; Sugita et al. 2005) to ∼50–80% in Hale-Bopp (60–80%, Harker et al. 2002, 2004; 50%, Moreno et al. 2003) and ∼70% in C/2001 Q4 (NEAT) (Wooden et al. 2004), implies that large scale outward radial transport in the protoplanetary disk is efficient.

2.3.4 Formation Scenarios for Mg-rich Crystalline Silicates

In the ISM, crystalline silicates are rare (<5%, Li and Draine 2001) to nearly absent ($\leq 1.1 \pm 1.1$% towards the Galactic Center, Kemper et al. 2004, 2005). Therefore, most of the crystalline silicates are from nebular sources. Mg-rich silicates either condense from the canonical low oxygen fugacity solar nebula or are annealed from amorphous silicates into crystals in low oxygen fugacity environs (Sect. 1.4.1). *Mg-rich crystalline silicates in comets is the strongest criterion for large scale radial transport of materials from the hot, inner regions to the icy cold, outer regions of the protoplanetary disk.*

The canonical solar nebula has a low oxygen fugacity, which (thermodynamically) preferentially condenses *extremely Mg-rich* [Mg_2SiO_4, $x \geq 0.99$] silicate crystalline mineral grains (Gail 2004; Krot et al. 2000; Grossman 1972; Sect. 1.4.1). Extremely Mg-rich silicate crystals dominate the olivines (forsterites) in *Stardust* samples (Zolensky et al. 2007), exist as forsterite and enstatite crystals ($x, y \geq 0.98$) in some anhydrous CP IDPs (Bradley et al. 1999b), exist in Halley (Schulze et al. 1997; Bradley et al. 1999b), and comprise the matrices of the most primitive chondrites (type 3.0, minimally-thermally and non-aqueously altered chondrites, e.g., Acfer 094, Wooden et al. 2005; Nuth et al. 2005; Zolensky et al. 2007), and are present as *relic* grains in chondrules (Bradley et al. 1999b; Weinbruch et al. 2000).

[8]The silicate crystalline mass fraction is [$f_{\rm cryst} \equiv$ crystalline/(crystalline + amorphous)], and is given for the submicron to micron-size portion of the grain size distribution (Harker et al. 2002; Moreno et al. 2003). If larger porous amorphous silicate grains are considered (as analogs to aggregates of submicron amorphous silicate subgrains), then the crystalline fraction is much smaller, only 4% (Min et al. 2005). Crystalline silicates as subgrains of larger (>5 μm) mixed aggregates is computationally challenged (Moreno et al. 2003). Low spectral resolution computations suggest crystals are discernible only in the most porous of aggregates (Kolokolova et al. 2007).

Mg-rich crystalline silicates ($\sim 0.97 \leq x \leq 0.9$) also are prevalent in cometary materials: enstatite crystals ($y \simeq 0.95$) in *Stardust* samples (Zolensky et al. 2007), in anhydrous CP IDPs (Bradley et al. 1992, 1999b; Zolensky and Barrett 1994). Such crystals can form by slower condensation in dust-laden nebular environs. Minor enhancements in the Fe-content of otherwise pure-Mg silicates are explained by condensation models that account for the progressive removal of Mg and Si from the gas phase (Petaev and Wood 1998). Models that include the vaporization of dust grains previously condensed from solar nebula gases and include slower cooling during condensation can yield Mg-contents of $x \simeq 0.95$–0.9 in the interiors of ~ 0.5 μm-radii grains and $x \simeq 0.94$–0.92 in the interiors of ~ 3 μm-radii grains (Fedkin and Grossman 2006). Dust loading and slower condensation allows Fe to inter-diffuse into grains that start condensing as extremely high Mg-content silicates. Condensing grains out of regions where aqueously altered grains or ice-coated grains have vaporized (10 wt% ice) increases the Fe-content only by a minor amount (Fedkin and Grossman 2006). Hence, condensation in nebular environs enriched in fine-grained dust (with or without ice coatings) can account for Mg-rich crystalline silicates in comets ($x \gtrsim 0.9$).

Alternatively, Mg-rich crystals ($x \simeq 0.9$) can form at $\gtrsim$1000 K by annealing of Fe-Mg amorphous silicates in low oxygen fugacity environs because Fe-reduction occurs at the same temperatures as annealing, albeit at slower rates (Wooden et al. 2007; Davoisne et al. 2006; Lemelle et al. 2001). Given near steady-state conditions ($\sim$1 Myr), there is sufficient time for Fe-reduction; Fe-Mg amorphous silicates transported into the inner low oxygen fugacity solar nebula will become reduced (Gail 2002). At these temperatures, these grains also anneal, yielding Mg-rich crystalline silicates (Gail 2002; Wooden et al. 2007).

Annealing in shocks is an attractive scenario for producing crystalline silicates because it can occur after the disk mass accretion rate ($\dot{M}$) declines and the region hot enough to condense crystalline silicates shrinks (e.g., mid-plane $T \lesssim 1500$ K at $\leq$1 AU for $\dot{M} = 10^{-6} M_{\odot}$ yr^{-1}, Gail 2002; mid-plane $T \lesssim 1400$ K at $\leq$1.5 AU for $\dot{M} = 10^{-6} M_{\odot}$ yr^{-1}, Bell et al. 2000). If Mg-rich crystals form in shocks (Harker and Desch 2002), and precursor amorphous silicates contain Fe (Sect. 2.3.1), then Fe-reduction is necessary for the annealing scenario to be consistent with the preponderance of Mg-rich crystalline silicates in comets (Wooden et al. 2007; Davoisne et al. 2006). Through exposure to a single shock energetic enough to crystalline an amorphous silicate grain, there probably is sufficient time in the pre- and post-shock radiation environment for Fe-reduction to proceed for submicron- to micron-sized amorphous silicates, but not larger ones (Wooden et al. 2007, based on inter-diffusion rates determined by Lemelle et al. (2001) and Chakraborty (1997), and compared with rates inferred from experimental heating of GEMS by Brownlee et al. 2005).

2.3.5 Evidence for Fe-Rich Crystalline Silicates

In cometary materials, Mg-rich crystalline silicates dominate, but Fe-bearing and Fe-rich crystalline silicates are present. Even though Mg-rich crystalline silicates dominate *Stardust* samples, there are crystalline olivines spanning pure-Mg to nearly pure-Fe, i.e., $[1.00 \leq x \leq 0.04]$ or [Fo100–Fo4] (cf., Sect. 2.3), and crystalline pyroxenes spanning pure-Mg to Fe-rich, i.e., $[1.00 \leq y \leq 0.65]$ or [En100–En65] (Zolensky et al. 2007). In other CP IDPs, both anhydrous and hydrous, there is a range of Fe-Mg contents spanning Mg-rich to moderately Fe-rich $[1 \leq x, y \leq 0.5]$, with a frequency peak in the range $x, y = 0.9$–1 (Zolensky and Barrett 1994). In one anhydrous CP IDP thin section, the wavelength positions of the far-IR spectral resonances reveal a domain of microcrystalline olivine of that has $x \simeq 0.75$ (Molster

et al. 2003). To date, Fe-rich crystalline silicates (fayalite and ferrosilite) are identified and assessed only in weighted-surface area models by Lisse et al. (2006, 2007).[9]

2.3.6 Formation Scenarios for Fe-rich Crystalline Silicates

We hypothesize that cometary Fe-rich crystalline silicates condensed, or are annealed, in high oxygen fugacity nebular environs (Sect. 1.4.2). High oxygen fugacity conditions cause Fe to inter-diffuse into Mg-rich crystals and increase the Fe-content of olivines to $x \simeq 0.20$ at 800 K (Fedkin and Grossman 2006). Evaporating asteroidal aqueously altered grains (C1 chondrites) and icy dust grains (10 wt% icy coatings) only increases the Fe-content by a small factor. Condensation of moderately Fe-rich to Fe-rich silicates ($0.8 \lesssim x, y \lesssim 0$) requires the environs to have enhanced water vapor, with or without dust loading (Fig. 3; Fedkin et al. 2008; Palme and Fegley 1989; Weinbruch et al. 1990).

Annealing of Fe-Mg amorphous silicates in high water vapor content nebular regions (Sect. 1.4.2) is expected to form Fe-rich crystalline silicates. In contrast, if (GEMS-like) Fe-Mg amorphous silicates are heated in low water vapor content nebular regions then Mg-rich crystalline silicates and reduced Fe-metal surface blebs result (Davoisne et al. 2006). Heating of GEMS to ∼1000 K for several hours in pure flowing nitrogen gas (nevertheless, an uncontrolled fugacity environment, see Sect. 1.4.3) produces moderately Fe-rich crystalline silicates and a silica rich glass (Brownlee et al. 2005). Annealing of pure-Fe amorphous silicates requires higher temperatures (∼1270 K) than annealing pure-Mg amorphous silicates (∼1000 K) (Brucato et al. 2002; cf., Table 1 in Wooden et al. 2005). Successful shock annealing of pure-Fe amorphous silicates occurs so closer to their evaporation temperatures that probably only submicron pure-Fe crystalline silicates remain (Nuth and Johnson 2006).

If the less numerous cometary Fe-rich crystalline silicates are GEMS annealed in high water vapor nebular regimes or annealed in humid shocks, yet GEMS are numerous in the outer disk, then high water vapor concentrations are less frequent, and/or the radial transport of high water vapor products is less efficient, and/or the epochs of high water vapor content are too late for radial transport to reach the comet-forming region prior to the completion of nuclear accretion. To summarize, moderately Fe-rich and Fe-rich crystalline silicates can form in the protoplanetary disk in episodes of hot, high water vapor content regions but not much of this material appears to be incorporated into cometary nuclei, especially when compared to primitive chondritic materials (Scott and Krot 2005a).

2.4 FeS

Iron-sulfides (troilite, FeS) are well documented components of anhydrous CP IDPs, are abundant in *Stardust* samples (Flynn 2008), are measured *in situ* in Halley's coma (Schulze et al. 1997), and have been included in some models fitting space-borne IR spectra of comets 9P/Tempel 1 (Lisse et al. 2006) and Hale-Bopp (Min et al. 2005; Lisse et al. 2007).

FeS is highly opaque and its IR absorptivity (Begemann et al. 1994; Semenov 2001) is featureless at near-IR wavelengths and has some structure in the mid-IR, with a resonance

[9]The relative mineral abundances depend on grain temperatures and model assumptions. In Lisse's models, grain temperatures are free parameters and best-fit temperatures are lower for Fe-rich crystalline silicates than for Mg-rich crystalline silicates. In contrast, computed radiative equilibrium temperatures are hotter because Fe-silicates are more absorbing in the visible and near-IR but equally emissive in the mid-IR (e.g., Dorschner et al. 1995). Hence, Lisse's models yield systematically higher abundances of Fe-rich crystalline silicates than SED models that compute radiative equilibrium temperatures.

at 23 μm. The 23 μm feature is observed in a few IDPs (Keller et al. 2000) and in two protoplanetary disks (Keller et al. 2002). The 23 μm feature is not identified yet in comet spectra, which is attributed to the presence of only large FeS grains in cometary comae ($a \geq 0.8$ μm, Min et al. 2005). FeS comprises 15 wt% of Halley's refractory dust (derived from Schulze et al. 1997), and are more abundant amongst the more massive particles (Fomenkova et al. 1992a, 1992b). FeS is a challenging species to detect with IR spectroscopy because of its lack of high contrast spectral features.

In the spectral decomposition of the *Deep Impact* ejecta, FeS is a significant component comprising 15% of the grain effective surface area (Lisse et al. 2006, 2007). In two models for Hale-Bopp's *ISO SWS* IR spectrum, FeS is assessed to be 16 wt-% (Min et al. 2005, using optical constants from Begemann et al. 1994 and Semenov 2001), and 15% of the weighted surface area (Lisse et al. 2007). Min et al.'s result of 16 wt% FeS is influenced by their additional constraints to match the chemical abundance of FeS in meteorites (17 wt%) and to achieve a total Fe-content (FeS plus Fe-grains and Mg-Fe amorphous silicates) equivalent with solar composition. For ∼micron-sized and larger grains, both FeS and amorphous carbon (Sect. 2.5.1) have featureless absorptivities, although FeS grains are more highly absorbing and so FeS grains will be warmer. Min et al. allow all grain species to have their own size distributions, so additional constraints provide a way to resolve degeneracies in their model fits between FeS and amorphous carbon.

In anhydrous CP IDPs and in *Stardust* samples, iron is contained in macroscopic (micron-sized) FeS crystals. Also, in GEMS (Sects. 2.3.1, 2.3.2) there is nanophase Fe and FeS, and sulphur is concentrated in Fe-sulfides (Flynn et al. 2004). FeS is most frequently observed toward the outer surfaces of GEMS than the centers. This gradient may be a consequence of S diffusion into the GEMS, while in the solar nebula (Keller, private communication). If GEMS are interstellar particles (Sect. 2.3.2), nanophase FeS occurring in the interior of aggregate GEMS (Keller et al. 2005) challenges the assessment that all S in diffuse ISM clouds is in the gas-phase (Jones et al. 2000). FeS is invoked as an opacity source in parent molecular clouds and accretion disks (Pollack et al. 1994), so FeS may exist in pre-protoplanetary clouds. On the other hand, kinetic condensation models suggest FeS forms in the solar nebula in ∼0.3 Myr (rather quickly) at temperatures at or below ∼700 K (Fegley 2000). More recent models show that FeS starts condensing at 1250 K, eventually consuming all available S (Fedkin and Grossman 2006).

In contrast to nanophase FeS in submicron-sized GEMS, FeS crystals in *Stardust* samples and in anhydrous CP IDPs are micron-sized and larger. In *Stardust* FeS grains or organics associated with FeS grains, there are significant He and Ne concentrations that indicate FeS particles were exposed to energetic particles while resident near the young Sun in the inner disk (Marty et al. 2008). *Stardust* results are consistent with the residence (and inferred formation) of FeS in the inner nebula.

2.5 Refractory Carbonaceous Species

In comparison to CI chondrites (solar composition), comets contain (at least) 2–3 times more atomic carbon. In chondrites, the primary form of carbon is macromolecular carbon, which is a complex refractory organic material robust to acid dissolution. From the interstellar medium to comets to chondrites, amorphous carbon dwindles and organic matter increases in robustness and complexity: amorphous carbon comprises 50% of ISM materials, 8–10% by mass of cometary materials, and only $\lesssim$2% of meteoritic materials (Fomenkova and Chang 1995).

2.5.1 Amorphous Carbon

In the following paragraphs, we highlight amorphous carbon as a cometary refractory grain component. The relative abundances of amorphous carbon range from 10–50 wt% of comae grains depending on the measurement techniques or modeling approaches. Measurements of the comae of comets 1P/Halley, 9P/Tempel 1 and C/2001 Q4 (NEAT) reveal their nuclei have heterogeneous compositions based on variable amorphous carbon-to-silicate ratios.

All cometary IR SEDs exhibit strong near-IR (∼3–5 μm) 'featureless' emission, which is well-fitted by amorphous (glassy) carbon (Hanner et al. 1994). Submicron-sized amorphous carbon grains are hot enough to produce the shape of this emission, which rises above declining spectral slope of scattered sunlight (Harker et al. 2002).[10] Grain models for cometary IR SEDs yield a range of amorphous carbon contents. Efforts to fit the same *ISO SWS* spectrum of comet Hale-Bopp at 2.8 AU (Crovisier et al. 1997) with different models yield different amorphous carbon abundances (relative to the other refractory grain components): thermal emission models for a size distribution with discrete compositions yield 21 wt% (Harker et al. 2002, 2004), 24 wt% (Min et al. 2005); irregularly-shaped particles of varied composition yields 27 wt% (Moreno et al. 2003); weighted-surface area with grain temperature as a free parameter yields 8 wt% (Lisse et al. 2007). Hale-Bopp's narrow band 10 μm photometry at 1.5 AU is fitted with the 'bird-nest' model for highly porous aggregates of silicate cores coated with carbonaceous materials and yields 25 wt% amorphous carbon, 25 wt% refractory organic and 50 wt% silicates (Li and Greenberg 1998); however, the best-fit 'birds-nest' model for narrow band photometry has less fidelity compared to the model fits of spectra at this epoch (see Moreno et al. 2003 or Harker et al. 2002, 2004). Most consistent comparisons between comets arise when comparing models with similar assumptions, e.g., compare different comets fitted by the 'bird-nest' model, or compare models for discrete or mixed mineral grains (not coated) for which radiative equilibrium temperatures are computed (Harker et al. 2004; Min et al. 2005; Moreno et al. 2003), or compare weighted surface area models (Lisse et al. 2006, 2007). Given this caveat, amorphous carbon-to-silicate ratios appear to vary amongst a handful of comets, with possibly higher ratios in ecliptic comets compared to isotropic comets.

2.5.2 Amorphous Carbon and Heterogeneity of Cometary Nuclei

In two comets, variable amorphous carbon-to-silicate ratios provide firm evidence for nuclear inhomogeneities. Over the duration of 2 hr, the amorphous carbon-to-silicate ratio in the coma of long-period nearly isotropic comet C/2001 Q4 (NEAT) increased by a factor of 2, possibly associated with the passage of jet-dominated material through the beam (Wooden et al. 2004).

Even more convincing are the Gemini, Subaru, and Lunin telescopic observations of the *Deep Impact* event that demonstrate the surface layer of comet 9P/Tempel 1 excavated by the *Deep Impact* event is fine-grained amorphous carbon (Harker et al. 2005, 2007; Kadono et al. 2007; Sugita et al. 2005; Furusho et al. 2007), to a depth of several tens of centimeters (Kadono et al. 2007). Moreover, during 3 hr post-impact the amorphous carbon abundances vary from 2–75 wt%, with a time average of ∼30 wt% that agrees with pre-impact coma (28 wt%) (Harker et al. 2007). With the exception of the faster moving amorphous carbon surface layer, the temporal evolution of the post-*Deep Impact* coma grain population is

[10] For ∼micron-sized and larger grains, both FeS and amorphous carbon have featureless absorptivities, although FeS grains are more highly absorbing and so FeS grains will be warmer (Sect. 2.4).

consistent with a temporary geyser dragging heterogeneous subsurface materials into the coma (Harker et al. 2007). For comet 9P/Tempel 1, *the nucleus is heterogeneous yet contains pockets of homogenous composition* on size scales smaller than the impact crater ($\lesssim$150–200 m, Busko et al. 2007) and the depth of release of $\sim$1 m (Kadono et al. 2007) to tens of meters (A'Hearn et al. 2005).

The nucleus of 1P/Halley also appears heterogeneous based on the coma's spatial distribution of C-only grains. These amorphous carbon grains peak at 20,000 km from the nucleus on the outbound leg of the Vega-2 spacecraft (Fomenkova 1997), and are not spatially correlated with any other organic component nor with any siliceous component (Fomenkova et al. 1994).

2.5.3 Interstellar Heritage for Amorphous Carbon

A few Halley C-only grains have presolar signatures of $^{12}C/^{13}C > 5000$ (Jessberger and Kissel 1991), which are characteristic of descendants of dust-forming winds of AGB carbon stars (Fomenkova and Chang 1995; Fomenkova et al. 1994). Equally important, amorphous carbon is an 'interstellar' refractory grain component because the oxidation state of the protoplanetary disk is too high to allow elemental carbon to condense into carbon grains (Sect. 1.4.1; Gail 2001; Fedkin and Grossman 2006). Since amorphous carbon is destroyed or transformed in the disk, it must be from a reservoir other than the disk, i.e., from an interstellar reservoir. Supporting evidence comes from the fact that carbon is depleted from the gas phase in the ISM (Jones 2000), graphitic carbon contributes to the interstellar extinction curve (Li and Draine 2001), and ion bombardment converts organics to amorphous carbon (Muñoz Caro et al. 2006). (The optical properties of graphitic carbon are similar to amorphous carbon and to pyrolyzed cellulose, Jäger et al. (1998).) Measuring the amorphous carbon abundance in comets and identifying amorphous carbon as 'interstellar' is significant because it identifies amorphous carbon as an *input* to nebular processing.

2.5.4 Semi-Refractory and Refractory Organics in Comae

In Halley, 85 wt% of the atomic carbon occurs in refractory and semi-refractory organics composed of C, H, O, and N in various combinations (Fomenkova 1999): 60 wt% complex organic matter, 20 wt% hydrocarbons, 5 wt% [C,N] and [C,O] polymers. The rest of the carbon is in amorphous carbon (10 wt%) and fine-grained carbonates (5 wt%, Sect. 2.8).

In 1P/Halley's coma, much of the complex organic matter is observed closer than 10,000–25,000 km of the nucleus (Fomenkova et al. 1994). If grains have typical coma speeds of 0.2 km s^{-1}, then these semi-refractory organic materials (Mann et al. 2005) have finite coma lifetimes of 14–34 hr. Similarly short lifetimes (3 hr and 17 hr) are deduced for 2 different organic components observed in visual- and near-IR scattered light in the coma of comet C/2000 WM_1 (LINEAR) (Tozzi et al. 2004).

2.5.5 Refractory Organics in Anhydrous CP IDPs and in Stardust

In anhydrous CP IDPs, the submicron- to micron-sized domains of siliceous material are bound together by carbonaceous material (Keller et al. 2000, 2004). Also, carbonaceous materials form thin coatings (0.01 μm thick) on discrete submicron to micron-size Mg-rich crystals (Keller et al. 2000). The lifetime of particles the interplanetary medium can be upwards of 40,000 yr, so organic material IDPs is refractory. Individual CP IDPs can vary widely in their carbon abundances from 1–47 wt% (Thomas et al. 1995, 1996), and

constitute up to 90% of the volume (Thomas et al. 1994b). For an average of 100 CP IDPs, carbon is ∼12 wt% (Thomas et al. 1993, 1994a, 1994c, 1995; Flynn et al. 2003; Keller et al. 2004), but it can range up to ∼13×CI (Thomas et al. 1993; Keller et al. 2004). The carbon is divided between aliphatic bonds, and aromatic bonds characteristic of poorly graphitized carbon or very large PAHs, as discussed below.

Laboratory measurements of the carbonaceous materials in anhydrous CP IDPs use a variety of techniques, including IR spectroscopy, Raman spectroscopy, transmission and scanning electron microscopy (TEM, SEM), NanoSIMS, and carbon-, nitrogen- and oxygen-XANES (X-ray Absorption Near Edge Structure) spectroscopy. C-XANES spectroscopy reveals the presence of C=C π^* bonds and C=O bonds (Flynn et al. 2003; Keller et al. 2004). IR transmission spectroscopy reveals a group of absorption bands at 3.3–3.6 μm (3000–2800 cm^{-1}), that correspond to aliphatic hydrocarbons chains of $-CH_2$ bonds with terminal ends of $-CH_3$ groups (Flynn et al. 2003; Keller et al. 2004). On the one hand, aliphatic hydrocarbon bands commonly are detected in IR spectroscopy of C-rich IDPs. In contrast, the 3.3 μm hydrocarbon features only occur in one strongly heated particle. On the other hand, the C-XANES spectra indicate a significant abundance of hydrocarbon C=C π^* bonds.[11] The presence of C=C π^* bonds but the absence of the spectroscopic C-H band (∼3.3 micron) indicates that much of the carbonaceous matter is very poorly graphitized carbon possessing only short range order (<2 nm) or very large PAH molecules (Keller et al. 2004).

Stardust flew by at only 234 km from the nucleus of 81P/Wild 2, and organic signatures appear diffused out into the aerogel capture medium from tracks laden with refractory grains, so the organics are *labile* (Sandford et al. 2006). Organics are found rarely as discrete clumps (one 5 μm region, De Gregorio et al. 2008). More often organics occur as C/N-rich zones in regions of the tracks, such as the Ada and Febo particles (Matrajt et al. 2007, 2008). Febo has a C-XANES spectrum that shows C=C π^* bonds (Matrajt et al. 2007) and a Raman spectrum characteristic of aromatic material like disordered graphite (Wopenka et al. 2008). However, Febo has no 3.3 μm PAH band and only a broad weak inflection in its 2.9–3.7 μm spectrum (Wopenka et al. 2008). Febo is enriched in $^{15}N/^{14}N$ ($\delta^{15}N = 420 \pm 160$ ‰), similar to other *Stardust* particles and organics in anhydrous CP IDPs, so Febo is a presolar cometary organic (Matrajt et al. 2007, 2008) (Febo's D/H $\lesssim 300$ ‰, Matrajt et al. 2007).

In anhydrous CP IDPs, aliphatic hydrocarbon is the carrier of the deuterium-enrichments (Keller et al. 2004). On submicron size scales, D-enrichments range from subchondritic (−400 ‰) to strongly enriched ($\gtrsim +10{,}000$ ‰) (Keller et al. 2004; Messenger et al. 1996). In one anhydrous CP IDP fragment, high $^{15}N/^{14}N$ isotopic ratios occur in a more refractory phase than the D-rich material, perhaps bonded to the relatively rare aromatic hydrocarbons (Keller et al. 2004). Large variations in the D- and ^{15}N-enrichments in the matrices of anhydrous CP IDPs indicates that the organic materials have experienced various degrees of thermal processing and are a mixture of presolar and protoplanetary disk materials (Keller et al. 2004). Organics in *Stardust* samples appear to span anhydrous CP IDPs and primitive meteorites (Sandford et al. 2006; Kerridge 1999). Comparisons of *Stardust* organics with organics in anhydrous CP IDPs are advancing.

[11] Diffuse ISM organics contains abundant aliphatic and aromatic bonds (Pendleton and Allamandola 2002). Hydrocarbon C=C π^* bonds constitute polycyclic aromatic hydrocarbons (PAHs) (Ehrenfreund and Charnley 2000; Ehrenfreund et al. 2004; Li and Draine 2001). Hydrocarbon bonds also constitute hydrogenated amorphous carbon, which can be produced by proton-bombardment of amorphous carbon (Muñoz Caro et al. 2006).

2.5.6 *Reconciling Amorphous Carbon with Refractory Organics in Cometary Materials as Probed by IR Spectroscopy*

There is no spectral trace for refractory complex organics in cometary IR SEDs, even though refractory complex organic matter dominates (85 wt%) the carbonaceous matter in 1P/Halley and C-only grains (amorphous carbon) constitute only 8–10 wt% (Fomenkova et al. 1994; Fomenkova 1997, 1999). Intimate mixtures of amorphous carbon and silicates do fit cometary IR SEDs (Hanner et al. 1996). In contrast, laboratory synthesized refractory organics have problems when fitting IR SEDs. Mayo Greenberg's highly absorbing refractory organics have resonances either in the 10 μm region (Greenberg and Hage 1990) or in the 3–8 μm region (EUREKA organics, Greenberg et al. 1996) that are absent from cometary IR SEDs (Greenberg and Li 1999 *vs.* Harker et al. 2002 or Moreno et al. 2003). Tholin (Khare et al. 1990) is a laboratory synthesized refractory organic commonly used to produce the reddish color of outer icy solar system bodies. Tholin does not fit the IR SED of Hale-Bopp, either as discrete grains or as intimate mixtures (using Brugemann theory) (Harker et al. 2002).

Earlier reports of 'organic' 3.4 μm features in comets 1P/Halley, C/1989 X1 (Austin), C/1990 K1 (Levy) are interpreted as gas-phase methanol and other gas-phase species (Bockelée-Morvan et al. 1995). Even so, an 'organic' 3.4 μm feature is 'identified' in the mothercraft spectrum of the *Deep Impact*-induced coma of 9P/Tempel 1 (A'Hearn et al. 2005; Feaga et al. 2007).

The spectroscopic appearance of abundant amorphous carbon in comet comae may be reconciled with the *in situ* and laboratory investigations of refractory complex organics in *Stardust* samples and in anhydrous CP IDPs (Sect. 2.5.4) if the refractory complex organics have absorptivities similar to amorphous carbon, i.e., if the spectroscopic features of aliphatics and aromatics[12] in refractory complex organics are so weak as to not be discernible in cometary IR SEDs.

2.6 Phyllosilicates and Their Formation in 'Humid' Shocks

Phyllosilicates occur in a few otherwise anhydrous CP IDPs (Nakamura et al. 2005; Rietmeijer 1998; Wooden 2002), but most phyllosilicates reside in the denser hydrated IDPs (Bradley 1988; Sandford and Walker 1985). Wooden et al. (1999) sets limits of $<1\%$ of phyllosilicates in the coma of comet C/1995 O1 (Hale-Bopp). In contrast, Lisse et al. (2006) attributes 10% (weighted surface area) of *Deep Impact* ejecta and 18% of Hale-Bopp to the phyllosilicate smectite nontronite. Phyllosilicates are mentioned as a possible minor phase in the analyses of flyby mass spectrometry of Halley (Fomenkova et al. 1992a; Rietmeijer et al. 1989). *Stardust* samples from comet 81P/Wild 2 do not contain phyllosilicates (Brownlee et al. 2006; D. Brownlee and M. Zolensky, private communication).

Phyllosilicates are abundant in aqueously altered asteroidal materials (Krot et al. 1995; Zolensky and Browning 1997; Krot et al. 2000; Brearley 2006). In order that phyllosilicates form by aqueous alteration in comet nuclei, water ice must be heated to liquidus. Models for comet nuclei heating by ^{26}Al imply comet nuclei $\geq$20 km in diameter can reach temperatures of liquidus water (Merk and Prialnik 2006; Prialnik et al. 2008; see review by

[12] Although the sole 6.2 μm PAH band is claimed for *Deep Impact* and Hale-Bopp (Lisse et al. 2006, 2007), the group of bands characteristic of carbon skeletal bonds in PAH macromolecules, i.e., 6.2, 6.8, and 7.7 μm, are not yet identified with high signal-to-noise in comets (Crovisier and Bockelée-Morvan 2008). Small isolated PAH molecules probably do not survive more than $\sim$20 s in cometary comae at 1 AU (Joblin et al. 1997).

McKinnon et al. 2008). This implies that comets are collisional fragments of larger differentiated bodies, and dynamical models are in conflict about this topic as well as models for the formation of comet nuclei based on images of comet nuclei (Sect. 1.3).

Collisions between large nuclei are speculated to produce aqueous processing (Flynn et al. 2008), but the *Deep Impact* impact experiment showed that collisions are ineffective in heating a significant fraction of nuclear material because nuclear densities and heat conductivities are extremely low (Sugita et al. 2005). Hence, aqueous alteration in comet nuclei, and more specifically, selective aqueous alteration on submicron scales to produce only phyllosilicates, Fe-rich crystalline silicates, and carbonates but not other products of aqueous alteration, is incompatible with important aspects of cometary nuclei structure and evolution.

As an alternative to aqueous alteration on parent bodies, some types of phyllosilicates can form in water-rich shocks in the gas-phase nebula (Ciesla et al. 2003). Shocks are a favored mechanism for chondrule formation (Connolly and Love 1998; Desch and Connolly 2002; Connolly et al. 2006) and annealing crystalline silicates (Sects. 2.3.4, 2.3.6). Shocks in the 2–3 AU region are driven by gravitational instabilities in the disk at 5–10 AU, near or beyond Jupiter's orbit (Boss and Durisen 2005). The breaking shock wave models of Boss and Durisen (2005) can contribute to radial transport. Shocks might be sustained for 1–0.1 Myr for disk accretion rates of 10^{-6}–$10^{-7} M_{\odot}$ yr^{-1} (Boss and Durisen 2005). Also, shocks are triggered by proto-Jupiter and by x-ray flares (Desch et al. 2005).

Shocks occurring beyond the ice line (or snow line at ∼5 AU, Fig. 1) can form transform anhydrous silicates to phyllosilicates, specifically, olivines to serpentines (Ciesla et al. 2003). The inward march of icy planetesimals can pump up the water vapor content by factors of >500, so humid shocks may occur interior of the snow line where pre-shock temperatures are warmer and shock temperatures are higher due to higher disk surface densities. However, the kinetics of hydration make smectite harder to form in shocks than serpentine (S. Krot, private communication). So, compared to serpentine, smectite is more likely to be an aqueous alteration product rather than a shock product. *Stardust* samples from comet 81P/Wild 2 do not contain phyllosilicates, in contradiction to the identification in IR spectra of 9P/Tempel 1 by Lisse et al. (2006, 2007). *Stardust* samples contain chondrules, as well as significantly more inner solar system products than any other comet (Ishii et al. 2008; D. Brownlee, private communication). Since chondrule-formation is a late-stage phenomena, addition of some aqueously altered asteroidal materials, e.g., achondrite fragments, to the accretion region of comet 81P/Wild 2 would not be surprising, but this is not the case.

2.7 Iron Oxides and Iron Carbonates

In 1P/Halley, 1% are Fe-metal grains are expected to have more Ni (by comparison with chondritic materials), so perhaps these (Ni-poor) Fe-metal grains are iron oxide grains (Fomenkova et al. 1992b). A similarly minuscule fraction (∼1%) of 1P/Halley's grains are Fe-rich grains with high C/Fe ratios, which may be Fe-carbonates.

One magnetite grain (Fe_3O_4) is seen in a *Stardust* track (Flynn 2008). It may be a consequence of impact heating upon collection (similar to IDPs, Keller et al. 2004), or a product of aqueous alteration on comet 81P/Wild 2 (Bridges et al. 2008). However, partial aqueous alteration in cometary nuclei is problematic (Sect. 2.6). In the solar nebula, the formation of magnetite proceeds so slowly at low temperatures that only thin rims could have formed on metal grains (Fegley 2000). Whether these conditions lead to submicron-sized iron oxides, or whether these reactions proceed more efficiently under high humidity conditions, is conjecture.

2.8 Carbonates

In contrast to the scant evidence for cometary phyllosilicates and oxides in 1P/Halley, ~5 wt% (~15% by number) is attributed to Mg-carbonates (Fomenkova 1999; Fomenkova et al. 1992a). In *Stardust* samples of comet 81P/Wild 2, rare (a handful) 0.1–0.7 μm-sized carbonate grains are extracted from the tracks. However, many more smaller carbonate grains (<0.02 μm) tentatively are identified in the tracks (Sect. 1.3; Flynn et al. 2008). The carbonates preferentially are amongst the smallest grains (Flynn et al. 2008), similar to carbonates in 1P/Halley (Fomenkova et al. 1992a, 1992b).

The carbonate feature is at 6.8 μm, which is in the 5–8 μm region obscured by telluric water from ground-based observations. Therefore, ground-based IR spectra of comets do not sample carbonates and they are not discussed (Hanner and Bradley 2004; Harker et al. 2002). However, the 6.8 μm feature is tentatively identified in Kuiper Airborne Observatory spectra of 1P/Halley (Bregman et al. 1987; Bregman, private communication). A carbonate feature is claimed in *Spitzer* spectra of the *Deep Impact* ejecta of comet 9P/Tempel 1, comprising ~10% of the surface area of the small grain emission (Lisse et al. 2006).

If cometary carbonates formed by parent body aqueous alteration, then other aqueous minerals (Sect. 1.4) should be found in *Stardust* tracks in association with carbonates. If carbonates do not appear in consort with outer aqueous alteration products, as currently appears to be the case, then carbonates may have formed by non-equilibrium processes in the vapor phase. The traditional understanding is that carbonates cannot have formed by nebular processes because the carbon dioxide concentration (f_{CO_2}) is never high enough in the solar nebula (Armstrong et al. 1982; Zolensky and Browning 1997). However, laboratory experiments indicate that carbonates can form by non-equilibrium condensation in circumstellar environments with water vapor (Toppani et al. 2005). We champion Flynn et al. (2008)'s suggestion that Toppani's experiments support the idea that carbonates in comets are nebular grains.[13] We clarify that Toppani's work suggests that the nebular conditions of carbonate formation require transient heating events, lower than nebular pressures, rapid cooling, all in the presence of water vapor. Such conditions seem similar to those in the shocks that may form phyllosilicates (Sect. 2.6).

In addition to transient heating events, carbonates may form in disk winds or on longer time scales in the nebula at heliocentric distances of 2 AU $\lesssim r \lesssim$ 4 AU. For example, an isolated calcium carbonate ($CaCO_3$) is stable in a solar composition gas at $T < 450$ K and $P < 10^{-7}$ bar (Trivedi 1987; Lewis et al. 1979). Lewis et al. (1979) derive f_{CO_2} stability curves for carbonates at low pressures and moderately low temperatures ($P < 10^{-6}$ bar, $T < 400$ K). Lewis et al.'s carbonate stability curves may apply to rarefied conditions at 2–4 AU, i.e., at disk heights near the disk photosphere (away from the mid-plane), where gas temperatures are ~300–450 K and where the f_{CO_2} may be enhanced (Tscharnuter and Gail 2007; Wooden et al. 2007). The CO_2 fugacity (f_{CO_2}) at these disk radii is pumped up by a combination of carbon combustion interior to this zone and outward radial transport. In Trivedi's condensing wind model, phyllosilicates and carbonates form at similar distances ($\gtrsim$1.7 AU). Note that carbonate condensation at lower pressures nearer to the disk photosphere (i.e., further from the disk midplane) also favors the growth of small grains, such as seen in *Stardust* tracks. The suggestion that carbonates might form as nebular condensates needs to be revisited in the context current models for the protoplanetary disk chemistry (like

[13] Laboratory-condensed calcium oxide has a 6.8 μm band, which is claimed to be the 7 μm band in the *Spitzer* spectrum of *Deep Impact* (Kimura and Nuth 2005).

Tscharnuter and Gail 2007; H.-P. Gail, private communication). The viability of this suggestion enriches the view that grains previously discussed as products of aqueous alteration on either asteroids or comets instead could be nebular refractory grains.

3 Discussion

3.1 The Role of 'Interstellar' Carbon in Condensing 'Nebular' Crystals

Amorphous carbon is an 'interstellar' source (Sect. 2.5.1). Amorphous carbon is a significant constituent of the surfaces of Centaurs and Trans-Neptunian Objects (TNOs), ranging from 10% to 90% of their surface compositions, with Centaurs having on average higher relative abundances (∼70%) than TNOs (∼30%) (statistics computed from articles by Boehnhardt et al. 2003 and Dotto et al. 2003). The reflection spectrum of the nucleus of comet 162P/Siding Spring suggest an amorphous carbon dominated surface (Campins et al. 2006). The composition of comets, KBOs, and Centaurs substantiates the concept that the outer disk is rich in carbon and that carbon is available to 'feed' the inner disk. The evidence that cometary nuclei are heterogeneous, and, specifically, the nucleus of 9P/Tempel 1 possesses surface layers and pockets dominated by amorphous carbon (Sect. 2.5.2), means that regions of the inner disk could have experienced fluctuating carbon enhancements.

When inward accretion carries carbon-rich grains interior to the water dissociation line ($\gtrsim$1000 K), OH^- radicals react with carbon on grain surfaces and oxidize the C to CO or CO_2 (Gail 2002). Since CO is very tightly bound, this removes oxygen from the gas phase, thus lowering the oxygen fugacity. As discussed in Sect. 1.4.1, the canonical solar nebula has a low oxygen fugacity, which favors the formation of extremely Mg-rich crystalline silicates (Sect. 2.3.4). Extremely Mg-rich olivines and pyroxenes are numerous in *Stardust* return samples from comet 81P/Wild 2 (Zolensky et al. 2007). They exist in select anhydrous CP IDPs (Bradley et al. 1999b), and comprise the matrix of the chondrite Acfer 094 (a type 3.0, least thermally and least aqueously altered chondrite) (Wooden et al. 2005; Scott and Krot 2005b; Zolensky et al. 2007). Slower condensation in dust-enriched, low oxygen fugacity environs forms submicron to 10 μm-sized Mg-rich crystalline silicates [$0.95 \lesssim x = y \lesssim 0.8$] (Sect. 1.4.1). In summary, the inward transport of amorphous carbon can contribute to the low oxygen fugacity conditions that produce the extremely Mg-rich and Mg-rich crystalline silicates, as well as enhancing CO and CO_2.

Carbonates can form in regions of enhanced f_{CO_2}, at moderate temperatures (2–3 AU) and closer to the disk photosphere at more rarefied pressures (Sect. 2.8). Historically, carbonates are thought to never condense from nebular gases because the carbon dioxide fugacity is always too low (in 'closed box' equilibrium models). However, we hypothesize carbonates condense from the nebula (Sect. 2.8), in the ∼2–3 AU region for the disk model in Fig. 1, assisted by high carbon-dioxide fugacity conditions that result from the combustion (oxidation) of carbon and outward radial transport (Sect. 1.4.1). According to disk models (Tscharnuter and Gail 2007), this could have happened at 0.5 Myr, prior to major chondrule-forming epochs.

3.2 Humid Conditions Produce Fe-Rich Silicates and Phyllosilicates

Recently, Fe-bearing crystalline silicates, and (possibly) phyllosilicates (Sect. 2.6), have become notable cometary refractory grains. Their placement in Fig. 1 is open for discussion.

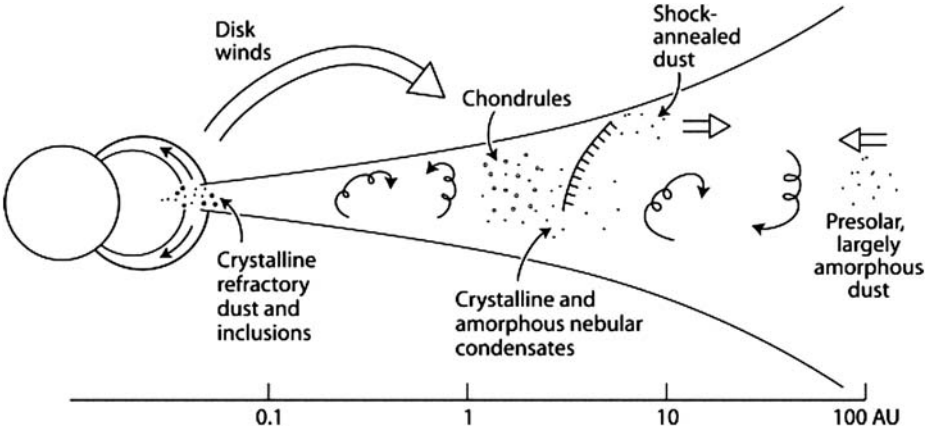

Fig. 4 Schematic diagram showing how interstellar largely amorphous dust (called 'presolar') may be thermally processed in the nebular disk prior to accretion into planetesimals. (Fig. 1 from Scott and Krot 2005a)

As an alternative to aqueous alteration, Fe-bearing crystalline silicates condense in the nebula under high oxygen fugacity conditions (Sects. 1.4.2, 2.3.6). If the high oxygen fugacity is a consequence of fluctuating very high water vapor content or high water vapor and the simultaneous evaporation of already existing dust grains, then Fe-rich crystalline silicates form interior to the ice line (*ice* in Fig. 1). The inward migration of icy bodies (Fig. 2) can stochastically bring water into the hotter regions where, under equilibrium conditions, water vapor is depleted (e.g., Tscharnuter and Gail 2007). Icy planetesimal formation predicates fluctuating nebular water vapor (Sect. 1.4), and implies nebular formation of Fe-bearing and Fe-rich crystalline silicates is possible (Sect. 1.4.2).

Outside the snow line, water-rich shocks can increase the Fe-content to yield moderately Fe-rich silicates (Fedkin et al. 2008). Humid shocks also form phyllosilicates from anhydrous precursors (Ciesla et al. 2003), with some caveats (Sect. 2.6). The time scales for Fe-bearing crystalline formation may be earlier than chondrule-forming events (Sect. 3.3), based on their high abundance relative to chondrules in *Stardust* samples.

3.3 Chondrules Suggest Oxygen Fugacity Lowered by the Influx of Carbon

When compared to comets, chondrites are deficient in amorphous or poorly graphitized carbon. Since chondrites were processed at high temperatures in the solar nebula, this suggests that carbon in grains is carried into the inner hot solar nebula and destroyed or transformed prior to its incorporation into asteroids.

There are two types of chondrules, type I (FeO-poor and Mg-rich) and type II (FeO-rich and Mg-poor). Only 5% of amorphous carbon needs to be added to the siliceous mixture to produce type I chondrules in the laboratory by melting (Connolly et al. 1994). Type I chondrules have about ten times more organic matter than type II (Hewins 1997). Hewins (1997) makes the case that type I chondrules formed under conditions that were either dryer and/or more rich in organics and type II chondrules formed under higher water vapor conditions and/or with less available carbon.

3.4 Many Comets Preferentially Contain Low Oxygen Fugacity Grains

If comets do not contain asteroidal materials and comets themselves were not aqueously altered, then we can conclude cometary refractory grains that are from 'nebular' sources

are predominantly grains present in the protoplanetary disk prior to and during chondrule melting, and during the accretion of (chondrules plus matrix into) chondrites. Cometary refractory nebular grains are *pre-accretionary* nebular grains (with respect to chondrites).

If low oxygen fugacity grains dominate comets, yet chondrules have grains of both low and high oxygen fugacity, then radial transport out to the comet forming zone is more efficient for low oxygen fugacity nebular grains. The outward radial transport efficiency diminishes as the disk evolves, with the declining mass accretion rate or by 'gaps' produced by giant planet formation. Taken together, the properties of refractory grains in comets might suggest that many comets accreted primary nebular condensates. *Stardust* samples from comet 81P/Wild 2, however, show this comet accreted CAI-grains and a few chondrules (type I and type II), so the accretion of 81P/Wild 2 had to extend to at least chondrule-forming epochs (∼1.5 Myr after CAIs).

4 Summary: Cometary Pre-Accretionary 'Nebular' Grains

By comparing cometary and chondritic materials, we deduce that cometary 'nebular' refractory grains are pre-accretionary grains. Setting the details of carbonate formation aside (Sect. 2.8), the Mg-rich crystalline silicates and the Fe-bearing crystalline silicates can be explained by their formation or transformation in the gas-phase nebula under variable water vapor content in the nebula.

Cometary phyllosilicates might be products of water-rich shocks. However, matrixes of primitive meteorites have Mg-Fe silicates but no phyllosilicates. Moreover, if the (contentious) identification of cometary smectite holds up (Sects. 1.3, 2.6), from the kinetics of hydration, smectites are more likely fragments of aqueously altered asteroids. Chondrule formation is a late-stage phenomena. This is why addition of some aqueously altered asteroidal materials, in particular asteroids dated the same age as the oldest CAIs, to the accretion regions of comets should not be a surprise. Nevertheless, chondrules are rare and phyllosilicates are absent in *Stardust* samples, so even though comet 81P/Wild 2 appears to have more inner solar system grains than any other comet, its grains appear to be dominantly pre-accretionary.

The canonical low oxygen fugacity solar nebula (low water vapor content) favors the condensation of Mg-rich crystalline silicates, and the annealing of Fe-Mg amorphous silicates into Mg-rich crystalline silicates with reduced Fe-metal. Arid shocks can anneal submicron to micron-sized amorphous Fe-Mg silicates into Mg-rich crystalline silicates (Wooden et al. 2007; Sect. 1.4.1). An low water vapor content solar nebula selectively produces Fe metal grains, which can react with sulfur in the gas phase to produce FeS.

Carbon combustion, which contributes to the low oxygen fugacity nebula, enhances the f_{CO_2} (as well as CO) and potentially provides a pathway for the formation of carbonates from the gas phase. Although carbonates previously are attributed to hydration processes on parent bodies, more specific modeling efforts are needed to assess whether tiny carbonates are 'nebular' refractory grains from more rarefied regions closer to the disk photosphere.

In chondrites, Fe-rich silicates and phyllosilicates can be ascribed to either nebular (high water vapor content, high oxygen fugacity) or aqueous alteration on parent bodies (asteroids). By contrasting comets with chondrites, the absence of other parent body aqueous alteration products in comets strongly suggests that these cometary 'nebular' grains formed by gas-phase processes characterized by high water vapor content. If comets do not contain parent-body aqueously altered materials (asteroidal materials), then cometary grains represent pre-accretionary (pre-asteroidal) materials. Only 4 out of ∼4000 asteroidal samples

are not aqueously or thermally altered by their residence inside asteroids (Scott and Krot 2005a). Cometary pre-accretionary refractory nebular grains better sample disk processes prior to and during chondrule- and asteroid-formation because they have suffered little or no post-accretion alteration in comet nuclei.

Acknowledgements I am grateful for discussions with colleagues including Michael S. Kelley, Gary Huss, Sasha Krot, Mike Zolensky, and Don Brownlee. I thank Sasha Krot for his time in reviewing this article, and to Toby Owen for his encouragement in preparing the manuscript. This treatise is dedicated to Hans Balsiger who motivated the convening of this ISSI workshop of a small group of scientists with diverse interests who gathered to discuss recent findings and from these discussions formulated new understandings. The author acknowledges participation in *Spitzer* GO comet programs for partial support in this work.

References

M.F. A'Hearn et al., Science **310**, 258–264 (2005)
C.M.O'd Alexander, A.P. Boss, L.P. Keller, J.A. Nuth, A. Weinberger, in *Protostars and Planets V*, ed. by B. Reipurth, D. Jewitt, K. Keil (University of Arizona Press, Tucson, 2007), pp. 801–813
J.T. Armstrong, G.P. Meeker, J.C. Huneke, G.J. Wasserburg, Geochim. Cosmochim. Acta **46**, 575–595 (1982)
B. Begemann, J. Dorschner, T. Henning, H. Mutschke, E. Thamm, Astrophys. J. **423**, L71–L74 (1994). http://www.astro.uni-jena.de/Laboratory/OCDB/index.html
K.R. Bell, P.M. Cassen, H.H. Klahr, Th. Henning, Astrophys. J. **486**, 372–387 (1997)
K.R. Bell, P.M. Cassen, J.T. Wasson, D.S. Woolum, in *Protostars and Planets IV*, ed. by V. Mannings, A.P. Boss, S.S. Russell (University of Arizona Press, Tucson, 2000), pp. 897
M.J. Belton, P. Thomas, J. Veverka et al., Icarus **191**, 573–585 (2007)
D. Bockelée-Morvan, T.Y. Brooke, J. Crovisier, Icarus **116**, 18–39 (1995)
D. Bockelée-Morvan, D. Gautier, F. Hersant, J.-M. Hure', F. Robert, Astron. Astrophys. **384**, 1107–1118 (2002)
H. Boehnhardt et al., Earth, Moon, Planets **92**, 145–156 (2003)
A.P. Boss, R.H. Durisen, in *Chondrites and the Protoplanetary Disk*, vol. 341, ed. by A.N. Krot, E.R.D. Scott, B. Reipurth (ASP, San Francisco, 2005), pp. 821–838
J.P. Bradley, Geochim. Cosmochim. Acta **52**, 889–900 (1988)
J.P. Bradley, Science **265**, 925–929 (1994a)
J.P. Bradley, H.J. Humecki, M.S. Germani, Astrophys. J. **394**, 643–651 (1992)
J.P. Bradley, Geochim. Cosmochim. Acta **58**, 2123–2134 (1994b)
J.P. Bradley, T. Snow, D.E. Brownlee, L.P. Keller, G.J. Flynn, M. Miller, Lun. Planet. Sci. **29**, 1737 (1998)
J.P. Bradley, L.P. Keller, J. Gezo, T. Snow, G.J. Flynn, D.E. Brownlee, J. Bowey, Lun. Planet. Sci. **30**, 1835 (1999a)
J.P. Bradley, T.P. Snow, D.E. Brownlee, M.S. Hanner, in *Solid Interstellar Matter: The ISO Revolution*, ed. by L. d'Hendecourt, C. Joblin, A. Jones (EDP Sciences and Springer, Les Houches, 1999b), pp. 297–315
J.P. Bradley, L.P. Keller, T.P. Snow, M.S. Hanner, G.J. Flynn et al., Science **285**, 1716–1718 (1999c)
A.J. Brearley, in *Meteorites and the Early Solar System II*, ed. by D.S. Lauretta, H.Y. McSween Jr. (University of Arizona Press, Tucson, 2006), pp. 587–624
J.D. Bregman, F.C. Witteborn, L.J. Allamandola, H. Campins, D.H. Wooden, D.M. Rank, M. Cohen, A.G.G.M. Tielens, Astron. Astrophys. **187**, 616–620 (1987)
J.C. Bridges, H.G. Changela, J.D. Carpenter, I.A. Franchi, Lun. Planet. Sci. **39**, 2193 (2008)
D.E. Brownlee, D.J. Joswiak, D.J. Schlutter, R.O. Pepin, J.P. Bradley, S.G. Love et al., Lun. Planet. Sci. **26**, 183–184 (1995)
D.E. Brownlee, D.J. Joswiak, J.P. Bradley, Lun. Planet. Sci. **30**, 2031 (1999)
D.E. Brownlee, D.J. Joswiak, J.P. Bradley, G. Matrajt, D.H. Wooden, Lun. Planet. Sci. **36**, 2391 (2005)
D. Brownlee et al., Science **314**, 1711 (2006)
D.E. Brownlee, D. Joswiak, G. Matrajt, J. Bradley, D.S. Ebel, Lun. Planet. Sci. **39**, 1978 (2008)
J.R. Brucato, V. Mennella, L. Colangeli, A. Rotundi, P. Palumbo, Planet. Space Sci. **50**, 829–837 (2002)
J.R. Brucato, G. Strazzula, G. Baratta, L. Colangeli, Astron. Astrophys. **413**, 395–401 (2004)
I. Busko, D. Lindler, M.F. A'Hearn, R.L. White, Icarus **191**, 210–222 (2007)
H. Campins, J. Ziffer, J. Licandro, N. Pinilla-Alonso, Y. Fernández, J. de León, T. Mothé-Diniz, R.P. Binzel, Astron. J. **132**, 1346–1353 (2006)
P. Carrez, K. Demyk, P. Cordier, L. Gengembre, J. Grimblot, L. d'Hendecourt, A.P. Jones, H. Lerouz, Meteor. Planet. Sci. **37**, 1599–1614 (2002)

P. Cassen, in *Workshop on Parent-Body and Nebular Modifications of Chondritic Materials*, ed. by M.E. Zolensky, A.N. Krot, E.R.D. Scott. LPI Tech. Report 97-02, Part 2 Summary of Technical Sessions (LPI, Houston, 1997), pp. 6–7
S. Chakraborty, J. Geophys. Res. **102**, 12317–12332 (1997)
S.B. Charnley, Space Sci. Rev. (2008), this issue
S. Charnoz, A. Morbidelli, Icarus **188**, 468–480 (2007)
I. Cherchneff, Astron. Astrophys. **224**, 379–382 (1995)
M. Chi, H. Ishii, A. Toppani, Z.R. Dai, D.J. Joswiak, H. Leroux, M. Zolensky, L.P. Keller, N.D. Browning, J.P. Bradley, Lun. Planet. Sci. **38**, 2010 (2007)
M. Chi, H. Ishi, Z.R. Dai, S.B. Simon, N.D. Browning, J.P. Bradley, Lun. Planet. Sci. **39**, 2321 (2008)
K.M. Chick, P.M. Cassen, Astrophys. J. **477**, 398–409 (1997)
H. Chihara, C. Koike, A. Tsuchiyama, S. Tachibana, D. Sakamoto, Astron. Astrophys. **391**, 267–273 (2002)
F.J. Ciesla, D.S. Lauretta, B.A. Cohen, L.L. Hood, Science **299**, 549–552 (2003)
L. Colangeli, Th. Henning, J.R. Brucato, D. Clément, D. Fabian et al., Astron. Astrophys. Rev. **11**, 97–152 (2003)
H.C. Connolly Jr., S.G. Love, Science, 62–67 (1998)
H.C. Connolly Jr., R.H. Hewins, R.D. Ash, B. Zanda, G.E. Lofgren, M. Bourot-Denise, Nature **371**, 136–139 (1994)
H.C. Connolly Jr., S.J. Desch, R.D. Ash, R.H. Jones, in *Meteorites and the Early Solar System II*, ed. by D.S. Lauretta, H.Y. McSween Jr. (University of Arizona Press, Tucson, 2006), pp. 383–397
J. Crovisier, K. Leech, D. Bockelée-Morvan, T.Y. Brooke, M.S. Hanner et al., Science **275**, 1904–1907 (1997)
J. Crovisier, in *Proc. XVIIIemes Rencontres de Blois. Planetary Science: Challenges and Discoveries*. eprint arXiv:astro-ph/0703785 (2007)
J. Crovisier, D. Bockelée-Morvan, Icarus (2008, in press)
J.N. Cuzzi, K.J. Zahnle, Astrophys. J. **614**, 490–496 (2004)
J.N. Cuzzi, M.I. Petaev, F.J. Ciesla, A.N. Krot, E.R.D. Scott, Lun. Planet. Sci. **36**, 2095 (2005a)
J.N. Cuzzi, F.J. Ciesla, M.I. Petaev, A.N. Krot, E.R.D. Scott, S.J. Weidenschilling, in *Chondrites and the Protoplanetary Disk*, vol. 341, ed. by A.N. Krot, E.R.D. Scott, B. Reipurth (ASP, San Francisco, 2005b), p. 732
K.E. Cyr, W.D. Sears, J.I. Lunine, Icarus **135**, 537–548 (1998)
C. Davoisne, Z. Djouadi, H. Leroux, L. d'Hendecourt, A. Jones, D. Deboffle, Astron. Astrophys. **448**, L1–L4 (2006)
B.T. De Gregorio, N.D. Bassim, G.D. Cody, L.R. Nittler, R.M. Stroud, T.J. Zega, Lun. Planet. Sci. **39**, 2139 (2008)
S.J. Desch, Astrophys. J. **671**, 878–893 (2008)
S.J. Desch, H.C. Connolly Jr., Meteor. Planet. Sci. **37**, 183–207 (2002)
S.J. Desch, F.J. Ciesla, L.L. Hood, T. Nakamoto, in *Chond* (2005), pp. 849–872
J. Dorschner, B. Begemann, T. Henning, C. Jaeger, H. Mutschke, Astron. Astrophys. **300**, 503–520 (1995)
E. Dotto, M.A. Barucci, C. de Bergh, Earth, Moon, Planets **92**, 157–167 (2003)
C. Dukes, R. Baragiola, L. McFadden, J. Geophys. Res. **104**, 1865–1872 (1999)
D.S. Ebel, L. Grossman, Geochim. Cosmochim. Acta **64**, 339–366 (2000)
C. Engrand, K.D. McKeegan, L.A. Leshin, J.P. Bradley, D.E. Brownlee, Lun. Planet. Sci. **30**, 1690 (1999)
P. Ehrenfreund, S.B. Charnley, Annu. Rev. Astron. Astrophys. **38**, 427–483 (2000)
P. Ehrenfreund, S.B. Charnley, D.H. Wooden, in *Comets II*, ed. by M.C. Festou, H.U. Keller, H.A. Weaver, (University of Arizona Press, Tucson, 2004), pp. 115–133
L.M. Feaga, O. Groussin, J. Sunshine, M.F. A'Hearn, AAS DPS **39**, #21.05 (2007)
A.V. Fedkin, L. Grossman, in *Meteorites and the Early Solar System II*, ed. by D.S. Lauretta, H.Y. McSween Jr. (University of Arizona Press, Tucson, 2006), pp. 279–294
A.V. Fedkin, F.J. Ciesla, L. Grossman, Lun. Planet. Sci. **39**, 1834 (2008)
B. Fegley Jr., Space Sci. Rev. **90**, 239–252 (1999)
B. Fegley Jr., Space Sci. Rev. **92**, 177–200 (2000)
B. Fegley Jr., H. Palme, Earth Planet. Sci. Lett. **72**, 311–326 (1985)
G.J. Flynn, L.P. Keller, M. Feser, S. Wirick, C. Jacobsen, Geochim. Cosmochim. Acta **67**, 4719–4806 (2003)
G.J. Flynn, H. Leroux, K. Tomeoka et al., Lun. Planet. Sci. **39**, 1979 (2008)
G.J. Flynn, L.P. Keller, C. Jacobsen, S. Wirick, Adv. Space Res. **33**, 57–66 (2004)
G.J. Flynn, Earth, Moon, Planets **102**, 447–459 (2008)
M.S. Fomenkova, in *From Stardust to Planetesimals*, vol. 122, ed. by Y.J. Pendleton, A.G.G.M. Tielens (ASP, San Francisco, 1997), pp. 415–421
M.S. Fomenkova, Space Sci. Rev. **90**, 109–114 (1999)
M.S. Fomenkova, S. Chang, Lun. Planet. Sci. **26**, 431–432 (1995)
M.N. Fomenkova, J.F. Kerridge, K. Marti, L.-A. McFadden, Science **258**, 266–269 (1992a)

M.N. Fomenkova, J.F. Kerridge, K. Marti, L. McFadden, Lun. Planet. Sci. **23**, 381–382 (1992b)
M.N. Fomenkova, S. Chang, L.M. Mukhin, Geochim. Cosmochim. Acta **58**, 4503–4512 (1994)
R. Furusho et al., Icarus **191**, 454–458 (2007)
H.-P. Gail, Astron. Astrophys. **378**, 192–213 (2001)
H.-P. Gail, Astron. Astrophys. **390**, 253–265 (2002)
H.-P. Gail, Astron. Astrophys. **413**, 571–591 (2004)
H.-P. Gail, E. Sedlmayr, Astron. Astrophys. **206**, 153–168 (1988)
H.-P. Gail, E. Sedlmayr, Astron. Astrophys. **347**, 594–616 (1999)
J.M. Greenberg, J.I. Hage, Astrophys. J. **361**, 260–274 (1990)
J.M. Greenberg, A. Li, Planet. Space Sci. **47**, 787–795 (1999)
J.M. Greenberg, A. Li, T. Yamamoto, T. Kozasa, in *Physics, Chemistry, and Dynamics of Interplanetary Dust*, vol. 104 (ASP, San Francisco, 1996), pp. 497–506
L. Grossman, Geochim. Cosmochim. Acta **36**, 567–619 (1972)
M.S. Hanner, D.K. Lynch, R.W. Russell, Astrophys. J. **425**, 274–285 (1994)
M.S. Hanner, D.K. Lynch, R.W. Russell, J.A. Hackwell, R. Kellogg, D. Blaney, Icarus **124**, 344–351 (1996)
M.S. Hanner, J.P. Bradley, in *Comets II*, ed. by M.C. Festou, H.U. Keller, H.A. Weaver (University of Arizona Press, Tucson, 2004), pp. 555–564
D.E. Harker, S. Desch, Astrophys. J. **565**, L109–L112 (2002)
D.E. Harker, D.H. Wooden, C.E. Woodward, C.M. Lisse, Astrophys. J. **580**, 579–597 (2002)
D.E. Harker, D.H. Wooden, C.E. Woodward, C.M. Lisse, Astrophys. J. **615**, 1081 (2004)
D.E. Harker, C.E. Woodward, D.H. Wooden, Science **310**, 278–280 (2005)
D.E. Harker, C.E. Woodward, D.H. Wooden, R.S. Fisher, C.A. Trujillo, Icarus **191**, 432–453 (2007)
Th. Henning, H. Mutschke, C. Jäger, in *Astrochemistry: Recent Successes and Current Challenges*, ed. by D.C. Lis, G.A. Blake, E. Herbst. IAU Symp., vol. 231 (Cambridge University Press, Cambridge, 2005), pp. 457–468
R.H. Hewins, Annu. Rev. Earth Planet. Sci. **25**, 61–83 (1997)
W.M. Irvine, F.P. Schloerb, J. Crovisier, B. Fegley Jr., M.J. Mumma, in *Protostars and Planets IV*, ed. by V. Mannings, A.P. Boss, S.S. Russell (University of Arizona Press, Tucson, 2000), pp. 1159–1200
H.A. Ishii, J.P. Bradley, Z.R. Dai, M. Chi, A.T. Kearsley, M.J. Burchell, N.D. Browning, F. Molster, Science **319**, 447–450 (2008)
C. Jäger, H. Mutschke, Th. Henning, Astron. Astrophys. **332**, 291–299 (1998)
C. Jäger, D. Fabian, F. Schrempel, J. Dorschner, Th. Henning, W. Wesch, Astron. Astrophys. **401**, 57–65 (2003)
E.K. Jessberger, J. Kissel, in *Comets in the Post-Halley Era*, vol. 2 (1991), pp. 1075–1092
C. Joblin, P. Boissel, P. de Parseval, Planet. Space Sci. **45**, 1539–1542 (1997)
A.P. Jones, J. Geophys. Res. **105**, 10257–10268 (2000)
D.J. Joswiak, G. Matrajt, D.E. Brownlee, A.J. Westphal, C.J. Snead, Lun. Planet. Sci. **38**, 2142 (2007)
T. Kadono, S. Sugita, S. Sako, T. Ootsubo, M. Honda, H. Kawakita, T. Miyata, R. Furusho, J. Watanabe, Astrophys. J. **661**, L89–L92 (2007)
C. Kaito, Y. Miyazaki, A. Kumamoto, Y. Kimura, Astrophys. J. **666**, L57–L60 (2007)
Ch. Keller, H.-P. Gail, Astron. Astrophys. **415**, 1177–1185 (2004)
L.P. Keller, S. Messenger, Lun. Planet. Sci. **35**, 1985 (2004)
L.P. Keller, S. Messenger, Lun. Planet. Sci. **39**, 2347 (2008)
H.U. Keller, L. Jorda, M. Küppers, P.J. Gutierrez, S.F. Hviid et al., Science **310**, 281–283 (2005)
L.P. Keller, J.P. Bradley, J. Bouwman, F.J. Molster, L.B.F.M. Waters, G.J. Flynn, T. Henning, H. Mutschke, Lun. Planet. Sci. **31**, 1860 (2000)
L.P. Keller, S. Hony, J.P. Bradley, F.J. Molster, L.B.F.M. Waters et al., Nature **417**, 148–150 (2002)
L.P. Keller, S. Messenger, G.J. Flynn, S. Clemett, S. Wirick, C. Jacobsen, Geochim. Cosmochim. Acta **68**, 2577–2589 (2004)
L.P. Keller, S. Messenger, R. Christoffersen, Lun. Planet. Sci. **36**, 2088 (2005)
M.S. Kelley, D.H. Wooden, Space Sci. Rev. (2008, submitted)
F. Kemper, L.B.F.M. Waters, A. de Koter, A.G.G.M. Tielens, Astron. Astrophys. **369**, 132–141 (2001)
F. Kemper, W.J. Vriend, A.G.G.M. Tielens, Astrophys. J. **609**, 826–837 (2004)
F. Kemper, W.J. Vriend, A.G.G.M. Tielens, Astrophys. J. **633**, 534–534 (2005)
J.F. Kerridge, Space Sci. Rev. **90**, 275–288 (1999)
B.N. Khare, W.R. Thompson, C. Sagan, E.T. Arakawa, C. Meisse, I. Gilmour, Lun. Planet. Sci. **21**, 627 (1990)
Y. Kimura, J.A. Nuth III, Astrophys. J. **630**, 637–641 (2005)
H. Kimura, T. Chigai, T. Yamamoto, Astron. Astrophys. **482**, 305–307 (2008)
N.T. Kita, G.R. Huss, S. Tachibana et al., in *Chondrites and the Protoplanetary Disk*, vol. 341, ed. by A.N. Krot, E.R.D. Scott, B. Reipurth (ASP, San Francisco, 2005), pp. 558–587

W. Kley, D.N.C. Lin, Astrophys. J. **397**, 600–612 (1992)
C. Koike, H. Chihara, A. Tsuchiyzma, H. Suto, H. Sogawa, H. Okuda, Astron. Astrophys. **399**, 1101–1107 (2003)
L. Kolokolova, H. Kimura, N. Kiselev, V. Rosenbush, Astron. Astrophys. **463**, 1189–1196 (2007)
A.N. Krot, E.R.D. Scott, M.E. Zolensky, Meteorit **30**, 748–775 (1995)
A.N. Krot, B. Fegley Jr., K. Lodders, H. Palme, in *Protostars and Planets IV*, ed. by V. Mannings, A.P. Boss, S.S. Russell (University of Arizona Press, Tucson, 2000), pp. 1019–1054
A.N. Krot, M.I. Petaev, P.A. Bland, Antarct. Meteor. Res. **17**, 154–172 (2004)
A.N. Krot, I.D. Hutcheon, H. Yurimoto, J.N. Cuzzi, K.D. McKeegan, E.R.D. Scott, G. Libourel, M. Chaussidon, J. Aléon, M.I. Pataev, Astrophys. J. **662**, 1333–1342 (2005)
A.N. Krot, K.D. McKeegan, G.R. Huss, K. Liffman, S. Sahijpal, I.D. Hutcheon, G. Srinivasan, Astrophys. J. **639**, 1227–1237 (2006)
M. Küppers, I. Bertini, S. Fornasier, P.J. Gutierrez, S.F. Fviid et al., Nature **437**, 987–990 (2005)
P. Lamy, I. Toth, Y.R. Fernandez, H.A. Weaver, in *Comets II*, ed. by M.C. Festou, H.U. Keller, H.A. Weaver (University of Arizona Press, Tucson, 2005), pp. 223–264
L. Lemelle, F. Guyot, H. Leroux, G. Libourel, Am. Min. **86**, 47–54 (2001)
J.S. Lewis, S.S. Barshay, B. Noyles, Icarus **37**, 190–206 (1979)
A. Li, B.T. Draine, Astrophys. J. **550**, L213–L216 (2001)
A. Li, J.M. Greenberg, Astrophys. J. **498**, L83–L87 (1998)
C.M. Lisse et al., Science **313**, 635–640 (2006)
C.M. Lisse, K.E. Kraemer, J.A. Nuth III, A. Li, D. Joswiak, Icarus **187**, 69–86 (2007)
I. Mann, A. Czechowski, H. Kimura, M. Köhler, T. Minato, T. Yamamoto, in *IAU Symp. 229, Asteroids, Comets, and Meteors*, ed. by L. Daniela, M.S. Ferraz, F.J. Angel (Cambridge University Press, Cambridge, 2005), pp. 41–65
B. Marty, R.L. Palma, R.O. Pepin, L. Zimmermann, D.J. Schlutter et al., Science **319**, 75–78 (2008)
G. Matrajt, S. Wirick, M. Ito, S. Messenger, D. Brownleee, D. Joswiak, Lun. Planet. Sci. **38**, 1201 (2007)
G. Matrajt, M. Ito, S. Wirick, S. Messenger, D.E. Brownlee, D. Joswiak, G. Flynn, S. Sandford, C. Snead, A. Westphal, Meteor. Planet. Sci. **43**, 315–334 (2008)
J. Matzel, Z.R. Dai, N. Teshich, I. Hutcheon, P. Weber, J.P. Bradley, Lun. Planet. Sci. **39**, 2525 (2008)
W.B. McKinnon, D. Prialnik, S.A. Stern, A. Coradini, in *The Solar System Beyond Neptune*, ed. by M.A. Barucci, H. Boehnhardt, D.P. Cruikshank, A. Morbidelli (University of Arizona Press, Tucson, 2008), pp. 213–242
R. Merk, D. Prialnik, Icarus **183**, 283–245 (2006)
S. Messenger, R.M. Walker, S.J. Clemett, R.N. Zare, Lun. Planet. Sci. **27**, 867–868 (1996)
S. Messenger, L.P. Keller, F.J. Stadermann, R.M. Walker, E. Zinner, Science **300**, 105–108 (2003)
T. Mikouchi, O. Tachikawa, K. Hagiya, K. Ohsumi, Y. Suzuki, K. Uesugi, A. Takeuchi, M.E. Zolensky, Lun. Planet. Sci. **38**, 1338 (2007)
M. Min, J.W. Hovenier, A. de Koter, L.B.F.M. Waters, C. Dominik, Icarus **179**, 158–173 (2005)
M. Min, L.B.F.M. Waters, A. de Koter, J.W. Hovenier, L.P. Keller, F. Marwick-Kemper, Astron. Astrophys. **462**, 667–676 (2007)
F.J. Molster, A. Demyk, L. d'Hendecourt, J.P. Bradley, L. Bonal, J. Borg, Lun. Planet. Sci. **34**, 1148 (2003)
A. Morbidelli, in *Trans-Neptunian Objects and Comets*, ed. by D. Jewitt, A. Morbidelli, H. Rauer. Saas-Fee Advanced Course, vol. 35 (Springer, Berlin, 2006). arXiv:astro-ph/0512256
F. Moreno, O. Muñoz, R. Vilaplana, A. Molina, Astrophys. J. **595**, 522–530 (2003)
G.M. Muñoz Caro, G. Matrajt, E. Dartois, M. Nuevo, L. D'Hendecourt, D. Deboffle, G. Montagnac, N. Chauvin, C. Boukari, D. Le Du, Astron. Astrophys. **459**, 147–159 (2006)
T. Nakamura, M. Zolensky, M. Sekiya, R. Okazaki, K. Nagao, Meteor. Planet. Sci. **38**, 243–350 (2003)
K. Nakamura, S. Messenger, L.P. Keller, Lun. Planet. Sci. **36**, 1824 (2005)
T. Nakamura, T. Noguchi, A. Tsuchiyama, T. Ushikubo, N.T. Kita et al., Lun. Planet. Sci. **39**, 1695 (2008)
J.A. Nuth III, A.J. Brearley, E.R.D. Scott, in *Ch* (2005), pp. 675–700
J.A. Nuth, N.M. Johnson, Icarus **180**, 243–250 (2006)
H. Palme, B. Fegley Jr., Earth Planet. Sci. Lett. **101**, 180–195 (1989)
Y.J. Pendleton, L.J. Allamandola, Astrophys. J. Suppl. **138**, 75–98 (2002)
M.I. Petaev, J.A. Wood, Meteor. Planet. Sci. **33**, 1123–1137 (1998)
J.B. Pollack, D. Hollenbach, S. Beckwith, D.P. Simonelli, T. Roush, W. Fong, Astrophys. J. **421**, 615–639 (1994)
D. Prialnik, M. Podolak, Space Sci. Rev. **90**, 169–178 (1999)
D. Prialnik, G. Sarid, E.D. Rosenberg, R. Merk, Space Sci. Rev. (2008), this issue. doi:10.1007/s11214-007-9301-4
F.J.M. Rietmeijer, in *Planetary Materials, Rev. in Mineralogy*, vol. 36, ed. by J.J. Papike (Mineral. Soc. Am. Washington, 1998), pp. 2-1–2-95

F.J. Rietmeijer, L.M. Mukhin, M.N. Fomenkova, E.N. Evlanov, Lun. Planet. Sci. **20**, 904 (1989)
F. Robert, in *Meteorites and the Early Solar System II*, ed. by D.S. Lauretta, H.Y. McSween Jr. (University of Arizona Press, Tucson, 2006), pp. 341–351
S.A. Sandford, R.M. Walker, Astrophys. J. **291**, 838–851 (1985)
S.A. Sandford et al., Science **314**, 1720–1724 (2006)
K.R. Savage, B.D. Sembach, Annu. Rev. Astron. Astrophys. **34**, 279–329 (1996)
S. Schmitz, F.E. Brenker, L. Vincze, B. Vekemans, M. Burghammer, C. Rielel, Lun. Planet. Sci. **39**, 1137 (2008)
H. Schulze, J. Kissel, E.K. Jessberger, in *From Stardust to Planetesimals*, vol. 122, ed. by Y.J. Pendleton, A.G.G.M. Tielens (ASP, San Francisco, 1997), pp. 397–414
E.R.D. Scott, A.N. Krot, Astrophys. J. **623**, 571–578 (2005a)
E.R.D. Scott, A.N. Krot, in *Chondrites and the Protoplanetary Disk*, vol. 341, ed. by A.N. Krot, E.R.D. Scott, B. Reipurth (ASP, San Francisco, 2005b), pp. 15–53
D. Semenov, http://www.mpia-hd.mpg.de/homes/henning/Dust_opacities/Opacities/opacities.html (2001)
L. Spitzer Jr., E.B. Jenkins, Annu. Rev. Astron. Astrophys. **13**, 133–164 (1975)
G. Strazulla, J.F. Cooper, E.R. Christian, R.E. Johnson, C. R. Phys. **4**, 791–801 (2003)
S. Sugita et al., Science **310**, 274–278 (2005)
K.L. Thomas, G.E. Blanford, L.P. Keller, W. Klock, D.S. McKay, Geochim. Cosmochim. Acta **57**, 1551–1566 (1993)
K.L. Thomas, L.P. Keller, G.E. Blanford, D.S. McKay, in *Analysis of Interplanetary Dust*, vol. 310 (AIP, 1994a), pp. 165–171
K.L. Thomas, L.P. Keller, G.E. Blanford, D.S. McKay, in *Workshop on the Analysis of Interplanetary Dust Particles*, ed. by M. Zolensky. LPI Tech. Report No. 94-02 (LPI, Houston, 1994b), pp. 49–50
K.L. Thomas, L.P. Keller, W. Klock, J. Warren, G.E. Blanford, D.S. McKay, Lun. Planet. Sci. **25**, 1393–1394 (1994c)
K.L. Thomas, L.P. Keller, D.S. McKay, Meteorit **30**, 587–588 (1995)
K.L. Thomas, L.P. Keller, D.S. McKay, in *Physics, Chemistry, and Dynamics of Interplanetary Dust*, vol. 104, ed. by B.A.S. Gustafson, M.S. Hanner (ASP, San Francisco, 1996), pp. 28–31
A.G.G.M. Tielens, L.B.F.M. Waters, T.J. Bernatowicz, in *Chondrites and the Protoplanetary Disk*, vol. 341, ed. by A.N. Krot, E.R.D. Scott, B. Reipurth (ASP, San Francisco, 2005), pp. 605–631
A. Toppani, F. Robert, G. Libourel et al., Nature **437**, 1121–1124 (2005)
J.-P. Tozzi, L.M. Lara, L. Kolokolova, H. Boenhardt, J. Licandro, R. Schulz, Astron. Astrophys. **424**, 325–330 (2004)
B.M.P. Trivedi, Astrophys. J. **320**, 430–436 (1987)
W.M. Tscharnuter, H.-P. Gail, Astron. Astrophys. **463**, 369–392 (2007)
J.T. Wasson, in *Workshop on Parent-Body and Nebular Modifications of Chondritic Materials*, ed. by M.E. Zolensky, A.N. Krot, E.R.D. Scott. LPI Tech. Report 97-02, Part 1 Abstracts (LPI, Houston, 1997), p. 64. http://www.lpi.usra.edu/meetings/chondrite/pdf/4065.pdf
M. Wehrstedt, H.-P. Gail, Astron. Astrophys. (2008, submitted)
S. Weinbruch, H. Palme, W.F. Müller, A. El Goresy, Meteorit **25**, 115–125 (1990)
S. Weinbruch, H. Palme, B. Spettel, Meteor. Planet. Sci. **35**, 161–171 (2000)
R.A. Wogelius, J.V. Walther, Chem. Geol. **97**, 101–112 (1992)
S.J. Wolk, F.R. Harnden Jr., E. Flaccomio, G. Micela, F. Favata, H. Shang, E.D. Feigelson, Astrophys. J. Suppl. **160**, 423–449 (2005)
J.A. Wood, A. Hashimoto, Geochim. Cosmochim. Acta **57**, 2377–2388 (1993)
D.H. Wooden, Earth, Moon, Planets **89**, 247–293 (2002)
D.H. Wooden, D.H. Harker, C.E. Woodward, H.M. Butner, C. Koike et al., Astrophys. J. **517**, 1034–1058 (1999)
D.H. Wooden, H.M. Butner, D.E. Harker, C.E. Woodward, Icarus **143**, 126–137 (2000)
D.H. Wooden, C.E. Woodward, D.E. Harker, Astrophys. J. **612**, L77–L80 (2004)
D.H. Wooden, A.J. Harker, D.E. Brearley, in *Chondrites and the Protoplanetary Disk*, vol. 341 (ASP, San Francisco, 2005), pp. 774–810
D. Wooden, S. Desch, D. Harker, H.-P. Gail, L. Keller, in *Protostars and Planets V* (University of Arizona Press, Tucson, 2007), pp. 815–833
B. Wopenka, G. Matrajt, D. Joswiak, D. Brownlee, Lun. Planet. Sci. **39**, 1827 (2008)
M.E. Zolensky, R.A. Barrett, Meteorit **29**, 616–620 (1994)
M.E. Zolensky, L. Browning, in *Workshop on Parent-Body and Nebular Modifications of Chondritic Materials*, ed. by M.E. Zolensky, A.N. Krot, E.R.D. Scott. LPI Tech. Report 97-02, Part 2, Summary of Technical Sessions (LPI, Houston, 1997), pp. 1–8
M. Zolensky, K. Nakamura, M.K. Weisburg, M. Prinz, T. Nakamura, K. Ohsumi, A. Saitow, M. Mukai, M. Gounelle, Meteor. Planet. Sci. **38**, 305 (2003)

M. Zolensky et al., Science **314**, 1735–1739 (2006a)
M. Zolensky, P. Bland, J. Bradley, A. Brearley, S. Brennan et al., Lun. Planet. Sci. **37**, 1203 (2006b)
M. Zolensky, T. Zega, M. Weisberg et al., Lun. Planet. Sci. **38**, 1481 (2007)
M. Zolensky, K. Nakamura-Messenger, F. Rietmeijer, H. Leroux, T. Mikouchi et al., Meteor. Planet. Sci. **43**, 261–272 (2008)

Section II: Reservoirs for Comets

Dynamical Origin of Comets and Their Reservoirs

Martin J. Duncan

Originally published in the journal Space Science Reviews, Volume 138, Nos 1–4.
DOI: 10.1007/s11214-008-9405-5

Abstract It is widely believed that cometary orbits contain important clues to both the outer solar system's current structure and its past dynamical evolution. The first part of this paper summarizes the results of numerical simulations designed to study the dynamical origins of observed comets and to link the observed populations to the reservoirs from which they are currently leaking. The second part reviews simulations which are designed to study the dynamical origin of the reservoirs themselves. The paper concludes with a brief discussion of the currently unresolved issue of where in the primordial solar nebula the different dynamical classes of observed comets originated.

Keywords Comets · Oort cloud · Transneptunian region

1 Introduction

The majestic display that often draws our attention to a comet is also a harbinger that its current orbit is short-lived. This is because the development of an easily observed coma and tails requires that the comet's perihelion be close enough to the Sun that the comet inevitably enters the dynamical realm of the planets (particularly that of Jupiter) in which its dynamical lifetime is typically much shorter than the age of the Solar System (see e.g. Levison and Duncan 1994). Thus, there must be one or more cometary reservoirs which are simultaneously sufficiently massive and long-lived to store comets for billions of years yet sufficiently 'leaky' to continuously replenish the population of currently observable comets. One of the goals of the work summarized below is to use simulations of the dynamical evolution of comets starting from various hypothetical reservoirs to compare the predicted properties of the resulting 'observable' comets with the real observed populations. The observed comets then provide important clues to the structure of the reservoirs.

M.J. Duncan (✉)
Department of Physics, Engineering Physics and Astronomy, Queen's University, Kingston, Ontario, Canada, K7L 3N6
e-mail: duncan@astro.queensu.ca

H. Balsiger et al. (eds.), *Origin and Early Evolution of Comet Nuclei*
DOI: 10.1007/978-0-387-85455-7_7

As might be expected, the cometary reservoirs appear to lie in the transneptunian region and enormous observational strides have been made in the last 15 years in discovering ∼1000 objects called transneptunian bodies (TNOs) which are presumably the larger cousins of comet-sized bodies. The orbits of the TNOs and some of their inferred physical characteristics are helping us to piece together the picture of what happened during the formation of the outer solar system. Thus, the second part of this paper briefly summarizes how the recently discovered reservoir properties provide some clues to the planet formation processes which in turn point to a rather radical upheaval in our models of outer solar system evolution. The last section summarizes what these new models may imply for the answer to the fundamental question: *Where in the primordial solar nebula did different dynamical classes of observed comets originate*?

This paper summarizes two invited talks given at the International Space Science Institute in Bern, Switzerland as part of a 2006 Workshop on the "Origin and Early Evolution of Comet Nuclei". For brevity, the talks and this paper focus on the work of the author and colleagues/students, although references are given to more complete reviews of the topic where possible. We begin with a mention of the dynamical classes into which comets are usefully sorted before proceeding to the three main themes described above.

2 Cometary Taxonomy

Historically, cometary taxonomy was based on orbital period, with comets of orbital period shorter than 200 years being termed 'short-period comets' and those with periods less than 20 years being further subdivided into the class called 'Jupiter-family' comets. However, numerical integrations such as those described below show that under such a scheme a given short-period comet typically shifts in and out of the 'Jupiter-family class' many times during its dynamical evolution. Carusi and Valsecchi (1987) first suggested that since the Tisserand parameter does not vary substantially during a typical comet's lifetime, a taxonomy based on this parameter might be more appropriate than one based on orbital period.

Recall that the Tisserand parameter with respect to Jupiter, T, is defined as

$$T = a_J/a + 2\sqrt{(1-e^2)a/a_J}\cos(i),$$

where a_J is Jupiter's semi-major axis, and a, e, and i refer to an object's semi-major axis, eccentricity, and inclination, respectively. It is an approximation to the Jacobi constant, which is an integral of the motion in the circular restricted three-body problem. It is also a measure of the relative velocity between a comet and Jupiter during close encounters, $v_{rel} = v_c\sqrt{3-T}$, where v_c is Jupiter's velocity about the Sun. Objects with T close to, but smaller than, 3 have very slow, and thus very strong, encounters with Jupiter. Objects with $T > 3$ cannot cross Jupiter's orbit in the circular restricted case, being confined to orbits either totally interior or totally exterior to Jupiter.

In what follows, we will adopt a taxonomic scheme based on that of Levison (1996), in which the most significant division is based on the Tisserand parameter. In this scheme comets with $T > 2$ are designated **ecliptic comets** because most members have small inclinations. Comets with $2 < T < 3$ are mainly on Jupiter-crossing orbits and are dynamically dominated by that planet. We call these **Jupiter-family comets** (hereafter called **JFC**s). As we shall see, these objects most likely originate in the Kuiper belt (Edgeworth 1949; Kuiper 1951; Fernandez 1980; Duncan et al. 1988) or the scattered disk described below (Torbett 1989; Duncan and Levison 1997). Comets with $T < 2$, which are believed to be

mainly comets that originated in the Oort cloud (Oort 1950; Everhart 1977) are designated **nearly isotropic comets** (**NIC**s), reflecting their inclination distribution (see below). The NICs with semi-major axes $a < 40$ AU are denoted **Halley-type comets** (**HTC**s) while those with $a > 40$ AU are called **long-period comets** (**LPC**s). LPCs with $a > 20{,}000$ AU typically come directly from the "outer" Oort cloud (see Sect. 4). Independent of other classifications, a comet is said to be **'visible'** if its perihelion distance is less than 2.5 AU.

3 Origin of Jupiter-Family Comets

Jupiter-family comets were originally thought to originate from nearly isotropic comets that had been captured into short-period orbits by gravitational encounters with the planets (Newton 1891, 1893; Everhart 1977; Bailey 1986). Joss (1973; see later work by Fernández and Gallardo 1994 and Levison et al. 2001) argued that this process is too inefficient and Fernandez (1980) suggested that a belt of distant icy planetesimals beyond Neptune could serve as a more efficient source of most of these comets. Duncan et al. (1988) strengthened this argument by performing dynamical simulations which showed that a cometary source beyond Neptune with small inclinations to the ecliptic was far more consistent with the observed orbits of most of these comets than the randomly distributed inclinations of comets in the Oort cloud (see also Quinn et al. 1990). They named this source the Kuiper belt (KB).

The size, extent, and eccentricity of the cometary orbits in this belt were left as open questions in (Duncan et al. 1988). Simulations by Levison and Duncan (1997: hereafter called LD97) showed that a flattened population of Neptune-encountering bodies produces an 'armada' of comets that diffuse in semi-major axis (a) and perihelion distance (q) due to planetary perturbations. Figure 1 shows that the properties of 'visible' comets resulting from the model are in excellent agreement with observed JFCs. Very few HTCs are produced in the simulations but LD97 stopped integrating comets when their semi-major axes exceeded 1000 AU (see Sect. 5).

Duncan and (1997: DL97) extended the LD97 integrations to 4 Gyr to obtain the remnant structure of the primordial planetesimal population which scattered during outer planet formation in the early solar system. They found that about 1% of the particles survive for 4 Gyr in what has come to be called the "scattered disk" (SD). Thus, some planetesimals originating in the Uranus/Neptune zone and/or the inner Kuiper belt could have been trapped in the SD for 4 Gyr and be currently leaking inward to make the JFCs. Trapping occurs in part because Neptune's mean motion resonances are 'sticky' in the sense of nonlinear dynamics—the effects of the near-resonant encounter can increase the perihelion distance and typically leave 32 AU $\leq q \leq 40$ AU. This process can continuously replenish JFCs if there are now $\sim 10^9$ objects with $D > 1$ km in the SD, corresponding to ~10–20 Earth masses originally scattered by Neptune. Interested readers are referred to Duncan et al. (2004) for a more comprehensive review of the dynamical evolution of ecliptic comets.

4 Origin of Long-Period Comets

In his historic paper, Oort (1950) proposed that the Sun was surrounded by a spherical cloud of comets (now called the Oort Cloud (OC)) with semi-major axes of tens of thousands of AU. In Oort's model, planetary perturbations (primarily by Jupiter) acting on small bodies placed the comets onto large, highly eccentric orbits, after which perturbations by passing stars raised the comets' perihelia from the planetary region. Oort showed that comets in

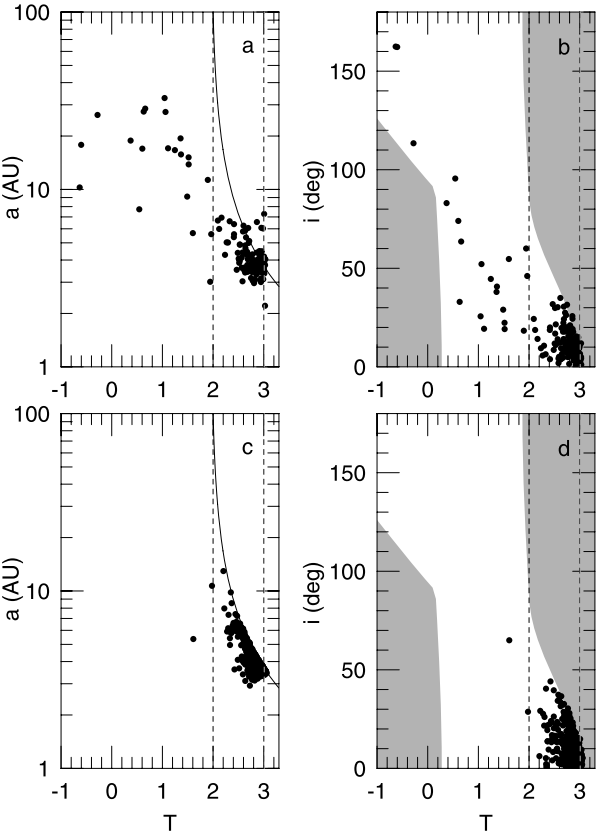

Fig. 1 **a** The semi-major axes, a, of observed comets with periods less than 200 years as a function of their Tisserand parameter with respect to Jupiter, T. The *dashed vertical lines* represent the boundaries of the Jupiter family at $T = 2$ and $T = 3$. Objects falling above the *solid curve* must have perihelia greater than 2.5 AU. **b** The inclination, i, of the same set of comets as in **a** as a function of T. Again, the *dashed lines* represent the boundaries of the Jupiter family. The *shaded areas* represent regions that are physically unattainable due to the relationship between i and T assuming $q \leq 2.5$ AU and apocenter $Q \geq a_J$. **c** The same as **a** except for simulated comets when they first become 'visible' i.e. when their perihelia first drop below 2.5 AU. **d** The same as **b** except for simulated comets when they first become visible. Reproduced from Levison and Duncan (1997)

the cloud are so far from the Sun that perturbations from random passing stars can change their orbital angular momenta significantly and occasionally send some comets back into the planetary system as potential LPCs. The process by which small bodies evolve to and from the planetary region involves several stages during which the body's path evolves under the gravitational effects of the Sun and the following potential perturbers.

4.1 Planets

Assuming that comets formed in the region of the giant planets, their orbits initially evolve due to gravitational scattering by the planets. At first, planetary perturbations produce comparable changes in the comets' semi-major axes (a) and perihelion distances (q) when cometary eccentricities (e) are small. Eventually, most comets are placed onto highly eccentric orbits with perihelia still in the planetary region. The planets continue to change the comets' orbital energies (i.e., a) via a random-walk (Yabushita 1980) while leaving their angular momenta (or, equivalently, q for highly eccentric orbits) nearly unchanged.

4.2 Stars

Stars with masses above the hydrogen-burning limit of 0.07 $M_\odot$ pass within 1 pc ($\sim 2 \times 10^5$ AU) of the Sun about once per 10^5 years (García-Sánchez et al. 1999, 2001).

The average mass of these stars is $\sim$0.5 $M_\odot$ (Chabrier 2001). In fractional terms, stars change q much more than they change a as a consequence of the long lever arm and slow speed of comets on highly eccentric orbits near aphelion. However, as we discuss next, tides from the Galactic disk are slightly more effective than stars in producing systematic changes in q. Nonetheless, passing stars do produce a random walk, or "diffusive" change, in cometary semi-major axes (Weinberg et al. 1987).

4.3 The Galactic Tidal Field

The importance of Galactic tides, i.e., the differential gravitational acceleration of OC comets relative to the Sun due to the disk and bulge of the Milky Way, was pointed out by Byl (1983, 1986, 1990), Smoluchowski and Torbett (1984), Heisler and Tremaine (1986), Delsemme (1987), and Matese et al. (1995). Slightly less than half of the local Galactic mass density is in stars. Thus at most times (i.e., at times other than during a strong comet shower), the rate at which comets are fed into the planetary region from the OC due to the Galactic tide is probably slightly larger than the influx due to stellar passages (Heisler and Tremaine 1986). Indeed, Heisler (1990) concluded that when stellar impulses are added to the Galactic tidal interaction the long-timescale average increase in the steady state flux due to the tide alone is only $\sim$20%.

Tides change comets' q at nearly constant a. The disk ("z") component of the Galactic tide causes q to oscillate in and out of the planetary region with a period T_z that is of order 1 Gyr for comets with $a \sim 10{,}000$ AU and initial $q \sim 25$ AU (Heisler and Tremaine 1986, Eq. 18; Duncan et al. 1988). The value of T_z scales as $a^{-3/2}$, i.e., inversely as the comet's orbital period. In addition, there is a "radial" component of the Galactic tide due to the mass interior to the Sun's orbit around the Galaxy. The amplitude of the radial tide is a factor of $\sim$8 smaller than the disk tide, but the radial tide is still important because it breaks conservation of J_z, the component of a comet's angular momentum perpendicular to the Galactic plane. Thus the radial tide modulates cometary perihelion distances and must be considered in studies of the influx of long-period and Halley-type comets (Matese and Whitmire 1996; Levison et al. 2006).

Combining the effects above, Fig. 2 shows that comets with perihelia in the Jupiter–Saturn zone ($q \sim$ 5–15 AU) will diffuse on timescales of 10^4–10^7 years to the point where the energy diffusion time t_d is comparable to the orbital period P ($a \sim$ several hundred to ten thousand AU, depending on q), at which point the diffusion approximation breaks down since the energy kick in one orbit is comparable to the binding energy of the orbit. Most comets in this range of q will subsequently be ejected, although due to the wide range in possible planetary "kicks" in energy, a small fraction (typically a few percent) can be launched to the region where the time for the perihelion to be lifted away from the Jupiter–Saturn region is less than an orbital period ($a \gtrsim 20{,}000$ AU as can be seen in Fig. 2). On the other hand, comets with perihelia in the Uranus-Neptune zone ($q \sim 25$ AU) will diffuse on 10^8 year timescales until they reach the region where the tidal torquing time is comparable to the period ($a \lesssim 10{,}000$ AU from Fig. 2). In the next orbit, depending on the argument of perihelion with respect to the Galactic plane, roughly half of the comets will be torqued outward to the relative safety of the Oort cloud and roughly half will be drawn into the Jupiter–Saturn zone, where they are likely to be ejected. Similarly, objects with $q \sim 35$ AU—i.e., those in the Scattered Disk—will evolve on billion year timescales to $a \sim 3000$ AU where their perihelia will be torqued in or out.

Figure 2 can also be used to understand the key observational bias concerning the OC noted by Hills (1981). Observed long-period comets come directly from the "outer" Oort

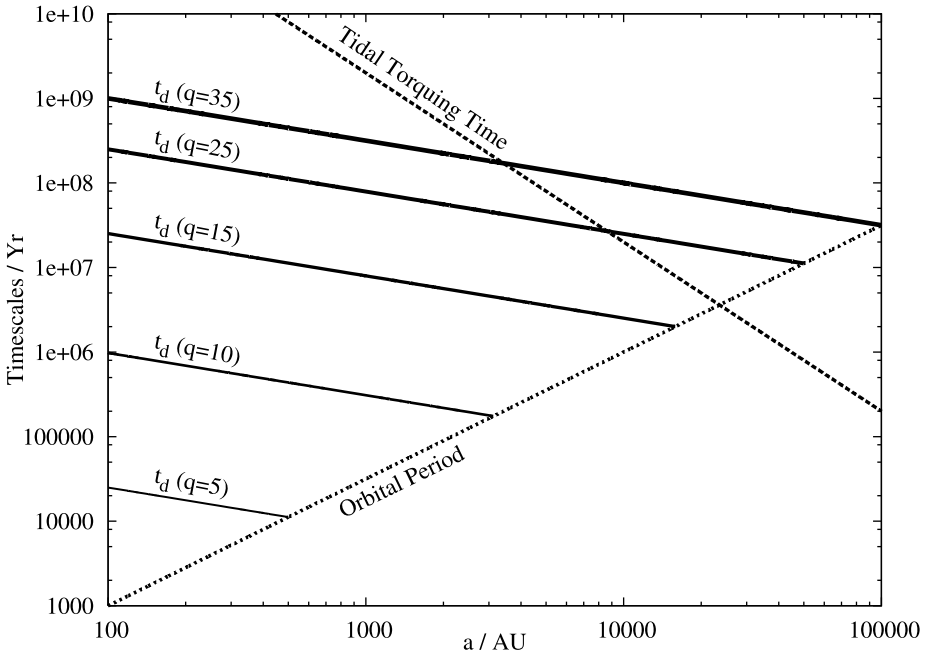

Fig. 2 Timescales relevant to the dynamical evolution of a comet in the current solar system are plotted against semi-major axis. These include (i) orbital period (*dotted line*) (ii) the energy diffusion time t_d (timescale for cumulative planetary perturbations near perihelion to change the comet's semi-major axis by roughly a factor of two) for several perihelion distances q (*solid lines*) and (iii) the tidal torquing time t_q (timescale for the Galactic tidal field to change q by roughly 10 AU) for the current Galactic disk density (*dashed line*)

cloud ($a > 20{,}000$ AU) where the Galactic tidal field can drive the perihelion distance from $q \sim 15$ AU to $q \lesssim 3$ AU (where they produce a visible coma) in one cometary orbital period. Comets with perihelia driven inward from the "inner" Oort cloud ($a < 20{,}000$ AU) in the current Galactic environment will do so over several orbits and thus at some time will pass through perihelion when q is near Jupiter and/or Saturn and the planetary perturbations almost inevitably drive such comets into interstellar space (or occasionally into the outer Oort cloud) or into much more tightly bound orbits where tidal torquing is negligible. Thus, Jupiter (and to a lesser extent Saturn) acts like a barrier preventing most objects from the inner Oort cloud from directly being observed as comets with perihelia near 1 AU. This effect is called the "Jupiter-barrier".

Since inner Oort cloud comets are rarely directly injected into visible orbits, the inner cloud could be quite massive. Indeed two members of the inner OC's population may recently have been found: the unusual body (90377) Sedna ($a = 501$ AU, $q = 76$ AU: Brown et al. 2004) may be a member of the inner OC as may be the object 2000 CR_{105} ($a = 224$ AU, $q = 44$ AU: Gladman et al. 2002). Whether the unusually large perihelia of these objects was produced by a passing star (Morbidelli and Levison 2004; Kenyon and Bromley 2004a) is a matter of some debate since other models for their origin exist (Matese et al. 2005; Gomes et al. 2006; Gladman and Chan 2006). However, if Sedna in particular is representative of the inner regions of the Oort cloud then the inner OC may be rather massive (containing as much as 5 $M_\oplus$ in the rough estimation of Brown et al. 2004). In Sect. 7 we

shall explore models of OC formation which produce a massive inner cloud as a byproduct of the Sun's presumed early history in the denser environment of an embedded star cluster.

5 Origin of Halley-Type Comets

Due to the "Jupiter-barrier", bodies from the inner OC for which the Galactic tide is driving their perihelion distances into the region of the giant planets will suffer perturbations which will inevitably drive such comets back into the outer Oort cloud (or interstellar space) or into much more tightly bound orbits where tidal torquing is negligible. A small fraction of the latter comets will eventually diffuse down into orbits with sufficiently small semi-major axes that their perihelia will begin to be substantially affected and they can then come sufficiently close to the Sun to produce comae. Numerical simulations (Duncan et al. 1988; Quinn et al. 1990; Emel'yanenko and Bailey 1998) have suggested that these objects may be an important source of Halley-type comets. Thus, it has been suggested that HTCs may represent our only currently observable link to the inner Oort cloud.

Levison et al. (2001; henceforth LDD01) attempted to constrain the structure of the inner OC by modeling the "capture" process by which OC comets evolve onto orbits like those of Halley-type comets (HTCs). While some HTCs, such as Halley and Swift-Tuttle, follow retrograde orbits, most (for example 19 of 26 with $q < 1.3$ AU in a recent compilation—see http://www.physics.ucf.edu/~yfernandez/cometlist.html) revolve on prograde orbits. LDD01 found that cometary inclinations were roughly conserved during the capture process, so that the source region had to be somewhat flattened. (An alternative, proposed by Fernández and Gallardo (1994), is that the observed preponderance of prograde orbits is due to cometary fading: when the number of perihelion passages is limited by physical causes, fewer retrograde comets are found in evolved states since they evolve dynamically more slowly than their prograde counterparts. However, LDD01 modelled this possibility in their detailed numerical integrations and found that for the range of fading times proposed by Fernández and Brunini, the simulated HTCs generally had larger semi-major axes than are observed.) Since the outer OC is roughly spherical, LDD01 concluded that most HTCs must derive from a flattened inner core which they associated with the inner OC. LDD01 found that models in which the median inclination of inner OC comets, i', is between 10° and 50° can fit the HTC orbital distribution.

However, Levison et al. (2006; henceforth LDDG06) subsequently realized that there was a problem in identifying the flattened outer source with a 'fossilized' inner OC. Recall that the other, more numerous, class of short period comets are the Jupiter Family comets. As we argued above, most of the JFCs are believed to leak in from the inner edge of the scattered disk, initially under the dynamical control of Neptune. As might be expected, the integrations of LDD01 showed that low inclination objects with initial semi-major axes in the inner OC also evolve into JFCs if their perihelia originated near Neptune. However, those low inclination comets from the inner OC with initial $q \lesssim 25$ AU generally evolved into HTCs. Thus, in order for a flattened inner Oort cloud to be the source of the low-inclination HTCs, inner Oort cloud comets must be able to evolve onto orbits with $q \lesssim 25$ AU and remain on low-inclination orbits in the inner Oort cloud for the age of the solar system.

LDDG06 showed that 1) only if $a \lesssim 3000$ AU are Galactic tides *weak* enough that orbital inclinations do not change significantly over the age of the Solar System (i.e. the Oort cloud remains disk-like), and 2) only if $a \gtrsim 12000$ AU are Galactic tides *strong* enough that an object can evolve from an orbit with $q > 30$ AU to one with $q \lesssim 25$ AU before perturbations from Neptune remove it from the Oort cloud. This obvious inconsistency is resolved

if the flattened source is itself being dynamically replenished, rather than being a fossilized remnant of the early history of the solar system. Thus, LDDG06 studied the dynamical evolution of objects that evolve off the outer edge of the scattered disk and have their perihelion distances driven inward by Galactic tides. They found that roughly 0.01% of these objects evolve onto HTC-like orbits. The orbital element distribution of the resulting HTCs is consistent with observations, including the requisite number of retrograde orbits, which are produced by the tidally-driven precession of the line of nodes in Galactic coordinates.

In order for the scattered disk to supply enough HTCs, the model predicts that it needs to contain 3 billion comets with diameters larger than 10 km. This value is larger than estimates inferred from observations of the scattered disk and it may be larger than that needed for the Jupiter-family comets. However, the structure of the scattered disk at large heliocentric distances, where the HTCs would come from, is not constrained by either the Jupiter-family comet models or observations. In addition, LDDG06's HTC model lacked passing stars and molecular clouds which could affect the delivery rates.

It should be noted that, in the simulations of LDDG06, comets coming off the outer edge of the scattered disk not only become HTCs, but contribute to the long-period comet (LPC) population, especially to those LPCs known as *dynamically new comets* (DNCs) ($a \gtrsim 10{,}000$ AU; see Levison 1996, although Dybczyński 2006 argues that $a \gtrsim 25{,}000$ AU is a better criterion). In particular, the models produce a population of DNCs with a median inclination of 40° and in which only 30% are retrograde. The observed inclination distribution of the DNCs is isotropic. However, one interesting aspect of the model DNCs is that they have large semi-major axes—75% of DNCs in LDDG06 have $a > 30{,}000$ AU. This is relevant because Fernández (2002) performed an analysis of the inclination distribution of LPCs in different ranges of semi-major axes and concluded that although the DNCs are isotropic, 68% of the DNCs with $a > 32{,}000$ AU are prograde. This is consistent with LDDG06's model if most of these objects are from the scattered disk. To test the latter requirement, future investigations combining the simulations just discussed together with a complete evolutionary model of the OC will be needed.

6 Origin of the Oort Cloud: The Standard Model

Dones et al. (2004: hereafter DWLD) present results of a comprehensive study of the "standard" model of OC formation—i.e., a model in which the planets are assumed to be fully formed, in their current orbits, in the current Galactic environment and in which the leftover planetesimals ("comets") begin on orbits with semi-major axes between 4 and 40 AU and initially small eccentricities and inclinations. The study integrated the orbits of 3,000 comets for times up to 4 billion years under the gravitational influence of the Sun, the four giant planets, the Galaxy, and random passing stars. Their model of the Galaxy included both the "disk" and "radial" components of the Galactic tide. The disk tide is proportional to the local density of matter in the solar neighborhood and exerts a force perpendicular to the Galactic plane, while the radial tide exerts a force within the Galactic plane (see Sect. 4.3). These simulations did not include other perturbers such as molecular clouds, a possible dense early environment if the Sun formed in a cluster (Gaidos 1995; Fernández 1997), or the effects of gas drag (de la Fuente Marcos and de la Fuente Marcos 2002; Higuchi et al. 2002). Studies involving the latter two effects are discussed below.

Figure 3 shows the resulting time evolution of the populations of the inner and outer Oort clouds and scattered disk individually. The population of the outer Oort cloud peaks around 600 Myr while the inner Oort cloud peaks around 1.8 Gyr. Because of the faster decline of

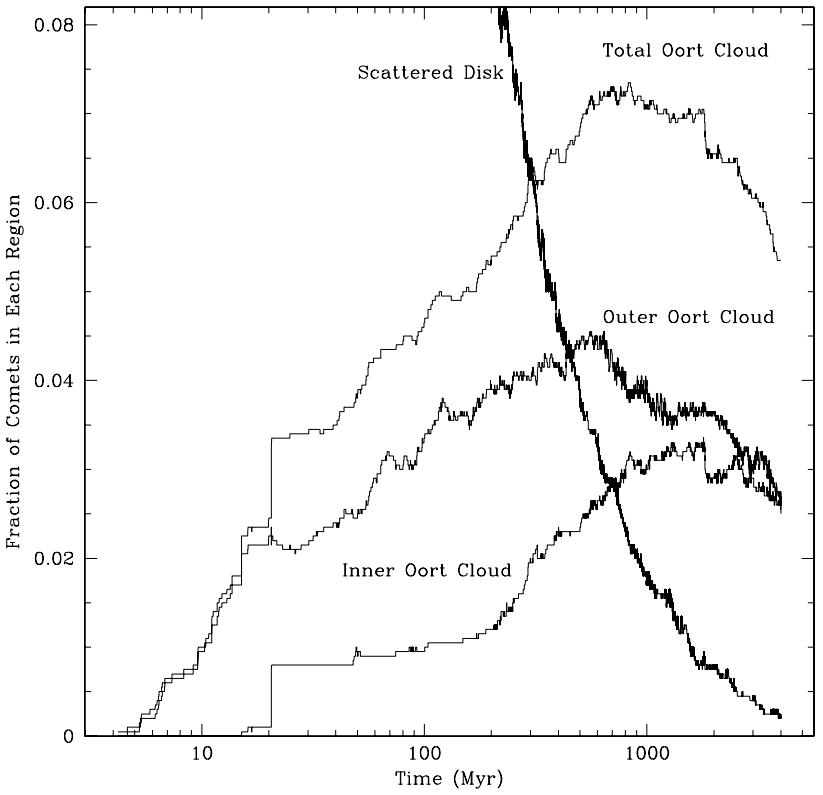

Fig. 3 In the simulations reported in DWLD the outer Oort cloud, which is originally populated by comets injected by Jupiter and Saturn, forms more rapidly than the inner Oort cloud. These simulations predict that the present populations of the inner and outer Oort clouds should be comparable and that of the scattered disk should contain roughly 10% as many comets as the outer OC

the outer Oort cloud, the ratio of numbers of inner to outer Oort cloud comets increases with time, to 1.1 at present. As noted above, only 2.5% of the comets that were initially in the simulation occupy the outer Oort cloud at 4 Gyr.

At face value, the low efficiency of OC formation in the simulations reported in DWLD implies a massive primordial protoplanetary disk. Assuming an outer OC mass of 2–40 $M_\oplus$ (Francis 2005) the simulation efficiency implies that the original mass in planetesimals between 4 and 40 AU was ∼80–1600 $M_\oplus$, some 2 to 40 times the mass in solids in a "minimum-mass" solar nebula. The amounts of mass at anything but the low end of this estimate likely would have produced excessive migration of the giant planets and/or formation of additional giant planets (Hahn and Malhotra 1999; Thommes et al. 2002; Gomes et al. 2004). However, the uncertainties in cometary mass estimates suggest that it is possible that the outer OC may currently contain ∼1 $M_\oplus$, in which case the disk mass inferred in DWDL does not present a problem.

The results may be inconsistent with observations in another way. The population of the scattered disk that DWLD predicted, of order 10% the population of the Oort cloud, may be much larger than the actual population of the scattered disk inferred from observations

of large bodies (Trujillo et al. 2000). Again, however, the large uncertainties in the observational estimates of both populations mean that there may be no problem.

However, we must certainly come to terms with the fact that none of the models described above will produce the orbits of the inner OC objects described above. For that, we will likely need the types of models discussed next.

7 Origin of the Inner Oort Cloud: The Embedded Cluster Phase

Tremaine (1993), Gaidos (1995), Fernández (1997), Eggers et al. (1997, 1998), Eggers (1999) and Fernández and Brunini (2000) have discussed star formation in different Galactic environments. These authors point out that the Sun may have formed in a denser environment than it now occupies (i.e., in a molecular cloud or star cluster), and found that a more tightly bound Oort cloud would form under these circumstances.

A comprehensive set of simulations has recently been performed by Brasser et al. (2006: hereafter BDL06). Their model assumes that the Sun formed in an embedded star cluster, which are clusters that are very young and heavily obscured by dust since the molecular gas is still present (Lada and Lada 2003). Most stars in the Galaxy probably form in embedded clusters with between 100–1000 members (Adams et al. 2006): indeed, typical populations of embedded clusters within 2 kpc of the Sun today are 50–1500 stars (Lada and Lada 2003). The lifetime of the gas in these clusters is typically 1–5 Myr: only 10% of embedded clusters last for 10 Myr (Lada and Lada 2003). Since the formation of unbound stellar clusters is the rule and not the exception (Lada et al. 1984), it is probable that the Sun formed in such a cluster and escaped from it within $\lesssim$5 Myr.

Many of the results can be understood by referring to Fig. 4, which is modelled after Fig. 2 and in which the symbols have the same meaning. In Fig. 4, the tidal torquing time from the Plummer potential is computed in BDL06 (and is confirmed by numerical integrations) and the energy diffusion timescales for the pre-LHB planetary configuration are numerically obtained as a function of q.

Recall (see e.g., Sect. 4) that once a comet is scattered to semi-major axes $a \gg q$, it tends to diffuse outward at fixed q along the lines of t_d, until it hits one of two lines. If it crosses the period line first, it tends to be ejected. If it crosses the tidal torquing time line first, the comet is usually lifted by the tide and stars and can thus be saved from being ejected. The intersection of the lines of t_d and t_q indicates the value of a at which the lifting is likely to begin and is a measure of the inner edge of the OC.

As it turns out, a mean density of at least $\langle\rho\rangle \sim 2000\ M_\odot\ \mathrm{pc}^{-3}$ is needed to save the comets from Saturn. As can be seen from Fig. 4, even when $\langle\rho\rangle = 10^5\ M_\odot\ \mathrm{pc}^{-3}$, the comets with perihelia close to Jupiter can barely be saved, because the mean kick in energy from this planet is too strong. However, for all the densities shown, a fair number of comets from around Saturn can be saved, with the subsequent OCs being formed ranging in size from a few hundred to several thousand AU.

Figure 5 shows snapshots at the end of five different runs in a–q space. The panels show one run selected from each of the different central densities respectively, with the lowest density in the bottom panel and the highest in the top, left one. On average 2–18% of the initial sample of comets end up in the OC after 1–3 Myr. A comet is defined to be part of the OC if it is bound and has $q > 35$ AU. The models show that the median distance of an object in the OC scales approximately as $\langle\rho\rangle^{-1/2}$ when $\langle\rho\rangle \gtrsim 10\ M_\odot\ \mathrm{pc}^{-3}$.

The models of BDL06 easily produce objects on orbits like that of (90377) Sedna (Brown et al. 2004) within $\sim$ 1 Myr in cases where the mean density is $10^3\ M_\odot\ \mathrm{pc}^{-3}$ or higher;

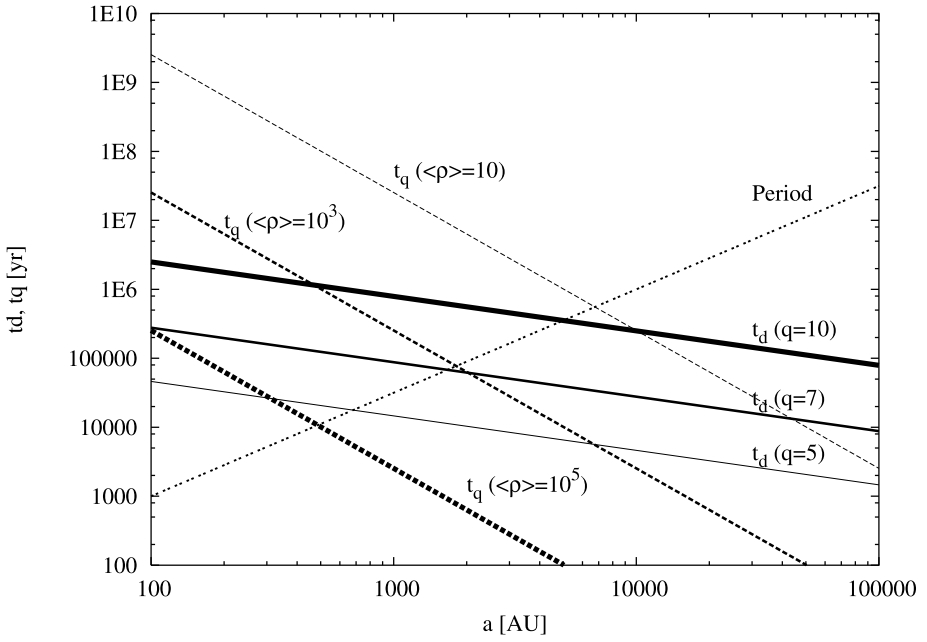

Fig. 4 Plot of the relevant timescales for a comet's evolution as a function of semi-major axis for the models of BDL06. The symbols have the same meaning as in Fig. 1. Three values of t_d are plotted (near-horizontal *solid lines*) for $q = 5$ (*thin*), 7 (*medium*) and 10 AU (*thick*). Three values of t_q are plotted (downward-sloping *broken lines*), for $\langle\rho\rangle = 10$ (*thin*), 10^3 (*medium*) and 10^5 $M_\odot$ pc^{-3} (*thick*). The orbital period is also plotted (upward-sloping, *dotted line*)

one needs mean densities of order 10^4 $M_\odot$ pc^{-3} to create objects like 2000 CR_{105} by this mechanism, which are reasonable given the observations of Gutermuth et al. (2005). Thus the latter object may also be part of the OC.

Close stellar passages can stir the primordial Kuiper Belt to sufficiently high eccentricities ($e \gtrsim 0.05$; Kenyon and Bromley 2002) that collisions become destructive. From the simulations performed it is determined that there is a 50% or better chance to stir the primordial Kuiper Belt to eccentricities $e \geq 0.05$ at 50 AU when $\langle\rho\rangle \gtrsim 10^5$ $M_\odot$ pc^{-3}. Note also that in the case of a close stellar encounter that actually truncates the belt at 50 AU, there would be a population of objects on orbits with perihelia like Sedna's, but much smaller semi-major axes. This seems inconsistent with the lack of detections of bodies on these orbits.

The orbit of the new object (136199) Eris (Brown et al. 2005) is only reproduced for mean cluster densities of the order of 10^5 $M_\odot$ pc^{-3}, but in the simulations of BDL06 it could not come to be on its current orbit by this mechanism without close stellar passages causing disruptive collisions among bodies in the primordial Kuiper Belt down to 20 AU. BDL06 concluded that it is therefore improbable that the latter object is created by this mechanism. It is possible, although by no means proven, that the Kozai mechanism (coupling between the argument of perihelion, eccentricity, and inclination) associated with mean motion resonances with Neptune, may be responsible for raising both the perihelion distances and the inclinations of relatively close-in objects such as Eris (Gomes et al. 2005a). If so, then the combined simulations of BDL06 and Gomes et al. may provide a rough delineation in (q–a) space between the inner OC and the region relatively unaffected by stellar perturbations.

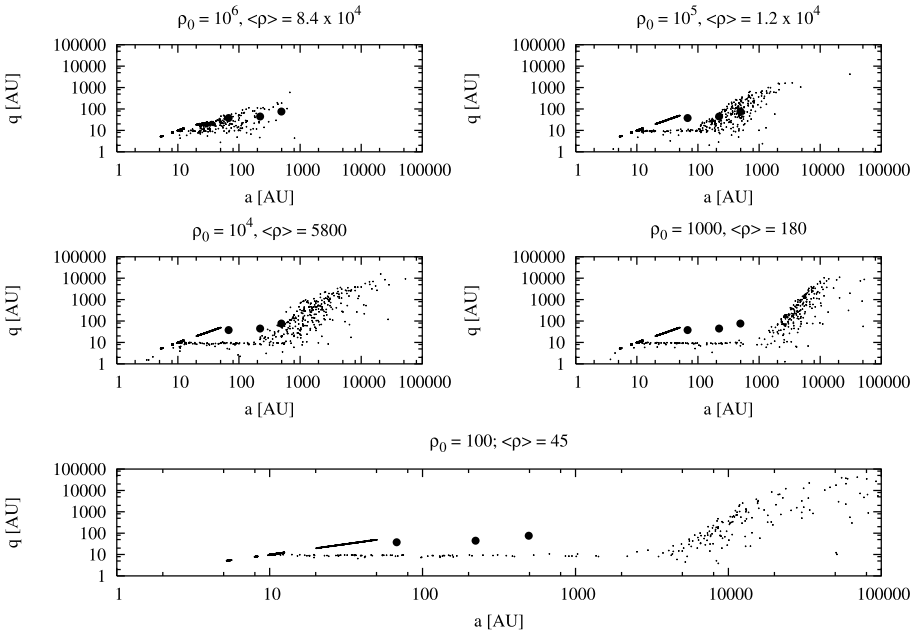

Fig. 5 Snapshots in a–q space are shown at the end of five different runs from BDL06, one from each set of runs with a different central density. The mean densities the Sun encountered are shown above *each panel*. The lowest density is at the *bottom*. Note that the extent and median values of a of the members of the OC increase with decreasing density, as is expected. The positions of (90377) Sedna, 2000 CR_{105} and (136199) Eris in order of descending semi-major axis are marked with bullets. Thus it can be seen that objects with orbits like (90377) Sedna and 2000 CR_{105} only form through this mechanism when the density is high

It should be noted that drag due to gas in the solar nebula may have been very important in the formation of the Oort cloud (de la Fuente Marcos and de la Fuente Marcos 2002; Higuchi et al. 2002). Brasser et al. (2007) (hereafter BDL07) built upon the work of BDL06 by incorporating the aerodynamic drag (adapting the results of Adachi et al. 1976) and gravitational potential of the primordial Solar nebula. The Solar nebula was approximated by the minimum-mass Hayashi model (Hayashi et al. 1985) with scale height $0.047s^{5/4}$ AU, where s is the cylindrical distance (in AU) from the Sun, and in which the inner and outer radii were truncated at various distances from the Sun. In all of the simulations, the density of the primordial Solar nebula decayed exponentially with an e-folding time of 2 Myr. Since the deceleration due to gas drag experienced by a comet is inversely proportional to its size, a typical comet radius of 1.7 km was adopted for most of the simulations (consistent with the LINEAR observations of LPCs of Francis (2005) and using the relation between mass and absolute magnitude of Weissman (1996)). The numerical simulations of BDL07 followed the evolution of comets subject to the gravitational influence of the Sun, Jupiter, Saturn, star cluster and primordial Solar nebula; some of the simulations included the gravitational influence of Uranus and Neptune as well.

The main effect of the gas drag (which roughly conserves angular momentum for disk density profiles like those of Hayashi models) was found to be the circularization of the orbits of km-sized bodies at semi-major axes 1.5–2 times their initial perihelion distances. As a result, the simulations of BDL07 show that when the primordial Solar nebula extends much beyond Saturn or Neptune, virtually no km-sized comets will end up in the inner OC

during this phase. Instead, slightly more than half of the material will be on circular orbits inside of Jupiter if the inner edge of the disk is well inside Jupiter's orbit. If the disk's inner edge is beyond Jupiter's orbit, most comets end up on orbits in exterior mean- motion resonances with Saturn when Uranus and Neptune are not present. In those cases where the outer edge of the disk is close to Saturn or Neptune, the fraction of material that ends up in the subsequently formed inner OC is much less than that found in BDL06 for the same cluster densities.

All of this implies that the presence of the primordial Solar nebula greatly reduces the population of km-sized comets to be expected in the inner OC. In order to determine the effect of the size of the comets on inner OC formation efficiency, a set of runs with the same initial conditions but different cometary radii have been performed by BDL07. It was determined that the threshold comet size to begin producing significant inner Oort clouds is roughly 20 km if the minimum-mass Hayashi model is present for $\sim$2 Myr. This implies that the presence of the primordial Solar nebula in the models studied acts as a size-sorting mechanism, with large bodies (such as Sedna) unaffected by the gas drag and ending up in the inner OC while km-sized comets remain in the planetary region (or in some models in the Saturn- or Uranus-Neptune scattered disks). It should be noted, however, that comets left on dynamically cold orbits just beyond the outermost planet are likely to be eventually scattered (typically to large semi-major axes in a manner reminiscent of the models described in Sect. 6) in the relatively gas-free environment in which Uranus and Neptune are thought subsequently to migrate. We now turn to a brief discussion of this phase.

8 Origin of the Kuiper Belt and Scattered Disk

Our picture of the structure of the region just beyond Neptune has been revolutionized in the past 15 years. The Kuiper Belt (KB) has an intricate structure in which several dynamical classes have been defined. Some of the proposed nomenclature is discussed in the review by Gladman et al. (2008) and theories for the origin of the constituents is reviewed in the chapter by Morbidelli et al. (2008) in the same book. Of key importance in the context of this paper is the fact that theory and simulations show that to grow TNOs to their observed sizes in their current locations on 10^7–10^8 yr timescales required 10–30 $M_\oplus$ of solid material in a dynamically cold disk (Stern 1996; Kenyon and Bromley 2004b). This is 100–1000 times more mass than is inferred from current observations (Bernstein et al. 2004; Gladman et al. 2001). It has proved very difficult to find models which can reduce the KB mass by such a large factor and yet explain the intricate dynamical structure which is observed (cf. Morbidelli et al. 2008).

There is a related problem: even with disk masses containing many tens of Earth masses, it is extremely difficult to accrete objects as large as Uranus and Neptune at 20 or 30 AU (Thommes et al. 2003). Furthermore, to produce the cores of Jupiter and Saturn before the gas goes away requires such large densities (5–10 times minimum mass) that one predicts 4–5 cores in the 5–10 AU range. This gave rise to the model of Thommes et al. (1999, 2002: hereafter TDL02) which suggested Uranus and Neptune formed in the Jupiter–Saturn region and were scattered out by the dynamical instability which inevitably ensued when Jupiter and/or Saturn accreted its massive gas envelope and became dynamically dominant. In the simulations of TDL02, the orbits of Uranus and Neptune were stabilized and circularized by the effects of dynamical friction produced by the scattering of a massive planetesimal disk. However, the disk in the models of TDL02 was sufficiently massive and extended that, on longer timescales than those studied by TDL02, Neptune was found to migrate well past its current location at 30 AU (Gomes et al. 2004).

A promising refinement of the model of TDL02 has recently been proposed (Tsiganis et al. 2005) which is often referred to as the *Nice model* since its proponents collaborated on the project at l'Observatoire de Nice. Like the TDL02 model, the Nice model begins with a compact planetary system with a dynamically cold planetesimal disk beyond the planets. In this case Jupiter and Saturn begin closer together than their mutual 1:2 mean-motion resonance and Uranus and Neptune are on initially circular orbits beyond Saturn but within 15 AU of the Sun. The passage of planetesimals from the outer disk down to Jupiter (where they are ejected) causes the slow inward migration of Jupiter and gradual outward migration of the outer planets due to angular momentum conservation. The instability in the Nice model is triggered by the passage of Jupiter and Saturn through their mutual 1:2 mean-motion resonance, which excites their eccentricities and also destabilizes the orbits of the outer planets and triggers their scattering of and migration through the outer disk.

In this scenario it is assumed that the disk of planetesimals was truncated near 30 AU. This assumption avoids the problem referred to above of the excessive migration of Neptune. It also obviously reduces the problem of explaining why the mass of the transneptunian region is currently so low! The disk mass interior to 30 AU in the Nice model ($\sim$35 $M_\oplus$) is also smaller than that of TDL02 because the instability is less violent so that less mass is required to retain the outer planets and circularize their orbits.

The Nice model is remarkably successful at reproducing the giant planets' orbital parameters (including eccentricities and inclinations), and has other consequences in accord with observations (see Morbidelli et al. 2008). A very important byproduct is that it reproduces many of the observed dynamical features of the KB (Levison et al. 2008) by 'transplanting' essentially all of the objects now found in the transneptunian region from primordial orbits interior to 35 AU. If confirmed, this scenario obvious complicates the answer to our overriding question of where in the disk the observed comets originally formed. We return to that issue now.

9 Summary

Where in the primordial solar nebula did the different dynamical classes of observed comets originate? On the observational side, there have of course been searches for differences in physical attributes that might distinguish among the dynamical classes. The talks presented at the 2006 ISSI workshop gave the impression that there are no easy handles to grab: diversity seems more the rule rather than the exception, even in a given dynamical class. A notable exception is the long-standing result of A'Hearn et al. (1995) that the majority of JFCs appear to be significantly depleted in the carbon-chain molecules that lead to the observed C_2 and C_3. However, the interpretation of this result is open to the usual 'nature vs. nurture' debate.

On the theoretical side, the issue of where the JFCs, HTCs and LPCs come from were addressed above. The best estimates are that: 1) JFCs almost certainly are leaking in from inner edge of the scattered disk. 2) HTCs may be leaking off the outer edge of the scattered disk, or may come from the classical Oort cloud. 3) LPCs most likely come from the classical Oort cloud but some may come from the outer edge of the scattered disk.

The question then becomes: where did the comets currently in these two reservoirs originally form in the protoplanetary disk? If some variant of the Nice model is correct then everything in the scattered disk formed between about 16–30 AU, hence all JFCs and possibly all HTCs formed in that region. As for the LPCs—some comets from the 16–30 AU disk will be emplaced in the Oort cloud during the scattering which produces Neptune's migration. But recall that there was an earlier phase (within the first 1–10 Myr) during which

Jupiter and Saturn accreted gas and rapidly approached their current masses. Such large masses very quickly scatter planetesimals in their vicinities. As we discussed in Sect. 7, if sufficient gas was present beyond ∼10 AU, gas drag would have deposited comet-sized bodies in the disk beyond the outermost planets in existence at that time. If sufficient gas was not present, passing stars may have lifted some of the cometary perihelia into the inner Oort Cloud. Passing stars and Giant Molecular clouds subsequently may have dynamically heated the inner cloud, thereby placing a substantial fraction of the Jupiter–Saturn planetesimals in the outer Oort cloud. Thus, at the moment it is difficult to predict the relative proportions of Jupiter–Saturn planetesimals in the two reservoirs. More detailed planet formation calculations need to be done.

Returning to the observational side, note that several ground-based telescopes (e.g. SkyMapper, PanSTARRS and LSST—see Francis 2005 for a review), each capable of studying large areas to deeper than 22nd magnitude, may yield several hundred new LPC detections over the next few years. Many of these will have perihelia out to and beyond 10 AU and will provide critically needed information about the inner OC. In addition, occultation observations (e.g. Chen et al. 2006; Roques et al. 2006) will provide constraints on the TNO population in general while proposals for occultation measurements from space (Lehner 2006) offer the tantalizing possibility of detecting comet-sized bodies within the Oort cloud itself! These observations and the continuing surveys of the Kuiper Belt will help us clarify the surprisingly complex structures in the transneptunian region and will provide important clues to the dynamical origin of cometary reservoirs.

Acknowledgements The continued financial support of the Natural Sciences and Engineering Research Council of Canada is gratefully acknowledged. Virtually all of the author's work described here was done in a long-lived collaboration with Hal Levison (supported in part by NASA's Origins and PGG programs), and much of it additionally with colleagues and students such as Ramon Brasser, Luke Dones, Brett Gladman and Paul Weissman.

References

I. Adachi, C. Hayashi, K. Nakazawa, The gas drag effect on the elliptical motion of a solid body in the primordial solar nebula. Prog. Theor. Phys. **56**, 1756–1771 (1976)
F.C. Adams, E.M. Proszkow, M. Fatuzzo, P.C. Myers, Early evolution of stellar groups and clusters. Astrophys. J. **641**, 504–525 (2006)
M.F. A'Hearn, R.L. Millis, D.G. Schleicher, D.J. Osip, P.V. Birch, The ensemble properties of comets: Results from narrowband photometry of 85 comets, 1976–1992. Icarus **118**, 223–270 (1995)
M.E. Bailey, The mean energy transfer rate to comets in the Oort cloud and implications for cometary origins. Mon. Not. R. Astron. Soc. **218**, 1–30 (1986)
G.M. Bernstein, D.E. Trilling, R.L. Allen, M.E. Brown, M. Holman, R. Malhotra, The size distribution of trans-Neptunian bodies. Astron. J. **128**, 1364–1390 (2004)
R. Brasser, M.J. Duncan, H.F. Levison, Embedded star clusters and the formation of the Oort cloud. Icarus **184**, 59–82 (2006)
R. Brasser, M.J. Duncan, H.F. Levison, Embedded star clusters and the formation of the Oort Cloud: II. The effect of the primordial Solar nebula. Icarus **191**, 413–433 (2007)
M.E. Brown, C. Trujillo, D. Rabinowitz, Discovery of a candidate inner Oort cloud planetoid. Astrophys. J. Lett. **617**, 645–649 (2004)
M.E. Brown, C. Trujillo, D. Rabinowitz, Discovery of a planet-sized body in the scattered Kuiper belt. Astrophys. J. **635**, L97–L100 (2005)
J. Byl, Galactic perturbations on nearly parabolic cometary orbits. Moon Planets **29**, 121–137 (1983)
J. Byl, The effect of the galaxy on cometary orbits. Earth, Moon, Planets **36**, 263–273 (1986)
J. Byl, Galactic removal rates for long-period comets. Astron. J. **99**, 1632–1635 (1990)
A. Carusi, G.B. Valsecchi, Dynamical evolution of short-period comets, in *European Regional Astronomy Meeting of the IAU*, vol. 2 (1987), pp. 21–28

G. Chabrier, The galactic disk mass budget. I. Stellar mass function and density. Astrophys. J. **554**, 1274–1281 (2001)
W.P. Chen et al., Search for small trans-Neptunian objects by the TAOS project, in *Proceedings IAU Symposium* No. 236, ed. by G.B. Valsecchi, D. Vokrouhickly (Cambridge Univ. Press, 2006), pp. 65–68
C. de la Fuente Marcos, R. de la Fuente Marcos, On the origin of comet C/1999 S4 LINEAR. Astron. Astrophys. **395**, 697–704 (2002)
A.H. Delsemme, Galactic tides affect the Oort cloud: An observational confirmation. Astron. Astrophys. **187**, 913–918 (1987)
L. Dones, P.R. Weissman, H.F. Levison, M.J. Duncan, Oort cloud formation dynamics, in *Comets II*, ed. by M. Festou, H.U. Keller, H.A. Weaver (2004), pp. 153–174
M.J. Duncan, H.F. Levison, A scattered comet disk and the origin of Jupiter family comets. Science **276**, 1670–1672 (1997)
M.J. Duncan, H.F. Levison, L. Dones, Dynamical evolution of ecliptic comets. In *Comets II*, ed. by M. Festou, H.U. Keller, H.A. Weaver (2004), pp. 193–204
M. Duncan, T. Quinn, S. Tremaine, The origin of short-period comets. Astrophys. J. **328**, L69–L73 (1988)
P.A. Dybczyński, Simulating observable comets. III. Real Stellar Perturbers of the Oort cloud and their output. Astron. Astrophys. **449**, 1233–1242 (2006)
K.E. Edgeworth, The origin and evolution of the Solar System. Mon. Not. R. Astron. Soc. **109**, 600–609 (1949)
S. Eggers, Cometary dynamics during the formation of the solar system. Ph.D. thesis, Max-Planck-Institut für Aeronomie (1999)
S. Eggers, H.U. Keller, P. Kroupa, W.J. Markiewicz, Origin and dynamics of comets and star formation. Planet. Space Sci. **45**, 1099–1104 (1997)
S. Eggers, H.U. Keller, W.J. Markiewicz, P. Kroupa, Cometary dynamics in a star cluster. Astronomische Gesellschaft meeting abstracts **14**, 5 (1998), abstract
V.V. Emel'yanenko, M.E. Bailey, Capture of Halley-type comets from the near-parabolic flux. Mon. Not. R. Astron. Soc. **298**, 212–222 (1998)
E. Everhart, in *Comets–Asteroids–Meteorites*, ed. by A.H. Delsemme (University of Toledo Press, Ohio, 1977)
J.A. Fernandez, On the existence of a comet belt beyond Neptune. Mon. Not. R. Astron. Soc. **192**, 481–491 (1980)
J.A. Fernández, The formation of the Oort cloud and the primitive galactic environment. Icarus **129**, 106–119 (1997)
J.A. Fernández, Changes in the inclination-distribution of long-period comets with the orbital energy, *ESA SP-500: Asteroids, Comets, and Meteors: ACM 2002* (2002), pp. 303–304
J.A. Fernández, A. Brunini, The buildup of a tightly bound comet cloud around an early Sun immersed in a dense galactic environment: Numerical experiments. Icarus **145**, 580–590 (2000)
J.A. Fernández, T. Gallardo, The transfer of comets from parabolic orbits to short-period orbits: Numerical studies. Astron. Astrophys. **281**, 911–922 (1994)
P.J. Francis, The demographic of long-period comets. Astrophys. J. **635**, 1348–1361 (2005)
E.J. Gaidos, Paleodynamics: Solar System formation and the early environment of the Sun. Icarus **114**, 258–268 (1995)
J. García-Sánchez, R.A. Preston, D.L. Jones, P.R. Weissman, J.F. Lestrade, D.W. Latham, R.P. Stefanik, Stellar encounters with the Oort cloud based on Hipparcos data. Astron. J. **117**, 1042–1055 (1999). Erratum in Astron. J. **118**, 600
J. García-Sánchez, P.R. Weissman, R.A. Preston, D.L. Jones, J.-F. Lestrade, D.W. Latham, R.P. Stefanik, J.M. Paredes, Stellar encounters with the Solar System. Astron. Astrophys. **379**, 634–659 (2001)
B. Gladman, C. Chan, Production of the extended scattered disk by rogue planets. Astrophys. J. **643**, L135–L138 (2006)
B. Gladman, J.J. Kavelaars, J.-M. Petit, A. Morbidelli, M.J. Holman, T. Loredo, The structure of the Kuiper belt: Size distribution and radial extent. Astron. J. **122**, 1051–1066 (2001)
B. Gladman, M. Holman, T. Grav, J. Kavelaars, P. Nicholson, K. Aksnes, J.-M. Petit, Evidence for an extended scattered disk. Icarus **157**, 269–279 (2002)
B. Gladman, G.G. Marsden, C. Van Laerhoven, Nomenclature in the outer Solar System, in *The Solar System Beyond Neptune*, ed. by M.A. Barucci, H. Boehnhardt, D.P. Cruikshank, A. Morbidelli (University of Arizona, Tucson, 2008), 43–57
R.S. Gomes, T. Gallardo, J.A. Fernandez, A. Brunini, On the origin of the high-perihelion scattered disk: The role of the Kozai mechanism and mean motion resonances. Cel. Mech. Dyn. Ast. **91**, 109–129 (2005a)
R.S. Gomes, J.J. Matese, J.J. Lissauer, A distant planetary-mass solar companion may have produced distant detached objects. Icarus **184**, 589–601 (2006)

R.S. Gomes, A. Morbidelli, H.F. Levison, Planetary migration in a planetesimal disk: Why did Neptune stop at 30 AU? Icarus **170**, 492–507 (2004)
R.A. Gutermuth, S.T. Megeath, J.L. Pipher, J.P. Williams, L.E. Allen, P.C. Myers, S.N. Raines, The initial configuration of young stellar clusters: A K-band number counts analysis of the surface density of stars. Astrophys. J. **632**, 397–420 (2005)
J.M. Hahn, R. Malhotra, Orbital evolution of planets embedded in a planetesimal disk. Astron. J. **117**, 3041–3053 (1999)
C. Hayashi, K. Nakazawa, Y. Nakagawa, Formation of the solar system, in *Protostars and Planets II* (University of Arizona Press, Tucson, 1985), pp. 1100–1153
J. Heisler, Monte Carlo simulations of the Oort comet cloud. Icarus **88**, 104–121 (1990)
J. Heisler, S. Tremaine, The influence of the galactic tidal field on the Oort comet cloud. Icarus **65**, 13–26 (1986)
A. Higuchi, E. Kokubo, T. Mukai, Cometary dynamics: Migration due to gas drag and scattering by protoplanets. ESA SP-500: *Asteroids, Comets, and Meteors*. ACM (2002), pp. 453–456
J.G. Hills, Comet showers and the steady-state infall of comets from the Oort cloud. Astron. J. **86**, 1730–1740 (1981)
P. Joss, Astron. Astrophys. **25**, 271 (1973)
S.J. Kenyon, B.C. Bromley, Collisional cascades in planetesimal disks. I. Stellar flybys. Astron. J. **123**, 1757–1775 (2002)
S.J. Kenyon, B.C. Bromley, Stellar encounters as the origin of distant Solar System objects in highly eccentric orbits. Nature **432**, 598–602 (2004a)
S.J. Kenyon, B.C. Bromley, The size distribution of Kuiper belt objects. Astron. J. **128**, 1916–1926 (2004b)
G.P. Kuiper, On the origin of the Solar System, in *Proceedings of a Topical Symposium, Commemorating the 50th Anniversary of the Yerkes Observatory and Half a Century of Progress in Astrophysics*, ed. by J.A. Hynek (McGraw-Hill, New York, 1951), pp. 357–414
C.J. Lada, E.A. Lada, Embedded clusters in molecular clouds. Annu. Rev. Astron. Astrophys. **41**, 57–115 (2003)
C.J. Lada, M. Margulis, D. Dearborn, The formation and early dynamical evolution of bound stellar systems. Astrophys. J. **285**, 141–152 (1984)
M.J. Lehner, The Whipple mission. Talk presented at 2006 TNO conference in Catania, Italy (2006)
H.F. Levison, Comet taxonomy, in *Completing the Inventory of the Solar System*. ASP Conf. Ser, vol. 107 (1996), pp. 173–191
H.F. Levison, M.J. Duncan, The long-term dynamical behavior of short-period comets. Icarus **108**, 18–36 (1994)
H.F. Levison, M.J. Duncan, From the Kuiper belt to Jupiter-family comets: The spatial distribution of ecliptic comets. Icarus **127**, 13–32 (1997)
H.F. Levison, L. Dones, M.J. Duncan, The origin of Halley-type comets: Probing the inner Oort cloud. Astron. J. **121**, 2253–2267 (2001)
H.F. Levison, A. Morbidelli, C. van Laerhoven, R. Gomes, K. Tsiganis, Origin of the structure of the Kuiper belt during a dynamical instability in the orbits of Uranus and Neptune (2008) astro-ph preprint
H.F. Levison, M.J. Duncan, L. Dones, B.J. Gladman, The scattered disk as a source of Halley-type comets. Icarus **184**, 619–633 (2006)
J. Matese, D. Whitmire, Tidal imprint of distant galactic matter on the Oort comet cloud. Astrophys. J. **472**, L41–L43 (1996)
J.J. Matese, D.P. Whitmire, J.L. Lissauer, A wide binary Solar companion as a possible origin of Sedna-like objects. Earth, Moon Planets **97**, 459–470 (2005)
J.J. Matese, P.G. Whitman, K.A. Innanen, M.J. Valtonen, Periodic modulation of the Oort cloud comet flux by the adiabatically changing galactic tide. Icarus **116**, 255–268 (1995)
A. Morbidelli, H. Levison, Scenarios for the origin of the orbits of the trans-Neptunian objects 2000 CR105 and 2003 VB12. Astron. J. **128**, 2564–2576 (2004)
A. Morbidelli, H. Levison, R. Gomes, The dynamical structure of the Kuiper belt and its primordial origin, in *The Solar System Beyond Neptune*, ed. by M.A. Barucci, H. Boehnhardt, D.P. Cruikshank, A. Morbidelli (University of Arizona, Tucson, 2008), 275–292
H.A. Newton, Astron. J. **11**, 73 (1891)
H.A. Newton, Mem. Natl. Acad. Sci. **6**, 7 (1893)
J.H. Oort, The structure of the cloud of comets surrounding the Solar System and a hypothesis concerning its origin. Bull. Astron. Inst. Neth. **11**, 91–110 (1950)
T. Quinn, S. Tremaine, M. Duncan, Planetary perturbations and the origins of short-period comets. Astrophys. J. **355**, 667–679 (1990)
F. Roques et al., Exploration of the Kuiper belt by high-precision photometric stellar occultations: First results. Astrophys. J. **132**, 819–822 (2006)

R. Smoluchowski, M. Torbett, The boundary of the Solar System. Nature **311**, 38–39 (1984)
S.A. Stern, On the collisional environment, accretion time scales, and architecture of the massive, primordial Kuiper belt. Astron. J. **112**, 1203–1217 (1996)
E.W. Thommes, M.J. Duncan, H.F. Levison, The formation of Uranus and Neptune in the Jupiter–Saturn region of the Solar System. Nature **402**, 635–638 (1999)
E.W. Thommes, M.J. Duncan, H.F. Levison, The formation of Uranus and Neptune among Jupiter and Saturn. Astron. J. **123**, 2862–2883 (2002)
E.W. Thommes, M.J. Duncan, H.F. Levison, Oligarchic growth of giant planets. Icarus **161**, 431–455 (2003)
M. Torbett, Astron. J. **98**, 1477 (1989)
S. Tremaine, The distribution of comets around stars, in *Planets Around Pulsars*, ed. by J.A. Phillips, S.E. Thorsett, S.R. Kulkarni. Astronomical Society of the Pacific conference series (1993), pp. 335–344
C.A. Trujillo, D.C. Jewitt, J.X. Luu, Population of the scattered Kuiper belt. Astrophys. J. Lett. **529**, L103–L106 (2000)
K. Tsiganis, R. Gomes, A. Morbidelli, H.F. Levison, Origin of the orbital architecture of the giant planets in the Solar System. Nature **402**, 635–638 (2005)
M.D. Weinberg, S.L. Shapiro, I. Wasserman, The dynamical fate of wide binaries in the solar neighborhood. Astrophys. J. **312**, 367–389 (1987)
P.R. Weissman, The Oort cloud. *Completing the Inventory of the Solar System*. ASP Conf. Ser., vol. 107 (1996), pp. 265–288
S. Yabushita, On exact solutions of diffusion equations in cometary dynamics. Astron. Astrophys. **85**, 77–79 (1980)

Reservoirs for Comets: Compositional Differences Based on Infrared Observations

Michael A. DiSanti · Michael J. Mumma

Originally published in the journal Space Science Reviews, Volume 138, Nos 1–4.
DOI: 10.1007/s11214-008-9361-0

Abstract Tracing measured compositions of comets to their origins continues to be of keen interest to cometary scientists and to dynamical modelers of Solar System formation and evolution. This requires building a taxonomy of comets from both present-day dynamical reservoirs: the Kuiper Belt (hereafter KB), sampled through observation of ecliptic comets (primarily Jupiter Family comets, or JFCs), and the Oort cloud (OC), represented observationally by the long-period comets and by Halley Family comets (HFCs). Because of their short orbital periods, JFCs are subjected to more frequent exposure to solar radiation compared with OC comets. The recent apparitions of the JFCs 9P/Tempel 1 and 73P/Schwassmann-Wachmann 3 permitted detailed observations of material issuing from below their surfaces—these comets added significantly to the compositional database on this dynamical class, which is under-represented in studies of cometary parent volatiles. This chapter reviews the latest techniques developed for analysis of high-resolution spectral observations from ∼2–5 μm, and compares measured abundances of native ices among comets. While no clear compositional delineation can be drawn along dynamical lines, interesting comparisons can be made. The sub-surface composition of comet 9P, as revealed by the Deep Impact ejecta, was similar to the majority of OC comets studied. Meanwhile, 73P was depleted in all native ices except HCN, similar to the disintegrated OC comet C/1999 S4 (LINEAR). These results suggest that 73P may have formed in the inner giant planets' region while 9P formed farther out or, alternatively, that both JFCs formed farther from the Sun but with 73P forming later in time.

Keywords Comets · Ices · Composition · Parent volatiles · Molecular spectroscopy · Infrared spectroscopy

ISSI Workshop on the Origin and Evolution of Cometary Nuclei, Bern, Switzerland, October 16-20, 2006.

M.A. DiSanti (✉) · M.J. Mumma
Solar System Exploration Division, NASA-Goddard Space Flight Center, Mail Stop 693, Greenbelt, MD 20771, USA
e-mail: michael.a.disanti@nasa.gov

H. Balsiger et al. (eds.), *Origin and Early Evolution of Comet Nuclei*
DOI: 10.1007/978-0-387-85455-7_8

Abbreviations

JFC Jupiter Family Comet
OC Oort Cloud
KB Kuiper Belt
HFC Halley Family Comet
RP Spectral Resolving Power
9P 9P/Tempel 1
73P 73P/Schwassmann-Wachmann 3
21P 21P/Giacobini-Zinner

1 Introduction

Comets formed relatively far from the Sun, where temperatures were low enough for ices to condense. They reside for long periods of time in the outer Solar System, so the ices contained in their nuclei (i.e., the native ices) retain a relatively well-preserved footprint of conditions when and where they formed, and their abundances can provide clues to the formation and evolution of the Solar System. The original structures and compositions of native ices should reflect local conditions (chemistry, temperature, degree of radiation processing) prevalent when and where they formed (Bockelée-Morvan et al. 2005; Irvine et al. 2000; Mumma et al. 1993).

Although comets contain relatively primitive icy material remaining from the epoch of Solar System formation, the extent to which they are modified from their initial state is a fundamental question in cometary science. The current orbits of comets provide information on their recent dynamical history, however tracing cometary origins is complicated by their radial migration in the protoplanetary disk and by dynamical interactions with the growing giant planets (Levison and Morbidelli 2003; Gomes et al. 2005; Tsinganis et al. 2005). Such interactions placed comets into two principal present-day reservoirs: the Oort cloud (OC) and the Edgeworth-Kuiper Belt (KB), where they remain largely unaltered until perturbed into the inner Solar System (Stern 2003; Gladman 2005). In concert with recent and ongoing dynamical modeling of Solar System formation and evolution, a more complete understanding of cometary origins can be gained through observations measuring the native ice compositions of comets from these reservoirs.

The OC population is sampled primarily through observations of long-period comets ($P > 200$ years) as well as comets perturbed into shorter period orbits such as those presently in the Halley dynamical family (HFCs). The KB population can be sampled spectroscopically through observations of comets in very short-period orbital resonance with Jupiter and the Sun. These represent the Jupiter family comets (JFCs), a transitional population fed primarily from the (recently recognized) scattered (i.e., higher orbital eccentricity) component of the Kuiper disk (Bernstein et al. 2004). Compared with OC comets, JFCs tend to have lower production rates and (perhaps) more highly processed surface layers due to their short orbital periods. It is therefore natural to investigate whether systematic compositional differences exist between JFCs and OC comets.

The comet nucleus warms when approaching the Sun, causing native ices to release "parent volatiles" into the coma where they can be sensed spectroscopically. A number of parent molecules have strong fundamental vibrational bands at near infrared (NIR) wavelengths ($\lambda \sim 2$–5 μm), and many have pure rotational transitions at radio (sub-millimeter and millimeter) wavelengths. Technological advances over the past 1–2 decades have led to tremendous progress in the study of parent molecules in comets, and this has formed the basis

for a new (and continually growing) cometary taxonomy based on native ice composition. Approximately two dozen parent species are identified to date (e.g., see Fig. 12 of Bockelée-Morvan et al. 2005), although most of the more complex (and generally less abundant) ones (including ethylene glycol; see Crovisier et al. 2004, and Fig. 3 of Crovisier 2006a) have been seen only in one unusually bright comet (C/1995 O1 Hale-Bopp).

This chapter emphasizes recent NIR results. The following section presents a brief overview of existing high-resolution NIR echelle spectrometers and the capabilities they afford. The latest techniques developed for efficiently measuring rotational temperatures ($T_{\rm rot}$) of parent molecules, for measuring spatially resolved ortho-to-para ratios (i.e., spin temperatures, $T_{\rm spin}$) for cometary H_2O in the coma, and for studying chemically related parent species that provide clues to cold gas-grain interstellar chemistry are then discussed. This is followed by integration of the latest compositional findings into the overall picture as represented previously by the reviews of Bockelée-Morvan et al. (2005) and Mumma et al. (2003); see also Crovisier (2006b). Finally, prospects for future advances in studies of cometary parent volatile composition are presented.

2 Near-Infrared Instrumentation and Capabilities

Modern NIR echelle spectrometers feature sufficiently high spectral resolving powers ($\mathrm{RP} \equiv \lambda/\Delta\lambda > 10^4$) to measure intensities of individual emission lines with high signal-to-noise. Because gas outflow speeds are typically $\sim$1 km s^{-1} in the coma, cometary lines are not resolved by NIR array spectrometers and so the line-to-continuum contrast increases with increasing RP. These instruments also have small (sub-arc-second) pixels, permitting the spatial distribution of line emission in the coma to be measured at high spatial resolution. The combination of their RP and small solid angle per pixel translates to a highly dispersed thermal background and therefore to increased sensitivity compared with instruments having lower RP and larger subtense per detector element. In contrast, radio spectrometers feature sufficient RP (typically $>10^5$) to resolve cometary emission lines and so provide a measure of gas kinematics in the coma and also reduced ambiguity in identifying line emissions that would otherwise be blended at lower spectral resolution, however they do not provide the spatial resolution available in the NIR (typically 1 arc-second or better; see below).

2.1 Instrumentation

The first instrument to deliver $\mathrm{RP} > 2 \times 10^4$ was CSHELL (Tokunaga et al. 1990; Greene et al. 1994) at the NASA-IRTF 3-m telescope. Commissioned in 1993, CSHELL incorporates a 256×256-pixel array with pixels subtending 0.2 arc-second square, a slit length of 30 arc-seconds, and achieves spectral coverage (spectral grasp per echelle setting) of $\sim 2.3 \times 10^{-3}$ times the central wavelength. The first detections of a cometary parent volatile (H_2O) achieved using CSHELL were in C/1991a1 (Shoemaker-Levy) and in 6P/d'Arrest. Spectral emission lines of the 2 μm hot-band ($\nu_1 + \nu_2 + \nu_3 - \nu_1$) of H_2O were identified in each comet, and water production rates were derived (Mumma et al. 1995). Observations of the bright long-period comet C/1996 B2 (Hyakutake) in spring 1996 first demonstrated the power of CSHELL for compositional studies of parent volatiles in comets (Mumma et al. 1996; Brooke et al. 1996).

The second major technological advance in the field came with the availability of NIRSPEC (McLean et al. 1998) at the Keck-2 (10-m) telescope. This instrument uses a 1024×1024 array, with pixel subtense similar to that of CSHELL; however the larger

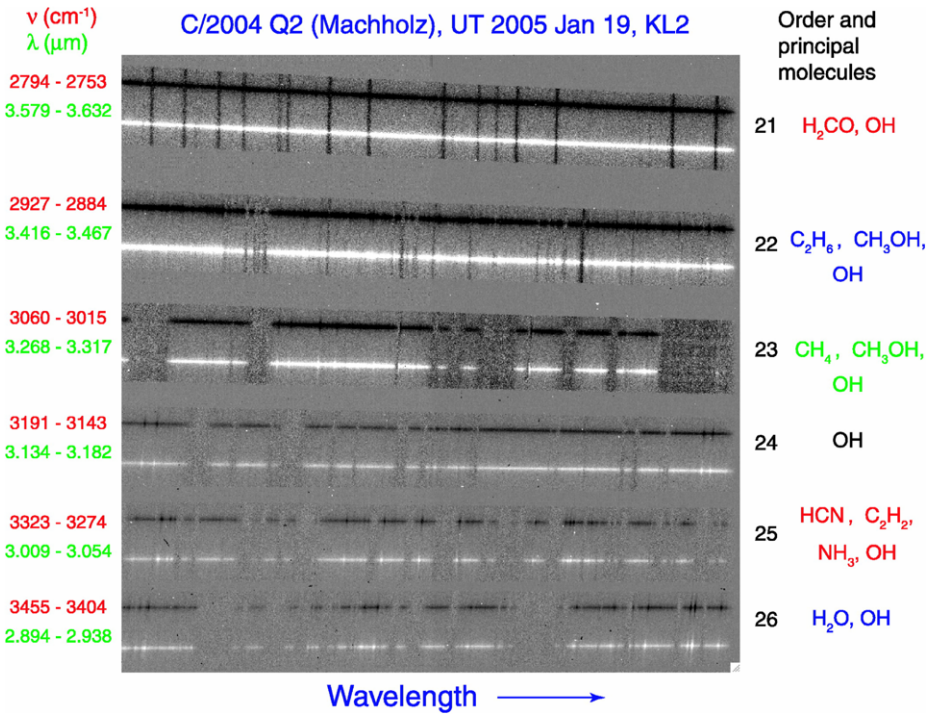

Fig. 1 NIRSPEC A-B difference frame, which cancels sky emission and reveals comet signal in A-beam (*white*) and B-beam (*black*) positions, plus terrestrial atmospheric absorptions (running vertically). Molecular emissions are bright features superimposed on the cometary continuum. This illustrates the piece-wise continuous spectral coverage (indicated to the left) afforded by NIRSPEC; all species listed on the right are measured simultaneously, eliminating important systematic uncertainties in the subsequent analysis. Note that lines of OH prompt emission are present in all six orders—these serve as a proxy for water production in the event that H_2O cannot be observed directly (e.g., see Fig. 3A). (Adapted from Bonev et al. 2006)

telescope aperture at Keck translates to a tighter point spread function and higher sensitivity. NIRSPEC achieves a RP similar to CSHELL, but is cross dispersed, so multiple echelle orders are sampled simultaneously with successive orders displaced spatially from each other by means of a lower-resolution grating oriented orthogonally to the echelle. Six orders are spanned in the L-band (Fig. 1), and three orders in the M-band, permitting multiple parent species (e.g., CO, CH_4, C_2H_6, C_2H_2, HCN, CH_3OH, H_2CO, NH_3) and daughter fragments such as OH (through both fluorescent and prompt emission), CN, and NH_2 to be targeted simultaneously with H_2O. A nearly-complete L-band spectral survey between ~2.8–3.7 μm can be obtained using only three echelle/cross-disperser settings, as was first demonstrated for comet C/1999 H1 (Lee) in 1999 (Mumma et al. 2001a; Dello Russo et al. 2006). The spectral coverage *per order* is approximately six times that of CSHELL (Fig. 2).

A cross-dispersed spectrometer (IRCS, Kobayashi et al. 2000) at the Subaru 8-m telescope has been used for NIR studies of parent volatiles in comets since 2002, when CH_4, CH_3D, and C_2H_6 were characterized in 153P/Ikeya-Zhang (Kawakita et al. 2003; see also Table 1). Since then, IRCS has been used to study parent volatiles, spin temperatures, and abundances of related isotopic (deuterated) species in several comets (Kawakita et al. 2005, 2006a, 2006b). It delivers somewhat lower spectral resolving power (RP ~ 1×10^4)

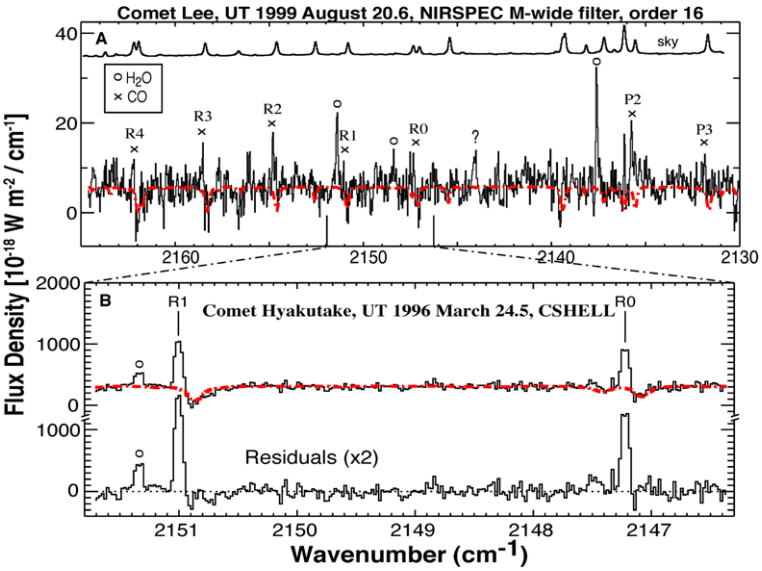

Fig. 2 Spectra showing emissions of CO (labeled by rotational designation) and H_2O near 4.7 μm. Note the vastly different abundances of CO relative to H_2O in these two comets (see Table 1), and the greater spectral coverage afforded by NIRSPEC. Subtracting the synthetic transmittance spectrum of the terrestrial atmosphere (*dashed line*) results in observed residual emission in excess of the continuum (the "Residuals" in panel B). (From Mumma et al. 2001a)

than CSHELL or NIRSPEC, but offers broader spectral coverage per order (by approximately a factor of two) compared with NIRSPEC.

2.2 Overview of Capabilities

In the past 10–15 years, the NIR spectral region has become fertile ground for the direct study of parent volatiles in comets using these instruments. There are several important areas in which the NIR is unique:

1. Measurement of symmetric hydrocarbons (e.g., C_2H_2, CH_4, C_2H_6, e.g., see Fig. 9 of Bockelée-Morvan et al. 2005), which lack a permanent dipole moment and therefore have no allowed pure rotational transitions, and whose electronic states pre-dissociate, precluding study at UV wavelengths.
2. Direct measurement of water production through non-resonant (or "hot-band") fluorescent emission (Weaver et al. 1986, 1987; Bockelée-Morvan and Crovisier 1989; Mumma et al. 1996; Dello Russo et al. 2000)—line intensities have been modeled over a range of T_{rot} for ten hot bands between ~2 and 5 μm (Dello Russo et al. 2005, 2006).
3. Use of OH prompt emission as a proxy for water production in cases when simultaneous direct observation of H_2O itself is not possible (Mumma et al. 2001a; Bonev 2005; Bonev et al. 2006), and as a means of studying unimolecular dissociation dynamics of H_2O under conditions not easily attainable in terrestrial laboratories (Bonev and Mumma 2006).
4. The small pixels and long slit allow release of parent volatiles (native sources) to be distinguished from potential extended release in the coma. For example, this permits

abundances of native CO, H_2CO, and CH_3OH to be quantified and compared a systematic way (see DiSanti et al. 2002, and discussion below).

5. The NIR provides a means to efficiently measure molecular excitation (i.e., T_{rot}) for a number of parent species, through simultaneous observation of lines sampling a range of rotational energies. The long-slit coverage also permits spatially resolved measures of T_{rot} for cometary parent molecules and, most recently, of T_{spin} for H_2O in the coma (Bonev et al. 2007).

2.3 Measurement of Rotational Temperatures

It is generally not possible to sample all quantum states in a given molecular band, owing to factors such as atmospheric extinction, limited instrumental sensitivity, and incomplete spectral coverage. Application of a quantum band model to encompassed lines can provide a measure of rotational temperature provided these lines sample a range of rotational energies. Once T_{rot} is known, this establishes the fluorescence efficiencies (g-factors) for the lines sampled, and so permits calculation of the total abundance (i.e., the production rate) for that species. For simple linear molecules (e.g., HCN, C_2H_2, CO), a Boltzmann analysis can be applied in which emitted line flux is graphed against upper state rotational energy. The negative inverse slope provides T_{rot} (Magee-Sauer et al. 1999; DiSanti et al. 2001; Mumma et al. 2001a).

For structurally more complex molecules, a general method (that also applies to linear molecules) has been developed that can be applied to any molecule having line intensities modeled over a range of rotational energies and temperatures. Observed and modeled emission line intensities are compared using two complementary approaches: (1) a correlation analysis, and (2) an excitation analysis. This latter approach was first applied to observations of H_2O in comet 153P/Ikeya-Zhang (Dello Russo et al. 2004). The two approaches were first combined to retrieve T_{rot} for H_2CO in C/2002 T7 (LINEAR) and for H_2O in C/2001 WM_1 (LINEAR) and C/2004 Q2 (Machholz) using streamlined software algorithms (see Fig. 3, and discussions in DiSanti et al. 2006 and Bonev 2005). Modeled g-factors are first multiplied by the terrestrial atmospheric transmittance at each Doppler-shifted line-center frequency, and are then convolved to the resolving power of the observations and compared with observed line intensities, stepping through a range in T_{rot} (Fig. 3).

2.4 Calculation of Native Production Rates

A general method for calculating production rates (Q, molecules s^{-1}) from line intensities contained in a square aperture that is stepped along the slit (the "Q-curve" method) has been described extensively in the literature (Dello Russo et al. 1998; Magee-Sauer et al. 1999; Dello Russo et al. 2000; DiSanti et al. 2001; Mumma et al. 2003). Owing to slit losses, production rates calculated in this manner invariably increase from a nucleus-centered value to a constant value (the "terminal Q," or "global Q") at some distance from the nucleus. A "growth factor" is defined as the ratio of terminal to nucleus-centered production rates; this factor is established from a summed (from multiple lines) emission profile, and is applicable to all concurrently obtained native volatile emissions. Applying this growth factor to nucleus-centered production rates measured for each individual line yields reliable global line-by-line production rates. The global production rate of a native volatile is then the mean of these global Q's, weighted by the stochastic noise associated with each line (see Dello Russo et al. 2005 and Bonev 2005 for detailed discussions).

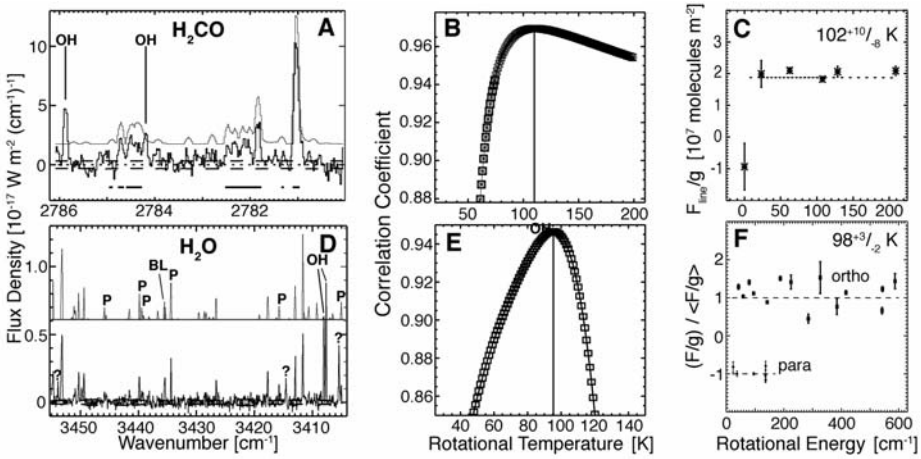

Fig. 3 Observations of (**A–C**) C/2002 T7 (from DiSanti et al. 2006) and (**D–F**) C/2004 Q2 (from Bonev et al. 2006) using CSHELL and NIRSPEC, respectively, illustrating the approach to measuring rotational temperatures of cometary molecules. **A**, **D**. Cometary residuals and convolved fluorescence model (*light trace*). In panel **D**, para lines are marked (*P*), as is an ortho-para blend (BL); all unlabeled lines are ortho, and these are used to measure $T_{\rm rot}$ (see Bonev et al. 2006). Comparing model and residuals for selected spectral regions in panel **A** (indicated by *horizontal lines*), and for unblended H_2O lines in panel **D**, yields consistent results from correlation (panels **B**, **E**) and excitation (panels **C**, **F**) analyses (in panel **F**, the para lines are offset vertically from the ortho lines for clarity). At the optimal $T_{\rm rot}$, the ratio $F_{\rm line}/g$ is independent of rotational energy; i.e., the best-fit linear slope is zero. *Dashed lines* in panels **A** and **D** represent the $\pm 1\sigma$ error. Panel **A** includes the H_2CO ν_1 Q-branch (the strong feature at 2781 $\rm cm^{-1}$) and simultaneously measured OH prompt emissions, used as a proxy for measuring H_2O production

2.5 Measurement of Chemically Related Parent Species in Comets

To explain the high C_2H_6 to CH_4 abundance observed in Comet Hyakutake, a scenario involving hydrogen atom addition (e.g., to C_2H_2) on surfaces of icy-mantled grains prior to their incorporation into the nucleus was proposed (Mumma et al. 1996), since the formation of C_2H_6 in the gas phase is energetically inhibited. This trend of high C_2H_6/CH_4 abundance has been observed in all comets characterized since then, suggesting that H-atom addition was a common and important process in the evolution of pre-cometary grains.

CO should also be hydrogenated on grain surfaces. Laboratory irradiation experiments on interstellar ice analogs have shown the yields of the chemically linked molecules H_2CO and CH_3OH resulting from this process to be highly dependent both on hydrogen density (i.e., fluence) and on temperature in the range ~10–25 K (Hiraoka et al. 2002; Watanabe et al. 2004). H-atom addition to CO produces the highly reactive formyl radical (HCO). This subsequently converts to monomeric formaldehyde (H_2CO) and then to CH_3OH, or alternatively to formic acid (HCOOH) (these three products have been confirmed in laboratory simulations; Hudson and Moore 1999). HCO can in principle also build formaldehyde polymers such as polyoxymethylene (POM) (Huebner et al. 1987; Meier et al. 1993; Cottin et al. 2001, 2004). Comparing the relative abundances of native CO, H_2CO, and CH_3OH in comets provides one test of the hydrogenation efficiency; this was exemplified through observations of 153P/Ikeya-Zhang using CSHELL (DiSanti et al. 2002). A range of efficiencies is suggested among comets measured to date (DiSanti et al. 2005, 2007a), and the laboratory yields provide a basis for comparison in assessing natal conditions.

2.6 Spatially Resolved Measurements of T_{spin} for H_2O in the Coma

The water molecule exists in two isomeric forms, depending whether the nuclear spins of its H-atoms are parallel (ortho-H_2O) or anti-parallel (para-H_2O). Radiative and collisional transitions between these isomers are strongly forbidden, but the probability of their interconversion is non-zero. Because the lowest level of ortho-H_2O has an energy 23.8 cm^{-1} above that of para-H_2O, the ratio of total populations in ortho and para states (the ortho-to-para ratio, OPR) is temperature-dependent, and the spin temperature is uniquely defined for OPR < 3.0 (the equilibrium value; e.g., see Fig. 1 in Mumma et al. 1987). The OPR for cometary H_2O has been reported in eleven comets, nine summarized in Bonev et al. (2007), plus fragments B and C of 73P (Dello Russo et al. 2007; Bonev et al. 2008). Crovisier (1984) and Mumma et al. (1987, 1993) explored the idea that T_{spin} for H_2O measured in comets reflects its chemical formation temperature (i.e., that the OPR is preserved in the nucleus); see also the extended discussion in Bockelée-Morvan et al. (2005).

To date, there is no definitive evidence that H_2O molecules undergo nuclear spin conversion during their long residence in the interior of a comet or in the coma after sublimation. As used previously for identification of extended sources and for spatially resolved measurements of T_{rot} in comets (Dello Russo et al. 1998; DiSanti et al. 1999, 2001, 2003), the small pixels and long-slit capability of modern NIR spectrometers permit T_{spin}-conversion in the coma to be tested. In the case of C/2004 Q2 (Machholz), the OPR of H_2O did not vary with cometocentric distance in the coma (Bonev et al. 2007; see Fig. 4).

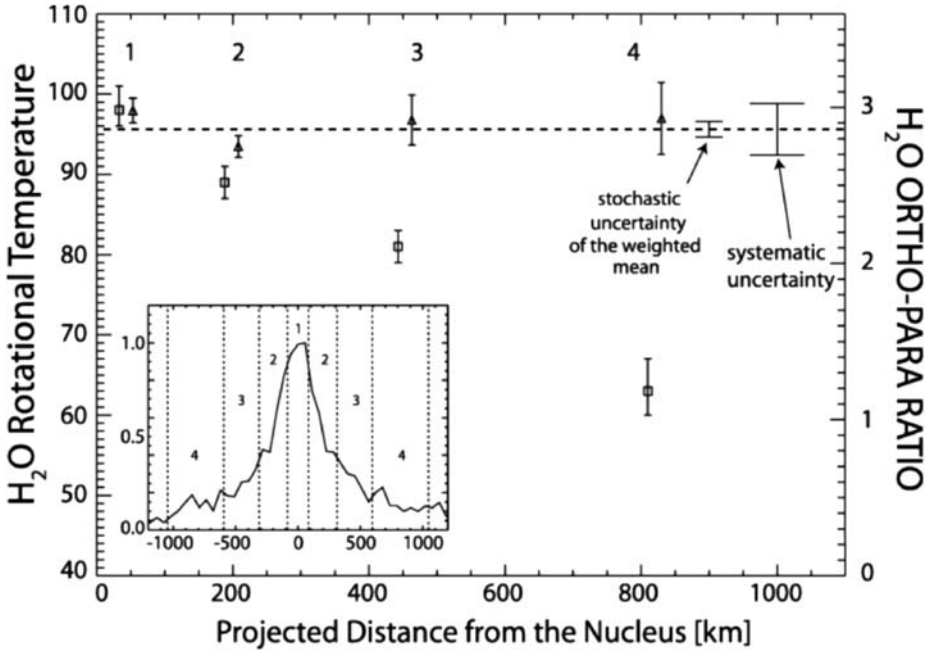

Fig. 4 Measured T_{rot} (*squares*) and OPRs (*triangles*) for H_2O in the inner coma of C/2004 Q2 (Machholz), along with the weighted mean OPR value (*dashed horizontal line*). *Inset*: Spatial profile (normalized intensity vs. projected nucleocentric distance, in km) of H_2O emission in C/2004 Q2, formed by summing (column by column) the signal of all detected water lines. Each measurement of T_{rot} and OPR corresponds to a range of cometocentric distances (averaged to either side of the nucleus), as indicated. (Adapted from Bonev et al. 2007)

Table 1 Organic parent volatile abundances in comets ($H_2O = 100$)*

OC comets[a]	CO**	CH_4	C_2H_6	C_2H_2	HCN	CH_3OH
C/1996 B2	15 ±1.9	0.79 ±0.08	0.62 ±0.07	0.16 ±0.08	0.18 ±0.04	1.7 ±0.4[b]
C/1995 O1	12 ±0.4	1.45 ±0.16	0.56 ±0.04	0.31 ±0.1	0.27 ±0.04	2.4 ±0.3[b,c]
C/1999 H1	1.8 ±0.2	1.45 ±0.18	0.67 ±0.07	0.27 ±0.03	0.29 ±0.02	2.1 ±0.5
153P/I-Z‡	4.7 ±0.8	0.51 ±0.06	0.62 ±0.18	0.18 ±0.05	0.18 ±0.05	2.5 ±0.5
Mean**	**1.8 – 15**	**0.5 – 1.5**	**0.59 ±0.03**	**0.24 ±0.03**	**0.26 ±0.03**	**2.2 ±0.2**
C/2001 A2	3.9 ±1.1[d]	1.2 ±0.2[e]	1.7 ±0.2[d]	0.5 ±0.1[d]	0.6 ±0.1[d]	3.9 ±0.4[d]
1P/Halley	3.5[f]	< 1[f]	∼ 0.4[f]	∼ 0.3[f]	∼ 0.2[f]	1.7 ±0.4[g]
C/1999 S4	< 0.4[h] 0.9 ±0.3	0.18 ±0.06	0.11 ±0.02	< 0.12	0.10 ±0.03	< 0.15
JF Comets						
9P						
Preimpact (ambient)			0.23 ±0.04[j]		0.18 ±0.06[i]	1.3 ±0.20[i]
Postimpact (amb.+ejecta)	4.3 ±1.7[i]	0.54 ±0.30[i]	0.40 ±0.04[j]	0.13 ±0.04[i]	0.22 ±0.03[j]	0.99 ±0.17[i]
(ejecta alone)			0.55 ±0.09[j]		0.24 ±0.07[j]	
73P-B[k]			< 0.3		< 0.2	
73P-B[l]	< 1.9		0.14 ±0.01	< 0.060	0.28 ±0.01	0.20 ±0.03
73P-C[k]	0.5 ±0.13[m]	< 0.25	0.15 ±0.04		0.18 ±0.02	< 0.51
73P-C[l]	< 2.6		0.11 ±0.01	< 0.033	0.22 ±0.01	0.19 ±0.05

*Uncertainties represent 1σ, and upper limits represent 3σ. Quantities in heavy solid boxes indicate depleted abundances, and those in the heavy dashed box indicate enhanced abundances, compared with the majority of Oort cloud comets measured

**Values for CO pertain to release solely from the nucleus (i.e., the *native* source)

‡ Using IRCS at Subaru, Kawakita et al. (2003) reported mixing ratios of $CH_4/H_2O = (0.52 \pm 0.10) \times 10^{-2}$ and $C_2H_6/H_2O = (0.43 \pm 0.12) \times 10^{-2}$ in Comet 153P/Ikeya-Zhang, using H_2O production rates from radio OH observations near the same heliocentric distance ($R_h \sim 1.5$ AU). Extrapolating IR hot-band measurements from $R_h \sim 0.5$–0.8 AU [$Q_{H_2O}(10^{28}$ molecules $s^{-1}) = (9.2 \pm 1.1) R_h{}^{-3.21 \pm 0.26}$; Dello Russo et al. 2004] results in $CH_4/H_2O = (0.91 \pm 0.22) \times 10^{-2}$ and $C_2H_6/H_2O = (0.74 \pm 0.24) \times 10^{-2}$

***Refers to combined values from the previous four comets. If the mean dispersion of values (i.e., their standard distribution about the mean, or the standard error) is more than twice the error in the mean associated with the individual uncertainties of each value (the stochastic error), the range of values is listed, as for CO and CH_4. (These two species are both highly volatile, yet their abundances are not correlated among comets, demonstrating that thermal considerations alone cannot explain cometary molecular abundances; see Gibb et al. 2003.) Otherwise, the mean and the larger of its stochastic and standard error are listed

[a]Unless otherwise noted, values for Oort cloud comets are taken from Mumma et al. (2003), and the original papers referenced therein should be cited; [b]Biver et al. (2002) and references therein; [c]Bockelée-Morvan et al. (2000); [d]Magee-Sauer et al. (2008); [e]Gibb et al. (2007); [f]Eberhardt (1999); [g]Eberhardt et al. (1987); [h]Weaver et al. (2001); [i]Mumma et al. (2005); [j]DiSanti et al. (2007b); [k]Villanueva et al. (2006); [l]Dello Russo et al. (2007); [m]DiSanti et al. (2007c)

3 Compositional Results and Comparisons

Recent review papers on parent volatiles in comets (Mumma et al. 2003; Bockelée-Morvan et al. 2005) reported abundances (production rates relative to H_2O) for several OC comets, revealing that all but one of these comets (C/1999 S4 LINEAR) had similar abundances for several key parent molecules (specifically, C_2H_2, C_2H_6, HCN, and CH_3OH; see Table 1, and also Fig. 5). C/1999 S4, which disintegrated during its apparition in 2000, showed relatively severe depletions of most parent volatiles relative to H_2O. Based on severely depleted CH_3OH together with only mildly depleted HCN (Mumma et al. 2001b) and H_2S/HCN (Bockelée-Morvan et al. 2001), and normal H_2CO/HCN (Bockelée-Morvan et al. 2001), chemical processing of its ices prior to accumulation in the Jupiter/Saturn nebular region (∼5–10 AU from the young Sun) was proposed (Mumma et al. 2001b; see Sect. 3.3 "Compositional Comparisons among Comets").

This section incorporates results for two JFCs that recently presented excellent opportunities for detailed observational study. These are 9P/Tempel 1 (9P), target of the NASA Deep Impact experiment (A'Hearn et al. 2005), and the recently split comet 73P/Schwassmann-Wachmann 3 (73P), whose nuclear fragments passed within 0.1 AU of Earth in spring 2006. The compositions of these JFCs are then compared with each other and with the ensemble of comets measured to date. Owing to their faintness, JFCs are observationally more challenging (compared with OC comets) and so are under-represented in studies of parent volatile composition. The existing detailed measurements of 9P and 73P are therefore extremely important for comparison with the more extensive database on OC comets.

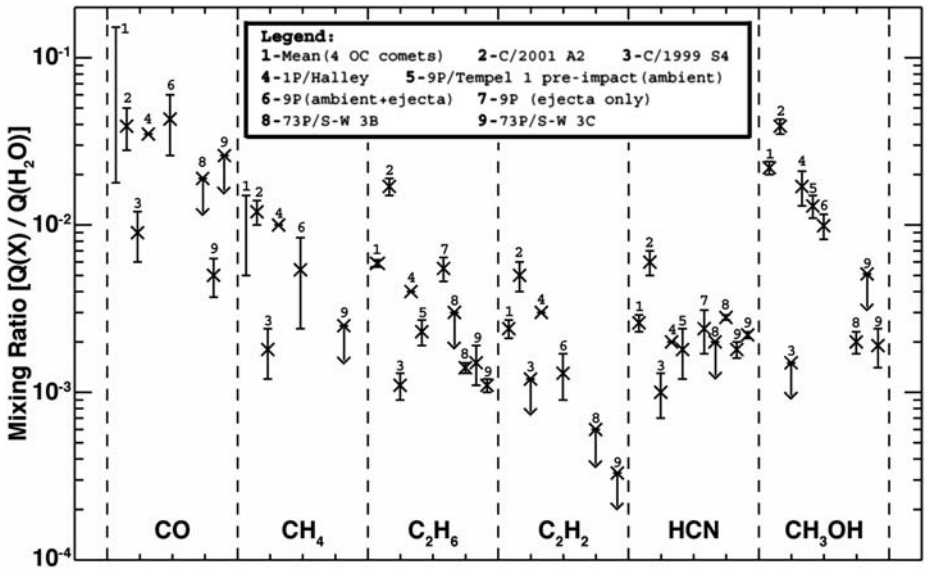

Fig. 5 Graphical representation of mixing ratios (abundances relative to H_2O) for the comets and parent molecules listed in Table 1. Numbers above each point are keyed in the legend inset. Note the low abundances of C_2H_6, C_2H_2, HCN, and CH_3OH for comets 3, 8, and 9, and the high abundances for comet 2, compared with the mean of four OC comets and 1P/Halley

3.1 Comet 9P/Tempel 1

The NASA Discovery mission Deep Impact (DI) to the JFC 9P provided the first opportunity to examine material issuing from below the surface of a cometary nucleus (see below) as a result of a deliberate collision (A'Hearn et al. 2005; Sunshine et al. 2006). A principal objective of the DI experiment was to compare the composition of dust and volatiles prior to and following the impact event. Compositional differences were revealed, both from ground-based and space-based data. NIR spectra from the DI spacecraft showed a very pronounced cometary organics (CH-X) feature (centered near 3.4–3.5 μm) post-impact, in contrast to its much weaker pre-impact intensity (A'Hearn et al. 2005). This suggested an enriched organics signature, and possibly heterogeneity in nucleus composition, however optical depth effects in co-measured H_2O and CO_2 emission precluded quantitative conclusions from being drawn (Feaga et al. 2007). Postimpact ground-based spectra (covering ~8–13 μm; Harker et al. 2005) and Spitzer Space Telescope spectra (5–35 μm; Lisse et al. 2006) indicated a large increase in grain emission within the first hour after impact, but declining in strength by 1.8 hours postimpact (Harker et al. 2005), although escape of material from the field of view may have also contributed to the observed decline. Ground-based NIR spectra revealed enriched C_2H_6 in the ejecta (by 3 ± 1 compared with its preimpact abundance, based on time-averaged preimpact and postimpact spectra), however the abundance ratios of HCN and CH_3OH were unchanged. The abundance ratio C_2H_6/H_2O in the ejecta was similar to that found in the majority of OC comets (Mumma et al. 2005).

Time-resolved measurements (Fig. 6) following the DI event revealed that the enhanced mixing ratio for C_2H_6, first seen about 25 minutes after impact, remained constant (within statistical uncertainty) for the duration of the C_2H_6 observations (~ 25 additional minutes; Fig. 6B). This analysis confirmed the results from Mumma et al. (2005)—the ratio C_2H_6/H_2O in the ejecta was enriched (by 2.4 ± 0.5) compared with its preimpact value, while HCN/H_2O was unchanged (see DiSanti et al. 2007b, and Table 1, Fig. 5). Also, as with C_2H_6, the mixing ratio for HCN in the ejecta remained constant with time. It was therefore concluded that the impact ejecta showed enhanced C_2H_6/H_2O but unchanged HCN/H_2O relative to the quiescent (preimpact) source, and that its composition did not change with time. The relatively sudden appearance of the volatile ejecta signature was attributed to heating of icy grains (perhaps to a threshold temperature) that were decreasingly shadowed by intervening (sunward) particles (DiSanti et al. 2007b). At optical wavelengths, disintegration of icy grains ejected by the impact was proposed based on filter imaging studies. The flux contained in a filter encompassing the OH (0-0) band at 308.6 nm peaked later than did the adjacent UV continuum flux (Schulz et al. 2006).

The DI results may indicate chemical fractionation within a homogeneous cometary nucleus, perhaps resulting from repeated perihelion passages. The surface or near-surface (i.e., at depths of ~ 1 m or less, based on thermal inertia modeling; Groussin et al. 2007) regions were more highly processed compared with the ejecta, thought to originate from 10–30 m below the surface (Lisse et al. 2007). Alternatively, the apparent heterogeneity may indicate a nucleus comprised of cometesimals from different formation regions and of diverse chemistry (Mumma et al. 2005).

3.2 Comet 73P/Schwassmann-Wachmann 3

In September 1995, 73P brightened suddenly by several magnitudes near perihelion (Crovisier et al. 1996). Subsequent imaging (in December 1995) revealed three main fragments and at least two smaller ones (Boehnhardt et al. 1995). During its subsequent apparition (in

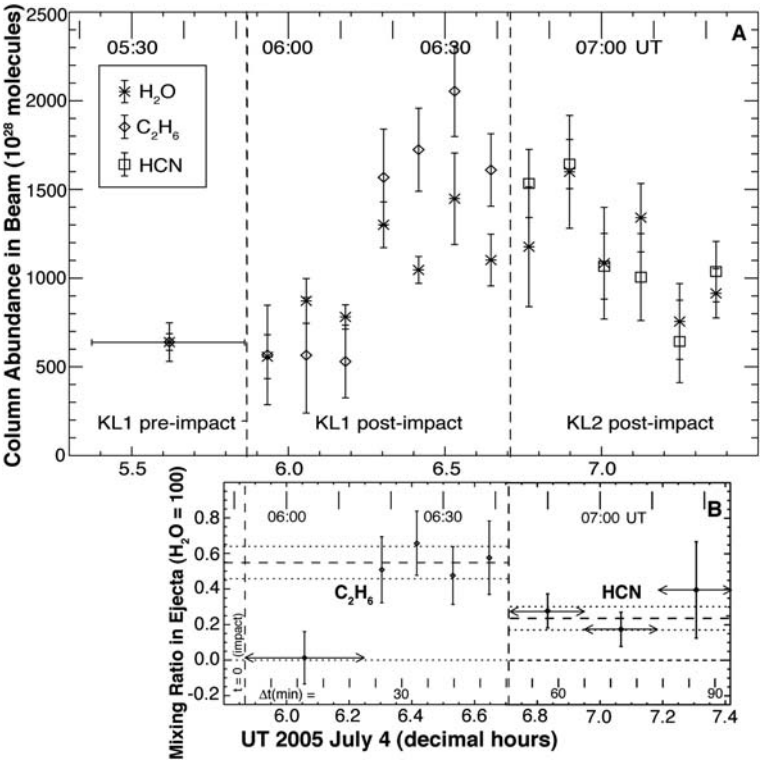

Fig. 6 **A** Measured column abundances for H_2O, C_2H_6, and HCN, tracking their evolution in JFC 9P/Tempel 1 resulting from the Deep Impact event, as observed with NIRSPEC. The preimpact point represents 16 minutes on source, and each postimpact point represents one ABBA sequence (4 minutes on source). The points for C_2H_6 and for HCN are scaled according to their respective preimpact mixing ratios relative to H_2O on July 4. **B** Corresponding mixing ratios (relative to H_2O) in the ejecta, obtained by subtracting preimpact column abundances from the total column abundances in panel **A**. The first point for C_2H_6 pertains to the mean of the first three postimpact points in panel **A**, and each point for HCN is the mean of two points from panel **A**. (Adapted from DiSanti et al. 2007b)

1999/2000), two of the previously observed major fragments (B and C) were recovered, and these revealed coma activity (Boehnhardt et al. 2002).

The 2006 apparition of 73P was awaited with the anticipation of studying relatively freshly exposed cometary material with close viewing geometry, and indeed the two brightest remaining fragments (B and C) received intense scrutiny. In 2006, fragment B exhibited several outbursts and rapid disintegration (Weaver et al. 2006), while fragment C showed more stable behavior. This stimulated searches for causal factors such as chemical heterogeneity, however no significant compositional differences between these fragments were seen in the NIR (Villanueva et al. 2006; Kawakita et al. 2006b; Dello Russo et al. 2007; Kobayashi et al. 2007) or radio (Biver et al. 2006).

This suggests a homogeneous nucleus for 73P, and that its composition primarily reflects formative conditions rather than evolutionary processing (Dello Russo et al. 2007). Evidence supporting homogeneity is also provided by the similar abundances measured from observations separated by several weeks, in 2006 April (Villanueva et al. 2006) and May (Kawakita et al. 2006b; Dello Russo et al. 2007; Kobayashi et al. 2007); i.e., no

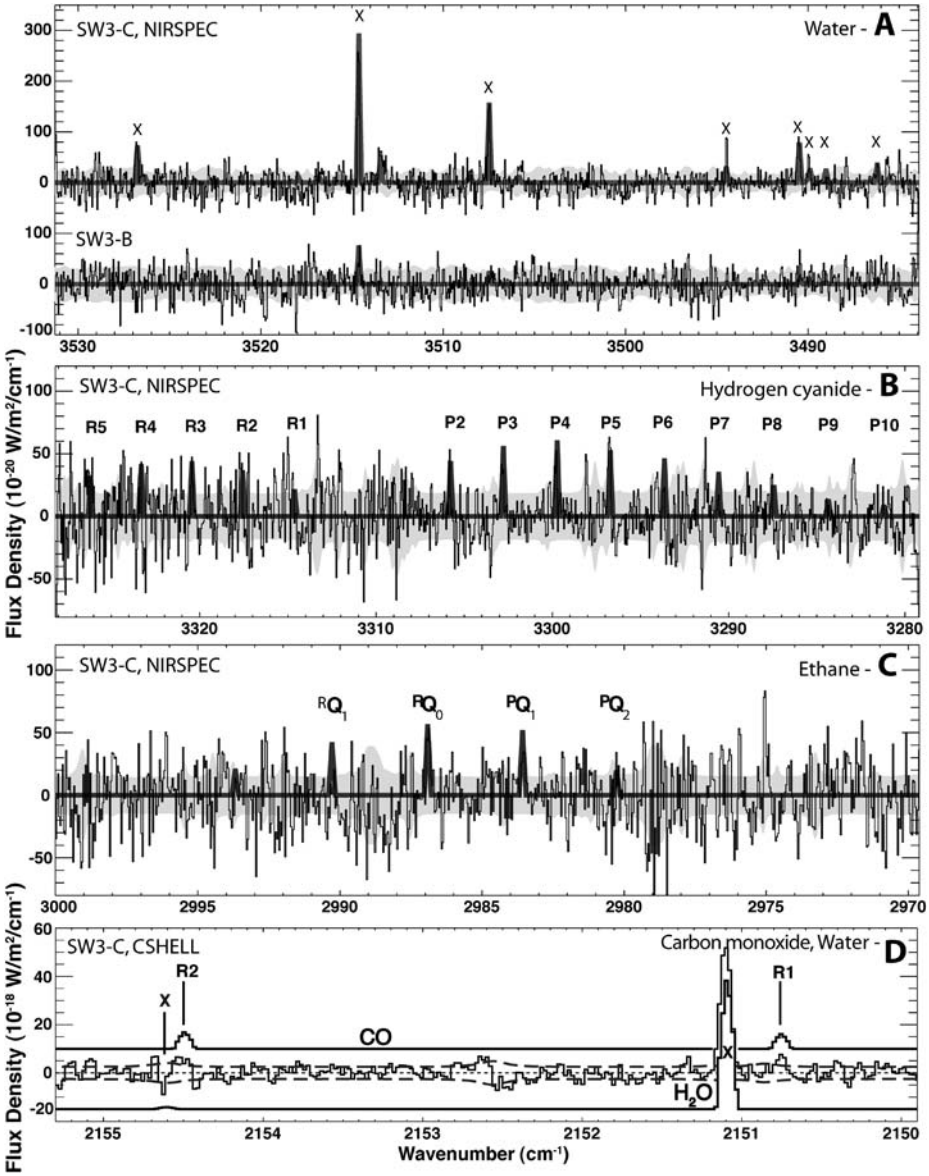

Fig. 7 Spectral residuals of parent volatiles detected in comet SW3 ($\lambda/\Delta\lambda \sim 2.5 \times 10^4$). **A–C** The *light-gray background* represents the 2σ stochastic noise envelope, and the *heavy gray traces* correspond to the modeled molecular emission multiplied by atmospheric transmittance and convolved to the instrumental resolving power (from Villanueva et al. 2006). **D** Comet residuals, convolved CO (above) and H_2O (below) models for $T_{\rm rot} = 80$ K, and 1σ stochastic noise envelope (*dashed traces*). (From DiSanti et al. 2007c)

evidence supporting serial evolution in composition was seen. In addition to revealing a homogeneous composition, 73P exhibited severe depletion of all parent volatiles except HCN (Villanueva et al. 2006; Kawakita et al. 2006a, 2006b; Dello Russo et al. 2007; DiSanti et al. 2007c; see Table 1, and also Figs. 5 and 7).

3.3 Compositional Comparisons Among Comets

The depleted abundance of C_2H_6 and the "normal" abundances of HCN and CH_3OH observed preimpact in 9P (Mumma et al. 2005) are similar to the C_2H_6 and HCN abundances seen in the JFC 21P/Giacobini-Zinner, the composition of which was partially characterized (Weaver et al. 1999; Mumma et al. 2000; Biver et al. 2002). This may indicate a similar processing history for the surface or near-surface material of 9P and 21P. The abundance of CO in 9P ($\sim 4\%$ on both July 4 and 5, at the 2–3σ confidence level; Mumma et al. 2005) may also fall in the normal range, provided the comet had returned to its quiescent (i.e., preimpact) state by July 5. Hubble Space Telescope observations of 9P prior to and following impact (Feldman et al. 2006) yielded an abundance of CO as high as 10%, suggesting this was likely the case. In 21P, NIR observations separated by approximately three weeks (for which R_H decreased from ~ 1.2 to 1.1 AU) suggested possible chemical heterogeneity within its nucleus, with reported CO (C_2H_6) abundances (relative to H_2O) of $\sim 10\%$ (0.2%) (Mumma et al. 2000), and < 2–3% (< 0.05–0.08%) (at the 3σ confidence level; Weaver et al. 1999). Future spectral observations of 21P will address both questions of processing history and of possible heterogeneous composition.

As with C/1999 S4 (LINEAR), which had a composition similar to 73P, thermal processing alone cannot explain the relatively low ratio CH_3OH/HCN, as these two species have similar volatility (e.g., see Crovisier and Encrenaz 2000, and Fig. 1.2 of Crovisier 2007). A composition influenced more by gas phase nebular processing than by condensation temperature was proposed for C/1999 S4 (see discussion in Mumma et al. 2001b). Comparison between C/1999 S4 and 73P demonstrates that comets from different present-day dynamical reservoirs (OC and KB, respectively) can display very similar parent volatile compositions (DiSanti et al. 2007c).

Another OC comet, C/2001 A2 (LINEAR), shed six observable fragments during its perihelion passage and underwent several major outbursts that were linked to fragmentation events (Sekanina et al. 2002). Compared with the majority of OC comets characterized to date, only C/2001 A2 showed enhanced abundances for several parent volatiles, including HCN (Magee-Sauer et al. 2008; see also Table 1, Fig. 5). This comet also displayed dramatic changes in CH_4/H_2O (increasing by approximately a factor of two postperihelion between $R_h \sim 1.2$ and $R_h \sim 1.6$ AU), and in H_2CO/H_2O on successive dates of observation near 1.2 AU (Gibb et al. 2007). Icy planetesimals are predicted to diffuse radially in the protoplanetary disk prior to being transported to the OC by gravitational scattering (Charnoz and Morbidelli 2003; Levison and Morbidelli 2003; Dones et al. 2005). This could lead to internal chemical heterogeneity if cometesimals that formed in different disk regions are later incorporated into a final cometary nucleus. C/2001 A2 may provide the best evidence yet in support of this hypothesis.

The lower abundances of parent volatiles (relative to H_2O) observed in 73P compared with the 9P ejecta may indicate that 73P formed closer to the Sun (as was proposed for C/1999 S4 LINEAR). Alternatively, it was suggested that both 73P and 9P may both have formed farther than 5–10 AU from the Sun, but that 73P formed later in time, after significant nebular clearing had allowed penetration of ionizing flux (producing higher H-atom densities) to greater distances with commensurate increased processing of its pre-cometary ices (Villanueva et al. 2006). In principle a similar formation scenario (farther from the Sun, but late) could also have applied to C/1999 S4 (LINEAR). However, based strictly on the principal source regions predicted by dynamical modeling (i.e., scattered KB for JFCs and giant planets' region for OC comets), the scenario proposed by Mumma et al. (2001b) would appear more likely for LINEAR S4. Regardless, it seems that the processing histories of the ices in 9P and 73P (as well as LINEAR S4) differ considerably.

How does this compare with studies of photodissociation products in comets? A dichotomy in the abundances of carbon-chain radicals was found in an optical survey of 85 comets (A'Hearn et al. 1995). Approximately one-half of the 39 JFCs studied were depleted in C_2/CN and C_3/CN, possibly indicative of differences in their long-chain carbon chemistries. It is interesting to note that 73P fell into the severely depleted category (based on its low C_2/CN; Fink and Hicks 1996), of which 21P is the prototypical comet, while 9P was classified as "typical" (albeit near the depleted end; A'Hearn et al. 1995). JFCs dominated the depleted class in this relatively large sample of comets, but it is not clear whether the reason for this is evolutionary (i.e., due to repeated and frequent perihelion passages) or primordial (traceable to formation conditions).

Potential abundance variations with heliocentric distance could contribute to this apparent dichotomy, particularly if a grain source contributes a portion of CN (Klavetter and A'Hearn 1994) or C_2 (Combi and Fink 1997). However, the A'Hearn et al. ensemble of comets showed at most a weak decrease in C_2/CN and no significant change in C_3/CN with increasing R_h, suggesting that the measured abundances of these daughter products to a large extent reflect their actual abundances. It is not known whether a similar trend will be borne out for potential parents, for example through the ratio C_2H_2/HCN, and in any case the parentages of C_2, C_3, and CN are not yet well established. These issues can only be addressed through measurement of parent volatiles in a large number of comets from both KB and OC reservoirs.

4 Current Status and Future Prospects

The current status of compositional studies of parent volatiles in comets reveals a range of abundances. These do not correlate with dynamical class and therefore presumably with formation region: giant planets' region for OC comets, trans-neptunian region for JFCs. This suggests that substantial radial mixing occurred in the proto-solar nebular environment, as predicted by current dynamical models. It also suggests that at least some fraction of comet nuclei should incorporate cometessimals that formed in different regions and so could contain distinct chemical signatures, consistent with results found for C/2001 A2 (LINEAR) and (possibly) for 9P, but apparently not for 73P.

While studies of parent volatiles in comets have provided very interesting comparisons, the sample size of well-characterized comets is still relatively small. In addition to those listed in Table 1, spectral observations are already in hand for six OC comets (including most recently the HFC 8P/Tuttle in late 2007/early 2008) and one KB comet (2P/Encke). Analysis of these data is proceeding, and studying these and future comets will add significantly to the results presented here, and will allow questions related to cometary composition versus place (and also time) of formation in the early Solar System to be addressed more completely.

Acknowledgements We thank D. Bockelee-Morvan and an anonymous referee for suggestions that improved this chapter, and also B. Bonev, G. Villanueva, and N. Dello Russo for their input. Support is acknowledged from the NASA Planetary Astronomy, Astrobiology, and Planetary Atmospheres Programs.

References

M.F. A'Hearn, R.L. Millis, D.G. Schleicher, D.J. Osip, P.V. Birch, The ensemble properties of comets: Results from narrowband photometry of 85 comets, 1976-1992. Icarus **118**, 223–270 (1995)

M.F. A'Hearn et al., Deep Impact: Excavating comet Tempel 1. Science **310**, 258–265 (2005)

G.M. Bernstein, D.E. Trilling, R.L. Allen, M.E. Brown, M. Holman, R. Malhortra, The size distribution of trans-Neptunian bodies. Astron. J. **128**, 1364–1390 (2004)
N. Biver, D. Bockelée-Morvan, J. Crovisier, P. Colom, F. Henry, R. Moreno, G. Paubert, D. Despois, D.C. Lis, Chemical composition diversity among 24 comets observed at radio wavelengths. Earth Moon Planets **90**, 323–333 (2002)
N. Biver, D. Bockelée-Morvan, J. Bossier, P. Colom, J. Crovisier, A. Lecacheux, D.C. Lis, B. Parise, K. Menton, Comparison of the chemical composition of fragments B and C of comet 73P/Schwassmann-Wachmann 3 from radio observations. Bull. Am. Astron. Soc. **38**(3), 484–485 (2006)
D. Bockelée-Morvan, J. Crovisier, The nature of the 2.8-μm emission feature in cometary spectra. Astron. Astrophys. **216**, 278–283 (1989)
D. Bockelée-Morvan et al., New molecules found in comet C/1995 O1 (Hale-Bopp). Investigating the link between cometary and interstellar material. Astron. Astrophys. **353**, 1101–1114 (2000)
D. Bockelée-Morvan et al., Outgassing behavior and composition of comet C/1999 S4 (LINEAR) during its disruption. Science **292**, 1339–1343 (2001)
D. Bockelée-Morvan, J. Crovisier, M.J. Mumma, H.A. Weaver, The composition of cometary volatiles, in *Comets II*, ed. by M.C. Festou, H.U. Keller, H.A. Weaver (University of Arizona Press, Tucson, 2005), pp. 391–423
H. Boehnhardt, H. Kaufi, R. Keen, P. Carmilleri, J. Carvajal, A. Hale, Comet 73P/Schwassmann-Wachmann 3. IAUC 6274, 1995
H. Boehnhardt, S. Holdstock, O. Hainaut, G.P. Tozzi, S. Benetti, J. Licandro, 73P/Schwassmann-Wachmann 3—one orbit after breakup: Search for fragments. Earth, Moon, and Planets **90**, 131–139 (2002)
B.P. Bonev, Towards a chemical taxonomy of comets: Infrared spectroscopic methods for quantitative measurements of cometary water (with an independent chapter on Mars polar science). Ph. D. thesis (U. Toledo), available on-line (2005). astrobiology.gsfc.nasa.gov/Bonev_thesis.pdf
B.P. Bonev, M.J. Mumma, M.A. DiSanti, N. Dello Russo, K. Magee-Sauer, R.S. Ellis, D.P. Stark, A comprehensive study of infrared OH prompt emission in two comets. I. Observations and effective g-factors. Astrophys. J. **653**, 774–787 (2006)
B.P. Bonev, M.J. Mumma, A comprehensive study of infrared OH prompt emission in two comets. II. Implications for unimolecular dissociation of H_2O. Astrophys. J. **653**, 788–791 (2006)
B.P. Bonev, M.J. Mumma, G.L. Villanueva, M.A. DiSanti, R.S. Ellis, K. Magee-Sauer, N. Dello Russo, A search for variation in the H_2O ortho-para ratio and rotational temperature in the inner coma of comet C/2004 Q2 (Maccholz). Astrophys. J. **661**, L97–L100 (2007)
B.P. Bonev, M.J. Mumma, H. Kawakita, H. Kobayashi, G.L. Villanueva, IRCS/Subaru observations of water in the inner coma of comet 73P- B/Schwassmann-Wachmann 3: Spatially resolved rotational temperatures and ortho-para ratios. Icarus (2008, in press)
T.Y. Brooke, A.T. Tokunaga, H.A. Weaver, J. Crovisier, D. Bockelee-Morvan, D. Crisp, Detection of acetylene in the infrared spectrum of comet Hyakutake. Nature **383**, 606–608 (1996)
S. Charnoz, A. Morbidelli, Coupling dynamical and collisional evolution of small bodies: an application to the early ejection of planetesimals from the Jupiter–Saturn region. Icarus **166**, 141–156 (2003)
M.R. Combi, U. Fink, A critical study of molecular photodissociation and CHON grain sources for cometary C_2. Astrophys. J. **484**, 879–890 (1997)
H. Cottin, M.C. Gazeau, Y. Benilan, F. Raulin, Polyoxymethylene as parent molecule for the formaldehyde extended source in comet Halley. Astrophys. J. **556**, 417–420 (2001)
H. Cottin, Y. Benilan, M.-C. Garzeau, F. Raulin, Origin of cometary extended sources from degradation of refractory organics on grains: polyoxymethylene as formaldehyde parent molecule. Icarus **167**, 397–416 (2004)
J. Crovisier, The water molecule in comets: Fluorescence mechanisms and thermodynamics of the inner coma. Astron. Astrophys. **130**, 361–372 (1984)
J. Crovisier, D. Bockelee-Morvan, E. Gerard, H. Rauer, N. Biver, P. Colom, L. Jorda, What happened to comet 73P/Schwassmann-Wachmann 3? Astron. Astrophys. **310**, L17–L20 (1996)
J. Crovisier, T. Encrenaz, *Comet Science: The Study of Remnants from the Birth of the Solar System* (Cambridge University Press, UK, 2000), p. 129
J. Crovisier, D. Bockelee-Morvan, N. Biver, P. Colom, D. Despois, D.C. Lis, Ethylene glycol in comet C/1995 O1 (Hale-Bopp). Astron. Astrophys. **418**, L35–L38 (2004)
J. Crovisier, The molecular composition of comets and its interrelation with other small bodies of the Solar System, in *Proceedings IAU Symposium No. 229, Asteroids, Comets, Meteors 2005*, ed. by D. Lazzaro, S. Ferraz-Mello, J.A. Fernandez (International Astronomical Union, 2006a), pp. 133–151
J. Crovisier, New trends in cometary chemistry. Faraday Disc. **133**, 1–13 (2006b)
J. Crovisier, Cometary diversity and cometary families (2007). ArXiv:astro-ph/0703785v1
N. Dello Russo, M.A. DiSanti, M.J. Mumma, K. Magee-Sauer, T.W. Rettig, Carbonyl sulfide in comets C/1996 B2 (Hyakutake) and C/1995 O1 (Hale-Bopp): Evidence for an extended source in Hale-Bopp. Icarus **135**, 377–388 (1998)

N. Dello Russo, M.J. Mumma, M.A. DiSanti, K. Magee-Sauer, R. Novak, T.W. Rettig, Water production and release in comet C/1995 O1 Hale-Bopp. Icarus **143**, 324–337 (2000)
N. Dello Russo, M.A. DiSanti, K. Magee-Sauer, E.L. Gibb, M.J. Mumma, R.J. Barber, J. Tennyson, Water production and release in comet 153P/Ikeya-Zhang (C/2002 C1): Accurate rotational temperature retrievals from hot-band lines near 2.9-μm. Icarus **168**, 186–200 (2004)
N. Dello Russo, B.P. Bonev, M.A. DiSanti, M.J. Mumma, E.L. Gibb, K. Magee-Sauer, R.J. Barber, J. Tennyson, Production rates, rotational temperatures and spin temperatures in comets C/1999 H1 (Lee), C/1999 S4, and C/2001 A2. Astrophys. J. **621**, 537–544 (2005)
N. Dello Russo, M.J. Mumma, M.A. DiSanti, K. Magee-Sauer, E.L. Gibb, B.P. Bonev, I.S. McLean, L.-H. Xu, A high-resolution infrared spectral survey of comet C/1999 H1 Lee. Icarus **184**, 255–276 (2006)
N. Dello Russo, R.J. Vervack Jr., H.A. Weaver, N. Biver, D. Bockelée-Morvan, J. Crovisier, C.M. Lisse, Compositional homogeneity in the fragmented comet 73P/Schwassmann-Wachmann 3. Nature **448**, 172–175 (2007)
M.A. DiSanti, M.J. Mumma, N. Dello Russo, K. Magee-Sauer, R. Novak, T.W. Rettig, Half the carbon monoxide of comet Hale-Bopp originates in nuclear ices. Nature **399**, 662–665 (1999)
M.A. DiSanti, M.J. Mumma, N. Dello Russo, K. Magee-Sauer, Carbon monoxide production and excitation in comet C/1995 O1 (Hale-Bopp): Isolation of native and distributed CO sources. Icarus **153**, 361–390 (2001)
M.A. DiSanti, N. Dello Russo, K. Magee-Sauer, CO, H_2CO, and CH_3OH in comet 2002 C1 (Ikeya-Zhang), in *Proceedings Asteroids, Comets, Meteors 2002*. ESA-SP, vol. 500 (Berlin, 2002), pp. 571–574
M.A. DiSanti, M.J. Mumma, N. Dello Russo, K. Magee-Sauer, D.M. Griep, Evidence for a dominant native source of CO emission in comet C/1996 B2 (Hyakutake). J. Geophys. Res. Planets **108**, 1–15 (2003)
M.A. DiSanti, M.J. Mumma, B.P. Bonev, N. Dello Russo, K. Magee-Sauer, W.M. Anderson, D.C. Reuter, E.L. Gibb, Abundances of carbon monoxide, formaldehyde, and methyl alcohol in comets: Measuring efficiencies for conversion of CO in grain mantles. Astrobiology **5**(2), 190 (2005). NAI AbSciCon 2005, Abstract # 935
M.A. DiSanti, B.P. Bonev, K. Magee-Sauer, N. Dello Russo, D.C. Reuter, M.J. Mumma, G.L. Villanueva, Formaldehyde emission in comet C/2002 T7 (LINEAR): Validation of a line-by-line fluorescence model at infrared wavelengths. Astrophys. J. **650**, 470–483 (2006)
M.A. DiSanti, M.J. Mumma, B.P. Bonev, G.L. Villanueva, K. Magee-Sauer, E.L. Gibb, W.M. Anderson, Y.L. Radeva, A comparison of oxidized carbon abundances among comets. Bull. Am. Astron. Soc. **39**(3), 507 (2007a)
M.A. DiSanti, G.L. Villanueva, B.P. Bonev, K. Magee-Sauer, J.E. Lyke, M.J. Mumma, Temporal evolution of parent volatiles and dust in comet 9P/Tempel 1 resulting from the Deep Impact experiment. Icarus **187**, 240–252 (2007b)
M.A. DiSanti, W.M. Anderson, G.L. Villanueva, B.P. Bonev, K. Magee-Sauer, E.L. Gibb, M.J. Mumma, Depleted carbon monoxide in fragment C of the Jupiter-family comet 73P/Schwassmann-Wachmann 3. Astrophys. J. **661**, L101–L104 (2007c)
L. Dones, P.R. Weissman, H.F. Levison, M.J. Duncan, Oort Cloud formation and dynamics, in *Comets II*, ed. by M.C. Festou, H.U. Keller, H.A. Weaver (University of Arizona Press, Tucson, 2005), pp. 153–191
P. Eberhardt, Comet Halley's gas composition and extended sources: Results from the neutral mass spectrometer on Giotto. Space Sci. Rev. **90**, 45–52 (1999)
P. Eberhardt et al., The CO and N_2 abundance in comet P/Halley. Astron. Astrophys. **187**, 481–484 (1987)
L.M. Feaga, M.F. A'Hearn, J.M. Sunshine, O. Groussin, Asymmetries in the distribution of H_2O and CO_2 in the inner coma of comet 9P/Tempel 1 as observed by Deep Impact. Icarus **191**, 134–145 (2007)
P.D. Feldman, R.E. Lupu, S.R. McCandliss, H.A. Weaver, M.F. A'Hearn, M.J.S. Belton, K.J. Meech, Carbon monoxide in comet 9P/Tempel 1 before and after the Deep Impact encounter. Astrophys. J. **647**, L61–L64 (2006)
U. Fink, M.D. Hicks, A survey of 39 comets using CCD spectroscopy. Astrophys. J. **459**, 729–743 (1996)
E.L. Gibb, M.J. Mumma, N. Dello Russo, M.A. DiSanti, K. Magee-Sauer, Methane in Oort cloud comets. Icarus **165**, 391–406 (2003)
E.L. Gibb, M.A. DiSanti, K. Magee-Sauer, N. Dello Russo, B.P. Bonev, M.J. Mumma, Methane and formaldehyde in comet C/2001 A2 (LINEAR): Search for heterogeneity within a comet nucleus. Icarus **188**, 224–232 (2007)
B. Gladman, The Kuiper Belt and the solar system's comet disk. Science **307**, 71–75 (2005)
R. Gomes, H.F. Levison, K. Tsiganis, A. Morbidelli, Origin of the cataclysmic Late Heavy Bombardment period of the terrestrial planets. Nature **435**, 466–469 (2005)
T.P. Greene, A.T. Tokunaga, J.S. Carr, High resolution spectroscopy with CSHELL at the IRTF, in *Infrared Astronomy with Arrays: The Next Generation*, ed. by I. McLean (Kluwer, Dordrecht, 1994), p. 511
O. Groussin, M.F. A'Hearn, J.-Y. Li, P.C. Thomas, J.M. Sunshine, C.M. Lisse, K.J. Meech, T.L. Farnham, L.M. Feaga, W.A. Delamere, Surface temperature of the nucleus of comet 9P/Tempel 1. Icarus **187**, 16–25

D.E. Harker, C.E. Woodward, D.H. Wooden, The dust grains from 9P/Tempel 1 before and after the encounter with Deep Impact. Science **310**, 278–280 (2005)
K. Hiraoka, T. Sato, S. Sato, N. Sogoshi, T. Yokoyama, H. Takashima, S. Kitagawa, Formation of formaldehyde by the tunneling reaction of H with solid CO at 10 K revisited. Astrophys. J. **577**, 265–270 (2002)
R.L. Hudson, M.H. Moore, Laboratory studies of the formation of methanol and other organic molecules by water + carbon monoxide radiolysis: Relevance to comets, icy satellites, and interstellar ices. Icarus **140**, 451–461 (1999)
W.F. Huebner, D.C. Boice, C.M. Sharp, Polyoxymethylene in comet Halley. Astrophys. J. **320**, L149–L152 (1987)
W.F. Irvine, F.P. Schloerb, J. Crovisier, B. Fegley Jr., M.J. Mumma, Comets: A link between interstellar and nebular chemistry, in *Protostars and Planets IV*, ed. by V. Mannins, A.P. Boss, S.S. Russel (University of Arizona Press, Tucson, 2000), pp. 1159–1200
H. Kawakita, J.-I. Watanabe, D. Kinoshita, M. Ishiguro, R. Nakamura, Saturated hydrocarbons in comet 153P/Ikeya-Zhang: Ethane, methane, and monodeuterio-methane. Astrophys. J. **590**, 573 (2003)
H. Kawakita, J.-I. Watanabe, R. Furusho, F. Tetsuharu, D.C. Boice, Nuclear spin temperature and deuterium-to-hydrogen ratio of methane in comet C/2001 Q4 (NEAT). Astrophys. J. **590**, L49–L52 (2005)
H. Kawakita et al., Ortho-to-para ratios of water and ammonia in comet C/2001 Q4 (NEAT): Comparison of nuclear spin temperatures of water, ammonia, and methane. Astrophys. J. **643**, 1337–1344 (2006a)
H. Kawakita, H. Kobayashi, M.J. Mumma, Observations of organic molecules in comet 73P-B/Schwassmann-Wachmann using IRCS/Subaru. Bull. Am. Astron. Soc. **38**(3), 503 (2006b)
J.J. Klavetter, M.F. A'Hearn, An extended source for CN jets in comet P/Halley. Icarus **107**, 322–334 (1994)
N. Kobayashi et al., IRCS: Infrared camera and spectrograph for the Subaru Telescope, in *Proc. SPIE 4008: Optical and IR Telescope Instrumentation and Detectors*, ed. by M. Iye, A.F. Moorwood (2000), pp. 1056–1066
H. Kobayashi, H. Kawakita, M.J. Mumma, B.P. Bonev, J.-I. Watanabe, T. Fuse, Organic volatiles in comet 73P-B/Schwassmann-Wachmann 3 observed during its outburst: A clue to the formation region of the Jupiter-family comets. Astrophys. J. **668**, L75–L78 (2007)
H.F. Levison, A. Morbidelli, The formation of the Kuiper belt by the outward transport of bodies during Neptune's migration. Nature **426**, 419–421 (2003)
C.M. Lisse et al., Spitzer spectral observations of the Deep Impact ejecta. Science **313**, 635–640 (2006)
C.M. Lisse, K.E. Kraemer, J.A. Nuth III, A. Li, D. Joswiak, Comparision of the composition of the Tempel 1 ejecta to the dust in comet C/Hale-Bopp 1995 O1 and YSO HD 100546. Icarus **187**, 69–86 (2007)
K. Magee-Sauer, M.J. Mumma, M.A. DiSanti, N. Dello Russo, T.W. Rettig, Infrared spectroscopy of the ν_3 band of hydrogen cyanide in comet C/1995 O1 Hale-Bopp. Icarus **142**, 498–508 (1999)
K. Magee-Sauer, M.J. Mumma, M.A. DiSanti, N. Dello Russo, E.L. Gibb, B.P. Bonev, The organic composition of comet C/2001 A2 (LINEAR). Icarus **194**, 347–358 (2008)
I.S. McLean et al., Design and development of NIRSPEC: a near-infrared echelle spectrograph for the Keck II telescope. Proc. SPIE **3354**, 566–578 (1998)
R. Meier, P. Eberhardt, D. Krankowsky, R.R. Hodges, The extended formaldehyde source in comet P/Halley. Astron. Astrophys. **277**, 677–690 (1993)
M.J. Mumma, H.A. Weaver, H.P. Larson, The ortho-para ratio of water vapor in comet P/Halley. Astron. Astrophys. **187**, 419–429 (1987)
M.J. Mumma, P.R. Weissman, S.A. Stern, Comets and the origin of the Solar System: Reading the Rosetta Stone, in *Protostars and Planets III*, ed. by E.H. Levy, J.I. Lunine (University of Arizona Press, Tucson, 1993), pp. 1177–1252
M.J. Mumma, M.A. DiSanti, E.E. Roettger, A.T. Tokunaga, Ground-based detection of water in comet Shoemaker-Levy 1992 XIX: Probing cometary parent molecules by hot-band fluorescence. Bull. Am. Astron. Soc. **27**, 1144 (1995)
M.J. Mumma, M.A. DiSanti, N. Dello Russo, M. Fomenkova, K. Magee-Sauer, C.D. Kaminski, D.X. Xie, Detection of abundant ethane and methane, along with carbon monoxide and water, in comet C/1996 B2 Hyakutake: Evidence for interstellar origin. Science **272**, 1310–1314 (1996)
M.J. Mumma, M.A. DiSanti, N. Dello Russo, K. Magee-Sauer, T.W. Rettig, Detection of CO and ethane in comet 21P/Giacobini-Zinner: Evidence for variable chemistry in the outer solar nebula. Astrophys. J. **531**, L155–L159 (2000)
M.J. Mumma et al., A survey of organic volatile species in comet C/1999 H1 (Lee) using NIRSPEC at the Keck Observatory. Astrophys. J. **546**, 1183–1193 (2001a)
M.J. Mumma et al., Organic composition of C/1999 S4 (LINEAR): A comet formed near Jupiter? Science **292**, 1334–1339 (2001b)
M.J. Mumma, M.A. DiSanti, N. Dello Russo, K. Magee-Sauer, E.L. Gibb, E.R. Novak, Remote infrared observations of parent volatiles in comets: A window on the early solar system. Adv. Space Res. **31**, 2563–2575 (2003)

M.J. Mumma et al., Parent volatiles in comet 9P/Tempel 1: Before and after impact. Science **310**, 270–274 (2005)
Z. Sekanina, E. Jehin, H. Boehnhardt, X. Bonfils, O. Schuetz, D. Thomas, Recurring outbursts and nuclear fragmentation of comet C/2001 A2 (LINEAR). Astrophys. J. **572**, 679–684 (2002)
R. Schulz, A. Owens, P.M. Rodriguez-Pascual, D. Lumb, C. Erd, J.A. Stuwe, Detection of water ice grains after the Deep Impact onto comet 9P/Tempel 1. Astron. Astrophys. **448**, L53–L56 (2006)
S.A. Stern, The evolution of comets in the Oort cloud and Kuiper belt. Nature **424**, 639–642 (2003)
J.M. Sunshine et al., Exposed water ice deposits on the surface of comet Tempel 1. Science **311**, 1453–1455 (2006)
A.T. Tokunaga, D.W. Toomey, J. Carr, D.N. Hall, H.W. Epps, Design for a 1–5 micron cryogenic echelle specrograph for the NASA IRTF. Proc. SPIE **1235**, 131–143 (1990)
K. Tsinganis, R. Gomes, A. Morbidelli, H.F. Levison, Origin of the orbital architecture of the giant planets of the Solar System. Nature **435**, 459–461 (2005)
G.L. Villanueva, B.P. Bonev, K. Magee-Sauer, M.A. DiSanti, C. Salyk, G.A. Blake, M.J. Mumma, The volatile composition of the split ecliptic comet 73P/Schwassman-Wachmann 3: A comparison of fragments C and B. Astrophys. J. **650**, L87–L90 (2006)
N. Watanabe, A. Nagaoka, T. Shiraki, A. Kouchi, Hydrogenation of CO on pure solid CO and CO–H_2O mixed ice. Astrophys. J. **616**, 638–642 (2004)
H.A. Weaver, M.J. Mumma, H.P. Larson, D.S. Davis, Post-perihelion observations of water in comet Halley. Nature **324**, 441–446 (1986)
H.A. Weaver, M.J. Mumma, H.P. Larson, Infrared investigation of water in comet 1P/Halley. Astron. Astrophys. **187**, 411–418 (1987)
H.A. Weaver, G. Chin, D. Bockelee-Morvan, J. Crovisier, T.Y. Brooke, D.P. Cruikshank, T.R. Geballe, S.J. Kim, R. Meier, An infrared investigation of volatiles in comet 21P/Giacobini-Zinner. Icarus **142**, 482–497 (1999)
H.A. Weaver et al., HST and VLT investigations of the fragments of comet C/1999 S4 (LINEAR). Science **292**, 1329–1334 (2001)
H.A. Weaver, C.M. Lisse, M.J. Mutchler, P. Lamy, I. Toth, W. Reach, Bull. Am. Astrophys. Soc. **38**(3), 490 (2006)

Section III: Evolution of Nuclei

Thermal and Chemical Evolution of Comet Nuclei and Kuiper Belt Objects

Dina Prialnik · Gal Sarid · Eric D. Rosenberg · Rainer Merk

Originally published in the journal Space Science Reviews, Volume 138, Nos 1–4.
DOI: 10.1007/s11214-007-9301-4

Abstract The structure and composition of comet nuclei are mainly altered during two short phases that are separated by a very long hibernation phase. Early evolution—during and immediately after formation—is the result of heating caused by radioactive decay, the most important source being ^{26}Al. Several studies are reviewed, dealing with evolution throughout this phase, calculated by means of 1-D numerical codes that solve the heat and mass balance equations on a fixed spherically symmetric grid. It is shown that, depending on parameters, the interior may reach temperatures above the melting point of water. The models thus suggest that comets are likely to lose the ices of very volatile species during early evolution; ices of less volatile species are retained in the cold subsurface layer. As the initially amorphous ice is shown to crystallize in the interior, some objects may also lose part of the volatiles trapped in amorphous ice. Generally, the outer layers are far less affected than the inner part, resulting in a stratified composition and altered porosity distribution. The second phase of evolution occurs when comet nuclei are deflected into the inner solar system and is dominated by the effect of solar radiation. Now the outer layers are those mostly affected, undergoing crystallization, loss of volatiles, and significant structural changes. If any part of a comet nucleus should retain its pristine structure and composition, it would be well below the surface and also well above the core.

Keywords Comets: general · Kuiper Belt

1 Introduction: Structure, Composition, and Energy Sources

The evolution of comets may be divided into three main stages: (a) formation and early thermal evolution, (b) dynamical evolution, and (c) late thermal evolution. The first and last are very brief on the evolutionary time scale of the solar system; thus during most of their lives comet nuclei may be considered as hibernating thermally and chemically, while their orbits may undergo significant changes that eventually carry them from their place of birth to the inner solar system. It is with stages (a) and (c) that we are concerned in this paper.

D. Prialnik (✉) · G. Sarid · E.D. Rosenberg · R. Merk
Department of Geophysics and Planetary Sciences, Tel Aviv University, Tel Aviv, Israel
e-mail: dina@planet.tau.ac.il

H. Balsiger et al. (eds.), *Origin and Early Evolution of Comet Nuclei*
DOI: 10.1007/978-0-387-85455-7_9

1.1 Initial Structure and Composition

Observed comets are believed to come from three main reservoirs: the Oort cloud (OC), the Kuiper belt (KB), and the scattered disk (SD). The OC is considered as the source of long-period and Halley-type comets (Stern 2003; Dones et al. 2005), which are thought to have formed between Jupiter and Neptune and scattered out mostly by Uranus and Neptune (Hahn and Malhotra 1999; Dones et al. 2005). Kuiper belt objects (KBOs) on the other hand, are believed to have formed in the belt, which is regarded as the source of Jupiter family comets (Levison and Duncan 1997; Duncan et al. 2005). The SD is intermediate: its objects formed in the region of the giant planets, as the OC objects, and were scattered into the trans-Neptunian zone, constituting an extension of the KB.

Observed comets and KBOs span a wide range of sizes, and size is a critical parameter for thermal evolution. All ground- and space-based observations indicate that the size of comet nuclei seldom exceeds a few kilometers, while KBOs are clearly larger. Recently, Lamy et al. (2005) collected a set of about 80 measured cometary radii. Due to the non-spherical shape of comet nuclei, they calculated effective radii of spheres having the same volumes as the nuclei. In this sample, the vast majority of comet nuclei have effective radii between 1 and 5 km. Only four objects have radii of 10 km and more.

By contrast, KBOs have diameters between a few tens and a few hundred km (Jewitt et al. 1998). Due to observational bias toward near and bright objects (as compared to remote and faint objects), a cumulative luminosity function is used to derive a more or less reliable size distribution of KBOs. With this method, Jewitt and Luu (2000) predicted a number of 10^5 bodies around 50 km radius and about 10 bodies of 1000 km radius and more, i.e. Pluto-sized bodies. Such trans-Neptunian objects (TNOs) were found recently. The largest object of the outer Solar System is presently Eris a SD object with a radius of about 1200 km (Brown et al. 2005).

The estimated equilibrium temperature at distances where comet progenitors formed ranges between 30–60 K. Although the orto-to-para ratio in H in cometary H_2O indicates temperatures around 30 K, this may reflect the temperature in the presolar nebula rather than the protoplanetary disk (see Kawakita et al. 2006 for a detailed discussion). This is above the condensation temperature of highly volatile species, such as CO, N_2, or CH_4, but low enough for moderately volatile species, such as CO_2, HCN, or NH_3, to condense, and also for water ice to be amorphous. Amorphous water ice traps volatiles, including the highly volatile species, and releases them upon crystallization (Bar-Nun et al. 1987). Thus indirect support for the originally amorphous nature of the H_2O ice is provided by observations of highly volatile species, in particular abundant CO, in the comae of comets. Since ice is rarely detected in comets, and since amorphous ice would only be preserved below the surface, there is little direct evidence for the amorphous state of cometary ice. Nevertheless, the ice in two new comets has been inferred to be amorphous from the absence of the 1.65-μm absorption feature of crystalline ice in their spectra: C/Hale-Bopp O1 at 7 AU (Davies et al. 1997) and C/2002 T7 (LINEAR) at 3.5 AU (Kawakita et al. 2004).

In conclusion, it is reasonable to assume that the initial composition of comet nuclei includes dust (rock) and gas laden amorphous water ice, possibly mixed with other ices. As in asteroids and other solid objects of the solar system, the dust should include radioactive species, and their abundances should be similar to those found in meteorites. Finally, comet nuclei are porous, their volume including a large fraction of voids. The high porosity (Ψ) of nuclei was first inferred from the close-up observations of comet Halley's nucleus and confirmed by every close encounter with a comet nucleus ever since (e.g., A'Hearn et al. 2005). The proportions of ice, dust and voids are constrained—as shown in Fig. 1 (left)—by

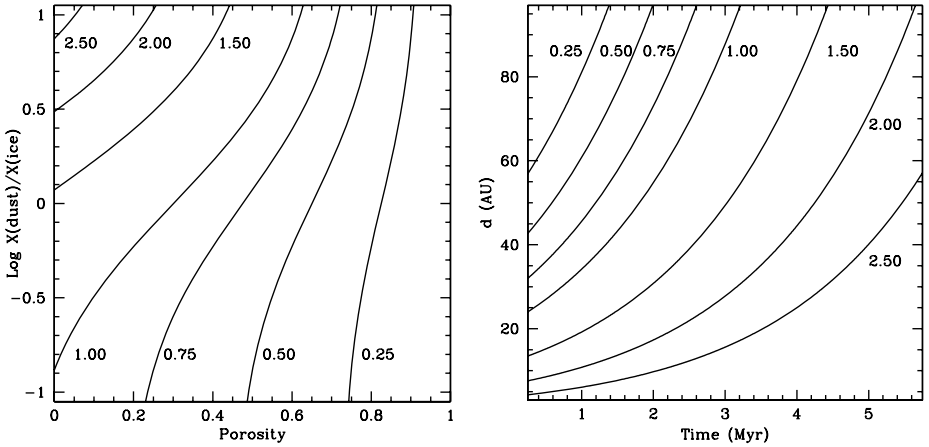

Fig. 1 *Left*: Relation between bulk density, porosity and dust to ice ratio. *Right*: Domains of dominance of radioactive power and solar power over the (t, d) plane for various body radii marked as $\log(R[\mathrm{km}])$ (e.g. 1.00 corresponds to 10 km; 2, to 100 km, *etc.*). Above the line corresponding to each radius radioactivity dominates; below it, solar radiation dominates

the bulk density (ρ_b) that may be derived from observations: defining $\mathcal{R} \equiv X_d/X_i$, where X_i and X_d are the ice and dust mass fractions, respectively, we have

$$1 - \Psi = \frac{\rho_b}{1+\mathcal{R}}\left(\frac{1}{\varrho_i} + \frac{\mathcal{R}}{\varrho_d}\right), \tag{1}$$

where ϱ_i and ϱ_d are the specific solid densities of ice and dust. This composition leads us directly to the internal energy sources and sinks available to comets.

1.2 Energy Sources

Internal energy sources are of three kinds: radiogenic energy, in proportion to the dust fraction, heat released upon crystallization, in proportion to the amorphous H_2O ice content, and latent heat of phase transition of the various volatiles. Clearly, the first two are energy *sources*, which are associated with irreversible processes. Latent heat, however, may be either released or absorbed, and if gases can flow through the porous medium, latent heat may be released in one place and absorbed in another, thereby acting as an effective means of heat transfer.

In terms of energy exchange, there is a significant difference between species that are originally frozen, as opposed to trapped in amorphous ice. If frozen, they represent a potential heat *sink*, since they absorb heat in order to melt or sublimate, although they may later return the absorbed heat, if refreezing occurs. Trapped gases released from amorphous ice, on the other hand, are a potential heat *source*, since they will release latent heat upon eventual condensation, although they may reabsorb it upon subsequent sublimation. This difference is particularly important in early evolution, when comet nuclei reside in cold environments, and hence have cold outer layers, where gases released in the interior are bound to refreeze.

In addition to internal sources, or rather ahead of them, there is the external source of solar energy. Stage (c) of the comet nucleus evolution is entirely dominated by it. Solar

energy and radioactivity are different from the other energy sources inasmuch as they are independent of internal conditions, while crystallization and phase transitions depend on temperature and pressure. Only in stage (a) does radioactivity compete with solar energy, since small bodies are not affected by the long-lived radioactive isotopes that release energy very slowly, but only by short-lived ones, ^{26}Al in particular (see below). Choi et al. (2002) compare these two complementary energy sources in terms of the distance from the sun $d_{\rm H}$, the radius of the object R, and the abundance of the radioactive source, the main one being ^{26}Al, which itself is a function of time t, in order to assess their relative power. Figure 1 (right panel) illustrates the effect of these factors as the solution of

$$(1-\mathcal{A})\pi R^2 \frac{L_\odot}{4\pi d_{\rm H}^2} = \frac{4\pi}{3} R^3 \rho \frac{X_0 \mathcal{H}}{\tau} {\rm e}^{-t/\tau}, \tag{2}$$

where $\mathcal{A}$ is the albedo (assumed 0.04), $L_\odot$ is the solar luminosity, ρ is the bulk density (assumed 700 kg m^{-3}), X_0 is the initial ^{26}Al mass fraction ($\sim 7 \times 10^{-7}$), τ is the characteristic radioactive decay time (1.06×10^6 yr) and $\mathcal{H}$ is the energy released per unit mass (1.48×10^{13} J/kg).

As the two thermal evolution stages of comet nuclei, (a) and (c), are widely separated in time and affected by different energy sources, they are usually studied separately. However, although changes in temperature that may occur during early evolution will be slowly erased during the long and inert stage (b), structural and compositional changes *will* be carried from stage (a) to stage (c). Some of the complex evolutionary effects have been investigated by numerical simulations and will be addressed in Sects. 3 and 4. However, since they depend crucially on a number of uncertain physical and initial parameters, to the extent that no systematic parameter study is as yet possible, it will be instructive to investigate comet nuclei in a more general, albeit less accurate manner, by some basic analytical considerations or simple models.

2 Theoretical Considerations

2.1 Heating versus Cooling

The extent to which small bodies of the solar system may have been affected by early radiogenic heating has been debated for four decades. The pioneering work towards answering this question is that of Whipple and Stefanik (1996), who considered the decay of long-lived radionuclides and found that it would lead to loss of the most volatile species. It was followed by the studies of Wallis (1980) and Irvine et al. (1980), who showed by simple calculations that liquid water could be obtained in the cores of comet nuclei.

Considering that small bodies cool far more effectively than large ones and form more quickly, they are mainly affected by high-power (short-lived) radioactive sources. The radioactive isotope ^{26}Al , with a decay time $\tau = 1.06 \times 10^6$ yr and decay energy per unit mass $\mathcal{H} = 1.48 \times 10^{13}$ J/kg, was recognized as a potential heat source capable of melting bodies of radii between 100 and 1000 km half a century ago (Urey 1955). Evidence for its existence was supplied by ^{26}Mg enhanced abundances found in Ca-Al inclusions of meteorites (e.g., MacPherson et al. 1995). Further support, from an independent source, was provided by the detection of interstellar 1.809 MeV γ-rays from the decay of ^{26}Al (Diehl et al. 1997). All this evidence points towards an interstellar isotopic ratio $^{26}{\rm Al}/^{27}{\rm Al} \approx 5 \times 10^{-5}$, implying an initial mass fraction $X_0 \approx 7 \times 10^{-7}$ in dust. Recently, other short-lived radionuclides, such as ^{60}Fe, have also been invoked (Mostefaoui et al. 2005).

Since Urey's early work, the role of ^{26}Al decay in the early heating of asteroids as well as small icy bodies has been intensively studied, discussed and reviewed, recent examples being Boss (2007), Schubert et al. (2007). Support for early heating of comet nuclei to the point of melting is provided by the detection of hydrated silicates in comets, suggesting the presence of abundant amounts of water in their parent bodies (Lisse et al. 2006).

The potential effect of radiogenic heating during the early evolution of icy bodies of different radii may be roughly estimated based on global energy considerations (cf. Prialnik 1998). If we represent such a body of mass M and radius R by a single internal temperature that changes with time, $T(t)$, the energy balance equation is simply

$$M\,\frac{du}{dt} = M\,\tau^{-1} X_0 \mathcal{H} \mathrm{e}^{-t/\tau} - 4\pi R^2(\sigma T_s^4 - \sigma T_e^4), \tag{3}$$

where the internal energy per unit mass u is obtained by $u = \int c(T)dT$, $c(T)$ being the heat capacity; $T_s = T(R)$ is the surface temperature and T_e is the temperature of the environment, or the equilibrium temperature at the corresponding heliocentric distance. The difference between T_e and T_s is due to heat conduction into or out of the nucleus. In the lowest approximation we may assume $-K\frac{dT}{dr} \sim K\frac{T}{R}$. Hence

$$c(T)\frac{dT}{dt} = \tau^{-1} X_0 \mathcal{H} \mathrm{e}^{-t/\tau} - \frac{3KT}{R^2\rho}. \tag{4}$$

The maximal heating rate, obtained at $t = 0$, is $\tau^{-1} X_0 \mathcal{H}$ and for the internal temperature to rise, the RHS of (4) must be positive at $t = 0$, a requirement that is determined by the body's radius and by the thermal conductivity of its material. As the heating rate declines with time, it eventually becomes lower than the rate of cooling in all cases. Hence, for suitably large comets the internal temperature rises at the beginning up to a maximal value T_{max} and then falls off, tending to T_e.

With the approximation $c(T) \propto T$—which is valid for $T \gtrsim 50$ K (Klinger 1980)—(4) may be solved analytically for $T(t)$, using the appropriate conductivities for amorphous and for crystalline ices. For given T_0 and X_0, a family of solutions $T_R(t)$ is obtained, with the radius R as parameter. Examples are given in Fig. 2, and show that above a certain radius, an icy body made of amorphous ice will start crystallizing ($T \gtrsim 120$ K), and above a still larger radius, melting of ice will eventually occur (see also Jewitt et al. 2006).

An example of the results obtained by detailed numerical simulations is given in the right panel of Fig. 2, confirming the general behavior derived analytically.

2.2 Accretion and Radioactive Heating

So far we have considered radioactive heating to take place in a body of given size, while in reality heating also occurs while the body grows. Following Merk and Prialnik (2003), we consider an accreting body of mass $M(t)$ and assume that the accreted material contains a mass fraction $X(t)$ of radioactive ^{26}Al, initially X_0. The available radioactive energy at any given time is thus $E = X\mathcal{H}M$ and the rate of energy supply for the heat balance equation is $Q = -\,dE/dt$. If accretion and radioactive heating are treated separately, a fixed mass M_f is assumed and the resulting rate of heating is

$$Q_F(t) = \frac{1}{\tau} X_0 \mathcal{H} M_f\, \mathrm{e}^{-t/\tau}. \tag{5}$$

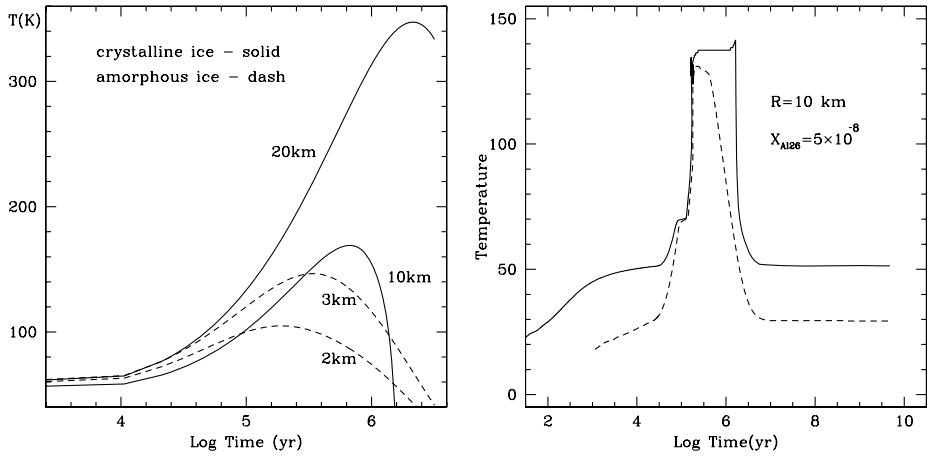

Fig. 2 Evolution of temperature as a function of time. *Left*: Analytical solution; parameter values are $T_0 = 50$ K, $X_0 = 5 \times 10^{-8}$. *Dashed lines* represent amorphous ice and show that in bodies with radii above ~2 km the peak temperature reached will be high enough for crystallization to occur. *Solid lines* represent crystalline ice and show that the lowest radius required for bodies to undergo melting is between 10 and 20 km (for the assumed parameters). *Right*: Numerical solution for maximal internal temperature as a function of time (data from Choi et al. 2002); $d_H = 30$ AU (*solid*); $d_H = 90$ AU (*dashed*), adopting the same initial abundance of ^{26}Al

On the other hand, if a growing mass is considered, with a given growing rate, the rate of heating is given by

$$Q_G(t) = \frac{1}{\tau} X_0 \mathcal{H} M_f \, \mathrm{e}^{-t/\tau} \frac{M(t)}{M_f} \left(1 - \tau \frac{\dot{M}}{M(t)}\right) \tag{6}$$

The variation with time of these rates differs considerably, as can be seen by considering a simple growth law that provides a reasonable approximation to detailed numerical results such as those of Weidenschilling (2000):

$$M(t) = M_f(1 - e^{-t/\theta}), \tag{7}$$

where θ is a time constant for accretion. Clearly, as $t \to \infty$, the body reaches the final mass M_f. The rate of internal heating is therefore

$$\begin{aligned} Q_G(t;\theta,\tau) &= -\dot{E} \\ &= -\dot{X}(t;\tau)\mathcal{H}M(t;\theta) - X(t;\tau)\mathcal{H}\dot{M}(t;\theta). \end{aligned} \tag{8}$$

Substituting (7) and (5) and rearranging terms, we obtain

$$Q_G(t;\theta,\tau) = Q_F(t;\tau)\left[1 - e^{-t/\theta}\left(1 + \frac{\tau}{\theta}\right)\right]. \tag{9}$$

As one would expect, very rapid (instantaneous) growth (or $\theta \ll \tau$) just yields $\lim_{\theta\to 0} Q_G(t;\theta,\tau) = Q_F(t;\tau)$, which means that the processes may be separated and treated in turn. On the other hand, if accretion is very slow ($\theta \gg \tau$), no heating should result, since the radioactive material would have decayed before any appreciable amount of

mass accumulated, and indeed according to (9), $\lim_{\theta\to\infty} Q_G(t;\theta,\tau) = 0$, and the processes, again, do not interfere with each other. However, in reality, $\theta \sim \tau$, and Q_G is very different from both zero and Q_F.

It is already obvious from (9) that $Q_G < Q_F$; therefore a diminished X_0 is adopted for compensation, when the processes are treated separately and a fixed mass is assumed at the onset of radioactive decay. This amounts to a constant correction factor for Q_F, equivalent to a delay time t_0, that is, $e^{-t_0/\tau}$, whereas according to (9), the correction factor Q_G/Q_F is very different from a constant.

In conclusion, if the characteristic timescales of accretion and radioactive decay are comparable, a growing body may be affected by radioactivity while it grows: at first, when the body is small, efficient cooling is compensated by the high radioactivity, later, diminished radioactivity is compensated by the less efficient cooling of a larger body.

2.3 Self Gravity

Comets are held together mostly by material forces, even if the material strength is low. However, when we consider the larger bodies of the KBO population, self-gravity becomes important and is bound to affect the internal structure. The question is, when should we take account of this effect? For a spinning spherical body of uniform density ρ and radius R, the hydrostatic pressure as a function of radial distance from the center is given by:

$$P(r) = 2\pi^2\rho R^2\left(\frac{G\rho}{3\pi} - \frac{1}{p_{\rm spin}^2}\right)\left[1 - \left(\frac{r}{R}\right)^2\right], \tag{10}$$

where ω is the angular velocity, $\omega = 2\pi/p_{\rm spin}$. This immediately sets limits to the spinning period, as function of density:

$$[p_{\rm spin}]_{\rm crit} = \begin{cases} 3.3\ {\rm hr}: & \rho = 1.0\ {\rm g/cm^3}, \\ 4.7\ {\rm hr}: & \rho = 0.5\ {\rm g/cm^3}. \end{cases} \tag{11}$$

Indeed, the spin period of comets is higher than these limits, and typically, much higher (Samarasinha et al. 2005).

If the central pressure $P(r=0)$ is lower than the compressive strength, then clearly self-gravity is negligible; on the other hand, when even close to the surface, say at $r = 0.9R$, the pressure given by (10) is higher than the compressive strength, then the body is bound to become compressed under its own gravity. There is ample evidence indicating that the tensile strength of small solar system bodies is low (see Blum et al. 2006). Even if we take the upper limit of the tensile strength range increased by an order of magnitude to take into account that the compressive strength may be higher than the tensile strength, the result is that self-gravity may be safely neglected only for bodies of radii below ~ 30 km, and it must certainly be considered above 100 km.

To account for hydrostatic equilibrium, an equation of state is required in order to calculate the density distribution throughout the body. Since the objects considered are cold and generally small compared to planets, a simple, temperature independent equation of state should suffice. Adopting a simple Birch-Murnaghan form for the $P(\rho)$ dependence (e.g., Cook 1980),

$$P(\rho) = K\left[\left(\frac{\rho}{\rho_0}\right)^{7/3} - \left(\frac{\rho}{\rho_0}\right)^{5/3}\right], \tag{12}$$

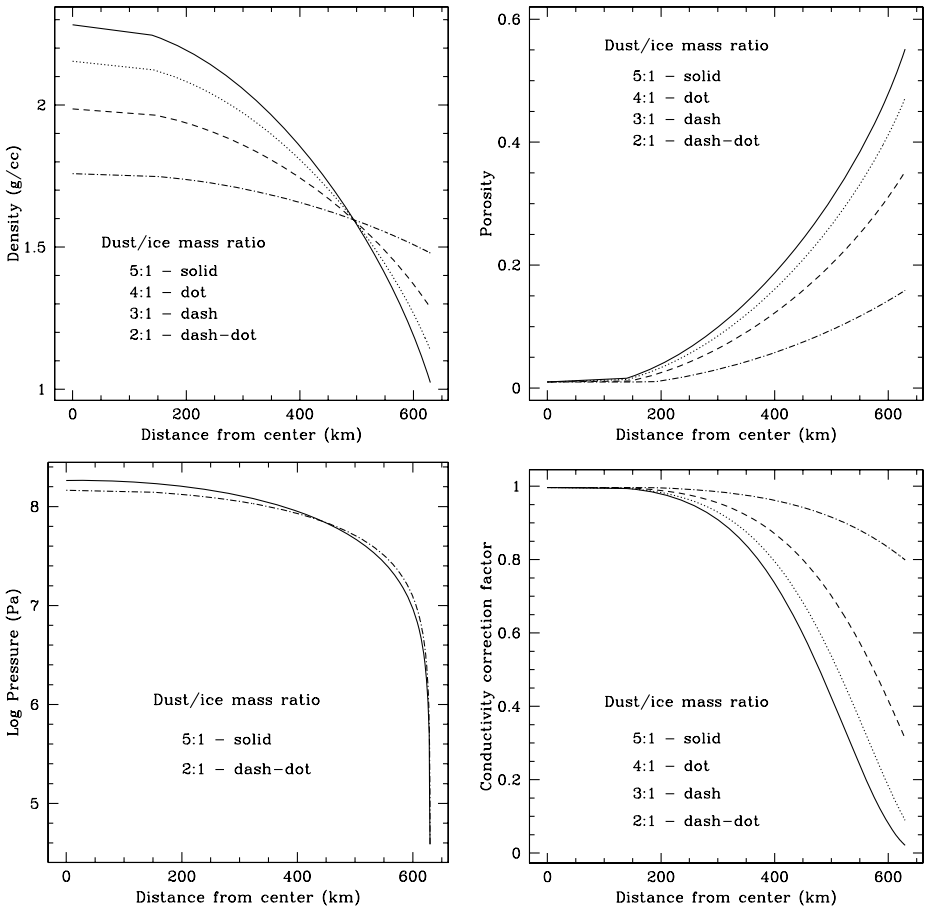

Fig. 3 Structure of a self-gravitating body having the mass and radius of 50000 Quaoar, for different compositions defined by the dust/ice mass ratio, as marked: *top-left*, density; *top-right*, porosity; *bottom-left*, pressure; *bottom-right*, correction factor for the thermal conductivity coefficient resulting from porosity

we can obtain $\rho(r)$ by solving numerically the hydrostatic equation combined with the mass conservation equation $dm/dr = 4\pi r^2 \rho$, that is,

$$\frac{d}{dr}\left[\frac{r^2}{\rho}\frac{dP(\rho)}{dr}\right] = -4\pi r^2 G\rho\,. \tag{13}$$

In order to obtain a solution, we have to determine two parameters (K and ρ_0) and two boundary conditions. One condition is $m(0) = 0$, and if the radius and average density (or mass) of a body are known from observations, there remains only one free parameter (or condition) to determine. Since the internal pressures are not expected to be sufficiently high for compressing the solid material (rock and ice), but only reduce the porosity, the highest central pressure will result by assuming the central porosity to vanish. Adopting this as the additional condition, we present in Fig. 3 an example based on the radius and estimated mass of a large KBO, 50000 Quaoar, 630 km and $\sim 1.7 \times 10^{21}$ kg, respectively. Results

are presented for different dust/ice mass ratios: 2, 3, 4 and 5. A unity mass ratio implies too large a specific volume to allow vanishing porosity at the center, as shown by (1).

Clearly, porosity increases with the dust/ice mass ratio, since the specific density of dust is much higher than that of ice, and thus, for a given bulk density, the volume occupied by solids decreases. We note the change in the correction factor for the thermal conductivity due to porosity (cf. Shoshany et al. 2002), ranging from unity at the center, to less than 3% near the surface. We also note that despite the relatively low *average* porosity, the porosity of the outer layers may be considerable, comparable to that encountered in comet nuclei.

2.4 Structural Changes

The structural parameters that affect the internal processes taking place in porous comet nuclei are the porosity Ψ, the surface to volume ratio S and the permeability ϕ. Assuming a structure of tortuous capillaries (Mekler et al. 1990) with tortuosity ξ and given a pore size distribution, where the number of capillaries with radii in the interval $[r, r+dr]$, crossing a unit area is $N(r)dr$, these parameters are obtained as moments of the distribution (Prialnik et al. 2005):

$$S = \xi \int 2\pi r N(r)dr, \qquad \Psi = \xi \int \pi r^2 N(r)dr, \qquad \phi = \frac{\pi}{\xi} \int r^3 N(r)dr. \tag{14}$$

For a known porosity, we have

$$S = 2\Psi \frac{\int r N(r)dr}{\int r^2 N(r)dr} = 2\Psi \left(\frac{\bar{1}}{r}\right), \qquad \phi = \frac{\Psi}{\xi^2} \frac{\int r^3 N(r)dr}{\int r^2 N(r)dr} = \frac{\Psi}{\xi^2}\bar{r} \tag{15}$$

and, as shown by Sarid et al. (2005), the relation between S and ϕ may be orders of magnitude different from that obtained for a uniform average pore size, where $S \propto 1/\phi$.

Pore sizes may shrink or grow as a result of condensation or sublimation, respectively. In this case pore radii change by a uniform amount Δ, negative or positive, but independent of r. If we assume $|\Delta| \ll r$, the new porosity Ψ' satisfies

$$\Psi' = \xi \int \pi (r+\Delta)^2 N(r)dr \approx \xi \int \pi r^2 N(r)dr + \xi \int \pi 2r\Delta\, N(r)dr = \Psi + S\Delta \tag{16}$$

and since it may be independently calculated from the mass conservation equations, we obtain $\Delta = (\Psi' - \Psi)/S$. Thus, the effect of pore size change caused by sublimation or condensation of ice may be easily incorporated in modeling. However, pores may also be squeezed or broken due to build-up of internal pressure. In this case, the changes are far more difficult to estimate and follow (Prialnik et al. 1993), since the material strength and its history become involved.

3 Early Evolution

Full-scale long-term simulations of the early evolution of comet nuclei, or more precisely, comet nucleus progenitors, are extremely demanding due to the interaction between the various thermal processes, which interfere with each other. Hence, to date, such calculations (e.g., Prialnik et al. 1987; Prialnik and Bar-Nun 1990; Yabushita 1993; Haruyama et al. 1993; Prialnik and Podolak 1995) have focused on one aspect of the evolution, as

determined by one key parameter, such as thermal conductivity, ^{26}Al content, or radius, neglecting or simplifying other effects. Even if limited, these calculations shed light and impose constraints on the interior structure of these bodies. More recently, models including mixtures of volatiles and gas flow through the porous medium have been considered by De Sanctis et al. (2001) and by Choi et al. (2002).

Numerical modeling involves the simultaneous solution of energy and mass conservation for all the components considered, assuming a spherical body. Since solar energy is not the major heat source, and since the orbital period is long and the orbital eccentricity relatively low, the assumption of spherical *symmetry* ("fast rotator") is acceptable for the early stages of evolution.

3.1 Heating During Accretion

Radioactive heating during the earliest stages of evolution of KBOs, concomitant with accretion, was studied by Merk and Prialnik (2003, 2006). Their numerical studies considered a composition of amorphous ice and dust in various proportions and allowed for heat exchange associated with crystallization and melting of the ice. They did not consider, however, other volatiles nor allow for flow (gas or liquid) through the porous medium.

Using the rates of growth supplied by an accretion algorithm, an extensive space survey was carried out for the parameter plane spanned by heliocentric distance and maximal radius R_{pmax} of the accreting object (planetesimal) in the outer region of the Solar System: 20 AU $\leq$ $d_H \leq$ 44 AU and 2 km $\leq R_{pmax} \leq$ 32 km. Of the three different compositions considered for the homogeneously growing body, we show in Fig. 4 the results obtained for a mixture of dust-to-ice $\sim$3.4 (by mass), in the form of contour plots. The *top-left* panel shows the accretion times, which span a wide range, and exceed the lifetime of ^{26}Al considerably at high radii.

The initially amorphous ice crystallizes upon heating by the decay of ^{26}Al. Figure 4-*bottom-left* shows the relative radius (that is, distance from the center divided by the object's radius) of the crystalline/amorphous ice boundary, when the crystallization process is completed. We note that large bodies formed in the Kuiper Belt zone retain the pristine amorphous ice throughout a considerable fraction of their mass (if the boundary is located at half the radius, meaning that above it the ice is amorphous, then only 1/8 of the mass has crystallized). Small bodies, as well as bodies formed closer to the sun, are bound to undergo complete crystallization for the high dust-to-ice ratio shown here. The results change significantly, however, if the ice content is much higher.

Figure 4-*bottom-right* shows the maximum extent of *liquid water* (in terms of relative radius r/R_{pmax}). The occurrence of liquid water in this calculation is tentative, since melting requires not only temperatures in excess of 273 K (disregarding possible lowering of the melting point in the presence of ammonia or methane), but also pressures in excess of $\sim$600 Pa. Since the pressure in the pores is not calculated, it is assumed that a sufficiently high pressure is obtained, implying that the material strength is high enough to sustain such a pressure. The occurrence of liquid water is limited in the parameter space considered, where beyond $\sim$30 AU (roughly, Neptune's present-day orbit), the fraction of liquid water becomes small regardless of R_{pmax}. Inward of 30 AU, melting is not found for the 2 km bodies, even if formed as close to the sun as 20 AU (and hence quickly accreting); these bodies remain permanently frozen. Comparing the bottom panels of Fig. 4, we point out the existence of bodies which may have liquid water in the deep interior, while retaining the pristine amorphous ice in their outer layers. These are bodies with radii in excess of 20 km, formed beyond 40 AU, which can be identified with KBOs.

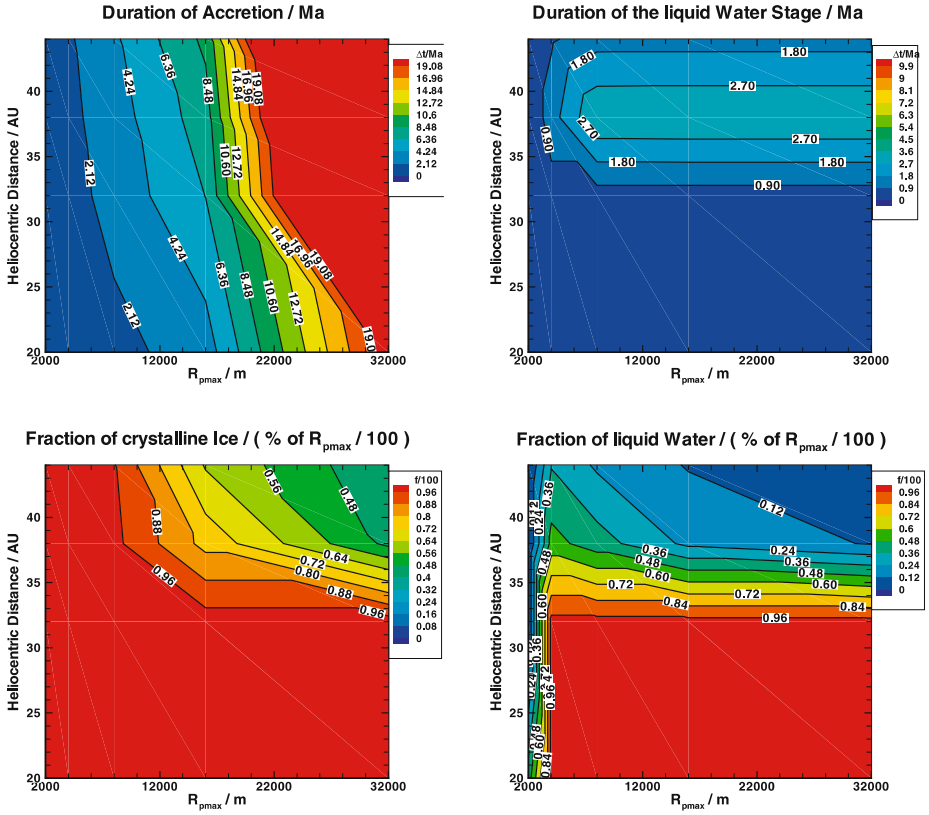

Fig. 4 Thermal evolution characteristics of growing bodies with a composition of ∼3:1 dust to ice by mass: *top-left*, accretion time; *top-right*, duration of accretion; *bottom-left*, extent of crystalline ice zone; *bottom-right*, maximal extent of liquid water. Radii are given in meters, heliocentric distances—in AU (adapted from Merk 2003)

The *top-right* panel of Fig. 4 shows the period of time during which liquid water is preserved, between melting as the temperature rises, and refreezing, as it drops with the decay of ^{26}Al. We note a relatively narrow intermediate region, just inward of the Kuiper Belt's inner boundary, where liquid water persists for the longest time (for the particular dust-to-ice ratio considered). Closer to the sun, temperatures become too high and the water may evaporate; farther away, accretion is too slow and hence cooling too fast.

In a different study, taking into account vapor flow through pores, Podolak and Prialnik (2006) have shown that although vapor can escape to the surface as well as serve as cooling agent, liquid water may still result from heating by ^{26}Al, with internal temperatures reaching ∼260 K and internal vapor pressures, ∼8 MPa. This demands a low permeability of the medium. Thus further exploration of the effects of structural parameters is required.

3.2 Survival of Volatile Ices

We now turn to other volatiles and consider the possible changes that are expected to occur due to internal heating by radioactivity. The main question is whether and to what extent can volatile ices survive in the interior of cometesimals. This question was investigated by Choi

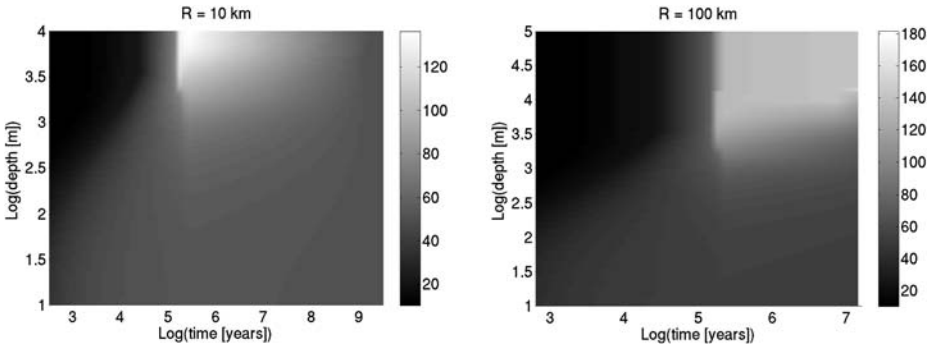

Fig. 5 Gray-scale map of the evolving temperature profile (adapted from Choi et al. 2002), for object radii of 10 km (*left*) and 100 km (*right*). The change in shade along a vertical line represents the radial temperature variation at the corresponding time. The change in shade along a horizontal line represents the change of temperature with time at the corresponding (fixed) depth. The time and depth scales are logarithmic, since changes are more pronounced during the early stages of evolution, and sharper, generally, towards the surface of the nucleus

et al. (2002), size and heliocentric distance being again the free parameters of the study. Here, however, the accretion phase is neglected and a diminished initial abundance of ^{26}Al is assumed instead (see Sect. 2.2), as another free parameter. Evolutionary calculations are carried out for very long times, up to 10^9 years; the decay of ^{40}K is thus considered as well. The composition includes CO and CO_2 ices, mixed with dust and amorphous water ice and volatile ices are allowed to sublimate and flow through the porous medium. The working assumption is that gases released in the interior can easily escape to the surface and out of the nucleus (high effective permeability). The detailed numerical solution yields temperature profiles and follows the evolution of temperature-dependent processes and the resulting changes in structure. An example of the results is shown in Fig. 5, for bodies of 10 km and 100 km radius.

For both radii considered, an outer layer about 1 km deep remains relatively cold at all times and thus preserves the ice in amorphous form. In all cases, however, the CO ice is lost, but this is bound to occur in the Kuiper Belt region even in the absence of ^{26}Al, as shown by De Sanctis et al. (2001). The complete loss of CO ice—and by analogy, all volatiles that sublimate below ∼50 K, which were initially included as *ices*—is common to all cases considered in this study. Moreover, less volatile ices are partially lost as well and from a depth of a few km down to the center the composition may become depleted of volatile ices.

Loss of volatiles from the interior is accompanied by changes in porosity, and presumably, in the tensile strength of the material as well. Internal stresses caused by steep temperature gradients and gas pressures up to a few 10^5 Pa (Prialnik et al. 1993) may contribute to weakening of the porous material. The main conclusion of the numerical simulations is that the internal composition emerging from the early stage of evolution is most probably not homogeneous, but stratified, with the outer layers being *less* altered, even almost pristine.

3.3 Gases Trapped in Amorphous Ice

The conclusion that volatile ices, even if included in the original composition, would be completely lost due to radiogenic heating leads us to consider the possibility that such volatiles may still be present, trapped in the amorphous water ice, which—we have seen—can survive radiogenic heating, at least in a thick outer layer. Otherwise it would be difficult

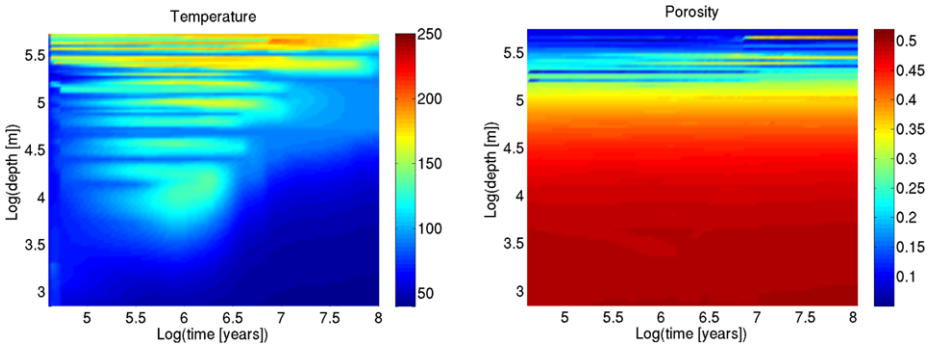

Fig. 6 Map of the temperature (*left*) and porosity (*right*) of a self-gravitating body having the bulk properties of 50000 Quaoar as it changes with time throughout the spherical body. Model parameters are: $R = 630$ km, $M = 1.6 \times 10^{21}$ kg, average porosity Ψ 0.25, dust mass fraction $X_d = 0.75$, $X_0(^{26}\mathrm{Al}) = 3 \times 10^{-8}$; mass fractions of occluded volatiles: CO—0.005, CO_2—0.005, HCN—0.0025; $X_0(^{26}\mathrm{Al}) = 3 \times 10^{-8}$; orbital properties: eccentricity—0.035, semimajor axis—42.95 AU

to reconcile observations of CO in comet comae with the hypothesis that comet nuclei are formed not further away than the outer edge of the KB (about 50 AU).

As mentioned in Sect. 1.2, trapped gases that are released from amorphous ice at relatively high temperatures (120–160 K), and migrate toward colder regions of the body where they refreeze, constitute an additional means of heat transfer. The processes of crystallization, freezing of the released gases and their subsequent sublimation, are all extremely temperature dependent and they all occur in the same temperature range on comparable timescales, thus interfering with each other. The result is a very complicated composition pattern, where layers enriched in various volatiles (in the form of ice) alternate.

A very recent numerical study of this complex phenomenon (Sarid and Prialnik 2007), which considers the evolution of relatively large KBOs and includes self-gravity, shows the resulting layered structure; as seen in Fig. 6-*left*, the temperature profile is not monotonic from the center outward. Volatiles that have been released in the interior and have migrated towards the surface, refreeze. The more volatile ices refreeze closer to the cold surface than the less volatile, so that the pristine mixture of amorphous ice and dust becomes enriched in volatile ices. The deep interior may be affected by loss of water ice, even to the extent that a water depleted core may form. The porosity is significantly affected by these processes, as illustrated in Fig. 6-*right*. If the surface layers will be heated at a later stage, either by a collision or by a change in orbit that brings them closer to the sun, sublimation of these ices may lead to enhanced activity. This may occur even if the temperature is not sufficiently high to trigger crystallization of the amorphous ice.

4 Late Evolution

For the late stages of evolution, when solar radiation is dominant, the non-uniform heating of the surface, combined with the low thermal inertia and low conductivity, require a 3-dimensional (3-D) approach, or some 3-D approximation (Prialnik et al. 2005). The evolution of active comets has been covered in numerous papers in recent years, and discussed in great detail by Huebner et al. (2006) and references therein. Inevitably, the orbit plays a major role, and also the spin rate and spin axis inclination; hence each comet has its own

evolution pattern. Here we focus on lasting changes in the structure of the nucleus, rather than on cyclic variations and cometary activity.

4.1 Internal Heating and Crystallization of Amorphous Ice

Internal heating of a comet nucleus is a very slow process, unless an internal heat source, such as crystallization of amorphous ice, is activated. One reason is that most of the solar radiation is spent in sublimation of volatiles, while only a small fraction is conducted to the interior. Another reason is that the orbital skin depth is of the same order of magnitude as the thickness of the outer layer that is lost during one perihelion passage. A third reason is that while a comet nucleus absorbs solar heat near perihelion, it emits thermal radiation in excess of the solar input along the distant part of its orbit.

The inhomogeneity of the internal structure is illustrated in Fig. 7, which shows the depth of the heat front and of the crystallization front propagating inward from the surface of a

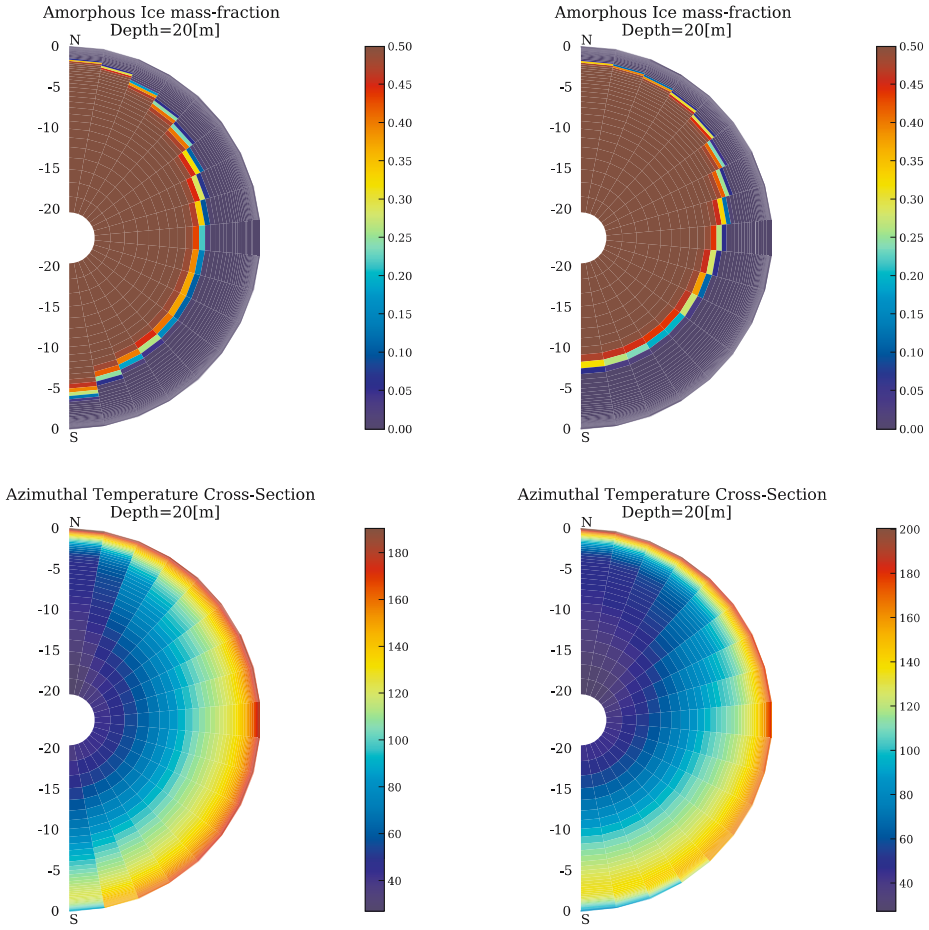

Fig. 7 Temperature profile at perihelion and depth of crystallization front after 5 revolutions for a model of a spherical comet nucleus composed of ice and dust in equal mass fractions, in the orbit of comet 67P/Churyumov-Gerasimenko, obtained with a fully 3-D code (without ablation): *left*—tilt angle of rotation axis 15°; *right*—tilt angle of rotation axis 40° (see Rosenberg and Prialnik 2007)

spinning nucleus. This is an upper limit, since ablation is not taken into account; it serves to stress differences between different latitudes, as well as the effect of the tilt angle of the spin axis (see Rosenberg and Prialnik 2007).

4.2 Loss of Volatiles and Dust Mantling

As the heat front generated by solar radiation propagates from the surface inward, gases are released either by sublimation of ices or by release from the crystallizing amorphous ice. These gases diffuse through the porous medium, driven by pressure and temperature gradients. Most of the gas escapes into the coma, but a fraction flows into the colder layers of the interior, where the gas eventually refreezes (cf. Benkhoff and Boice 1996). Since below the skin depth the temperature decreases monotonically with depth, the more volatile species will refreeze deeper down and a stratified structure will result. This is illustrated in Fig. 8, which shows the subsurface stratified structure obtained for a model for comet 9P/Tempel 1, where H_2O, HCN, and CO_2 follow in succession (stratified structure was also obtained by De Sanctis et al. 2007).

The escaping gas drags with it dust particles; however, the larger particles that cannot be lifted by the gas accumulate on the surface and gradually a dust mantle builds up. When the mantle becomes as thick as the diurnal skin depth, it seals the interior, as illustrated in Fig. 8, showing that the temperature change is largely confined to the very thin dust mantle (see Prialnik and Mekler 1991). The thin dust mantle of the model is in excellent agreement with the results of the *Deep Impact* mission: from the surface temperature distribution, Groussin et al. (2007) deduced that the thermal inertia—at least of the surface layer—is very low, of order several 10's W K m^{-2} $s^{1/2}$, which leads to the conclusion that the diurnal skin depth is no more than a few cm and since diurnal response to sunlight has been clearly detected (Schleicher et al. 2006), it means that the dust layer that covers the surface extends to skin depth, but not deeper. The delayed response to solar radiation is seen in the lower right-hand panel of Fig. 8. The second peak in production rate, occurring at dawn, may explain the observed sunrise outbursts (A'Hearn et al. 2005). It is caused by sublimation of ice deposited in the dust mantle by vapor migrating outward during the night.

The interior of the nucleus does evolve—and this explains the stratified structure extending over a much larger depth scale—but at a very slow rate. The heat diffusion time for a whole nucleus is larger than the life-time of an active comet in the inner solar system. Hence it is possible that a layer that has avoided both early and late evolution may still be present in a comet nucleus.

5 Conclusions: The History of a Comet Nucleus

The calculations presented here, both as analytical estimates and as complex numerical simulations, should be taken to indicate evolutionary trends and provide constraints, and the results should be regarded more as qualitative than strictly quantitative. An uneven shape, rotation, orbital migration, and collisions, are only a few among the factors that may affect the structure of comets and KBOs, but are difficult—if not impossible—to be accounted for in a systematic manner.

But we may attempt a sketch of a plausible evolutionary history of a typical comet nucleus (if such exists!). It forms in the outskirts of the solar system, in a relatively cold environment, growing by accretion on a time scale of Myrs. The main components are water ice and dust, but moderately volatile gases may condense and mix with the water and dust. It is

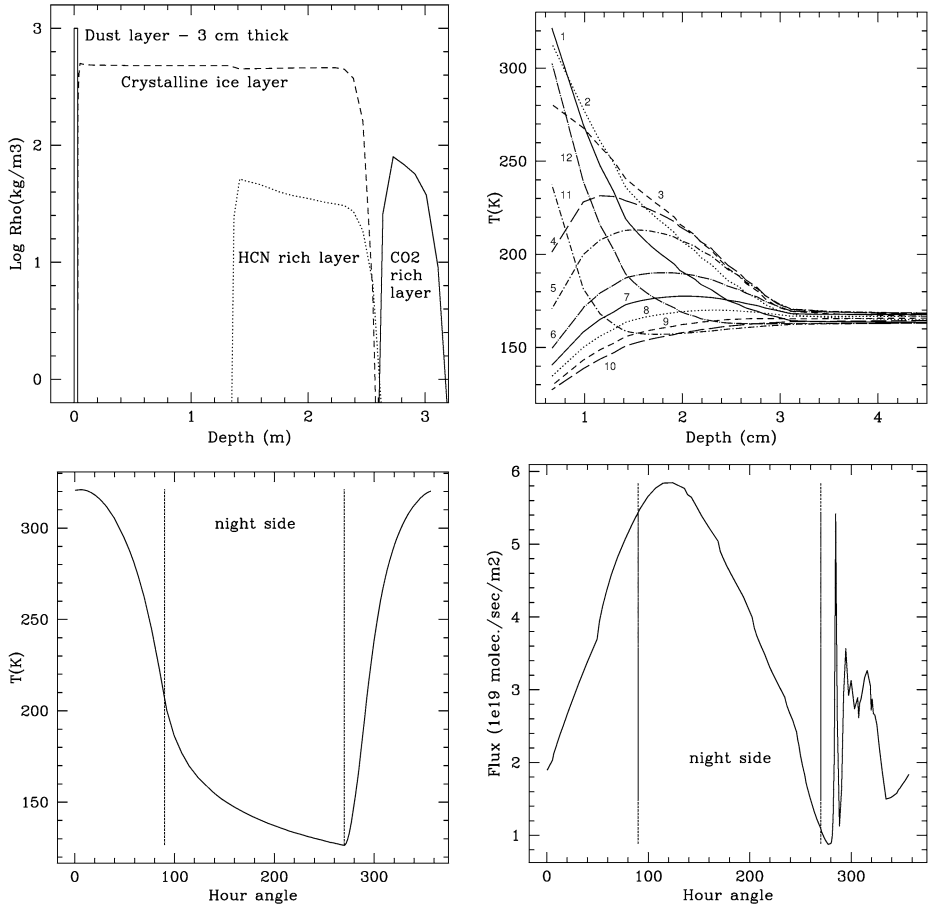

Fig. 8 Model of comet 9P/Tempel 1, with initially equal mass fractions of amorphous ice and dust and trapped CO_2 and HCN, 5% each. *Top-left*: Densities of volatile ices in the outer 3 m; outer dust layer (marked) is depleted of volatiles. *Top-right*: Diurnal temperature variation within the outer dust layer; profiles are shown at 30° hour angle intervals, starting with 1 at local noon. *Bottom-left*: Diurnal surface temperature variation at the spherical nucleus equator; between vertical lines (night-side) there is no absorption of solar radiation. *Bottom-right*: Diurnal variation of the H_2O molecular flux at the equator

unlikely that extremely volatile species be included as ices, but all volatiles may be trapped (occluded) in amorphous water ice. The body emerging from accretion at low velocities is highly porous, and presumably homogeneous, unless it is big enough to contract under its own gravity.

During these early stages, heating by short-lived radioactive species will cause several changes, altering the initial homogeneity: extremely volatile species, if present as ices, will be lost. Moderately volatile species will sublimate in the central part of the body, migrate outward, and eventually refreeze in the pores of the outer layers: the more volatile, the *closer* to the surface. Crystallization of the amorphous ice, releasing more volatiles, will propagate from the center up to several hundred meters to a few km below the surface. In the central part, the H_2O ice may be heated to such an extent that it will sublimate, or, if the permeability is low and sufficient pressure builds up, melt. Vapor or liquid will diffuse

outwards and refreeze, thus blocking the pores and significantly reducing the initially high porosity. In extreme cases, the very deep interior may become depleted of *all* volatiles.

Gradually, on a time scale of millions of years, radioactivity will decay, the body will start cooling, and all the processes induced by the brief period of high temperatures will subside. The body will be left, however, with a stratified structure, both in terms of composition (e.g., alternating layers enriched in different volatiles), and in structure (e.g., uneven porosity). The outer layers, down to a considerable depth, will nevertheless retain most of the initial properties. The body will now enter a long period of thermal hibernation.

Billions of years later, if the body (or a fragment produced by collision) will be thrown into the inner solar system, thus becoming an active comet, thermal and chemical evolution will resume, but in reverse direction: from the surface inwards, and accompanied by ablation rather than growth. Otherwise the processes will be similar: sublimation of volatiles, inward migration of the gas that does not escape through the surface, refreezing at some depth below the surface, as well as crystallization of amorphous ice, with the crystallization front advancing inwards, toward the center, at an irregular rate. Complete depletion of volatiles will now create an outer dust mantle rather than a rocky core. Beneath it, a layered structure will emerge, but the more volatile species will now be found *further down* from the surface.

Not surprisingly, such a complicated structure will exhibit an equally complicated activity pattern, and a great diversity among active comets, even beyond that attributed to differences in orbit. The task of deciphering the internal structure and its causes by means of the observed activity becomes an art.

Acknowledgements We are grateful to an anonymous referee for a very careful reading of the manuscript and many helpful suggestions and comments. We acknowledge support for this work from the Israeli Science Foundation grant 942/04 and from the German-Israeli Foundation grant 859-25.7/2005.

References

M.F. A'Hearn et al., Science **310**, 258 (2005)
A. Bar-Nun, J. Dror, E. Kochavi, D. Laufer, Phys. Rev. B **35**, 2427 (1987)
J. Benkhoff, D.C. Boice, Planet. Space Sci. **44**, 665 (1996)
J. Blum, R. Schräpler, B.J.R. Davidsson, J.M. Trigo-Rodríguez, Astrophys. J. **652**, 1768 (2006)
A.P. Boss, Astrophys. J. **660**, 1707 (2007)
M.E. Brown, C.A. Trujillo, D.L. Rabinowitz, Astrophys. J. **635**, L97 (2005)
Y.-J. Choi, M. Cohen, R. Merk, D. Prialnik, Icarus **160**, 300 (2002)
A.H. Cook, *Interiors of the Planets* (Cambridge University Press, Cambridge, 1980), pp. 94–107
J.K. Davies, T.L. Roush, D.P. Cruikshank, M.J. Bartholomew, T.R. Geballe, T. Owen, C. de Bergh, Icarus **127**, 238 (1997)
M.C. De Sanctis, M.T. Capria, A. Coradini, Astron. J. **121**, 2792 (2001)
M.C. De Sanctis, M.T. Capria, A. Coradini, E. Ammannito, Astron. J. **133**, 1836 (2007)
R. Diehl, U. Oberlack, J. Knodlseder, H. Bloemen, W. Hermsen, D. Morris, J. Ryan, V. Schonfelder, A. Strong, P. von Ballmoos, C. Winkler, in *AIP Conference Proceedings*, vol. 410, ed. by C.D. Dermer, M.S. Strickman, and J.D. Kurfess (1997), p. 1114
L. Dones, P.R. Weissman, H.F. Levison, M.J. Duncan, in *Comets II*, ed. by M. Festou, H.U. Keller, H.A. Weaver (University of Arizona Press, Tucson, 2005), p. 153
M.J. Duncan, H.F. Levison, L. Dones, in *Comets II*, ed. by M. Festou, H.U. Keller, H.A. Weaver (University of Arizona Press, Tucson, 2005), p. 193
O. Groussin, M.F. A'Hearn, J.-Y. Li, P.C. Thomas, J.M. Sunshine, C.M. Lisse, K.J. Meech, T.L. Farnham, L.M. Feaga, W.A. Delamere, Icarus **191**, 93 (2007)
J.M. Hahn, R. Malhotra, Astron. J. **117**, 3041 (1999)
J. Haruyama, T. Yamamoto, H. Mizutani, J.M. Greenberg, J. Geophys. Res. **98**, 15079 (1993)
W.F. Huebner, J. Benkhoff, M.-T. Capria, A. Coradini, C. De Sanctis, R. Orosei, D. Prialnik, *Heat and Gas Diffusion in Comet Nuclei* (ISSI/ESA Publications, The Netherlands, 2006)
W.M. Irvine, S.B. Leschine, F.P. Schloerb, Nature **283**, 748 (1980)

D. Jewitt, L. Chizmedia, R. Grimm, D. Prialnik, in *Protostars and Planets V*, ed. by B. Reipurth, D. Jewitt, K. Keil (University of Arizona Press, Tucson, 2006), p. 863
D.C. Jewitt, J.X. Luu, in *Protostars and planets IV*, ed. by V. Mannings, A.P. Boss, S.S. Russell (University of Arizona Press, Tucson, 2000), p. 1201
D. Jewitt, J.X. Luu, C.A. Trujillo, Astron. J. **115**, 2125 (1998)
H. Kawakita, N. Dello Russo, R. Furusho, T. Fuse, J.-I. Watanabe, D.C. Boice, K. Sadakane, N. Arimoto, M. Ohkubo, T. Ohnishi, Astrophys. J. **643**, 1337 (2006)
H. Kawakita, J.-I. Watanabe, T. Ootsubo, R. Nakamura, T. Fuse, N. Takato, S. Sasaki, T. Sasaki, Astrophys. J. **601**, L191 (2004)
J. Klinger, Science **209**, 271 (1980)
P.L. Lamy, I. Toth, Y.R. Fernandez, H.A. Weaver, in *Comets II*, ed. by M. Festou, H.U. Keller, H.A. Weaver (University of Arizona Press, Tucson, 2005), p. 223
H.F. Levison, M.J. Duncan, Icarus **127**, 13 (1997)
C.M. Lisse, J. VanCleve, A.C. Adams, M.F. A'Hearn, Y.R. Fernández, T.L. Farnham, L. Armus, C.J. Grillmair, J. Ingalls, M.J.S. Belton et al., Science **313**, 635 (2006)
G.J. MacPherson, A.M. Davis, E.K. Zinner, Meteoritics **30**, 365 (1995)
Y. Mekler, D. Prialnik, M. Podolak, Astrophys. J. **356**, 682 (1990)
R. Merk, PhD thesis, University of Muenster, 2003
R. Merk, D. Prialnik, Earth Moon Planets **92**, 359 (2003)
R. Merk, D. Prialnik, Icarus **183**, 283 (2006)
S. Mostefaoui, G.W. Lugmair, P. Hoppe, Astrophys. J. **625**, 271 (2005)
M. Podolak, D. Prialnik, in *Comets and the Origin and Evolution of Life*, ed. by P.J. Thomas, R.D. Hicks, C.F. Chyba, C.P. McKay (Springer, Berlin, 2006), p. 303
D. Prialnik, in *Minor Bodies in the Outer Solar System*, ed. by A. Fitzsimmons, D. Jewitt, R.M. West (1998), p. 33
D. Prialnik, A. Bar-Nun, Astrophys. J. **355**, 281 (1990)
D. Prialnik, A. Bar-Nun, M. Podolak, Astrophys. J. **319**, 992 (1987)
D. Prialnik, J. Benkhoff, M. Podolak, in *Comets II*, ed. by M.C. Festou, H.U. Keller, H.A. Weaver (University of Arizona Press, Tucson, 2005), p. 359
D. Prialnik, U. Egozi, A. Bar-Nun, M. Podolak, Y. Greenzweig, Icarus **106**, 499 (1993)
D. Prialnik, Y. Mekler, Astrophys. J. **366**, 318 (1991)
D. Prialnik, M. Podolak, Icarus **117**, 420 (1995)
E.D. Rosenberg, D. Prialnik, *New Astron.* doi: 10.1016/j.newast.2007.03.002 (2007)
N.H. Samarasinha, B.E.A. Mueller, M.J.S. Belton, L. Jorda, in *Comets II*, ed. by M.C. Festou, H.U. Keller, H.A. Weaver (University of Arizona Press, Tucson, 2005), p. 281
G. Sarid, D. Prialnik, in preparation, 2007
G. Sarid, D. Prialnik, K.J. Meech, J. Pittichova, T.L. Farnham, Pub. Astron. Soc. Pac. **117**, 796 (2005)
G. Schubert, J.D. Anderson, B.J. Travis, J. Palguta, Icarus **188**, 345 (2007)
Y. Shoshany, D. Prialnik, M. Podolak, Icarus **157**, 219 (2002)
D.G. Schleicher, K.L. Barnes, N.F. Baugh, Astron. J. **131**, 1137 (2006)
S.A. Stern, Nature **424**, 639 (2003)
H.C. Urey, Proc. Natl. Acad. Sci. **41**, 127 (1955)
M.K. Wallis, Nature **284**, 431 (1980)
S.J. Weidenschilling, in *Lunar Planet. Sci. Conf. XXXI* (2000) p. 1684
F.L. Whipple, R.P. Stefanik, Mem. R. Soc. Liege (Ser. 5) **12**, 33 (1996)
S. Yabushita, Mon. Not. R. Astron. Soc. **260**, 819 (1993)

Loss of the Surface Layers of Comet Nuclei

N. Thomas · C. Alexander · H.U. Keller

Originally published in the journal Space Science Reviews, Volume 138, Nos 1–4.
DOI: 10.1007/s11214-008-9332-5

Abstract The Deep Impact observations of low thermal inertia for comet 9P/Tempel 1 are of profound importance for the observations to be made by the Rosetta spacecraft at comet 67P/Churyumov-Gerasimenko. While sub-surface sublimation is necessary to explain the observations, the depth at which this occurs is no more than 2–3 cm and possibly less. The low thermal conductivity when combined with local surface roughness (also observed with Deep Impact) implies that local variations in outgassing rates can be substantial. These variations are likely to be on scales smaller than the resolution limits of all experiments on the Rosetta orbiter. The observed physico-chemical inhomogeneity further suggests that the Rosetta lander will only provide a local snapshot of conditions in the nucleus layer.

Keywords Comets: surface · Comets: nuclei · Comets: emission

1 Introduction

High resolution observations of the surface of comet 9P/Tempel 1 returned by the Deep Impact mission (A'Hearn et al. 2005; Thomas et al. 2007; Belton et al. 2007) have added considerably to our knowledge of the surface layer of cometary nuclei. Although much remains to be learned, in conjunction with observations of Comet 1P/Halley (Giotto; Keller et al. 1996), Comet 19P/Borrelly (Deep Space 1; Soderblom et al. 2002) and Comet 81P/Wild 2 (Stardust; Brownlee et al. 2004), we can begin to place tighter constraints on the structure of the surface layer and the mass emission mechanisms from this layer. However, a feature of these new observations is that they indicate significant inhomogeneity.

N. Thomas (✉)
Physikalisches Institut, Universität Bern, Sidlerstrasse 5, 3012 Bern, Switzerland
e-mail: nicolas.thomas@space.unibe.ch

C. Alexander
Jet Propulsion Laboratory, Pasadena, CA, USA

H.U. Keller
Max-Planck-Institut für Sonnensystemforschung, Katlenburg-Lindau, Germany

H. Balsiger et al. (eds.), *Origin and Early Evolution of Comet Nuclei*
DOI: 10.1007/978-0-387-85455-7_10

While this was to be expected, the implications are that models require yet another degree of complexity and yet more parameters.

In this paper, we address the surface layer as a specific entity. We review the evidence for inhomogeneity and attempt to describe the forms (both physical and chemical) this inhomogeneity takes. We then discuss the surface heat balance and its implications for the mass emission mechanism. Here, we also discuss scale lengths and relate them to the resolutions of remote sensing instruments on the Rosetta orbiter. In doing so, we use a highly simplified thermal model to illustrate the importance of certain processes. In the following section, we describe our current concept of the structure of the surface layer and the relative distribution of volatile and non-volatile material in the uppermost few centimetres. Finally, we discuss how physical and chemical inhomogeneity naturally leads to further physical inhomogeneity in that the topography of the surface is affected by inhomogeneous physical and chemical properties. We conclude by reviewing possible strategies for the investigation of Comet 67P/Churyumov-Gerasimenko by the Rosetta spacecraft.

Throughout, we draw heavily on the recent book by Huebner et al. (2006) which provides an excellent review of the current status of thermal models of the surface layer.

2 Evidence for Inhomogeneity

Four comet nuclei have been investigated during close fly-bys by spacecraft in recent years. In interpreting these images, it is necessary to recall that the images were acquired by different imaging systems under different circumstances.

At first glance, it is clearly apparent that the surfaces of the nuclei exhibit different surface structures and features (Basilevsky and Keller 2006). 81P/Wild 2 is covered with circular and elliptical depressions. (Indeed this work was prompted by a challenge to explain these structures.) 19P/Borrelly, and, in particular, the central section of the observed nucleus, is relatively smooth with no obvious counterpart to the depressions seen on 81P/Wild 2. 9P/Tempel 1 is an intermediate. There are circular depressions but there are also large remarkably smooth areas. 1P/Halley, too, shows a circular depression and a large smooth region in the centre of the visible hemisphere. It is necessary to conclude therefore that topographically, the nuclei are different.

Furthermore, a single cometary nucleus can exhibit varied terrain. Britt et al. (2004) attempted to make a geomorphological map of 19P/Borrelly. They identified several regions on the nucleus with different surface properties. Smooth terrain dominated the central region of the nucleus while "mottled" terrain and dark spots were evident on the two ends of the elongated body. Nelson et al. (2004) attempted to determine whether these dark spots were albedo features or shadowed depressions. The central, smooth region appeared to show some vertical relief, which Britt et al. (2004) referred to as "mesas".

Deep Impact revealed remarkably varied terrain on the surface of 9P/Tempel 1. Smooth regions which may resemble the "mesas" in 19P/Borrelly images were clearly evident (although the surfaces of these features are relatively dark on 19P/Borrelly but relatively bright on 9P/Tempel 1). Rough surfaces were also seen. Variations in surface reflectance were prominent in several non-circular depressions. These were the only regions where water absorption features could be observed in infrared spectra of the nucleus (Sunshine et al. 2006). A central band of slightly lower reflectivity material could also be seen. From these observations, one must conclude that most nuclei are not physically homogeneous.

The spatial variation of activity on cometary nuclei also points to physical inhomogeneity. Dust emission from nuclei is not spatially uniform. The clearest example of this

is 19P/Borrelly which, at the time of the DS1 fly-by in September 2001, exhibited a main jet roughly perpendicular to its long axis. This jet contributed 19–24% of the total dust brightness (when compared to the whole at a fixed distance from the nucleus centre) and yet the full width at half maximum was only 18° (Ho et al. 2007). The highest resolution images from DS1 show that this jet has three components at its base.

Several explanations of the origin of dust brightness enhancements in the inner coma of comets have been presented in the literature. Yelle et al. (2004) have suggested sub-surface emission through a vent (similar to a Laval nozzle) as a means of collimating the observed jet features. Keller et al. (1994) and Knollenberg (1994), following unpublished work by Kitamura in the 1980s (see also Kitamura 1986, 1987), investigated the effect of active areas surrounding an inactive central region. In this case, the gas, which drags the dust away from the nucleus, responds to the pressure gradient and "fills" the central region from all sides producing an enhancement in gas and dust density above the inactive surface. (In practise, the central region need not be completely inactive but merely of much lower activity than its surroundings.) Collimation of dust emission by concave topographic features has also been investigated by Knollenberg and has been shown to be a viable means of producing enhancements in dust brightness. Irrespective of the mechanism, whether it is topographic or a response to emission variations, the dust brightness variations seen in cometary comae indicate physical differences across the surface. It should be noted, however, that the gas, which drives the dust emission, cannot be seen with conventional imaging systems and Deep Impact observations of 9P/Tempel 1 suggest that the relationship between the spatial distribution of gas emission and that of dust emission is by no means trivial (M. A'Hearn et al., this issue).

The variations in surface reflectance may also point to chemical inhomogeneity. Although we know very little about the surface composition, there are measurable reflectance changes evident in the observations of 9P/Tempel 1. Reflectance variations might also be attributable to surface roughness and hence this is somewhat ambiguous. On the other hand, ground-based and spacecraft observations of jets in comets have been frequently made which show the jets to be rich (or poor) in CN, C_2, and C_3 when compared to other jets from the same comet. Examples from diverse techniques include those given by Clairemidi et al. (1990), Schulz (1992), Henry et al. (2002), and Farnham et al. (2007). These radicals are minor species when compared to the total gas and dust production rate but they nonetheless indicate that one cannot assume that outgassing regions are chemically homogeneous.

From the above, it must be concluded that comet nuclei are neither uniform physically nor chemically. If we accept that comet nuclei are not merely different from each other but are also physically and chemically inhomogeneous in themselves, then it is apparent that surface features on a nucleus can be altered and modified as a result of this inhomogeneity. Hence, features on the surface are dynamic—the surface is not a uniformly shrinking iceball.

3 Surface Heat Balance

To address the importance of inhomogeneity for the surface layer in a more quantitative manner, we require a simple model to investigate numerous parameters. We begin by using the thermal conductivity equation in one-dimension for the internal heat transport, i.e.

$$\rho c \frac{\delta T}{\delta t} = \kappa \frac{\delta^2 T}{\delta x^2} \tag{1}$$

where ρ is the bulk density of the nucleus material, c is its specific heat capacity, and κ is the thermal conductivity such that the thermal diffusivity may be defined as $d_t = \kappa / \rho c$ and

the thermal inertia, Γ, as $(\kappa\rho c)^{1/2}$. Here we ignore gas flow as a heat and mass transport mechanism within the nucleus and we also ignore effects such as amorphous–crystalline ice transition (which may or may not be a significant heat source) and radioactive decay heating. We keep open the possibility of explicitly describing conductivity changes within the nucleus. We do not attempt to describe further details of the heat transport as this would introduce further free parameters which cannot be constrained now (and indeed we have little hope of constraining them with Rosetta).

It is necessary to set boundary conditions. For the purposes of this study, we set explicitly the internal temperature of the nucleus. As this is still an unknown quantity, values in the range 30 K to 100 K can be easily justified. The surface boundary condition is the critical element in the study. The net energy flux excluding conduction is given by (Huebner et al. 2006)

$$F_{\mathrm{surf}} = \frac{S(1 - A_H)}{{r_h}^2} \cos\iota - \epsilon\sigma T^4 - Q\Delta H \tag{2}$$

where S is the solar flux at 1 AU, r_h is the heliocentric distance [AU], ι is the zenith angle of the Sun at the surface under consideration ($\cos\iota$ cannot of course be negative), A_H is the hemispherical albedo[1], ϵ is the IR emissivity (which is poorly known), σ is the Stefan-Boltzmann constant, Q is the mass loss rate resulting from sublimation and ΔH is the enthalpy of sublimation.

In principle, the system can now be solved using a discrete grid. However, Huebner et al. (2006) have shown the importance of being precise in specifying how the grid is treated. Here, for simplicity and ease of comparison, we use an explicit scheme and recognize that the Courant criterion

$$\delta t \leq \frac{\rho c(\Delta r)^2}{2\kappa} \tag{3}$$

where δt is the timestep, must be fulfilled. This results in timestep sizes of tens of seconds. Huebner et al. (2006) define the diurnal thermal skin depth, l_s, through the equation

$$l_s = \sqrt{\frac{2\kappa}{\omega\rho c}} \tag{4}$$

where ω is the angular velocity of the nucleus spin ($= 2\pi/\tau$ s^{-1} where τ is the spin period). By substituting values for compact ice and for what one might refer to as a highly porous material we arrive at the results in Table 1. It is generally appropriate to assume a grid size smaller than at least 1/4 of one skin depth (Spencer et al. 1989).

The Deep Impact spacecraft has given considerable support to the idea that the surface layers of comets are highly porous, low conductivity and therefore insulating. Groussin et al. (2007) report an estimated thermal inertia, Γ, of $<$50 W m^{-2} s$^{-1/2}$ K^{-1} (and therefore close to the values in the right hand column of Table 1). The thermal skin depth in this case must therefore be close to 2 cm—a quite remarkable result which has significant implications.

It will be immediately recognized that the thermal skin depth applies not merely in the vertical directions (into the interior) but also horizontally. This implies that, for example, a column into the interior will hardly be influenced by the thermal properties of a second column just a few centimetres away (at least on diurnal timescales).

[1] This is the ratio of the total photon power reflected to that incident. If one assumes a Lambertian surface, then $A_H = 3p/2$ where p is the geometric albedo.

Table 1 Comparison of parameters of compact ice and highly porous material. Note the large difference in the thermal skin depth

Quantity	Compact ice	Units	Highly porous
κ	1	[W m^{-1} K^{-1}]	0.01
ρ	600	[kg m^{-3}]	400
c	800	[J kg^{-1} K^{-1}]	400
τ	6	[h]	6
d_t	2×10^{-6}	[m^2 s^{-1}]	6.2×10^{-8}
Γ	700	[W m^{-2} s$^{-1/2}$ K^{-1}]	40
l_s	12	[cm]	2.1

The Rosetta spacecraft is equipped with an orbiter and a lander. Considering the orbiter experiments first, the highest spatial resolution experiment onboard is the imaging system, OSIRIS (Keller et al. 2007). OSIRIS is foreseen to have a pixel scale of 1.86 cm px^{-1} when 1 km above the surface (the expected closest distance of the spacecraft when preparing for the ejection of the lander) leading to an effective resolution of ≈ 4 cm. For most normal operations, however, Rosetta may be several kilometres away and at periods of peak cometary activity it may be as much as 100–300 km from the nucleus. Hence, even under optimum conditions, OSIRIS will not resolve distances comparable to the thermal scale length.

While we have no evidence of inhomogeneity at the 10 cm scale, it is not unlikely based on observations so far. Furthermore, the highest resolution images we have from Deep Impact suggest that the surface is extremely rough in places (the "mesas" may be an exception but even this is not clear at 2 cm resolution). The low albedo of the surface would also suggest that this roughness continues down to sub-mm scales. The presence of the $\cos\iota$ term in the boundary condition implies that 2 cm scale roughness has a significant influence on the thermal balance. We must conclude that what we will see with Rosetta, even at the highest resolution, is an unresolved ensemble of discrete surface elements which barely influence each other and hence future thermal models must treat comet nucleus surfaces as such.

Naturally, the imaging system on the lander has spatially superior resolution. But it will only observe at one position on the nucleus and, given the expected inhomogeneity, these results will not be easy to extrapolate to other areas on the nucleus.

As discussed by Orosei et al. (1999) and re-iterated in Huebner et al. (2006), the treatment of the surface element in any numerical scheme of thermal diffusion can have significant influence on the results (particularly the predicted nighttime temperatures) if the thermal diffusivity is very low. A further problem arises, however, in that comet nucleus surfaces are unlikely to be smooth—more probably they are a rough accumulation of irregular particles. As has been pointed out by Davidsson (this issue), scattering in the uppermost layer will lead to absorption below the true surface. The importance of this will depend upon the particle properties of the uppermost layer. It is perfectly possible that significant energy deposition can occur up to several millimetres (several tenths of a scale length) below the surface. Hence, the use of a surface boundary for a grid element actually at the physical surface is also probably unrealistic.

We study a system with the properties shown in Table 2 to illustrate the importance of the boundary description.

In Fig. 1, we show the result of a simple calculation where we have integrated from aphelion to perihelion. For perihelion, we show the temperature with depth at the chosen position at midday and at midnight. Sublimation is excluded. The plot shows that the temperature drops with depth with a gradient of more than 3 K mm^{-1} at midday. While the code here has not been fully iterated to a steady state over the orbital period, it is also apparent

Table 2 Parameters used for the evaluation of the examples shown herein

Orbit	
Perihelion distance	1.2923384 AU
Eccentricity	0.6315284
Rotation parameters	
North pole vector wrt orbit normal	[0.5,0.,0.866]
Rotation period	24 h
Surface constants	
IR emissivity	0.9
Hemispherical albedo	0.04
Thermal conductivity	0.01 W m^{-1} K^{-1}
Specific heat–density product	2.4 10^5 J m^{-3} K^{-1}
Area under investigation	
Longitude	0.0°
Latitude	+20.0°
Numerical quantities	
Depth step size	2.99 mm
Timestep	100 s
Courant criterion	107 s
Lower boundary temperature	90 K
Depth of lower boundary	5.98 m
Orbital skin depth	1.66 m
Diurnal skin depth	3.38 cm

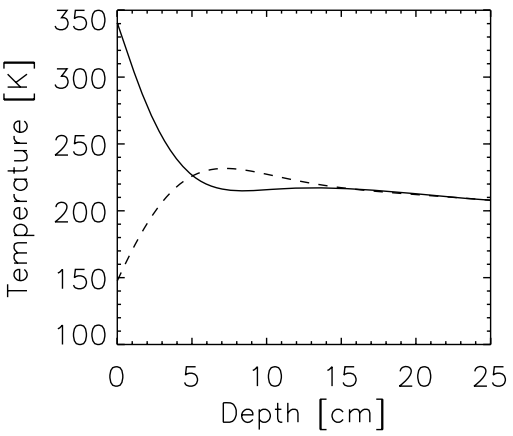

Fig. 1 The temperature–depth profile at perihelion for the parameters shown in Table 2, excluding sublimation. *Solid line*: Midday. *Dashed line*: Midnight

that the internal temperatures are below about 230 K only 5 cm below the surface and we note that we have used a relatively high temperature for the lower boundary condition.

The small thermal skin depth has major implications for theories of sub-surface sublimation. Several authors have suggested that sublimation occurs from below the visible surface. The Deep Impact observations by Sunshine et al. (2006) clearly established that the areal coverage of water ice on the surface of 9P/Tempel 1 was insufficient to explain the total water gas production rate of the comet and hence outgassing had to be occurring from below

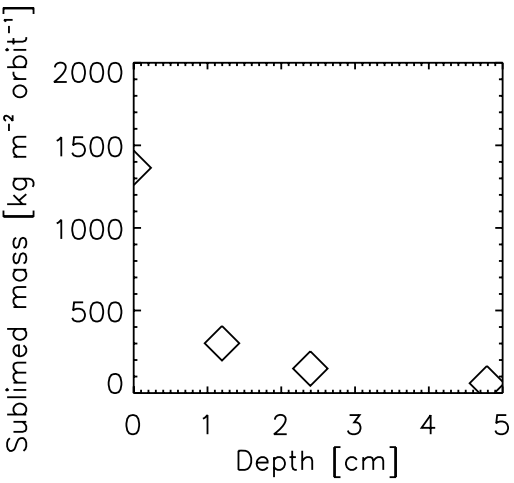

Fig. 2 The production rate of water gas computed for various depths of a low thermal conductivity surface layer. As the layer becomes thicker, the effective production rate per unit area decreases rapidly. Calculation parameters are those shown in Table 2

the observed surface in most regions. However, to be compatible with the thermal inertia observations and the implied thermal skin depth, this outgassing cannot be from depths greater than a couple of centimetres.

In Fig. 2, we show the total water gas production over one orbit plotted against the depth from which the emission occurs. We use the parameters given in Table 2. It should be noted that the inclusion of sublimation leads to numerical instability which in an explicit scheme must be compensated for by reducing the time step to well below (more than a factor of 10 below) the Courant criterion.

If the emission is at the surface, around 3 m of material is eroded per orbit which is equivalent to approximately 100 thermal skin depths. At peak production, one thermal skin depth would be eroded in no more than 2 nucleus rotations. Near-surface outgassing is therefore a highly dynamic process which can be strongly influenced on timescales of days by local inhomogeneities with depth.

The production rate per square metre drops rapidly and is reduced to only 4.4% of the production rate for a surface emission model just 4.8 cm below the surface. Let us take Comet 67P/Churyumov-Gerasimenko here as an example. The water gas production rate is around 10^{28} molecule s^{-1} at perihelion from an object with an average radius of 1.98 km. Assuming free sublimation around 3% of the surface must be active to match the observed production rate. If we now demand sublimation from more than 2.5 cm below the surface, we reach a point where the whole illuminated nucleus must be uniformly active to match the production rate. As discussed above, Deep Impact, Deep Space 1, and Giotto have all shown that this is, even in the most optimistic interpretation, questionable for comets observed to date. Hence, we have a strict limit for the depth of any sub-surface outgassing.

4 The Surface Layer

Sublimation is occurring from a layer within 2.5 cm of the surface. This emitting layer is masked from view by an optically thick layer of non-volatile or considerably less volatile material (which we refer to, for brevity, as non-volatile material or NVM). The free sublimation rate of water ice at perihelion suggests erosion at a rate comparable to one skin depth in about 1 day. If emission is sub-surface then this rate might be reduced by up to a factor of 10

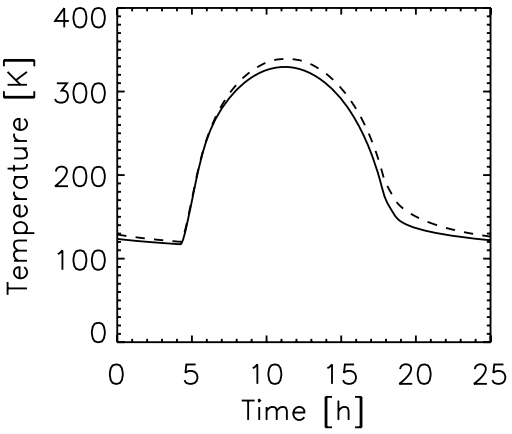

Fig. 3 The surface temperature over one rotation at perihelion for two cases. Sublimation is modelled to occur below the surface at constant depth. *Solid line*: Sublimation occurring 1.2 cm below the surface. *Dashed line*: 4.8 cm below the surface

but no more, otherwise emission ceases as insufficient heat can be transported to maintain the outgassing rate necessary to match observed production rates. The NVM must therefore be removed on timescales of 10 days or less. Hence, the surface structure of the nucleus is continuously being modified even where NVM is present at the surface—it is dynamic.

Although sublimating ice is within 2.5 cm of the surface, it is mostly invisible to optical and infrared remote sensing. While Sunshine et al. (2006) made a detection of surface water ice, the areal coverage was completely insufficient to explain the observed gas production rate. This might be explained if the subliming material is at a depth of the order of a few hundred microns. Such a layer would be thin enough to support significant heat transport while masking, at optical and IR wavelengths, the ice below. The subliming material is then able to exert maximum pressure on the uppermost layer of crust or dust particles leading to their ejection. Gas sublimed actually at the surface does not collide with NVM and hence exerts little or no force on it.

If sublimation were to occur from 2 cm depth, for example, the sublimation, already reduced by the reduction in heat input, would have to be sufficient to disrupt the 2 cm thick layer above. (It is not reasonable to assume that deep sub-surface sublimation can pass through a 2 cm thick layer and then selectively erode a micron thick layer at the surface. If the surface were sufficient loose to be eroded by such a low gas flow rate, it should have been eroded earlier when the sublimation rate per unit area was higher.) It seems to be possible that such a process can occur. Observations of "chunks" of emitting material have been made on many occasions (e.g., Rodionov et al. 1998). However, this leads to ice being at the surface immediately after the ejection and may be a mechanism for small outbursts. It may also indicate inhomogeneity in the tensile strength of NVM with depth. The reproducibility of cometary emission over many rotations (e.g., Millis and Schleicher 1986) and the stability of total dust emission over many hours (Keller et al. 1996) suggests that such outbursts are not the "common" means of mass ejection (although it is not clear whether this is the dominant mass loss mechanism or not).

It is important to recognize that the depth of sub-surface sublimation will be extremely difficult to deduce from the observed surface temperature. In Fig. 3 we show the temperature of the surface in two cases. The solid line and the dashed line show the surface temperatures over one rotation when sublimation is occurring 1.2 cm and 4.8 cm below the surface respectively. The difference, under perfect model conditions, is typically only 5 K.

5 Effects of Inhomogeneity

5.1 Surface Physical and Chemical Inhomogeneity

The inhomogeneity of the comet nucleus, clearly evident in Deep Impact data, now allows us to build model structures and modify the outgassing properties of these structures in an infinite number of ways since the constraints are almost non-existent. The importance of exact knowledge of the surface properties is illustrated by increasing the thermal conductivity by a factor of 4 (from 0.01 to 0.04 $\mathrm{W\,m^{-1}\,K^{-1}}$) which corresponds to a doubling of the thermal inertia. If emission were to be from a depth of 2.5 cm, the production over one orbit would increase by a factor of about 3.1.

The peak emission rate with the higher conductivity is 0.675 $\mathrm{g\,m^{-2}\,s^{-1}}$ and is around a factor of 3.4 higher than obtained with the lower conductivity. Hence, two adjacent regions with such a difference in thermal conductivity would produce an elevation difference of 2.9 mm in just one hour. The small-scale variations in conductivity of the surface layer would rapidly become evident in the local topography. There are additional non-linear feedbacks (both positive and negative) resulting from the production of surface slopes through such an inhomogeneity.

5.2 Conductivity Changes with Depth

Given the observed surface inhomogeneity, a change in thermal conductivity with depth is clearly possible. A simple model can be used to assess what influence this has on the surface temperature. In Fig. 4, the surface thermal conductivity has been set to 0.01 $\mathrm{W\,m^{-1}\,K^{-1}}$. At a depth of 1.3 cm, the conductivity is abruptly changed to 0.04 $\mathrm{W\,m^{-1}\,K^{-1}}$. A comparison with a constant κ of 0.01 $\mathrm{W\,m^{-1}\,K^{-1}}$ gives the following results. At perihelion, the midday temperature is 1.6 K higher if κ is higher internally. The midnight temperature is, however, nearly 15 K lower. The reason for this is that, with the higher κ, the surface is more closely connected to the internal temperature (which has been set at 90 K). Hence, investigations of the heat balance require accurate nighttime measurements of the surface temperature to place constraints not merely on the internal temperature but also the conductivity variation with depth.

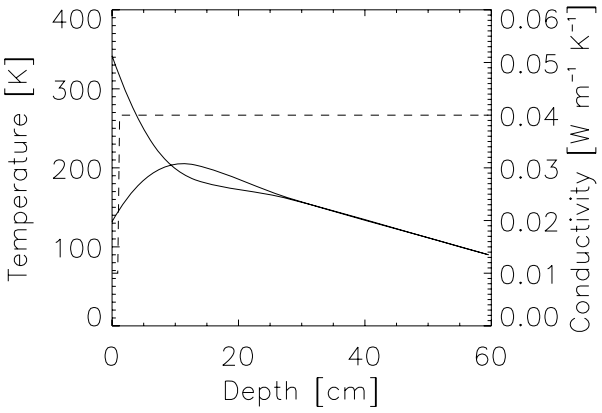

Fig. 4 The depth dependence of temperature at midday and midnight at perihelion assuming a factor of 4 increase in thermal conductivity 1.3 cm under the surface. The *dashed line* shows the conductivity using the right-hand scale

5.3 Topographic Inhomogeneity

We have already seen that the influence through thermal conduction of one nucleus element on another more than about 10 cm away is almost negligible because of the small thermal skin depth. This implies that as far as direct solar input is concerned, surface elements can be treated independently. This leads to independent development of that topography with time. For an initially spherical nucleus with zero obliquity, a homogeneous nucleus will sublime predominantly at equatorial latitudes to produce a "waist" (e.g., Dziak-Jankowska et al. 2002). (This situation is of course unstable to a change in the rotation axis so that the comet spins about the axis of minimum moment of inertia.) However, here we look at local effects.

Consider the geometry in Fig. 5. If the surface structure were located at the equator of a comet with zero obliquity, it is trivial to conclude that, integrated over one orbital period, the central, flat section of the structure will lose more mass than the surrounding inclined planes. This would result in the deepening of the pit until self-shadowing becomes significant. This picture rapidly becomes more complicated for moderate to high obliquities when combined with the eccentricity and the effective latitude of the active region. A relatively simple example is shown in Fig. 6. Here, we plot the cumulative sublimation over one orbit for the five surfaces in Fig. 5—a flat surface and four 45° slopes arranged orthogonally to each other surrounding the flat surface. The direction to the nucleus north pole is also marked in the figure. (We note that Kossacki et al. (2003) have investigated a similar geometry applied to Mars.) It can be seen that the flat surface sublimes the most and hence the model structure should deepen as expected. The two slopes parallel in latitude (east and west facing slopes) behave in a rather similar way but lose 13% less mass. The slopes that are parallel to lines of longitude (north and south facing) show markedly different behaviour as one might expect because they strongly depend upon the latitude and the orientation of the rotation axis. In this case, the loss rates are lower and hence the pit expands asymmetrically. Over one orbit the expansion is 25% slower in the north-south direction than east-west.

This shows that, for example, an originally circular depression can then become elliptical on relatively short timescales. While this is not a demonstration of a production mechanism for the structures on 81P/Wild 2, it certainly shows that, given the number of free parameters available, an interpretation in terms of sublimation pits is feasible. It should also be noted that the rate of expansion differs through the orbit with the evolution of the southern slope occurring more slowly than the northern slope. Furthermore, the present example is rather

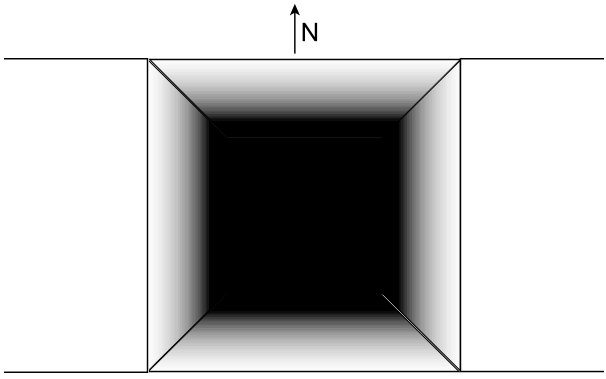

Fig. 5 A model geometry to demonstrate the effects of topography. The black central section is depressed but flat. The sides are at an angle of 45° with respect to the local zero gradient

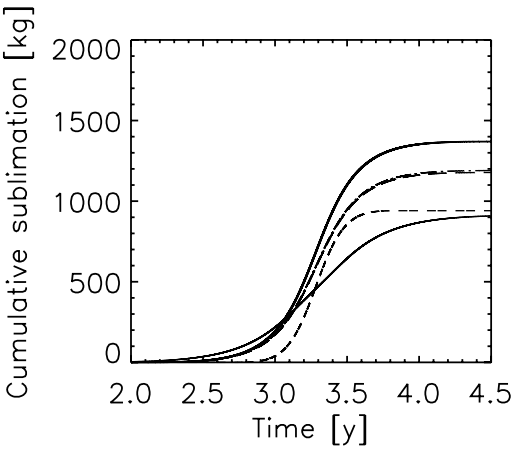

Fig. 6 Modelled cumulative sublimation of five surfaces on a comet with the orbital parameters given in Table 2. *Solid*: A flat surface. *Other lines* are for surfaces inclined at 45°. *Dash-dot-dot* and *short dashed lines* are for surfaces with slopes aligned to lines of longitude. *Dash-dot* and *long dashed lines* are for surface with slopes aligned to line of latitude

simple. Models with moderate obliquity and intermediate latitude sources can show more extreme behaviour. Investigation of these is on-going.

In this discussion, we have ignored "self-heating" of the nucleus. Topography will result in light being reflected from one surface element onto another. It is probably possible to ignore this because of the low hemispherical albedo of the nucleus. However, the nucleus surface can rise to temperatures close to 400 K when the comet is at 1 AU. This produces significant thermal IR emission which can add to the solar heat input of other surfaces within the emitting hemisphere. Ivanova and Shulman (2002, 2006) have studied this problem as have Kossacki et al. (2006) while Russell and Hecht (pers. comm.) have incorporated this physics into models of sublimation in mid-latitude Martian craters. What is not known here is the emission angular distribution function (which may be but is probably not isotropic because of sub-millimetre sized roughness) and hence more uncertainties remain.

6 Strategies for Rosetta

The implications for Rosetta of the Deep Impact results are quite profound.

Firstly, the lander carries several experiments to probe the interior of the nucleus. To constrain the sublimation process, however, penetration and measurement at very shallow depths is primarily required. Naturally, determination of the low boundary temperature and the interior structure support these observations but the dynamic nature of nucleus activity is governed by the upper 3 cm.

Secondly, given the probable inhomogeneity of the nucleus, efforts must be made to place the lander in a representative region on the nucleus. This places a strong requirement on data acquisition and particularly analysis prior to lander site selection.

Thirdly, the importance of the microwave spectrometer, MIRO, for investigations of the surface layer have increased considerably. We can assume that the infrared spectrometer, VIRTIS, will fail to detect the source of the sublimation directly over most of the surface. It may also fail to place significant constraints on the depth of sublimation (within the first 3 cm) via the temperature and thermal inertia. MIRO penetrates the surface to approximately this depth and can probe the temperature. While interpretation is unlikely to be straightforward it may be the only means of probing this critical region over most of the nucleus. It is necessary to get the spacecraft as close as possible to the nucleus to minimize the scale of

the measurement. (The angular resolution of MIRO is equivalent to a spatial resolution of 5 m from a distance of 2 km.)

Fourthly, the OSIRIS imaging system must be used to observe the nucleus at <10 cm resolution near perihelion. This implies sending the spacecraft close to the nucleus while significant activity is on-going. The difficulties and dangers of this manoeuvre have not, to our understanding, been assessed in a complete way.

Finally, future modelling studies must take account of the fact that a 1-D representation of nucleus activity ignores unresolved roughness and inhomogeneity which will play a critical role in determining the local gas and dust emission which in turn will influence the near-nucleus coma structure.

7 Conclusions and Discussion

The Deep Impact observations have added considerably to our understanding of the surface layer of cometary nuclei. Observations of surface inhomogeneity, both topographical and chemical, have been made (A'Hearn et al. 2005; Belton et al. 2007) and the thermal inertia of the uppermost layer is extremely low (Groussin et al. 2007). Sub-surface chemical heterogeneity cannot be ruled out. This leads to a series of important consequences.

The thermal skin depth is of the order of 2 cm. But, sub-surface sublimation must be occurring to explain the limited surface area coverage of water ice seen by Deep Impact (Sunshine et al. 2006). The depth below the surface of sublimation is therefore limited to a few centimetres at most. The surface layer is highly dynamic with disruption of a thickness equivalent to one thermal skin depth in less than one day occurring at perihelion for typical Jupiter-family nuclei. Inhomogeneity on scalelengths comparable to the thermal skin depth results in modifications to local topography which can significantly affect the local heat balance on similar timescales. The resolution of the Rosetta imaging system, OSIRIS, will typically be five times greater than the thermal skin depth. Hence, inhomogeneities on the scale of the skin depth will be observed as an ensemble of different emission properties which must be modelled as such. One-D calculations (or multi-dimensional calculations using surface grid sizes much larger than the thermal skin depth) will fail to give an accurate picture of the parameters providing the emission unless some approach to compensating for the effects of inhomogeneity is taken.

The temperature variation with depth can be probed best by MIRO and this is likely to provide the most significant constraints on the thermo-physical properties of the surface layer. Variations in thermal conductivity with depth have a limited effect on the surface daytime temperature but might be addressed by measuring the thermal IR from the nightside if VIRTIS is capable of this task.

Models clearly show that surface structures similar to some of those observed on comet nuclei can be produced by sublimation processes together with topographic effects. The observed inhomogeneity in comets gives an enormous number of additional free parameters for thermo-physical modelling. This implies that, at the present time, our knowledge is so limited that essentially any realistic structure can be produced by using the correct mix of input parameters. Progress in this field will be somewhat arbitrary until further constraints become available.

Acknowledgements The authors thank the organizers, both referees for accurate comments, and in particular Elmar Jessberger for asking a provocative question!

References

M.F. A'Hearn et al., Science **310**, 258 (2005)
A.T. Basilevsky, H.U. Keller, Planet. Space Sci. **54**, 808 (2006)
M.J.S. Belton et al., Icarus **187**, 332 (2007)
D.T. Britt et al., Icarus **167**, 45 (2004)
D.E. Brownlee et al., Science **304**, 1764 (2004)
J. Clairemidi, G. Moreels, V.A. Krasnopolsky, Icarus **86**, 115 (1990)
B. Dziak-Jankowska, J. Leliwa-Kopystyński, M.E. Królikowska, Earth, Moon, Planets **90**, 35 (2002)
T.L. Farnham, N.H. Samarasinha, B.E.A. Mueller, M.M. Knight, Astron. J. **133**, 2001 (2007)
O. Groussin et al., Icarus **187**, 16 (2007)
F. Henry, D. Bockelée-Morvan, J. Crovisier, J. Wink, Earth, Moon, Planets **90**, 57 (2002)
T.-M. Ho, N. Thomas, D.C. Boice, M. Combi, L.A. Soderblom, V. Tenishev, Planet. Space Sci. **55**, 974 (2007)
W.F. Huebner, J. Benkhoff, M.T. Capria, A. Coradini, C. De Sanctis, R. Orosei, D. Prialnik, Heat and gas diffusion in comet nuclei. ISSI Scientific Report, SR-004, 2006, ISBN 1608-280X
A. Ivanova, L. Shulman, Earth, Moon, Planets **90**, 249 (2002)
A.V. Ivanova, L.M. Shulman, Adv. Space Res. **38**, 1932 (2006)
H.U. Keller et al., Space Sci. Rev. **26** (2007)
H.U. Keller, J. Knollenberg, W.J. Markiewicz, Planet. Space Sci. **42**, 367 (1994)
H.U. Keller, W. Curdt, J.R. Kramm, N. Thomas, Images of the Nucleus of Comet Halley. ESA-SP 1127, vol. 1, 1996
Y. Kitamura, Icarus **66**, 241 (1986)
Y. Kitamura, Icarus **72**, 555 (1987)
J. Knollenberg, Ph.D. Thesis. Univ. Göttingen, 1994
K.J. Kossacki, W.J. Markiewicz, M.D. Smith, Planet. Space Sci. **51**, 569 (2003)
K.J. Kossacki, J. Leliwa-Kopystyński, S. Szutowicz, Icarus **184**, 221 (2006)
R.L. Millis, D.G. Schleicher, Nature **324**, 646 (1986)
R.M. Nelson, L.A. Soderblom, B.W. Hapke, Icarus **167**, 37 (2004)
R. Orosei, F. Capaccioni, M.T. Capria, A. Coradini, M.C.D. Sanctis, C. Federico, M. Salomone, J.-P. Huot, Planet. Space Sci. **47**, 839 (1999)
A.V. Rodionov, L. Jorda, G.H. Jones, J.F. Crifo, F. Colas, J. Lecacheux, Icarus **136**, 232 (1998)
R. Schulz, Icarus **96**, 198 (1992)
L.A. Soderblom et al., Science **296**, 1087 (2002)
J.R. Spencer, L.A. Lebofsky, M.V. Sykes, Icarus **78**, 337 (1989)
J.M. Sunshine et al., Science **311**, 1453 (2006)
P.C. Thomas et al., Icarus **187**, 4 (2007)
R.V. Yelle, L.A. Soderblom, J.R. Jokipii, Icarus **167**, 30 (2004)

Section IV: New Results from Laboratory Measurements and Modeling

Distributed Sources in Comets

Hervé Cottin · Nicolas Fray

Originally published in the journal Space Science Reviews, Volume 138, Nos 1–4.
DOI: 10.1007/s11214-008-9399-z

Abstract The distribution of some molecules and radicals (H_2CO, CO, HNC, CN, ...) in the atmosphere of several comets cannot be explained only by a direct sublimation from the nucleus, or by gas phase processes in the coma. Such molecules are in part the result of a distributed source in the coma, which could be the photo and thermal degradation of dust. We present a review of the degradation processes and discuss possible interpretations of the observations in which the degradation of solid complex organic material in dust particles seems to play a major role. The knowledge of such gas production mechanisms provides important clues on the chemical nature of the refractory organic material contained in comet nuclei.

Keywords Comets · Distributed source · Extended source · Composition · Organic chemistry · Modelling

Introduction

Our current knowledge of the composition of the comet nuclei derives from observations made in their atmospheres, and from our understanding of the physico-chemical processes governing the emission of material into the atmosphere (sublimation of ices contained in the nucleus releasing gaseous molecules and dragging along solid particles), and its evolution once out-gassed or lifted. Recently, Stardust spacecraft captured cometary grains in the atmosphere of Comet 81P/Wild 2. Those grains were brought back to Earth in 2006 and were analysed in the laboratory where it has been shown they were made of a complex mineral and organic mixture (Brownlee et al. 2006). The grains collected during this mission are representative of the most refractory component of comets, emitted from the nucleus, that survived the collection process. Until the *Rosetta* mission succeeds in landing the *Philae* probe at the surface of Comet 67P/Churyumov–Gerasimenko in 2014, the only way to study

H. Cottin (✉) · N. Fray
Laboratoire Interuniversitaire des Systèmes Atmosphériques, Universités Paris 12 et Paris 7, UMR CNRS 7583, 61 Av. du Général de Gaulle, Créteil 94010, France
e-mail: cottin@lisa.univ-paris12.fr

the whole unaltered molecular composition of cometary nuclei will be in an indirect way, reconstructing the composition of the nuclei from what we can probe in their atmospheres.

The simplest way to describe chemistry within cometary atmospheres is the application of Haser's model which supposes that 'parent molecules' are released only by the nucleus ices sublimating and that 'daughter molecules' are produced solely by the photodissociation of a single gaseous species. Moreover, this simple model requires many hypotheses: radial expansion of molecules at constant velocity, stationary state of the gas production, spherical symmetry around the nucleus, and destruction of the 'parent' species by photodissociation (Haser 1957). More advanced hypothesis have to be introduced into models to take into account a chemistry more elaborated than simple photolysis (proton transfer, dissociative recombination, etc.), and more elaborated physics than radial transport at constant velocity (hydrodynamic models, magnetohydrodynamic & Monte Carlo models (Rodgers et al. 2004; Ip 2004; Combi et al. 2004)). However, approaching the distribution of parent molecules in comets via a Haser distribution is usually sufficient, while the study of species formed in the coma requires the other kind of modelling.

The present paper focuses specifically on distributed sources, also called sometimes 'extended' sources in the literature. Properly speaking, this term could apply to any compound formed in the coma from a parent molecule by any kind of process (photolysis, electron impact, charge exchange reactions, dissociative electron recombination . . .). However, such mechanisms are considered as normal coma chemistry, and do not require the introduction of an additional term. In common cometary terminology, the use of "distributed sources" or "extended sources" can be confusing as it is not really associated to a clear and self consistent definition. It often refers to the production of a molecule in the coma through an unknown process, with no associated known parent. In the book Comets II (Festou et al. 2004), the following definition is given in the glossary:

> Extended source – Most stable molecular species (as opposed to radicals, atoms and ions) appear to be emitted directly from the nucleus. Some stable molecular species appear to have at least one component that is produced in the coma from another source. Processes that have been suggested are sublimation from grains or large polymerized molecules, photon-induced desorption or photo-sputtering from grains or large molecules, gas-phase chemistry in the coma, or photodissociation of other parent molecules. Well known examples in comets are extended source components of H_2CO and CO. The term "distributed source" is also often used.

We do not endorse this definition as it excludes radicals while CN, C_2 and C_3 radicals are also often associated with a distributed source, and including these species in the present definition would also include any compound produced in the coma through the mechanisms mentioned above. Moreover, the term "extended source" is rather ambiguous as it is also used to describe the extended nature of the gas and dust release across the nucleus surface (for example in Thomas et al. 1988). This problem is clarified by using the word *distributed.* It also makes sense to favour this term since it is the common mathematical word used to describe inhomogeneous terms in differential equations, e.g., the right-hand-sides of the conservation equations presented later in this paper. Therefore, using the word *distributed* causes less confusion and is more consistent with common science/mathematics usage.

Taking into account the previous discussion, we propose the following definition:
A *distributed source* is an additional source of a gaseous species being produced in the coma from the grains. It is an exchange of mass between the dust and the gas inventory of the coma. Henceforth, we restrict the expression "distributed source" to the production of gaseous species in the coma from solid materials. In this usage, mechanisms that simply

change one gaseous molecule to another, keeping the mass budget unchanged, are understood as chemistry, and not distributed sources. We propose the use of the term "secondary source" in this case as opposed to distributed to avoid any confusion and the use of "additional source" to cover both distributed and secondary sources. The present definition of the distributed sources seems rather consistent, for future use and with its historical use in the literature. Of course, it may not be known from observations alone whether an enhancement in the density of a species in the coma is due to a dust (distributed) source, but such a situation can't be avoided at present.

To date, the origins of observed species tagged as "distributed" are unknown or at least uncertain. The first section of this paper is a review of the observations of distributed species while interpretations of these observations are discussed in the second section.

1 Observations

The best way to reveal the origin of the production of a gaseous species detected in the atmosphere of a comet, and whether it is directly released from the nucleus, produced by chemistry in the gas phase, or by a distributed source, is to determine its radial distribution in the coma. Moreover, to make a distinction between a production by chemistry or a distributed source, the spatial distributions have to be carefully analysed. In some cases, densities of gaseous species as a function of the distance from the nucleus were measured in-situ by mass spectroscopy. This technique has revealed for the first time the existence of distributed sources in the coma of Comet 1P/Halley (Meier et al. 1993). Nevertheless, the spatial distribution of gas species is generally determined by long-slit spectroscopy at infrared, visible and ultraviolet wavelengths as well as by coarse mapping or interferometry at millimeter wavelengths (Bockelée-Morvan et al. 2004).

Others observational clues on the existence of distributed sources can be found. Indeed generally, the heliocentric evolution of the production rates of molecules produced by a distributed source is steeper than the one of molecules produced from the nucleus (Bockelée-Morvan and Rickman 1997). Moreover, the line shape at millimeter wavelengths, which is characteristic of the motion of gas species in the coma, could give clues on the production mechanism (Gunnarsson et al. 2002; Womack et al. 1997).

In this chapter, we review the observational evidences for some of the distributed source for H_2CO, CO, HNC, CN and some sulfur compounds. Concerning C_2 and C_3 radicals, for which the nature of the parents is uncertain, some information can be found in Combi and Fink (1997), Festou (1999) and Helbert et al. (2005).

1.1 Distributed Source for H_2CO

The radial distribution of H_2CO in the coma of 1P/Halley has been deduced from in-situ measurements by the Neutral Mass Spectrometer (NMS) onboard the Giotto spacecraft (Meier et al. 1993; Eberhardt 1999). It has been shown that its density profile cannot be reconciled with its only source in the nucleus. The additional source for the H_2CO production has been confirmed by coarse mapping at radio wavelengths in Comets C/1990 K1 (Levy), C/1989 X1 (Austin) (Colom et al. 1992) and C/1996 B2 (Hyakutake) (Biver et al. 1999). In Comet C/1995 O1 (Hale-Bopp), interferometric observations have also shown that H_2CO had an additional source (Wink et al. 1997; Bockelée-Morvan and Crovisier 2000; Milam et al. 2006). All these observations suggest that the production scale length for H_2CO is about 7000 km at 1 AU, which does not fit with the photodissociation of any known

possible gaseous parent (see Sect. 2). These observations have been performed for heliocentric distances lower than 1.5 AU. Moreover, the H_2CO production rates measured in C/1995 O1 (Hale-Bopp) present a very steep heliocentric evolution which suggests that the origin of some H_2CO is distributed out to 4 AU (in and outbound) (Biver et al. 2002a; Bockelée-Morvan and Rickman 1997).

1.2 Distributed Source for CO

In a similar manner than for H_2CO, an additional and potentially distributed source for CO has been discovered in the coma of 1P/Halley thanks to in situ measurements by mass-spectrometry (Eberhardt et al. 1987; Eberhardt 1999). These measurements indicate that approximately one third of the total CO is produced directly from the nucleus, while the remainder of CO comes from an additional source located in the innermost 25 000 km of the coma (Eberhardt 1999). Determination of the CO spatial distribution by infrared long-slit spectroscopy has confirmed the existence of a CO additional source in Comet C/1996 B2 (Hyakutake) (DiSanti et al. 2003). This observation suggests a parent scale length of about 1000 km and a release rate from nucleus that accounts for about 80% of total observed CO. A coarse map of the CO spatial distribution has also been obtained at millimetre wavelengths in this comet (Biver et al. 1999). Both observations are compatible with most of the CO being released from the nucleus, at least within the innermost 1000 km in the coma. As these observations do not extend farther than 7000 km in the coma, they are not sensitive to other sources with a scale length as large as the one observed in Comet 1P/Halley. In Comet C/1995 O1 (Hale-Bopp), the spatial distribution of CO has been determined by infrared long slit spectroscopy by numerous authors (Brooke et al. 2003; Disanti et al. 2001, 1999; Weaver et al. 1997) for heliocentric distances smaller than 2 AU. These observations suggest that the production of additional CO reaches its terminal value at a distance of about 7000 km from the nucleus at 1.49 AU and 5000 km at 1.06 AU (Brooke et al. 2003; Disanti et al. 2001). The ratio of nucleus to additional sources release rates determined from these infrared observations remains controversial. Indeed, according to different authors, the release of CO from additional source could represent 50% (Disanti et al. 2001) or 90% (Brooke et al. 2003) of the total. Beyond 2 AU from the Sun, only the nucleus source was seen by infrared long slit spectroscopy (Disanti et al. 2001). Nevertheless, this observation seems to be contradictory with the ones performed in the radio domain, which probe larger fractions of the coma than the infrared observations. The radio observations show that at large heliocentric distances, the profiles of the CO radio lines in Comet C/1995 O1 (Hale-Bopp) could be fitted assuming a production by a distributed source (Gunnarsson et al. 2003). Interferometric maps of the CO spatial distribution have been obtained when the comet was close to perihelion (Henry et al. 2002). They show strong deviations from those expected for an isotropic distribution of CO, probably caused by the existence of CO jets. One may also note that the heliocentric evolution of the CO production rates in Comet C/1995 O1 (Hale-Bopp) is not as steep as for H_2CO, HNC or CS (Biver et al. 2002a) as one might expect from distributed sources. First coarse mapping at millimeter wavelengths of CO in Comet 29P/Schwassmann–Wachmann 1 at 6.2 AU seems to reveal a strong additional source at such heliocentric distances (Gunnarsson et al. 2002). Nevertheless, new observations and analysis of the CO line profile indicate that the additional source, if present, is very weak (Gunnarsson et al. 2008). Since the observations seem to be inconsistent, a summary of them is given in Table 1.

Table 1 Summary of the observations of the CO additional source

Comet	References	Observational method	R_H (AU)	Remarks
1P/Halley	Eberhardt et al. 1987	(1)	0.9	• Production of CO at $\rho < 20\,000$ km
	Eberhardt 1999	(1)	0.9	• $Q_{nucleus}(CO)/Q_{nucleus}(H_2O) = 3.5\%$
				• $Q_{total}(CO)/Q_{nucleus}(H_2O) = 11\%$
				• Production of CO at $\rho < 25\,000$ km
C/1996 O2 (Hyakutake)	DiSanti et al. 2003	(2)	0.64–1.06	• $Q_{nucleus}(CO) = 14.9\%$
				• $Q_{total}(CO) = 19.1\%$
				• Production of CO at $\rho < 10^3$ km for $R_H = 0.64$ AU
				• Production of CO at $\rho < 2$–$3 \cdot 10^3$ km for $R_H = 1.06$ AU
	Biver et al. 1999	(4)	1.24	• $Q_{nucleus}(CO) \approx Q_{total}(CO)$
				• $L_P \approx 400$ km (*)
C/1995 O1 (Hale-Bopp)	Weaver et al. 1997	(2)	1.1	• Detection of a CO distributed source
	Disanti et al. 1999 and 2001	(2)	0.93–4.11	• Detection of a CO distributed source only for $R_H < 2$ AU
				• $Q_{nucleus}(CO)/Q_{total}(CO) \approx 50\%$ for $R_H < 2$ AU
				• Production of CO at $\rho < 6$–$7 \cdot 10^3$ km for $R_H = 1.49$ AU and at $\rho < 5 \cdot 10^3$ km for $R_H = 1.06$ AU
	Brooke et al. 2003	(2)	1.02–1.05	• Detection of a CO distributed source
				• $Q_{nucleus}(CO)/Q_{total}(CO) \approx 10\%$
				• $L_P \approx 5000$ km (*)
	Gunnarsson et al. 2003	(3)	3.7–10.8	• Detection of a CO distributed source
				• $Q_{nucleus}(CO)/Q_{total}(CO) \approx$ 10–60%
	Henry et al. 2002	(5)		• Presence of a spiral CO jet
	Biver et al. 2002a	(6)		• No steep heliocentric evolution of $Q(CO)$

(1) In-situ mass spectrometry
(2) Long slit spectroscopy at infrared wavelengths
(3) Analysis of the radio line profile
(4) Coarse mapping at radio wavelengths
(5) Interferometry at radio wavelengths
(6) Determination of the production rates at radio wavelengths
(*) L_p: production scale length of the distributed molecule. See precisions in Sect. 2.1

1.3 Distributed Source for HNC

HNC, which is an isomeric form of HCN, was detected for the first time in Comet C/1996 B2 (Hyakutake) (Irvine et al. 1996) at millimeter wavelengths. It was then observed in C/1995

O1 (Hale-Bopp) (Biver et al. 2002a; Irvine et al. 1998a) and in other comets (Biver et al. 2002b, 2006). In Comet C/1995 O1 (Hale-Bopp), interferometric observations made it possible to measure the HNC spatial distribution (Wink et al. 1997), which deviates from that of HCN in the innermost coma, and indicates production of HNC in the coma. Nevertheless, the main indication of an HNC distributed source is the heliocentric dependence of the HNC/HCN ratio. Indeed, as for the H_2CO production rates, this ratio increases with decreasing heliocentric distance in Comet C/1995 O1 (Hale-Bopp) (Biver et al. 2002a), C/2002 C1 (Ikeya-Zhang) (Irvine et al. 2003) as well as for other comets (Biver et al. 2006).

1.4 Distributed Source for CN

Reviews about the existence of the CN additional source have already been published (Festou 1999; Fray et al. 2005). It is clear that at least some of the CN radicals are produced in the coma through HCN photodissociation. Nevertheless, it is not clear if this mechanism could solely explain the abundance of CN. Indeed CN and HCN production rates have the same order of magnitude in most of the comets and considering the uncertainties in their production rates, we cannot conclude if HCN is the only parent molecule of CN or not in most of the comets. In comets, the $^{14}N/^{15}N$ isotopic ratios in CN is about two times lower than on Earth (Hutsemékers et al. 2005). First measurements of the $^{14}N/^{15}N$ in HCN (Jewitt et al. 1997; Ziurys et al. 1999) lead to values close to the terrestrial one. This was a major indication that HCN could not be the unique parent molecule of CN radicals until new measurements in comet 17P/Holmes and reanalysis of the older observations show that the $^{14}N/^{15}N$ isotopic ratio in CN and HCN are about the same (Bockelée-Morvan et al. 2008). Nevertheless, from this new result, we cannot exclude that CN has other major progenitors, than HCN, sharing the same low $^{14}N/^{15}N$ isotopic ratio (Bockelée-Morvan et al. 2008). The spatial distribution of CN has been measured in numerous comets by long-slit spectroscopy at UV wavelengths. From these observations, it seems that CN radicals could be entirely produced by the HCN photodissociation for heliocentric distances greater than 3 AU. Nevertheless, closer to the Sun, the CN spatial distribution is too narrow to be explained only by this process (Bockelee-Morvan and Crovisier 1985; Fray et al. 2005). Indeed for heliocentric distance less than 3 AU, the CN parent scale length is lower than the HCN photodissociation scale lengths (see Fig. 1).

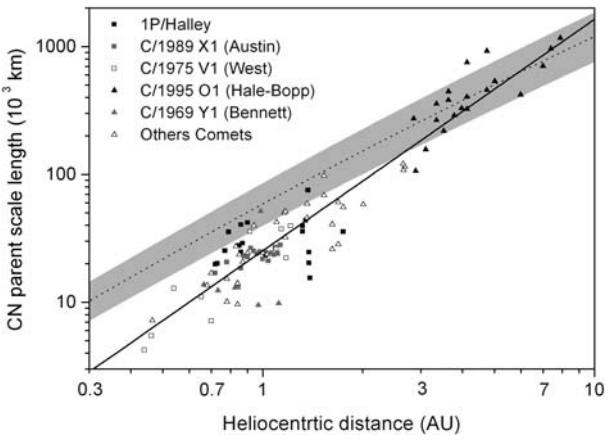

Fig. 1 Measured CN parent scale lengths as a function of the heliocentric distance. The CN parent scale lengths have been normalized to the minimum of solar flux and the *black line* is the best fit to these data. The *dashed line* is the effective CN parent scale length assuming that CN is produced exclusively by photodissociation of HCN. The *grey region* represents the error on the effective CN parent scale lengths due to uncertainties in the photodissociation rate of HCN and in the expansion velocity (figure from Fray et al. 2005)

1.5 Distributed Sources for Other Species

The radial distribution of OCS has been determined in Comet C/1995 O1 (Hale-Bopp) at about 1 AU from the Sun by infrared long-slit spectroscopy (Dello Russo et al. 1998). This observation suggests that about 70% of the total production of OCS comes from an additional source having a parent scale length of 3000–3500 km. The fact that most sulfur is contained in the refractory CHON grains suggests that OCS may be derived from refractory grains by a distributed source. However, as the mechanism for a distributed source for OCS is unknown, an additional contribution from other gaseous species cannot be ruled out.

CS has been observed in different comets at millimeter and ultraviolet wavelengths. The CS/HCN and CS/H_2O production rate ratios increase with decreasing heliocentric distance in all the comets for which CS has been observed (Biver et al. 2000, 2002a, 2006). The spatial distribution of CS has been determined thanks to coarse mapping at millimeter wavelengths in Comet C/1996 B2 (Hyakutake) at 0.7 AU (Biver et al. 1999) suggesting a parent scale length of about 1200 km. Whereas this value is roughly in agreement with the photodissociation scale length of CS_2, which has been tentatively detected in Comet P/122 de Vico (Jackson et al. 2004), the increase of CS abundance with decreasing heliocentric distance suggests that CS is also produced by an additional mechanism (Biver et al. 2006).

In Comet C/1995 O1 (Hale-Bopp), the SO spatial distribution has been measured by interferometry at millimeter wavelengths (Wink et al. 1997). This observation shows clearly that SO is a daughter species. SO is at least produced in part by the photodissociation of SO_2. Nevertheless, its production rate is greater than the one of SO_2, suggesting an additional production mechanism of SO (Bockelée-Morvan et al. 2000; Boissier et al. 2007).

First detection of radical NS is reported in Comet C/1995 O1 (Hale-Bopp) (Irvine et al. 2000). In their paper, the authors state that whether NS itself is present in the nucleus or has a distributed source in the coma is unknown.

2 Interpretations

2.1 General Discussion

Understanding the chemistry of comets is quite a difficult task. The additional sources, including distributed and secondary sources, do not have an origin based on the same mechanism. Some physical and chemical mechanisms which could explain the origin of secondary and distributed (i.e. additional) sources are summarized in Fig. 2. Some production of gaseous species may result from the dissociation (photolysis or other chemical processes including electron impact (Helbert et al. 2005)) of several gaseous parents (among which some may not have been detected to date) or chemistry between two gaseous compounds in the innermost coma. Distributed sources include sublimation of icy grains in the coma or the production of gaseous compounds during the degradation of solid organic material contained in cometary dust particles.

Indeed, it is now established that the organic content of comets is more complex than what is seen in the gaseous phase alone. Most of the detections presented in the above section are all remote sensing observations, probing the gaseous phase of comets, leading to the detection of about 20 stable gaseous molecules (Bockelée-Morvan et al. 2004). However in 1986, Vega 1 & 2 and Giotto spacecrafts probed the atmospheres of Comet 1P/Halley. Molecular analyses of solid particles in the coma were conducted by mass spectrometry and resulted in the detection of solid organic compounds much more complex than the gaseous

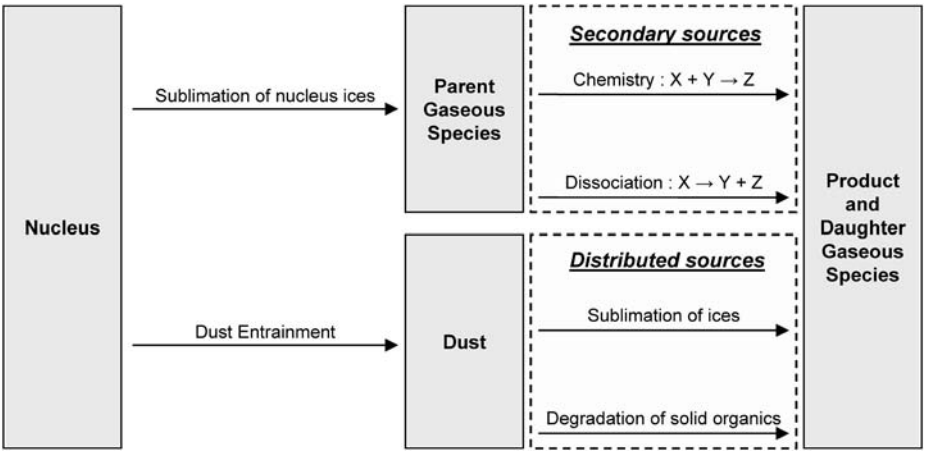

Fig. 2 Chemical mechanisms of production of the gaseous species in the cometary environment. The 'secondary' and 'distributed' sources have been clearly distinguished

ones securely detected from the Earth. It showed that more organic material is present, in the solid state, and that its molecular mass can reach value above 150 amu (Kissel and Krueger 1987; Mitchell et al. 1992). In-situ results from the Stardust mission (with the CIDA mass spectrometer) have confirmed these observations (Kissel et al. 2004). Recently, the analysis of grains captured from Comet 81P/Wild 2 by the Stardust spacecraft has also enabled the detection of complex organic material made of aliphatic and aromatic hydrocarbons, and molecules bearing a large range of organic functions (hydroxyl, carbonyl, amide, nitrile . . .) with high molecular weight (up to 300 amu) (Keller et al. 2006; Sandford et al. 2006).

For an even better insight into the most complex and less volatile material, one can turn to experimental laboratory work. The principle of such experiments is the following: from observations of the most abundant species in comae and in the interstellar medium, one can infer probable compositions of the nucleus ices. A gaseous sample of the key species is condensed under near vacuum conditions on a cold substrate and irradiated by UV photons or charged particles. Sometimes, condensed ices are also simply warmed up slowly without irradiation. These processes are similar to the ones precometary ices may have encountered in the Solar Nebula or in the interstellar medium and they allow the synthesis of complex organic compounds from the initial simple ice. When the sample is warmed up for analysis, a refractory organic residue remains on the substrate at ambient temperature. The diversity of organic compounds synthesized during those experiments is remarkable (Greenberg 1982; Colangeli et al. 2004; Despois and Cottin 2005), and this mixture of molecules can be considered as an analogue of the solid organic component of comets.

In the frame of the study of distributed sources, a new generation of cometary laboratory experiments has been developed. Proceeding in an opposite direction than the 'classical' ice experiments, they study the production of gaseous compounds during the photo-degradation (induced by the solar UV flux) and the thermal-degradation (induced by dust particles heating) of complex solid molecules suspected to be present in cometary dust particles, once they are ejected in the coma. Such experiments are described in Cottin et al. (2000), Fray et al. (2004a, 2004b) and an example is given in Fig. 3.

These experiments are not actually meant to *simulate* the cometary environment, but rather to measure physico-chemical data, such as production quantum yields (photo-

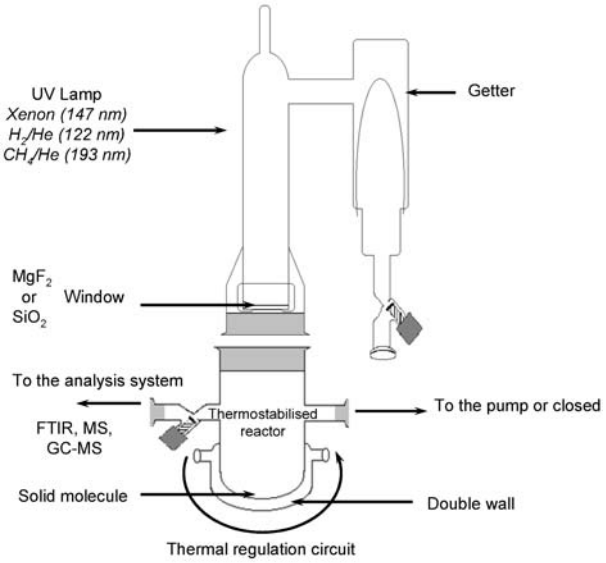

Fig. 3 Experimental setup dedicated to the study of the degradation of solid organic material into gaseous fragments. The solid organic molecule is deposited at the bottom of a Pyrex reactor where it can be heated with a thermal regulation circuit or photolyzed (at different wavelengths) with a UV lamp located at the top of the reactor. Gaseous degradation products can then be analyzed by infrared spectroscopy, direct mass spectrometry or gas chromatography coupled with a mass spectrometer (more details in Cottin et al. 1999, 2000)

degradation), Arrhenius constants and activation energies (thermal-degradation), characteristic of the gaseous production resulting from the decomposition of some specific targeted solid material. Results obtained after that kind of experiments, which were not necessarily conducted in a cometary context, are summarized in Table 2.

These quantitative data are then included into numerical models simulating the production of gaseous species during the degradation of solid compounds ejected in the cometary atmosphere on dust particles. The purpose of these models is to calculate the spatial distribution of the gaseous species produced by these mechanisms. With hypotheses similar to the classical Haser's approach, these models are based on the equation of conservation.

If a gaseous species is produced solely by the photodissociation of a unique parent molecule, then the conservation equation can be written:

$$\frac{\partial n_D}{\partial t} + div(n_D.v_{gas}) = \beta_P.n_P - \beta_D.n_D. \tag{1}$$

Here n_P and n_D are the number density (m^{-3}) of the parent and daughter molecules respectively, β_P and β_D the photodissociation rates (s^{-1}) of the parent and daughter molecules and v_{gas} the gas expansion velocity in the coma ($m\,s^{-1}$) assumed to be constant. In the frame of the Haser's model, the parent (l_P) and daughter (l_D) scale lengths are defined as the product of the gas expansion and the photo-lifetime (reciprocal of the photodissociation rate). The distribution of daughter molecules produced by the photo processes of a single gaseous parent is shown in (2), where Q_P and Q_D are the spherically symmetric production rates of parent and daughter molecules (s^{-1}).

$$n_D(r) = \frac{1}{r^2}\left(\frac{Q_P}{4\pi\, v_{gas}}\frac{l_D}{l_P - l_D}(e^{-r/l_P} - e^{-r/l_D}) + \frac{Q_D}{4\pi\, v_{gas}}e^{-r/l_D}\right). \tag{2}$$

In most cases, the parent and daughter scale lengths are measured by adjustment of the observations with (2). This parent scale length is then compared to the photodestruction rate of a candidate parent molecule. This comparison gives important clues on the nature

Table 2 Summary of data available on the degradation of potential precursors of distributed sources

	Photodegradation			Thermal degradation		
POM	Products and production quantum yields for various wavelength from Cottin et al. (2000)			H_2CO is the only product. Kinetic parameters for its production as a parameters for its production as a function of T (Arrhenius law) for two different POM polymers are given below. From Fray et al. (2004a).		
	λ (nm)	122	147	193	Ea (J mol^{-1})	A (molec g^{-1} s^{-1}
	H_2CO	0.75 ± 0.21	0.96 ± 0.19	<0.16	POM 1	81×10^3 ±0.76%	1.2×10^{30} +28%/−22%
	HCOOH	0.13 ± 0.05	0.26 ± 0.10	ε			
	CO	NE	∼ 1	ε	POM 2	99×10^3 ±2.3%	7.2×10^{32} +140%/−60%
	CO_2	NE	∼ 0.3	ε			
	CH_3OH	∼ 0.05	∼ 0.05	ε			
	NE : Present but not estimated						
HMT	Some HCN detected at 147 nm but at level too low to be quantified (Cottin et al. 2002)			No thermal degradation. HMT sublimates when heated under vacuum (Fray 2004)		
HCN polymer	Some HCN, CH_4 and C_2H_2 are produced with quantum yields lower than 0.03 at 122 and 147 nm (Fray 2004; Fray et al. 2004b)			NH_3 and HCN are the major products of the thermal degradation (Fray et al. 2004b). The production kinetics have been measured for $T > 420$ K (Fray 2004). Nevertheless, for lower T, the production declines to very low value (unpublished results)		
C_3O_2 polymer	No data available			For $T > 400$ K: release of CO_2 For $T > 500$ K: increased efficiency in the degradation, with release of CO_2 and CO. CO/CO_2 ratio increases with T. From Blake and Hyde (1964) and Smith et al. (1963)		

of the gaseous parent molecule. Nevertheless, one should keep in mind that the ejection velocity acquired by the daughter species during the photolysis of the parent is neglected. This actually changes the physical meaning of the parent scale length (Combi and Delsemme 1980), but as a first approximation this results in estimations usually sufficient to suggest a possible parent.

In the case of a production from the degradation of solid material in cometary dust particles, the conservation equation is:

$$\frac{\partial n_D(r)}{\partial t} + div(n_D(r) \cdot v_{gaz}) = \left(n_{grain}(r) \cdot \sigma_\alpha(r) \cdot C_D\right) + \left(n_{grain}(r) \cdot m_\alpha(r) \cdot k_D(T)\right) - \left(\beta_D \cdot n_D(r)\right). \quad (3)$$

In the right side of this equation, the first two terms are the production of the considered gaseous species by the photo- and the thermal-degradation of the solid material. In this equation, n_{grain} is the grain density in the coma (m^{-3}), σ_α the surface of material exposed to the

Solar flux and C_D the production rate of gaseous species by photo-degradation ($m^{-2}\,s^{-1}$), m_α the mass of solid material in each particles and k_D the production rate of the gaseous species by thermal-degradation ($kg^{-1}\,s^{-1}$).

With classical Haser's hypotheses regarding the dynamics in the coma, two scale lengths related respectively to the thermal- (l_T) and photo-degradation (l_P) can be defined (Cottin et al. 2004; Fray et al. 2006) and (3) is integrable analytically. Then, n_D can be written:

$$n_D(r) = \frac{1}{4\pi r^2 v_{gas}} \left\{ \begin{array}{l} \frac{3Q_{grain}\beta^3 m_\alpha}{m_D l_T X} \left[\begin{array}{l} l_D(1-X)(1-e^{-\frac{r}{l_D}}) \\ +\frac{(3X-2)(1+1/\beta)}{(1/l_D-1/l_T)}(e^{-\frac{r}{l_T}}-e^{-\frac{r}{l_D}}) \\ +\frac{(1-3X)(1+1/\beta)^2}{(1/l_D-2/l_T)}(e^{-\frac{2r}{l_T}}-e^{-\frac{r}{l_D}}) \\ +\frac{X(1+1/\beta)^3}{(1/l_D-3/l_T)}(e^{-\frac{3r}{l_T}}-e^{-\frac{r}{l_D}}) \end{array} \right] \\ +Q_D\, e^{-\frac{r}{l_D}} \end{array} \right\}. \quad (4)$$

Where Q_{grain} is the production of grains of a specific size and composition, β is the ratio l_T/l_P, m_D the mass of the daughter molecule, X is related to the photoproduction of the daughter compound, and Q_D the contribution from the nucleus to the production of the molecule (more details can be found in Cottin et al. (2004)).

Even if this equation can be simplified in the case that either thermal or photo degradation is not relevant (one being negligible compared to the other), (4) has to be integrated over the whole size distribution of dust particles, taking into account the velocity and temperature for each size range. Moreover, the scale lengths related to the degradation of solid material depend on the initial composition of the cometary dust particles: they are not characteristic for a specific solid material. Therefore, parent scale length, as the one used with gaseous parents (2) has no direct equivalent here and a discussion about this parameter is useless for identifying a parent compound in the solid phase. As an example, measuring the scale length of the parent of formaldehyde, which is about 7000 km at 1 AU as mentioned in Sect. 1.1, is purely formal and unfortunately of no help in assessing the nature of the parent if it is in the solid phase.

2.2 Origin of H_2CO

Adjusting the spatial distribution of formaldehyde in Comet 1P/Halley would be quite simple considering the photodissociation of CH_3OH. If H_2CO is considered as the main CH_3OH photoproduct (for rate coefficients see Huebner et al. 1992), methanol would have to be produced from the nucleus at a level of 16% relative to water to obtain a good fit to measurements (Cottin et al. 2004). But methanol is only produced in amounts ranging from ~ 1 to 6% in comets (Bockelée-Morvan et al. 2004). Moreover, as discussed in Bockelée-Morvan et al. (1994), formaldehyde is not the main dissociation product of methanol, but rather the CH_3O methoxy radical. Thus, the additional source of cometary H_2CO is not consistent with a production from the CH_3OH photodissociation.

Formaldehyde is known to polymerize into long linear molecules (–$(CH_2$–O$)_n$–) called polyoxymethylene (POM) (Fig. 4). This polymer was invoked in the cometary context to interpret a mass spectrum obtained with the PICCA instrument on board the Giotto spacecraft, between 8200 and 12600 km from the nucleus of Comet 1P/Halley. Indeed, Huebner (1987) suggested that the alternation of patterns with $\Delta m/z = 14$ and 16 shown in the PICCA spectrum is consistent with a sequence of –CH_2– ($m = 14$) and –O– ($m = 16$). But few years later, Mitchell et al. (1992) showed that the PICCA mass spectrum is not

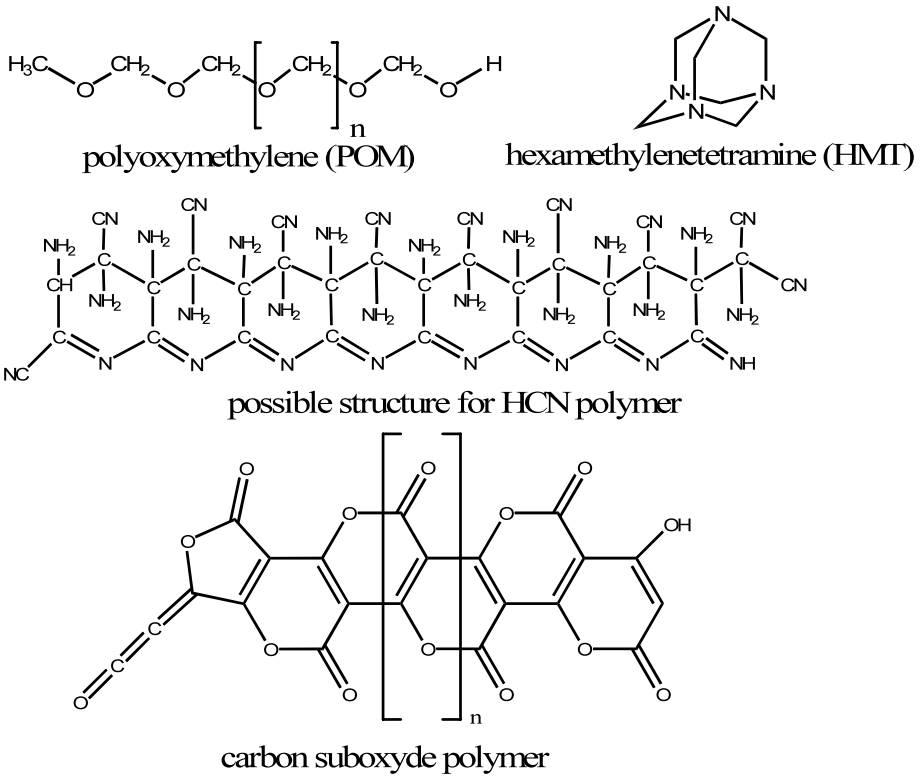

Fig. 4 Molecular structures of molecules evoked in this paper as possible parents for observed distributed sources. Structure of HCN polymer is one possible among others (see Minard et al. 1998 for more structures). Structure of carbon suboxide polymers proposed by Ballauff et al. (2004)

specifically characteristic of POM: the regular pattern observed is only the signature of a mixture of organic molecules composed of C, H, O, N atoms. Thus, even if the observed spectrum is not sufficient to establish its presence definitively, the presence of POM in cometary nucleus and dust particles cannot be ruled out at this stage. Furthermore, its production is possible under certain conditions in laboratory simulated interstellar and precometary ices (Schutte et al. 1993). Therefore, polyoxymethylene has often been suggested as the H_2CO distributed source (see, e.g. Boice et al. 1989, 1990; Meier et al. 1993; Eberhardt 1999). Boice et al. (1990) tried to estimate the production of formaldehyde from POM, but with the hypothesis that short polymer chains are emitted from dust particles and photodissociated in the gas phase. Because of the lack of experimental data, photodissociation rates were estimated from formaldehyde and related molecular bond strengths, without any direct laboratory measurement. Meier et al. (1993) showed that this does not fit the *Giotto* measurements.

First quantitative data considering the production of gaseous H_2CO by photo- and thermal-degradation of solid polyoxymethylene have been measured with the experimental setup shown Fig. 3 and described by Cottin et al. (2000) and Fray et al. (2004a). It has been shown that the major gaseous species produced by the photo-degradation of POM at 122 and 147 nm was H_2CO and CO and their production quantum yields have been measured (Cottin et al. 2000 and Table 2). Moreover, H_2CO is the sole gaseous species produced

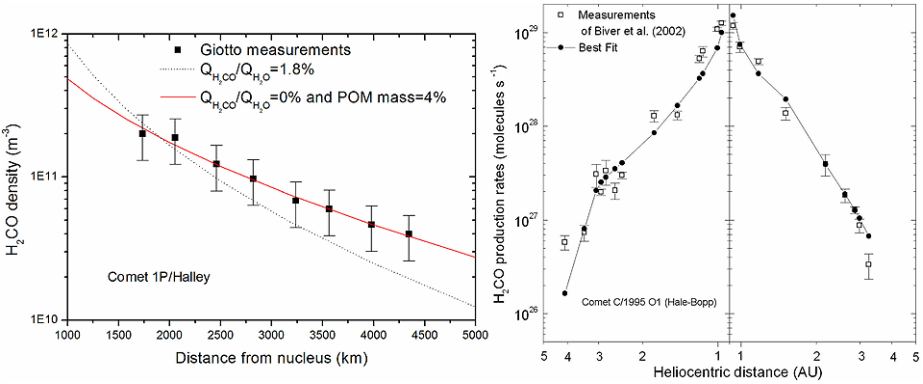

Fig. 5 *On the left*: H_2CO density profile in Comet 1P/Halley: measured by Giotto spacecraft (*squares*), and calculated considering a distributed source from solid polyoxymethylene (*continuous line*). This fit is obtained if POM represents 4% in mass of dust particles and H_2CO is not released from the nucleus. *Dotted line* is the best fit with no distributed source, obtained if 1.8% of H_2CO (relative to H_2O) is released from the nucleus. *On the right*: H_2CO production rates as a function of heliocentric distance in Comet C/1995 O1 (Hale-Bopp). The measurements of H_2CO are represented as open squares and the computed values as *black circles*. The latter have been obtained considering a POM mass fraction in the dust particles of 3.1% and H_2CO production at the surface of the nucleus equal to 3% of HCN production (i.e. $Q(H_2CO)/Q(H_2O) = 0.0075\%$)

by the thermal-degradation of POM. Its production kinetics follows an Arrhenius law and the Arrhenius constants and activation energies have been measured (Fray et al. 2004a and Table 2).

The production of gaseous formaldehyde in the coma from solid polyoxymethylene has been modelled using these quantitative data. If we consider that a few percent in mass of POM is present on dust particles when they are ejected from the nucleus, the spatial distribution of H_2CO in 1P/Halley as well as the steep heliocentric evolution of the H_2CO production rates in Comet C/1995 O1 (Hale-Bopp) are quite well reproduced (Cottin et al. 2004; Fray et al. 2006) (Fig. 5).

The fact that POM can account for the distributed source of formaldehyde in two comets, within the same abundance range, and for observations as a function of the nucleus distance and also as a function of the heliocentric distance, strengthens the probability of its presence without being an actual detection of the polymer in comets. The presence of POM (or POM-like polymers) in the solid state on cometary dust particles is to date the best interpretation of observations.

2.3 Origin of CO

The case of the additional source for CO is more controversial than for H_2CO. As shown in Sect. 1.2, not all the observations are consistent. The photodissociation of several gaseous molecules (C_3O_2, H_2CO and CO_2) have been proposed to explain the origin of CO in the coma.

In Comet 1P/Halley, it has been proposed that gaseous carbon suboxide (C_3O_2) could be a precursor for CO by photodissociation (Huntress et al. 1991). If present in the atmosphere of comets, C_3O_2 would be photodissociated into CO and C_2O, C_2O being photodissociated into CO and C, and be a parent molecule at least for some CO (Crovisier 1994). Nevertheless, its upper limit in this comet ($< 0.1\%$) is far from the amount required to produce the CO from secondary sources (7.5%) (Crovisier et al. 1991). Thus,

photodissociation of gaseous C_3O_2 cannot alone explain the formation of CO, even if it has been shown in the laboratory that it can be present in cometary ices (Brucato et al. 1997; Gerakines and Moore 2001). Looking for another gaseous parent, Meier et al. (1993) suggests that H_2CO is a precursor of 2/3 of the CO from an additional source, while later reanalysis of the data led to the conclusion that distributed formaldehyde produced from degradation of polyoxymethylene could fully explain all of the additional CO under certain assumptions such as the kinetics of POM degradation which were not known at that time (Eberhardt 1999). A comprehensive modelling with current knowledge of POM properties has yet to be done to settle this question for Comet 1P/Halley. If one considers CO_2 as a parent for CO, the CO Cameron system in the UV wavelength domain would be expected. It has been observed in several comets (Biermann 1976; Weaver et al. 1994; Bockelée-Morvan et al. 2004). This structure is thought to be produced mainly by prompt emission following the photodissociation of CO_2. Therefore it is clear that the photodissociation of CO_2 also contributes to the CO production in the coma. Nevertheless, as the photodissociation rate of CO_2 is very low ($\beta_{CO_2} = 2 \cdot 10^{-6}$ s^{-1}) (Huebner et al. 1992), this mechanism cannot explain the observed scale length of the CO distributed source. In Comet 1P/Halley, it is not yet settled whether a mechanisms different than the photodissociation of other gaseous molecules has to be considered to explain the CO additional source.

In Comet C/1995 O1 (Hale-Bopp), the additional source of the CO in the atmosphere seems to be triggered at 2 AU (Disanti et al. 2001). The photolysis of a gaseous parent would not result in the same kind of observation, which suggests some thermal threshold from which a solid precursor might start to decompose and release CO in the gas phase. Looking for a solid precursor leads one to consider if POM could also be the origin of the additional CO. But even if photo-degradation of POM yields a small amount of CO (about the same order of magnitude than for H_2CO (Cottin et al. 2000), no CO is produced by thermal-degradation, which is the dominant degradation mechanism of POM for most of dust particles. Also, if CO from distributed sources in C/1995 O1 (Hale–Bopp) originated from POM degradation, then one should expect H_2CO production from distributed sources to at least equal that for CO, and more probably be larger by perhaps as much as one or two orders of magnitude. This would result in more H_2CO than CO in the coma, which is not the case. Thus, POM cannot be the main precursor for carbon monoxide.

As we already discussed in this section, gaseous carbon suboxide is not sufficient to produce the observed amount of CO from additional sources. But its polymer (carbon suboxide polymer, shown in Fig. 4) is known to decompose into CO_2 and CO when pyrolysed. The polymer starts to release some gas (CO_2) at about 400 K, but only due to structural changes, the mass loss is low. Above 500 K the polymer degrades with increased efficiency as the temperature rises and with an additional production of CO. The CO/CO_2 ratio tends to 1/1 above 700 K and with increasing time (Blake and Hyde 1964; Smith et al. 1963). These studies show that if the same kind of polymers is present in comets, a distributed CO_2 source should also be observed, which, to date, is not the case. But laboratory synthesised polymer are extremely unstable as the compound is extremely hygroscopic (Schmedt auf der Günne et al. 2005). Exposed to air, it takes up atmospheric water within seconds and undergoes chemical modifications. Therefore, before reaching final conclusions about the relevance of this molecule in the cometary environment, new laboratory measurements have to be undertaken in controlled environment. Furthermore, no data about the photo-degradation of C_3O_2 polymers in VUV are currently available.

In Comet 29P/Schwassmann–Wachmann, located at large heliocentric distance , the temperature of the grains is so low that the distribution of CO in the coma can be explained by the slow sublimation of CO frozen on grains ejected from the nucleus (Gunnarsson et al. 2002, 2008). In this case, sublimation of the CO ice is a distributed source.

Because of the potential for multiple precursors, understanding the origin of CO from secondary and/or distributed sources requires probably a complete modelling work taking into account several gaseous and solid parents. Different compositions between comets, resulting in comets enriched or depleted in one or several precursors, and the use of different measurement methods probing different regions of the coma at different scales, could be an explanation for the contradictory observations.

2.4 Origin of HNC

In Comet C/1995 O1 (Hale-Bopp), Rodgers and Charnley (1998, 2005) and Irvine et al. (1998a, 1998b) show that the additional source for HNC could be accounted for by superthermal chemistry driven by fast hydrogen atoms ($HCN + H_f \rightarrow HNC + H$, with H_f = fast H). This would then be a secondary source. But this mechanism is only efficient in the relatively dense environment of Comet C/1995 O1 (Hale-Bopp), and due to the failure of such superthermal reactions to produce efficiently HNC in less active comets (Irvine et al. 2003; Rodgers and Charnley 2001, 2005), it seems more reasonable to look for other processes for the origin of HNC from additional sources.

Therefore, these authors propose the degradation of an unknown solid organic parent as the origin for the HNC from distributed sources. Candidates are the same as the ones presented and discussed in the next section for the parents of CN from distributed sources. However, quantitative and even qualitative data about its production by thermal or photo-degradation of refractory parents are rather difficult to obtain, since HNC is not easy to detect because of its rapid isomerisation into HCN in laboratory.

2.5 Origin of CN

The CN radicals may be produced by HCN photodissociation and another unknown mechanism. As the observed spatial distribution of CN is less distributed than the predicted distribution of CN produced solely by HCN photodissociation (Fig. 1), the scale length of the unknown production process has to be shorter than the observed production scale lengths (Fray et al. 2005). If the unknown mechanism is the photodissociation of a gaseous molecule, its lifetime has to be shorter than that of HCN. This is the case for HC_3N and C_2N_2. Nevertheless, the HC_3N production rate measured in Comet C/1995 O1 (Hale-Bopp) does not seem to be sufficient to explain the CN distribution and C_2N_2 has never been detected in comets (Fray et al. 2005). Another hypothesis is a direct production of CN radical by degradation of complex refractory organic compounds present on cometary dust particles. This hypothesis has originally been proposed by A'Hearn et al. (1986) and Lamy and Perrin (1988). Hexamethylenetetramine (HMT) could be a candidate since it is easily synthesized from H_2CO and NH_3 during laboratory simulations of interstellar and precometary ices (Bernstein et al. 1995; Cottin et al. 2001; Muñoz Caro et al. 2004). But it has been shown that this compound is quite stable when photolyzed (Cottin et al. 2002) and no degradation has been observed when heated (HMT sublimates when heated) (Fray 2004). Thus HMT is surely not the parent molecule of CN. It has also been shown that HCN polymers, which have been proposed to be present in cometary nuclei (Rettig et al. 1992), produce HCN and NH_3 when heated (Fray et al. 2004b). Under certain circumstances, such polymers can be synthesized in interstellar or precometary ices (Gerakines et al. 2004). If one turns to other candidates, it must be noted that thermal-degradation of polyacrylonitrile leads to the formation of HCN, NH_3 and CH_4 (Xue et al. 1997) and that thermal-degradation of numerous synthetic nitrogen polymers also leads to

the formation of HCN (Michal 1982). As numerous nitrogenated compounds can produce HCN by thermal-degradation, more experiments have to be implemented to measure quantitative data needed for proper modelling.

Nevertheless, one should keep in mind that since CN parent scale length is shorter than the HCN photodissociation scale length (Fig. 1), CN has to be directly produced from the dust particles without HCN as an intermediary species (Fray et al. 2005). So far, all the experimental studies investigating the volatile compounds produced during photo- or thermal-degradation of nitrogenated organic matter have been performed in conditions in which CN radicals were not detectable, even if it was produced. Indeed, in laboratory conditions CN radicals are very reactive species turning very rapidly into HCN.

2.6 Origin of Sulfur Compounds

A recent analysis of SO interferometric observations in Comet C/1995 O1 (Hale-Bopp) concludes that the discrepancy between measured and computed values of the SO photodissociation rate may indicate that SO_2 is not the sole parent of SO, or that SO_2 is itself created by an additional source in the coma (Boissier et al. 2007). Whether this results from coma chemistry or a distributed source remains unknown.

Concerning NS detection in the same comet, Canaves et al. (2002, 2007), have published a detailed modelling of the chemistry of NS in cometary comae. Their most recent results conclude that the amount of detected NS in Comet C/1995 O1 (Hale-Bopp) can be explained by gas phase chemistry in the atmosphere. They call it a distributed source, but it would rather be a secondary source if we stick to the definitions proposed in the present paper.

Very limited interpretation can be given for distributed sources of sulfur bearing species. Indeed, except the recent references given hereabove, the literature lacks discussion about the origin of these species. If, much work remains to be done in the laboratory for C, H, O, N molecules, almost everything has to be done for C, H, S (and possibly O and N) molecules.

3 Conclusions

We are far from being able to understand the origin of distributed sources in comets. They are for sure a signature of complex chemistry in both gaseous and solid phases, but we still lack crucial data characterizing the physico-chemical properties of candidate parent compounds to reach final interpretations. More laboratory work is needed, mostly to measure how the complex refractory organic component of comets behaves on dust particles (photo- and thermal-degradation).

The discussions developed in the present paper should not leave the impression that all the distributed sources could be explained evoking the convenient degradation of some unknown solid material. If this process seems to be quite adapted to the case of formaldehyde, it is possible that it actually hides our current ignorance of some other chemical processes in the atmosphere of comets. Work remains before a conclusion can be formed. However, as our knowledge of the composition of the nucleus of comets derives from what we observe in their atmosphere, distributed sources are precious, though tangled, Ariadne's threads to follow.

Acknowledgements The authors wish to thanks the two referees for their extensive work on the paper. Their valuable reviews greatly help to improve its clarity as well for the English than for its science content.

References

M.F. A'Hearn, S. Hoban, P.V. Birch, C. Bowers, R. Martin, D.A. Klinglesmith, Nature **324**, 649–651 (1986). doi:10.1038/324649a0

M. Ballauff, S. Rosenfeldt, N. Dingenouts, J. Beck, P. Krieger-Beck, Angew. Chem. Int. Ed. **43**(43), 5843–5846 (2004). doi:10.1002/anie.200460263

M.P. Bernstein, S.A. Sandford, L.J. Allamandola, S. Chang, M.A. Scharberg, Astrophys. J. **454**, 327–344 (1995). doi:10.1086/176485

L. Biermann, NASA STI/Recon technical report N 77, 22023 (1976)

N. Biver, D. Bockelée-Morvan, J. Crovisier, J.K. Davies, H.E. Matthews, J.E. Wink et al., Astron. J. **118**, 1850–1872 (1999). doi:10.1086/301033

N. Biver, D. Bockelée-Morvan, J. Crovisier, F. Henry, J.K. Davies, H.E. Matthews et al., Astron. J. **120**, 1554–1570 (2000). doi:10.1086/301529

N. Biver, D. Bockelée-Morvan, P. Colom, J. Crovisier, F. Henry, E. Lellouch et al., Earth Moon Planets **90**, 5–14 (2002a). doi:10.1023/A:1021599915018

N. Biver, D. Bockelée-Morvan, J. Crovisier, P. Colom, F. Henry, R. Moreno et al., Earth Moon Planets **90**, 323–333 (2002b). doi:10.1023/A:1021530316352

N. Biver, D. Bockelée-Morvan, J. Crovisier, D.C. Lis, R. Moreno, P. Colom et al., Astron. Astrophys. **449**, 1255–1270 (2006). doi:10.1051/0004-6361:20053849

A.R. Blake, A.F. Hyde, Trans. Faraday Soc. **60**, 1775–1782 (1964). doi:10.1039/tf9646001775

D. Bockelee-Morvan, J. Crovisier, Astron. Astrophys. **151**, 90–100 (1985)

D. Bockelée-Morvan, J. Crovisier, P. Colom, D. Despois, Astron. Astrophys. **287**(2), 647–665 (1994)

D. Bockelée-Morvan, H. Rickman, Earth Moon Planets **79**, 55–77 (1997). doi:10.1023/A:1006225030955

D. Bockelée-Morvan, J. Crovisier, Earth Moon Planets **89**, 53–71 (2000). doi:10.1023/A:1021530016410

D. Bockelée-Morvan, D.C. Lis, J.E. Wink, D. Despois, J. Crovisier et al., Astron. Astrophys. **353**, 1101–1114 (2000)

D. Bockelée-Morvan, J. Crovisier, M.J. Mumma, H.A. Weaver, in *Comets II*, ed. by M. Festou, H.U. Keller, H.A. Weaver (University of Arizona Press, Tucson, 2004), p. 391

D. Bockelée-Morvan, N. Biver, E. Jehin, A.L. Cochran, H. Wiesemeyer, J. Manfroid et al., Astrophys. J. **679**, L49–L52 (2008). doi:10.1086/588781

D.C. Boice, D.W. Naegeli, W.F. Huebner, Physics and mechanics of cometary materials. ESA SP **302**, 83–88 (1989)

D.C. Boice, W.F. Huebner, M.J. Sablik, I. Konno, Geophys. Res. Lett. **17**, 1813–1816 (1990). doi:10.1029/GL017i011p01813

J. Boissier, D. Bockelee-Morvan, N. Biver, J. Crovisier, D. Despois, B.G. Marsden et al., Astron. Astrophys. **475**, 1131–1144 (2007). doi:10.1051/0004-6361:20078380

T.Y. Brooke, H.A. Weaver, G. Chin, D. Bockelée-Morvan, S.J. Kim, L.H. Xu, Icarus **166**, 167–187 (2003). doi:10.1016/j.icarus.2003.08.008

D. Brownlee, P. Tsou, Aléon et al., Science **314**, 1711–1716 (2006). doi:10.1126/science.1135840 Medline

J.R. Brucato, A.C. Castorina, M.E. Palumbo, M.A. Satorre, G. Strazzulla, Planet. Space Sci. **45**(7), 835–840 (1997). doi:10.1016/S0032-0633(97)00071-8

M.V. Canaves, A.A. De Almeida, D.C. Boice, G.C. Sanzovo, Earth Moon Planets **90**, 335–347 (2002). doi:10.1023/A:1021582300423

M.V. Canaves, A.A. de Almeida, D.C. Boice, G.C. Sanzovo, Adv. Space Res. **39**, 451–457 (2007). doi:10.1016/j.asr.2006.09.040

L. Colangeli, J.R. Brucato, A. Bar-Nun, R.L. Hudson, M.H. Moore, in *Comets II*, ed. by M. Festou, H.U. Keller, H.A. Weaver (University of Arizona Press, Tucson, 2004), pp. 695–717

P. Colom, J. Crovisier, D. Bockelee-Morvan, D. Despois, G. Paubert, Astron. Astrophys. **264**, 270–281 (1992)

M.R. Combi, A.H. Delsemme, Astrophys. J. **237**, 633–640 (1980). doi:10.1086/157909

M.R. Combi, U. Fink, Astrophys. J. **484**, 879–890 (1997). doi:10.1086/304349

M.R. Combi, W.M. Harris, W.H. Smyth, in *Comets II*, ed. by M. Festou, H.U. Keller, H.A. Weaver (University of Arizona Press, Tucson, 2004), pp. 523–552

H. Cottin, M.C. Gazeau, J.F. Doussin, F. Raulin, Phys. Chem. Earth **24**, 597–602 (1999)

H. Cottin, M.-C. Gazeau, J.-F. Doussin, F. Raulin, J. Photochem. Photobiol. Chem. **135**(1), 53–64 (2000). doi:10.1016/S1010-6030(00)00274-4

H. Cottin, C. Szopa, M.H. Moore, Astrophys. J. Lett. **561**(1), L139–L142 (2001). doi:10.1086/324575

H. Cottin, S. Bachir, F. Raulin, M.C. Gazeau, Adv. Space Res. **30**(6), 1481–1488 (2002). doi:10.1016/S0273-1177(02)00508-2

H. Cottin, Y. Bénilan, M.-C. Gazeau, F. Raulin, Icarus **167**, 397–416 (2004). doi:10.1016/j.icarus.2003.10.009

J. Crovisier, T. Encrenaz, M. Combes, Nature **353**, 610 (1991). doi:10.1038/353610a0 Medline
J. Crovisier, J. Geophys. Res. **99**(E2), 3777–3781 (1994). doi:10.1029/93JE02088
N. Dello Russo, M.A. Disanti, M.J. Mumma, K. Magee-Sauer, T.W. Rettig, Icarus **135**, 377–388 (1998). doi:10.1006/icar.1998.5990
D. Despois, H. Cottin, in *Lectures in Astrobiology*, ed. by M. Gargaud, B. Barbier, H. Martin, J. Reisse (Springer, Berlin, 2005), pp. 289–352
M.A. Disanti, M.J. Mumma, N. dello Russo, K. Magee-Sauer, R. Novak, T.W. Rettig, Nature **399**, 662 (1999). doi:10.1038/21378 Medline
M.A. Disanti, M.J. Mumma, N. Dello Russo, K. Magee-Sauer, Icarus **153**, 361–390 (2001). doi:10.1006/icar.2001.6695
M.A. DiSanti, M.J. Mumma, N. Dello Russo, K. Magee-Sauer, D.M. Griep, J. Geophys. Res. Planets **108f**, 15–11 (2003)
P. Eberhardt, D. Krankowsky, Schulte et al., Astron. Astrophys. **187**, 481–484 (1987)
P. Eberhardt, Space Sci. Rev. **90**(1/2), 45–52 (1999). doi:10.1023/A:1005221309219
M.C. Festou, Space Sci. Rev. **90**, 53–67 (1999). doi:10.1023/A:1005225426057
M.C. Festou, H.U. Keller, H.A. Weaver, *Comets II* (University of Arizona Press, Tucson, 2004)
N. Fray, PhD thesis. Université Paris 12 (2004)
N. Fray, Y. Bénilan, H. Cottin, M.-C. Gazeau, J. Geophys. Res. Planets **109**, E07S12 (2004a). doi:10.1029/2003JE002191
N. Fray, Y. Bénilan, H. Cottin, M.-C. Gazeau, R.D. Minard, F. Raulin, Meteorit. Planet. Sci. **39**, 4 (2004b)
N. Fray, Y. Bénilan, H. Cottin, M.C. Gazeau, J. Crovisier, Planet. Space Sci. **53**, 1243–1262 (2005). doi:10.1016/j.pss.2005.06.005
N. Fray, Y. Bénilan, N. Biver, D. Bockelée-Morvan, H. Cottin, J. Crovisier et al., Icarus **184**(1), 239–254 (2006). doi:10.1016/j.icarus.2006.04.014
P.A. Gerakines, M.H. Moore, Icarus **154**(2), 372–380 (2001). doi:10.1006/icar.2001.6711
P.A. Gerakines, M.H. Moore, R.L. Hudson, Icarus **170**, 202–213 (2004). doi:10.1016/j.icarus.2004.02.005
J.M. Greenberg, in *Comets*, ed. by L.L. Wilkening (University of Arizona Press, Tuscon, 1982), pp. 131–163
M. Gunnarsson, H. Rickman, M.C. Festou, A. Winnberg, G. Tancredi, Icarus **157**, 309–322 (2002). doi:10.1006/icar.2002.6839
M. Gunnarsson, D. Bockelée-Morvan, A. Winnberg et al., Astron. Astrophys. **402**, 383–393 (2003) doi:10.1051/0004-6361:20030178
M. Gunnarsson, D. Bockelée-Morvan, N. Biver, J. Crovisier, H. Rickman, Astron. Astrophys. **484**, 537–546 (2008)
L. Haser, Bulletin de l'académie royale de Belgique **43**, 740–750 (1957)
J. Helbert, H. Rauer, D.C. Boice, W.F. Huebner, Astron. Astrophys. **442**, 1107–1120 (2005). doi:10.1051/0004-6361:20041571
F. Henry, D. Bockelée-Morvan, J. Crovisier, J. Wink, Earth Moon Planets **90**, 57–60 (2002). doi:10.1023/A:1021508216836
W.F. Huebner, Science **237**(August), 628–630 (1987). doi:10.1126/science.237.4815.628 Medline
W.F. Huebner, J.J. Keady, S.P. Lyon, Astrophys. Space Sci. **195**, 1–294 (1992). doi:10.1007/BF00644558
W.T. Huntress Jr., M. Allen, M. Delitsky, Nature **352**, 316–318 (1991). doi:10.1038/352316a0
D. Hutsemékers, J. Manfroid, E. Jehin, C. Arpigny, A. Cochran, R. Schulz et al., Astron. Astrophys. **440**, L21–L24 (2005). doi:10.1051/0004-6361:200500160
W.H. Ip, in *Comets II*, ed. by M. Festou, H.U. Keller, H.A. Weaver (University of Arizona Press, Tucson, 2004), pp. 605–629
W. Irvine, D. Bockelee-Morvan, Lis et al., Nature **382**, 418–420 (1996). doi:10.1038/383418a0
W.M. Irvine, E.A. Bergin, J.E. Dickens, D. Jewitt, A.J. Lovell, H.E. Matthews et al., Nature **393**, 547 (1998a). doi:10.1038/31171 Medline
W.M. Irvine, J.E. Dickens, A.J. Lovell, F.P. Schloerb, M. Senay, E.A. Bergin et al., Faraday Discuss. **109**, 475–492 (1998b). doi:10.1039/a709289j Medline
W.M. Irvine, M. Senay, A.J. Lovell, H.E. Matthews, D. McGonagle, R. Meier, Icarus **143**(2), 412–414 (2000). doi:10.1006/icar.1999.6281 Medline
W.M. Irvine, P. Bergman, T.B. Lowe, H. Matthews, D. McGonagle, A. Nummelin et al., Orig. Life Evol. Biosph. **33**, 609–619 (2003). doi:10.1023/A:1025791101127 Medline
W.M. Jackson, A. Scodinu, D. Xu, A.L. Cochran, Astrophys. J. **607**, L139–L141 (2004). doi:10.1086/421995
D.C. Jewitt, H.E. Matthews, T. Owen, R. Meier, Science **278**, 90–93 (1997). doi:10.1126/science.278.5335.90 Medline
L.P. Keller, S. Bajt, G.A. Baratta et al., Science **314**, 1728–1731 (2006). doi:10.1126/science.1135796 Medline
J. Kissel, F.R. Krueger, J. Silén, B.C. Clark, Science **304**, 1774–1776 (2004). doi:10.1126/science.1098836 Medline

J. Kissel, F.R. Krueger, Nature **326**, 755–760 (1987). doi:10.1038/326755a0
P.L. Lamy, J.-M. Perrin, Icarus **76**, 100–109 (1988). doi:10.1016/0019-1035(88)90142-X
R. Meier, P. Eberhardt, D. Krankowsky, R.R. Hodges, Astron. Astrophys. **277**, 677–690 (1993)
J. Michal, Fire Mater. **6**(1), 13–15 (1982). doi:10.1002/fam.810060105
S.N. Milam, A.J. Remijan, Womack et al., Astrophys. J. **649**, 1169–1177 (2006). doi:10.1086/506501
R.D. Minard, P.G. Hatcher, R.C. Gourley, C.N. Matthews, Orig. Life Evol. Biosph. **28**, 461–473 (1998). doi:10.1023/A:1006566125815 Medline
D.L. Mitchell, R.P. Lin, C.W. Carlson, A. Korth, H. Reme, D.A. Mendis, Icarus **98**, 125–133 (1992). doi:10.1016/0019-1035(92)90213-Q
G.M. Muñoz Caro, U. Meierhenrich, W.A. Schutte, W.H.-P. Thiemann, J.M. Greenberg, Astron. Astrophys. **413**, 209–216 (2004). doi:10.1051/0004-6361:20031447
T.W. Rettig, S.C. Tegler, D.J. Pasto, M.J. Mumma, Astrophys. J. **398**, 293–298 (1992). doi:10.1086/171857
S.D. Rodgers, S.B. Charnley, Astrophysical J. Lett. **501**(2), L227–L230 (1998). doi:10.1086/311459
S.D. Rodgers, S.B. Charnley, Mon. Not. R. Astron. Soc. **323**(1), 84–92 (2001). doi:10.1046/j.1365-8711.2001.04099.x
S.D. Rodgers, S.B. Charnley, W.F. Huebner, D.C. Boice, in *Comets II*, ed. by M. Festou, H.U. Keller, H.A. Weaver (University of Arizona Press, Tucson, 2004), pp. 505–522
S.D. Rodgers, S.B. Charnley, Mon. Not. R. Astron. Soc. **356**(4), 1542–1548 (2005). doi:10.1111/j.1365-2966.2004.08606.x
S.A. Sandford, J. Aléon, C.M.O.D. Alexander et al., Science **314**, 1720 (2006)
J. Schmedt auf der Günne, J. Beck, W. Hoffbauer, P. Krieger-Beck, Chem. Eur. J. **11**, 4429–4440 (2005). doi:10.1002/chem.200401133
W.A. Schutte, L.J. Allamandola, S.A. Sandford, Icarus **104**, 118–137 (1993). doi:10.1006/icar.1993.1087 Medline
R.N. Smith, D.A. Young, E.N. Smith, C.C. Carter, Inorg. Chem. **2**(4), 829–838 (1963). doi:10.1021/ic50008a041
N. Thomas, D.C. Boice, W.F. Huebner, H.U. Keller, Intensity profiles of dust near extended sources on comet Halley. Nature **332**(6159), 51–52 (1988) doi:10.1038/332051a0
H.A. Weaver, P.D. Feldman, J.B. McPhate, M.F. A'Hearn, C. Arpigny, T.A. Smith, Astrophys. J. **422**, 374–380 (1994). doi:10.1086/173732
H.A. Weaver, T.Y. Brooke, G. Chin, S.J. Kim, D. Bockelée-Morvan, J.K. Davies, Earth Moon Planets **78**, 71–80 (1997). doi:10.1023/A:1006227530238
J. Wink, D. Bockelée-Morvan, D. Despois, P. Colom, N. Biver, J. Crovisier et al., Earth Moon Planets **78**, 63–63 (1997). doi:10.1023/A:1006263026604
M. Womack, M.C. Festou, S.A. Stern, Astron. J. **114**, 2789–2796 (1997). doi:10.1086/118687
T.J. Xue, M.A. McKinney, C.A. Wilkie, Polym. Degrad. Stabil. **58**(1–2), 193–202 (1997). doi:10.1016/S0141-3910(97)00048-7
L.M. Ziurys, C. Savage, M.A. Brewster, A.J. Apponi, T.C. Pesch, Wyckoff, Astrophys. J. Lett. **527**(1), L67–L71 (1999). doi:10.1086/312388

How Well Do Experimental Results on Large Samples of Gas-Laden Amorphous Ice Duplicate Deep Impact's Findings?

A. Bar-Nun · I. Pat-El · D. Laufer

Originally published in the journal Space Science Reviews, Volume 138, Nos 1–4.
DOI: 10.1007/s11214-008-9307-6

Abstract The findings of Deep Impact on the structure and composition of Tempel-1 are compared with our experimental results on large (20 cm diameter and up to 10 cm high) samples of gas-laden amorphous ice which does not contain dust. The mechanical ∼tensile strength inferred for Tempel-1: up to 12 kPa is close to our experimental findings of 2–4 kPa. This means that Tempel-1 is as fluffy as our very fluffy, talcum like, ice sample. The thermal inertia: $30 < I < 100$ W K^{-1} m^{-2} s$^{1/2}$ is close to our value of 80. The density of 350 ± 250 kg m^{-3}, is close to our value of 250–300 kg m^{-3}, taking into account an ice/silicate ratio of 1 in the comet, while we study pure ice. Surface morphological features, such as non-circular depressions and chaotic terrain, were observed in our experiments. The only small increase in the gas/water vapor ratio pre- and post-impact, suggest that in the area excavated by the impactor, the 135 K front did not penetrate deeper than a few meters. Altogether, the agreement between the findings of Deep Impact and our experimental results point to a loose agglomerate of ice grains (with a silicate-organic core), which was formed by a very gentle aggregation of the ice grains, without compaction.

Keywords Comets: general · Comets: Tempel-1

PACS 90

1 Introduction

Deep Impact (DI) provided a unique opportunity to obtain *in situ* information on the structure and composition of the outer layer of a comet (e.g., A'Hearn et al. 2005; Mumma et al. 2005; A'Hearn and Combi 2007; Groussin et al. 2007; Holsapple and Housen 2007; Busko et al. 2007). A 372 kg projectile impacted comet Tempel-1 at a speed of 10.3 km sec^{-1},

Workshop on Origin and Early Evolution of Comet Nuclei.

A. Bar-Nun (✉) · I. Pat-El · D. Laufer
Department of Geophysics and Planetary Sciences, Tel-Aviv University, Tel-Aviv 69978, Israel
e-mail: akivab@post.tau.ac.il

excavated a crater whose dimensions could be 150–200 m and formed a large plume. Deep Impact also provided an opportunity to see whether our experimental results on large samples of gas-laden amorphous ice, though not containing dust represent the DI findings.

2 Experimental

The experimental procedure is described in detail by Bar-Nun and Laufer (2003). Briefly, a ∼200 μm thick layer of gas-laden amorphous ice is deposited on a cold plate at 80 K by flowing a water vapor–gas mixture onto the plate in a 80 K chamber at 10^{-6} torr. This ice layer is scrapped by a 80 K knife and falls as ∼200 μm ice grains into a 20 cm diameter, 80 K sample container. This process is repeated until a few cm thick agglomerate of ∼200 μm ice grains is accumulated in the container.

At 80 K, the ice deposited from the vapor is amorphous, having many pores in which the gas which was flowed together with the water vapor is trapped (Bar-Nun et al. 1985, 1987, 1988). The ice sample is then heated uniformly by IR radiation (which is completely absorbed by the ice) from above by an aluminum cap preheated to 330 or 430 K, providing ∼0.37 or 1.1 Solar Constants respectively. The temperatures of the ice at various distances from the surface are monitored by thermocouples, to measure the penetration of the heat wave, enabling the calculation of the thermal conductivity coefficient. The evolution of the trapped gases and water vapor from the surface is monitored by a mass-spectrometer.

The massive release of gas such as argon, which does not freeze at 80 K, upon warming up of the ice sample, shows that the gas is trapped in *amorphous ice* (Bar-Nun and Laufer 2003).

Surface features are photographed through windows in the chamber and after opening it under a vigorous flow of nitrogen. While the chamber is open, a force-meter with a 1.5 cm diameter half-sphere penetrates slowly the ice sample, measuring its compressive strength. The ice density is measured by collecting it in a cuvette during deposition, monitoring its height and, again, when the ice melts.

3 Experimental Results and Comparison with DI

3.1 Density

The density of the upper layer of comet Tempel-1 was calculated by A'Hearn et al. (2007) to be $350 \pm 250\ \mathrm{kg\,m^{-3}}$ while Richardson et al. (2007) suggest $400 + 600/-200\ \mathrm{kg\,m^{-3}}$, as compared with a density of 250–300 $\mathrm{kg\,m^{-3}}$ found in our experiments on pure ice. This density was measured at the end of the experiment of IR irradiation. It includes a thin crust about 3 times denser then the underlying fluffy ice (this article). A higher density could be expected for Tempel-1, in view of the cometary grains being composed of ice: silicate and organics ≈ 1:1:1. Nevertheless, both values point to a *very loose agglomerate of grains*.

3.2 Surface Morphology

Circular impact craters with elevated rims were observed on comet Tempel-1 (A'Hearn et al. 2005; Thomas et al. 2007), comet Wild-2 the target of the Stardust mission (Brownlee et al. 2004), and on many icy satellites. Circular impact craters do not need further elaboration.

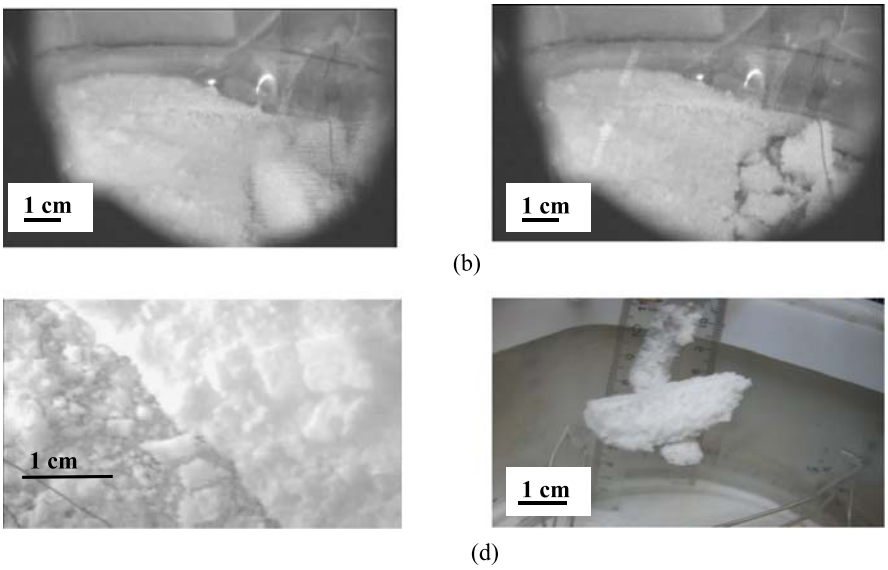

Fig. 1 (**a**) Swelling of a smooth ice dome by an underlying gas pocket at the lower right hand section and (**b**) its collapse and shattering. (**c**) Chaotic terrain and collapse of the ice after a vigorous gas release (from Laufer et al. 2005). (**d**) An ice crust 1.5 cm thick which was removed from the top of an ice sample irradiated by 1.1 Solar Constants for 1.5 hours

In addition, *rough terrain and non-circular depressions* were observed on both comets, the only ones photographed at close range (Thomas et al. 2007; Basilevsky and Keller 2007). On Tempel-1, regions of *smooth terrain*, 3 km long (Thomas et al. 2007) and elevated by about 20 m above the surface, were also observed. The mechanism of their formation was proposed by Bar-Nun et al. (2007).

Laufer et al. (2005) showed that very rough terrain and non-circular depressions are formed when a large enough pressure is built up in underlying gas pockets, resulting in the formation of *bulges*, which collapse to form *non-circular craters or shatter to form very rough terrain*. This happens when quiescent gas release through dynamic percolation cannot accommodate anymore the flow of gas from below (Fig. 1a–c).

3.3 Crust Formation

The very low albedos of comets Halley: $0.04 + 0.02/-0.01$ (Keller and Thomas 1997; Lamy et al. 2004) Tempel-1: 0.04 (A'Hearn et al. 2005) and Wild-2: 0.03 ± 0.015 (Brownlee et al. 2004) show that the surface is covered by a dark layer of silicate particles cemented by organics, both of which were left behind when the ice sublimated, and insulates thermally the pristine gas-laden ice underneath. Nevertheless, more vigorous gas evolution in certain small areas, which cannot be accommodated by quiescent dynamic percolation, shatters or blows off sections of this layer. Thus activity in comets Halley and Wild-2 is from sparse areas, and only $6 \pm 3\%$ of the surface of Tempel-1 which was observed by Deep Impact is exposed ice (Sunshine et al. 2006). *In these areas,* the overlying insulating dust layer has been shattered or blown off by massive gas flow, similar to the process which formed the rough terrain and non-circular craters on these comets and in our experiments.

Another surface phenomenon observed in our experiments is the build-up of a crystalline *ice crust*, which is denser and tougher than the underlying amorphous ice. Such ice crust is

formed when a fraction of the water vapor which sublimates from the comet's surface flows *inward*, into cooler layers and freezes there, thus hardening the upper layers. Being close to the surface and having experienced $T \geq 135$ K, this amorphous ice was already transformed to the crystalline structure. Theoretical calculations by Prialnik and Mekler (1991) suggest that in pure ice without a dust layer there should not be a build-up of a pure ice crust, because the rate of recession of the upper ice layer by sublimation is faster than the build-up of a dense layer. In our recent experiments this was proven to be wrong. An ice crust about 1.5 cm thick was formed at the top of the sample after irradiation by 1.1 Solar Constant during ∼1.5 hours. It was strong enough to be removed from the top of the ice sample as seen in Fig. 1d. The crust is an agglomerate of small grains which were cemented together by the condensing water vapor. On Tempel-1, the $6 \pm 3\%$ of exposed ice is composed of 30 ± 20 μm ice grains (Sunshine et al. 2006) as compared with the sub-micron to micron grains seen in the plume (A'Hearn et al. 2005; Meech et al. 2005).

3.4 Mechanical Strength

The "strength" of the upper layer of comet Tempel-1 was found to be ∼65 Pa (A'Hearn et al. 2005). Meaning that the structure is a *very loose agglomerate of ice particles*, "like talcum powder" (A'Hearn et al. 2005). This strength is close to but not exactly a tensile strength in a loose weak material (e.g., Richardson et al. 2005; Schultz et al. 2005). It was calculated by the DI team as (density) × (minimum ejection velocity) squared (J. Melosh, private communication). Holsapple and Housen (2007) argue that any strength from 0 to 12 kPa could furnish the amounts of total mass ejected, as estimated from observations by the DI spacecraft and from the ground. In our experiments (Bar-Nun and Laufer 2003, Fig. 6), during the slow penetration of a force-meter, we measured the compressive strength of a loose aggregate of ∼200 μm ice particles with a harder crust on its surface. The compressive strength rose quickly in the first few mm during the penetration through the crust and then more slowly until a limiting value of ∼20 kPa was reached, when the sample was compacted. After this point, the force rose very steeply. A comparison between compressive strength and tensile strength for a loose aggregate with high porosity was done by Sirono and Greenberg (2000). A ratio (compressive strength) / (tensile strength) of ∼10 is found in their Fig. 5 for a density of ∼250 kg m^{-3}. A factor of 5 was found by Housen and Holsapple (2003, Fig. 4). Dividing our measured compressive strength of ∼20 kPa by 10 or 5, we obtain a tensile strength of ∼2 or 4 kPa, comparable to the upper limit of 12 kPa calculated by Holsapple and Housen (2007). Even this upper limit value together with the low density, attest to the comet being a very loose aggregate of grains, probably ice-coated mineral–organic grains, which aggregated very slowly without compaction. In our experiment, the energy of each 200 μm ice particle falling in vacuum a distance of 10 cm is 1×10^{-9} kg m^2 sec^{-2}. Since the density and strength of our ice sample are similar to those of Tempel-1, it is suggested that the energy of impact of the ice grains which agglomerated to form the nucleus was of the same order of magnitude, although other scenarios might produce a nucleus with the same properties.

3.5 Thermal Inertia

The Thermal Inertia of the surface layer of comet Tempel-1 was calculated by Groussin et al. (2007) to be $I < 50$ W K^{-1} m^{-2} s$^{1/2}$. Davidsson et al. (2007) calculated a value between $30 < I < 100$ W K^{-1} m^{-2} s$^{1/2}$ for the active areas. Our measured thermal conductivity coefficient for an agglomerate of gas-laden amorphous ice grains is $\kappa = 0.03$ W K^{-1} m^{-1} s^{-1}

(Bar-Nun and Laufer 2003). With $Cp = 840\ \mathrm{J\,kg^{-1}\,K^{-1}}$ (Klinger 1981) and the measured density $\rho = 250\ \mathrm{kg\,m^{-3}}$, $I = (K\rho Cp)^{1/2} = 80\ \mathrm{W\,K^{-1}\,m^{-2}\,s^{1/2}}$. This value is in good agreement $30 < I < 100\ \mathrm{W\,K^{-1}\,m^{-2}\,s^{1/2}}$ calculated by Davidsson et al. (2007) for the active areas on Tempel-1.

This close agreement, however, does not mean that the upper, several cm thick, layer of Tempel-1 is composed of ice. This $I = 80\ \mathrm{W\,K^{-1}\,m^{-2}\,s^{1/2}}$ could well be the thermal inertia of a loose agglomerate of the dust, which was left on the surface after the water ice sublimated. This is suggested by the observation that the bulk of the water vapor appears to be coming from generally near the sub-solar region, where there is no ice on the surface ((Feaga et al. 2006) and A'Hearn, private communication). This loose dust layer should be thin enough, of the order of a few cm, to transmit enough energy to the underlying layer. This leads to sublimation of the water ice, while penetration of the heat wave to deeper layers releases the gases which are trapped in the ice.

It is not clear whether adding dust to our ice would increase or decrease its thermal inertia. Interplanetary dust particles (IDPs) are thought to be cometary particles which were processed for a long time in space. They are a loose agglomerate of silicate grains which were presumably covered by a now absent organic coating. We do not know whether they were originally a loose agglomerate or agglomerated only in the dust layer which formed on the surface of the nucleus. We also do not know what kind of contact exists between the silicates and the organics and between the organics and the ice. However, the differences between an agglomerate of pure ice grains and ice grains with dust could be shadowed by the large effect of the gas flowing in the ice. The thermal conductivity of an agglomerate of ~200 μm *pure amorphous ice* grains was measured by Bar-Nun and Laufer (2003) to be $8 \pm 1 \times 10^{-3}\ \mathrm{W\,m^{-1}\,K^{-1}}$ while that of an agglomerate of ~200 μm *gas-laden amorphous ice* grains was measured to be $3\text{–}5 \times 10^{-2}\ \mathrm{W\,m^{-1}\,K^{-1}}$.

3.6 Gas and H_2O Evolution

From the ratios of gases to H_2O observed pre-impact and post-impact, one can obtain an idea on the depletion of these gases in the outer layer of comet Tempel-1. Bar-Nun and Laufer (2003) showed that the gas/water vapor ratio in the experimental coma is *larger* than the gas/ice ratio in the nucleus, because the gas trapped in the amorphous ice is released from deeper layers due to the transformation of the amorphous ice to crystalline ice at 135 K, while water vapor sublimates only from the surface, and part of it migrates inward to form the denser crust. A small amount of trapped gas is released also between 35 and 120 K, by the slow stepwise annealing of the amorphous ice, before its transformation at 135 K (Laufer et al. 1987). Therefore, it is expected that all underlying ice layers which were heated to 135 K, where the transformation from amorphous to crystalline ice occurs, will be depleted of gases. The observations of Feaga et al. (2006), Farnham et al. (2007) and in the inner coma, support this model. While the H_2O distribution shows a distribution with sunward enhancement, the CO_2 shows enhancement in the anti-sunward direction. This is due to the rotation of the nucleus together with the time required for the heat wave to reach a deeper layer, consisting of amorphous ice with gases trapped in it. When this layer reaches ~135 K, the amorphous ice transforms into cubic ice and releases the trapped gases (Bar-Nun et al. 1985; Bar-Nun and Laufer 2003).

Our experiments measured gas and water vapor output with only 5 cm thick ice samples, while a tens of meters ice layer was excavated by DI. Only a *small* increase in HCN/H_2O and CO_2/H_2O after impact was observed by A'Hearn et al. (2005) and in CH_3OH/H_2O and HCN/H_2O by Mumma et al. (2005). The constancy or small increase can be explained by

the excavation reaching deeper layers, where the temperature of ∼135 K which induces gas release by the transformation of the amorphous to crystalline ice, did not reach. Apparently, the cratered area was previously covered by an insulating dust layer, which prevented the penetration of the heat wave into ice. An increase in the ratio C–H organics/ H_2O observed by A'Hearn et al. (2005) might be explained by evaporation and photolysis in the plume of part of the frozen heavy organics which surround the silicates grains.

4 Conclusions

The agreement between the findings of Deep-Impact and our experimental results on large (20 cm diameter and up to 10 cm high) samples of gas-laden amorphous ice demonstrates the adequacy of the simulation experiments in predicting and explaining cometary phenomena.

The measured thermal conductivity coefficient $\kappa = 0.03\ \mathrm{W\,K^{-1}\,m^{-1}\,sec^{-1}}$, results in a thermal inertia $I = 80\ \mathrm{W\,K^{-1}\,m^{-2}\,sec^{1/2}}$, in good agreement with the value of $30 < I < 100$ derived for Tempel-1. This thermal inertia however, can be that of few cm thick loose dust layer, which covers almost all the comet's surface and through which the ice is heated and sublimates. The measured tensile strength of ∼2–4 kPa is in the range of up to 12 kPa derived for Tempel-1 by Holsapple and Housen (2007). The surface morphological features observed in Tempel-1: Chaotic terrain and non-circular depressions, were observed in the simulation experiments. They arise from bulging of smooth sections of the surface by the build-up of pressure in underlying ice layers, followed by collapse to form non-circular craters or by shattering to form chaotic terrain. An ice crust, stronger than the underlying ice, was observed to form when part of the water vapor sublimating from the surface migrated back into the ice and condensed there, cementing the ice grains together. This is also in agreement with the observation of 30 ± 20 micron ice particles on the clean ice surfaces on Tempel-1, while the ejecta is composed of sub-micron to micron size particles.

The only small increase in the gas/ice ratios pre- and post-impact show that the 135 K heat wave did not penetrate beyond a few meters from the surface, while the impact excavated a tens of meters deep crater. The large increase in C_2H_6/H_2O can not be explained.

All the DI observations and experimental results point to a very loose agglomerate of ice particles (with silicate-organic cores), which was formed by very gentle agglomeration of the ice grains having kinetic energies of the order of $1 \times 10^{-9}\ \mathrm{kg\,m^2\,sec^{-2}}$, although other scenarios might have produced a nucleus with the same properties.

Acknowledgements This research was supported by the Israel Ministry of Science, through the Israel Space Agency and by the US–Israel Binational foundation (BSF). We thank Kevin Housen and Michael A'Hearn for helpful comments.

References

M.F. A'Hearn et al., Science **310**, 265 (2005)
M.F. A'Hearn, M.R. Combi, Icarus **187**, 1 (2007)
A. Bar-Nun, G. Herman, D. Laufer, M.L. Rappaport, Icarus **63**, 317 (1985)
A. Bar-Nun, J. Dror, E. Kochavi, D. Laufer, Phys. Rev. B **35**, 2427 (1987)
A. Bar-Nun, I. Kleinfeld, E. Kochavi, Phys. Rev. B **38**, 7749 (1988)
A. Bar-Nun, D. Laufer, Icarus **161**, 157 (2003)
A. Bar-Nun, F. Pállson, H. Bjornsson, Icarus (2007, submitted)
A.T. Basilevsky, H.U. Keller, Sol. Syst. Res. **41**, 109 (2007)
D.E. Brownlee et al., Science **304**, 1764 (2004)
I. Busko, D. Lindler, M.F. A'Hearn, R.L. White, Icarus **187**, 56 (2007)

B.J.R. Davidsson, P.J. Gutiérrez, H. Rickman, Icarus **187**, 306 (2007)
T.L. Farnham, D.D. Wellnitz, D.L. Hampton, J.-Y. Li, J.M. Sunshine, O. Groussin, L.A. McFadden, C.J. Crockett, M.F. A'Hearn, M.J.S. Belton, P. Schultz, C.M. Lisse, Icarus **187**, 26 (2007)
L.M. Feaga, M.F. A'Hearn, J.M. Sunshine, O. Groussin, Deep Impact Science Team, 37th Annual Lunar and Planetary Science Conference, March 13–17, 2006, League City, Texas, abstract no. 2149
O. Groussin, M.F. A'Hearn, J.-Y. Li, P.C. Thomas, J.M. Sunshine, C.M. Lisse, K.J. Meech, T.L. Farnham, L.M. Feaga, W.A. Delamere, Icarus **187**, 16 (2007)
K.R. Housen, K.A. Holsapple, Icarus **163**, 102 (2003)
K.A. Holsapple, K.R. Housen, Icarus **187**, 345 (2007)
H.U. Keller, N. Thomas, Adv. Space Res. **19**, 187 (1997)
J. Klinger, Icarus **47**, 320 (1981)
D. Laufer, E. Kochavi, A. Bar-Nun, Phys. Rev. B **36**(0), 9219 (1987)
D. Laufer, I. Pat-El, A. Bar-Nun, Icarus **178**, 248 (2005)
P.L. Lamy, I. Toth, Y.R. Fernandez, H.A. Weaver, in *Comets II*, ed. by M.C. Festou, H.U. Keller, H.A. Weaver (University of Arizona Press, Tucson, 2004), pp. 223
K.J. Meech, N. Ageorges, M.F. A'Hearn, C. Arpigny, A. Ates, J. Aycock, S. Bagnulo, J. Bailey, R. Barber, L. Barrera et al., Science **310**, 265 (2005)
M.J. Mumma et al., Science **310**, 270 (2005)
D. Prialnik, Y. Mekler, Astrophys. J. Part 1 **366**, 318 (1991)
J.E. Richardson, H.J. Melosh, N.A. Artemeiva, E. Pierazzo, Space Sci. Rev. **117**, 241 (2005)
J.E. Richardson, H.J. Melosh, C.M. Lissec, B. Carcich, Icarus **190**, 357 (2007)
P.H. Schultz, C.M. Ernst, J.L.B. Anderson, Space Sci. Rev. **117**, 207 (2005)
S. Sirono, J.M. Greenberg, Icarus **145**, 230 (2000)
J.M. Sunshine et al., Science **311**, 1453 (2006)
C.P. Thomas et al., Icarus **187**, 4 (2007)

Comet Knudsen Layers

Björn J.R. Davidsson

Originally published in the journal Space Science Reviews, Volume 138, Nos 1–4.
DOI: 10.1007/s11214-008-9305-8

Abstract This paper reviews some important results about Knudsen layers obtained in theoretical gas kinetics research in the last few decades, focusing on the weak and strong evaporation problems in two-surface, half-space, and spherical geometries. Furthermore, the application of such results in cometary science is reviewed. In order to illustrate some properties of the half-space evaporation problem for water ice surfaces at temperatures relevant for active comets, a number of numerical Direct Simulation Monte Carlo calculations are presented.

Keywords Comets: coma · Comets: gas kinetics

1 Introduction

Cometary nuclei are highly porous km-sized remnants from planetary formation, rich in μm-sized grains of silicates and organics, as well as frozen volatiles, such as H_2O, CO, and CO_2. When heated sufficiently by the Sun, the near-surface ices evaporate and the vapor forms an extended atmosphere, rich in dust that has been entrained by the gas. The composition and physical properties of such *cometary comae* provide important observational constraints on the properties of the (often unobservable) nucleus. The scientific interest in cometary nuclei steams from the fact that they are primitive in nature, and therefore contain clues to Solar Nebula properties as well as planetesimal formation processes.

Knudsen layers, or equivalently, *kinetic boundary layers* form when a gas is interacting with a solid boundary, unless particular conditions apply. The Knudsen layer is characterized by a break-down of local thermodynamic equilibrium, i.e., the distribution function is far from Maxwellian within $\sim$ 10–100 mean free paths λ from the boundary. An example when a Knudsen layer does *not* form, is when an equilibrium gas without bulk motion is interacting with a non-absorbing surface which scatters molecules diffusively. In this case,

B.J.R. Davidsson (✉)
Department of Physics and Astronomy, Uppsala University, Box 515, 75120 Uppsala, Sweden
e-mail: bjorn.davidsson@astro.uu.se

H. Balsiger et al. (eds.), *Origin and Early Evolution of Comet Nuclei*
DOI: 10.1007/978-0-387-85455-7_13

the number of molecules just about to impact the surface equals the number of recently scattered molecules, and the distribution of velocity vectors for the two groups of particles are exact mirrored images of each other. For the gas, the solid boundary therefore does not behave differently than any (imaginary) test surface placed in the midst of the gas, and the gas simply does not "feel" the presence of the boundary. However, in other cases, e.g., when the gas mentioned above has a bulk motion tangentially to the diffusively scattering surface, the detailed symmetry is broken, and a Knudsen layer forms. Since Knudsen layers also form when there is a broken balance between the number of molecules approaching and leaving a surface, as is the case for *net evaporation* and *net condensation* (see, e.g., Cercignani 2000), it also means that the part of a cometary coma closest to the nucleus will constitute a Knudsen layer.

There are several reasons to study comet Knudsen layers, including the following.

1. In hydrodynamical modeling of cometary comae (see Sect. 3), the initial number density, temperature, and drift velocity of gaseous species must be specified and linked to the conditions prevailing on the nucleus. This requires knowledge about processes taking place within the Knudsen layer.
2. Accurate thermophysical modeling of cometary nuclei requires knowledge about parameters like surface gas density and the flux of recondensating coma molecules (Davidsson and Skorov 2004), which only are available if the Knudsen layer is modeled together with the nucleus.
3. Estimates of comet nucleus masses and bulk densities from non-gravitational force modeling requires that an accurate calculation of the force acting on the nucleus due to outgassing can be made (Davidsson and Gutiérrez 2004, 2005, 2006; Davidsson et al. 2007).
4. The European Space Agency spacecraft *Rosetta* carries the lander probe *Philae*, which will be situated inside the Knudsen layer of Comet 67P/Churyumov–Gerasimenko. In order to analyze and interpret data collected by the lander, Knudsen layer properties must be known in detail, and tools to model this environment must be available.

In Sect. 2, basic gas kinetic concepts are recapitulated and a brief overview of Knudsen layer research is made. Section 3 reviews application of results from Knudsen layer research in *cometary science*. This is followed by a brief summary of the Direct Simulation Monte Carlo (DSMC) technique in Sect. 4, used to make the calculations presented in Sect. 5, which serves the purpose of illustrating and exemplifying various Knudsen layer properties.

2 Physical Background

The *distribution function* $f(\mathbf{x}, \mathbf{v}, t)$ times $d\mathbf{x}\,d\mathbf{v}$ describes the number of molecules located within the volume $d\mathbf{x}$ (centered on $\mathbf{x}$), which have their velocity vectors in the range $[\mathbf{v}, \mathbf{v} + d\mathbf{v}]$, at time t. The *Boltzmann equation*,

$$\frac{\partial f}{\partial t} + \mathbf{v}\frac{\partial f}{\partial \mathbf{x}} = Q(f, f) \tag{1}$$

describes the time evolution of f (first term on the left hand side) caused by changes in the number of molecules in $d\mathbf{x}$ with velocities $[\mathbf{v}, \mathbf{v} + d\mathbf{v}]$. Changes are due to a *net inflow or outflow* of such molecules from surrounding volume elements (second term on the left hand side), or due to net removal or creation of such molecules by *molecular collisions* within $d\mathbf{x}$ (the *collision integral* on the right hand side). A vanishing collision integral $Q(f, f) \to 0$ means that collisions (locally) have no effect on f, and the gas is then in *local*

thermodynamical equilibrium. The collision integral only vanishes if f is identical to the *Maxwell–Boltzmann distribution*,

$$f_{\mathrm{M}} = \frac{n\beta^3}{\pi^{3/2}} \exp(-\beta^2 |\mathbf{v} - \mathbf{W}|^2), \tag{2}$$

where

$$\beta = \sqrt{\frac{m}{2kT}}, \tag{3}$$

where m is the molecular mass, k is the Boltzmann constant, while n, T, $\mathbf{W}$ are the number density, temperature, and drift speed vector, respectively. The latter parameters are calculated from an arbitrary f as

$$\{n,\ \mathbf{W},\ T_i\} = \left\{ \int_{R^3} f\, d\mathbf{v},\ \frac{\int_{R^3} \mathbf{v} f\, d\mathbf{v}}{\int_{R^3} f\, d\mathbf{v}},\ \frac{m}{kn} \int_R |\mathbf{v}_i - \mathbf{W}_i|^2 f\, d\mathbf{v}_i \right\}, \quad i = x,\ y,\ z \tag{4}$$

where $T_{\mathrm{tr}} = \frac{1}{3}(T_x + T_y + T_z)$ is the translational temperature of a general gas, and $T = T_x = T_y = T_z$ is the temperature of an equilibrium gas. The integrals in (4) are the three first *moments* of the distribution function.

The general Boltzmann equation is difficult to solve, therefore it is common to apply various simplifying assumptions to make calculations easier. A frequently used approximative collision integral is the *BGK model* (Bhatnagar et al. 1954),

$$Q(f, f) \approx \nu(f_{\mathrm{M}} - f(\mathbf{x},\ \mathbf{v},\ t)), \tag{5}$$

where $f(\mathbf{x},\ \mathbf{v},\ t)$ is the actual (generally non-Maxwellian) distribution function, f_{M} is a Maxwellian distribution evaluated for the parameters $\{n,\ T,\ \mathbf{W}\}$ obtained by applying (4) on $f(\mathbf{x},\ \mathbf{v},\ t)$, and ν is the collision frequency.

It is also common to approximate the distribution function by performing a *Hilbert expansion*,

$$f = \sum_{i=0}^{\infty} \varepsilon^i f_i, \tag{6}$$

where ε is a small parameter (e.g., the mean free path). If (6) is truncated after the second term, and if we take $f_0 = f_{\mathrm{M}}$, we obtain $f \approx f_{\mathrm{M}}(1 + h)$ for some function h. If this is inserted into the steady-state version of (1), the *linearized Boltzmann equation* is obtained,

$$\mathbf{v} \frac{\partial h}{\partial \mathbf{x}} = \frac{2Q(f_{\mathrm{M}},\ hf_{\mathrm{M}})}{f_{\mathrm{M}}}. \tag{7}$$

Naturally, solutions to (7) only make physical sense for steady-state problems where the distribution function only deviates slightly from a Maxwellian. Therefore, if evaporation (or condensation) problems are considered, a distinction is often made between *weak evaporation* problems, where (7) is sufficiently accurate, and *strong evaporation* problems, where (1) must be solved.

After this recapitulation of basic concepts it is time to briefly review some important results regarding the properties of Knudsen layers, formed near surfaces where a vapor interacts with its condensed (solid or liquid) phase. Over the years, the *two-surface problem* has attracted considerable interest, consisting of two parallel infinite plates separated by

some distance. Using the linearized Boltzmann equation combined with the BGK model, Pao (1971a) studied the flow of mass and energy from a warm plate towards a cooler plate, thereby discovering the *inverted temperature gradient paradox*, which means that the vapor near the cool plate may be warmer, than the vapor near the warm plate. This is possible because of a *microscopic temperature jump*, i.e., a temperature discontinuity when going from the plate to the adjacent vapor, caused by a break-down of thermodynamic equilibrium. The difference between actual vapor density, and the saturation density evaluated for the plate temperature, forms a corresponding *microscopic density jump*. As discussed by Aoki and Cercignani (1983), the temperature gradient result depends on the latent heat of the solid (e.g., water ice at 200 K is indeed capable of producing an inverted temperature gradient), but does not seem to be an artifact of the simplified (5) and (7).

Matsushita (1977) studied the effect of including a second noncondensable species in the vapor (e.g., CO molecules trapped between two plates of water ice), using a linearized Boltzmann equation and a BGK collision integral (modified to apply to multicomponent vapor). He found that the noncondensable molecules reduce the mass flux between the plates, and may also reverse the inverted temperature gradient. Furthermore, the noncondensable molecules have a strong tendency to concentrate near the cool plate. These results where confirmed by Soga (1982), considering the nonlinear problem (steady-state limit of (1)).

If the plate distance is large enough in a two-surface problem, an intermediate region forms where local thermodynamic equilibrium holds, i.e., it is fully described by (2) evaluated for some parameters $\{n_\infty,\, T_\infty,\, W_\infty\}$, where $\mathbf{W} = [0, 0, W_\infty]$ (arbitrarily taking the $\hat{z}$–axis to be perpendicular to the plates). That is to say, two Knudsen layers adjacent to the plates, are separated by a hydrodynamic region. Such a behavior is seen both in laboratory experiments (e.g., Mager et al. 1989) as well as in numerical solutions to the nonlinear Boltzmann equation (e.g., Yen and Akai 1977). If one of the plates is moved to infinity (or is explicitly neglected), the important and well-studied *half-space evaporation (or condensation) problem* is obtained, to be discussed in the following.

The differences between $\{T_\infty,\, n_\infty\}$ and the plate surface temperature and corresponding saturation density, $\{T_\mathrm{s},\, n_\mathrm{s} = n_\mathrm{sat}(T_\mathrm{s})\}$ are referred to as the *macroscopic temperature and density jumps*, respectively. Naturally, the problem of relating the downstream vapor properties $\{n_\infty,\, T_\infty,\, W_\infty\}$ with the surface plate properties has attracted substantial interest over the years. The half-space problem was studied by Pao (1971a, 1971b), assuming weak evaporation and a BGK model. For a given net mass flux, Pao could evaluate the microscopic temperature and density jumps exactly. Numerical solutions to the linearized Boltzmann equation using a hard-sphere molecular model (Sone et al. 1989) demonstrate that these results are not highly dependent on the assumed collision model.

Naturally, weak evaporation problems have a limited applicability, therefore we move on to consider strong evaporation. When attempting to solve the steady-state nonlinear Boltzmann equation, it is very common to make a distribution function *Ansatz*, i.e., to guess the general shape of f and form a closed set of equations by taking the appropriate number of moments of (1). In a pioneering study, Shankar and Marble (1971) used a *bimodal (Liu–Lee) Ansatz*,

$$\begin{cases} f^+ = f_\mathrm{M}(n_1(z),\, T_1(z),\, W_1(z)) \\ f^- = f_\mathrm{M}(n_2(z),\, T_2(z),\, W_2(z)), \end{cases} \tag{8}$$

i.e., at each height z from the plate, the distribution function for molecules moving away from the plate (f^+) is a semi-Maxwellian characterized by some parameters $\{n_1,\, T_1,\, W_1\}$, while at the same point, molecules moving towards the plate (f^-) are characterized by *another* semi-Maxwellian evaluated for a different parameter set $\{n_2,\, T_2,\, W_2\}$. Shankar and

Marble (1971) first assumed $W_1(z) = W_2(z) = 0$ (i.e., non-drifting semi-Maxwellians), resulting in four unknown parameters at each z. Consequently, four moments were considered (assuming Maxwell molecules when evaluating the nonconserved fourth moment). Considering a vapor (with $\{n_0, T_0\}$) initially in equilibrium with a surface, and letting the plate temperature increase from T_0 to T_s at $t = 0$, Shankar and Marble (1971) studied the $t \to \infty$ behavior of the vapor. They found a pressure wave propagating at the sound speed into the ambient vapor, and most importantly, a *constant mass production rate* of the surface,

$$\dot{m} = 0.148\sqrt{\frac{2\pi m}{kT_0}}\Delta p, \tag{9}$$

where Δp is the difference between the saturation pressure corresponding to T_s, and the ambient pressure p_0. Shankar and Marble (1971) also considered the $W_1 \neq 0$ and $W_2 \neq 0$ cases with a six moment method, only finding minor corrections to (9).

Mager et al. (1989) also used a bimodal Ansatz of the type (8), reducing the number of moments to five by explicitly assuming $W_1(z) = W_2(z)$ and using a collision integral for Maxwell molecules. The solutions were compared with experimental data. Their laboratory investigation considered plates of iodine (one evaporating at $225 \leq T_s \leq 263\,\mathrm{K}$, the other acting as a condensation plate cooled by liquid nitrogen). Focusing on the equilibrium region in the midst of the slab, the measured values $\{n_\infty,\ T_\infty,\ W_\infty\}$ were very well reproduced by theory, illustrating the applicability of both the collision model and the Ansatz.

Another approach is based on the *Mott–Smith Ansatz*, given by

$$\begin{cases} f^+ = a(z)\, f_{\mathrm{M}}^+(n_s,\ T_s,\ 0) + \big(1 - a(z)\big) f_{\mathrm{M}}^+(n_\infty,\ T_\infty,\ W_\infty) \\ f^- = \big(1 - (1 - \beta^-)a(z)\big) f_{\mathrm{M}}^-(n_\infty,\ T_\infty,\ W_\infty) \end{cases} \tag{10}$$

where $a(z)$ is some function satisfying $a(0) = 1$ and $a(\infty) = 0$. Hence, the $v_z > 0$ half of the distribution function gradually changes from the stationary semi-Maxwellian at $z = 0$ (dictated by surface evaporation), to the downstream ($z \to \infty$) drifting semi-Maxwellian $f_{\mathrm{M}}^+(n_\infty,\ T_\infty,\ W_\infty)$. The $v_z < 0$ half of the distribution function always has the functional *shape* given by $f_{\mathrm{M}}^-(n_\infty,\ T_\infty,\ W_\infty)$, but the number density is boosted by a factor β^- at the surface, compared to the downstream value. Anisimov (1968) was the first to apply (10) for strong evaporation in a half-space, using three moments, and forming a closed set of equations by assuming that the Mach number,

$$M = W\sqrt{\frac{m}{\gamma kT}} \tag{11}$$

(where γ is the specific heat ratio), approached unity as $z \to \infty$, i.e., assumed $M_\infty = 1$. Doing so, he obtained the macroscopic temperature and density jumps for monatomic vapor ($\gamma = 5/3$),

$$\begin{cases} \dfrac{T_\infty}{T_s} = 0.67 \\ \dfrac{n_\infty}{n_s} = 0.31, \end{cases} \tag{12}$$

Furthermore, Anisimov (1968) obtained $\beta^- = 6.29$, i.e., the number of molecules with $v_z < 0$ is about ~ 6 times more common close to the surface, compared to the conditions at large z.

In a famous paper, Ytrehus (1977) used (10) and the first three moments of (1), just like Anisimov (1968), but not applying any assumption regarding M_∞. He then obtained (see also Cercignani 2000) the macroscopic temperature and density jumps, as well as β^-, as functions of the *downstream speed ratio* $S_\infty = \sqrt{5/6} M_\infty$,

$$\begin{aligned}
\sqrt{\frac{T_\infty}{T_\mathrm{s}}} &= -\frac{1}{8}\sqrt{\pi} S_\infty + \sqrt{1 + \frac{\pi}{64} S_\infty^2} \\
\frac{n_\infty}{n_\mathrm{s}} &= \frac{F^- + \sqrt{\frac{T_\infty}{T_\mathrm{s}}} G^-}{2\exp(-S_\infty^2)} \\
\beta^- &= \frac{2(2S_\infty^2 + 1)\sqrt{\frac{T_\infty}{T_\mathrm{s}}} - 2\sqrt{\pi} S_\infty}{F^- + \sqrt{\frac{T_\infty}{T_\mathrm{s}}} G^-}
\end{aligned} \tag{13}$$

where the auxiliary functions F^- and G^- are given by

$$\begin{aligned}
F^- &= -\sqrt{\pi} S_\infty \operatorname{erfc}(S_\infty) + \exp(-S_\infty^2) \\
G^- &= (2S_\infty^2 + 1)\operatorname{erfc}(S_\infty) - \frac{2}{\sqrt{\pi}} S_\infty \exp(-S_\infty^2),
\end{aligned} \tag{14}$$

where erfc is the complimentary error function.

Next, Ytrehus (1977) considered the fourth moment of (1), assuming Maxwell molecules, and could thereby obtain a differential equation for $a(z)$ itself (see (10)). He then found, that in order to fulfill the boundary condition $a(z \to \infty) = 0$ (i.e., to ensure that local thermodynamic equilibrium indeed *is* obtained at infinity), there must be an upper limit on the Mach number, $M_\infty \leq 0.992$. Vapor outflow from a plane into a half-space is therefore always a *subsonic flow*. Equations (13)–(14) can also be used to show that the *backflux*, i.e., the ratio of condensing to evaporating molecules at the surface, decreases from 100% at $M_\infty = 0$ (when the vapor is in equilibrium with the surface) to $\sim 18\%$ at $M_\infty \approx 1$, i.e., a *near-sonic downstream condition maximizes the net evaporation rate of the surface*.

Yen and Akai (1977) calculated numerical solutions to the nonlinear steady-state Boltzmann equation for both hard sphere and Maxwell molecules, verifying the analytical solution of Ytrehus (1977) for a wide range of subsonic downstream Mach numbers. As shown by Soga (1977), the results by Ytrehus (1977) are also in good agreement with his own investigation, in which the Rankine–Hugoniot shock wave relation was used together with the first three moments of (1) to calculate the macroscopic temperature and density jumps versus the net mass flux. Soga (1977) also reproduce numerical simulations by Kogan and Makashev (1971), which also are in reasonable agreement with the results of Ytrehus (1977).

Following the finding of $M_\infty \leq 0.992$ by Ytrehus (1977), i.e., a numerical value close but not equal to unity, substantial efforts were made to investigate whether the upper limit in fact was exactly unity. Arthur and Cercignani (1980) demonstrated that the limit indeed was $M_\infty < 1$ by using a linearized Boltzmann equation with a BGK model, and speculated that the result might be extended to include $M_\infty \leq 1$ for the nonlinear case. Alternative mathematical techniques applied to the same linear problem by Siewert and Thomas (1981) and Loyalka et al. (1981) confirmed the $M_\infty < 1$ limit. Siewert and Thomas (1982) also obtained this result, using a three-dimensional BGK model rather than the standard one-dimensional version. An important generalization of the problem, was also performed by Greenberg and van der Mee (1984).

Another problem of fundamental importance is that of *evaporation from a sphere into vacuum*. In the $K = 0$ limit (where $K = \lambda/R$ is the Knudsen number and R is the sphere radius), isentropic expansion leads to the behavior (see, e.g., Cercignani 2000)

$$\begin{cases} n(r) \propto r^{-2} \\ T(r) \propto r^{-4/3} \\ W(r) \propto W_\infty(1 - r^{-4/3}) \\ M \propto r^{2/3}, \end{cases} \tag{15}$$

i.e., n is diluted with the distance r from the surface due to expansion, W increases towards the terminal speed W_∞ until all kinetic energy is used for bulk motion instead of random motion (as a consequence T approaches zero), and the Mach number tends towards infinity. However, this behavior depends critically on the capability of the vapor to actually decrease molecular random motion and increase the drift speed—which requires collisions. But as n decreases, the vapor approaches free molecular flow. As a consequence, (15) is not fulfilled for large r. Instead, T and M *freeze out* at some values T_f and M_f, while $n(r) \propto r^{-2}$ is still valid. The exact values of T_f and M_f will depend on K at the surface of the sphere. Sone and Sugimoto (1993) performed a large number of numerical solutions to the nonlinear Boltzmann equation with a BGK model, to investigate, e.g., the dependence of T_f and M_f on K. They found, e.g., that freeze-out typically takes place for $r < 10$–$100\,\mathrm{R}$, for a wide range of Knudsen numbers.

As emphasized by Sone and Sugimoto (1993), the Knudsen layer just above the spherical surface (with a Mach number limited by $M \leq 1$ according to the half-space problem, if K is sufficiently small), must merge smoothly with the exterior flow, which expands isentropically until $v \to 0$ leads to free molecular flow. Since the isentropic expansion is *supersonic*, the only way to guarantee a smooth transition is to have a *Knudsen layer with* $M = 1$ *on its upper boundary*. That is to say, of all $M \leq 1$ solutions theoretically possible for the planar half-space problem, only the $M = 1$ solution is applicable if the surface has a convex curvature. The same observation was made by Cercignani (1981, 2000), when discussing jets emanating from a finite evaporating area on a plane, which has a core solution resembling that of evaporation from a sphere.

3 Knudsen Layers in Comet Research

The solution of Ytrehus (1977), extended by Cercignani (1981) to polyatomic vapor ((13)–(14) represent the monatomic $\gamma = 5/3$ case), has proven to be most useful in modeling of cometary comae. As explained by, e.g., Crifo (1995), it can be used to assign the appropriate values of $\{n, T, W\}$ on top of the Knudsen layer (needed as boundary conditions for a hydrodynamical model). The procedure includes the determination of the local nucleus temperature, which depends on, e.g., solar illumination and the backflux, which is turn depends on the unknown Mach number (speed ratio). The Mach number is obtained by an iterative procedure, continuing until the properties of the nucleus, Knudsen layer, and the exterior hydrodynamic model are physically consistent with each other. Application of the half-space problem solution (assuming a planar surface) is possible also for curved surfaces, as long as the curvature radius is large compared to the local mean free path (see, e.g., Crifo and Rodionov 1999; Crifo et al. 2002). Henceforth, the Mach number on top of the Knudsen layer will be referred to as the "initial" Mach number.

Naturally, it is of great interest to find out what solutions (of all possible subsonic cases included in the half-space problem), that actually are obtained in practical cometary applications. Crifo (1995) studied an active area shaped as a spherical cap with curvature radius $R = 4\,\mathrm{km}$, located on an irregular comet at a heliocentric distance of $r_\mathrm{h} = 1\,\mathrm{AU}$. He found that surface outgassing resulted in the initial Mach number $M = 0.99$. In addition, the spherical ($R = 6\,\mathrm{km}$, $r_\mathrm{h} = 1\,\mathrm{AU}$) nucleus studied by Crifo and Rodionov (2000) had a *dayside* initial outflow characterized by $M \approx 1$. Due to subsequent isentropic expansion, the Mach number gradually increased beyond that point, e.g., being $M = 1.2$ about 126 m above the surface. These initially sonic outflows are consistent with the previously mentioned statement by Sone and Sugimoto (1993)—the transition from the Knudsen layer to the isentropically expanding coma must pass through the sonic point. It was also pointed out by Rodionov et al. (2002), when working with non-spherical but chemically homogeneous model comet nuclei, that the maximum net evaporation rates (equivalent to initial sonic outflow) where obtained on the "hills" of the comet, i.e., in areas having a convex curvature.

Therefore, one can generally assume that a slightly convex local geometry, nominally will result in a Knudsen layer characterized by $M \approx 1$ at the exterior boundary. However, there are *important exceptions* to this rule, also for simple convex geometries like the sphere. Crifo and Rodionov (1999) studied a chemically heterogeneous spherical nucleus ($R = 1.4\,\mathrm{km}$, $r_\mathrm{h} = 1\,\mathrm{AU}$), containing three areas rich in surface ice, surrounded by areas only containing very little ice. The initial Mach numbers right above the ice-rich areas were close to unity, but the regions above the *ice-poor* areas where characterized by very slow ($\sim 100\,\mathrm{m\,s^{-1}}$) and relatively warm ($\sim 180\,\mathrm{K}$) vapor, so that the initial Mach number was $M \leq 0.1$. This solution to (the polyatomic extension of) (13)–(14) predicts a substantial backflux to the surface, being on the order of the local vapor production rate—the coma is nearly in equilibrium with the nucleus, and the net vapor production is very low.

Surface topography is another mechanism that may produce clearly subsonic initial Mach numbers. This was exemplified by Crifo and Rodionov (1997, 1999), when studying a chemically homogeneous non-spherical nucleus (with $R \leq 1.5\,\mathrm{km}$ and $r_\mathrm{h} = 1\,\mathrm{AU}$), shaped as a bean, so that a deep valley (directly exposed to solar illumination) is surrounded by two hills. Although the flows from the hills initially were sonic, the initial flow from the deeper part of the valley was pronouncedly subsonic, with $M \leq 0.5$. This led to a relatively high backflux, and a reduced net vapor production rate from the valley floor, compared to the hill tops, *in spite of the fact that these areas received the same solar flux*.

Naturally, it is of great importance to test whether the half-space solution indeed is applicable to curved surfaces (the criterion $K = \lambda/R \ll 1$ is, after all, only a guide line). One important test was made by Crifo et al. (2002), who compared solutions based on the Euler equations combined with the kinetic half-space Knudsen layer solution, to DSMC calculations, e.g., for a large sphere far from the Sun ($R = 24.5\,\mathrm{km}$, $r_\mathrm{h} = 5.37\,\mathrm{AU}$). They found an excellent agreement between the two solutions, demonstrating the applicability of the (plane-parallel) half-space solution. Another test was made by Crifo et al. (2003), now comparing Navier–Stokes solutions (combined with the half-space Knudsen layer solution), to DSMC calculations. First, an apple-shaped nucleus was studied, with $R \leq 0.5\,\mathrm{km}$, having a sunlit "crater" on the top (opening radius $\sim 0.4\,\mathrm{km}$, depth $\sim 0.2\,\mathrm{km}$), its surface having a 6% ice concentration, and placed at $r_\mathrm{h} = 2.5\,\mathrm{AU}$. From the crater bottom up to the surrounding hills, the agreement between the two solutions was excellent. However, when moving from the subsolar point on the hill tops towards the terminator, the backflux predicted by the half-space solution was off by up to 50%. The reason for this, was that the sonic point was reached *before* the flow had reached local thermodynamic equilibrium. This can *never*

happen over a plane surface (since $M \leq 1$ must be fulfilled), but is possible for a convex surface. Crifo et al. (2003) also performed a test for a similarly shaped nucleus, but having $R \leq 6.95\,\mathrm{km}$, $r_\mathrm{h} = 5.789$, and 100% ice coverage (the directly illuminated crater had an opening radius $\sim 3\,\mathrm{km}$ and depth $\sim 2\,\mathrm{km}$). Here, they found excellent agreement near the crater floor, but a 50% error in the backflux on parts of the crater walls, as well as in the area between surrounding hill tops and the terminator (for the same reason as before). In addition, Crifo et al. (2003) found an area on the crater wall where *net condensation* took place, for which (13)–(14) are not applicable. In spite of such examples of break-down, taking place locally and under special geometric conditions, the half-space solution is generally indeed very useful.

When applying results from the research on kinetic boundary layers, in cometary science (as in the coma models described above), it is often sufficient to know the final downstream flow properties, without worrying about the *detailed behavior of the flow throughout the Knudsen layer itself*. However, in some applications, it is of interest to also follow the gradual evolution of the vapor versus height *within* the Knudsen layer (e.g., when studying the acceleration of dust grains within the Knudsen layer). One may also want to relax some of the inherent assumptions in the analytical solutions (i.e., regarding the initial distribution function for particles leaving the surface). A suitable numerical technique for performing such detailed solutions to the Boltzmann equation is the DSMC, mentioned previously and briefly summarized in Sect. 4. As seen in Sect. 2, numerical solution techniques to the Boltzmann equation has been applied in Knudsen layer research numerously during the last few decades, but Bisikalo et al. (1989) were apparently the first to apply DSMC simulations explicitly targeting *cometary* conditions. They investigated the evaporation of pure water ice at $T_\mathrm{s} = 180{-}200\,\mathrm{K}$, and noted that the backflux increased from 11.5% to 14% with temperature, and that the downstream Mach number was $M = 1.15{-}1.16$. In a similar DSMC investigation by Skorov and Rickman (1998) for $T_\mathrm{s} = 200\,\mathrm{K}$ water ice, they found 18% backflux and a downstream Mach number $M \approx 1.2$. In both cases, equilibrium was claimed to take place $\sim 10\lambda$ from the surface.

Unfortunately, these results reveal more about the importance of using the appropriate number of Monte Carlo test particles, as well as sufficient spatial and temporal resolution in DSMC simulations, rather than describing physically real properties about the system. From the discussion in Sect. 2, it is clear that outflow from a plane surface by no means can be supersonic (this applies also for polyatomic vapor). Furthermore, the solution of Ytrehus (1977) shows that equilibrium is reached at *infinity* when $M_\infty \approx 1$. As pointed out by Cercignani (2000), the local thermodynamic equilibrium is reached to within 90% at a distance of $20\,\lambda$ from the surface, and to within 99% at a distance $200\,\lambda$ from the surface. Hence, one should never talk about "distance where equilibrium is reached" in a plane-parallel geometry, but only of "distance where divergence from equilibrium drowns in numerical errors".

Another illustration of the sensitivity of physical parameters to small errors was provided by Huebner and Markiewicz (2000). They set out to determine the downstream flow properties in the limiting case of *negligible return flux*. It means that the surface net fluxes of mass, energy, and momentum, $\{\dot{m},\ \dot{e},\ \dot{p}\}$, are (artificially) *only* allowed to be functions of the surface temperature. The problem consists of connecting the semi-Maxwellian near the surface, with the downstream drifting Maxwellian through conservation of mass, energy and momentum. For polyatomic molecules, Huebner and Markiewicz (2000) found a single solution with a downstream Mach number of $M_\infty = 1.141$. The approximation that results in a single supersonic flow is the following. Molecules leave the surface according to a semi-Maxwellian evaluated for T_s, carrying with them the fluxes $\{\dot{m},\ \dot{e},\ \dot{p}\}$. Due to

intermolecular collisions, the molecules re-arrange energy and momentum between themselves, so that a drifting Maxwellian is formed—this is of course made in such a way that the *net* fluxes at a large height still are $\{\dot{m},\ \dot{e},\ \dot{p}\}$. Now, consider the backscattered molecules hitting the surface. They are not allowed to change any of the local net fluxes (this is the true meaning of the "negligible return flux" approximation). The original mass flux can easily be retained by neglecting condensation, i.e., all particles scatter. The original energy flux can also be retained, by forcing the particles to keep their speeds (as in specular reflection). However, there is no way (in reality) to avoid changing the *momentum* of the scattered particles, since this is a vectorial property that by necessity must change (sign) during reflection. The approximation made, in order to obtain a *single supersonic solution*, is therefore to ignore momentum reversal for scattered particles. In spite the fact that the error in momentum introduced by this simplification is very small (since the backflux is very small in the first place), the result is quite remarkable—it reduces an infinite number of solutions to *one single solution*, and furthermore, this solution is located *outside* the $M_\infty \leq 1$ region, which must apply if mass, energy, and momentum are truly conserved! The extreme sensitivity of half-space problem downstream solutions, to small numerical errors in the momentum flux in particular, has also been noted by the author while performing DSMC calculations.

Another set of DSMC calculations were performed by Davidsson and Skorov (2004). The purpose of these simulations was to produce realistic boundary conditions to be used in *thermophysical nucleus modeling*. Typically, the mass conservation equation in such models is solved by assuming either zero coma density or saturation density. Furthermore, the condensing backflux is rarely included in the energy conservation equation in such models. Davidsson and Skorov (2004) wanted to provide an alternative to such simplifications. Moreover, it was considered important to evaluate the pressure acting on the surface due to outgassing, since rather arbitrary values previously had been used when estimating nucleus masses in non-gravitational force modeling. The DSMC modeling was performed with a downstream condensation plate. The vanishing backflux at large distances, resulting from using such a boundary condition, is equivalent to the $M_\infty = 1$ limiting case of the half-space problem, since it *reproduces the effect of having a mild surface curvature*, as discussed previously (the diluted flow in a spherical geometry eventually leads to zero backflux). Therefore, the approach by Davidsson and Skorov (2004) is accurate as long as $0 \leq \lambda/R \lesssim 1$ near the surface, and as long as there are *no important changes in surface production rate and/or topography* near the surface facet in question. Such conditions may of course break down in reality, for very irregular and chemically heterogeneous nuclei.

An important feature of the work by Davidsson and Skorov (2004), was to allow the distribution function of molecules exiting from the porous surface structure to *deviate from the semi-Maxwellian*. In fact, the initial half-space distribution function was calculated numerically, allowing for a temperature gradient of the medium, as well as a temperature-dependent sub-surface vapor production rate and condensation coefficient. As a result, Davidsson and Skorov (2004) obtained interpolation tables for the near-surface vapor number density, recondensing backflux, and pressure acting on the surface due to outgassing, as functions of both the surface temperature, and the near-surface temperature gradient. Since the thermophysical model uses these interpolation tables iteratively during a numerical simulation, a *quasi-parallel nucleus/coma model is obtained*. This model was used by Davidsson and Gutiérrez (2004, 2005, 2006) and by Davidsson et al. (2007) to estimate the nucleus masses of Comets 19P/Borrelly, 67P/Churyumov–Gerasimenko, 81P/Wild 2, and 9P/Tempel 1 through non-gravitational force modeling.

4 Direct Simulation Monte Carlo (DSMC)

For illustrative purposes, a number of numerical calculations for the half-space problem are presented in Sect. 5. These were made by using a one-dimensional DSMC code written by Bird (1994), but modified by the author to, e.g., allow arbitrary initial ($v_z > 0$) distribution functions.

In the DSMC framework, the vapor is modeled at a molecular level by considering a large number of Monte Carlo test particles, each representing a certain number of real molecules. Each test particle is characterized by its position coordinates $\{x, y, z\}$, its velocity vector $\{v_x, v_y, v_z\}$, and its rotational energy E_{rot}.

The time-development of the vapor is modeled by alternating between a *translation phase* and a *collision phase*. During the translation phase (with a duration given by the time step Δt), the test particles are moved linearly in accordance with their velocity vectors. During the translation phase, no intermolecular collisions are considered, but if a boundary is encountered, this is accounted for. During the collision phase, the test particles are considered stationary, while their velocity vectors and rotational energies are updated, as a result of collisions.

In order to treat collisions (and to calculate macroscopic quantities from (4) from the numerically obtained f), the considered volume is divided into a number of *cells*, which in turn are divided into a number of *sub-cells*, from which collision partners are selected. In this work, the Variable Hard Sphere (VHS) model is applied to describe collisions.

Inelastic collisions are here treated according to the phenomenological Larsen–Borgnakke model, assuming three internal degrees of freedom. It does not consider the detailed rotational energy levels of any particular molecular species. It only guarantees that an equilibrium gas has equipartition between translational and rotational energies, that the translational and internal energy distributions for a large sample of test particles both are Maxwellian, and that the total energy and momentum are conserved in each collision. A finite relaxation rate for nonequilibrium vapor is introduced by only considering every fifth collision as inelastic.

The calculated macroscopic quantities are prone to fluctuate violently with time, since the instantaneous number of test particles per cell generally is a very small, constantly changing number. Therefore, the flow properties are *sampled* a large number of times during the course of simulation.

The current simulations considered a $15-20\,\mathrm{m}$ separation between the surface and a downstream condensation plate. The slab was divided into 1500–2000 cells to guarantee a cell size smaller than λ, and a time step of $\Delta t = 5 \cdot 10^{-6}\,\mathrm{s}$ was used to assure cell crossing in more than ~ 4 time steps. At any given moment, the slab contained $\sim 4 \cdot 10^4$ test particles. The steady-state flow is sampled $2 \cdot 10^5$ times, leading to typical errors in $\{n,\ T,\ W\}$ of 0.2%, $0.1\,\mathrm{K}$ and $0.5\,\mathrm{m\,s^{-1}}$, respectively. External energy sources such as solar radiation have not been considered.

Calculations are performed in a two-step procedure. First, a calculation is made with a downstream condensation plate, while sampling the fluxes of mass, energy, and momentum $\{\dot{m}_0, \dot{e}_0, \dot{p}_0\}$ reaching the downstream condensation plate. This calculation results in two Knudsen layers separated by an equilibrium region, as discussed in Sect. 2. To remove the outer Knudsen layer caused by the condensation plate, one calculates the values of $\{n_\infty,\ T_\infty,\ W_\infty\}$, associated with a downstream drifting Maxwellian *that will not change the prevailing flux balance at the surface*. One can show, that these parameters are functions

of the sampled $\{\dot{m}_0, \dot{e}_0, \dot{p}_0\}$, as follows,

$$T_\infty = \frac{m}{2k}\left(-\frac{1}{2}\mathcal{A} \pm \sqrt{\frac{1}{4}\mathcal{A}^2 - \mathcal{B}}\right) \tag{16}$$

$$W_\infty = \left(\frac{2\dot{e}_0}{\dot{m}_0} - \frac{2kT_\infty}{m}\left(\frac{5}{2} + \frac{\zeta}{2}\right)\right)^{1/2} \tag{17}$$

$$n_\infty = \frac{\dot{m}_0}{m W_\infty}, \tag{18}$$

where $\zeta = 3$ is the number of internal degrees of freedom, and the auxiliary functions $\mathcal{A}$ and $\mathcal{B}$ are given by

$$\mathcal{A} = -\frac{4\dot{e}_0}{\left(2 + \frac{\zeta}{2}\right)\dot{m}_0} + \frac{\left(\frac{5}{2} + \frac{\zeta}{2}\right)\dot{p}_0^2}{\left(2 + \frac{\zeta}{2}\right)^2 \dot{m}_0^2} \tag{19}$$

$$\mathcal{B} = \left(\frac{2\dot{e}_0}{\left(2 + \frac{\zeta}{2}\right)\dot{m}_0}\right)^2 - \frac{2\dot{e}_0 \dot{p}_0^2}{\left(2 + \frac{\zeta}{2}\right)^2 \dot{m}_0^3}. \tag{20}$$

As it turns out, the sampled $\{\dot{m}_0, \dot{e}_0, \dot{p}_0\}$ are such that $\mathcal{A}^2 = 4\mathcal{B}$, i.e., (16)–(20) yield a unique solution $\{n_\infty, T_\infty, W_\infty\}$. Consistent with our expectations (given that the condensation plate simulates a mild degree of surface curvature), the corresponding downstream Mach number is extremely close to unity. The simulation is then *repeated*, now using a drifting Maxwellian evaluated for $\{n_\infty, T_\infty, W_\infty\}$ as boundary condition, which removes the outer Knudsen layer.

5 Numerical Examples

Table 1 shows the properties of seven considered nucleus models, characterized by their surface temperatures T_s, temperature change ΔT over the uppermost 7 grain radii of the medium, and the corresponding vapor production rates $\dot{m}_{\rm prod}$ (before backflux correction).

All model nuclei except #4 and #5 are isothermal. All nuclei are assumed to consist of a 0.73 : 0.27 mixture of crystalline water ice and dust grains, by volume in compacted material (the dust does not participate in the outflow). The porosity of the surface material is 70%. The probability of molecular condensation at the surface is around 50% for the considered surface temperatures. The production rates and the distribution functions of molecules

Table 1 Properties of the nucleus media

Case	T_s [K]	ΔT [K]	$\dot{m}_{\rm prod}$ [10^{21} molec m^{-2} s^{-1}]
1	190	0	1.014
2	195	0	2.335
3	200	0	5.030
4	200	−20	3.535
5	200	+20	7.730
6	205	0	9.727
7	210	0	15.723

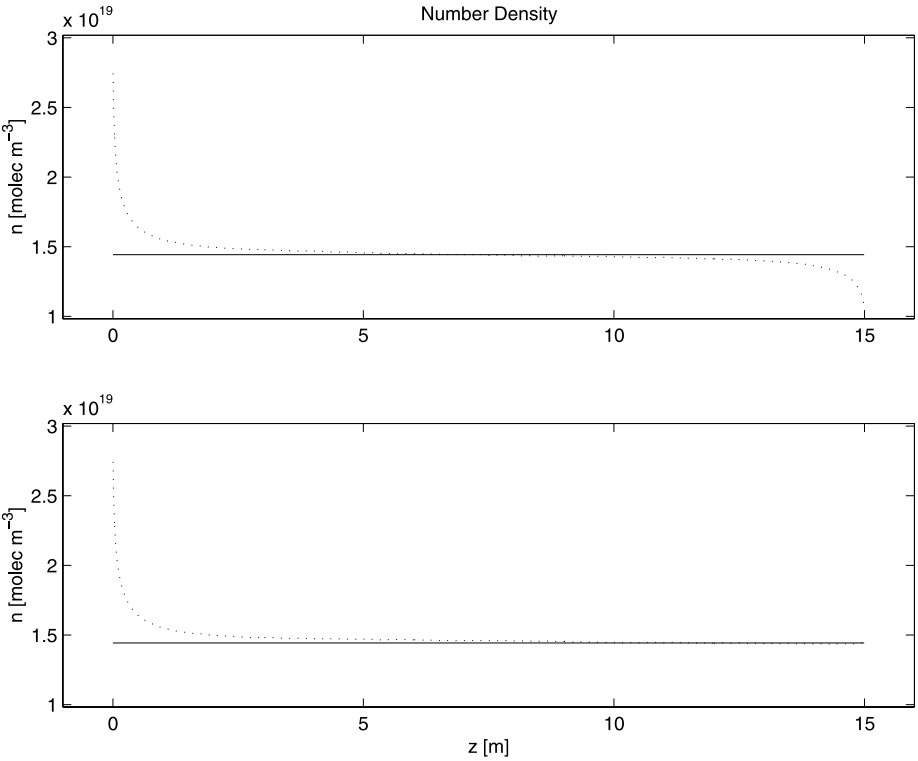

Fig. 1 Vapor density of model #3 as function of height z. For the *upper panel*, a downstream condensation plate was used. The *solid line* is the expected n_∞ obtained from (18). The *lower panel* show the density versus height when using a drifting Maxwellian as outer boundary condition, characterized by $\{n_\infty,\ T_\infty,\ W_\infty\}$ as determined by (16)–(20)

leaving the media were calculated by using the method described by Davidsson and Skorov (2004). Note that the three models with the same surface temperature (#3–#5) have quite different production rates, due to differences in the sub-surface temperatures.

Figures 1, 2, and 3 show the number density, drift speed, and temperature versus height, respectively, for model #3. The upper panels of Figs. 1–2 show the results when a condensation plate is used as outer boundary condition. We see two Knudsen layers, separated by an equilibrium region. Based on the sampled values of $\{\dot{m}_0,\ \dot{e}_0,\ \dot{p}_0\}$ absorbed by the condensation plate, (16)–(20) are used to calculate the parameters $\{n_\infty,\ T_\infty,\ W_\infty\}$ as described previously. These values are shown as straight horizontal lines in Figs. 1–3. The lower panels of Figs. 1–2 show what happens in a second simulation, where a drifting Maxwellian evaluated for $\{n_\infty,\ T_\infty,\ W_\infty\}$ is used at the exterior boundary. The outer Knudsen layer disappears, whereas n, W (as well as T) tend to their asymptotic values.

Table 2 summarizes the conditions prevailing close to the evaporating surface for the various models. Note that $T_z < T_{x,y}$, indicating relatively little kinetic energy in motion along the surface normal, and more kinetic energy in motion parallel to the surface—the molecules are *decollimated*. With height (see Fig. 3), T_z grows at the expense of $T_{x,y}$, illustrating that *collimation* is occurring. Also note that the rotational temperatures in Table 2 are a few degrees smaller than the corresponding T_s values—already within the first cell have a certain

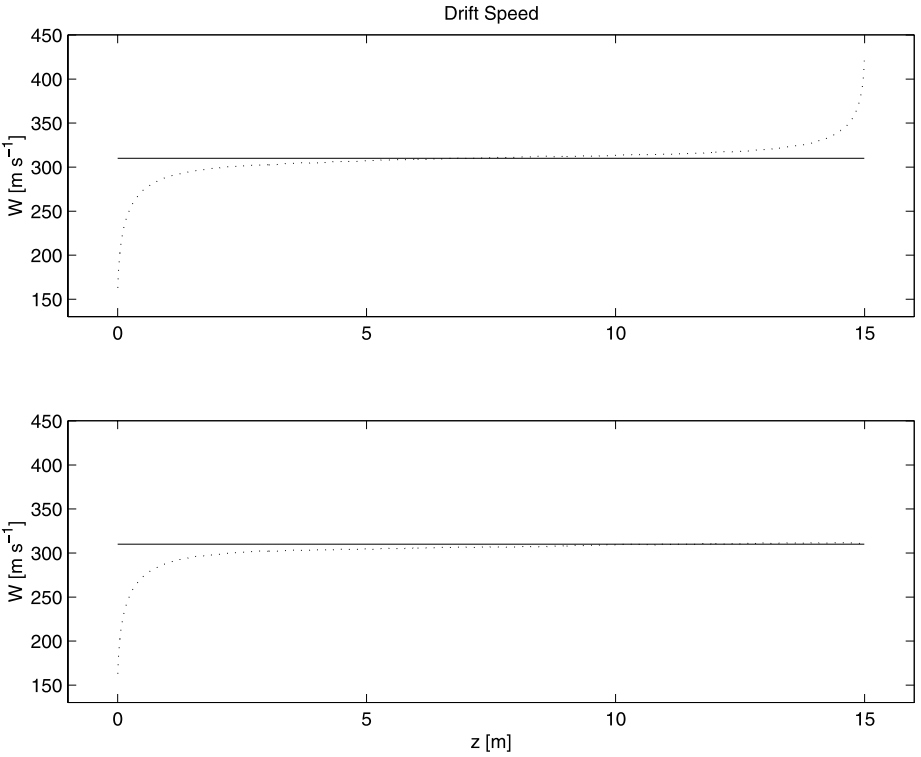

Fig. 2 Drift speed of model #3 as function of height z. For the *upper panel*, a downstream condensation plate was used. The *solid line* is the expected W_∞ obtained from (17). The *lower panel* shows the drift speed versus height when using a drifting Maxwellian as outer boundary condition, characterized by $\{n_\infty,\ T_\infty,\ W_\infty\}$ as determined by (16)–(20)

Table 2 Near-surface vapor properties. These numbers are valid 5 mm ($\sim 0.3\lambda$) above the surface. The number density n [10^{19} molec m^{-3}], the temperatures $T_{\mathrm{x,\,y,\,z}}$ (see (4)), the translational temperature T_{tr}, rotational temperature T_{rot} and overall temperature T_{ov} (all in [K]) and the drift speed W [m s^{-1}] are given. The condensing backflux B_{cond} is given in [%] of $\dot{m}_{\mathrm{prod}}$, and p_{tot} [mPa] is the pressure acting on the surface due to outgassing, molecular scattering and condensation

Case	n	T_{x}, T_{y}	T_{z}	T_{tr}	T_{rot}	T_{ov}	W	B_{cond}	p_{tot}
1	0.596	178.8	123.5	160.3	186.5	173.4	150	11.9	14.1
2	1.327	182.1	129.1	164.4	190.6	177.5	156	11.5	33.1
3	2.743	184.7	135.9	168.5	194.5	181.5	163	11.0	72.7
4	2.052	190.8	129.9	170.5	194.9	182.7	151	11.9	50.5
5	3.933	178.7	142.8	166.7	193.5	180.1	177	9.9	113.3
6	5.085	187.1	143.5	172.4	197.6	185.0	171	10.5	143.1
7	7.926	189.3	151.1	176.5	200.8	188.7	178	10.1	235.2

re-distribution from rotational energy to translational energy taken place. As seen in the lower panel of Fig. 3 this re-distribution proceeds rapidly throughout the Knudsen layer.

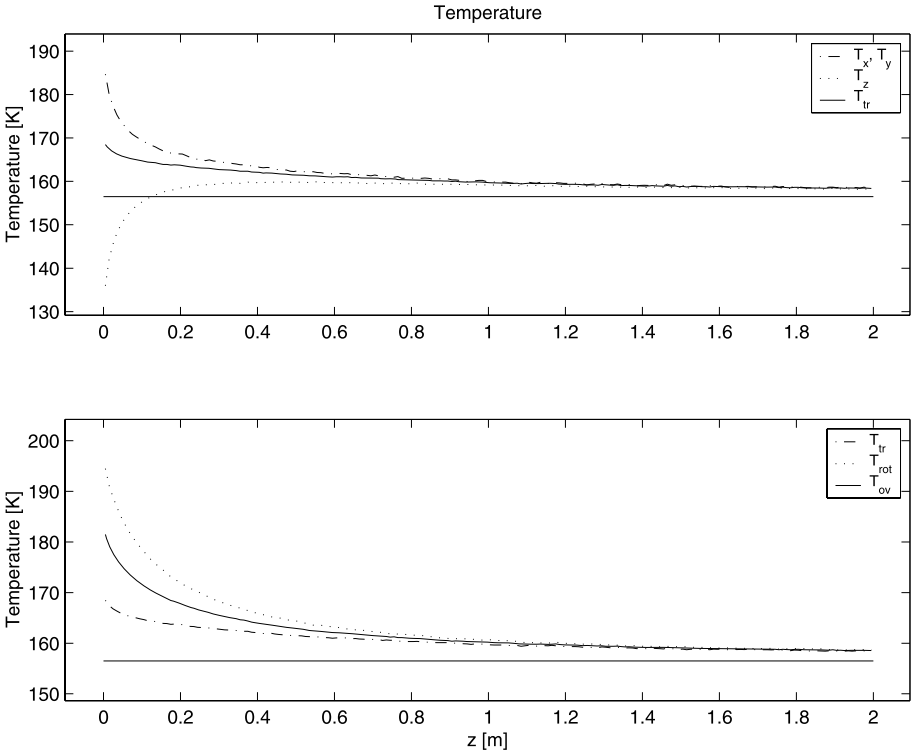

Fig. 3 Temperature for model #3, within 2 m from the surface. The *upper panel* shows the components $T_x = T_y$, T_z and the translational temperature T_{tr}. The *lower panel* shows the translational and rotational (T_{rot}) temperatures, as well as the overall temperature T_{ov}. The *solid straight lines* indicate the downstream equilibrium temperature T_∞

Note that the overall temperatures in Table 2 represent the *microscopic temperature jumps*. As can be seen, the drift speed is rather low ($150 \lesssim W \lesssim 180\ \mathrm{m\,s^{-1}}$) near the surface, but increases with height (see Fig. 2). This is due to a redistribution of energy from *random motion* to *bulk motion*. The reduction of random motion automatically leads to a reduction in temperature, why T_{ov} is falling in Fig. 3. Note that the backfluxes in Table 2 are substantially lower than the $\sim 18\%$ backflux predicted by Anisimov (1968) and Ytrehus (1977). This is because Table 2 only shows the fraction of the backflux actually *recondensing*. Finally, it is worth to note the pressure acting on the surface due to outgassing, which is not even amounting to one Pascal!

Table 3 shows the conditions near the outer boundary, where the vapor is close to equilibrium. Here, the temperature T_∞ (compared with T_s) represents the *macroscopic temperature jump*. Notice that the drift speeds roughly have doubled, compared to the near-surface values. Of course, due to isentropic expansion beyond the Knudsen layer, the gas velocities at very large distances from the nucleus will be substantially higher than the values around $310\ \mathrm{m\,s^{-1}}$ see here. The downstream backflux is around 5%, which is enough to cause, e.g., the substantial difference between the two versions of model #3 seen in the upper and lower panels of Figs. 1 and 2. Finally, note that the downstream Mach number is extremely close to (but somewhat smaller than) unity, just as expected.

Table 3 Downstream vapor properties. The downstream number density n_∞, temperature T_∞ and drift speed W_∞ are given in units of $[10^{19}$ molec $\mathrm{m}^{-3}]$, [K], and $[\mathrm{m\,s}^{-1}]$, respectively. The backflux at the *exterior* boundary is given as a percentage of the flux in the forward direction. The downstream Mach number, M_∞ is extremely close to unity, and in all cases on the subsonic side. The distance z_{asym} measured in [m] is the distance where divergence from local thermodynamic equilibrium *no longer is detectable*

Case	n_∞	T_∞	W_∞	B [%]	M_∞	z_{asym}
1	0.298	149.0	300	5.2	0.9909	16.0
2	0.677	152.8	306	5.1	0.9960	11.4
3	1.443	156.5	310	5.1	0.9989	8.9
4	1.005	156.3	310	5.1	0.9990	9.2
5	2.238	157.2	311	5.1	0.9997	5.4
6	2.770	160.4	314	5.1	0.9999	5.3
7	4.448	164.2	318	5.1	0.9997	6.6

Acknowledgements I thank Prof. Hans Balsiger and the SOC for inviting me to present this paper at the Workshop on the Origin and Early Evolution of Comet Nuclei, at ISSI, Bern, Switzerland, on 17–20 October, 2006. I acknowledge financial support from the Swedish National Space Board (SNSB) grant 135/06:1.

References

S.I. Anisimov, Sov. Phys. JETP **27**(1), 182 (1968)
K. Aoki, C. Cercignani, Phys. Fluids **26**(5), 1163 (1983)
M.D. Arthur, C. Cercignani, J. Appl. Math. Phys. (ZAMP) **31**, 634 (1980)
P.L. Bhatnagar, E.P. Gross, M. Krook, Phys. Rev. **94**(3), 511 (1954)
G.A. Bird, *Molecular Gas Dynamics and the Direct Simulation of Gas Flows* (Oxford University Press, London, 1994)
D.V. Bisikalo, M.Ya. Marov, V.I. Shematovich, V.S. Strel'nitskij, Adv. Space Res. **9**(3), 53 (1989)
C. Cercignani, in S.S. Fisher (ed.), Rarefied gas dynamics. Prog. Astronaut. Aeronaut. **74**, 305 (1981)
C. Cercignani, *Rarefied Gas Dynamics* (Cambridge University Press, Cambridge, 2000)
J.-F. Crifo, Astrophys. J. **445**, 470 (1995)
J.-F. Crifo, A.V. Rodionov, Icarus **129**, 72 (1997)
J.-F. Crifo, A.V. Rodionov, Planet. Space Sci. **47**, 797 (1999)
J.-F. Crifo, A.V. Rodionov, Icarus **148**, 464 (2000)
J.-F. Crifo, G.A. Lukianov, A.V. Rodionov, G.O. Khanlarov, V.V. Zakharov, Icarus **156**, 249 (2002)
J.-F. Crifo, G.A. Loukianov, A.V. Rodionov, V.V. Zakharov, Icarus **163**, 479 (2003)
B.J.R. Davidsson, P.J. Gutiérrez, Icarus **168**, 392 (2004)
B.J.R. Davidsson, P.J. Gutiérrez, Icarus **176**, 453 (2005)
B.J.R. Davidsson, P.J. Gutiérrez, Icarus **180**, 224 (2006)
B.J.R. Davidsson, Y.V. Skorov, Icarus **168**, 163 (2004)
B.J.R. Davidsson, P.J. Gutiérrez, H. Rickman, Icarus **187**, 306 (2007)
W. Greenberg, C.V.M. van der Mee, J. Appl. Math. Phys. (ZAMP) **35**, 156 (1984)
W.F. Huebner, W.J. Markiewicz, Icarus **148**, 594 (2000)
M.N. Kogan, N.K. Makashev, Fluid Dyn. **6**, 913 (1971)
S.K. Loyalka, C.E. Siewert, J.R. Thomas, J. Appl. Math. Phys. (ZAMP) **32**, 745 (1981)
R. Mager, G. Adomeit, G. Wortberg, in E.P. Muntz, D.P. Weaver, D.H. Campbell (eds.), Rarefied gas dynamics. Prog. Astronaut. Aeronaut. **117**, 460 (1989)
T. Matsushita, in J.L. Potter (ed.), Rarefied gas dynamics. Progr. Astronaut. Aeronaut. **51**, 1213 (1977)
Y.-P. Pao, Phys. Fluids **14**(2), 306 (1971a)
Y.-P. Pao, Phys. Fluids **14**(7), 1340 (1971b)
A.V. Rodionov, J.-F. Crifo, K. Szegö, J. Lagerros, M. Fulle, Planet. Space Res. **50**, 983 (2002)
P.N. Shankar, F.E. Marble, Phys. Fluids **14**(3), 510 (1971)
C.E. Siewert, J.R. Thomas, J. Appl. Math. Phys. (ZAMP) **32**, 421 (1981)
C.E. Siewert, J.R. Thomas, J. Appl. Math. Phys. (ZAMP) **33**, 202 (1982)

Y.V. Skorov, H. Rickman, Planet. Space Sci. **46**(8), 975 (1998)
T. Soga, in J.L. Potter (ed.), Rarefied gas dynamics. Prog. Astronaut. Aeronaut. **51**, 1185 (1977)
T. Soga, Phys. Fluids **25**(11), 1978 (1982)
Y. Sone, H. Sugimoto, Phys. Fluids A **5**(6), 1491 (1993)
Y. Sone, T. Ohwada, K. Aoki, Phys. Fluids A **1**(2), 363 (1989)
S.-M. Yen, T.J. Akai, in J.L. Potter (ed.), Rarefied gas dynamics. Prog. Astronaut. Aeronaut. **51**, 1175 (1977)
T. Ytrehus, in J.L. Potter (ed.), Rarefied gas dynamics. Prog. Astronaut. Aeronaut. **51**, 1197 (1977)

Section V: New Results from Observations

Morphology–Composition–Isotopes: Recent Results from Observations

R. Schulz

Originally published in the journal Space Science Reviews, Volume 138, Nos 1–4.
DOI: 10.1007/s11214-007-9237-8

Abstract This article presents some recent imaging and spectroscopic observations that led to results which are significant for understanding the properties of comet nuclei. The coma morphology and/or composition were investigated for 12 comets belonging to different dynamical classes. The data analysis showed that the coma morphology of three non-periodic comets is not consistent with the general assumption that dynamically new comets still have a relatively uniform nucleus surface and therefore do not exhibit gas and/or dust jets in their coma. The determination of carbon and nitrogen isotopic ratios revealed the same values for all comets investigated at various heliocentric distances. However, the relative abundance of the rare nitrogen isotope ^{15}N is about twice as high as in the Earth's atmosphere. Observations of comets at splitting events and during outbursts led to indications for differences between material from the nucleus surface and the interior. The monitoring of the induced outburst of 9P/Temple revealed that under non-steady state conditions the fast disintegration of species is detectable.

Keywords Comets · Coma morphology · Composition · Outbursts · Split comets

1 Introduction

It has been repeatedly suggested that the nuclei of the observable comets may be at different evolutionary stages depending on how much time they have spent in the inner solar system or, in other words, on how much they have been altered by heating through solar radiation. If this is so, a statistically relevant characterization of the nuclei of the ensemble of comets within reach for observations would provide information on their evolutionary train, which in turn will lead to clues on the conditions under which our solar system has formed and evolved. The best method for such a characterization would, of course, be to send space probes to a number of comets which are suspected, on the basis of their orbits and orbital

R. Schulz (✉)
ESA Research and Scientific Support Department, ESTEC, Postbus 299, 2200 AG Noordwijk, The Netherlands
e-mail: rschulz@esa.int

history, to be at different evolutionary stages, and analyze their nuclei in-situ in all detail. However, we can visit a comet only once in a while and therefore have to rely for the most part on what can be measured by remote sensing observations. Hence, we have to define and develop methods to determine the properties of the nucleus without seeing it. Consequently, a number of assumptions have been adopted over the years on the relation between a comet nucleus and its coma, in view to composition as well as correlation between nucleus surface and coma morphology. With increasing numbers of observed comets the validity of some of these assumptions has started to become doubtful. This paper presents and discusses some recent observational results which provide relevant new evidence that supports or refutes some assumptions which became common notion over the past three decades. The data presented and discussed in this overview only cover observations in the optical and the UV. The latest results from comet research in the infrared and sub-millimeter are covered elsewhere in these proceedings.

2 Techniques and Targets

From Earth-based telescopes the visible and near-ultraviolet spectral range (300–900 nm) is easily accessible. It is therefore not surprising that the methods for observation and analysis of data at these wavelengths have become most sophisticated and manifold. For comets this wavelengths range is used mostly to investigate the morphological, brightness and compositional evolution of coma and tail in gas and dust. As many coma gas species show strong fluorescence emission bands in the visible and ultraviolet, this spectral range is most suitable for two-dimensional monitoring of the coma in selected emission bands of neutral and ionized gas species as well as the continuum reflected by sub-micron dust grains. The observations discussed here were obtained with ground- and space-based telescopes and various instruments and techniques including coma imaging with broad-band and narrow-band filters, high-resolution spectroscopy and high-speed photon counting spectrophotometry. Each of these techniques is being used for specific investigations of certain properties of the chosen target comets. The short-term evolution of the coma brightness and morphology can be well studied by imaging observations with special cometary filters (Schleicher and Farnham 2004). The coma compositional evolution is best monitored with spectrophotometric techniques (Schulz 2005) and isotopic ratios are determined from high-resolution spectroscopy (Hutsemékers et al. 2005).

The investigations cover various comets with different dynamical characteristics, such as non-periodic comets as well as long- and short-period comets of both the Jupiter and the Halley family. Many of them were studied with various techniques at different heliocentric distances along their pre- and post-perihelion orbits in order to find clues on whether specific characteristics change as the comet moves along its orbit. In addition, when possible, comets have been studied during specific events such as outbursts and/or nucleus splitting, which provide the opportunity to characterize sub-surface material ejected under non-steady state conditions. In cases such as major outbursts or splitting events, this material may come from tens to hundreds of meters below the surface.

3 Observational Results in Steady-State Conditions

Most comets are studied while they are ejecting material under steady state conditions through the sublimation of frozen gases. This continuous ejection of gas and dust into the comet's atmosphere is usually defined as the quiescent level of the nucleus activity. As it

is directly related to the intensity of the solar radiation, it increases with decreasing heliocentric distance. The investigation and comparison of specific properties of the coma under quiescent conditions—such as morphology, dust color, dust-to-gas ratio, composition and isotopic ratios—can lead to clues about intrinsic differences between the individual comets. If such studies cover a statistically relevant sample, they enable us to reveal whether there is a relation between the physical and the dynamical properties of comets, and hence to find clues on the origin of comets.

3.1 Coma Morphology

It is generally supposed that the surface properties of a comet nucleus should be correlated with its dynamical characteristics. Specifically, there has been the hypothesis that dynamically new comets would have a relatively uniform nucleus surface whereas for periodically returning comets the surface would be more heterogeneous, being divided into active and inactive areas. From observations it seemed that new comets have a generally structureless coma, with no dust (or gas) jets and associated active regions on the nucleus surface (Sekanina 1991; Donn 1991). This concept remained a common notion for more than a decade although only a handful of dynamically new comets had been imaged and analyzed with sophisticated structural enhancement techniques, and these indeed did not show any hints of jet activity (e.g. Schulz et al. 1993). A comparative study of coma morphologies in gas and dust revealed that coma structures were present in seven of nine comets investigated (Schulz 2002). A featureless coma was found for the only dynamically new comet in the sample and surprisingly a Jupiter-family comet.

The year 2004 provided the opportunity to observe three bright, non-periodic comets in retrograde orbits, namely, C/2001 Q4 (NEAT), C/2002 T7 (LINEAR), and C/2003 K4 (LINEAR), which have been designated as dynamically new comets. All three comets were imaged with a high enough signal-to-noise ratio to allow the detailed investigation of their coma morphologies and the search for distinct features that may be superimposed on the general two-dimensional coma profile. None of them showed the expected featureless coma. Instead, all three comets displayed distinct coma features, which were very different from one comet to the next, in shape as well as in terms of the presence or non-presence of short-term variability (Schulz et al. 2005). A single, broad feature perpendicular to the sun-tail direction dominated the coma of C/2003 K4 in all filters, whereas the coma of Comet C/2002 T7 exhibited different features in blue and red filters. C/2001 Q4 showed rather complex coma morphology with clear short-term variability in coma brightness (Fig. 1). In conclusion, these dynamically new comets neither show the featureless coma nor any similarities in coma morphology that may have been expected for dynamically similar comets. If distinct coma features are produced through active areas on a rotating comet nucleus, the nuclei of these three comets would be divided already into active and passive regions, which is in contrast with the evolutionary models. However, Crifo and Rodionov (1997) demonstrated that distinct coma features could form as a result of the shape of the comet nucleus with shadowed valleys having a lower material production rate than areas that are well exposed to solar radiation. The detection of distinct coma features in these three dynamically new comets therefore indicates that more than one process can produce coma jets. Hence, the widely accepted interpretation that coma jet structures are being produced by active areas on a rotating nucleus might not be unique.

3.2 Isotopic Composition

The solar nebula grew out of material from various stellar sources that underwent different nuclear synthetic processes. Isotopic abundance ratios of the stable isotopes of the light

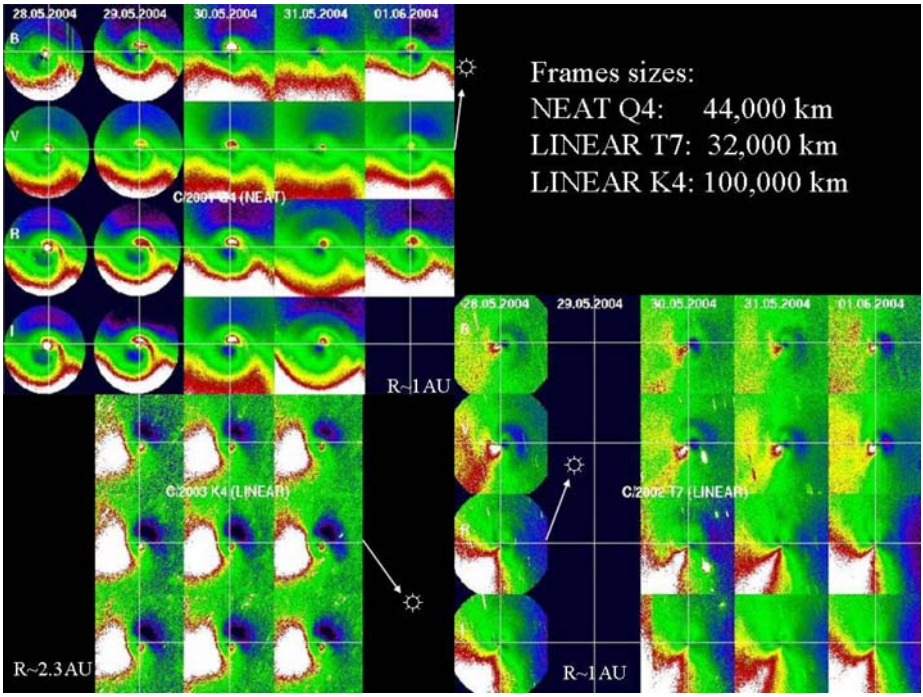

Fig. 1 Structurally enhanced images in broadband BVRI filters of comets C/2001 Q4 (NEAT), C/2002 T7 (LINEAR), and C/2003 K4 (LINEAR). The white cross marks the coma center in each image. The projected sun direction is indicated

elements in small solar system bodies are therefore excellently suited to probe the origin of solar system matter. In particular comets are believed to have preserved unprocessed material of the solar nebula from the time of the planetary system's formation. Therefore in spite of the great difficulties encountered, the determination of isotopic ratios in comets has been attempted for almost half a century. They can be measured either via in-situ mass spectroscopy obtained from a spacecraft, or from the ground by means of high-resolution spectroscopy, whereby the intensities of spectral features of various isotopic species are compared. For Carbon and Nitrogen the observed molecules are CN and C_2 in the optical and HCN in the sub-millimeter range. Such measurements are very difficult mainly because of the weakness of the emissions of the rare species. Therefore high-resolution spectroscopy was for a long time possible only on very bright comets close to perihelion. This changed when efficient high-resolution spectrographs became available on large telescopes, such as the Ultraviolet and Visual Echelle Spectrograph (UVES) at the ESO Very Large Telescope (VLT). Table 1 summarizes the ground-based measurements of isotopic ratios of carbon and nitrogen in the gas coma that were published before the first UVES observations in 2002. While the $^{12}C/^{13}C$ ratio had been determined in a number of comets by various methods, the $^{14}N/^{15}N$ ratio had been measured for only one comet, C/1995 O1 (Hale–Bopp), using spectra of the HCN band at sub-millimeter range. For both, the carbon and the nitrogen isotopic ratio, the telluric values had been confirmed in principle, although in some cases with rather large uncertainties.

In 2002, the first observation of a comet with the UVES spectrograph led to the clear detection of $^{12}C^{15}N$ emission features of the B-X $(0, 0)$ band at 388 nm, and hence per-

Table 1 Carbon and Nitrogen isotopic ratios derived from gas coma measurements before 2002

$^{12}C/^{13}C$	Species	Comet	Reference
70 ± 15	C_2	C/1963 A1 Ikeya	Stawikowski and Greenstein (1964)
100 ± 20	C_2	C/1969 T1 Tago–Sato–Kosaka	Owen (1973)
$115^{+30}{}_{-20}$	C_2	C/1973 E1 Kohoutek	Danks et al. (1974)
$135^{+65}{}_{-45}$	C_2	C/1973 E1 Kohoutek	Danks et al. (1974)
$100^{+20}{}_{-30}$	C_2	C/1975 N1 Kobayashi–Berger–Milon	Vanysek (1977)
95 ± 12	CN	1P/Halley	Kleine et al. (1995)
111 ± 12	HCN	C/1995 O1 Hale–Bopp	Jewitt et al. (1997)
90 ± 15	HCN	C/1995 O1 Hale–Bopp	Lis et al. (1997a)
109 ± 22	HCN	C/1995 O1 Hale–Bopp	Ziurys et al. (1999)
34 ± 12	HCN	C/1996 B2 Hyakutake	Lis et al. (1997b)
89		telluric value	Anders and Grevesse (1989)
$^{14}N/^{15}N$			
323 ± 46	HCN	C/1995 O1 Hale–Bopp	Jewitt et al. (1997)
330 ± 98	HCN	C/1995 O1 Hale–Bopp	Ziurys et al. (1999)
272		Telluric value	Anders and Grevesse (1989)

Table 2 Carbon and Nitrogen isotopic ratios derived in the CN gas coma since 2002

Comet	Type	R_h (AU)	$^{12}C/^{13}C$	$^{14}N/^{15}N$	Reference
122P/de Vico	HT	0.66	90 ± 10	140 ± 20	Jehin et al. (2004a)
C/1995 O1 (Hale–Bopp)	OC	2.73	80 ± 20	140 ± 30	Manfroid et al. (2005)
		0.93	95 ± 40	140 ± 45	Manfroid et al. (2005)
		0.92	90 ± 30	160 ± 40	Manfroid et al. (2005)
C/1999 S4 (LINEAR)	OC	0.88	100 ± 30	150 ± 40	Hutsemékers et al. (2005)
C/1999 T1 (McNaught–Hartley)	OC	1.35	75 ± 15	120 ± 15	Jehin et al. (2004b)
C/2000 WM1 (LINEAR)	OC	1.21	115 ± 20	140 ± 30	Arpigny et al. (2003)
153P/Ikeya–Zhang	OC	0.92	90 ± 25	170 ± 50	Jehin et al. (2004a)
C/2002 V1 (NEAT)	OC	1.20	100 ± 15	140 ± 15	Jehin et al. (2004b)
		1.01	100 ± 15	140 ± 15	Jehin et al. (2004b)
C/2002 X5 (Kudo–Fujikawa)	OC	0.71	90 ± 15	140 ± 15	Jehin et al. (2004b)
		1.09	90 ± 15	140 ± 15	Jehin et al. (2004b)
C/2002 Y1 (Juels–Holvorcem)	OC	1.15	90 ± 20	140 ± 20	Jehin et al. (2004b)
C/2001 Q4 (NEAT)	OC	0.98	90 ± 15	135 ± 20	Manfroid et al. (2005)
		3.70	70 ± 30	130 ± 40	Manfroid et al. (2005)
C/2003 K4 (LINEAR)	OC	1.21	90 ± 15	135 ± 20	Manfroid et al. (2005)
		2.61	85 ± 20	150 ± 35	Manfroid et al. (2005)
88P/Howell	JF	1.41	90 ± 10	140 ± 15	Hutsemékers et al. (2005)
9P/Tempel 1 (pre-impact)	JF	1.51	95 ± 15	145 ± 20	Jehin et al. (2006)
(impact + 1–4 hours)		1.51	95 ± 15	165 ± 30	Jehin et al. (2006)

mitted not only determination of the $^{12}C/^{13}C$ ratio, but also the $^{14}N/^{15}N$ isotopic ratio in this molecule (Arpigny et al. 2003). The determination of the $^{14}N/^{15}N$ ratio is of particular interest because, contrary to the $^{12}C/^{13}C$ ratio, no measurement is available in the Sun

and different values are found among the different bodies of the solar system. By now, the $^{12}C/^{13}C$ and $^{14}N/^{15}N$ ratios have been determined from high-resolution spectroscopy of the CN coma in more than a dozen comets of different dynamical classes and at different heliocentric distances (e.g. Jehin et al. 2004a; Manfroid et al. 2005; Hutsemékers et al. 2005; Jehin et al. 2006; Schulz et al. 2007). All these comets have the same $^{12}C/^{13}C$ and $^{14}N/^{15}N$ ratios within the error margin (Table 2). The average $^{12}C/^{13}C$ ratio of 91 ± 21 is consistent with the telluric value, but the average $^{14}N/^{15}N$ ratio of 141 ± 29 is not. In fact the $^{14}N/^{15}N$ isotopic ratio determined from the CN molecule in comets is almost a factor of 2 lower than the telluric value (272). The $^{14}N/^{15}N$ ratio determined in HCN on the other hand appears to be consistent with or even slightly higher than the telluric value. $^{14}N/^{15}N$ ratios of 323 ± 46 and 330 ± 98 have been determined from sub-millimeter measurements of the HCN molecule in comet C/1995 O1 (Hale–Bopp) by two independent teams (Jewitt et al. 1997; Ziurys et al. 1999). So at least for comet C/1995 O1 (Hale–Bopp) the rare isotope ^{15}N seems to be more than twice as abundant in CN as in HCN, which is most puzzling, because HCN is usually considered to be a major parent molecule of CN. Unfortunately, no measurements of the $^{14}N/^{15}N$ ratio in HCN exist for other comets. Attempts have been made to derive this ratio in comets C/2001 Q4 (NEAT), C/2002 T7 (LINEAR) and 9P/Tempel from sub-millimeter observations of the HCN band obtained with the James Clark Maxwell Telescope on Hawaii, but $HC^{15}N$ was not detected (see Coulson et al. 2005, 2007 for a summary of the 9P/Tempel observations).

The isotopic ratios in comets help to constrain the temperature and pressure conditions in the early solar nebula if they are representative remnants of the proto-solar nebula. The values of the $^{14}N/^{15}N$ ratio derived from CN in 13 comets at different heliocentric distances are remarkably similar, especially considering that this ratio varies strongly among the different solar system objects. Figure 2 shows the $^{14}N/^{15}N$ ratio as derived for various solar system objects as well as the interstellar medium and the Large Magellanic Cloud. The $^{14}N/^{15}N$ ratio in the atmosphere of Jupiter (~ 450) was proposed to be representative of the proto-solar value (Owen et al. 2001; Fouchet et al. 2004). If this is the case, the $^{14}N/^{15}N$ ratio in comets cannot be explained in a straightforward way, but rather indicates that more than one $^{14}N/^{15}N$ isotope ratio may have existed in the proto-solar nebula characterizing different components. Furthermore the very different ratios for CN and HCN present additional evidence for the long-suspected existence of at least one additional parent of CN.

4 Results from Outbursts and Split Comets

Being much less processed by solar radiation and cosmic rays, the interior of a comet nucleus is believed to be different from the surface crust and the material sublimating thereof. Direct measurements of the interior of a kilometer-sized body are, however, very difficult to obtain. However, in principle we have opportunity to get a glimpse into the interior of a comet nucleus by means of remote sensing observations every time a comet splits or has a major outburst. These events are not as rare as was assumed a few decades ago, when telescope sizes and observation techniques were more limited. In fact about 20 split comets have been reported over the past 25 years (Boehnhardt 2005) and many more outbursts. Unfortunately, the fresh material released immediately after an outburst or nucleus splitting would mix within a short time with that being released from what was the original surface. Therefore, to be able to unambiguously distinguish the fresh interior material from that sublimating from the upper surface layers, observations have to be obtained before and within a few hours after the outburst or splitting event, which is a problem, because usually nobody

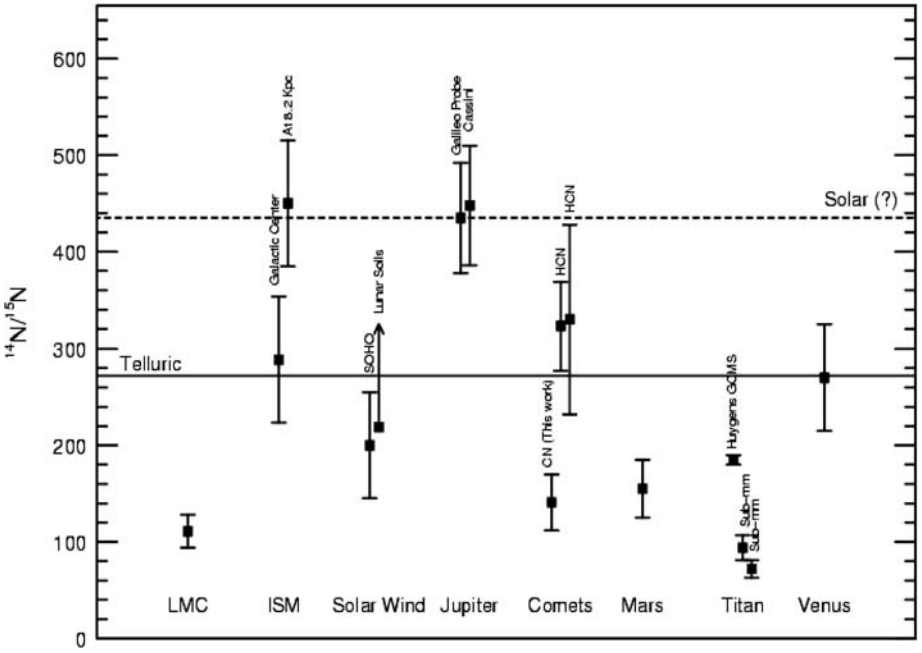

Fig. 2 LMC = Large Magellanic Cloud HC15N; ISM = Interstellar Medium HCN; Solar wind from SOHO and upper layers of lunar soils; Jupiter from Galileo Probe and Cassini/CIRS; Comets CN, HCN; Mars; Titan Huygens GCMS, Sub-mm HCN; Venus

knows in advance that an outburst or a nucleus splitting would occur. Nevertheless in a few cases it was possible to compare the coma properties during the early phases of gas and dust expansion after outburst or splitting events with the pre-event quiescent properties. For comet C/1999 S4 (LINEAR), for instance, evidence was found for a change in the dust size distribution, i.e. an increased abundance of smaller dust particles (Schulz and Stüwe 2002) when it was, by lucky coincidence, observed a few hours after its probably initial break-up that led to the complete disintegration of this comet a few weeks later (Weaver et al. 2001).

An increased abundance of small dust particles in fresh comet material was also found as a result of the observation of the only comet nucleus outburst that was ever known in advance, the outburst of comet 9P/Tempel induced by the Deep Impact event (A'Hearn et al. 2005). The comet was monitored with the XMM-Newton Observatory 15.5 hours before and again during and until 17.3 hours after the impact with both the X-ray instruments and the Optical Monitor (Schulz et al. 2006). These observations led to the discovery of rapidly disintegrating small icy grains shortly after the impact that proved the long-standing assumption that the water in comets does not exclusively sublimate directly from the comet nucleus, but is also ejected in form of small icy grains (Huebner and Weigert 1966). Figure 3 shows the two-dimensional evolution of the coma observed as a result of the impact. Three filters were used reflecting sub-micron sized grains in the visible (B filter) and in the UV, as well as covering the OH emission band at 308 nm. Before impact (right-hand side images) the comet was detected in the B and the OH filter, whereas there is no detection in UV continuum. After impact the coma is clearly detected in all three filters. In the B and OH filter it remains visible for the next eight hours until the end of the observing run, whereas in the UV continuum filter the comet was clearly detected only up to about two hours after the

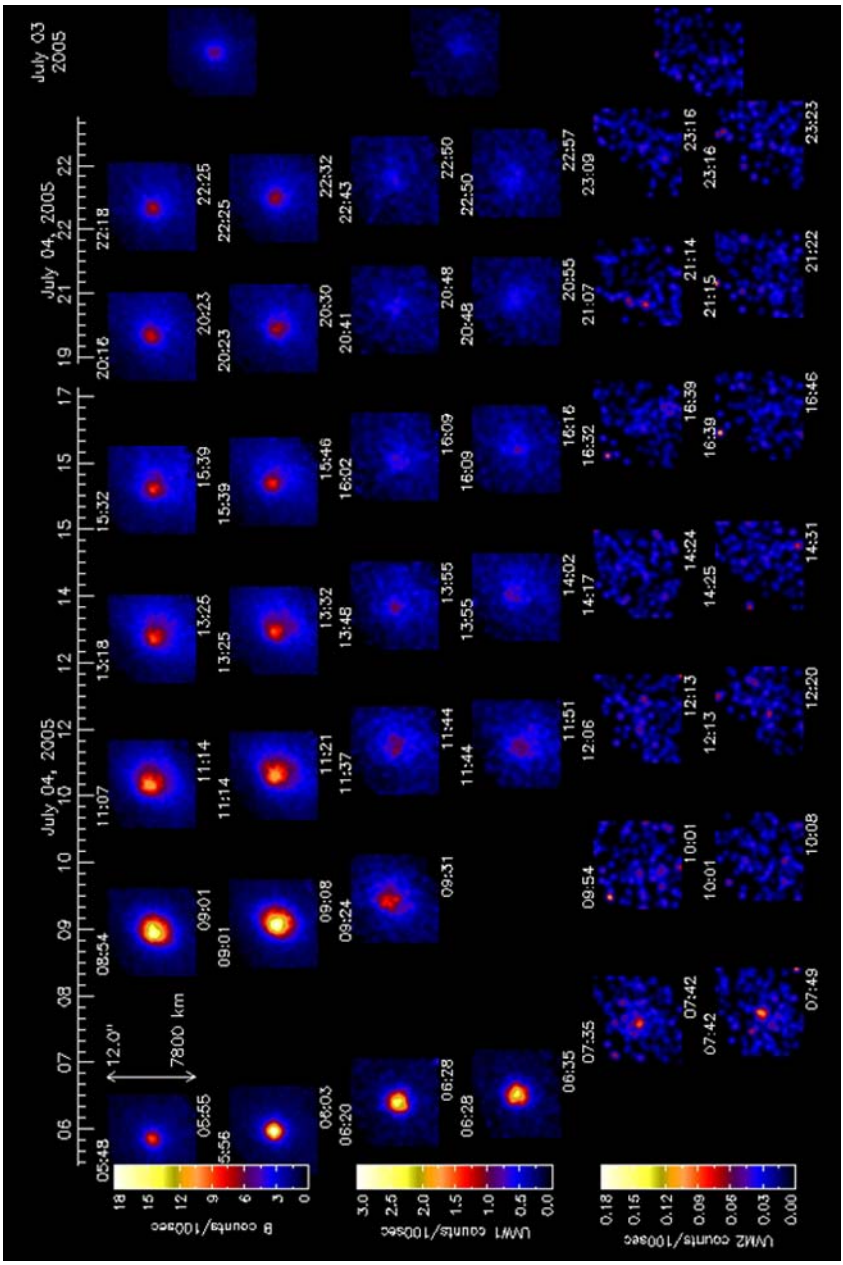

Fig. 3 The two-dimensional coma evolution of comet 9P/Tempel observed after the Deep Impact event (impact time: July 4, 2005, at 5:52 UT) in three filters. B: broad-band blue filter; UVM1: OH filter; UVM2: UV continuum filter. A pre- impact observation in each filter is added on right hand side (see text for details)

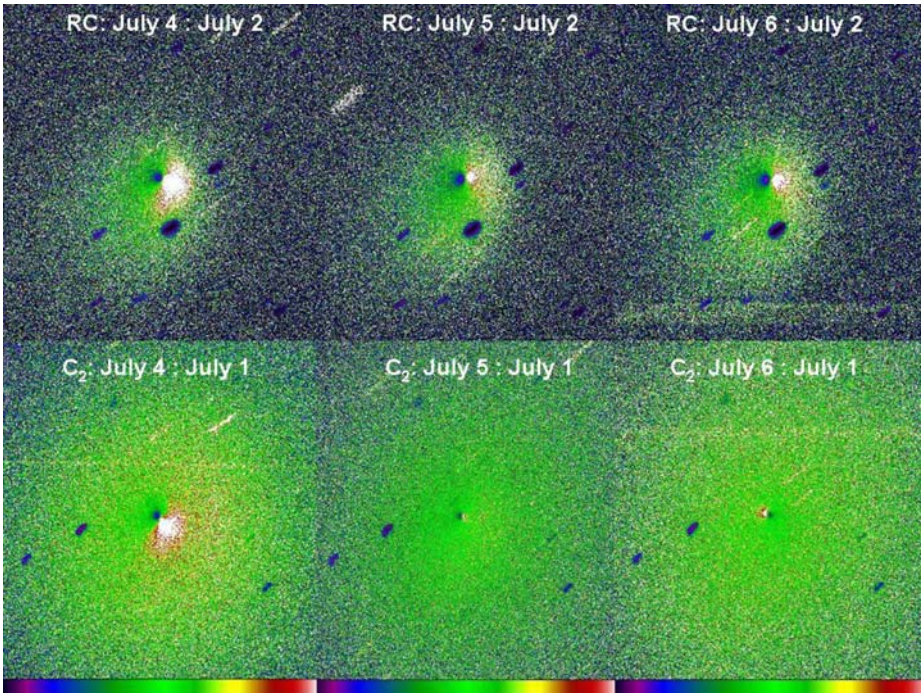

Fig. 4 Quotient images of comet 9P/Tempel in red continuum and C_2. Images obtained on three consecutive nights after the impact are divided by a pre-impact image taken with the same filter. A jet structure is visible on July 4, about 15 hours after the impact in the continuum as well as in the C_2 filter. In the dust coma the jet structure persists over July 5–6, whereas in the C_2 it is visible only on July 4. Assuming a gas expansion velocity of 1 km/s the C_2 has left the field of view of the image within 18.5 hours, hence the C_2 produced on July 4 and visible as a jet structure has left the field of view on July 5 and no further C_2 was produced in the form of a jet. Image scale: 133000 km

impact, after which time the icy grains had disintegrated (Schulz et al. 2006). After the outburst the comet was also detected by the X-ray instrument, EPIC, onboard XMM-Newton, while there was no detection before impact. This indicates the release of very small dust particles, which scatter solar X-rays. Hence, the induced outburst of comet 9P/Tempel was in this regard similar to a natural one of comet C/1995 O1 (Hale–Bopp) in September 1996 which had produced a dust-rich cloud that was clearly correlated with a ten-fold increase of the X-ray luminosity in this comet (Schulz et al. 2000).

Additional observations of comet 9P/Tempel—obtained from the ground at the 1-m ESA Optical ground Station telescope using special narrow-band comet filters—show that a jet-like coma structure was produced as a result of the impact. It shows that the feature remains visible in the dust coma for several days, whereas in the C_2 coma it is visible only on the image taken 15.8 hours after the impact and has vanished when the coma was observed again in the following night. Figure 4 shows the evolution of the structure in red continuum and C_2 on July 4–6. The observational evidence strongly supports that the C_2 in the feature observed on July 4, 2005, was produced from fresh dust particles released by the outburst and forming an extended source for the production of the C_2 radical. This indicates that the disintegration of C_2-bearing dust species can be directly observed during the non-steady state conditions present immediately after outbursts and/or nucleus splitting.

5 Discussion and Conclusions

In spite of the obvious advantages of space missions to comets that provide knowledge gathered from close-up observations and in-situ measurements, remote-sensing observations from Earth and Earth orbit continue to make important contributions to our understanding of comets. Major technical advances, such as increased telescope sizes, sophisticated detectors for multi-wavelengths coverage and computer processing capabilities have helped ensure that the biggest advantages of remote-sensing observations remain competitive, namely, the possibility of studying a statistically relevant sample of comets and the availability of equipment on short notice if key opportunities arise to advance our knowledge. Investigations of coma morphology have started becoming statistically relevant and show that the connection between distinct coma features and the properties of the comet nucleus surface may not be as straightforward as originally assumed (hoped for). The anomalous nitrogen isotopic abundance ratio certainly came as a great surprise and needs to be explained in the context of solar system formation as a whole. Observations of comet activity under non-steady state conditions have proven to be most promising in testing certain hypothesis concerning compositional differences of surface and subsurface material as well as the existence of short-lived species, such as icy grains.

The observations summarized in this paper provide only a glimpse into the possibilities that open up when increasing the amount of dedicated comet monitoring observations from ground by sophisticated remote-sensing methods. For the future it will be crucial to continue such observations on a large scale, but particularly for space mission targets, in order to establish the proper relation between the results that will be furnished by the space mission and the data that can be obtained by remote observations of the target comet from Earth, and to transfer what we learn to other comets.

Furthermore, the effort to establish a statistically relevant classification scheme for comets needs to be continued, because only that will allow us to understand their diversity and similarities. It should not be based only on coma abundances, but also take into account the information available from the analysis of coma morphology. Both can be extracted from remote-sensing observations at various wavelengths. Most of the necessary observations are rather uncomplicated and can therefore be gathered for a great number of comets including the targets of the forthcoming space missions. For the latter, in-situ measurements at least of the coma composition as well as images of the nucleus will also exist. Thus, these comets can serve as a reference for the interpretation and modeling of the physical and chemical processes relevant for the formation of a comet coma.

References

M.F. A'Hearn, M.J.S. Belton, A. Delamere, J. Kissel, K.P. Klaasen, L.A. McFadden, K.J. Meech, H.J. Melosh, P.H. Schultz, J.M. Sunshine, P.C. Thomas, J. Veverka, D.K. Yeomans, M.W. Baca, I. Busko, C.J. Crockett, S.M. Collins, M. Desnoyer, C.A. Eberhardy, C.M. Ernst, T.L. Farnham, L. Feaga, O. Groussin, D. Hampton, S.I. Ipatov, J.-Y. Li, D. Lindler, C.M. Lisse, N. Mastrodemos, W.M. Owen Jr., J.E. Richardson, D.D. Wellnitz, R.L. White, Science **310**, 258–264 (2005)

E. Anders, N. Grevesse, Geochim. Cosmochim. Acta **53**, 197–214 (1989)

C. Arpigny, E. Jehin, J. Manfroid, D. Hutsemékers, R. Schulz, J.A. Stüwe, J.-M. Zucconi, I. Ilyin, Science **301**, 1522–1524 (2003)

H. Boehnhardt, in *Comets II*, ed. by M.C. Festou, H.U. Keller, H.A. Weaver (University of Arizona Press, Tucson, 2005), pp. 301–316

I.M. Coulson, H.M. Butner, G. Moriarty-Schieven, L.M. Woodney, S.B. Charnley, S.D. Rodgers, J. Stüwe, R. Schulz, K. Meech, Y. Fernandez, P. Vora, Deep Impact: submillimetre spectrocopic HCN observations of 9P/tempel-1 from JCMT. *Protostars and Planets*, vol. V, Hawaii, USA, #8524, 2005

I.M. Coulson, H.M. Butner, G. Moriarty-Schieven, L.M. Woodney, S.B. Charnley, S.D. Rodgers, J. Stüwe, R. Schulz, K. Meech, Y. Fernandez, P. Vora, in *Proc. Deep Impact Workshop* (Brussels, 2007 in press)
J.F. Crifo, A.V. Rodionov, Icarus **129**, 72–93 (1997)
A.C. Danks, D.L. Lambert, C. Arpigny, Astrophys. J. **194**, 745–751 (1974)
B. Donn, in *Comets in the Post-Halley Era*, vol. 1, ed. by R.L. Newburn, M. Neugebauer, J. Rahe (Kluwer Academic, Dordrecht, 1991), pp. 335–359
T. Fouchet, P.G.J. Irwin, P. Parrish, S.B. Calcutt, F.W. Taylor, C.A. Nixon, T. Owen, Icarus **172**, 50–58 (2004)
W.F. Huebner, A. Weigert, Z. Astrophys. **64**, 185–201 (1966)
D. Hutsemékers, J. Manfroid, E. Jehin, C. Arpigny, A. Cochran, R. Schulz, J.A. Stüwe, J.-M. Zucconi, Astron. Astrophys. **440**, L21–L24 (2005)
E. Jehin, J. Manfroid, A.L. Cochran, C. Arpigny, J.-M. Zucconi, D. Hutsemékers, W.D. Cochran, M. Endl, R. Schulz, Astrophys. J. **613**, L161–L164 (2004a)
E. Jehin, J. Manfroid, A.L. Cochran, C. Arpigny, D. Hutsemékers, J.-M. Zucconi, R. Schulz, The nitrogen isotope ratio $^{14}N/^{15}N$ ratio in Oort cloud comets. Presented at the 35th COSPAR Scientific Assembly, Paris, France, 18–25 July 2004, Abstract (2004b), p. 4342
E. Jehin, J. Manfroid, D. Hutsemékers, A. Cochran, C. Arpigny, W.M. Jackson, H. Rauer, R. Schulz, J.-M. Zucconi, Astrophys. J. **641**, L145–L148 (2006)
D.C. Jewitt, H.E. Matthews, T. Owen, R. Meier, Science **278**, 90–93 (1997)
M. Kleine, S. Wyckoff, P.A. Wehinger, B.A. Peterson, Astrophys. J. **439**, 1021–1033 (1995)
D.C. Lis, D.M. Mehringer, D. Benford, M. Gardner, T.G. Phillips, D. Bockelée-Morvan, N. Biver, P. Colom, J. Crovisier, D. Despois, H. Rauer, Earth Moon Planets **78**, 13–20 (1997a)
D.C. Lis, J. Keene, K. Young, T.G. Phillips, D. Bockelée-Morvan, J. Crovisier, P. Schilke, P.F. Goldsmith, E.A. Bergin, Icarus **130**, 355–372 (1997b)
J. Manfroid, E. Jehin, D. Hutsemékers, A. Cochran, J.-M. Zucconi, C. Arpigny, R. Schulz, J.A. Stüwe, Astron. Astrophys. **432**, L5–L8 (2005)
T. Owen, Astrophys. J. **184**, 33–44 (1973)
T. Owen, P.R. Mahaffy, H.B. Niemann, S. Atreya, M. Wong, Astrophys. J. **553**, L77–L79 (2001)
D.G. Schleicher, T.L. Farnham, in *Comets II*, ed. by M.C. Festou, H.U. Keller, H.A. Weaver (University of Arizona Press, Tucson, 2004), pp. 449–469
R. Schulz, ESA-SP **500**, 553–556 (2002)
R. Schulz, in *Asteroids, Comet, Meteors*, ed. by D. Lazzaro, S. Ferraz-Mello, J.A. Fernández. IAU Symp. and Coll. Ser. (Cambridge University Press, Cambridge, 2005), pp. 413–423
R. Schulz, J.A. Stüwe, Earth Moon Planets **90**, 195–203 (2002)
R. Schulz, M.F. A'Hearn, P.V. Birch, C. Bowers, M. Kempin, R. Martin, Icarus **104**, 206–225 (1993)
R. Schulz, J.A. Stüwe, G.P. Tozzi, A. Owens, Astron. Astrophys. **361**, 359–368 (2000)
R. Schulz, J.A. Stüwe, C. Erd, Earth Moon Planets **97**, 387–397 (2005)
R. Schulz, A. Owens, P.M. Rodriguez-Pascual, D. Lumb, C. Erd, J.A. Stüwe, Astron. Astrophys. **448**(3), L53–L56 (2006)
R. Schulz, E. Jehin, J. Manfroid, D. Hutsemékers, A. Cochran, J.-M. Zucconi, C. Arpigny, Isotopic abundances in the CN coma of comets—10 years of measurements. AOGS 4th Annual Meeting, Bangkok, 2007
Z. Sekanina, Astron. J. **100**, 1293–1314 (1991)
A. Stawikowski, J.L. Greenstein, Astrophys. J. **140**, 1280–1291 (1964)
V. Vanysek, in *Comets, Asteroids, Meteorites: Interrelations, Evolution and Origins*. Proceedings of the Thirty-Ninth International Colloquium, Lyons, France, August 17–20, 1976, A78-19751 06-88 (University of Toledo, Toledo, 1977), pp. 499–503
H.A. Weaver, Z. Sekanina, I. Toth, C.E. Delahodde, O.R. Hainault, P.L. Lamy, J.M. Bauer, L. Jorda, M.S.W. Keesey, C.M. Lisse, B.G. Marsden, K.J. Meech, G.P. Tozzi, R. West, Science **292**, 1329–1333 (2001)
L.M. Ziurys, C. Savage, M.A. Brewster, A.J. Apponi, T.C. Pesch, S. Wyckoff, Astrophys. J. **527**, L67–71 (1999)

Deep Impact and the Origin and Evolution of Cometary Nuclei

Michael F. A'Hearn

Originally published in the journal Space Science Reviews, Volume 138, Nos 1–4.
DOI: 10.1007/s11214-008-9350-3

Abstract The Deep Impact mission revealed many properties of comet Tempel 1, a typical comet from the Jupiter family in so far as any comet can be considered typical. In addition to the properties revealed by the impact itself, numerous properties were also discovered from observations prior to the impact just because they were the types of observations that had never been made before. The impact showed that the cometary nucleus was very weak at scales from the impactor diameter (∼1 m) to the crater diameter (∼100 m) and suggested that the strength was low at much smaller scales as well. The impact also showed that the cometary nucleus is extremely porous and that the ice was close to the surface but below a devolatilized layer with thickness of order the impactor diameter. The ambient observations showed a huge range of topography, implying ubiquitous layering on many spatial scales, frequent (more than once a week) natural outbursts, many of them correlated with rotational phase, a nuclear surface with many features that are best interpreted as impact craters, and clear chemical heterogeneity in the outgassing from the nucleus.

Keywords Comets · Space missions · Nuclei · Chemical composition

1 Introduction

Deep Impact consisted of two spacecraft, a flyby and an impactor, which were launched on 12 Jan 2005 and which took just under 6 months to travel to comet 9P/Tempel 1. Somewhat over one day before impact, the two spacecraft were on a trajectory as close to impacting the comet's nucleus as was possible at that range (in retrospect, they would have missed by about 1 km) and from that point until well after the flyby passed the nucleus all actions were conducted autonomously. The two spacecraft separated from one another on 3 July 2005 and from that point each carried out its own navigation and operations. In the several hours before impact, which occurred at 5:52 UTC (as seen from Earth) on 4 July 2005, the impactor made 3 maneuvers to ensure that it would impact a sunlit part of the nucleus visible

M.F. A'Hearn (✉)
Department of Astronomy, University of Maryland, College Park, MD 20742-2421, USA
e-mail: ma@astro.umd.edu

from the flyby spacecraft. Impact velocity was 10.3 km s^{-1}. Meanwhile, the flyby spacecraft diverted by several meters per second to fly past the nucleus with a closest approach (CA) distance of ~500 km. The flyby spacecraft also fired thrusters to change its orbital speed by 100 m s^{-1}, a large maneuver by normal interplanetary standards. This provided a window of 800 seconds from the time of impact until the last opportunity for the flyby spacecraft to view the impact site. Images from the impactor were transmitted to the flyby, which relayed them to Earth. The flyby spacecraft itself turned back to look at the nucleus after flying past and continued to make observations for two days. Further details on the encounter were presented by A'Hearn et al. (2005).

At the time of writing this article, the analyses based on work carried out in the first year, both by the Deep Impact team and by very many collaborators, have been published. Those still working on data analyses are either doing more detailed modeling or searching for new phenomena in the data or refining the existing analyses.

2 The Impact

The mass of the impactor, including roughly 7 kg of unused hydrazine (N_2H_4) fuel, was 372 kg. The mass was nearly 50% copper, most of that in a spherical cap at the front of the impactor, in a structure that was hollowed out in successive layers much like a light-weighted telescope mirror in order to reduce the bulk density by nearly a factor 2 compared to that of bulk copper. With the impact velocity of 10.3 km s^{-1}, the energy delivered was just under 20 GJoule or 5 tons of TNT. This is a million times less than the energy of the well known Tunguska airburst and within the range of impact energies delivered to the moon during the Apollo program (up to 40 GJoule).

Based on the shape model for the nucleus deduced after the encounter, the impact trajectory was very roughly 30° from horizontal, an angle that was not planned (it could not be planned because of lack of knowledge of the shape of the nucleus) but which, in retrospect, was almost ideal for our experiment. The impact occurred in stratigraphically low terrain which contains a variety of features, including two large (200–300 m diameter) features that appear to be residual impact craters as well as bounding scarps, hills, and trenches.

2.1 Self-Luminous Flash

The initial observation of the impact from the flyby was a brief (<120 msec), relatively faint flash uprange of the impact point. This was presumably hot material expelled up the entry tunnel. This flash was immediately followed by a much brighter flash located more or less at the impact site, which evolved into a rapidly moving (5 km s^{-1} projected on the sky) downrange plume. All these phenomena were entirely self-luminous but were not observable from Earth or from other spaceborne platforms.

The luminous efficiency was extremely low, estimated at 7×10^{-5} or up to a factor 2 larger when allowing for saturated pixels. Studying the strong dependence of luminosity on porosity of the target, Ernst and Schultz (2007) conclude that the measured luminous efficiency suggests a porosity >75% in the surface layers of the comet. If this is coupled with our global density of 0.4 g cm^{-3} (see below), we get a density of <1.6 g cm^{-3} for the solid material of the surface layers, a quite reasonable number for a mix of ice, carbonaceous material, and silicates.

The long (>100 ms) duration of the flash, particularly in the downrange plume, requires the presence of some hard material such as silicates in the mix of materials. On the other

hand, Sunshine et al. (2007) show from spectroscopy that volatiles (water ice) are clearly present in the downrange plume and thus reasonably near the surface. The water ice is not present in the uprange rays, which must come from the topmost layer with thickness of order the size of the impactor (Schultz et al. 2007). Thus the ice is depleted very close to the surface but clearly present a meter or so down.

A very simplified model of the downrange, hot plume (Melosh 2006) indicates that the mass was of order 1 to 5 tons and that it may have started at a temperature above 3000 K, although the temperature was not measured until it passed in front of the spectrometer slit, by which time it had already cooled to very roughly 1000 K. These simple models predict that the hot plume takes up all the kinetic energy of the impactor and possibly even more than all the energy, depending largely on the assumptions used to derive the mass of silicates and related (molten) dust in the hot plume. It is still an open question whether an internal energy source is needed, as suggested by Holsapple and Housen (2007 and see Sect. 2.2), but further work is needed on the energy balance. As a side note, most of the momentum is in the slow ejecta discussed below, not in the hot plume.

2.2 Excavated Ejecta

The longer term evolution has been modeled more extensively by Richardson et al. (2007), while Holsapple and Housen (2007) have made a detailed comparison of the observations with their laboratory studies. Observationally the ejecta cone was never seen to detach from the surface of the nucleus. This means that one can, in principle, set an upper limit to the yield strength of the material. Considering the limitations of the data and the fact that the crater is just over the limb in the look-back images, Richardson et al. conclude that the upper limit on yield strength is roughly 1–10 kPa, while Holsapple and Housen suggest that it could be as much as 65 kPa. The latter is comparable to the strength of shattered ice, but much less than that of block ice, which is in turn much less than that of competent rock. Thus the cometary material is not strong, but we can not say where the strength lies between zero and tens s of kPa. Holsapple and Housen further argue that the motion of the ejecta can not be explained just on the basis of cratering and that there must have been an acceleration mechanism providing energy and momentum. This might have been the release of a large quantity of trapped volatiles or some exothermic reaction.

Richardson et al. have also modeled the fall-back of ejecta onto the surface to deduce the local surface gravity. This then yields the overall average density of the nucleus as 400 $\mathrm{kg\,m^{-3}}$. Hydrodynamic drag effects on the ejecta have been ignored since the distribution of the gas is unclear. Sublimation of ejected ice in the interior of the cone leads to gas that would accelerate the ejecta tangentially, leading to an overestimate of the density. Ambient sublimation surrounding the impact site leads to radial acceleration and an underestimate of the density. Unfortunately, the data do not constrain the distribution and motion of gas so the size and even the direction of the effect is not clear. For any value of the rock/ice ratio within the range commonly considered, the resultant porosity is well above 50% averaged over the entire nucleus. This value for the bulk porosity is consistent with the 75% porosity of the surface layers discussed above on the basis of the luminous efficiency of the impact. The bulk density of the nucleus, 400 $\mathrm{kg\,m^{-3}}$, is also consistent with the value 450 $\mathrm{kg^{-3}}$ derived from modeling the non-gravitational acceleration of the nucleus in its orbit around the sun (Davidsson et al. 2007). Results for other comets by Rickmann, Davidsson, and others (see review by Weissman et al. 2005), primarily based on non-gravitational accelerations of the orbital motion, generally range downward from roughly 1000 $\mathrm{kg\,m^{-3}}$, but the results are even more strongly dependent on model assumptions than are the results

for Tempel 1 and, e.g., two independent analyses of Borrelly (Farnham and Cochran 2002; Davidsson and Gutiérrez 2004) yield non-overlapping error bars (1-σ) and their resulting bulk densities span the range from 180 to 830 kg m^{-3}.

After the hot plume passed in front of the slit of the spectrometer, the slower-moving mechanically excavated material passed in front of the slit. These ejecta included, within 2 seconds after impact, a large quantity of ice (Sunshine et al. 2007). Based on analogy with laboratory experiments (Schultz et al. 2007), these downrange ejecta are primarily derived from material within a couple of impactor diameters of the surface, i.e. with a few meters of the surface. It is possible that the icy grains dominate the total mass of the downrange ejecta. Subsequent spectral maps of the ejecta in all directions showed that the uprange rays contained little if any ice (Sunshine et al. 2007). These uprange rays are derived primarily from material within less than one impactor diameter of the surface, i.e. they are composed entirely of material from <1 m deep in the nucleus. This suggests a surface layer of thickness <1 m that is depleted in ice. It may eventually be possible to refine our determination of the layering near the surface, but this is the limit of our current understanding. The ejected ice was also seen in several ground-based measurements (Schulz et al. 2006; Knight et al. 2007). Nearly all the water ejected must have been ejected in the form of ice since there was not enough energy in the impact to sublime the amount of water observed. Kadono et al. (2007) have used ground-based observations of the spatio-temporal distribution of the ejecta and the variations in albedo to conclude that there is a surface layer of tens of cm enriched in carbonaceous material and suggest that the material below this layer is unprocessed since formation of the cometary nucleus.

A wide variety of species were detected in the ejecta using both ground-based data and data from spaceborne observatories. In general, the ejecta showed very little change in the relative composition of volatiles compared to the pre-impact, ambient outgassing. The only significant change reported was a large increase in ethane (C_2H_6; DiSanti et al. 2007). Many observers, including DiSanti et al., reported very little change in the relative abundance of numerous other species. The observations of particulates, however, did show significant differences above and beyond those reported by Kadono et al. Lisse et al. (2006) reported detection in spectra from Spitzer Space Observatory of several species that had not been previously reported in comets, including carbonates and phyllosilicates. Since then, most of the species except phyllosilicates have been detected in the coma grains returned by Stardust. There is still disagreement on relative abundances between the Stardust grains and the infrared observations of the ejecta from Tempel 1, but there are many possible reasons for such discrepancies. The differences from ambient outgassing might suggest that the subsurface grains are different from those on the surface, but other effects may be more important.

Fitting mid-IR spectra is sensitive to the sizes of the particles producing the radiation. Another conclusion from fitting the spectra before and after impact is that the size distribution of particles after impact was different from that before impact (Lisse et al. 2006, on-line supplementary material). Relative to the ambient outgassing, the size distribution of the ejecta was peaked near 1 micron and dropped toward both larger and smaller sizes. This made a significant change in the size of particles that dominated the emitting cross section. Thus the size distribution of the ejecta was different from the size distribution of the ambient ejecta in such a way as to increase the importance of particles smaller than a wavelength, thus making emission features more readily detectable. As will be discussed further below, it is plausible to assume that the particles in the ejecta had been subjected to sufficient shock forces that aggregates fragmented into their component pieces and that there is no intrinsic difference between the surface material and the interior material.

How much material was excavated *in toto*? This is best determined from remote sensing since the *in situ* observations do not have sufficient field of view nor do they have a

sufficiently long temporal window to determine this. The amount of ice ejected is readily determinable because it sublimes in sunlight producing H_2O, which can be observed directly and which further photodissociates to produce OH and H, which can also be observed. The sublimation of small grains takes many hours and the subsequent photodissociation takes a day or more so that observations over several days are needed in order to integrate the total amount of ice that was excavated in a matter of minutes. Observations of OH reported by Keller et al. (2007) and by Schleicher et al. (2006) and of H_2O reported by Biver et al. (2007) are all consistent in concluding that 4000 to 9000 tons of ice was excavated to produce this gas. CO and CO_2 and other abundant volatiles such as methanol (CH_3OH) can add a few tens of percent to this. The amount of refractory dust is much less well determined since, even with the fragmented grains implied by Lisse et al. (2006) the total mass is still dominated by the largest particles and none of the observations are sensitive to the largest particles. Dust/volatile ratios of order unity are consistent with most data, indicating a total mass of 10–20 ktons of material escaped the comet. Noting that in typical cratering events most of the material eventually falls back to the surface, a total excavated mass of twice the mass of ejected ice, say 2×10^7 kg, would be a very conservative number. At the bulk nuclear density, this corresponds to a volume of 5×10^4 m^3. This volume corresponds to a hemispherical instantaneous crater of nearly 30 m radius and is a reasonable lower limit on the size of the actual impact crater.

3 The Ambient Comet

Many of the interesting results from Deep Impact came from observing the comet in ways in which a comet had never been observed previously. These results would have been obtained independent of the existence of an impact. However, it is the combination of both types of results that leads us to our real insights.

3.1 The Nucleus

One striking conclusion about the nucleus comes from comparison with the other nuclei that have been imaged. They all have very different gross shapes and they all have very different topographic signatures. Comet Tempel 1 has a few, very large, nearly flat surfaces (Thomas et al. 2007) so that one can think of it as being more like a pyramid than an ellipsoid. By comparison, the structure of comet 19P/Borrelly is more like a banana, with a distinct, large-scale curvature (Kirk et al. 2004), while comet 81P/Wild 2 is the only one of the three comets recently visited to be plausibly thought of as an ellipsoid (Duxbury et al. 2004) and even it has significant deviations from an ellipsoid. The shape of 1P/Halley is not as well determined but it is probably best approximated as a bi-axial ellipsoid while Wild 2 is clearly triaxial with b nearly the geometric mean of a and c. The source of these different shapes is an open question.

The nuclei also have very different topographic features. Tempel 1 is the only one that has numerous features that might be impact craters (Thomas et al. 2007). All of the nuclei do show some signs of layering as discussed by Belton et al. (2007) while Basilevsky and Keller (2007) argue for the ubiquity of smooth flows. We note that the obvious most smooth area on Borrelly is a stratigraphically and gravitationally high feature characterized as a mesa (Britt et al. 2004), whereas the largest smooth area on Tempel 1 is a gravitationally low feature with adjacent stratigraphically higher layers. The other smooth areas on Tempel 1 are also stratigraphically relatively low. On Wild 2 the smooth areas are all stratigraphic lows and associated with depressions but without any signs of flows, unlike those on Tempel 1.

This first detection of ice on the surface of a cometary nucleus (Sunshine et al. 2006) was important not for showing where the water comes from, but for showing that the water in the coma does NOT come from ice on the surface. Ice anywhere on the nucleus at a level of 1% coverage per pixel in our spectral maps should have been detectable and the total ice found on the surface (3% coverage of pixels covering 0.5 km^2) was totally inadequate to explain the observed outgassing. There are still many questions about the surface ice due to the limitations of our spatio-temporal coverage. Since the ice is seen only in the morning areas of the nucleus and is composed of 50-μm grains, it could be ice redeposited during the previous night. Alternatively, it could be very small exposures of more extensive blocks of ice. The ice is generally in locally stratigraphically low areas.

The first detailed thermal map of a cometary nucleus (Groussin et al. 2007) showed that over most of its surface the comet is in local equilibrium with the instantaneous solar flux, i.e., that thermal inertia is negligibly small. In the coldest areas, toward the morning terminator and toward the terminator at the shadowed pole, the surface is warmer than expected from local equilibrium. Various physical processes, including surface roughness need to be examined to explain this effect. At the resolution of the spectral maps (120-m pixels), the temperature of the icy regions is much too high (270 K) for the ice to remain solid. We must conclude, therefore, that the ice is not in thermal contact with the dark material that is at this high temperature. This can be due to ice as frost with negligible contact points with solid surface or it could mean a large number of patches of contiguous ice with the only contact with dark material being at the very edges or it could mean narrow columns of ice that can sustain some sublimation from the top. As noted previously in the discussion of excavated ice, pure grains of ice last many hours and the icy areas on the surface are seen only a few hours after sunrise, so the first hypothesis above is as plausible as the others that involve bulk ice. The upper limits on thermal inertia, using reasonable assumptions about conductivity and heat capacity, imply a diurnal skin depth for thermal penetration of only 3 cm and an annual skin depth of 90 cm.

3.2 The Gaseous Coma

Near infrared spectral maps of the inner coma show that the water in the innermost coma, presumably just released from the nucleus is concentrated in the sunward direction (Feaga et al. 2007). Given the geometry, the result is consistent with water outgassing peaked along the subsolar meridian. The water shows very little indication of jets, although jets of very low brightness (column density) contrast would not be detected. The water is optically thick in the strongest lines of the principal band out to a distance of about 20 km from the nucleus. Beyond that distance, even the strongest lines have $\tau < 1$. Using the column densities in the optically thin region, we obtain a water production rate consistent with those obtained with several Earth-based techniques prior to impact (e.g., Biver et al. 2007; Schleicher et al. 2006).

The spatial distribution of CO_2 in the coma is very different from that of H_2O (Feaga et al. 2007). The strongest lines in the CO_2 band are also optically thick in the innermost coma, but through a fortunate cancellation among the rotational distribution of molecules and the line strengths, the effects of optical depth are similar in H_2O and CO_2. In the pre-impact image plane, the CO_2 is predominantly above the negative rotational pole, which has been in winter (permanent darkness) for several months. There is virtually no CO_2 detectable above the positive rotational pole, which has been in summer for the same several months. The ratio of CO_2 to H_2O brightnesses, and thus column densities, varies by a factor >4 around the nucleus. The strongest dust jet, also visible from Earth, is also far south and, as noted

in the next section, the dust is better correlated with CO_2 than with H_2O, although it is not well correlated with either. The outgassing of CO_2 is roughly 5–10% that of H_2O, assuming that variations in outflow velocity are not significant, similar to that of CO (Feldman et al. 2006).

The fact that the H_2O release seems concentrated near the sub-solar meridian implies that the ice, at whatever depth, is responding very rapidly to the diurnal thermal wave. Thus the thermal skin depth of 3 cm implies that ice is generally within about 10 cm (3 skin depths) of the surface. This is rather shallower than inferred from analysis of the impact ejecta above. Does this mean that ice in the impact region is deeper than average? Or is there this much uncertainty in all the results?

Is the CO_2 ejection from high negative latitudes an indication of annual thermal phase lag? Is it still warm enough at depth for the CO_2 to sublime but not warm enough for the H_2O to sublime? Or is the region around the negative pole a primordial cometesimal that formed in a colder part of the protoplanetary disk than the cometesimal near the positive rotational pole? There is essentially no sublimation of CO_2 in the region above the positive rotational pole although this has been in continuous sunlight for several months so the seasonal effect must also require that the CO_2 there is also deep enough that no summer heating has penetrated deeply enough. There have been several suggestions of heterogeneity in remote sensing of other comets, typically via variations in relative abundances as a function of rotation, but the lack of adequate spatial resolution has always limited their interpretability. The existence of primordial cometesimals inferred from the extensive layering seen on the nucleus of Tempel 1 has been discussed by Belton et al. (2007; see Sect. 4 below) as the TALPS model.

3.3 The Dust

The dust in the coma was observable at some level for the entire two months of approach to the comet. During the latter part of approach, discrete jets could be traced in motion as the nucleus rotated (Farnham et al. 2007). Very weak jets, visible only near closest approach when the patches of ice were very near the limb, could be traced directly to the icy patches. It is unclear whether those jets are normal, refractory cometary grains or icy grains, but the amount of material in those jets is insignificant compared to what is in the larger, prominent jets. These weak jets are the only ones that can be traced to specific surface features.

The more prominent jets can be traced nearly to the surface, but there is considerable ambiguity in associating any of them with specific surface features. We note that stereoscopy shows that all but two of the jets are in front of the plane of the sky and should therefore be emanating from the visible surface of the nucleus. The most prominent jet seen in the dust can be traced to middle southern latitudes and it projects as a fan centered on the negative rotational pole. This jet is also seen in Earth-based imaging. Since the rotation is seen easily but no spiral structure develops, the grains must be moving unusually slowly so that the range of ejection angles and velocities is enough to smear successive rotations into one another. At this point it is still unclear whether this jet is physically associated with the excess CO_2 seen in the region of this pole-centered fan.

The prominent jets have a variety of angular widths, some large enough to project back to large areas on the nucleus but none can be associated with specific surface features, and in particular none of them come from icy areas. Thus any picture of jet formation can not rely on excess local sublimation due to locally exposed ice. It is not yet clear whether any of the prominent jets can be associated with cavities that could produce collimation but this author is skeptical of this idea also.

Table 1 Selected results

Effective radius	3.0	km	Thomas et al. 2007
Maximum diameter	7.5	km	Thomas et al. 2007
Minimum diameter	5.0	km	Thomas et al. 2007
Surface area	119	km^2	Thomas et al. 2007
Volume	113	km^3	Thomas et al. 2007
Surface gravity	0.34	$mm\,s^{-2}$	Richardson et al. 2007
Mass	4.50E+13	kg	Richardson et al. 2007
Density	400	$kg\,m^{-3}$	Richardson et al. 2007
Excavated mass	2.E+07	kg	this paper
Porosity of surface	>0.75		Ernst and Schultz 2007
Yield strength	<65	kPa	Holsapple and Housen 2007
Crater diameter	>30	m	this paper

On its approach to the nucleus, the impactor encountered 4 dust particles large enough to be detected and corrected for by the Attitude Determination and Control System (ADCS). A'Hearn et al. (2008) showed that these are perfectly consistent with the power law assumed to fit a variety of remote sensing data. Sand-blasting of the primary mirror in the Impactor Targeting Sensor (ITS) led to reduced transmission during the last minute before impact. Models of the size distribution have not yet quantitatively reproduced the reduction in responsivity, but this is almost certainly due to order of magnitude uncertainties in the damage model at these high speeds. This pre-impact distribution, which agrees very well with the distribution needed to explain the pre-impact mid-infrared spectrum, is very different from that needed to explain the post-impact mid-infrared spectrum (Lisse et al. 2006, on-line supplementary material). A likely interpretation is that the cometary grains lifted by ambient outgassing are fragile aggregates and the shock wave that excavated material from the impact site was sufficient to fragment the aggregates into their individual components.

Both a photometric light curve extracted from the approach imaging (A'Hearn et al. 2005) and the study of the movies used to study the jets (Farnham et al. 2007) showed that spontaneous outbursts of material, not connected to the periodic jets, are very frequent, averaging more than once a week. The outbursts can easily be grouped by their rotational phase indicating that there are about 3 specific areas on the nucleus that repeatedly have outbursts, although the outbursts do not occur on every rotation. One of these groups may be correlated with sunrise on the east facet of the nucleus (the extensive surface that includes the icy patches) and images of one of those outbursts show clearly that the material is ejected to the northeast quadrant projected on the sky. The outbursts are more or less instantaneous, i.e. material emerges from the nucleus for less than about 10 minutes, and a clump of material moves away from the nucleus, gradually dissipating.

Some key numerical results, from Sects. 2 and 3, are summarized in Table 1.

4 Interrelationships and Origins

The wide variety of phenomena that have been seen at Tempel 1 provide a lot of information that can be used to constrain the internal structure of comets. Combining all the data into a coherent picture is still in the future. Observations of other comets are also crucial for understanding the pattern that must underlie all of the phenomenology. Detailed physical

modeling is required to explain simultaneously a) the natural outbursts, b) the chemical heterogeneity in the coma, c) the response of the water outgassing to the diurnal insolation, and d) the formation of jets of dust.

The numerous phenomena described above have led Belton et al. (2007) to argue that the comet preserves the primordial layering produced by the aggregation of cometesimals. This requires a rather gentle aggregation with relatively little interpenetration of the cometesimals. If the compositional heterogeneity is primordial, then it suggests eccentric orbits during the late stages of accumulation of the nucleus, but large eccentricities usually imply relatively large encounter speeds, which might be inconsistent with little interpenetration. Furthermore, the accumulation must proceed with relatively little compression of the components in order to preserve the high porosity (low density) determined for the whole nucleus and also for the surface layer at the impact site.

Basilevsky and Keller (2007) have similarly argued that the nucleus preserves the primordial cometesimals and pointed out the cratering record. They emphasize that the landforms are a mixture of primordial ones and much more recent landforms produced on recent perihelion passages. They have also argued that avalanche-type flows may be important. In producing the structures seen in the images.

The evidence is reasonably clear that the highly evolved layers of the comet are very thin, certainly no more than a few meters and comparable in thickness to the amount of material that is lost in a typical passage through perihelion. Theoretical models that predict evolution to very deep layers appear to be excluded by the results from Deep Impact. The results also suggest that remote sensing of the volatiles, at least when water dominates the outgassing, is a valid way to estimate the nuclear abundances of many volatile species.

Resolution of the evolutionary effects from the primordial situation requires observations of other comets, a key goal of the extended mission of the Deep Impact flyby spacecraft. This mission, recently approved by NASA, will fly past comet 103P/Hartley 2 in late 2010. This comet has a much smaller nucleus than those previously visited but it has a very large active fraction and will provide better SNR for both imaging and spectroscopy than did comet Tempel 1.

Acknowledgements This work was supported by NASA through the Discovery Program and specifically through contract NASW00004 to the University of Maryland. This paper summarizes work done by the team of many scientists and engineers who worked on Deep Impact and would not have been possible without their contributions.

References

M.F. A'Hearn et al., Deep Impact: excavating comet Tempel 1. Science **310**, 258–264 (2005)

M.F. A'Hearn, M.J.S. Belton, T.L. Farnham, L.M. Feaga, O. Groussin, C.M. Lisse, K.J. Meech, P.H. Schultz, J.M. Sunshine, Deep Impact and sample return. Earth, Planets, Space **60**, 61–66 (2008)

A.T. Basilevsky, H.U. Keller, Craters, smooth terrains, flows, and layering on the comet nuclei. Sol. Sys. Res. **41**, 109–117 (2007)

M.J.S. Belton et al., The internal structure of Jupiter family cometary nuclei from deep impact observations: The talps or "layered pile" model. Icarus **187**, 332–344 (2007)

N.D. Biver et al., Radio observations of comet 9P/Tempel 1 before and after deep impact. Icarus **187**, 253–271 (2007)

D.T. Britt, D.C. Boice, B.J. Buratti, H. Campins, R.M. Nelson, J. Oberst, B.R. Sandel, S.A. Stern, L.A. Soderblom, N. Thomas, The morphology and surface processes of comet 19/P Borrelly. Icarus **167**, 45–53 (2004)

B.J.R. Davidsson, P.J. Gutiérrez, Estimating the nucleus density of comet 19P/Borrelly. Icarus **168**, 392–408 (2004)

B.J.R. Davidsson, P.J. Gutiérrez, H. Rickman, Nucleus properties of 9P/Tempel 1 estimated from non-gravitational force modeling. Icarus **187**, 306–320 (2007)
M.A. DiSanti, G.L. Villanueva, B.P. Bonev, K. Magee-Sauer, J.E. Lyke, M.J. Mumma, Temporal evolution of parent volatiles and dust in comet 9P/Tempel resulting from the Deep Impact experiment. Icarus **187**, 240–252 (2007)
T.C. Duxbury, R.L. Newburn, D.E. Brownlee, Comet 81P/Wild 2 size, shape, and orientation. J. Geophys. Res. **109**, E12S02 (2004)
C.M. Ernst, P.H. Schultz, Evolution of the Deep Impact flash: Implications for the nucleus surface based on laboratory experiments. Icarus **190**, 334–344 (2007)
T.L. Farnham, A.L. Cochran, A McDonald observatory study of Comet 19P/Borrelly: Placing the Deep Space 1 observations into a broader context. Icarus **160**, 398–418 (2002)
T.L. Farnham, D.D. Wellnitz, D.L. Hampton, J.-Y. Li, J.M. Sunshine, O. Groussin, L.A. McFadden, C.J. Crockett, M.F. A'Hearn, M.J.S. Belton, P. Schultz, C.M. Lisse, Dust coma morphology in the Deep Impact images of comet 9P/Tempel 1. Icarus **187**, 26–40 (2007)
L.M. Feaga, M.F. A'Hearn, J.M. Sunshine, O. Groussin, T.L. Farnham, Asymmetries in the distribution of H_2O and CO_2 in the inner coma of comet 9P/Tempel 1 as observed by Deep Impact. Icarus **190**, 345–356 (2007)
P.D. Feldman, R.E. Lupu, S.R. McCandliss, H.A. Weaver, M.F. A'Hearn, M.J.S. Belton, K.J. Meech, Carbon monoxide in Comet 9P/Tempel 1 before and after the Deep Impact Encounter. Astrophys. J. **647**, L61–L64 (2006)
O. Groussin, M.F. A'Hearn, J.-Y. Li, P.C. Thomas, J.M. Sunshine, C.M. Lisse, K.J. Meech, T.L. Farnham, L.M. Feaga, W.A. Delamere, Surface temperature of the nucleus of comet 9P/Tempel 1. Icarus **187**, 16–25 (2007)
K.A. Holsapple, K.R. Housen, A crater and its ejecta: An interpretation of Deep Impact. Icarus **187**, 345–356 (2007)
T. Kadono, S. Sugita, S. Sake, T. Ootsubo, M. Honda, H. Kawakita, T. Miyata, R. Furusho, J. Watanabe, The thickness and formation age of the surface layer on comet 9P/Tempel 1. Astrophys. J. **661**, L89–L92 (2007)
H.U. Keller et al., Observations of comet 9P/Tempel 1 around the Deep Impact event by the OSIRIS cameras onboard Rosetta. Icarus **187**, 87–103 (2007)
R.L. Kirk, E. Howington-Kraus, L.A. Soderblom, B. Giese, J. Oberst, Comparison of USGS and DLR topographic models of comet Borrelly and photometric applications. Icarus **167**, 54–69 (2004)
M.M. Knight, K.J. Walsh, M.F. A'Hearn, R.A. Swaters, B.A. Zauderer, N. Samarasinha, R. Vazquez, H. Reitsema, Ground-based visible and near-IR observations of the Deep Impact encounter. Icarus **187**, 199–207 (2007)
C.M. Lisse et al., Spitzer spectral observations of the Deep Impact ejecta. Science **313**, 635–640 (2006)
H.J. Melosh, Deep Impact: The first second. Proc. Lunar Sci. Conf. **XXXVII** Abstract #1165 (2006)
J.E. Richardson, H.J. Melosh, C.M. Lisse, B. Carcich, A ballistics analysis of the Deep Impact Ejecta plume: Determining comet Tempel 1's gravity, mass, and density. Icarus **190**, 357–390 (2007)
D.G. Schleicher, K.L. Barnes, N.F. Baugh, Photometry and imaging results for comet 9P/Tempel 1 and Deep Impact: Gas production rates, postimpact light curves, and ejecta plume morphology. Astron. J. **131**, 1130–1137 (2006)
R. Schulz, A. Owens, P.M. Rodriguez-Pascual, D. Lumb, C. Erd, J.A. Stüwe, Detection of water ice grains after the DEEP IMPACT onto comet 9P/Tempel 1. Astron. Astrophys. **448**, L53–L56 (2006)
P.H. Schultz, C.A. Eberhardy, C.M. Ernst, M.F. A'Hearn, J.M. Sunshine, C.M. Lisse, The Deep Impact oblique cratering experiment. Icarus **190**, 295–333 (2007)
J.M. Sunshine et al., Exposed water ice deposits on the surface of comet 9P/Tempel 1. Science **311**, 1453–1455 (2006)
J.M. Sunshine, O. Groussin, P.H. Schultz, M.F. A'Hearn, L.M. Feaga, T.L. Farnham, K.P. Klaasen, The distribution and structure of water ice in the interior of comet Tempel 1. Icarus **190**, 284–294 (2007)
P. Thomas et al., The shape, topography, and geology of Tempel 1 from Deep Impact observations. Icarus **187**, 4–15 (2007)
P.R. Weissman, E. Asphaug, S.C. Lowry, Structure and density of cometary nuclei, in *Comets II*, ed. by M.C. Festou, H.U. Keller, H.A. Weaver (U. Arizona Press, Tucson, 2005), pp. 337–357

Assessing the elemental composition of comet 81P/Wild 2 by analyzing dust collected by Stardust

Thomas Stephan

Originally published in the journal Space Science Reviews, Volume 138, Nos 1–4.
DOI: 10.1007/s11214-007-9291-2

Abstract One of the prime objectives in the analysis of cometary dust collected by the Stardust space mission is to determine the elemental composition of comet 81P/Wild 2. For this analysis, samples captured by two sampling media, silica aerogel and Al foil, were available. While aerogel was qualified to sample the dust almost intact, particles impinging on Al foils produced hypervelocity impact craters with residual cometary matter. Both sample types delivered valuable information on the cometary inventory, even though a slight loss of volatiles was observed for impact residues on Al foils. Altogether an elemental composition close to solar elemental abundances was observed, indicating that the early solar system was chemically rather homogeneous from the innermost regions close to the sun to the outer edge of the solar system, the presumed region of cometary origin.

Keywords Comets · Stardust · Wild 2 · Element composition

1 Introduction

In January 2004, the Stardust spacecraft collected cometary matter during passage of the coma of comet 81P/Wild 2 and returned it to Earth in January 2006 for laboratory investigation (Brownlee et al., 2006, 2003; Tsou et al. 2003). Hence, Stardust was the first mission to return solid samples from a specific astronomical body other than the Moon. Stardust's trajectory took it within 234 km of the surface of Wild 2, and the cometary dust was collected at a relative velocity of 6.1 km/s. Stardust also collected a sample of contemporary interstellar dust during the cruise phase before the cometary encounter.

The primary capture medium for both cometary and interstellar dust was low-density silica aerogel with density gradients varying from 5 to 50 mg/cm^3 and a total surface area of

T. Stephan
Institut für Planetologie, Wilhelm-Klemm-Str. 10, 48149 Münster, Germany

Present address:
T. Stephan (✉)
University of Chicago, 5734 South Ellis Avenue, Chicago, IL 60637, USA
e-mail: tstephan@uchicago.edu

H. Balsiger et al. (eds.), *Origin and Early Evolution of Comet Nuclei*
DOI: 10.1007/978-0-387-85455-7_16

1,039 cm^2 exposed to the comet (Tsou et al. 2003). Aerogel was used to gently decelerate the impacting particles in an effort to preserve them more or less intact.

In addition to aerogel, 153 cm^2 of aluminum foils (Al 1100; >99% pure) were also exposed to the comet. These foils were primarily used to fix the aerogel tiles and to facilitate their removal from the modular sample tray assembly. On these Al foils, in contrast to aerogel, the impacting cometary dust particles came to an abrupt halt and hypervelocity impact craters were produced. However, residual cometary matter was found associated with the foils, typically as discontinuous layers of shock-produced melts, inside crater cavities or on crater rims (Hörz et al. 2006). Certainly, impact residues on metal foils are expected to be more severely altered from their initial properties than cometary matter captured by aerogel.

After recovery of the Stardust return capsule in the Utah desert, a multitude of cometary samples became available. These samples offered the unprecedented chance to analyze authentic cometary matter from a known source here on Earth. These samples should contain the preserved building blocks from the edge of the solar system, the presumed region of cometary origin, and therefore provide the first opportunity to compare these materials with fragments of small bodies (asteroids) that formed more than an order of magnitude closer to the Sun and that are available in the meteorite collection.

During an initial six-month period, the captured cometary samples were first studied by nearly 200 investigators around the world organized in six topical teams (Brownlee et al. 2006). The results of this preliminary examination (PE) were recently reported with respect to impact features (Hörz et al. 2006), organics (Sandford et al. 2006), isotopic compositions (McKeegan et al. 2006), infrared spectroscopic properties (Keller et al. 2006), elemental composition (Flynn et al. 2006), and mineralogy and petrology (Zolensky et al. 2006).

In the present study, the elemental compositions of samples investigated during PE are discussed comparatively to extract a firm data set from various sources, and from there conclusions are drawn on the Wild 2 composition. Contrary to previous work (Flynn et al. 2006), this study also includes results from particles extracted from aerogel and it provides a more comprehensive overview of the available data set so far.

2 Samples of Cometary Matter

Samples of cometary matter from the Stardust collection come from craters on Al foil with impact residues, pieces of aerogel with complete or fractional particle tracks, and fragments of cometary matter extracted from aerogel. All the different sample types have their particular advantages and disadvantages for the investigation of cometary properties.

2.1 Particle Tracks in Aerogel

Low-density silica aerogel was the major capture medium used by Stardust to collect cometary dust. Aerogel was chosen since it provides the highest probability for a particle to survive intact hypervelocity impact (Tsou et al. 2003). However, most of the cometary particles captured by Stardust disintegrated during their passage through the aerogel (Hörz et al. 2006). Fine-grained materials decelerate more rapidly and disperse over the first parts of the penetration tracks, often forming a bulbous cavity, while more massive and dense components of the impacting particles penetrate more deeply.

Figure 1 shows an example of a large track formed by hypervelocity impact of a Wild 2 particle into Stardust aerogel. The impacting particle probably consisted of an intimate mixture of mineral grains embedded in an icy matrix, highly volatile matter probably containing organics. During Stardust collection, while penetrating the aerogel, the ice may have

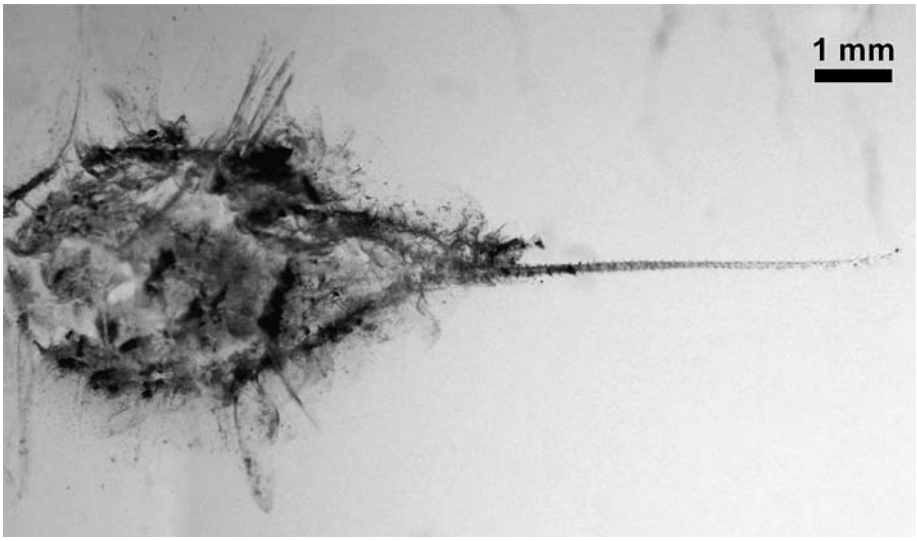

Fig. 1 Track 35 from Stardust aerogel cell C2054 is an example of a large particle track in aerogel. The cometary particle impacted from the left, producing a large bulbous cavity with several minor tracks originating from the bulb and a major track in forward direction leading to the terminal particle

vaporized explosively, thus distributing fine-grained material into the walls of the emerging bulbous part of the track. Some coarser fragments, probably more robust grains, were less affected by the explosive vaporization and continued their path through the aerogel. These fragments were found as terminal particles or larger fragments in side tracks originating from the bulb.

To determine the impactor composition, ideally all the cometary matter deposited along the track should be analyzed. It is obvious that extraction of all the material in a track like the one shown in Fig. 1 is impossible with available technology (Westphal et al. 2002). Therefore, in situ analytical methods are most advantageous. On the other hand, in situ analysis has to be performed within the aerogel, often through a relatively large volume of aerogel that may compromise the sensitivity for the analysis of cometary matter and inhibit or even prevent the measurement of elements that are also present as impurities in the aerogel.

For the analysis of tracks in aerogel, so-called keystones were produced, small chips of aerogel containing entire particle tracks (Westphal et al. 2004).

The cometary matter can also be analyzed without extraction, by preparation of dissected aerogel keystones with a significant part of the particle track exposed to the very surface of the aerogel (Westphal et al. 2004). These samples can directly be investigated with surface-sensitive analytical techniques. However, a complete suppression of the aerogel background cannot be achieved, since most of the cometary matter is heavily intermingled with compressed and partly shock-melted aerogel. Therefore, neither cometary Si nor O can be analyzed in these samples since these elements are the major constituents of Stardust aerogel.

Other elements are also affected by the aerogel background, since they are often present as trace impurities (Stephan et al. 2007c). Therefore, blank correction is crucial for analyses in or on aerogel.

2.2 Fragments Extracted from Aerogel

Terminal particles or larger fragments along the tracks can be extracted using methods described by Westphal et al. (2002). With these techniques, more than 90 particle fragments have been extracted from the aerogel track displayed in Fig. 1. Most particle fragments extracted from aerogel tracks are enclosed by condensed and often partly melted aerogel. To investigate their cometary components, sections of particles have to be produced, e.g., by microtoming. But even particle sections are often dominated by silica from aerogel that is intimately mixed with the cometary matter. It seems that the impacting particles were rather fluffy and that void spaces were filled with aerogel during the deceleration process. As a result, cometary Si and O concentrations were very difficult to constrain during this investigation, and the effects of aerogel impurities have to be considered.

2.3 Al Foil Craters

On Al foils, impacting particles come to an abrupt stop and hypervelocity craters formed. However, in all cases investigated so far, residual cometary matter was found, typically as discontinuous layers of impact-produced melts, inside crater cavities and on crater rims. These samples provide the sole opportunity to study Si in Wild 2 material. On the other hand, Al measurements on these samples are prevented because the target material itself is Al. In addition, the Al foils seems to be even more contaminated than the aerogel (Leitner et al. 2007a).

3 Analytical Methods

3.1 SXRF

The predominant analytical technique to study entire tracks in aerogel so far has been synchrotron X-ray fluorescence analysis (SXRF). This technique, however, allows to measure only the abundances of elements with atomic numbers $Z \geq 16$ (S). In SXRF, synchrotron radiation that completely penetrates an aerogel keystone is used to excite X-ray fluorescence (Flynn et al. 1996). With SXRF, elemental analysis was performed on keystones containing 23 tracks, which were selected to sample the diversity on the collector, by seven research groups with the use of six different instruments (Flynn et al. 2006).

3.2 TOF-SIMS

Time-of-flight secondary ion mass spectrometry (TOF-SIMS), contrary to SXRF, allows to analyze the light elements as well. Because it is a surface-analytical technique, TOF-SIMS requires cometary matter to be exposed on the sample surface. Details of this technique were described by Stephan (2001). During PE, TOF-SIMS was used to investigate cometary track material on dissected aerogel keystone fragments (Rost et al. 2007; Stephan et al. 2007c), particles extracted from aerogel (Stephan et al. 2007a, 2007b), as well as impact residues on Al foils (Leitner et al. 2007a, 2007b). Unfortunately, the TOF-SIMS investigation of crater residues is mainly confined to material sitting on crater rims, since crater bottoms typically are not accessible with this technique due to shadowing of the primary or secondary ions (Hoppe et al. 2006).

3.3 SEM-EDS

Residues in Al foil craters were also analyzed by scanning electron microscopy using energy-dispersive X-ray spectroscopy (SEM-EDS). The relative insensitivity to beam-sample-detector geometry makes EDS especially useful, as it can yield compositional information even from within complex-shaped depressions such as craters (Kearsley et al. 2007). However, EDS detection limits are relatively poor, and quantities of less than 0.2 wt% of many elements often cannot be determined reliably (Kearsley et al. 2007). Another disadvantage of SEM-EDS is that either high electron acceleration voltages (e.g., 20 kV) are used that result in relatively deep sampling of X-ray emission from several micrometers in depth, or low acceleration voltages (e.g., 5 kV) are applied that allow much shallower excitation of a residue layer of less than 500 nm in depth, but do not allow analysis of minor elements heavier than Ca (Kearsley et al. 2007).

During PE, the chemical composition of the residue in each of seven large craters (57–238 μm in diameter) in Al foil was determined, using a high acceleration voltage of 20 kV (Flynn et al. 2006).

4 Results

Figures 2 and 3 summarize the element compositions of various samples analyzed during Stardust PE. All data are presented as element ratios relative to Fe for samples captured by aerogel and relative to Si for impact residues on Al foils. Usually Si is used as the reference element in cosmochemistry, but could not be used for the samples that were captured by silica aerogel. In principle, Mg and Fe would both be suitable as reference elements, since they are both major elements and the aerogel shows only trace abundances of these elements (Stephan et al. 2007c). However, since Mg cannot be measured with SXRF, Fe was selected for normalization in this study.

All element ratios were then normalized to chondritic (CI) element ratios that are used as an approximation for bulk solar system abundances (Anders and Grevesse 1989).

Geometric mean values for all element ratios from samples from aerogel and Al foil, respectively, are also displayed in Figs. 2 and 3. These geometric mean values should be used as a first approximation for the bulk composition of Wild 2 dust.

Geometric mean values are more robust against statistical outliers than arithmetic means. Especially for ratios, arithmetic mean values easily become meaningless, since they would overestimate elements that show an anti-correlation to the normalization element. Finally, arithmetic means of ratios in general differ from ratios of arithmetic means. These shortcomings are all eliminated when using geometric means.

Variations in sample size or mass were not taken into account, since mass-weighted averages would be easily dominated by one or two large samples. This is of special importance, since the samples analyzed during PE are certainly not an unbiased sample of Wild 2 dust. Due to the strict time limitations during PE, samples that were easily accessible were preferentially selected. Therefore, large particles, tracks, and craters are certainly overrepresented in these analyses.

For the data treatment used in this study, it was rather assumed that each analysis represents an independent measurement of the cometary composition represented by a sample released from the comet's surface and certainly altered in a somehow unpredictable way during passage from the cometary nucleus to the space craft, during capture, and later during sample preparation. None of the impact tracks analyzed with SXRF were investigated

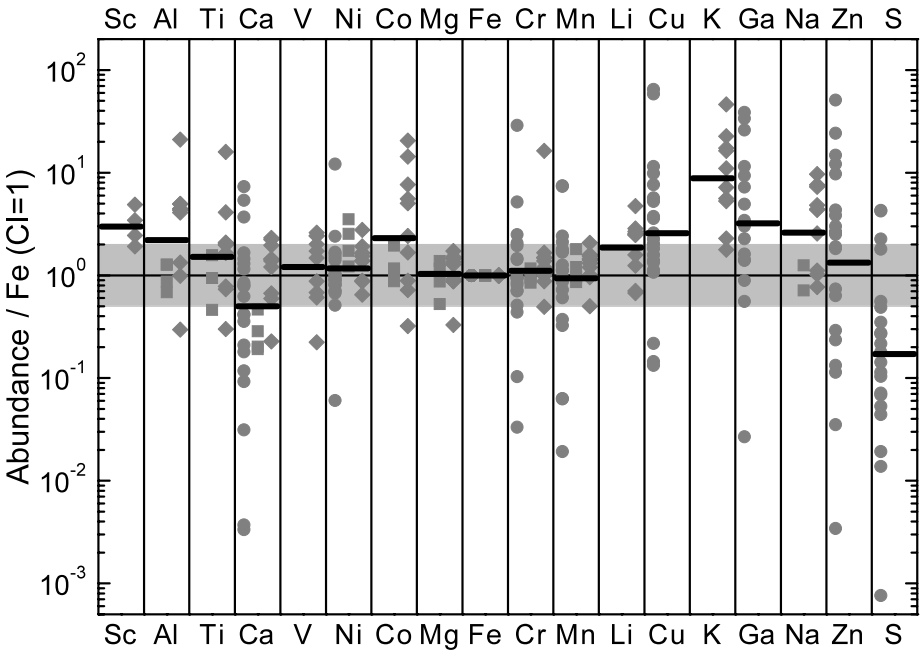

Fig. 2 Element ratios relative to Fe and normalized to CI chondritic abundances of cometary matter captured by Stardust aerogel. Elements are ordered according to their decreasing condensation temperatures (50% condensation for a solar-system composition gas according to Lodders 2003) as a measure of volatility. *Gray circles* denote individual SXRF analyses of entire tracks in aerogel (from Flynn et al. 2006, Supporting Online Material), *squares* represent TOF-SIMS analyses of residual cometary matter in aerogel tracks (from Stephan et al. 2007c), and *diamonds* indicate results from extracted particles (from Stephan et al. 2007b). *Black horizontal bars* designate geometric mean values calculated from all available data represented by the individual data points

more than once for this study. TOF-SIMS analyses, however, were in some cases performed on various portions of the same track or the same extracted particles (for details see Stephan et al., 2007b; 2007c), and several craters were analyzed by SEM-EDS as well as by TOF-SIMS, some of them even from different directions by TOF-SIMS (for details see Flynn et al. 2006; Leitner et al. 2007a). Nevertheless, each measurement was treated as an *individual* analysis in these cases, since no atom was counted more than once by TOF-SIMS, and TOF-SIMS and SEM-EDS usually accessed different portions of the craters. Since most samples from aerogel as well as from Al foils show heterogeneities typically on a submicrometer scale, it cannot be expected that measurements of different portions of one sample would yield matching results.

4.1 Dust Captured by Aerogel

Although huge variations that span up to more than three orders of magnitude were observed for some elements in Fig. 2, most geometric mean values are within a factor of two (light gray area in Fig. 2) of CI values.

The strongest average enrichment was observed for K (Fig. 2). However, K is a known contaminant in aerogel (Stephan et al. 2007c) and was found at least in some particles that

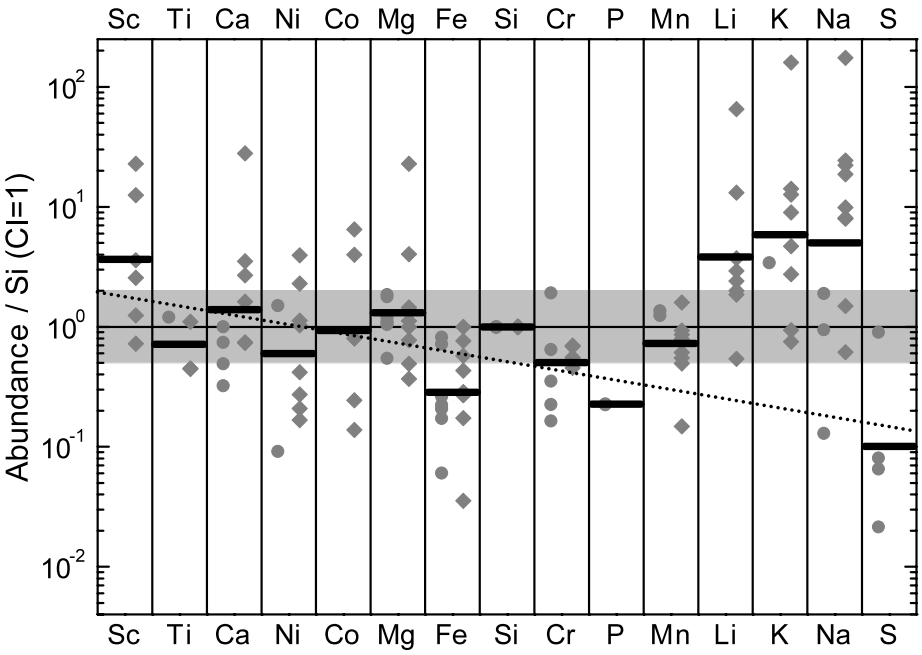

Fig. 3 Element ratios relative to Si and normalized to CI chondritic abundances of cometary matter captured by Stardust Al foil. Elements are ordered with increasing volatility. *Gray circles* denote SEM-EDS analyses of individual crater residues, mainly from the crater bottoms (from Flynn et al. 2006, Supporting Online Material), *diamonds* represent TOF-SIMS analyses of impact residues mainly from crater rims (from (Leitner et al. 2007a)). *Black horizontal bars* designate geometric mean values calculated from all available data represented by the single data points. The *dotted line* is a linear fit through all geometric mean values except those for Li, K, and Na

lead to the high geometric mean to be laterally correlated with Si from aerogel (Stephan et al. 2007b).

The apparent Sc enrichment can be fully attributed to the fact that Sc was only detectable in particles with high concentrations. Nondetections were not accounted for while calculating the geometric mean values, a shortcoming of this way of averaging.

Al, Co, Cu, Ga, and Na are just above the factor-of-two margin shown in Fig. 2. Some of these elements may also be enriched due to contamination. Al, Co, and Na especially show enrichments in extracted particles where blank correction was not possible (Stephan et al. 2007b), while they are nearly perfectly chondritic in fine-grained matter analyzed in tracks for which blank correction was possible (Stephan et al. 2007c).

Contamination is a major problem during analysis of all Stardust samples. The aerogel shows various kinds of contamination. Besides a general impurity of the aerogel (Tsou et al. 2003), both aerogel and Al foil show a heterogeneous distribution of various contaminants. The best way to assess this contamination level is to investigate the purity of the surrounding capture medium (Stephan et al. 2007c; Leitner et al. 2007a). For this study, however, analysis of the aerogel surrounding the extracted particles was not feasible. Thus, only general assumptions on background levels can be made (Stephan et al. 2007b). For samples captured by aerogel, C, H, O, N, and Si cannot be detected. This is due to the fact that aerogel is SiO_2 and contains large amounts of C (up to several wt.%; G.F. Herzog, priv. communication) often associated with N.

Ca and S are the only elements that show a visible depletion of their geometric mean values compared to CI abundances (Fig. 2). Due to their difference in geochemical behavior, reasons for the depletions are expected to be different for these two elements.

From the pattern observed in Fig. 2, most element ratios show a slight enrichment over CI. This can also be explained by a depletion of the reference element Fe that would lead to an overestimation of all element ratios relative to Fe. If a slight Fe depletion is real, Ca and S would be more depleted than shown in Fig. 2, while apparent enrichments in Sc, Al, Co, Cu, Ga, and Na would almost disappear.

4.2 Impact Residues on Al foil

A similar correlation with chondritic element ratios was also observed for impact residues on Al foils (Fig. 3). The highest enrichments compared to CI were observed for alkalis, K, Na, and Li, again maybe due to contamination. Also Sc shows once more an enrichment, while S is strongly depleted. Other elements that are significantly depleted include P and Fe, while Ca is close to chondritic. Despite the apparent enrichment of some volatiles due to contamination, there seems to be a slight general trend of increasing depletion with increasing volatility (dotted line Fig. 3). Such a trend was not observed for cometary matter captured by aerogel although S showed a similar depletion in Fig. 2.

This depletion might be the result of volatilization during hypervelocity impact on the Stardust Al foil that led to a preferential loss of volatiles. Especially, the volatilization of iron sulfide, troilite (stoichiometric FeS) or pyrrhotite ($Fe_{1-x}S$) that were both observed in Stardust samples (Zolensky et al. 2006), could easily explain a significant loss of S and also the significant but less-pronounced Fe depletion. It has been reported previously that many sulfides with nonstoichiometric, low-S compositions were found in Wild 2 particles, probably also reflecting capture heating (Zolensky et al. 2006).

4.3 Comparison with CI and Halley Data

To enable a comparison of the data shown in Figs. 2 and 3, Table 1 provides the geometric means for all element ratios from samples from aerogel and Al foil, respectively. These data were renormalized to a common major element, in this case Mg, because Fe seemed to be not suited due to the obvious Fe depletion in Fig. 3. Data are shown without normalization to CI chondritic values but CI ratios are provided for comparison as well as data for dust of comet 1P/Halley (Jessberger et al. 1988).

4.4 Discussion

Cometary matter collected by the Stardust mission revealed an overall chondritic composition of most elements in samples from comet Wild 2.

Some observed enrichments of alkali elements might result from contamination of the capture media aerogel and Al foil. Other element enrichments are less evident and might be attributed also to contamination or to data normalization.

On the other hand, S seems to be unambiguously depleted in both sample types. This might be due to volatilization of sulfides during particle capture. While such a loss seems to be plausible during generation of hypervelocity impact craters on Al foils, it is somehow surprising for particle tracks in aerogel, since aerogel tracks are often considered as closed systems that do not show significant loss of volatiles including even organics. However, track analysis using SXRF is confined to areas rich in Fe, since mapping of Fe is used to

Table 1 Comparison of geometric mean values for element ratios normalized to Mg = 100 for Wild 2 samples captured by aerogel and from impact residues on Al foils, recalculated from data shown in Figs. 2 and 3, with element ratios from comet Halley's dust (Jessberger et al. 1988) and CI chondrites (Anders and Grevesse 1989)

Element	Wild $2_{aerogel}$	Wild $2_{Al\text{-}foils}$	Halley	CI
Li	0.0096	0.015	—	0.0053
Na	13	20	10	5.3
Mg	≡ 100	≡100	≡100	≡100
Al	16	—	6.8	7.9
Si	—	71	185	93
P	—	0.17	—	0.97
S	7.9	3.7	72	48
K	2.9	1.6	0.2	0.35
Ca	2.8	6.0	6.3	5.7
Sc	0.0093	0.0089	—	0.0032
Ti	0.34	0.12	0.4	0.22
V	0.031	—	—	0.027
Cr	1.3	0.48	0.9	1.26
Mn	0.80	0.49	0.5	0.89
Fe	81	18	52	84
Co	0.45	0.15	0.3	0.21
Ni	5.2	2.1	4.1	4.6
Cu	0.12	—	—	0.049
Zn	0.15	—	—	0.117
Ga	0.011	—	—	0.0035

determine the boundaries of particle tracks in aerogel (Ishii et al. 2007). If highly volatile elements like S penetrate more deeply into the aerogel than Fe, these elements would be underestimated in the total track composition determined by SXRF. At least in some cases this was observed for another highly volatile element, namely Zn (Ishii et al. 2007). This model would also explain why Fe, probably from iron sulfide, is significantly depleted in foil crater residues but not to a similar extent in aerogel tracks. It should also be mentioned that contrary to the SXRF analyses of entire particle tracks, small grains extracted from aerogel and recently analyzed by transmission electron microscopy (TEM) EDS seem to show no substantial S depletion (Leroux et al. 2007).

Ca, on the other hand, displays a chondritic abundance in crater residues, but is depleted by a factor of two in aerogel tracks. In Stardust samples extracted from aerogel, Ca was found to be concentrated in Ca,Al-rich minerals, resembling CAIs (Ca,Al-rich inclusions) in meteorites (Zolensky et al. 2006; Stephan et al. 2007b). These might be underrepresented in the Fe-correlated track material investigated by SXRF and the extremely fine-grained cometary matter observed in a track bulb analyzed with TOF-SIMS (Stephan et al. 2007c). Therefore, the low geometric mean for Ca in Fig. 2 may be misleading. In extracted particles (Stephan et al. 2007b) as well as in crater residues (Fig. 3), Ca seems to be chondritic, probably reflecting an actually chondritic Ca concentration of Wild 2 itself.

5 Conclusions

Cometary samples collected by Stardust and investigated by various techniques on Earth suggest a CI-like element composition of comet 81P/Wild 2. Unambiguous deviations, which cannot be explained either by contamination of the sampling materials or by loss of volatiles during capture heating, were not observed.

However, for a better assessment of Wild 2 in comparison with other primitive solar system matter like meteorites, interplanetary dust particles (IDPs), or Halley's dust, quantitative analyses of light cometary volatiles like C, H, O, and N, so-called CHON elements, are highly desired. Unfortunately, concentrations of these elements are not easily determined in cometary matter residing in Stardust aerogel that itself show relatively high abundances of these elements. During formation of hypervelocity craters on Al foils, these elements are not expected to survive in large quantities. Therefore, impact residues are also not suited to determine the abundances of CHON elements.

The compositional results seem to indicate that no large-scale element fractionation occurred in the early solar system but rather large-scale mixing. Solar element abundances except for CHON elements were found aside from the solar photosphere, in primitive meteorites (CI carbonaceous chondrites) that probably originated in the asteroid belt, in IDPs, in both comets Halley and now also in Wild 2.

Acknowledgements The Stardust mission to comet 81P/Wild 2 was sponsored by NASA and executed jointly by the Jet Propulsion Laboratory and Lockheed Martin Space Systems. The author is greatly indebted to many individuals who assured a successful comet encounter and who safely returned the Stardust collectors and their precious samples to Earth. The manuscript benefited from thorough reviews by two anonymous reviewers and from careful reading and constructive contributions by Carolyn H. van der Bogert.

References

E. Anders, N. Grevesse, Abundances of the elements: Meteoritic and solar. Geochim. Cosmochim. Acta **53**, 197–214 (1989)

D. Brownlee, P. Tsou, J. Aléon, C.M.O'D. Alexander, T. Araki, S. Bajt, G.A. Baratta, R. Bastien, P. Bland, P. Bleuet, J. Borg, J.P. Bradley, A. Brearley, F. Brenker, S. Brennan, J.C. Bridges, N.D. Browning, J.R. Brucato, E. Bullock, M.J. Burchell, H. Busemann, A. Butterworth, M. Chaussidon, A. Cheuvront, M. Chi, M.J. Cintala, B.C. Clark, S.J. Clemett, G. Cody, L. Colangeli, G. Cooper, P. Cordier, C. Daghlian, Z. Dai, L. d'Hendecourt, Z. Djouadi, G. Dominguez, T. Duxbury, J.P. Dworkin, D.S. Ebel, T.E. Economou, S. Fakra, S.A.J. Fairey, S. Fallon, G. Ferrini, T. Ferroir, H. Fleckenstein, C. Floss, G. Flynn, I.A. Franchi, M. Fries, Z. Gainsforth, J.-P. Gallien, M. Genge, M.K. Gilles, P. Gillet, J. Gilmour, D.P. Glavin, M. Gounelle, M.M. Grady, G.A. Graham, P.G. Grant, S.F. Green, F. Grossemy, L. Grossman, J.N. Grossman, Y. Guan, K. Hagiya, R. Harvey, P. Heck, G.F. Herzog, P. Hoppe, F. Hörz, J. Huth, I.D. Hutcheon, K. Ignatyev, H. Ishii, M. Ito, D. Jacob, C. Jacobsen, S. Jacobsen, S. Jones, D. Joswiak, A. Jurewicz, A.T. Kearsley, L.P. Keller, H. Khodja, A.L.D. Kilcoyne, J. Kissel, A. Krot, F. Langenhorst, A. Lanzirotti, L. Le, L.A. Leshin, J. Leitner, L. Lemelle, H. Leroux, M.-C. Liu, K. Luening, I. Lyon, G. MacPherson, M.A. Marcus, K. Marhas, B. Marty, G. Matrajt, K. McKeegan, A. Meibom, V. Mennella, K. Messenger, S. Messenger, T. Mikouchi, S. Mostefaoui, T. Nakamura, T. Nakano, M. Newville, L.R. Nittler, I. Ohnishi, K. Ohsumi, K. Okudaira, D.A. Papanastassiou, R. Palma, M.E. Palumbo, R.O. Pepin, D. Perkins, M. Perronnet, P. Pianetta, W. Rao, F.J.M. Rietmeijer, F. Robert, D. Rost, A. Rotundi, R. Ryan, S.A. Sandford, C.S. Schwandt, T.H. See, D. Schlutter, J. Sheffield-Parker, A. Simionovici, S. Simon, I. Sitnitsky, C.J. Snead, M.K. Spencer, F.J. Stadermann, A. Steele, T. Stephan, R. Stroud, J. Susini, S.R. Sutton, Y. Suzuki, M. Taheri, S. Taylor, N. Teslich, K. Tomeoka, N. Tomioka, A. Toppani, J.M. Trigo-Rodríguez, D. Troadec, A. Tsuchiyama, A.J. Tuzzolino, T. Tyliszczak, K. Uesugi, M. Velbel, J. Vellenga, E. Vicenzi, L. Vincze, J. Warren, I. Weber, M. Weisberg, A.J. Westphal, S. Wirick, D. Wooden, B. Wopenka, P. Wozniakiewicz, I. Wright, H. Yabuta, H. Yano, E.D. Young, R.N. Zare, T. Zega, K. Ziegler, L. Zimmermann, E. Zinner, M. Zolensky, Comet 81P/Wild 2 under a microscope. Science **314**, 1711–1716 (2006)

D.E. Brownlee, P. Tsou, J.D. Anderson, M.S. Hanner, R.L. Newburn, Z. Sekanina, B.C. Clark, F. Hörz, M.E. Zolensky, J. Kissel, J.A.M. McDonnell, S.A. Sandford, A.J. Tuzzolino, Stardust: Comet and interstellar dust sample return mission. J. Geophys. Res. **108**, E8111 (2003)

G.J. Flynn, P. Bleuet, J. Borg, J.P. Bradley, F.E. Brenker, S. Brennan, J. Bridges, D.E. Brownlee, E.S. Bullock, M. Burghammer, B.C. Clark, Z.R. Dai, C.P. Daghlian, Z. Djouadi, S. Fakra, T. Ferroir, C. Floss, I.A. Franchi, Z. Gainsforth, J.-P. Gallien, Ph. Gillet, P.G. Grant, G.A. Graham, S.F. Green, F. Grossemy, P.R. Heck, G.F. Herzog, P. Hoppe, F. Hörz, J. Huth, K. Ignatyev, H.A. Ishii, K. Janssens, D. Joswiak, A.T. Kearsley, H. Khodja, A. Lanzirotti, J. Leitner, L. Lemelle, H. Leroux, K. Luening, G.J. MacPherson, K.K. Marhas, M.A. Marcus, G. Matrajt, T. Nakamura, K. Nakamura-Messenger, T. Nakano, M. Newville, D.A. Papanastassiou, P. Pianetta, W. Rao, C. Riekel, F.J.M. Rietmeijer, D. Rost, C.S. Schwandt, T.H. See, J. Sheffield-Parker, A. Simionovici, I. Sitnitsky, C.J. Snead, F.J. Stadermann, T. Stephan, R.M. Stroud, J. Susini, Y. Suzuki, S.R. Sutton, S. Taylor, N. Teslich, D. Troadec, P. Tsou, A. Tsuchiyama, K. Uesugi, B. Vekemans, E.P. Vicenzi, L. Vincze, A.J. Westphal, P. Wozniakiewicz, E. Zinner, M.E. Zolensky, Elemental compositions of comet 81P/Wild 2 samples collected by Stardust. Science **314**, 1731–1735 (2006)

G.J. Flynn, F. Horz, S. Bajt, S.R. Sutton, In-situ chemical analysis of extraterrestrial material captured in aerogel. Lunar Planet. Sci. **27**, 369–370 (1996) (abstr.)

P. Hoppe, F.J. Stadermann, T. Stephan, C. Floss, J. Leitner, K.K. Marhas, F. Hörz, SIMS studies of Allende projectiles fired into Stardust-type aluminum foils at 6 km/sec. Meteorit. Planet. Sci. **41**, 197–209 (2006)

F. Hörz, R. Bastien, J. Borg, J.P. Bradley, J.C. Bridges, D.E. Brownlee, M.J. Burchell, M. Chi, M.J. Cintala, Z.R. Dai, Z. Djouadi, G. Dominguez, T.E. Economou, S.A.J. Fairey, C. Floss, I.A. Franchi, G.A. Graham, S.F. Green, P. Heck, P. Hoppe, J. Huth, H. Ishii, A.T. Kearsley, J. Kissel, J. Leitner, H. Leroux, K. Marhas, K. Messenger, C.S. Schwandt, T.H. See, C. Snead, F.J. Stadermann, T. Stephan, R. Stroud, N. Teslich, J.M. Trigo-Rodríguez, A.J. Tuzzolino, D. Troadec, P. Tsou, J. Warren, A. Westphal, P. Wozniakiewicz, I. Wright, E. Zinner, Impact features on stardust: Implications for comet 81P/Wild 2 dust. Science **314**, 1716–1719 (2006)

H.A. Ishii, S. Brennan, J.P. Bradley, K. Luening, K. Ignatyev, P. Pianetta, Refining the quantitative elemental composition of comet Wild 2 dust in aerogel. Lunar Planet. Sci. **38** (2007), #1736 (abstr.)

E.K. Jessberger, A. Christoforidis, J. Kissel, Aspects of the major element composition of Halley's dust. Nature **332**, 691–695 (1988)

A.T. Kearsley, G.A. Graham, M.J. Burchell, M.J. Cole, Z.R. Dai, N. Teslich, J.P. Bradley, R. Chater, P.A. Wozniakiewicz, J. Spratt, G. Jones, Analytical scanning and transmission electron microscopy of laboratory impacts on Stardust aluminum foils: Interpreting impact crater morphology and the composition of impact residues. Meteorit. Planet. Sci. **42**, 191–210 (2007)

L.P. Keller, S. Bajt, G.A. Baratta, J. Borg, J.P. Bradley, D.E. Brownlee, H. Busemann, J.R. Brucato, M. Burchell, L. Colangeli, L. d'Hendecourt, Z. Djouadi, G. Ferrini, G. Flynn, I.A. Franchi, M. Fries, M.M. Grady, G.A. Graham, F. Grossemy, A. Kearsley, G. Matrajt, K. Nakamura-Messenger, V. Mennella, L. Nittler, M.E. Palumbo, F.J. Stadermann, P. Tsou, A. Rotundi, S.A. Sandford, C. Snead, A. Steele, D. Wooden, M. Zolensky, Infrared spectroscopy of comet 81P/Wild 2 samples returned by Stardust. Science **314**, 1728–1731 (2006)

J. Leitner, T. Stephan, A.T. Kearsley, F. Hörz, G.J. Flynn, S.A. Sandford, TOF-SIMS analysis of crater residues from Wild 2 cometary particles on Stardust aluminum foil. Meteorit. Planet. Sci. (2007a, in press)

J. Leitner, T. Stephan, A.T. Kearsley, F. Hörz, G.J. Flynn, S.A. Sandford, TOF-SIMS analysis of Wild 2 cometary matter collected by Stardust aluminum foil. Lunar Planet. Sci. **38** (2007b), #1591 (abstr.)

H. Leroux, F.J.M. Rietmeijer, M.A. Velbel, A.J. Brearley, D. Jacob, F. Langenhorst, J.C. Bridges, T.J. Zega, R.M. Stroud, P. Cordier, R.P. Harvey, M. Lee, M. Gounelle, M.E. Zolensky, A TEM study of thermally modified comet 81P/Wild 2 dust particles by interactions with the aerogel matrix during the Stardust capture process. Meteorit. Planet. Sci. (2007, in press)

K. Lodders, Solar system abundances and condensation temperatures of the elements. Astrophys. J. **591**, 1220–1247 (2003)

K.D. McKeegan, J. Aléon, J. Bradley, D. Brownlee, H. Busemann, A. Butterworth, M. Chaussidon, S. Fallon, C. Floss, J. Gilmour, M. Gounelle, G. Graham, Y. Guan, P.R. Heck, P. Hoppe, I.D. Hutcheon, J. Huth, H. Ishii, M. Ito, S.B. Jacobsen, A. Kearsley, L.A. Leshin, M.-C. Liu, I. Lyon, K. Marhas, B. Marty, G. Matrajt, A. Meibom, S. Messenger, S. Mostefaoui, S. Mukhopadhyay, K. Nakamura-Messenger, L. Nittler, R. Palma, R.O. Pepin, D.A. Papanastassiou, F. Robert, D. Schlutter, C.J. Snead, F.J. Stadermann, R. Stroud, P. Tsou, A. Westphal, E.D. Young, K. Ziegler, L. Zimmermann, E. Zinner, Isotopic compositions of cometary matter returned by Stardust. Science **314**, 1724–1728 (2006)

D. Rost, T. Stephan, E.P. Vicenzi, E.S. Bullock, G.J. MacPherson, A.J. Westphal, C.J. Snead, G.J. Flynn, S.A. Sandford, M.E. Zolensky, TOF-SIMS analysis of cometary matter in Stardust aerogel tracks. Lunar Planet. Sci. **38** (2007), #2346 (abstr.)

S.A. Sandford, J. Aléon, C.M.O'D. Alexander, T. Araki, S. Bajt, G.A. Baratta, J. Borg, J.P. Bradley, D.E. Brownlee, J.R. Brucato, M.J. Burchell, H. Busemann, A. Butterworth, S.J. Clemett, G. Cody, L. Colangeli, G. Cooper, L. d'Hendecourt, Z. Djouadi, J.P. Dworkin, G. Ferrini, H. Fleckenstein, G.J. Flynn, I.A. Franchi, M. Fries, M.K. Gilles, D.P. Glavin, M. Gounelle, F. Grossemy, C. Jacobsen, L.P. Keller, A.L.D. Kilcoyne, J. Leitner, G. Matrajt, A. Meibom, V. Mennella, S. Mostefaoui, L.R. Nittler, M.E. Palumbo, D.A. Papanastassiou, F. Robert, A. Rotundi, C.J. Snead, M.K. Spencer, F.J. Stadermann, A. Steele, T. Stephan, P. Tsou, T. Tyliszczak, A.J. Westphal, S. Wirick, B. Wopenka, H. Yabuta, R.N. Zare, M.E. Zolensky, Organics captured from comet 81P/Wild 2 by the Stardust spacecraft. Science **314**, 1720–1724 (2006)

T. Stephan, TOF-SIMS in cosmochemistry. Planet. Space Sci. **49**, 859–906 (2001)

T. Stephan, G.J. Flynn, S.A. Sandford, M.E. Zolensky, TOF-SIMS analysis of comet Wild 2 particles extracted from Stardust aerogel. Lunar Planet. Sci. **38** (2007a), #1126 (abstr.)

T. Stephan, G.J. Flynn, S.A. Sandford, M.E. Zolensky, TOF-SIMS analysis of cometary particles extracted from Stardust aerogel. Meteorit. Planet. Sci. (2007b, in press)

T. Stephan, D. Rost, E.P. Vicenzi, E.S. Bullock, G.J. MacPherson, A.J. Westphal, C.J. Snead, G.J. Flynn, S.A. Sandford, M.E. Zolensky, TOF-SIMS analysis of cometary matter in Stardust aerogel tracks. Meteorit. Planet. Sci. (2007c, in press)

P. Tsou, D.E. Brownlee, S.A. Sandford, F. Hörz, M.E. Zolensky, Wild 2 and interstellar sample collection and Earth return. J. Geophys. Res. **108**, E8113 (2003)

A.J. Westphal, C. Snead, J. Borg, E. Quirico, P.-I. Raynal, M.E. Zolensky, G. Ferrini, L. Colangeli, P. Palumbo, Small hypervelocity particles captured in aerogel collectors: Location, extraction, handling and storage. Meteorit. Planet. Sci. **37**, 855–865 (2002)

A.J. Westphal, C. Snead, A. Butterworth, G.A. Graham, J.P. Bradley, S. Bajt, P.G. Grant, G. Bench, S. Brennan, P. Pianetta, Aerogel keystones: Extraction of complete hypervelocity impact events from aerogel collectors. Meteorit. Planet. Sci. **39**, 1375–1386 (2004)

M.E. Zolensky, T.J. Zega, H. Yano, S. Wirick, A.J. Westphal, M.K. Weisberg, I. Weber, J.L. Warren, M.A. Velbel, A. Tsuchiyama, P. Tsou, A. Toppani, N. Tomioka, K. Tomeoka, N. Teslich, M. Taheri, J. Susini, R. Stroud, T. Stephan, F.J. Stadermann, C.J. Snead, S.B. Simon, A. Simionovici, T.H. See, F. Robert, F.J.M. Rietmeijer, W. Rao, M.C. Perronnet, D.A. Papanastassiou, K. Okudaira, K. Ohsumi, I. Ohnishi, K. Nakamura-Messenger, T. Nakamura, S. Mostefaoui, T. Mikouchi, A. Meibom, G. Matrajt, M.A. Marcus, H. Leroux, L. Lemelle, L. Le, A. Lanzirotti, F. Langenhorst, A.N. Krot, L.P. Keller, A.T. Kearsley, D. Joswiak, D. Jacob, H. Ishii, R. Harvey, K. Hagiya, L. Grossman, J.N. Grossman, G.A. Graham, M. Gounelle, Ph. Gillet, M.J. Genge, G. Flynn, T. Ferroir, S. Fallon, D.S. Ebel, Z.R. Dai, P. Cordier, B. Clark, M. Chi, A.L. Butterworth, D.E. Brownlee, J.C. Bridges, S. Brennan, A. Brearley, J.P. Bradley, P. Bleuet, P.A. Bland, R. Bastien, Mineralogy and petrology of comet 81P/Wild 2 nucleus samples. Science **314**, 1735–1739 (2006)

Section VI: Future – The Rosetta Mission

Composition Measurements of a Comet from the Rosetta Orbiter Spacecraft

S. Gulkis · C. Alexander

Originally published in the journal Space Science Reviews, Volume 138, Nos 1–4.
DOI: 10.1007/s11214-008-9335-2

Abstract The European Space Agency (ESA) Rosetta Spacecraft, launched on March 2, 2004 toward Comet 67P/Churyumov-Gerasimenko (C-G), carries a complementary set of instruments on both the orbiter and lander (Philae) portions of the spacecraft, to measure the composition of the Comet C-G. The primary composition measuring instruments on the Orbiter are Alice, COSIMA, ICA, MIRO, OSIRIS, ROSINA and VIRTIS. These instruments collectively are capable of providing compositional information, including temporal and spatial distributions of important atomic, molecular, and ionic species, minerals, and ices in the coma and nucleus. The instruments utilize a variety of techniques and wavelength ranges to accomplish their objectives. This paper provides an overview of composition measurements that will be possible using the suite of orbiter composition measuring instruments. A table is provided that lists important species detectable (depending on abundances) with each instrument.

Keywords Comets · Rosetta · Composition · Spectroscopy · Spacecraft instruments

1 Introduction

The processes that led to the formation of comets are currently unknown. Advancing our knowledge of cometary formation beyond the widely used statements that a) comets formed from interstellar material and b) comets are among the oldest and most pristine objects in the solar system is difficult because one is confronted with both an incomplete knowledge of the physical and chemical pathways leading from interstellar clouds (and the interstellar medium) to the current dynamical reservoirs of comets (e.g., Oort Cloud and Kuiper belt, scattered disk), and because we have an incomplete knowledge of comets themselves. Both of these areas of research will need to advance considerably before we can have a clear picture of the formation history of comets. Central to the question of how comets formed

S. Gulkis (✉) · C. Alexander
Jet Propulsion Laboratory, California Institute of Technology, 4800 Oak Grove Drive, MS 169-506, Pasadena, CA 91109, USA
e-mail: Samuel.Gulkis@jpl.nasa.gov

H. Balsiger et al. (eds.), *Origin and Early Evolution of Comet Nuclei*
DOI: 10.1007/978-0-387-85455-7_17

is 1) whether comets are conglomerates of unprocessed interstellar grains, 2) whether they formed from interstellar material energetically processed in such a way that obscures the connection with the interstellar medium, or 3) whether they represent chemical disequilibrium assemblages of the cold, low-density regions of the solar nebula rather than the interstellar environment itself. An objective of the European Space Agency (ESA) Rosetta Spacecraft, launched on March 2, 2004 toward Comet 67P/Churyumov-Gerasimenko (C-G) is to obtain a comprehensive set of measurements of C-G that will greatly increase our knowledge of this comet and help to illuminate the processes and pathways leading to the origin of comets in general.

Many molecules identified in molecular clouds are also found in cometary comae thereby suggesting a link between the two. However, this correlation by itself does not prove that comets formed from interstellar clouds (i.e. Irvine et al. 2000; Ehrenfreund et al. 2004 and references therein). A few examples from the literature illustrate this point. Ehrenfreund et al. (2004) mention that the molecules CS_2 and C_2H_6 have been observed in cometary comae although they have not yet been identified in molecular clouds. Ehrenfreund et al. also mention the existence of crystalline silicates in comets, detected in IR spectra, as an argument for the presence of "high-temperature" materials in comets. Crystalline silicates appear to have a low abundance in the interstellar medium. The presence of crystalline silicates, "high-temperature" materials, in comets along with an abundant presence of "low-temperature" volatile material suggests a complex formation history. As a final example, Irvine et al. (2000) discuss the observations of the ortho/para ratios (OPR) of cometary water in the comets 1P (Halley), C/1995 O1 (Hale-Bopp), 103 P (Hartley 2) and C/1986 P1 (Wilson). The spin temperatures derived from OPR measurements for the first three of these comets is 25–35 K, whereas it is >50 K for C/1986 P1 (Wilson). Since C/1986 P1 (Wilson) is the only dynamically new comet in the list above, it has been suggested that the high temperature derived from the OPR measurement for C/1986 P1 (Wilson) was probably reset by radiation damage while the comet was in the Oort Cloud. Irvine et al. (2000) also note that the derived temperatures for 1P (Halley) and C/1995 O1 (Hale-Bopp) are significantly lower than those derived from the [D]/[H] ratio in the solar nebula thereby suggesting an uncertainty in the meaning of the OPR derived temperatures. These and other examples of confusing or conflicting data have led to suggested explanations (e.g., Irvine et al. 2000; Notesco and Bar-Nun 1996; Notesco and Bar-Nun 1997) in terms of chemical fractionation during sublimation, trapping of gases as ice particles, and condensation; all point toward the possibility of a complex relationship between comets and the interstellar medium. Untangling the relationships between comets and interstellar clouds is an important research area that will be addressed by the Rosetta Spacecraft.

Ehrenfreund et al. (2004), Wooden et al. (2007) and others have discussed certain markers that can be used to compare the material in comets with interstellar cloud material. These markers can be used in general to help establish relationships between cometary and interstellar material, and specifically they can help to guide future composition measurements. A few examples illustrate specific markers that can be studied. These include:

1) comparing coma molecules that originate directly from the nucleus, sometimes called native molecules, with observations of interstellar ices and gases found in dark molecular clouds and in regions of star formation. A cometary measurement objective is to discriminate between native molecules and those that form in the coma from large organic particles or molecules;
2) comparing the ice phases (amorphous, crystalline, clathrates) that are believed to be associated with interstellar grain mantles and cometary ices. If ice from interstellar grains is incorporated into comets, it may be searched for directly or by studying the outgassing

pattern of volatiles as a function of heliocentric distance. Carbon dioxide and CH_3OH are suggested as possible tracer gases to study for an interstellar/cometary link;
3) establishing the abundance of N_2 in comets and comparing it with the N_2 in the interstellar medium where it is efficiently produced;
4) establishing isotopic fractionation in comets and comparing that with the interstellar medium values;
5) determining the source of HNC and other isomeric molecules in comets. Are they native to the nucleus or are they formed from large organic compounds in the coma; and
6) determining the ortho-to-para ratios in cometary molecules. The measurements may provide an estimate of the temperature of the gas and dust that formed comets and these can be compared with temperatures in cold interstellar clouds.

The Rosetta Spacecraft will rendezvous, go into orbit, and send a lander to the surface of Comet 67P/Churyumov-Gerasimenko in 2014. Glassmeier et al. (2007) have provided an overview of the Rosetta Mission. The mission will produce an extensive inventory of the composition of the target Comet C-G, including atomic, molecular, isotopic, organic and mineralogical (in the case of dust) compounds. Gas observations can be obtained in a manner that captures the energy states (rotational and vibrational levels) for some of the detected species. The measurements, once obtained, will provide constraints on the sources of the volatiles detected in the C-G coma. Parent and daughter molecules will be identified by their sources of origin. Parent molecules originate from the nucleus; daughter molecules are expected to be formed from heavy molecules in extended regions in the coma. The Rosetta observations will greatly improve our knowledge of a single comet, and with this knowledge will come a better understanding of the processes that formed all comets.

This paper provides an overview of composition measurements that will be possible using the orbiter instruments Alice, COSIMA, ICA, MIRO, OSIRIS, ROSINA, and VIRTIS. Emphasis is placed on the importance of using the collective data from all the instruments as a means to cross check assumptions that go into the analysis of data from the individual instruments.

2 Brief Descriptions of the Instruments

2.1 Alice

The Alice instrument is an imaging UV spectrograph, designed to obtain spatially-resolved spectra of the target comet in the 700–2050 Å spectral range. Stern et al. (2007) provide a detailed description of the instrument and the science objectives. Table 1 provides a summary of key characteristics of the Alice instrument. The spectral range covered by the instrument includes parts of the extreme-ultraviolet (EUV) and far-ultraviolet (FUV) wavelength ranges. Feldman et al. (2004) discuss spectroscopic observations in this wavelength range. The spectral resolution, $\Delta\lambda$, is between 8 Å and 12 Å ($\lambda/\Delta\lambda = 70$–$170$) for extended sources that fill the instrument's $\sim 0.05 \times 6.0^\circ$ field of view. The Principal Investigator of the Alice investigation is J. Parker (The initial Principal Investigator of Alice was S. A. Stern) of the Southwest Research Institute (SwRI) in Boulder, Colorado.

Four categories of composition are emphasized by the Alice team (Stern et al. 2007). These are the 1) noble gases, 2) parent molecules, 3) atoms, and 4) coma ions. Table 2 provides examples of species associated with these four categories. The parent molecule abundances of CO and CO_2 are determined indirectly in the Alice experiment. The total CO abundance is determined by measuring the fluorescence emission in the 1300–1900 Å

Table 1 Characteristics of the Alice instrument from Stern et al. (2007). Additional characteristics are provided in the same reference

Parameter	Description
Total spectral passband	680 Å to 2060 Å
Spectral resolution	8–12 Å (extended source)
Spatial resolution	$0.05° \times 0.6°$ (35×420 m^2 at 40 km from nucleus
Effective area (flight)	.02 cm^2 at 1575 Å and .05 cm^2 at 1125 Å
Stray light attenuation	-40 dB and -90 dB at $>4°$ and $>60°$ from boresight respectively
Telescope	Off-axis paraboloidal
Spectrograph	Rowland circle
Detector type	2-D Microchannel Plate w/double delay line readout

Table 2 This table provides examples of species that will be searched for with the Alice instrument. The table provides the wavelength in angstroms (Å) of the searched for transition, the type of transition, and the category identification according to the type of species

Atom or molecule	Wavelength, Å	Transition type	Category
He I	584	Resonance	Noble gas
Ne I	736/744	Resonance	Noble gas
Ar I	1048/1067	Resonance	Noble gas
Kr I	1236	Resonance	Noble gas
N_2	850–900/1000–1100	Electronic	
H_2O		Absorption in UV	Parent molecule
CO	1300–1900	Fluorescence	Parent molecule
	1900–2050	Cameron bands	
CO_2		Determined from CO Cameron bands	Parent molecule
H I	1216	Resonance	Atoms
	973		
	1025		
O I	1304	Resonance	Atoms
	989		
C I	1561	Resonance	Atoms
	1657		
	1931		
N I	1134	Resonance	Atoms
	1200		
S I	1813	Resonance	Atoms
	1474		
	1425		
O^+	834		Coma ions
N^+	1085		Coma ions
S^+	910, 1256		Coma ions
C^+	1036, 1335		Coma ions

Table 3 Characteristics of the COSIMA instrument from Kissel et al. (2007). Additional characteristics are provided in the same reference

Parameter	Description
Atomic mass range	1–3500 amu
Atomic mass resolution	$m/\Delta m$ (at $m = 100$ amu) > 2000 at 50% peak width
Indium ion pulse duration	<3 ns
Indium ion energy	8 keV
Ion beam width	~50 μm FWHM

spectral range; the Cameron bands of CO are observed between 1900–2050 Å. From these two sets of observations, a model is used to estimate abundances of the parent molecules CO and CO_2. Weaver et al. (1994) discuss various sources which contribute to the Cameron band emission. For comet P/Hartley 2 (1991 XV), they estimate that ~60% of the total excitation of the Cameron band emission is due to photodissociative excitation of CO_2. Stern et al. (2007) mention the high volatility of the noble gases, and their importance to the determination of the thermal history of comets. Planetary models requiring noble gas contributions from comets will also benefit from the knowledge of noble gases in comets.

2.2 COSIMA

The COSIMA (Cometary Secondary Ion Mass Analyser) instrument is a high-resolution, time-of-flight (TOF), secondary ion mass spectrometer (SIMS). Kissel et al. (2007) provide a detailed description of the instrument and the science objectives. The experiment's goal is *in situ* analysis of the elemental composition (and isotopic composition of key elements) of cometary grains (dust particles). This instrument allows a mass analysis of individual dust particles. The Principal Investigator of the COSIMA investigation is M. Hilchenbach (The initial Principal Investigator of COSIMA was J. Kissel) of the Max-Planck-Institut für Sonnensystemforschung in Katlenburg-Lindau, Germany.

Cometary dust is collected in this instrument on metal covered targets. Although the dust grains themselves are collected *in situ*, they are not individually time tagged thereby making it difficult to know where and when the grains were collected. Following identification on the targets, individual dust grains are illuminated by a pulsed primary indium ion beam, which releases secondary ions from the grains. These ions, either positive or negative, are selected and accelerated by electrical fields and travel a well-defined distance through a drift tube and an ion reflector. A micro-sphere plate with dedicated amplifier is used to detect the ions and measure their exact arrival times. As the flight times of the ions depend on their masses, the time-of-flight spectra can be converted into mass spectra. The instrument covers a very large mass range, from 1 to 3500 amu, with a mass resolution $m/\Delta m$ @ 50% of 2000 at mass 100 amu. Table 3 provides a summary of key characteristics of the COSIMA instrument.

The chemical characterization will include the main organic components, present homologous and functional groups, as well as the mineralogical and petrographical classification of the inorganic phases. Laboratory calibration measurements of the major expected mineral and chemical classes and groups are being conducted as part of the instrument calibration. Table 4 provides a partial list of the first in-flight species measurements with the COSIMA instrument.

Table 4 Partial list of first positive and negative in flight detections with the COSIMA instrument (Kissel et al. 2007). Data represent the target material as no dust was collected so far

Classification	Detection	Type
Unique ID	$^{12}CH_3$, H_3O, NO, C_4H_7, ^{107}Ag, ^{108}Ag	SIM + ion
Mixed organic and inorganic	N, O, Si, SiH, ^{38}K, ^{41}K, $SiCH_3$, ^{56}Fe, ^{57}Fe	SIM + ion
Organic (mostly hydrocarbons)	$^{12}CH_2$, $^{13}CH_3$, C_2H_4, C_3H_3, C_3H_7, C_4H_8	SIM + ion
Elemental	^{12}C, ^{13}C, ^{16}O, ^{17}O, ^{18}O, ^{35}Cl, ^{37}Cl, ^{79}Br, ^{81}Br	SIM − ion

2.3 ICA

The Rosetta Plasma Consortium (RPC) instrument on the ESA Rosetta orbiter is composed of five distinct instruments: the Ion Composition Analyser (ICA), the Ion and Electron Sensor (IES), the dual Langmuir Probes (LAP), a dual, tri-axial Fluxgate Magnetometer (MAG), and the Mutual Impedance Probe (MIP), in addition to the Plasma Interface Unit (PIU). The combined set of instruments is designed to measure the hot and cold plasma density, velocity, temperature, wave activity, magnetic field, and ion composition near the Comet C-G. Two of the five sensors, ICA and IES are designed to measure ions in the solar wind and cometary plasmas, and of these two only the ICA instrument provides a measurement of ion mass. The IES instrument is not discussed here since it measures energy/charge and not explicitly mass. Nilsson et al. (2007) provide a detailed description of the ICA instrument and the science objectives. The Principal Investigator of the ICA investigation is Dr. Rickard Lundin of the Swedish Institute for Space Physics in Kiruna, Sweden.

The ICA instrument on Rosetta is almost identical (Nilsson et al. 2007) to the ASPERA-3 IMA instrument on the Mars Express spacecraft (Lundin and Barabash 2004). The instrument operates (Nilsson et al. 2007) using three sequential sorting operations on positive ions. Incident ions are first selected by arrival angle, then by energy range, and finally by mass. The positive ions passing through the system eventually hit a microchannel plate and are detected by an anode system. ICA measures ions in the energy range from 25–40 keV/e. The instrument has an energy resolution of 7% (Nilsson et al. 2007) and a mass range from 1 to 10^6 amu. The mass-resolution is a function of the ion energy, and is better at low energies. The mass-resolution is sufficient to enable the distinction between major cometary and solar wind ion constituents (e.g., H^+, He^{++}, He^+, O^{++}, O^+, CO_2^+) although not all species can be resolved at all energies. Very large ionized molecules and charged dust particles can be detected with this instrument because of its large mass range, up to a million amu. This instrument has the largest mass range of all of the instruments discussed in this paper.

2.4 MIRO

The MIRO (Microwave Instrument for the Rosetta Orbiter) instrument is a dual frequency, heterodyne radiometer, designed for remote sensing of the target comet nucleus and coma. MIRO uses a 30-cm diameter, offset parabolic reflector telescope to sense remotely the coma and nucleus. Center-band operating frequencies are near 190 GHz (1.6 mm) and 562 GHz (0.5 mm). Broadband, total power continuum channels are implemented in both bands to measure the nucleus brightness temperatures. Radiometric calibration of the MIRO instrument is obtained by switching the input to the receivers between the sky and two blackbody targets, each maintained at a different temperature. A 4096 channel CTS (Chirp Transform

Table 5 Characteristics of the MIRO instrument from Gulkis et al. (2007). Additional characteristics are provided in the same reference

Parameter	Millimeter	Submillimeter
Instrument type	Continuum	Continuum and Spectral
Beam size (FWHM)	23.7 × 24.7 arc min	7.7 arc min
Foot-print at 10 km distance	75 m	25 m
Frequency	190 GHz	547.5–580.5 GHz
IF bandwidth	550 GHz	1100 MHz continuum
Spectral resolution		44 kHz
Number of channels		4096 (spectroscopic)
DSB noise temp	800 K	3800 K
Continuum sensitivity	<1 K/s continuum	<1 K/s continuum
Spectroscopic sensitivity		2 K/120 s @ 300 kHz

Table 6 Molecules and eight transition frequencies observable with MIRO instrument (Gulkis et al. 2007). Species are grouped according to ordinary names (water, carbon monoxide, ammonia, and methanol)

Molecules	Frequency (MHz)	Transition
$H_2{}^{16}O$	556936.002	1(1,0)–1(0,1)
$H_2{}^{17}O$	552020.960	1(1,0)–1(0,1)
$H_2{}^{18}O$	547676.440	1(1,0)–1(0,1)
CO	576267.9305	J(5-4)
NH_3	572498.3784	J(1-0)
CH_3OH	553146.296	8 (1)–7 (0) E
CH_3OH	568566.054	3 (−2)–2(−1) E
CH_3OH	579151.005	12 (−1)–11(−1) E

Spectrometer) having a resolution of 44 kHz is connected to the submillimeter receiver. The absolute frequency of the MIRO instrument is maintained through the use of an ultra stable oscillator (USO) reference signal. Gulkis et al. (2007) provide a detailed description of the instrument and the science objectives. Table 5 provides a summary of key characteristics of the MIRO instrument. The Principal Investigator of the MIRO investigation is S. Gulkis of the Jet Propulsion Laboratory (JPL), California Institute of Technology in Pasadena, California.

The CTS is fixed tuned to measure simultaneously four volatile species—CO, CH_3OH, NH_3 and three isotopologues of water, $H_2{}^{16}O$, $H_2{}^{17}O$ and $H_2{}^{18}O$ in the comet coma. The corresponding transitions are shown in Table 6. The MIRO experiment will use these species as probes of the physical conditions within the nucleus and coma. The basic quantities measured by MIRO are surface temperature, gas production rates and relative abundances, and velocity and excitation temperature of each species, along with their spatial and temporal variability. The spectral resolution is sufficient to observe individual, thermally broadened spectral lines ($T \geq 10$ K). During spectroscopic observations, the submillimeter wave re-

ceiver is operated in a frequency switched mode to eliminate residual baseline ripple and long-term (>5 s) gain variations.

2.5 OSIRIS

The OSIRIS (Optical, Spectroscopic, and Infrared Remote Imaging System) instrument is a dual camera system comprised of a narrow angle camera (NAC) and a wide-angle camera (WAC). Keller et al. (2007) provide a detailed description of the instrument and the science objectives. The NAC has been designed to perform high spatial resolution (angular resolution of 18.6 μrad/px) mapping of the nucleus. The WAC provides a large field of view for the observation of dust and gas in the vicinity of the nucleus. The angular resolution is 104 μrad/px with a field of view (FOV) of 12.1° × 12.7°. The WAC has good stray-light properties to allow observation of faint gas and dust emissions close to the relatively bright nucleus. The NAC FOV is approximately at the centre of the WAC FOV. Table 7 (Keller et al. 2007) gives the optical properties of the OSIRIS cameras. The Principal Investigator of the OSIRIS investigation is U. Keller of Max-Planck-Institut für Sonnensystemforschung in Katlenburg-Lindau, Germany.

The NAC and WAC cameras are both equipped with a dual filter wheel system having 16 positions. The filters were optimized for the two cameras individually. A list of filters for both cameras is shown in Table 8. The NAC has a series of broad band (≈50 nm) interference filters that cover a wavelength range of 250 to 1000 nm. The spectral resolution of the NAC is insufficient to detect any emission from radicals in this wavelength range because of the presence of the dust continuum. The WAC is designed to measure a number of important radicals including CS, OH, NH, CN, NH_2, and O I. A broadband green filter is used in both the NAC and WAC cameras.

For composition measurements at Comet C-G, OSIRIS can study the 2-D distribution of several important radicals including the dissociation product of water, OH. Working in combination with ROSINA and MIRO, OSIRIS should be able to place constraints on the gas flow field near the nucleus. Work is still needed in the definition of effective "g-factors" (emission rates) for some radicals before they have reached fluorescence equilibrium. Accurate dissociation rates are also needed.

Dust continuum data must be acquired to allow removal of the contribution of scattered sunlight from the gas filter images. The WAC filters were selected with this application in mind. After subtraction of the continuum, the inversion to produce column densities through use of the "g-factor" (i.e., Bockelée-Morvan et al. 2004) is possible. At large cometocentric distances, column densities can be derived reliably. For small cometocentric distances, the

Table 7 Optical properties of the OSIRIS Narrow Angle Camera (NAC) and Wide Angle Camera (WAC)

Property	NAC	WAC
Angular scale at centre of field [μrad/px]	18.6	104.0
Field of view [°]	2.2 × 2.2	12.1 × 12.7
Point spread function (FWHM) [px]	1.4	1.4
Optimum focus range [km]	1–∞	0.2–∞
$F\#$	8	5.6
Nominal minimum exposure time [ms]	50	50
Limiting magnitude	12	16

Table 8 NAC and WAC filters and provisional sensitivities

NAC filter	Wavelength [nm]	Sensitivity [(W/m^2/sr/nm)/(DN/s)] $\times 10^{-8}$	WAC filter	Wavelength [nm]	Sensitivity [(W/m^2/sr/nm)/(DN/s)] $\times 10^{-8}$
FUV	270	32	UV245	245	51
NUV	359	8.4	CS	257	150
Blue	480	2.1	UV295	295	130
Green	535	1.9	OH	308	270
Orange	645	1.0	UV325	325	32
Red	740	1.4	NH	335	250
Ortho	800	3.5	UV375	375	25
NIR	880	2.5	CN	388	13
Fe_2O_3	940	6.5	green	535	0.85
IR	990	14	NH_2	571	4.9
			Na	589	10
			Vis	610	3.8
			O I	630	13
			R	640	0.28

"g-factor" may be difficult to compute for certain radicals such as CN, NH, NH_2 and probably CS. If the timescale to reach fluorescence equilibrium is short in comparison to the time it takes the outflow to cross the field of view of the WAC, then an effective "g-factor" will need to be calculated. This is likely to introduce uncertainties close to the nucleus.

2.6 ROSINA

The Rosetta Orbiter Spectrometer for Ion and Neutral Analysis (ROSINA) instrument (Balsiger et al. 2007) consists of two mass spectrometers (DFMS and RTOF) having complementary capabilities, and a pressure sensor (COPS) which provides density and velocity measurements of the coma gas. DFMS and RTOF measure the composition of the volatile material (ions and molecules) in the coma; we limit the discussion of ROSINA to these two mass spectrometers. The Principal Investigator of the ROSINA investigation is H. Balsiger from the Physikalisches Institut, Universität Bern, in Bern, Switzerland.

DFMS is a double focusing mass spectrometer with a mass range from 12 to 150 amu. The design is optimized for very high mass resolution and dynamic range. The mass resolution is 3000 at 1% peak height. Two basic operation modes allow this sensor to analyze both neutral coma gases and primary ions. RTOF is a reflection type time-of-flight mass spectrometer with a mass range 1 to >300 amu. The design is optimized for high sensitivity over a very broad mass range. The mass resolution is better than 500 at 1% peak height. The main characteristics of the two instruments are given in Table 9.

ROSINA's very wide mass range will allow it to observe from 1 amu (Hydrogen) to >300 amu (organic molecules). DFMS's very high mass resolution (>3000 $m/\Delta m$) is needed to resolve molecules having closely similar masses (Balsiger et al. 2007) such as CO and N_2, $^{40}Ar^{++}$(19.9812) and $^{20}Ne^{+}$(19.9024), and $^{13}C^{+}$(13.0033) and $^{12}CH^{+}$(13.0078). The instrument has a very wide dynamic range (10^{10}) and high sensitivity ($>10^{-5}$ A/mbar) to accommodate very large differences in ion and neutral gas concentrations and large

Table 9 Characteristics of the ROSINA instrument from Balsiger et al. (2007). Additional characteristics are provided in the same reference

Name	Mass range [amu]	Mass resolution $m/\Delta m$ (at 1%)	Sensitivity gas [A/mbar] (1)	Ion (2)	Dynamic range (3)	Pressure range [mbar] (4)	FOV	Highest time resolution for full spectrum
DFMS (5)	12–150	3000	10^{-5}	10^4	10^{10}	10^{-5}–10^{-15}	$20° \times 20°$ $2° \times 2°$ (6)	120 s
RTOF	1–>300	>500	10^{-4}	10^3	$10^6/10^8$	10^{-6}–10^{-17}	$10° \times 40°$	4 s

(1) 1×10^{-3} A/mbar corresponds to 0.2 counts/s if density is 1 cm^{-3}.
Emission current of the ion source at 10 mA, can be increased (up to a factor of 5) or decreased
(2) Counts per second for cometary ion density of 1 cm^{-3}
(3) Ratio of highest to lowest peak in one measurement cycle
(4) Total measurement range
(5) High resolution mode
(6) Narrow field of view entrance

Table 10 Spectral ranges and resolutions of the three data channels in the VIRTIS instrument

Parameter	VIRTIS-M-Visible	VIRTIS-M-Infrared	VIRTIS-H
Spectral range (nm)	220.1–1046.0	952.8–5059.2	2000–5000
Spectral resolution ($\lambda/\Delta\lambda$)	100–380	70–360	1300–3000

changes in the ion and gas flux as the comet changes activity between aphelion and perihelion.

To ensure that absolute gas densities can be determined, each mass-spectrometer carries a reservoir of a calibrated gas mixture allowing in-flight calibration. Furthermore identical flight-spares of all three sensors serve for detailed analysis of all relevant parameters, in particular the sensitivities for complex organic molecules and their fragmentation patterns in electron bombardment.

2.7 VIRTIS

The Visual IR Thermal Imaging Spectrometer (VIRTIS) instrument on Rosetta (Coradini et al. 2007) has three different data channels housed together in a single instrument. Two of the data channels are devoted to spectral mapping and are housed in the Mapper(-M) optical subsystem. The two data channels are referred to as VIRTIS-M Visible and VIRTIS-M InfraRed. The third channel is used solely for high-resolution spectroscopy; it is a single pixel spectrometer and uses an independent, High (-H) resolution optical system. This channel is referred to as VIRTIS-H. Key characteristics of the VIRTIS instrument are shown in Table 10. The Principal Investigator of the VIRTIS investigation is A. Coradini of INAF, Istituto di Fisica Dello Spazio Interplanetario in Roma, Italy.

The VIRTIS instrument is designed to study ices, silicate, and hydrocarbon solid materials on the nucleus and volatile gases in the coma. The overall bandwidth of VIRTIS (0.22–5

microns) contains spectral bands diagnostic of ices, minerals, and organic compounds that might be present on the nucleus surfaces. Examples of ices that might be detected on the surface include H_2O, CO_2, CH_4, CO, NH_3, H_2S, SO_2, and N_2. Diagnostic features of ferric and ferrous minerals, Olivine, Pyroxene, hydrated minerals, clay minerals, Phyllosilicates Carbonates and Magnetite are also located within the VIRTIS band. The reflectance spectra of solid hydrocarbons (CH_4, C_2H_2, C_2H_4, C_2H_6, C_3H_8, etc.) are also found in the VIRTIS band making the identification of solid hydrocarbons possible.

The wide wavelength coverage of VIRTIS combined with its high spectral resolution makes it a powerful instrument for studying the coma. The IR portion of the spectrum is rich in fundamental rotational-vibrational bands of parent molecules such as CO, CO_2, CH_3OH, H_2CO, CH_4, NH_3, HCN, H_2S; VIRTIS-H will be able to detect isotopic species such as ^{13}CO, $H_2{}^{17}O$, $H_2{}^{18}O$, HDO. In the UV and VIS VIRTIS can observe OH, CN, NH, CH, C_2, NH_2, O I plus many ions CH^+, CO^+, H_2O^+, N_2^+.

3 Conclusions

The Rosetta orbiter composition-measuring instruments Alice, COSIMA, ICA, MIRO, OSIRIS, ROSINA, and VIRTIS, all very capable instruments by themselves, are even more capable when considered as a group. This suite of Rosetta instruments will provide composition measurements of the volatile (Alice, MIRO, OSIRIS, ROSINA, and VIRTIS) and dust (COSIMA) components of Comet 67P/Churyumov-Gerasimenko, and determine the ion distribution functions (ICA) for the major cometary and solar wind ion species. The composite data sets will include composition measurements of parent molecules, noble gases, atomic species, ions, heavy (organic) molecules and various isotopic abundances, as well as measurements of ices and minerals. Very heavy ions, up to a million amu, may be detected with the ICA instrument. Two of the instruments (MIRO and VIRTIS) will measure the surface and near surface temperatures of the nucleus (as well as the coma gases) thereby helping to understand the source of the volatile species in terms of the saturation pressures of various species at the nucleus surface.

The five coma gas instruments Alice, MIRO, OSIRIS, ROSINA, and VIRTIS use a variety of techniques and analysis approaches to determine the coma composition. The spectral wavelength range of the remote sounding instruments Alice, OSIRIS, VIRTIS and MIRO (arranged from the shortest to the longest wavelength coverage) is 680 Å to 0.5 mm (68 to 500,000 nm). This range includes the spectral bands from the EUV (Extreme Ultraviolet) to the FIR (far infrared) or submillimeter, as illustrated in Fig. 1. Generally speaking, the shortest wavelength observations (UV and optical) include observations of fragment species, including radicals and ions (Feldman et al. 2004) produced by the photolysis of parent molecules. In the infrared and submillimeter, the spectrum is rich is fundamental rotation and vibration spectra from parent molecules (i.e., Bockelée-Morvan et al. 2004). ROSINA is an *in situ* measuring instrument.

Many of the gaseous coma species will be detected with more than one instrument thereby providing important redundancy by way of observation technique and data analysis. Two factors provide the independent interpretations of the data; first, the wide wavelength coverage of the observations insures that different processes are involved in the states of excitation of the species, and secondly, some measurements are *in situ* and others remote. Redundant measurements allow various assumptions and parameters used in the analysis for each instrument to be cross checked for consistency. Molecular and atomic cross-sections, emission rate (g-factors), density and temperature variations along the line of sight, the

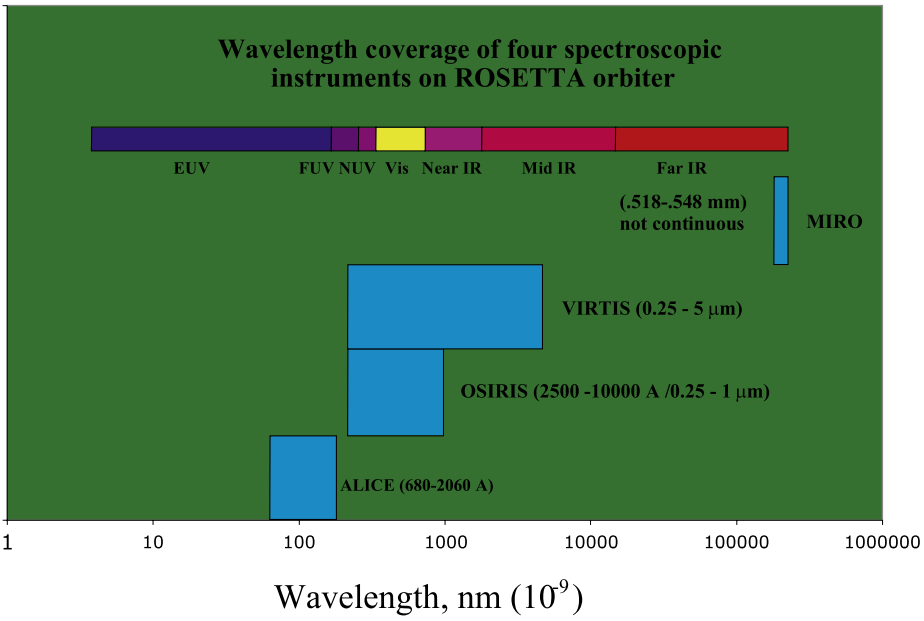

Fig. 1 Figure shows the wavelength coverage of the four spectroscopic instruments on the Rosetta orbiter. The Alice and VIRTIS instruments have full spectroscopic capability over the ranges shown. The OSIRIS and MIRO instruments use fixed frequency filters to search for particular species within the bands indicated

presence or absence of equilibrium conditions, and instrument calibration are typical factors needed to turn the remote sensing observations into abundances. Table 11, inspired by a tabular comparison of identified cometary and interstellar neutral molecules (Huebner et al. 2006), gives a partial list of atomic and molecular species that can be observed with the instruments Alice, OSIRIS, VIRTIS, MIRO, and ROSINA. Table 11 can be used to identify species observable with more than one instrument. For example, Table 11 shows that water can be detected by four instruments including three remote sounding instruments and one *in situ* instrument. OSIRIS can detect the closely related species OH. We note that various isotopic ratios, such as the O^{17}/O^{18} ratio, will be determined using different molecules and approaches, and this will test the consistency of the data. Table 11 can also be used to compare the Rosetta orbiter payload capabilities with the Huebner et al. (2006) pre-Rosetta table. Although COSIMA species are not included in Table 11, it should not be inferred that there is little connection between gas and dust measurements. Isotopic ratio measurements or ortho to para ratios in gas and dust may well have a bearing on the origin of the materials out of which comets formed.

As a final comment, we mention the engineering value of having this complementary set of instruments. It is possible and even likely, due to power limitations, overheating, or equipment failure, that not all of the payload will be powered on simultaneously all the time. We conclude from both scientific and engineering considerations, that the combined data set from all of the instruments will greatly aid in the reliability and interpretation of the data from Rosetta.

Even though Rosetta will study a single comet, Comet 67P/Churyumov-Gerasimenko, the trajectory, orbit, and suite of instruments on the Rosetta Spacecraft are well suited toward making significant advances in our knowledge of comets in general. The trajectory and

Table 11 This table gives a partial list of atomic and molecular species that can be observed with the four remote sounding instruments (Alice, OSIRIS, VIRTIS, MIRO) and the mass spectrometer ROSINA. A "√" mark in a column cell indicates that a particular species is detectable by that instrument, assuming the signal-to-noise is sufficient for detection. A "+" or "++" mark in a column cell indicates that the species is detectable as a positive ion (e.g., H_2O^+ or H_2O^{++}). Ions are not indicated for the ROSINA instrument. A blank cell has the possible two meanings: 1) species not detectable or 2) detectability not known by the authors

Species	Alice	OSIRIS	VIRTIS	MIRO	ROSINA
Atomic					
H	√				√
He	√				√
C	√				√
^{13}C					√
N	√				√
^{15}N					√
O	√				√
$^{17}O/^{18}O$				√	√
Ne	√				√
Si					√
S	√				√
Ar	√				√
Br					√
Kr	√				√
I					√
Diatomic					
H_2					√
CH	√	√	√+		√
NH			√		√
OH		√	√		√
HF					√
C_2			√		√
CN		√	√		√
CO	√		√+	√	√
^{13}CO			√		√
N_2	√		√+		√
NO					√
HCl					√
CS		√			√
NS					√
SO					√
NaCl					√
S_2					√
KCl					√
O I			√		√
Triatomic					
CH_2					√
NH_2		√	√		√
H_2O	√		√+	√	√
HDO			√		√

Table 11 (*Continued*)

$H_2{}^{17}O$		√	√	√
$H_2{}^{18}O$		√	√	√
C_2H				√
HCN		√		√
HNC				√
HCO				√
H_2S		√		√
C_3				√
C_2O				√
CO_2	√	√		√
N_2O				√
OCS				√
SO_2				√
CS_2				√
Quadatomic				
NH_3		√	√	√
HC_2H		√		√
C_2H_2		√		√
H_2CN				√
H_2CO		√		√
HNCO				√
H_2CS				√
Pentatomic				
CH_4		√		√
CH_2NH				√
HCOOH				√
C_4H				√
HC_3N				√
$\gg$5 atoms				
C_2H_4		√		√
C_2H_6		√		√
CH_3OH		√	√	√
CH_3CN				√
CH_3NC				√
CH_2CHO				√
C_3H_8		√		√
NH_2CHO				√

orbit of Rosetta will provide the first opportunity to observe a comet up close for an extended period of time ($>$18 months), and over a wide range of heliocentric distances from $\sim$4.2 AU to perihelion near 1.28 AU. Measurements will be made over cometocentric distances ranging from 2 km to 30 thousand km, or more. In extrapolating Rosetta observations of C-G to conditions in the solar nebula, the problem will be to identify generic comet traits from

unique Churyumov-Gerashimenko properties. Rosetta will provide an excellent data base (as a function of time and heliocentric distance) of the relative abundances of a very large number of species in the coma and nucleus. This Rosetta data base can be used as a reference to address issues related also to the diversity of comets. With its high resolution remote sounding instruments, Rosetta should be able to distinguish between the native composition of the nucleus, and species generated by chemistry or fragmentation in the coma, thereby providing a handle on the parent and daughter processes. Studies of outgassing rates as a function of heliocentric distance may provide evidence of the physical state of the ices that lie below the surface of the nucleus. Rosetta will measure isotopic ratios of elements and ortho/para ratios using different techniques. Consistent results using different techniques will boost our confidence in the interpretation and guide future observations, both ground based and from spacecraft. The Rosetta instruments will be able separate N_2 from CO, and ^{13}C from CH, elements that have heretofore been too difficult to distinguish from one another. N_2 will be distinguished from CO even if the abundance of N_2 is less than 1% of that of CO. Other key markers will be distinguished from one another: HNC/HCN; HDO/H_2O; DCN/HCN. Rosetta will be able to distinguish ^{28}Si from ^{29}Si (an element that is enriched in grains generated in supernovae) in comet grains for the first time, and in other ways gather the isotopic evidence that may distinguish the origin of cometary grains from those of meteorites. In summary, Rosetta observations of Comet 67P/Churyumov-Gerashimenko will provide in-depth knowledge of a single comet. It is our belief that this knowledge can be used to help understand the origins of comets in general.

Acknowledgements The authors thank the following individuals for providing information about their individual investigations prior to publication: K. Altwegg, H. Balsiger, F. Capaccioni, A. Coradini, K.-H. Glassmeier, R. Goldstein, M. Hilchenbach, H.U. Keller, J. Kissel, J.W. Parker, R. Lundin, S.A. Stern, and N.'Thomas. We also thank two reviewers for their careful reading of the manuscript, and for their numerous comments, all of which helped to improve the manuscript. We thank the International Space Science Institute (ISSI) for supporting us to attend a series of workshops related to the subject of this paper. The work at the Jet Propulsion Laboratory, California Institute of Technology was supported by NASA.

References

H. Balsiger, K. Altwegg, P. Bochsler, P. Eberhardt, J. Fischer et al., Space Sci. Rev. (2007). doi:10.1007/s11214-006-8335-3

D. Bockelée-Morvan, J. Crovisier, M.J. Mumma, H.A. Weaver, in *Comets II*, ed. by M.C. Festou, H.U. Keller, H.A. Weaver (University of Arizona Press, Tucson, 2004), p. 391

A. Coradini, F. Capaccion, P. Drossart, G. Arnold, E. Ammannito et al., Space Sci. Rev. (2007). doi:10.1007/s11214-006-9127-5

P. Ehrenfreund, S.B. Charnley, D.H. Wooden, in *Comets II*, ed. by M.C. Festou, H.U. Keller, H.A. Weaver (University of Arizona Press, Tucson, 2004), p. 115

P.D. Feldman, A.L. Cochran, M.R. Combi, in *Comets II*, ed. by M.C. Festou, H.U. Keller, H.A. Weaver (University of Arizona Press, Tucson, 2004), p. 425

K.-H. Glassmeier, H. Boehnhardt, D. Koschny, E. Kuhrt, I. Richter, Space Sci. Rev. (2007)

S. Gulkis, M. Frerking, J. Crovisier, G. Beaudin, P. Hartogh et al., Space Sci. Rev. (2007). doi:10.1007/s11214-006-9032-y

W.F. Huebner, J. Benkhoff, M.-T. Capria, A. Coradini, C. De Sanctis, R. Orosei, D. Prialnik, ISSI Scientific Report SR-004. ESA Publications Division (2006), p. 13

W.M. Irvine, F.P. Schloerb, J. Croisier, B. Fegley Jr., M.J. Mumma, in *Protostars and Planets IV*, ed. by V. Manning, A. Boss, Russell (University of Arizona Press, Tucson, 2000), p. 1159

H.U. Keller, C. Barbieri, P. Lamy, H. Rickman, R. Rodgigo et al., Space Sci. Rev. (2007). doi:10.1007/s11214-006-9128-4

J. Kissel, K. Altwegg, B.C. Clark, L. Colangeli, H. Cottin et al., Space Sci. Rev. (2007). doi:10.1007/s11214-006-9083-0

R. Lundin, S. Barabash, Planet. Space Sci. **52**, 1059 (2004)

H. Nilsson, R. Lundin, K. Lundin, S. Barabash, H. Borg, O. Norberg, A. Fedorov, J.-A. Sauvaud, H. Koskinen, E. Kallio, P. Riihelä, J.L. Burch, Space Sci. Rev. **128**, 671 (2007)
G. Notesco, A. Bar-Nun, Icarus **122**, 118 (1996)
G. Notesco, A. Bar-Nun, Icarus **126**, 336 (1997)
S.A. Stern, D.C. Slater, J. Scherrer, J. Stone, M. Versteeg et al., Space Sci. Rev. (2007). doi:10.1007/s11214-006-9035-8
H.A. Weaver, P.D. Feldman, J.B. McPhate, M.F. A'Hearn, C. Arpigny, T.E. Smith, Aastrophys. J. **422**, 374 (1994)
D. Wooden, S. Desch, D. Harker, H.P. Gail, L. Keller, Comet grains and implications for heating and radial mixing in the protoplanetary disk, in *Protostars and Planets V*, ed. by B. Reipurth, D. Jewitt, K. Keil (University of Arizona Press, Tucson, 2007)

Capabilities of Philae, the Rosetta Lander

J. Biele · S. Ulamec

Originally published in the journal Space Science Reviews, Volume 138, Nos 1–4.
DOI: 10.1007/s11214-007-9278-z

Abstract In situ (and sample return) space missions are the most promising tools to investigate the origin and evolution of comet nuclei. We present the instruments and investigations that will be performed with PHILAE (the ROSETTA Lander) on comet 67P Churyumov–Gerasimenko, starting in November 2014, ten years after launch. The rationale and the performance of the scientific instruments is briefly presented along with a description of the Lander mission (separation, descent, landing, operation on the comet surface both short-term and long-term) and the status of the mission (results of commissioning and cruise check-outs and science investigations).

Keywords Comets: individual (67P Churyumov–Gerasimenko) · In situ analysis · Rosetta · Philae · Lander · Missions

1 Introduction

The ESA mission ROSETTA, launched March 2, 2004, with an Ariane 5, will reach its target comet in 2014. As part of the Rosetta mission, the "Philae" Lander will be released from the Orbiter and make a soft landing on the nucleus of 67P/Churyumov–Gerasimenko at a heliocentric distance of 3 Astronomical Units (AU).

The Rosetta mission will be an important milestone in comet research and, thus, shed new light on the origin and evolution of cometary nuclei.

The name "Philae" was chosen prior to launch to remember an inscription on an obelisk from Philae (an island near Aswan/Egypt) which confirmed the decipherment of the Rosetta stone (Andrews 1981).

Jens Biele has been the Payload Manager for Philae until commissioning, S. Ulamec is the Project Manager. Current Lead Scientists are Jean-Pierre Bibring (IAS, Paris, France) and Herrmann Böhnhardt (MPS, Katlenburg-Lindau, Germany).

J. Biele (✉) · S. Ulamec
Institute for Planetary Research, DLR, German Aerospace Center, Rutherfordstr. 2, 12489 Berlin, Germany
e-mail: jens.biele@dlr.de

H. Balsiger et al. (eds.), *Origin and Early Evolution of Comet Nuclei*
DOI: 10.1007/978-0-387-85455-7_18

The Rosetta Lander is a contribution to the European Space Agency (ESA) mission by a European consortium.[1] ESA contributed to the project with substantial technical and financial support.

2 Mission Overview

After the postponement of the 2003 launch (the original target was comet 47P/Wirtanen—see Schwehm and Schulz 1999; Ulamec et al. 2006), Rosetta launched successfully with an Ariane 5 G+ from Kourou on March 2, 2004, to comet 67P/Churyumov–Gerasimenko.

After swing-by maneuvers at Earth (March 2005, November 2007, and November 2009) and Mars (February 2007), and asteroid flybys at 2,867 Steins (September 2008) and 21 Lutetia (July 2010), the target comet, 67P/Churyumov–Gerasimenko shall be reached in 2014 (see Fig. 1 and Table 1).

In 2004 the Lander underwent commissioning and was later also switched on during the first Earth swing-by, the Mars swing-by, and various checkout phases.

In 2014, after a phase of close comet investigation with the Orbiter remote-sensing instruments, including high-resolution global mapping of the nucleus, a safe and scientifically relevant landing site will be selected (Ferri 2003).

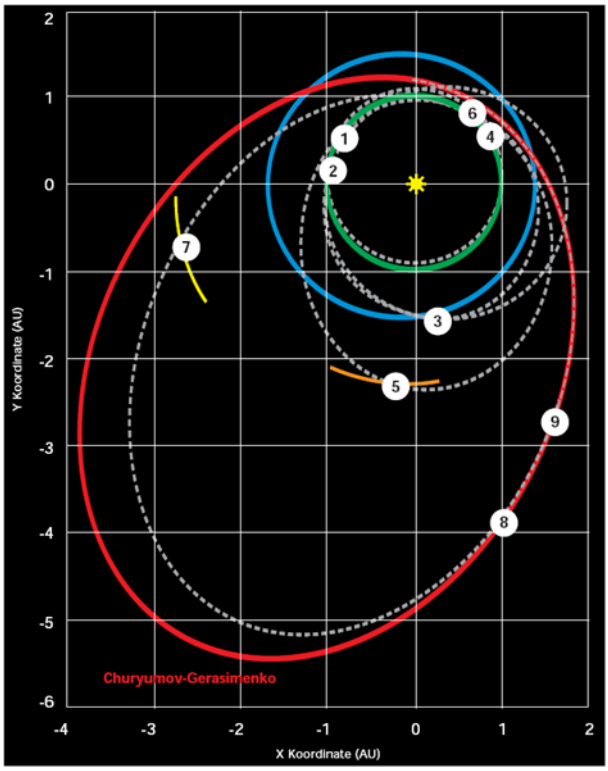

Fig. 1 Trajectory of Rosetta. *1* Launch, March 2004, *2* Earth swing-by, March 2005, *3* Mars swing-by, February 2007, *4* Earth swing-by, November 2007, *5* flyby at 2867 Steins, September 2008, *6* Earth swing-by, November 2009, *7* flyby at 21 Lutetia, July 2010, *8* rendezvous with Churyumov–G., May 2014, and *9* landing, November 2014

[1] DLR, MPS, MPE, CNES, ASI, KFKI, RAL, FMI, STIL, IWF Graz.

Table 1 Summary of Rosetta Mission Calendar RO-ESC-PL-5026 Issue 1, May 2005

Activity	Duration	Type	Time
Launch	–	–	02.03.2004
Commissioning block1	94 days	Active	05.03.–06.06.2004
Commissioning block2	41 day	Active	06.09.–16.10.2004
Cruise phase			
Earth swing-by #1	–	–	04.03.2005
P/L checkout 0	5 days	Passive	28.03.–01.04.2005
P/L checkout 1	5 days	Passive	30.09.–04.10.2005
P/L checkout 2	5 days	Passive	03.03.–07.03.2006
P/L checkout 3	5 days	Passive	25.08.–29.08.2006
P/L checkout 4	25 days	Active	27.11.–21.12.2006
Mars swing-by	–	–	25.02.2007
P/L checkout 5	5 days	Passive	18.05.–22.05.2007
P/L checkout 6	15 days	Active	17.09.–01.10.2007
Earth swing-by #2	–	–	13.11.2007
P/L checkout 7	5 days	Passive	04.01.–08.01.2008
P/L checkout 8	25 days	Active	07.07.–31.07.2008
Steins flyby	–	–	05.09.2008
P/L checkout 9	5 days	Passive	30.01.–03.02.2009
P/L checkout 10	15 days	Active	21.09.–05.10.2009
Earth swing-by #3	–	–	13.11.2009
P/L checkout 11	5 days	Passive	04.12.–08.12.2009
P/L checkout 12	25 days	Active	10.05.–03.06.2010
Lutetia flyby	–	–	10.07.2010
P/L checkout 13	5 days	Passive	03.12.–07.12.2010
RVM #1	–	–	23.01.2011
Deep space hibernation	917 days	–	14.07.2011–22.01.2014
RVM #2	–	–	22.05.2014
Pre-			
Comet approach	211 days	Active	23.01.2014–21.08.2014
Comet mapping & close observation	59 days	Active	22.08.2014–19.10.2014
Lander delivery preparation	27 days	Active	20.10.2014–10.11.2014
S-D-L			
Lander separation	6 h	Active	10.11.2014
On-comet			
First science sequence	5 days	Active	10.11.2014–15.11.2014
Extended mission	411 days;	Active	16.11.2014–31.12.2015
	Lander up to ∼90 days		(Lander: until ∼Feb. 2015)

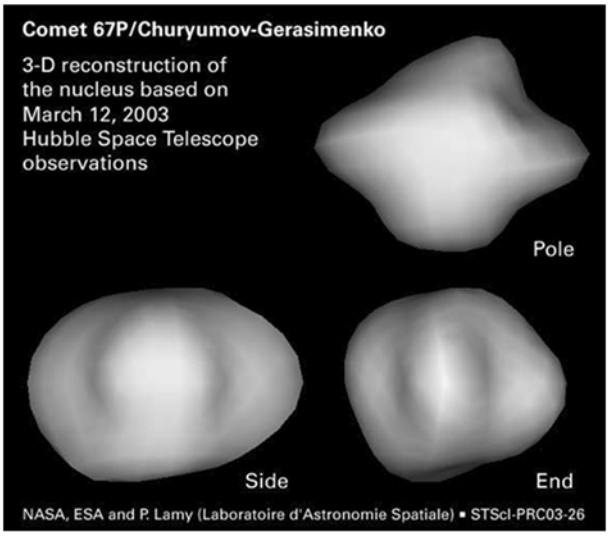

Fig. 2 Comet 67P/Churyumov–Gerasimenko, 3-D reconstruction of the nucleus based on March 12, 2003, Hubble Space Telescope observations. NASA, ESA and P. Lamy (Laboratoire d'Astronomie Spatiale) (Lamy et al. 2003)

From the comet orbit the spacecraft will provide detailed information on the properties of the comet nucleus to parameterise the Lander separation and descent sequence. The delivery of the Lander to the surface of the comet is foreseen in November 2014 at a distance of about 3 AU to the Sun.

The change of the target comet does have a certain effect on the Lander mission, since the expected touchdown velocity of around 1 m/s (depending on the actual comet properties) is higher than would have been expected for Wirtanen and implies a higher risk at landing. This is due to the considerably larger size (and mass) of Churyumov–Gerasimenko as compared to Wirtanen (Lamy et al. 2007). However, the design is flexible, and there is highest confidence for a successful mission (Ulamec et al. 2006).

Few properties of comet Churyumov–Gerasimenko are known: e.g., that it has a shape about 3×5 km and a rotation period of 12.3 h with a surface gravity of approximately 10^{-4} g. A possible shape has been reconstructed from precise photometric measurements from Hubble by Lamy et al. (2007); see Fig. 2.

The surface temperatures during the day are estimated to be in the range $-80\,^{\circ}$C to $+20\,^{\circ}$C; during the night the temperature is $>-200\,^{\circ}$C. The surface strength is estimated to be of the order of a few kPa (Biele et al. 2006b).

The Rosetta Lander will separate from the Orbiter (that will be on a dedicated delivery trajectory) with an adjustable velocity of 0.05 to 0.52 m/s. Its descent to the comet's surface will be stabilised by an internal flywheel and (if required) supported by a cold gas system. Figure 3 illustrates the landing scenario.

The descent time will be in the range of about 30 min, depending strongly on the actual comet properties and the selected delivery orbit.

3 Science Objectives

The Rosetta Lander's general tasks are to get a first in situ analysis of primitive material from the early solar system and to study the structure of a cometary nucleus which reflects growth processes in the early solar system and to provide ground truth for Rosetta Orbiter instruments (see also Biele et al. 2006a). The scientific objectives of the Lander are:

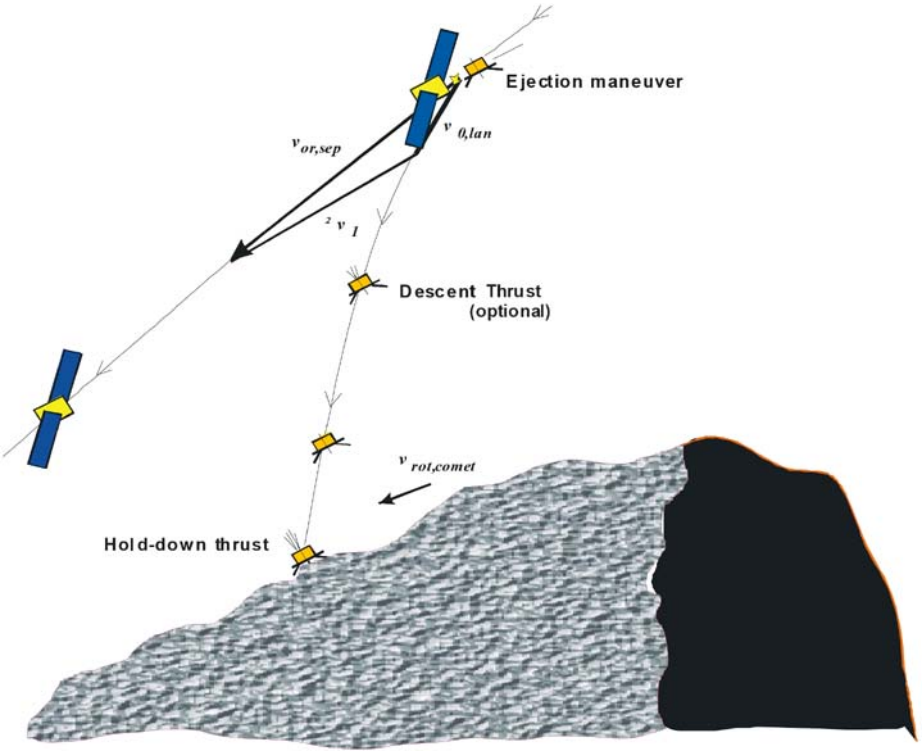

Fig. 3 Philae landing scenario. The ejection maneuver takes place at an altitude of the order of 1 km only; the Lander eject velocity partly cancels Rosetta's orbital velocity, such that Philae moves on an comet-surface crossing ellipse, stabilised by a flywheel and the optional use of a cold-gas thrusters (in z direction). After touchdown on the moving comet surface, the cold-gas system is activated to provide a hold-down thrust until the harpoons have safely anchored the Lander

- determining the composition (elemental, isotopic, mineralogical and molecular) of the cometary surface material
- measuring the physical properties (thermal, electrical, mechanical) of the cometary surface material
- describing the large-scale structure (panoramic imaging, particles and magnetic field, and internal heterogeneity)
- monitoring the cometary activity (day/night cycle, changing distance to the Sun, outbursts)

4 Schematic Views of the Philae Spacecraft

Figure 4 shows a schematic view of Philae as deployed on the comet's surface. The main body rests on a tripod landing gear, with ice screws and sensors integrated in the feet. All instruments and the drill are depicted in their deployed configuration. The open face of Philae with instruments exposed to the cometary environment is colloquially termed "balcony".

Figure 5 is a close-up of the inner, or "warm" compartment (with solar hood and thermal blankets (MLI) taken away).

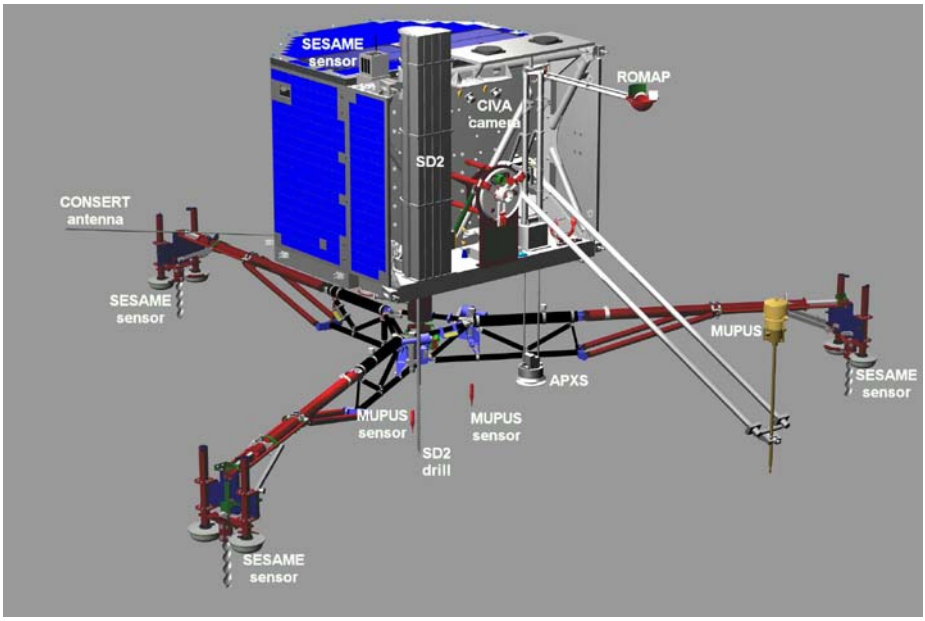

Fig. 4 A schematic view of the Philae spacecraft. The figure shows the overall structure, the subsystems and the experiment compartment of the Lander. Some instruments are not visible in the drawing: specifically, the instruments in charge of analysing the samples distributed by the SD2 (ÇIVA, COSAC, PTOLEMY), and the down-looking camera (ROLIS)

Fig. 5 Side view schematics of the inner structure of the lander compartment showing the location of COSAC and PTOLEMY systems, the CONSERT antennas, the SESAME dust sensor and various ÇIVA cameras

For details about the design and the subsystems of Philae, see Ulamec et al. (1997, 2005, 2007); Wittmann et al. (1999); and Biele et al. (2002).

For the collection of samples and the deployment of instruments it is important to note that the Lander can be rotated around its z (vertical) axis by 360° defining a "working circle" around the Lander body axis. Thus, arbitrary locations can be accessed by the sampling drill (SD2), the down-looking camera (ROLIS), and the APXS sensor; the MUPUS-PEN and the SESAME-PP electrodes are attached to the latter two instruments. Also the stereo camera pair of ÇIVA will be able to image a full panoramic of 360° using the Lander rotation capability.

Note that the landing gear also provides a tilting capability. This capability had to be drastically reduced in range (to ±5°) after the change of target comet in 2003 to ensure a safe landing.

5 Instruments—overview

The scientific investigations will be carried out through ten instruments, each under the responsibility of a principal investigator (Table 2). They will cover a very broad variety of investigations and are presented thoroughly in *Space Science Reviews*, special issue on Rosetta, 128/1–4 (2007).

Compare Figs. 4 and 5 for a schematic view of the location of the various experiments within Philae.

Philae's science objectives will complement those of the Orbiter investigations, in characterizing, by in situ measurements and observations, the composition of the cometary material down to its microscopic scale, the physical properties of the nucleus, its environment, its large-scale structure and its interior. Philae will also contribute to the monitoring of the long-term evolution (activity) of the comet.

With respect to the composition of the cometary material, the Lander will constitute a sophisticated and miniaturized laboratory operating in situ.

Using the SD2 (Sample Drill and Distribution) system, surface and subsurface (about 20 cm depth) samples, a few mm^3 in volume, will be acquired, controlled by a volume checker and distributed to 26 dedicated ovens, mounted on a carousel. Ten ovens ("Medium-temperature ovens", up to +180 °C) are equipped with IR-transparent sapphire windows: ÇIVA-M will obtain microscopic three-colour images (7 μm spatial sampling) and a complete near-IR (1 to 4 μm) high-resolution spectrum (40 μm spatial sampling, spectral resolution 10 nm at 4 μm) of the samples, to assess the scale of their heterogeneity, and to determine nondestructively the mineralogical and molecular composition of all cometary phases (ices, minerals, refractories). Then each sample will be step-wise heated, and the output gas piped to the PTOLEMY and COSAC instruments in order to identify its elemental, molecular and isotopic composition. Note that there are also 16 "High-temperature ovens" (without optical windows) that can be heated up to +800 °C.

PTOLEMY and COSAC are complementary, but both combinations of gas chromatographs (GC) and mass spectrometers (MS) (i.e., GCMS instruments for short) rely on different measurement strategies. Where COSAC contains an analytic GC and a time-of-flight mass spectrometer that can be used in multireflection mode for higher resolution, PTOLEMY uses a GC designed to separate various compounds and isotopes chemically for subsequent detection with an ion trap MS that only needs to resolve 1 amu. More specifically, PTOLEMY will measure by chemistry and mass analysis the H, C, N, O and S stable isotopes, the main target isotope ratios being $^{12}C/^{13}C$, $^{14}N/^{15}N$, $^{16}O/^{18}O$, $^{16}O/^{17}O$ and D/H.

Table 2 The 10 scientific experiments on board Philae

Instrument	Instrument type	PI: Principal investigator[a]	Science investigation	Mass (kg)
APXS	Alpha X-ray spectrometer	G. Klingelhöfer (R. Rieder, J. Brückner, R. Gellert, Jordi Gironés López)	Elemental composition of surface material	1.3
ÇIVA	–P: panoramic and stereo camera (b/w); –M/V: microscope, optical –M/I: microimaging IR spectrometer	J.-P. Bibring	Panoramic imaging. Microscopic imaging and analysis of the sample composition	3.4 (sharing parts with ROLIS)
CONSERT (lander unit)	Radio wave sounding transponder	W. Kofman	Internal structure of the nucleus by radio-wave sounding	1.8
COSAC	GCMS	H. Rosenbauer/F. Goesmann	Molecular composition and chirality of samples	4.9
MUPUS	PEN: hammering device with thermal and mechanical sensors; TM: IR thermal mapper; ANC: acceleration and thermal sensors and in anchors	T. Spohn	Physical properties of the subsurface (density, porosity, thermal properties)	2.2
PTOLEMY	GCMS	C. Pillinger/I. Wright	Isotopic composition of light stable elements in samples	4.5
ROLIS	Descent and close up down-looking camera, 3 colours active illumination	S. Mottola	Descent and down-looking imaging	1.4
ROMAP	Magnetometer and electron/ion sensor; Pressure sensors (1 Pirani, 1 Penning)	U. Auster	Magnetic and plasma monitoring	0.7
SESAME	CASSE: acoustic transmitters and receivers; PP: permittivity probe; DIM: 3D dust impact monitor	D. Möhlmann/K. Seidensticker	Electric and acoustic sounding, dust impact monitoring	1.8
SD2	Sample drill, sample volume check and transfer device; soil strength inference	A. Finzi	Sample acquisition (drill) and transfer	4.7
Total				26.7

[a]In case the PI changed over the development, both names are indicated.

It will measure the overall abundances of volatiles to a few % precision and isotopic ratios with 0.5–5% precision in a mass range of 12–150 amu. In the analytical part the sample can be analysed directly in the MS or via three analytical channels with GC columns and reactors (e.g., fluorination of cometary silicates, oxygenation of carbon) for chemical processing. For

discrimination of isotopes, hydrogen gas from a discrete supply can be injected into the ion trap to produce hydride species. Absolute values of the isotopic rations (in term of the delta notation) are obtained by in situ comparison with an onboard reference gas. The instrument uses stepped heating of the samples in the ovens and can analyse the cometary atmosphere by means of a carbon molecular sieve that acts as a gas-trapping medium.

COSAC, on the other hand, will use eight-column gas chromatography and high-resolution time-of-flight (TOF) mass spectrometry to identify the molecular composition of the material, in particular of the complex organics. COSAC has also the possibility (with two dedicated GC columns) to measure chirality of organic molecules, with the aim of addressing the prebiotic relevance of cometary material. The mass range for the COSAC MS is 1–1,500 amu; its resolution in "single" mode is $\Delta M/M = 350$ at $M = 70$ and accordingly higher for the multireflection modes (but with a loss of sensitivity).

Elemental abundances of the surface material (all elements from carbon to nickel) will also be measured by the APXS instrument in a small (few cm^2) area below the Lander by analysis of backscattered X-ray and Alpha-spectra. APXS contains a ^{96}Cm-244 (α, X, n) source (activity 1.1 GBq = 30 mCi, main emissions are 5.5 MeV alpha particles and 14 keV X-rays), a silicon drift X-ray detector (1–15 keV, resolution 180 eV at 6.4 keV) and six medium-resolution α-detectors.

Alpha-(PIXE, low z) and X-ray (XRF, higher z) induced X-ray spectroscopy is used to identify mainly characteristic K-lines, while the Rutherford backscattering of alpha particles is also used to remove ambiguities and to extend the element range to lower z (down to $z = 6$, while PIXE is sensitive down to $z = 11$). The sensitivity of APXS is about 0.1–1% in elemental abundance; it has been calibrated against a standard geological sample (SSK-1). Note that a significant fraction of organic compounds may "dilute" siliceous concentrations and needs to be corrected for.

The sample area of APXS is a circle with a diameter of 25 mm, situated on the "common working circle" of the Lander; by rotation of the latter, APXS may observe locations that have been looked at with ROLIS. The required integration time lies between three hours for X-ray spectroscopy and 10–24 hours for alpha spectroscopy.

Physical properties of the surface and subsurface material will be derived from optical images (ÇIVA-P and ROLIS) and will be accurately determined by direct measurements (MUPUS and SESAME).

More specifically, MUPUS consists of several sets of sensors. MUPUS-PEN is a rod-shaped thermal sensor with a hammering device on top; the soil density can be recovered indirectly (see the following). PEN is deployed on command after analysis of the first panoramic image by the ÇIVA-P cameras and hammers itself down to 32 cm deep into the cometary surface; depth can be measured to 2–3 mm accuracy and the energy per hammer stroke to a few percent, from which the mechanical strength of the upper surface can be derived. After complete deployment, 16 temperature sensors (absolute accuracy about 2 K, precision 0.5 K) in different depths monitor the temperature profile and its variations with the diurnal cycle and the approach to the Sun; the same 16 sensors can also be heated independently to induce thermal waves for subsequent measurement of thermal diffusivity. Thermal conductivity λ can, therefore, be observed directly from measurements of temperature amplitude, power and the known geometry to an accuracy of 15–20%; thermal diffusivity k can also be measured directly from the temporal variations of induced heat waves, but the accuracy of k is estimated to be worse due to partly unknown thermal contact resistances. However, the k measurement together with the known heat capacity of the soil (estimated with the measured water and dust content from other Philae instruments) may be used to derive the density of the cometary surface material.

MUPUS-TM is a thermal IR mapper (thermopile radiometer) sitting on the balcony and having a FOV of 60°, covering 0.5–1 m^2 that are centred on the PEN sensor. It will measure the surface temperature with a precision of 0.1 K and an accuracy of better than about 3 K; analysis of the temporal variations is a direct measure of the thermal inertia of the cometary surface material while a comparison with the uppermost PEN temperature sensor will give directly the thermal conductivity of the uppermost centimetre.

MUPUS-ANC consists of acceleration and thermal sensors in the anchors. The former will measure the strength during penetration and potential layering during penetration of the harpoons down to a maximum depth of 2.2 m (depending on the surface strength) with an accuracy of the order of 10%. After anchoring, the ANC temperature sensor (Pt-100, 1–2 K accuracy) will extend the PEN temperature measurements to a ideally much greater depth.

All three MUPUS sensors together will accurately determine the energy balance of the nucleus.

The SESAME experiment suite will focus on measuring the mechanical and electrical properties of the surface (CASSE and PP), typically down to two metres depth, and the dust environment (DIM) along with its diurnal and long-term variations.

CASSE is an acoustic surface sounding experiment with emitters (stacked piezoelectric actuators) and sensors (three-axis accelerometers) in each "foot" of the landing gear. By emitting mechanical waves across different feet in the range 100 Hz to a few kHz and timing the travel time and amplitude, shear and longitudinal wave velocities and damping parameters can be measured directly. With known density (MUPUS), Young's modulus E and the Poisson ratio υ and their daily and seasonal variations can be determined directly. In passive mode, the CASSE sensors monitor thermally and impact-caused cometary activity and can localize activity spots. During low orbit and descent, they can detect impacting particles. Signals generated during SD2 drilling and MUPUS-PEN hammering may be used as secondary signal sources. The use of CASSE to obtain refraction/reflection seismograms for the determination of the macro-structure of the cometary surface with potential layering and embedded in homogeneities is presently under study.

The Dust Impact Monitor (DIM) cube on top of the Lander balcony is a dust sensor with three active orthogonal (50 × 16) mm piezo sensors. From the measurement of the transient peak voltage and half contact duration, velocities and radii of impacting dust particles can be calculated. Particles with radii from about 0.5 μm to 3 mm and velocities from 0.025–0.25 m/s can be measured. If the background noise is very high, or the rate and/or the amplitudes of the burst signal are too high, the system automatically switches to the so-called Average Continuous mode; i.e., only the average signal will be obtained, giving a measure of the dust flux.

The Permittivity Probe (PP) experiment consists of capacitively coupled electrodes (three in the Lander feet, one each with MUPUS-PEN and APXS) and AC sine generators and detectors. It will measure (by the quadrupole array technique) the complex permittivity ε down to ∼2 m below the surface with a spatial resolution of ∼10% of the electrode distance used (0.5–2 m). The AC frequency can be varied from 10 Hz to 10 kHz with a peak to peak voltage of ≤20 V. The signal is sampled with 20 kHz; U/I amplitudes can be determined to 5–15% (signal to noise dependent) and the phase angles to about 1°.

The imaginary part of ε is a measure of the electrical conductivity of the subsurface material of the nucleus; given that the permittivity of ice varies by one order of magnitude in the temperature range between −80 °C and 0 °C, the measurement of static permittivity ε_∞, the transition frequency and the soil temperature (by MUPUS) allows us to determine the water content in the subsurface.

The global to large-scale structure of the nucleus will be studied by the CONSERT experiment, analysing the propagation of electromagnetic waves transmitted between a unit

onboard the Rosetta Orbiter and a transponder onboard Philae and travelling through the interior of the comet. A carrier frequency of 90 MHz with a bandwidth of 8 MHz is used. One measurement consists of sending a 200 ms pulse from the Orbiter to Philae, where it is received for 26 ms. The signal consists of a repeated 25.5 μs binary code which is accumulated coherently in that 26 ms window and then sent back to the Orbiter with a known instrument delay. The Orbiter unit finally receives the signal generated by Philae with a sampling rate of 10 MHz and determines the peak (delay) and signal form. With the given bandwith, a spatial resolution of 30 m (free space) or 20 m (comet material) can be achieved theoretically. The immediate information contained in the measured delay (given the known geometric positions of Orbiter and Lander at each point in time) is the mean relative dielectric constant ε_{r} (at 90 MHz) constraining the nucleus composition. By also analysing the wave front distortion, the polarisation change, the amplitude loss and properly solving the inverse problem of wave propagation, it is possible to reconstruct the interior of the nucleus. The amount of detail depends on the number of independent orbits. Even with one orbit, however, fundamental properties of the nucleus can be determined; i.e., whether it is homogeneous or layered or an accumulation of several blocks. Note that the CONSERT signal-to-noise ratio for the much larger nucleus of Churyumov–Gerasimenko, compared to the size of Wirtanen, is possibly marginal and might constrain the usable orbit configurations.

The large-scale topography and will be studied through panoramic stereoscopic images of the landing site after touch down (ÇIVA-P), and through images acquired during descent (ROLIS).

The ÇIVA-P camera system consists of seven identical cameras (60° FOV, 1.1 mrad angular sampling IFOV), implemented as five single cameras and one stereo pair (optical axis displacement: 10 cm) on the "Balcony", thus filling the 360° panorama. The spectral response of each camera extends from 400 to 100 nm with a maximum around 700 nm. The panoramic camera will characterize the surface topography and provide an albedo mapping of the landing site, with the aim of describing the interfaces between dark mantle materials and brighter surface ices at all scales from 1 mm at the distance of the landing legs and a few metres at the horizon. It will identify structures (microcracks, vents, faults) and erosion features linked to cometary processes; it will also reconstruct the local three-dimensional structure of the surface. With the rotation of Philae, the stereoscopic reconstruction can be obtained for the full panorama. If operations of ÇIVA-P are repeated several times along the cometary activity, surface changes and faint dust emissions will be detected at scales not achievable by the Orbiter.

The ROLIS camera is a down-looking camera with a 1024×1024 CCD sensor, an aperture of $f/5$ and a unvignetted FOV of $57.7° \times 57.7°$. The optics consist of a modified Hologon design with four fixed and one movable lens; during descent, it uses an "infinity lens" (IFL) to focus between 1.4 m and infinity and to obtain panchromatic images of the landing site a few times from great height and then every 5 s immediately before landing. The stored images will be transmitted immediately after touchdown.

After landing, ROLIS can obtain close-up multispectral images of the cometary surface the Lander. This is achieved by swivelling the IFL out of the optical path, whence the camera is focused at an object distance of 30 cm $(+10; -8)$ cm. The field of view now is 30×30 cm with a resolution of 0.3 mm; stereoscopic information can be obtained by rotation of the Lander. ROLIS contains an illumination device (four LED arrays with centre wavelengths of 470, 530, 640 and 870 nm with FWHM between 50 and 80 nm) for broadband multispectral imaging.

The ROLIS electronics use wavelet integer decomposition and zero-tree coding for image compression; compression ratios can be commanded between uncompressed and $\sim$20. Lossless compression (compression ratio $\sim$2 for most image scenes) is possible as well.

Multispectral images acquired by ROLIS bridge the resolution gap between ÇIVA-P and ÇIVA-M and allow a broad characterisation of the solid surface phases and enable at least carbonaceous, silicates and organics to be distinguished. Colour ratios will indicate the degree of soil heterogeneity at small scales. By Lander rotation, SD2 and APXS sampling sites can be observed because all instruments lie on the common working circle.

The magnetic and plasma environment of the nucleus will be measured by the magnetic, electron and ion detectors of the ROMAP experiment onboard Philae. The near-surface plasma environment (and the surface pressure) are important observables to constrain comet models and Orbiter measurement, the surface being the source of the cometary atmosphere. If ROMAP discovers an intrinsic magnetic field of Churyumov–Gerasimenko, it would be the first detection of magnetism at a comet and would yield important insights about its composition and evolution.

ROMAP consists of three sensors: a magnetometer (MAG) and plasma analyser (SPM) combined in one housing that can be deployed by a 60-cm boom, and two pressure sensors mounted on the baseplate of the balcony.

MAG searches for the comet nucleus magnetic field by measuring close to the surface. It consists of a fluxgate magnetometer with a dynamic and compensation range of $\pm$2,000 nT, 10 pT resolution, <5 pT/$\sqrt{\text{Hz}}$ noise, an offset drift of <0.1 nT/K and a sampling rate between 1 and 64 Hz. The static offset will be calibrated during cruise by comparison with the Orbiter magnetometer (RPC-MAG). Magnetic disturbances due to Lander operations can be corrected for to a large extent.

The plasma or electron and ion analyser SPM is a combination of an electrostatic, hemispherical analyser and a Faraday cup sensor with moderate directional sensitivity that allows us to determine the flux directions. It can detect electrons with an energy range from 0.35–4,200 eV (7% resolution), ions from 40–8,000 eV (15% resolution) in 32–64 logarithmically scaled energy steps. Extremely high ion fluxes can be measured by the Faraday cup, which measures the ion integrated energy distribution up to 2 keV in 16 energy levels.

The pressure sensor assembly consist of a Pennig sensor (ionising system, pressure range $10^{-8}..10^{-3}$ mbar) and a miniature Pirani sensor (a heated resistor in a bridge circuit, pressure range $10^{-3}..10$ mbar).

ROMAP measurements at decreasing heliocentric distances will allow to monitor the increasing activity (production rates) and the changing solar wind interaction with the coma.

6 Operations

The science operations of Philae are divided into various phases.

During the 10 year cruise, check-ups, calibrations, software and command up-loads are scheduled as well as occasional observation campaigns for ÇIVA-P (flybys and ROMAP (flybys, solar wind, comet tail crossings). After arrival at the comet, global mapping by the Orbiter instruments and the selection of a landing site, the Separation–Descent–Landing phase begins. Immediately before release from the Orbiter, thermal preparation and battery charging are foreseen. Immediately after the eject, the Landing Gear is unfolded, thereby releasing the CONSERT antennas. Then, the ROMAP boom is deployed. A telemetry contact to the Orbiter will be established a few minutes after release until well after landing. During descent (30–60 min) to the comet's surface, scientific measurements (images by ROLIS, magnetic field measurements by ROMAP-MAG, dust impact by SESAME-DIM and -CASSE, calibrations of SESAME-CASSE and MUPUS-TM) will be performed to monitor the cometary environment between the Orbiter and the surface of the nucleus, to observe

the nucleus while approaching, to characterize remotely the landing site and to document the touchdown event of the Lander at the surface. ROLIS descent images will be taken until touchdown and MUPUS-ANC measurements during the actual anchoring.

During the "first science sequence" of approximately five days, Philae will be operated mainly on primary batteries, thus minimizing sensitivity to landing geometry (solar irradiance of the cells). In the first 60 hours following the touch-down, all instruments will work in their baseline mode at least once at full completion of their relevant science goals. In particular a full panorama of the landing site will be taken by ÇIVA-P immediately after landing and cometary samples will be acquired by SD2, both from the surface and from the maximum depth reachable with drill (i.e., about 0.2 m); these samples will then be processed by the relevant instruments (COSAC, PTOLEMY, ÇIVA-M). MUPUS-PEN and APXS will be deployed and thermal conductivity, thermal diffusivity, strength measurements be made by MUPUS and the first X-ray and alpha spectra will be recorded by APXS. CONSERT will sound the nucleus over at least one full Orbiter orbit relative to the Lander. ROMAP will observe the daily variation of magnetic field and the plasma properties. All three parts of SESAME will perform measurements (PP only after MUPUS-PEN and/or APXS have been deployed). The Lander resources should enable at least a partial redo of this sequence over the following 60 hours, if partial failure (e.g., in data transmission) had happened. If performed successfully, the first sequence will secure a "minimum science success" of the Lander mission.

During the "long-term science mission" (up to three months until $r = 2$ AU is reached) all instruments will be operated mostly sequentially, powered by the solar cells and buffered by the secondary (rechargeable) batteries. The Lander has enough flexibility to allow—by rotation around its body axis—the optimized orientation of the solar cells with respect to the local time, to drill several boreholes, and to measure physical properties all around the landing site.

The presently guaranteed data volume to be uplinked to Earth is 235 Mbit during descent and the first five days and 65 Mbits during each subsequent 60-hour period. However, depending on actual telemetry coverage and Orbiter requirements, a significantly larger data volume is expected.

With the current best estimate of the comet environment, about 52–65 hours of primary mission operations are feasible (incl. a 30% system margin). Primary power during the first science sequence is 15–20 W; the solar cells generate 10 W during the day at 3 AU.

The long-term operations then rely entirely on the solar generator; the end of life will be determined either by overheating (the thermal system is designed for a range of 2–3 AU) or by insufficient power if the solar cell degradation (mainly by dust deposition) becomes too severe.

7 Conclusions

The Rosetta Lander "Philae" is a unique device. For the first time, a robotic system will land on a comet nucleus with the goal of deciphering, by direct in- situ measurements and observations, so far unknown key properties (such as chemical and isotopic composition, dust and gas emission mechanisms) of a comet nucleus—a body conceived as having preserved pristine material and conditions that drove the evolution of the Solar System.

Forming a highly integrated instrument complement, the package of Philae experiments has been developed and is operated in very close cooperation by ten scientific teams in charge of the investigations, and a technical, operational and managing team, responsible

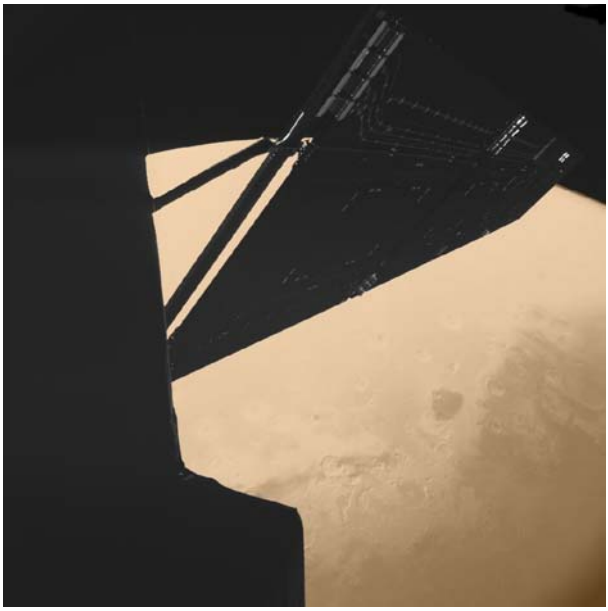

Fig. 6 ÇIVA image of Mars, February 25, 2007, showing portions of the Rosetta spacecraft with Mars in the background. This image was taken just four minutes before the spacecraft reached closest approach, about 1,000 kilometres from the planet's surface. A portion of the spacecraft and one of its solar arrays are visible in nice detail. Beneath, an area close to the Syrtis region is visible on the planet's disk. Courtesy of J.-P. Bibring (IAS), © ÇIVA/Philae/ESA

for the Lander as an autonomous vehicle. In the Philae mission success, the Rosetta Orbiter plays a major role: as the carrier and host during the ten-year cruise phase, to model the nucleus and select the landing site (with the OSIRIS cameras and other instruments), for the release and the descent phases and as a relay for all Lander commands and data transmission during on comet operations. In addition, it will contribute to the CONSERT investigation, as this instrument is mounted on and operated from both the Lander and the Orbiter.

After launch, Philae was undergoing, in total, four commissioning phases and showed to be in good health (Biele et al. 2006a). The tests showed nominal behaviour of subsystems and instruments. The only unit that may not be useable is a Penning pressure sensor (a subinstrument of ROMAP); the respective atmospheric pressure measurement will be performed (with lower accuracy) with the mass spectrometer of COSAC.

During Earth and Mars swing-bys (Fig. 6) some experiments (e.g., ÇIVA, ROMAP) have delivered data that will be used for calibration purposes. ROMAP is also used during the asteroid flybys and serendipitous events like passages through comet tails.

Philae has the ambition to provide a major contribution to the global success of the Rosetta mission.

Acknowledgements The author thanks the complete Rosetta Lander team for its support in preparing this contribution and extend special thanks to Jean-Pierre Bibring and Hermann Böhnhardt.

References

C. Andrews, *The Rosetta Stone* (The British Museum Press, London, 1981)

J. Biele, S. Ulamec, B. Feuerbacher, H. Rosenbauer, R. Mugnuolo, D. Moura, J.-P. Bibring, Current status and scientific capabilities of the Rosetta Lander payload. Adv. Space Res. **29**(8), 1199–1208 (2002)

J. Biele, R. Willnecker, J.P. Bibring, H. Rosenbauer, the Philae team, Philae (Rosetta Lander): experiment status after commissioning. Adv. Space Res. **38**, 2025–2030 (2006a)

J. Biele, S. Ulamec, L. Richter, E. Kührt, J. Knollenberg, D. Möhlmann, the Philae team, The strength of cometary surface material: relevance of deep impact results for Philae Landing on a comet, in *Deep Impact as a World Observatory Event*, ed. by H.U. Käufl, C. Sterken. Proceedings of Workshop, Bruxelles, 7–10 August 2006. ESO Astrophysics Symposia (Springer, Berlin, 2006b)

P. Ferri, Mission operations for the new Rosetta, in *54th International Astronautical Congress*, IAF-Q. 5.01, Bremen, 2003

P. Lamy et al., The nucleus of comet 67P/Churyumov–Gerasimenko, the new target of the Rosetta mission. Bull. Am. Astron. Soc. **35**(4), 970 (2003)

P.L. Lamy, I. Toth, B.J.R. Davidsson, O. Groussin, P. Gutiérrez, L. Jorda, M. Kaasalainen, S.C. Lowry, A portrait of the nucleus of comet 67P/Churyumov–Gerasimenko. Space Sci. Rev. **128**(1–4), 23–66 (2007)

G. Schwehm, R. Schulz, Rosetta goes to comet Wirtanen. Space Sci. Rev. **90**, 313–319 (1999)

S. Ulamec, J. Block, M. Fenzi, B. Feuerbacher, G. Haerendel, P. Hemmerich, M. Maibaum, H. Rosenbauer, B. Schiewe, H.P. Schmidt, R. Schütze, K. Wittmann, RoLand: a long term lander for the Rosetta mission. Space Technol. **17**(1), 59–64 (1997)

S. Ulamec, S. Espinasse, B. Feuerbacher, D. Moura, H. Scheuerle, Philae–Rosetta Lander, a new strategy to realize space systems, in *6th ICLCPM*, Kyoto, 2005

S. Ulamec, S. Espinasse, B. Feuerbacher, M. Hilchenbach, D. Moura, H. Rosenbauer, H. Scheuerle, R. Willnecker, Rosetta Lander–Philae: implications of an alternative mission. Acta Astronaut. **58**(8), 435–441 (2006)

S. Ulamec et al., Rosetta Lander Philae: System overview, Space Sci. Rev. **128** (2007)

K. Wittmann, B. Feuerbacher, S. Ulamec, H. Rosenbauer, J.P. Bibring, D. Moura, R. Mugnuolo, S. diPippo, K. Szegö, G. Haerendel, Rosetta Lander, in situ characterization of a comet nucleus. Acta Astronaut. **45**(4–9), 389–395 (1999)

Closure

Rapporteur Paper on the Composition of Comets

Kathrin Altwegg

Originally published in the journal Space Science Reviews, Volume 138, Nos 1–4.
DOI: 10.1007/s11214-008-9408-2

Abstract The ISSI workshop on "Origin and evolution of comet nuclei" had the goal to put together recent scientific findings concerning the "life" of a comet from the formation of the material in a dark molecular cloud to the accretion in the early solar system, from cometesimals to comet nuclei which were shaped and altered by cosmic rays, by radioisotopic heating, to their sublimation in the inner solar system. Astronomers, space researchers, modelers and laboratory experimentalists tried to draw the coherent picture. However, it became clear that there are still a lot of open questions, findings which seem to contradict each other, missing laboratory data, and experimental biases not taken into account. The Rosetta mission will make a big step forward in cometary science, but it will almost certainly not be able to resolve all questions. The main outcome of this workshop was the fact that comets are much more diverse than commonly thought and they are not only different from comet to comet but may consist of morphologically and chemically inhomogeneous cometesimals which may even have different places of origin.

Keywords Comets · Comet composition · Cometary evolution

1 Introduction

Comets are commonly believed to be the most pristine bodies of our solar system. Although this may well be true this doesn't mean that comets consist solely of original, unaltered material from the dark molecular cloud from which our solar system emerged. Comets and their material have been changed by the accretion shock, shaped by the solar nebula, mixed with material from the inner solar system which has experienced strong heating, and undergone processing while travelling through the inner solar system. When Oort postulated the existence of a cloud of comets surrounding the solar system (Oort 1950) it was understood for quite some time that this is where comets come from. Later, this picture was disturbed by the detection of the Kuiper belt, followed by the scattered disk (see e.g. Morbidelli and

K. Altwegg (✉)
Physikalisches Institut, University of Bern, Sidlerstr. 5, 3012 Bern, Switzerland
e-mail: altwegg@space.unibe.ch

H. Balsiger et al. (eds.), *Origin and Early Evolution of Comet Nuclei*
DOI: 10.1007/978-0-387-85455-7_19

Valsecchi 1997). By then it was acknowledged that Jupiter family comets have their origin in the scattered disk and therefore originate from the Neptune–Pluto region whereas long period comets are from the Oort cloud and have therefore their place of birth in the Saturn–Uranus region. Such models could have been confirmed by observing compositional differences between the two comet classes, e.g. different isotopic ratios. However, so far no clear compositional differences between comets have been observed. Rather it has been observed that comets are individually chemically inhomogenous (DiSanti and Mumma 2008). Recent models show that comets can change their dynamical group quite easily (Fernandez 2007). It is therefore no longer possible to clearly distinguish the birthplace of comets either by their dynamical class or probably by there overall composition.

Comets have undergone processing by intrinsic features like radioactive isotopes and cosmic rays, but also by heating, sublimation and chemical evolution during their travel through the inner solar system. Furthermore, what we know of comets is subject to quite strong experimental biases, be it that some molecules can be observed much more easily than others or that big, new comets are accessible to many more telescopes than small, less active ones. Coma dust samples collected by the STARDUST mission have already had quite a long history before they end up in a laboratory to be analyzed and in situ measurements are restricted to very few comets which may not necessarily represent the bulk comet distribution. The ISSI workshop on "Origin and evolution of comet nuclei" had the goal to bring together experts on all stages of the "life" of a comet, from the presolar grains, the processes in the molecular clouds to the accretion in the solar nebula and the subsequent processing in the solar system.

2 Origin of Cometary Material

Comets have been accreted in the solar nebula somewhere between Jupiter and the Kuiper belt. The material itself originates from the molecular cloud from which our solar system emerged. This cloud got its material from stars and supernovae which ejected gas and dust into interstellar space. In the solar nebula material was processed by the young sun and by heating through the accretion shock. Material was flowing inwards and outwards with time. Material was subsequently altered by heat from the Sun, from radioactive isotopes or from chemical processing such as crystallization of water ice or sublimation processes. Which traces can we find in comets from which period?

2.1 How Many Presolar Grains Do We Find in Comets?

It is well established that primitive meteorites and interstellar dust particles contain small amounts of dust grains with highly anomalous isotopic compositions (Hoppe 2007). So far, a few of these grains have also been detected in comet 1P/Halley (Jessberger and Kissel 1991). The only other comet where such studies can be performed is comet 81P/Wild 2. To date, only one so-called presolar dust grain has been found among the many STARDUST grains collected. This may of course be an experimental bias. Presolar grains are very often very fragile and fluffy. They may not have survived the impact of a few km/s into the aerogel of the STARDUST dust collector (Brownlee et al. 2006). Elemental abundance measurements of Halley dust (Jessberger and Kissel 1991) show, for heavy elements, the same abundance as C1 meteorites within a factor of two. The light elements H, C, O and N are clearly overabundant in Halley dust. From STARDUST we know that the elemental abundance for refractory elements of individual grains, however, vary a lot, up to a factor of 10000

(Stephan 2007). How many of the grains survived the accretion into the solar nebula and are therefore also "presolar" grains although they may not exhibit anomalous isotopic ratios, remains to be investigated.

2.2 Traces of the Molecular Cloud in Comets

How do we recognize a dark molecular cloud origin of cometary material? Table 1 lists some of the evidence collected so far.

The strongest argument for a dark molecular cloud origin of cometary matter is probably the high deuterium content in water ($D/H = 300 \times 10^{-6}$) in comets (e.g. Balsiger et al. 1995). Water in the solar system cannot be a product of thermal (neutral) reactions occurring in the solar nebula (Robert et al. 2000; Drouart et al. 1999). According to these authors water was initially synthesized by interstellar chemistry with a high D/H ratio $\geq 720 \times 10^{-6}$ which corresponds to the highest D/H value found in meteorites (in clay minerals from LL3 chondritic meteorites). When in the solar nebula, the D/H ratio decreases via an isotopic exchange with H_2. The isotopic homogenization of the solar nebula was completed in no more than 10^6 years, reaching a D/H ratio of 88×10^{-6} (found in chondrules of LL3 chondritic meteorites). Cometary water has suffered a partial isotopic re-equilibration with H_2 before its condensation but still contains the signature of a molecular cloud origin.

Another puzzling isotopic ratio is the $^{14}N/^{15}N$ in CN in comets. Whereas this ratio is 120–160 in the CN radical it is twice as high in HCN (Schulz 2007, and references therein). This points to a different parent for at least part of the CN. So far this parent is unknown.

Table 1 Evidence for a dark molecular origin of cometary material (after Altwegg and Huntress 2001)

Observed species	Evidence for interstellar origin
H_2O	Low spin temperature (ortho/para ratio of 2.45 for water, e.g. Weaver et al. 1987 and 3.03 for NH_2, Kawakita et al. 2001)
DHO/DCN	High deuterium content in water and HCN
Carbon	• Large part of the carbon is in complex organic molecules
abundance	• Molecular abundance is very similar to abundance in molecular clouds and hot cores
	• Distribution among saturated and unsaturated species is consistent with interstellar origin.
	• Distribution between dust and gas is consistent with interstellar origin.
CO	• Abundance is consistent with interstellar origin and with a condensation temperature of 25–50 K.
CH_4	• Low abundance not compatible with origin in solar nebula.
CO/CH_4	High ratio compatible with interstellar origin.
H_2CO	• Abundance is compatible with interstellar origin and is higher than expected for a solar nebula origin.
	• Polymer as a source for formaldehyde points to an interstellar origin.
CH_3OH	Abundance not compatible with solar nebula origin.
N	Low nitrogen abundance is consistent with interstellar origin where nitrogen is most abundant in the form of N_2. The sublimation temperature of N_2 is 25 K. So it was most probably not condensed in comets or it was lost during the comet lifetime. In the solar nebula one would expect a much higher NH_3 abundance.

This parent has to have a very low $^{14}N/^{15}N$ ratio which again points to a unequilibrated chemistry and therefore to molecular cloud origin.

It is well known that dark molecular clouds and hot cores contain a large reservoir of organic molecules. The chemistry is governed by gas-phase chemistry, accretion on grains and post-evaporation gas chemistry (Rodgers and Charnley 2003). So far 230 species have been detected in space http://www.astrochemistry.net/. 50 of these species have also been detected in comets. There is a strong similarity between the abundances in young stellar objects (YSO) and comets with a few notable exceptions (Charnley and Rodgers 2008).

The physics and chemistry of low-mass star formation provides the boundary conditions for the chemical evolution of both protostellar and protoplanetary disks (e.g. Van Dishoeck and Blake 1998). It is now possible to observe in detail the organic composition of each phase prior to disk formation, a chemical sequence analogous to that which led to the protosolar nebula (Charnley 2001). The organic chemistry of protoplanetary accretion disks is of fundamental importance for understanding the composition and origin of comets and meteorities. Future theoretical models of disk fractionation chemistry will be important to highlight the differences and similarities between the molecular inventory of the natal cloud, the disk, and that detected in primitive solar system material.

2.3 Processing and Mixing of Cometary Material in the Solar Nebula

Elemental abundance measurements for dust captured by STARDUST at comet 81P/Wild 2 show an almost solar abundance of elements which have not a high volatility (Stephan 2007), at least if averaged over a lot of dust grains. The author draws the conclusion that the early solar system did not show a large-scale element fractionation. Individual grains, however, show quite a large diversity in elemental abundance. Furthermore CAIs (Ca, Al-rich inclusions) have been identified in the STARDUST sample which are attributed to high temperature phases and therefore to coming from the innermost solar system. This points to a strong mixing of at least some of the material in the early solar system, but contradicts for example the high deuterium content in cometary water. Another, possibility for the existence of CAIs far out in the solar system is given by Shu et al. (2001). Ordinary CAIs and chondrules might have formed by flare heating of primitive rocks interior to the inner edge of a gaseous accretion disk that has been truncated by magnetized funnel flow onto the central proto-Sun. The evaporation of the moderately volatile mantles above large refractory cores, or the dissolving of small refractory cores inside thick ferromagnesian mantles before launch, plus extended heating in the X-wind produce the CAIs or chondrules that end up at planetary distances in the parent bodies of chondritic meteorites or comets. The physical addition of the hot rock components into a reservoir of cool rock and unequilibrated volatile components results from the action of the X-wind.

A puzzling aspect of cometary composition is the parallel existence of crystalline and amorphous silicates. ISM's (interstellar material) and molecular cloud cores contain about 1.1% crystalline silicates compared to amorphous silicates (Kemper et al. 2005), which are in the form of amorphous Mg–Fe silicates. Comets on the other hand show distinct features of crystalline silicates. Silicates in comets appear to be a mix of high-temperature crystalline enstatite and forsterite plus glassy or amorphous grains that formed at lower temperatures (Hanner 1999). The mineral identifications from the 10 and 20 μm cometary spectra are consistent with the composition of anhydrous chondritic aggregate IDPs (interplanetary dust particles) (Wooden 2008). The origin of the cometary silicates remains puzzling. If they formed in the inner solar nebula, then their presence in comets requires significant mixing in the solar nebula. If they are circumstellar in origin, one has to explain

why their spectral features are not visible in interstellar dust. Oort cloud comets seem to contain a much higher abundance of crystalline silicates than Jupiter family comets' (crystalline/crystalline+amorphous = 0.7 vs. 0.3). Furthermore, the observed crystalline feature in comets varies with heliocentric distance and with jet activity. In 9P/Temple 1 there was no crystalline feature observable before the impact of the Deep Impact probe. Shortly after the impact a clear crystalline signature could be observed which later on disappeared again (Wooden 2008). Crystals therefore seem to originate from below the mantle of comets and are not uniformly distributed in cometary nuclei. This could be at least partly due to an observational bias because of the grain size distribution as the grains lifted by the impact and probably also in jets are smaller than the undisturbed grain size distribution observed in relatively inactive comets.

2.4 The Last 4.5 Gy

Once cometesimals have formed their material can be altered by many processes. It is quite obvious from the four different comet nuclei observed so far at close distances that the morphological diversity among comets is large (A'Hearn 2008; Basilevsky and Keller 2006).

The first steps in the life of a comet after the condensation of its material were the accumulation from small dust and icy grains into cometesimals and finally into comets. It is not clear if the region where cometesimals formed is identical to the region where finally the comet formed.

9P/Temple 1 points to a very gentle accumulation of small cometesimals into a comet nucleus (A'Hearn 2008). Other scenarios also include cometary nuclei which are the result of collisions of bigger parent bodies (Fernandez 2007). It is entirely possible that the compositional and structural differences between comets and even within comets are quite large: from very low density, fluffy, porous objects with very low tensile strength to much more compact objects. The origin of the individual cometesimals forming a comet may have been at quite different locations in the solar nebula and may thus reflect samples of a radially inhomogenous disk.

Once comets have formed they are subject to heating by incorporated radioactive material which may even have led to liquid water in the interior of large (>10 km) comets (Prialnik et al. 2008). Their surfaces are changed by cosmic rays and, once inside the Jupiter orbit, also by solar UV. So far, little is known about their initial state and each model which describes their evolution faces the problem of selecting the "right" initial structure (e.g. rubble pile, capillary tubes, aggregation of grains).

One of the big, still open questions is the nature of the surface layer of a comet. Sublimation of a comet in the inner solar system is rapid. Balancing energy input and latent heat, rates of 10^{22} molecules $m^{-2}\,s^{-1}$ are typical, leading to depth loss rates of 1 cm per few hours (Thomas et al. 2008). The thermal inertia of the uppermost layer is extremely low (Groussin et al. 2007). The thermal skin depth is of the order of 2 cm. Sub-surface chemical heterogeneity cannot be ruled out. That means that the surface must be disrupted every few hours to maintain the observed constancy/repeatability of emission (e.g. the emission of 1P/Halley observed by HMC (Halley Multicolor Camera) was constant to 1% over 3 hours). The surface layer must therefore have the following qualities (Thomas et al. 2008; A'Hearn 2008):

- Surface layer thickness: ~cm at most
- Very good insulation properties
- But, sub-surface sublimation must be occurring to explain the limited surface area coverage of water ice seen by Deep Impact (Sunshine et al. 2006). The depth below the surface of sublimation is therefore limited to a few centimetres at most.

- Sublimation from a sub-surface layer below 1 thermal skin depth cannot match cometary production rates.

The observed inhomogeneity in comets gives an enormous number of additional free parameters for thermo-physical modelling. This implies that, at the present time, our knowledge is so limited that essentially any realistic structure can be produced by using the correct mix of input parameters (Thomas et al. 2008). Laboratory experiments on amorphous ice (Bar-Nun et al. 2008) agree quite well with Deep Impact data (A'Hearn 2008; A'Hearn et al. 2005). Both result in an extremely low tensile strength of a few hundred Pa. On the other hand, the tensile strength could also be much bigger, up to 12 kPa (Holsapple and Housen 2007) for 9P/Temple 1 and the measurements done on amorphous ice in the lab suffer from the unknown influence of gravity.

The nature of the insulation layer is not yet understood. It is an open question if indeed, as has been postulated after the Halley encounter, the material on top of a comet could contain Polyoxymethylene (POM) (Huebner et al. 1987). Laboratory measurements show that the extended formaldehyde source (Eberhardt 1999) at comet Halley would be compatible with POM's (Cottin 2008), but this is clearly not a proof for a surface layer consisting of POM's.

3 Experimental Biases

What we know of comets is limited and is subject to many significant observational biases, e.g.:

- Not all molecules can be detected by remote sensing
- Bright comets can more easily be observed than faint comets
- STARDUST samples may be contaminated by the impact (e.g. Spencer and Zare 2007), they have already a history of heating before they are captured (what we see is only what is left over), it is unclear which part of the nucleus they represent.
- Spectrophotometric observations depend heavily on models
- The coma of a comet is not fully representative of the nucleus
- In situ measurements are limited to very few comets which may have a very different origin in the solar nebula and a very different history since.
- Models, especially nucleus models suffer from an unknown initial state and too many free parameters.

These shortcomings have to be balanced by a strong interdisciplinary community effort including e.g.:

- Studies of mineralogy and organic volatility versus heliocentric distance r_h in select Jupiter family and Oort Cloud comets (amorphous vs. crystalline ice)
- Measure thermal conductivity of porous material in the lab (restrict evolution models)
- Look for the extended CN source and for possible parents of the anomalous $C^{14}N/C^{15}N$ in comets with lab experiments
- Revisit data used for analyzing spectroscopic measurements
- Measure changes of surface during one comet orbit!
- Look for "interstellar" molecules in comets (there are more than 1000 unidentified lines waiting for a patient researcher to be identified!). Look for molecules detected in cometary analogues.

New instrumentation for remote sensing on the Earth and space like e.g. ALMA and JWST (James Webb Space Telescope) will help to overcome some of the experimental biases.

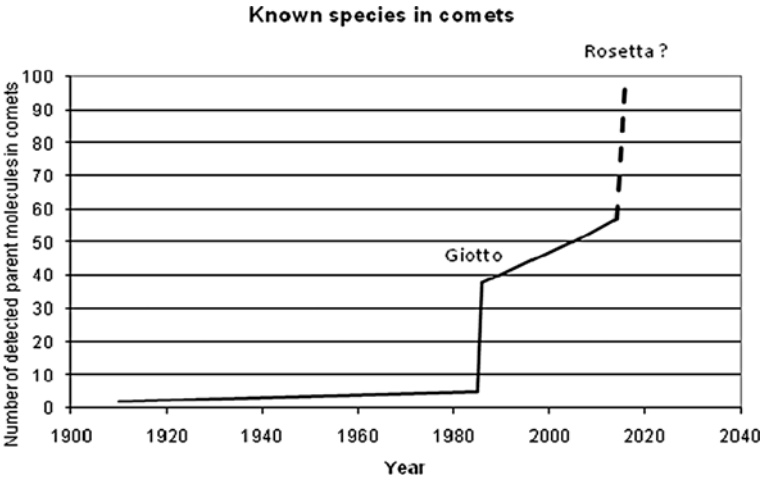

Fig. 1 Number of detected parent molecules in comets as a function of time

4 What Answers Can We Expect from Rosetta

The European spacecraft Rosetta on its way to comet 67P/Churyumov-Gerasimenko will for the first time study a Jupiter family comet in situ over almost a full orbit (Glassmeier et al. 2007). This spacecraft is well equipped with instruments to study the composition of the comet. Spectrometers from the UV to the microwave region will cover the lines of many molecules and minerals. Mass spectrometers will be able to detect molecules, isotopes and elements with very high mass ranges and mass resolutions of the volatiles as well as in the dust particles (Gulkis and Alexander 2008). Figure 1 shows the evolution of detected parent molecules in comets so far. It is evident that already the Giotto mission to comet 1P/Halley was extremely successful in identifying parent molecules as well as elemental and isotopic abundances in a comet. Rosetta's capabilities are far superior. With the Rosetta lander we hope to get "ground truth" for the first time. All measurements so far on composition have been made in the coma, or as in the case of STARDUST, on particles which have spent quite some time in the coma and which have furthermore been altered by the impact. The Rosetta lander will sample the nucleus material directly Of course also the lander has its limits. It will sample only one very small portion of the nucleus. It will sample material only from the nucleus surface or very close to it. But together with the measurements in the coma it will at least help to unravel the mystery of the comet surface layer and the near subsurface composition.

5 Open Questions

The ISSI workshop on "Origin and evolution of comet nuclei" made it very clear that there are plenty of open questions in cometary science. Some of them will be answered by Rosetta or by forthcoming remote sensing, but there will remain quite a few for future generations of cometary scientists. Below is a list of open questions. This list is not complete by far and it is clear that the list will even get longer, once Rosetta reaches its goal.

- Inhomogeneity of nuclei (between nuclei and in one single nucleus)

Table 2 Most important molecules detected in young stellar objects (YSO) and comets. In bold are the few species where there is a discrepancy between the abundances in YSO's and comets

	High-mass YSO	Low-mass YSO	Comets
H_2O	100	100	100
CO	1–20	1–60	5–20
CO_2	~20	15–40	2–10
CH_4	1–4	–	0.2–1.2
CH_3OH	1–35	**1–30**	**0.3–2**
H_2CO	3	–	0.2–1
OCS	**0.05–0.18**	**<0.08**	**0.5**
NH_3	<5	–	0.6–1.8
C_2H_6	<0.4	–	0-4–1.2
HCOOH	**3**	**9**	**0.05**
O_2	<20	–	0.5, upper limit
N_2	?	?	?
XCN	0.3–2.9	–	–
HCN	<3	–	0.2

- N_2 and CO have the same vapor pressure, but only CO is condensed
- $^{15}N/^{14}N$ ratio in HCN and CN differ by a factor of 2. What is the parent of CN?
- What is the parent of the extended CN emission?
- Silicates: where do the crystals come from (transport / annealing)
- Why are the crystalline and the amorphous silicates unevenly distributed in comets
- GEMS: Why are they sub-chondritic in composition (S, Mg, Ca, Fe compared to Si) (large flux of solar cosmic rays?)
- Evolution of nuclei
  - Surface layer:
    - Thickness
    - Composition
  - Dust emission
  - Porosity
  - Thermal conductivity
- What part of the nucleus is represented in the coma?
- Why is the dust production of comets stable over very long times?
- The dust ejection mechanism remains a subject of speculation
- What is the mass of a comet (depends on models) and with it what is the density, the porosity and the gravitation?
- What is the dust/ice ratio in comets?
- Etc., etc.

6 Conclusions

During the ISSI workshop on "Origin and evolution of comet nuclei" the life of a comet from the origin of the cometary material through the accretion of cometesimals in the solar nebula and to the evolution during its stay in the inner solar system was analyzed. Comets show a much bigger variety of morphological structures than previously assumed. However, their

overall composition so far shows not much diversity, even when comparing Oort cloud with Jupiter family comets. It became evident that a comet can be quite inhomogenous by itself, at least from a morphological point of view. It remains to be investigated if comets also show a chemical inhomogeneity inside their nuclei. STARDUST results point to a good mixing of solar nebula material while isotopic ratios of water and CN point to unaltered molecular cloud material. One of the most puzzling aspects is the surface layer of comets which has to be an extremely good thermal insulator while at the same time allowing outgassing from subsurface layers. It is still not clear if a comet surface is "hard" or very "fluffy". This question has to be solved by the Rosetta lander, at least for one comet Another unsolved mystery is the amorphous versus crystalline silicates found in comets. There remain plenty of open questions; some of them will be addressed by Rosetta whereas others will only be solved by future interdisciplinary community efforts in remote sensing, experimental laboratory work, models and in situ analyses.

References

M. A'Hearn, Deep Impact and the origin and evolution of cometary nuclei. Space Sci. Rev. (2008), this issue. doi:10.1007/s11214-008-9350-3

M.F. A'Hearn et al., Deep Impact: Excavating comet Tempel 1. Science **310**(5746), 258 (2005)

K. Altwegg, W.T. Huntress Jr., The constituents of cometary nuclei, in *The Century of Space Science*, ed. by J. Bleeker, J. Geiss, M. Huber (Kluwer, Dordrecht, 2001), pp. 1277–1294

H. Balsiger, K. Altwegg, J. Geiss, D/H and $^{18}O/^{16}O$ ratio in the hydronium ion and in neutral water from in situ ion measurements in comet Halley. J. Geophys. Res. **100**(A4), 5827–5834 (1995)

A. Bar-Nun, I. Pat-El, D. Laufer, How well do experimental results on large samples of gas-laden amorphous ice duplicate Deep Impact's findings? Space Sci. Rev. (2008), this issue. doi:10.1007/s11214-008-9307-6

A.T. Basilevsky, H.U. Keller, Comet nuclei: Morphology and implied processes of surface modification. Planet. Space Sci. **54**(8), 808–829 (2006)

D. Brownlee et al., Comet 81P/Wild 2 under a microscope. Science **314**(5806), 1711 (2006)

S.B. Charnley, S.D. Rodgers, Interstellar reservoirs of cometary matter. Space Sci. Rev. (2008), this issue. doi:10.1007/s11214-008-9331-6

S. Charnley, Interstellar Organic Chemistry The bridge between the big bang and biology: Stars, planetary systems, atmospheres, volcanoes: their link to life. International workshop, Stromboli, Italy, September 13–17, 1999 Rome. Consiglio Nazionale delle Ricerche, 440 p. Edited by Franco Giovanelli, p. 139 (2001)

H. Cottin, Distributed sources in comets. Space Sci. Rev. (2008), this issue. doi:10.1007/s11214-008-9399-z

A.M. DiSanti, M.J. Mumma, Reservoirs for comets: Compositional differences based on infrared observations. Space Sci. Rev. (2008), this issue. doi:10.1007/s11214-008-9361-0

A. Drouart, B. Dubrulle, D. Gautier, F. Robert, Structure and transport in the solar nebula from constraints on deuterium enrichment and giant planets formation. Icarus **140**(1), 129–155 (1999)

P. Eberhardt, Comet Halley's gas composition and extended sources: Results from the neutral mass spectrometer on Giotto. Space Sci. Rev. **90**(1), 45–52 (1999)

J.A. Fernandez, Origin of comet nuclei and dynamics. Space Sci. Rev. (2007)

K.-H. Glassmeier, H. Boehnhardt, D. Koschny, E. Kührt, I. Richter, The Rosetta mission: Flying towards the origin of the solar system. Space Sci. Rev. **128**(1), 1–21 (2007)

O. Groussin, M.F. A'Hearn, J.-Y. Li, P.C. Thomas, J.M. Sunshine, C.M. Lisse, K.J. Meech, T.L. Farnham, L.M. Feaga, W.A. Delamere, Surface temperature of the nucleus of Comet 9P/Tempel 1. Icarus **187**(1), 16 (2007)

S. Gulkis, C. Alexander, Composition measurements of a comet from the Rosetta orbiter spacecraft. Space Sci. Rev. (2008), this issue. doi:10.1007/s11214-008-9335-2

M.S. Hanner, The silicate material in comets. Space Sci. Rev. **90**, 99–108 (1999)

K.A. Holsapple, K.R. Housen, A crater and its ejecta: An interpretation of deep impact. Icarus **187**(1), 345–356 (2007)

P. Hoppe, Reservoir for comet material: Circumstellar grains. Space Sci. Rev. (2007), this issue. doi:10.1007/s11214-007-9238-7

W.F. Huebner, D. Boice, C.M. Sharp, Polyoxymethylene in comet Halley. Astrophys. J. **320**(2), L149 (1987)

E.K. Jessberger, J. Kissel, Chemical properties of cometary dust and a note on carbon isotopes, in *Comets in the Post-Halley Era*, vol. 2, 1991 (A93-13551 02-90), pp. 1075–1092

H. Kawakita, J. Watanabe, H. Ando, W. Aoki, T. Fuse, S. Honda, H. Izumiura, T. Kajino, E. Kambe, S. Kawanomoto, K. Noguchi, K. Okita, K. Sadakane, B. Sato, M. Takada-Hidai, Y. Takeda, T. Usuda, E. Watanabe, M. Yoshida, The spin temperature of NH_3 in comet C/1999S4 (LINEAR). Science **294**(5544), 1089 (2001)

F. Kemper, W.J. Vriend, A.G.G.M. Tielens, Erratum: "The absence of crystalline silicates in the diffuse interstellar medium". Astrophys. J. **633**(1), 534 (2005)

A. Morbidelli, G.B. Valsecchi, Neptune scattered planetesimals could have sculpted the primordial Edgeworth–Kuiper belt. Icarus **128**, 464–468 (1997)

M.A. Weaver, M.J. Mumma, H.P. Larson, Infrared investigation of water in comet P/Halley. Astron. Astrophys. **187**, 411–419 (1987)

J.H. Oort, The structure of the cloud of comets surrounding the Solar System and a hypothesis concerning its origin. Bull. Astron. Inst. Neth. **11**, 91 (1950)

D. Prialnik, G. Sarid, E.D. Rosenberg, R. Merk, Thermal and chemical evolution of comet nuclei and Kuiper belt objects. Space Sci. Rev. (2008), this issue. doi:10.1007/s11214-007-9301-4

F. Robert, D. Gautier, B. Dubrulle, The solar system d/h ratio: Observations and theories. Space Sci. Rev. **92**, 201–224 (2000)

S.D. Rodgers, S.B. Charnley, Chemical evolution in protostellar envelopes: Cocoon chemistry. Astrophys. J. **585**, 355–371 (2003)

F.H. Shu, H. Shang, M. Gounelle, A.E. Glassgold, T. Lee, The origin of chondrusles and refractory inclusions in chondritic meteorites. Astrophys. J. **548**, 1029–1050 (2001)

R. Schulz, Morphology–composition–isotopes. Space Sci. Rev. (2007), this issue. doi:10.1007/s11214-007-9237-8

M.K. Spencer, R.N. Zare, Comment on "Organics captured from comet 81P/Wild 2 by the STARDUST spacecraft". Science **317**(5845), 1680 (2007)

T. Stephan, Assessing the elemental composition of comet 81P/Wild 2 by analyzing dust collected by Stardust. Space Sci. Rev. (2007), this issue. doi:10.1007/s11214-007-9291-2

J.M. Sunshine, M.F. A'Hearn, O. Groussin, J.-Y. Li, M.J.S. Belton, W.A. Delamere, J. Kissel, K.P. Klaasen, L.A. McFadden, K.J. Meech, H.J. Melosh, P.H. Schultz, P.C. Thomas, J. Veverka, D.K. Yeomans, I.C. Busko, M. Desnoyer, T.L. Farnham, L.M. Feaga, D.L. Hampton, D.J. Lindler, C.M. Lisse, D.D. Wellnitz, Exposed Water Ice Deposits on the Surface of Comet 9P/Tempel 1. Science **311**(5766), 1453–1455 (2006)

N. Thomas, C. Alexander, H.U. Keller, Loss of the surface layers of comet nuclei. Space Sci. Rev. (2008), this issue. doi:10.1007/s11214-008-9332-5

E.F. Van Dishoeck, G.A. Blake, Chemical evolution of star forming regions. Ann. Rev. Astron. Astrophys. **36**, 317–368 (1998)

D.H. Wooden, Cometary refractory grains: interstellar and nebular sources. Space Sci. Rev. (2008)

Colloquium

The Contributions of Comets to Planets, Atmospheres, and Life: Insights from Cassini-Huygens, Galileo, Giotto, and Inner Planet Missions

Tobias Owen

Originally published in the journal Space Science Reviews, Volume 138, Nos 1–4.
DOI: 10.1007/s11214-008-9306-7

Abstract Comets belong to a group of small bodies generally known as icy planetesimals. Today the most primitive icy planetesimals are the Kuiper Belt objects (KBOs) occupying a roughly planar domain beyond Neptune. KBOs may be scattered inward, allowing them to collide with planets. Others may move outward, some all the way into the Oort cloud. This is a spherical distribution of comet nuclei at a mean distance of ∼50,000 AU. These nuclei are occasionally perturbed into orbits that intersect the paths of the planets, again allowing collisions. The composition of the atmosphere of Jupiter—and thus possibly all outer planets—shows the effects of massive early contributions from extremely primitive icy bodies that must have been close relatives of the KBOs. Titan may itself have a composition similar to that of Oort cloud comets. The origin and early evolution of its atmosphere invites comparison with that of the early Earth. Impacts of comets must have brought water and other volatile compounds to the Earth and the other inner planets, contributing to the reservoir of key ingredients for the origin of life. The magnitude of these contributions remains unknown but should be accessible to measurements by instruments on spacecraft.

Keywords Comets · Collisions · Origins: solar system · Icy planetesimals

1 Introduction

The possibility that comets may have played an important role in the development of planets was independently proposed by Edmond Halley and Isaac Newton in the late 17th century (Genuth 1997). Halley thought a collision with a comet would have caused a chaos on Earth that could have produced the Biblical flood. Newton suggested that the vapors from comet tails would be collected by planetary atmospheres, thereby delivering water that would sustain terrestrial life. Considering that no one knew the composition or structure of comets at that time, these were bold conjectures indeed!

T. Owen (✉)
University of Hawaii, Institute for Astronomy, Honolulu, HI 96822, USA
e-mail: owen@ifa.hawaii.edu

The steady increase in knowledge about comets made these hypotheses even more attractive, but not because they might explain the need for Noah's ark! The discovery of the radicals CN, C_2, and C_3 in the spectra of comets implied the presence of parent molecules that could be simple or even complex organics. This chain of reasoning in turn led to the hypothesis that impacts by comets could have aided or even initiated the pre-biological chemistry that ultimately resulted in the origin of life on Earth. In fact, similar impacts must have occurred on Venus and Mars, thereby providing them with the same chemicals. This idea represents a modern form of Newton's hypothesis. More recently, we have further broadened the possible influences of comets by suggesting that the accretion of these objects may have been responsible for the formation of giant planet cores, thereby enabling the formation of the planets themselves. The accretional impacts thus represent a modern version of Halley's idea.

2 Comets as Icy Planetesimals

An idealized pathway from the interstellar medium to the origin of life is given in Fig. 1. The current conception of the actual situation for cometary deliveries appears in Fig. 2. This figure is still idealized, but closer to reality.

It is evident from this figure that there are multiple opportunities for all types of comets to collide with planets and satellites. Some of these collisions can contribute to the composition of these objects and their atmospheres. Others will simply make craters as they explode upon impact.

The common feature in all these suggestions is the use of comets to aid in the explanation of some otherwise intractable yet fascinating problem. But does any of this make sense?

Figure 2 shows that the spectacular comets with which people are most familiar because of their bright comae and immensely long tails are actually a subset of a class of icy planetesimals that have originated in different places in the early solar nebula. Ever since Whipple's epochal study of the problem (Whipple 1950), it has become clear that a traditional comet is actually an ice-rich small body called the nucleus that has wandered close enough to the Sun to produce a coma and tail by sublimation. Millions if not billions of these icy nuclei form a spherical shell around the plane of the solar system at a mean distance of 50,000 AU. This shell is known as the Oort cloud, after its discoverer. These nuclei are commonly thought to have been scattered from their hypothesized place of origin among the giant planets. Another reservoir of icy objects extends outward in a disk beyond the orbit of Neptune. This is the Kuiper Belt, home of the Kuiper Belt objects (KBOs). The largest KBOs are far larger

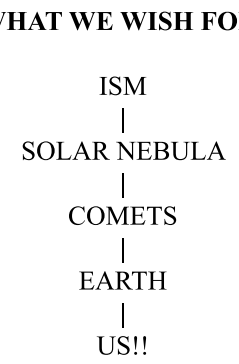

Fig. 1 The simple track we would prefer

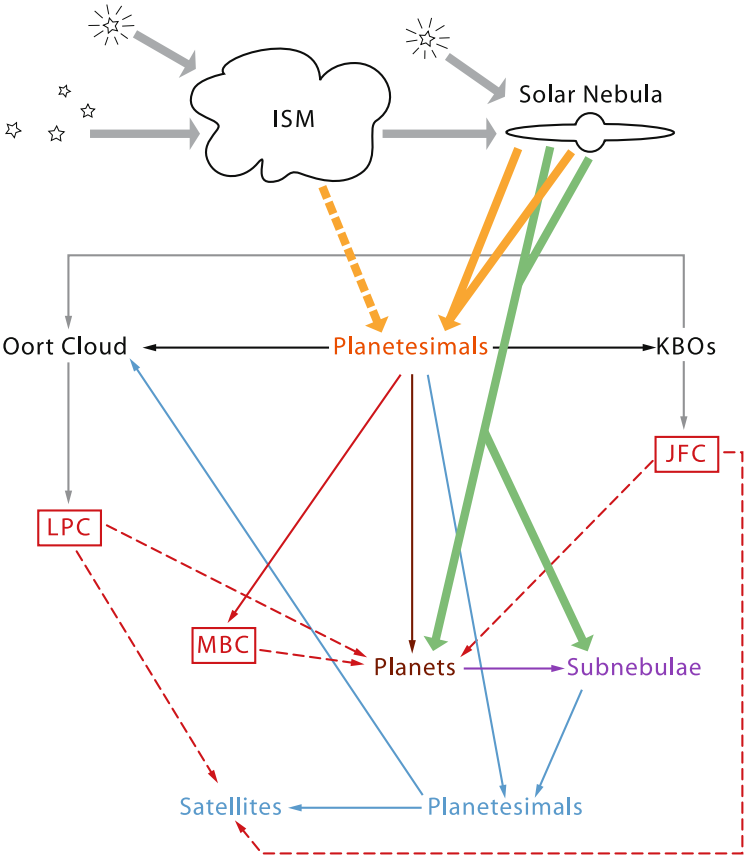

Fig. 2 A still incomplete depiction of the actual situation!

than any Oort cloud comets seen so far. They include Pluto and often have satellites. Some KBOs could have been scattered into the Oort cloud, from which they could occasionally visit the inner solar system.

The comet most likely to fit this description is Comet Sarabat (1729). This is the brightest comet ever observed, reaching naked-eye visibility at its perihelion of 4.0 AU (Hurst 1997). Could this comet have been a KBO? Unfortunately, we will never know.

Icy planetesimals also originated in the subnebulae surrounding the giant planets at the time they formed. Some of these accreted to form the icy satellites; others crashed into the forming planets, and still others could have been scattered into the Oort cloud.

Finally, several objects in the outer region of the main asteroid belt have recently been discovered to exhibit cometary characteristics (Hsieh and Jewitt 2006).

These different locations for the origins of icy planetesimals imply different compositions as well, largely determined by the temperature of the environments in which they formed. Thus we can expect bodies ranging from nearly pure ice—formed by collisions among differentiated objects—to extremely primitive objects containing all the elements except He and Ne, formed at temperatures below 30 K. But ground-based observations have not yet found such variations with the possible exception of some differences in abundances of organic compounds (Mumma et al. 2007).

To understand these differences we need to start at the beginning—the interstellar cloud fragment that collapsed to form the solar nebula. Here we find that C/N $\sim$ 4, the solar value, but the disposition of these two cosmically abundant elements is very different. We can therefore use them to track the processes of comet formation. C is mostly (>50%) present in solid form—as amorphous carbon, macromolecular carbon, and frozen simple compounds such as CO_2. In contrast, N is primarily ($\sim$90%) in the form of a highly volatile gas—N_2 or even atomic N. This means that it will be much easier for a forming planetesimal to capture carbon than nitrogen, so we may expect the ratio C/N > 4 in these objects.

Given the possibilities of fractionation by atmospheric escape, formation of compounds locked in planetary interiors including sequestration in high density cores, C/N by itself is a rather blunt instrument. Nevertheless, it is at least a beginning, and indeed we find a significant depletion of nitrogen in Oort cloud comets, exactly as predicted (Fig. 3). Because N_2 is commonly assumed to have been the dominant form of nitrogen in the solar nebula, the inability of ice to trap this molecule at $T > 30$ K (Owen and Bar-Nun 1995) has been identified as the probable cause of the nitrogen deficiency in comets. This conclusion obviously requires that Oort cloud comets scattered from the region of the giant planets formed at $T > 30$ K. A discussion of the compounds that carry the nitrogen in comets is given in the next section. As we shall see, the isotopes of nitrogen provide another way of distinguishing Oort cloud comets from other icy planetesimals.

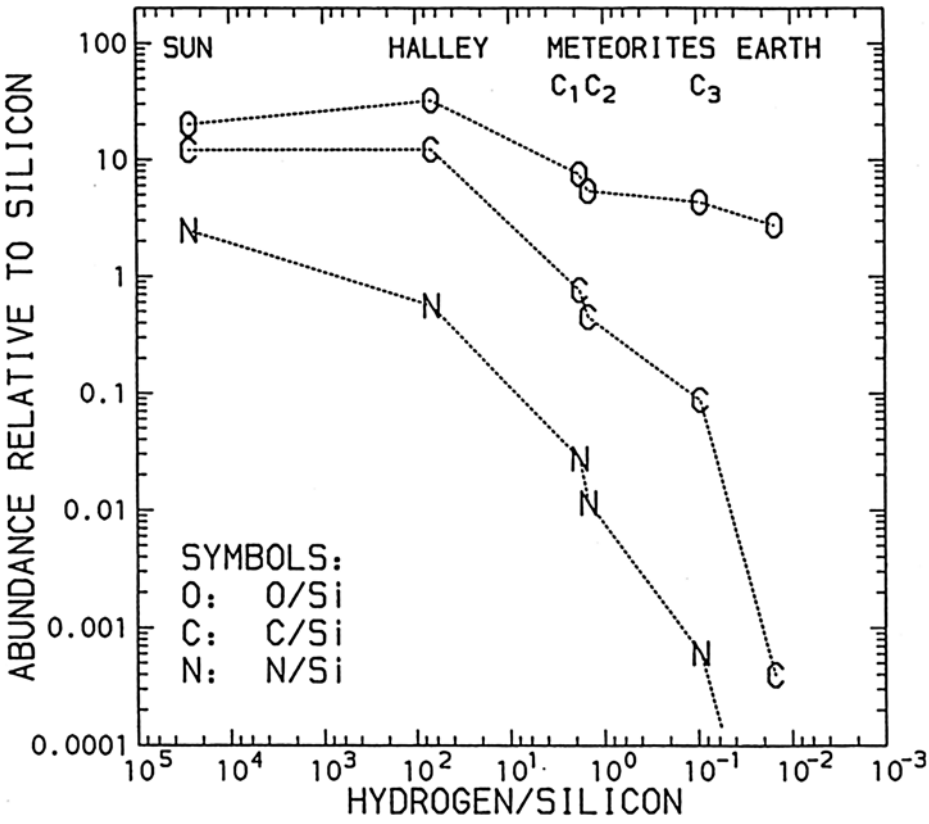

Fig. 3 Abundances in Halley's Comet (Geiss 1988)

3 The Giant Planets

Having established what to expect for the composition of comets, we can see whether the same value of C/N shows up in the atmospheres of the planets, testifying to cometary impact. In the case of the giant planets, it was widely assumed that it would, since comets were considered to be the major source of the planets' heavy elements (Pollack and Bodenheimer 1989).

The mass spectrometer on the Galileo probe revealed that this was definitely not the case for Jupiter (Niemann et al. 1998). Instead both carbon and nitrogen were found to be enriched by the same amount compared with solar values relative to hydrogen. Thus C/N was solar, and both C/H and N/H were $4 \pm 2 \times$ solar (Owen et al. 1999; Owen and Encrenaz 2006; see Fig. 4). Assuming these heavy elements were all delivered by solid bodies, these carriers must have been formed at very low temperatures ($T \leq 30$ K) to trap the N_2. This holds true whether the gas was trapped as clathrates, by adsorption on amorphous ice grains, or simply condensed on grains.

Such low-temperature objects are very different from the comets we have studied in the inner solar system so far, as these have all been deficient in nitrogen (Fig. 3; Cochran 2002). Owen and Encrenaz (2003) coined the term "SCIPs" (solar composition icy planetesimals) to describe these low-temperature planetesimals. These objects are essentially identical to the type III comets postulated by Owen and Bar-Nun (1995). If the outer Kuiper Belt objects were formed where we find them today, they may represent remnant SCIPs. We may yet

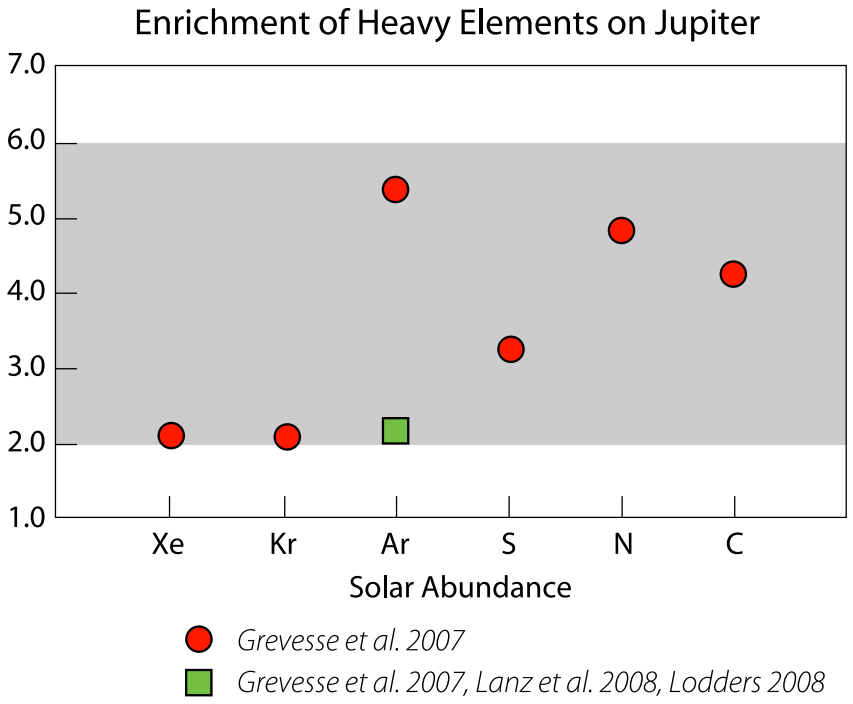

Fig. 4 The enrichment of heavy elements/hydrogen on Jupiter compared to solar abundances. *Red circles*, Grevesse et al. (2007); *green square*, from average of Lanz et al. (2008) and Lodders (2008). Error bars deleted for clarity

observe one of these objects in the inner solar system if indeed some of them were scattered out to the Oort cloud. They could then be perturbed into orbits that bring them in, just like the bright long-period comets that give such spectacular displays when they appear in our skies. This is the intriguing possibility offered by Comet Sarabat.

We can make one further test of this model if we can prove that the nitrogen on Jupiter arrived as N_2. This would show that the planetesimals that carried in the nitrogen must have formed at the low temperatures required to trap N_2. In this case, they would be SCIPs. To make this test, we have evaluated the nitrogen isotopes in Jupiter's NH_3, using the Galileo Probe Mass Spectrometer. NH_3 is the major product of nitrogen chemistry in the planet's accessible atmosphere, starting from N_2.

The results of that determination are shown in Fig. 5 (Owen et al. 2001). Here we see the isotopic ratio $^{15}N/^{14}N$ in the atmospheres of Jupiter, Titan, and the inner planets. The Jovian value is clearly lower than the others, exactly what we would expect if Jovian nitrogen were contributed by N_2 (Owen and Bar-Nun 1995; Terzieva and Herbst 2000), while nitrogen on the inner planets came from condensed compounds such as NH_3. The atmospheres of Titan and Mars show the fractionation of isotopes that can occur when bodies have sufficiently small masses that the lighter isotope can escape. Rocks from Mars also contain nitrogen that has not participated in the escape process and reveals the same isotope ratio we find on Earth. There is further support that the Jovian value of $^{15}N/^{14}N$ represents the nitrogen that dominated the solar nebula from a measurement of these same isotopes in the nitrogen in TiN found in a high-temperature CaAl inclusion of a meteorite (Meibom et al. 2007). The inclusion number agrees with the Jovian value (Fig. 5).

The nitrogen we find in comets—like that on Earth and other solid bodies—is predominantly derived from condensable nitrogen compounds, most probably primarily NH_3, but including minor compounds such as HCN. The Oort cloud comets studied so far are distinctly different from SCIPs, which must include N_2 as well as NH_3.

Comets contain another type of nitrogen that is even more different from the solar nitrogen trapped in SCIPs. Arpigny et al. (2003) have discovered and Jehin et al. (2004, 2006) and Cochran et al. (2007 and references therein) have confirmed in 15 comets, embracing all types, that $^{15}N/^{14}N$ in the CN radical in comets is consistently close to 7×10^{-3} (Fig. 5). This and higher values are seen in the organic components of cometary interplanetary dust particles (Messenger 2000). Higher values of D/H are also found in these materials. Both of these isotopic anomalies point toward the interstellar medium as their source. In comets, the CN radical must be derived from a minor component relative to NH_3, while in the interplanetary dust particles, the NH_3 is missing owing to its high volatility. Thus we can assume with some confidence that any nitrogen delivered to solid bodies by comets—or trapped in any ices forming at $T > 35$ K—will predominantly exhibit the ratio of $^{15}N/^{14}N$ we find in the atmospheres of Earth and Venus and in rocks protected from the atmosphere on Mars (Fig. 5).

Adopting their hypothesis that SCIPs delivered heavy elements to all the giant planets, Owen and Encrenaz (2003) predicted that the enrichment of heavy elements on Saturn would follow the pattern on Jupiter. Unfortunately, only remotely detected carbon (in methane) could be evaluated on Saturn because no atmospheric probe has yet been sent there to measure additional species. The value of C/H for Saturn determined by the IR spectrometer on the Cassini orbiter indeed shows the value predicted by the model we have just described (Flasar et al. 2005). It appears that the mass of heavy elements delivered to Saturn is the same as that delivered to Jupiter. The smaller mass of the planet then requires the enrichment to be correspondingly greater. This pattern is repeated for C/H on Uranus and Neptune, where the observed values of D/H also match the values predicted by the SCIP hypothesis (Owen and Encrenaz 2006).

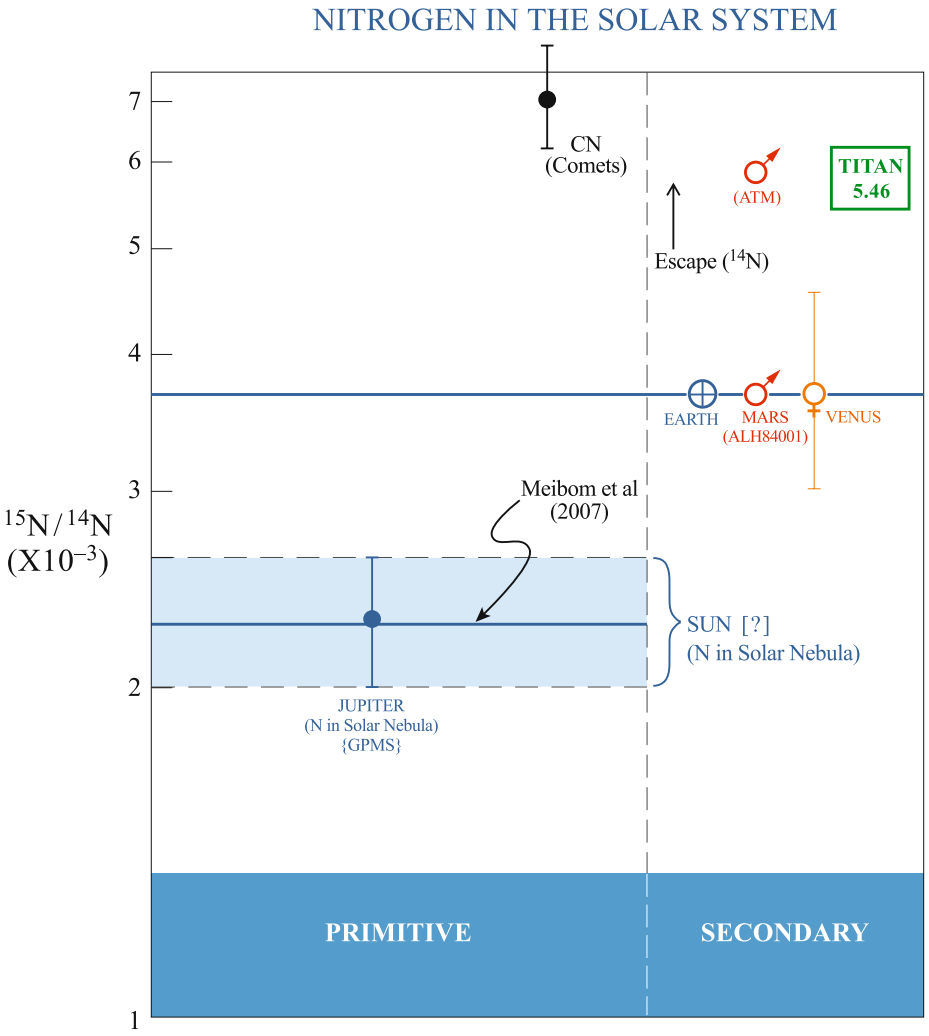

Fig. 5 The ratio $^{15}N/^{14}N$ in the solar system. Note low value for Jupiter, formerly considered to be the "solar" value and the high value for CN in comets (Owen et al. 2001; Arpigny et al. 2003)

The Jupiter results already indicate that SCIPs represent a distinct type of comet nucleus, one formed at sufficiently low temperatures to capture all the heavy elements. Are SCIPs required to explain abundances and isotope ratios on Saturn, Uranus, and Neptune? If so, this discovery would demonstrate that these low-temperature comet nuclei were the most abundant form of solid matter in the early solar system.

4 Titan

We turn now to a consideration of Titan, Saturn's biggest satellite. It is slightly larger than the planet Mercury, has a surface temperature of 94 K, and a nitrogen-dominated atmosphere with a surface pressure of 1.5 bars. The density of Titan indicates that it is approximately

half ice and half rock by mass, which is close to the solar ratio for these materials. Thus in bulk composition, this satellite is similar to a comet.

As determined by the mass spectrometer on the Huygens Probe, the atmosphere of Titan is 98% N_2 and 1.6% methane, with a trace of ^{40}Ar (Niemann et al. 2005). Here is an object that appears to violate our early paradigm of C/N $\sim$ 15 on small bodies. Yet Titan must have been built from planetesimals containing more carbon than nitrogen, even if they were SCIPs. So where is Titan's carbon?

Earth also has an atmosphere in which nitrogen dominates carbon; N/C $= 80/3.5 \times 10^{-4}$. On Earth we know exactly where the missing carbon is. Most of it is buried as carbonate rocks such as huge deposits of limestone. A smaller amount is buried organic material, the most well-known being coal and petroleum.

To produce the carbonates, it is necessary to have liquid water; the buried organics are contributed by long-dead organisms. Since neither of these agents are available on Titan, we must look elsewhere. All the methane presently in the atmosphere of Titan will be destroyed by photochemistry in 10–20 million years, so there must be an internal source that replenishes it.

At present, there are two competing hypotheses: delivery of carbon as methane in clathrate hydrates that get trapped in the planet's interior, and delivery in the form of CO_2, organics, and other forms of solid carbon that are converted to methane in a two-step process (Niemann et al. 2005). Hydrogen is first produced by a water-rock reaction known as serpentinization and then reacts with the various forms of carbon in a kind of Fischer-Tropsch reaction to produce methane.

To see what Titan can tell us about cometary contributions, we can again consult the atmosphere. Here we find from the fractionation of the nitrogen isotopes in N_2 (Fig. 5) that Titan must have produced $\sim$5$\times$ the amount of nitrogen we now find in the atmosphere. This tells us that the ice on Titan could not have been contributed by SCIPs, because N/Ar on Titan is $\sim 10^8$ instead of 30, as it would be if the ice had trapped gases while maintaining solar abundances. In fact, to reach the observed ratio from an initial mixture of NH_3 and ^{36}Ar, the temperature at which the ice formed must have been close to 100 K, based on the laboratory work of Bar-Nun et al. (1988). This may be compared to the $\sim$50 K temperature at which the Oort cloud comets appear to have formed (Owen and Bar-Nun 1995). Evidently, the icy planetesimals that accreted to form Titan originated in Saturn's "warm" subnebula rather than in the solar nebula as is postulated for the Oort cloud comets.

This conclusion can be tested eventually by examining D/H in Titan's H_2O in some future mission that will heat the surface of the satellite to vaporize some of the ice. Oort cloud comets have D/H $= 3.1 \times 10^{-4}$ (Balsiger et al. 1995; Eberhardt et al. 1995), whereas we might expect Titan's ice to have a lower value, representing isotope exchange with H in the $\sim$100 K subnebula.

5 Venus, Earth, and Mars

We now return to the question first posed by Newton and Halley: What role did comets play in bringing water and other volatiles to Earth?

We can begin with an investigation of C/N in inner planet atmospheres to establish a context for the source(s) of water. We choose Venus as our standard, as this planet appears to have all its volatile carbon and nitrogen in its atmosphere. The massive atmosphere consists of 96.5% CO_2 and 3.5% N_2, with small amounts of Ar and other gases. The surface pressure is 90 bars. The ratio C/N in this atmosphere is then $\sim$15 (Donahue and Pollack

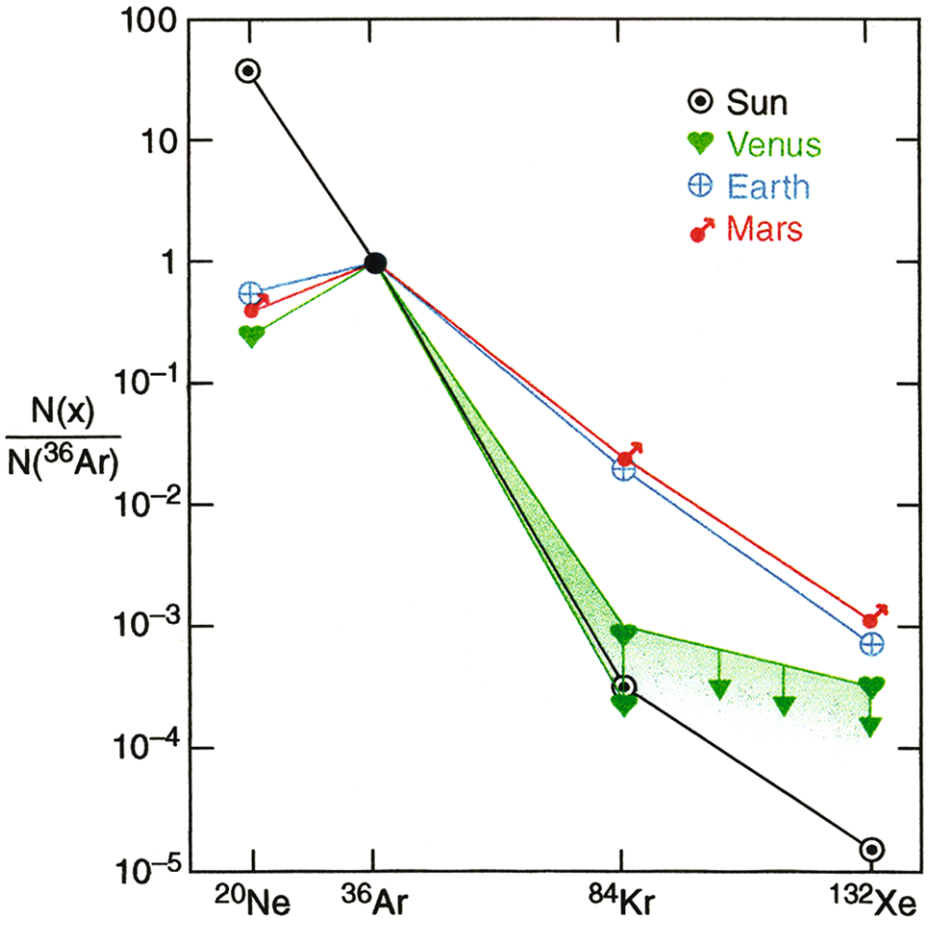

Fig. 6 Noble gases in the atmospheres of Venus, Earth, and Mars. Kr and Xe on Venus still poorly determined. Note similarity between Mars and Earth, and unusually high value of ^{36}Ar on Venus, giving Ar/Kr a nearly solar value

1983), consistent with the value found in comets (cp. Sect. 2). However, this same ratio is also found in meteorites, so this is not a proof that cometary bombardment produced the atmosphere of Venus, merely a positive consistency check. Any original water on Venus has been dissociated with the subsequent escape of hydrogen. We know this because of the huge fractionation of D/H, which is now 150 times the value in seawater on Earth (Donahue et al. 1982).

Thus there is no hope of using the residual water we find as vapor in the atmosphere to search for evidence of cometary bombardment.

However, a possible fingerprint left by one or more comets can be found in the abundances of the noble gases (Fig. 6). The ratio Ar/Kr $= 10^3$ is much closer to the solar value of 2×10^3 than to the value of 30 found in Earth's atmosphere. Recall that SCIPs are postulated to contain solar abundances. Furthermore, the abundance of Ar per gram of planetary rock is the highest found anywhere in the solar system. Both of these results could be explained by the impact of one or more SCIPs. Assuming that to be the case, one can easily show that

the amounts of C and N delivered with the noble gases would be far too small to account for the CO_2 and N_2 presently found in the atmosphere. Furthermore, if these elements were also delivered by SCIPs, C/N would be solar instead of 15× solar, as observed.

Evidently, there must be a noncometary source for the bulk of the planet's volatiles. It could be either meteorite bombardment or outgassing of the rocks making up most of the planet's mass. In either case, some "seasoning" must be added to produce the noble gases, and SCIPs provide an attractive source.

Turning to Earth, we may anticipate a similar story because Venus and Earth are such similar planets, located in the same part of the solar system. At first glance, the two atmospheres appear totally different. Earth's atmosphere has a surface pressure of only 1 bar and is 78% N_2, 21% O_2, and 1% of radiogenic Ar. As we saw in Section 4, however, the missing carbon is largely bound up in carbonate rocks and deposits of coal and petroleum. If this carbon were returned to the atmosphere as CO_2, it would produce surface pressure of about 70 bars that would be 98% carbon dioxide. The present 23% O_2 would disappear in the absence of life. We would find a ratio of C/N = 20 ± 10, again consistent with our scenario for the capture of these two elements by planetesimals, but not conclusive evidence for cometary delivery.

On the other hand, the noble gases in the atmosphere argue against the meteorites as a source. The ratio Kr/Xe is distinctly different from that found in meteorites. We don't yet know whether this pattern also exists in comets as no noble gases have yet been detected in any icy planetesimals. A search for these gases is one of the prime objectives of the Rosetta mission to Comet 67P/Churyumov-Gerasimenko.

The abundances of the noble gases are important because they provide a standard that can be used to calculate the contribution of comets to all the volatiles on Earth. The possibility that these volatiles may have included compounds that were important to the origin of life on Earth has been proposed by Oro (1961) and developed in detail by Delsemme (1998, 2000). Unfortunately, it is not possible to search for complex organic compounds in comets by remote observations. The Rosetta Mission will help, but returned samples will probably be required to provide a definitive answer. However, in the specific case of water, we can search for evidence of cometary bombardment directly by measuring D/H in seawater and comparing it to D/H in the water that forms cometary ice. Pristine comets are ∼50% water ice; the question is how much of the water on Earth was contributed by this celestial delivery system.

D/H in seawater is well determined as 1.6×10^{-4}. Measuring this ratio in comets has proved to be much more difficult. The most precisely determined value thus far is D/H = 3.1 ± 0.2 determined for Halley's comet by Balsiger et al. (1995) and Eberhardt et al. (1995). These measurements were made by mass spectrometers that were carried through the coma of Halley's comet. Ground-based observations using telescopes at submillimeter wavelengths led to the same result with greater uncertainty in two other comets (Fig. 7).

All three of these icy planetesimals came from the Oort cloud, leaving open the possibility that comets from other reservoirs might be made of ice with different values of D/H. In particular, the comets found in the outer part of the main belt of asteroids have been suggested as a source of Earth's water (Hsieh and Jewitt 2006). This hypothesis may run into trouble with the noble gases in these comets if they have the same proportions as noble gases found in carbonaceous chrondrite meteorites. These volatile rich meteorites are commonly thought to originate from the same region of the asteroid belt as the newly discovered comets. Their noble gases have a distinctly different abundance pattern than noble gases found in Earth's atmosphere.

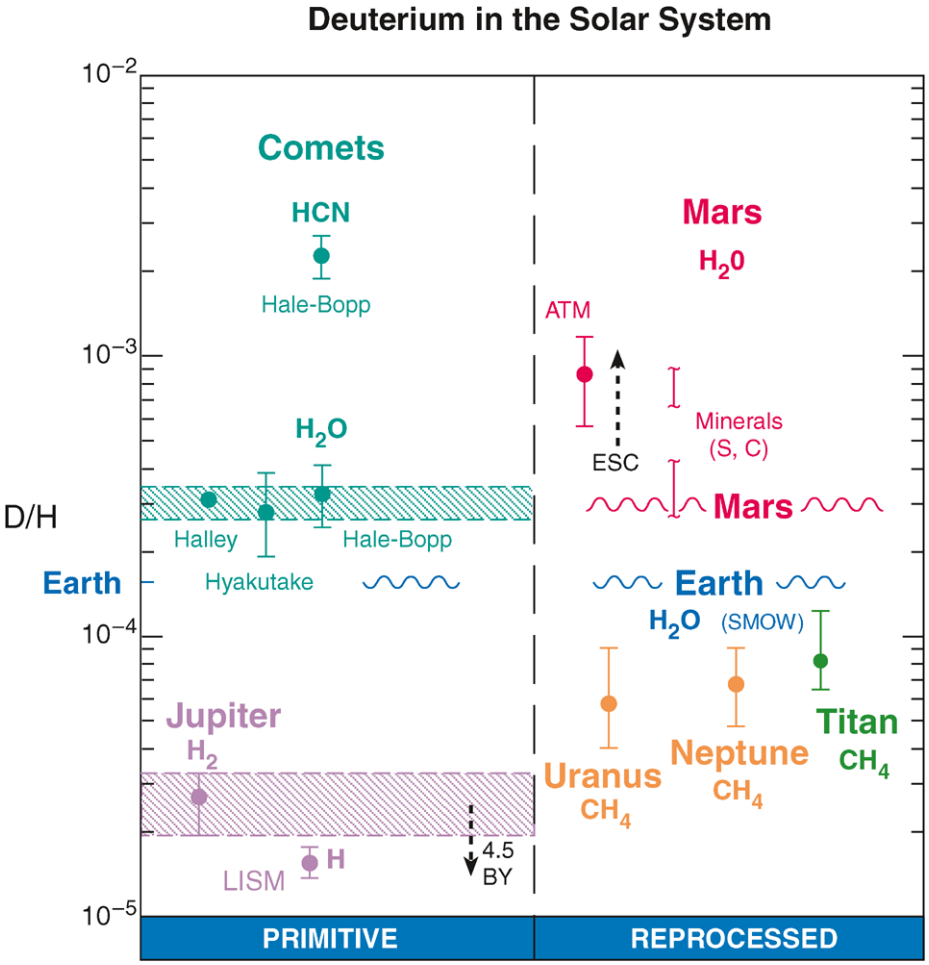

Fig. 7 D/H in the planets and comets of the solar system. Major differences exist between Jupiter, presumed to represent the primordial value in the solar nebula, the fractionated values among the inner planets, and the mixture of primordial D/H with D/H from the icy cores of Uranus and Neptune. The origin of the value on Titan remains uncertain

But perhaps the noble gases in these comets are different from those in the meteorites. The noble gases in meteorites are concentrated in the carbon found in a curious macromolecular compound called "Q" for quintessence, that comprises a tiny fraction (<0.04%) of the meteorite (Swindle 1988). The noble gases in the much greater mass of ice originally in these comets could be both more abundant and different in their relative abundances.

On the basis of existing evidence, we must conclude that comets by themselves could not have supplied Earth's water. Once again we look to the rocks that made the planet. In this case, we must postulate that the grains that made these rocks adsorbed water vapor in the inner solar nebula, where isotope exchange between H_2O and HDO could produce low values of D/H in H_2O. Mixing this water with cometary water would then produce the observed D/H in the ocean water. This isotope exchange rate has been measured by Lecluse and Robert (1994) and appears to be sufficiently efficient to produce the desired effect.

What about other volatiles? We have suggested that Earth's nitrogen was delivered as NH_3. This compound appears to be the major carrier of nitrogen in comets. Unfortunately, the value of $^{15}N/^{14}N$ in cometary NH_3 is unknown—another project for Rosetta. If it turns out that $^{15}N/^{14}N$ in this NH_3 has the same value as the ratio found in CN, instead of the value found in the nitrogen we breathe, we can rule out comets as the source of Earth's nitrogen (Fig. 5).

There is one more approach we can use to assess cometary contributions to Earth and the other inner planets. This involves the planet Mars.

On Mars we find small amounts of water vapor in the atmosphere, plus a ratio of C/N = 15. Here we have to admit that this value is probably a coincidence as a huge amount of CO_2 has evidently been blown off the planet by impact erosion (Melosh and Vickery 1989), while approximately 10 × the present amount of post-impact nitrogen has left the planet by nonthermal escape (McElroy et al. 1977).

We therefore turn once again to the noble gases for enlightenment. Here we find a remarkable correspondence between the abundance patterns of Ar/Kr/Xe found in the atmospheres of Earth and Mars (Fig. 6). Furthermore, the relative abundances of xenon isotopes are also the same for the two planets, again different from any other source (Owen and Bar-Nun 2000; Fig. 8). We emphasize once more that the Rosetta mission will tell us if the ices in comets have trapped noble gases with the same pattern of abundances and isotope ratios, thereby furnishing a crucial test of the cometary bombardment hypothesis.

Could it be that we are seeing the result of a post-impact cometary contribution on Mars? If so, near-surface water on Mars that has not been exposed to the atmosphere might exhibit the cometary value of D/H. The existing measurements of D/H in H_2O from Martian meteorites indicate that the lowest values of D/H in water not subject to escape may have cometary rather than terrestrial value (Leshin et al. 1996; Fig. 9). It is worthy of note that a single comet with a diameter of just 10 km could supply all the water that exchanges seasonally between the two Martian polar caps. It is also important to realize that there is apparently no exchange between surficial water and water in silicates (Karlsson et al. 1992). Evidently, the lack of plate tectonics on Mars keeps the hydrosphere separated from the lithosphere, unlike the situation on Earth.

Thus we have the fascinating possibility that the surface of Mars is lightly frosted by a thin layer of cometary water. The Mars Science Laboratory Mission planned for 2012 will be able to determine if that is the case by studying D/H in the surface water.

6 Conclusions

We can summarize the evidence for cometary contributions to planets as follows:

Outer Planets: Low-temperature, icy planetesimals with solar relative abundances (SCIPs) have apparently delivered the heavy elements to Jupiter and possibly all of the giant planets. If this is correct, SCIPs would have been the most abundant form of solid matter in the early solar system. While we don't find any evidence of SCIPs among the comets we have studied thus far, they may be identical to the most primitive Kuiper Belt objects we find in orbits beyond that of Neptune. We may characterize both of these families as comets of Type III formed at $T < 30$ K and thus containing solar abundances of heavy elements.

Titan: The ice making up ∼50% of Titan's mass was apparently formed from planetesimals that originated at $T \approx 100$ K in Saturn's subnebula. This conclusion follows from the high value of N/Ar in the satellite's atmosphere. This high ratio also excludes N_2 as the source of Titan's nitrogen, indicating that both N_2 and ^{36}Ar must be strongly depleted on the

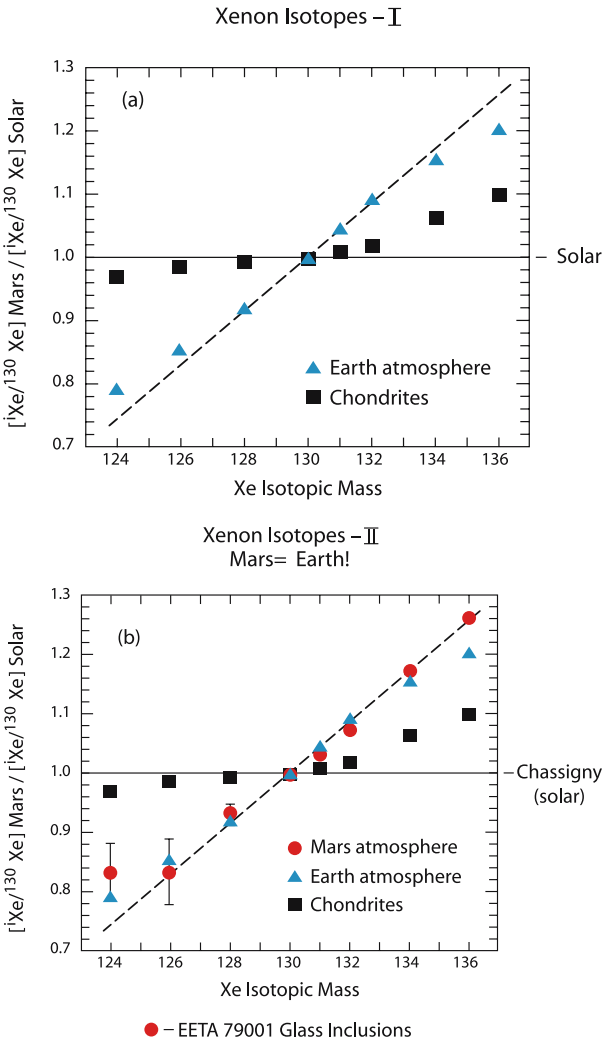

Fig. 8 A comparison of xenon isotopes I (**a**) Earth, Sun, meteorites, and II (**b**) Earth, Mars, meteorites (Bogard et al. 2001). Mars and Earth are remarkably similar and distinctly different from the Sun and meteorites

planet. However, carbon will be trapped in these "warm" planetesimals in the form of solid CO_2, amorphous grains, and macromolecular compounds, all of which can serve as sources for the atmospheric CH_4.

Inner Planets: The abundances of noble gases on Venus offer a hint that collisions with one or more SCIPs could have occurred. However, the dominant sources of N and C appear to be the rocks making up the planet. The water initially present on Venus has almost completely disappeared, removed by a combination of photodissociation in the upper atmosphere and escape of the resulting hydrogen.

On Earth the noble gas abundance pattern is distinctly different from that of Venus, the Sun, or the meteorites. Water in the oceans on Earth exhibits a value of D/H that is clearly lower than that in comets, indicating that cometary water, if it exists on Earth at all, must be

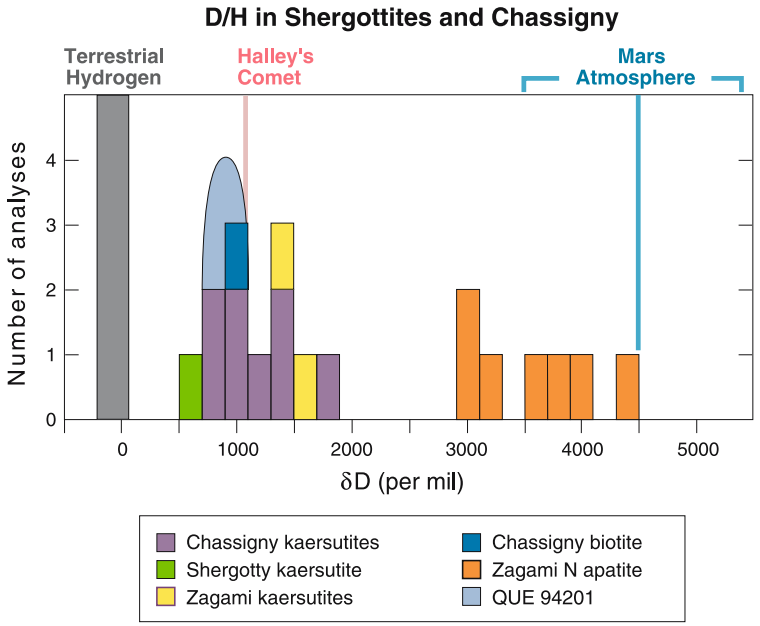

Fig. 9 D/H determined from minerals in Martian meteorites. The lowest value observed in these rocks from Mars is clearly closer to the cometary value than to D/H in Earth's oceans (Fig. 5) (Leshin et al. 1996; Greenwood et al. 2007)

mixed with water having a lower value of D/H. That water presumably came from the rocks making up the planet, as did the bulk of the C and N, just as for Venus. On Mars, we find the same abundance pattern for noble gases and Xe isotopes as on Earth, suggesting that both planets received their noble gases from the same source.

Water in the atmosphere of Mars has a fractionation of D/H caused by atmospheric escape, which has also affected the nitrogen isotopes. Water in the rocks of Mars has a minimum value of D/H that is identical with the cometary value, about 2× the value in Earth's oceans. Unlike Venus and Earth, Mars exhibits no signs of communication between crustal and interior volatiles, offering the possibility that cometary water may still be present as an extremely thin veneer on the Martian surface.

7 Future Work: Some Key Experiments

- Detailed analysis of the composition of nuclei and comae of several comets. Once the critical Rosetta results are in hand, plan for missions to comets with different source regions and especially dynamically new comets coming into the inner solar system as close as possible to the first time and ultimately comet sample return. These analyses must include abundances and isotope ratios of noble gases, H, C, O, N, and other major elements. These elements should be studied in all compounds in which they are found.
- Atmospheric probes for all of the major planets to investigate isotopes and abundances of noble gases and other major elements.
- Surface investigations on Titan to enable comparison of D/H in Titan's subcrustal water ice with D/H in atmospheric methane and hydrogen.

- Detection and abundance measurements of Kr, Xe, and their isotopes on Titan, Venus, and comets for comparison with solar and terrestrial/Martian values.
- Further investigation of D/H in Martian water isolated from the atmosphere.
- All of the existing measurements mentioned in the text would benefit from increased precision with the brilliant exception of the N isotopes measured in a high-temperature inclusion in a meteorite (Meibom et al. 2007).

Acknowledgements Thanks must go to and NASA and ESA for developing and flying the hugely successful Cassini-Huygens spacecraft, as well as the other spacecraft that supplied the data used here. I am grateful to George Gloeckler, Nicolas Grevesse, and the referees for their helpful comments and to Louise Good for her extensive and timely help with the manuscript.

This paper was written to honor the eightieth birthday of Johannes Geiss, whose contributions to our knowledge of the physics and chemistry of the solar system defy enumeration. The author expresses his personal thanks for many instructive and enjoyable conversations with our honoree.

References

C. Arpigny, E. Jehin, J. Manfroid, D. Hutsemékers, R. Schulz, J.A. Stüwe et al., Science **301**, 1522 (2003)
H. Balsiger, J. Altwegg, J. Geiss, J. Geophys. Res. **100**, 5827 (1995)
A. Bar-Nun, A.I. Kleinfeld, E. Kochavi, Phys. Rev. **38**, 7749 (1988)
D.D. Bogard, R.N. Clayton, K. Marti, T. Owen, G. Turner, in *Chronology and Evolution of Mars*, ed. by R. Kallenbach, J. Geiss, W.K. Hartmann (Kluwer, Dordrecht, 2001), pp. 425–458
A.L. Cochran, Astrophys. J. Lett. **576**, L165 (2002)
A.L. Cochran et al., in *Precision Spectroscopy in Astrophysics*, ed. by N. Santos (Springer, Berlin, 2007), 263–265 in press)
A.H. Delsemme, in *The Molecular Origins of Life*, ed. by A. Brack (Cambridge University Press, Cambridge, 1998), pp. 100–118
A.H. Delsemme, Icarus **146**, 313 (2000)
T.M. Donahue, J.H. Hoffman, R.R. Hodges Jr., A.J. Watson, Science **216**, 630 (1982)
T.M. Donahue, J.B. Pollack, in *Venus*, ed. by D.M. Hunten, L. Colin, T.M. Donahue, V.I. Moroz (University of Arizona, Tucson, 1983), pp. 1003–1036
P.M. Eberhardt, D. Reber, D. Krankowsky, R.R. Hodges, Astron. Astrophys. **302**, 301 (1995)
M. Flasar, R.K. Achterberg, B.J. Conrath, J.C. Pearl, G.L. Bjoraker, D.E. Jennings, P.N. Romani et al., Science **307**, 1247 (2005)
J. Geiss, Rev. Mod. Astron. **1**, 1 (1988)
S.S. Genuth, *Comets, Popular Culture and the Birth of Modern Cosmology* (Princeton University Press, Princeton, 1997). 365 pp
J.P. Greenwood, S. Itoh, N. Sakamoto, E.P. Vicenzi, H. Yurimoto, 38th Lunar and Planetary Science Conference (Lunar and Planetary Science XXXVIII), LPI Contribution No. 1338, 2007, p. 2134
N. Grevesse, M. Asplund, A.J. Sauval, Space Sci. Rev. **130**, 105 (2007)
H. Hsieh, D. Jewitt, Science **312**, 561 (2006)
G. Hurst, The Astronomer, Electronic Circ. No. 1177, 22 March, 1997
E. Jehin, J. Manfroid, A.L. Cochran, C. Arpigny, J.-M. Zucconi, D. Hutsemékers et al., Astrophys. J. Lett. **613**, L161 (2004)
E. Jehin, J. Manfroid, D. Hutsemékers, A.L. Cochran, C. Arpigny, W.M. Jackson et al., Astrophys. J. Lett. **641**, L145 (2006)
H.R. Karlsson, R.N. Clayton, E.K. Gibson Jr., T.K. Mayeda, Science **255**, 1409 (1992)
T. Lanz, K. Cunha, J. Holtzman, I. Hubeny, Astrophys. J. (2008, in press)
C. Lecluse, F. Robert, Geochim. Cosmochim. Acta **58**, 2297 (1994)
L.A. Leshin, S. Epstein, E.M. Stolper, Geochim. Cosmochim. Acta **60**, 2635 (1996)
K. Lodders, Astrophys. J. (2008, in press)
M.B. McElroy, T.Y. Kong, Y.L. Yung, J. Geophys. Res. **82**, 4379 (1977)
A. Meibom, A.N. Krot, F. Robert, S. Mostefaoui, S.S. Russell, M.I. Petaev et al., Astrophys. J. **656**, L33 (2007)
H.J. Melosh, A.M. Vickery, Nature **338**, 487 (1989)
S. Messenger, Nature **404**, 968 (2000)
M. Mumma et al., IAU Circ. 8890, July 11, 2007

H.B. Niemann, S.K. Atreya, S.J. Bauer, G.R. Carignan, J.E. Demick, R.L. Frost et al., Nature **438**, 779 (2005)
H.B. Niemann, S.K. Atreya, G.R. Carignan, T.M. Donahue, J.A. Haberman, D.N. Harpold, J. Geophys. Res. **103**, 22,831 (1998)
J. Oro, Nature **190**, 389 (1961)
T. Owen, A. Bar-Nun, Icarus **116**, 215 (1995)
T. Owen, A. Bar-Nun, in *Origin of the Earth and Moon*, ed. by R.M. Canup, K. Righter (University of Arizona Press, Tucson, 2000), pp. 459–471
T. Owen, Th. Encrenaz, Space Sci. Rev. **106**, 121 (2003)
T. Owen, Th. Encrenaz, Planet. Space Sci. **54**, 1188 (2006)
T. Owen, P. Mahaffy, H.B. Niemann, S. Atreya, T. Donahue, A. Bar-Nun et al., Nature **402**, 269 (1999)
T. Owen, P. Mahaffy, H.B. Niemann, S. Atreya, M. Wong, Astrophys. J. **553**, L77 (2001)
J.B. Pollack, P. Bodenheimer, in *Origin and Evolution of Planetary and Satellite Atmospheres*, ed. by S.K. Atreya, J.B. Pollack, M.S. Matthews (University of Arizona Press, Tucson, 1989), pp. 564–602
T.D. Swindle, in *Meteorites and the Early Solar System*, ed. by J.F. Kerridge, M.S. Matthews (University of Arizona Press, Tucson, 1988), pp. 541–542
R. Terzieva, E. Herbst, Monthly Not. Roy. Astron. Soc. **317**, 563 (2000)
F.L. Whipple, Astrophys. J. **111**, 375 (1950)

Space Science Series of ISSI

1. R. von Steiger, R. Lallement and M.A. Lee (eds.): *The Heliosphere in the Local Interstellar Medium*. 1996 ISBN 0-7923-4320-4
2. B. Hultqvist and M. Øieroset (eds.): *Transport Across the Boundaries of the Magnetosphere*. 1997 ISBN 0-7923-4788-9
3. L.A. Fisk, J.R. Jokipii, G.M. Simnett, R. von Steiger and K.-P. Wenzel (eds.): *Cosmic Rays in the Heliosphere*. 1998 ISBN 0-7923-5069-3
4. N. Prantzos, M. Tosi and R. von Steiger (eds.): *Primordial Nuclei and Their Galactic Evolution*. 1998 ISBN 0-7923-5114-2
5. C. Fröhlich, M.C.E. Huber, S.K. Solanki and R. von Steiger (eds.): *Solar Composition and its Evolution – From Core to Corona*. 1998 ISBN 0-7923-5496-6
6. B. Hultqvist, M. Øieroset, Goetz Paschmann and R. Treumann (eds.): *Magnetospheric Plasma Sources and Losses*. 1999 ISBN 0-7923-5846-5
7. A. Balogh, J.T. Gosling, J.R. Jokipii, R. Kallenbach and H. Kunow (eds.): *Co-rotating Interaction Regions*. 1999 ISBN 0-7923-6080-X
8. K. Altwegg, P. Ehrenfreund, J. Geiss and W. Huebner (eds.): *Composition and Origin of Cometary Materials*. 1999 ISBN 0-7923-6154-7
9. W. Benz, R. Kallenbach and G.W. Lugmair (eds.): *From Dust to Terrestrial Planets*. 2000 ISBN 0-7923-6467-8
10. J.W. Bieber, E. Eroshenko, P. Evenson, E.O. Flückiger and R. Kallenbach (eds.): *Cosmic Rays and Earth*. 2000 ISBN 0-7923-6712-X
11. E. Friis-Christensen, C. Fröhlich, J.D. Haigh, M. Schüssler and R. von Steiger (eds.): *Solar Variability and Climate*. 2000 ISBN 0-7923-6741-3
12. R. Kallenbach, J. Geiss and W.K. Hartmann (eds.): *Chronology and Evolution of Mars*. 2001 ISBN 0-7923-7051-1
13. R. Diehl, E. Parizot, R. Kallenbach and R. von Steiger (eds.): *The Astrophysics of Galactic Cosmic Rays*. 2001 ISBN 0-7923-7051-1
14. Ph. Jetzer, K. Pretzl and R. von Steiger (eds.): *Matter in the Universe*. 2001 ISBN 1-4020-0666-7
15. G. Paschmann, S. Haaland and R. Treumann (eds.): *Auroral Plasma Physics*. 2002 ISBN 1-4020-0963-1
16. R. Kallenbach, T. Encrenaz, J. Geiss, K. Mauersberger, T.C. Owen and F. Robert (eds.): *Solar System History from Isotopic Signatures of Volatile Elements*. 2003 ISBN 1-4020-1177-6
17. G. Beutler, M.R. Drinkwater, R. Rummel and R. von Steiger (eds.): *Earth Gravity Field from Space – from Sensors to Earth Sciences*. 2003 ISBN 1-4020-1408-2
18. D. Winterhalter, M. Acuña and A. Zakharov (eds.): *"Mars" Magnetism and its Interaction with the Solar Wind*. 2004 ISBN 1-4020-2048-1
19. T. Encrenaz, R. Kallenbach, T.C. Owen and C. Sotin: *The Outer Planets and their Moons* ISBN 1-4020-3362-1
20. G. Paschmann, S.J. Schwartz, C.P. Escoubet and S. Haaland (eds.): *Outer Magnetospheric Boundaries: Cluster Results* ISBN 1-4020-3488-1
21. H. Kunow, N.U. Crooker, J.A. Linker, R. Schwenn and R. von Steiger (eds.): *Coronal Mass Ejections* ISBN 978-0-387-45086-5

22. D.N. Baker, B. Klecker, S.J. Schwartz, R. Schwenn and R. von Steiger (eds.): *Solar Dynamics and its Effects on the Heliosphere and Earth* ISBN 978-0-387-69531-0
23. Y. Calisesi, R.-M. Bonnet, L. Gray, J. Langen and M. Lockwood (eds.): *Solar Variability and Planetary Climates* ISBN 978-0-387-48339-9
24. K.E. Fishbaugh, P. Lognonné, F. Raulin, D.J. Des Marais, O. Korablev (eds.): *Geology and Habitability of Terrestrial Planets* ISBN 978-0-387-74287-8
25. O. Botta, J.L. Bada, J. Gomez-Elvira, E. Javaux, F. Selsis, R. Summons (eds.): *Strategies of Life Detection* ISBN 978-0-387-77515-9
26. A. Balogh, L. Ksanfomality, R. von Steiger (eds.): *Mercury* ISBN 978-0-387-77538-8
27. R. von Steiger, G. Gloeckler, G.M. Mason (eds.): *The Composition of Matter* ISBN 978-0-387-74183-3
28. H. Balsiger, K. Altwegg, W. Huebner, T.C. Owen, R. Schulz (eds.): *Origin and Early Evolution of Comet Nuclei, Workshop honouring Johannes Geiss on the occasion of his 80th birthday* ISBN 978-0-387-85454-0
30. F. Leblanc, K.L. Aplin, Y. Yair, R.G. Harrison, J.P. Lebreton and M. Blanc (eds.): *Planetary Atmospheric Electricity* ISBN 987-0-387-87663-4

Springer – Dordrecht / Boston / London